THE ROLE OF PALMITIC ACID ON ENDOPLASMIC RETICULUM STRESS: IMPLICATION IN CANCER CELL SURVIVAL

Thesis submitted to

UNIVERSITY OF CALICUT

For the degree of

DOCTOR OF PHILOSOPHY IN ZOOLOGY

(Faculty of Science)

By

Soumya V.V., M.Sc., B.Ed., CSIR-NET (JRF)

Under the Guidance of

Dr. T.D. Babu., Ph.D. (Guide)

&

Dr. C.F. Binoy., Ph.D. (Co-Guide)

AMALA CANCER RESEARCH CENTRE

THRISSUR, KERALA, INDIA

February 2025

DECLARATION

I hereby declare that the thesis entitled "THE ROLE OF PALMITIC ACID IN ENDOPLASMIC RETICULUM STRESS: IMPLICATION IN CANCER CELL SURVIVAL" is an authentic record of the original research work carried out by me under the guidance of Dr. T.D. Babu, Associate Professor, Department of Biochemistry, Amala Cancer Research Centre, Thrissur, Kerala, India, and co-guidance of Dr. C.F. Binoy, Professor, Department of Zoology, St. Thomas College, Thrissur, Kerala, India, and has not been included in any other thesis submitted previously for the award of any degree. This thesis has been subjected to plagiarism checks using iThenticate software at C.H.M.K. Library, University of Calicut, and the similarity index was found within the permissible limit. I also declare that the thesis is free from AI-generated content.

Place: Thrissur **SOUMYA V. V**

Date: 15.02.2025

Amala Cancer Research Centre Society
(A Society Registered T.C. Act, XII of 1955 Sl. No. 56 of 1984)
Amala Nagar- 680 555, Thrissur, Kerala, India

Ref.No. ACRC/REG(b1)/500/2025

Date: 03.10.2025

CERTIFICATE

This is to certify that all the corrections/suggestions recommended by the adjudicators in the Ph D thesis of Ms. Soumya V V (Reg No: U.O. No.15237/2017/Admn. Dated 11.12.2017) entitled 'THE ROLE OF PALMITIC ACID ON ENDOPLASMIC RETICULUM STRESS: IMPLICATION IN CANCER CELL SURVIVAL' have been duly incorporated and the contents in the thesis and the soft copy are one and the same.

3/10/25

Dr. T D Babu
Supervising Guide

Dr. T. D. Babu, Ph.D
Asso. Professor, Dept. of Biochemistry
Amala Cancer Research Centre
Amala Nagar P.O., Thrissur-680 555
Kerala, India

RESEARCH & POSTGRADUATE DEPARTMENT OF ZOOLOGY
ST.THOMAS COLLEGE (AUTONOMOUS), TRICHUR- 680 001, KERALA, INDIA.
(NAAC ACCREDITED WITH CGPA 3.70/4 AT 'A++' GRADE - 4TH CYCLE)

Date : 04th October 2025

Prof. (Dr.) C. F. Binoy
Professor & Research Guide

E.Mail: drcfbinoy@gmail.com
Mobile: 8921645795

CERTIFICATE

This is to certify that all the corrections/suggestions recommended by the adjudicators in the Ph D thesis of Ms. Soumya V V (Reg No: U.O. No.15237/2017/Admn. Dated 11.12.2017) entitled 'THE ROLE OF PALMITIC ACID ON ENDOPLASMIC RETICULUM STRESS: IMPLICATION IN CANCER CELL SURVIVAL' have been duly incorporated and the contents in the thesis and the soft copy are one and the same.

Yours faithfully,

Dr. C.F Binoy

Research Co-Guide

Prof. (Dr.) C. F. BINOY, Ph.D.
Professor & Dean of Science
Research & Postgraduate Department of Zoology
St. Thomas' College, Thrissur - 680 001, Kerala
E-mail: drcfbinoy@gmail.com

Amala Cancer Research Centre Society
(A Society Registered T.C. Act, XII of 1955 Sl. No. 56 of 1984)
Amala Nagar- 680 555, Thrissur, Kerala, India

Ref.No. ACRC/REG(b1)/079/2025

Date: 14.02.2025

CERTIFICATE

This is to certify that the thesis entitled "THE ROLE OF PALMITIC ACID ON ENDOPLASMIC RETICULUM STRESS: IMPLICATION IN CANCER CELL SURVIVAL" is a bonafide record of research work carried out by Mrs. Soumya V V under my guidance and supervision at Department of Biochemistry, Amala Cancer Research Centre, Thrissur, Kerala and no part thereof has been presented for the award of any other degree, diploma or other similar titles. The contents of the thesis have been subjected to plagiarism check and the similarity index was found to be within the acceptable maximum limit.

14/2/25

Dr. T D Babu

Supervising Guide

Dr. T. D. Babu, Ph.D
Asso. Professor, Dept. of Biochemistry
Amala Cancer Research Centre
Amala Nagar P.O., Thrissur-680 555
Kerala, India

Phone: + 91 (0) 487 2420435-Extn-212

RESEARCH & POSTGRADUATE DEPARTMENT OF ZOOLOGY
ST.THOMAS COLLEGE (AUTONOMOUS), TRICHUR- 680 001, KERALA, INDIA.
(NAAC ACCREDITED WITH CGPA 3.70/4 AT 'A++' GRADE - 4TH CYCLE)

Prof. (Dr.) C. F. Binoy
Dean of Science
Professor & Head

E.Mail: drcfbinoy@gmail.com
Mobile: 8921645795

Date: 14-02-2025

CERTIFICATE

This is to certify that the thesis entitled **"THE ROLE OF PALMITIC ACID ON ENDOPLASMIC RETICULUM STRESS: IMPLICATION IN CANCER CELL SURVIVAL"** submitted by Mrs. Soumya V V, is an authentic record of the work carried out by her under my supervision and guidance at Department of Biochemistry, Amala Cancer Research Centre, Thrissur, Kerala, India. The work has been presented to plagiarism check and found to be within the permitted limit. Further, it is certified that no part has been presented for the award of any degree, diploma, or other similar titles previously.

14/02/2025

Prof. (Dr.) C.F. Binoy (Co-Guide)
Professor, Dept. of Zoology
St. Thomas College, Thrissur

E-mail: amalacancerresearch@gmail.com
Phone: 0487 2307968

Institutional Animal Ethics Committee (IAEC)

(Reg. No. 149/PO/Rc/S/1999/CPCSEA)

Amala Cancer Research Centre Society

AMALANAGAR - 680 555, THRISSUR, KERALA, INDIA

Ref :

Date: 02.12.2021

Certificate

This is to certify that the project proposal no. ACRC/IAEC/21(2)–P11 entitled 'Role of palmitic acid on endoplasmic reticulum stress: Implication in cancer cell survival' submitted by Dr. T D Babu (on behalf of Ms. Soumya V V) has been approved by the IAEC of Amala Cancer Research Centre in its meeting held on 02.12.2021 and 56 BALB/c mice have been sanctioned under this proposal.

Authorized by	Name	Signature	Date
Chairman:	Dr. T D Babu	.....	02.12.2021
Member Secretary:	Dr. Achuthan C R	.....	02.12.2021
Main Nominee of CPCSEA:	Dr. C B Devanand	.....	02.12.2021

UNIVERSITY OF CALICUT

CERTIFICATE ON PLAGIARISM CHECK

1.	Name of the Research Scholar	**SOUMYA V V.**	
2.	Title of thesis / dissertation	THE ROLE OF PALMITIC ACID ON ENDOPLASMIC RETICULUM STRESS: IMPLICATION IN CANCER CELL SURVIVAL	
3.	Name of the Supervisors	**Dr. T. D. Babu (Supervising- Guide)** **Dr. C. F. Binoy (Co-Guide)**	
4.	Department/Institution	Department of Biochemistry, Amala Cancer Research Centre, Amala Nagar, Thrissur,	
5.	Similar content (%) identified	**Non-core** **Introduction/ Theoretical overview/Review of literature/ Materials & Methods/ Methodology**	**Core** **Analysis/Result/Discussion/ Summary/Conclusion/ Recommendations**
		7	1
	Acceptable maximum limit (%)	10	10
6.	Software used	iThenticate	
7.	Date of verification	Feb 13,2025,8:10AM GM+5:30	

**Report on plagiarism check, specifying included/excluded items with % of similarity to be attached.*

Checked by (with name, designation & signature)

for Dr. Naisiudheen T.
SEEMA M.V.
Assistant Librarian
University of Calicut
Malappuram - 673 635

C.H. MOHAMMED KOYA LIBRARY
P.O. CALICUT UNIVERSITY
UNIVERSITY OF CALICUT

Name and signature of the Researcher: **SOUMYA V V**

Name and signature of the Supervisor:

14/2/25

Prof. (Dr.) C. F. BINOY, Ph.D
Professor & Dean of Science
Research & Postgraduate Department of Zoology
St. Thomas' College, Thrissur - 680 001, Kerala
E-mail: drcfbinoy@gmail.com

Dr. T. D. Babu, Ph.D
Asso. Professor, Dept. of Biochemistry
Amala Cancer Research Centre
Amala Nagar P.O., Thrissur-680 555
Kerala, India

The Doctoral Committee* has verified the report on plagiarism check with the contents of the thesis, as summarized above and appropriate measures have been taken to ensure originality of the Research accomplished herein.

Name & Signature of the HoD/HoI (Chairperson of the Doctoral Committee):

**In case of languages like Malayalam, Tamil etc. On which no software is available for plagiarism check, a manual check shall be made by the Doctoral Committee, for which an additional certificate has to be attached.*

Dr. V. RAMAN KUTTY
RESEARCH DIRECTOR

AMALA CANCER RESEARCH CENTRE SOCIETY
THRISSUR 680 555

ACKNOWLEDGEMENT

First and foremost, I thank the Almighty for His countless blessings and guidance throughout my life, and for His unwavering support throughout the journey of my research.

I am deeply indebted to my Ph.D. supervisor, **Dr. T.D. Babu**, Associate Professor, Department of Biochemistry, Amala Cancer Research Centre, for his exceptional mentorship, unwavering support, and constant encouragement. His guidance provided me with the confidence to explore new ideas, and his insightful feedback was crucial throughout the entire course of my research and the preparation of this thesis.

I would also like to extend my heartfelt thanks to my co-supervisor, **Dr. C.F. Binoy**, Professor, Department of Zoology, St. Thomas College, Thrissur, for his valuable suggestions and continuous encouragement. His motivation and unwavering support played a vital role in the success of my research.

I sincerely appreciate the guidance and support provided by **Dr. Ramankutty V**, Ph.D, Research Director at Amala Cancer Research Centre, during this research.

I deeply appreciate **Dr. Achuthan C.R,** for his subject-specific guidance, expert advice, and unwavering support. The confidence they have instilled in me has been invaluable during this journey.

I would like to extend my heartfelt thanks to all the members of the Amala Cancer Research Centre for their invaluable contributions. Special gratitude goes to **Dr. Ramadasan Kuttan** (former Research Director**), Dr. Suraj K** (Assistant Professor), **Dr. Manu K A** (Assistant Professor), **Dr. K.K. Janardhanan** (Professor), the late **Dr. Jose Padikkala** (former Professor), and **Dr. Girija Kuttan** (former Professor) for generously offering their time, expertise, and knowledge. Their professional insights and consistent support have played a crucial role in enriching my research experience.

I would like to express my deepest gratitude to the late Padma Bhushan **Rev. Gabriel, CMI**, the esteemed Founder-Director of Amala Cancer Research Centre, Thrissur. His relentless dedication and visionary leadership were instrumental in establishing the Centre, and his unwavering commitment to excellence continues to inspire its success and growth.

I would like to extend my sincere gratitude to **Rev. Julius Arakkal CMI**, Managing Director, **Rev. Fr. Francis Kurissery CMI**, former Managing Director, and **Fr. Antony Perinchery CMI**, Joint Director of Amala Cancer Hospital and Research Centre, for granting me the opportunity to conduct my research at this esteemed institution.

I am grateful to **Dr. Elyas K.K.,** Professor at the University of Calicut, and **Dr. Ramnath V.,** Professor at Kerala Veterinary and Animal Science University, for their valuable support and guidance. My heartfelt thanks also go to Prof. **Dr. Joy Augustine,** Head of Pathology at Amala Institute of Medical Sciences, for his expertise and insightful suggestions that greatly contributed to this work

I would also like to express my sincere thanks to **Dr. Rajkumar Banerjee,** CSIR-Indian Institute of Chemical Technology and **Dr. Bipasha Bose**, Professor & Faculty-In-Charge & PI of the Stem Cells and Regen Med Centre at Yenepoya University, for their invaluable support and guidance, which played an important role in the success of this research.

A special thanks to my dear friends **Dr. Arunaksharan N.**, **Dr. Soorya P.I.**, **Dr. Remya V.**, **Dr. Veena Raveendran**, **Ms. Sruthi P.K**. and **Mrs Aswathi C. V.,** for their unwavering support and companionship during challenging times. Their encouragement and presence have been truly invaluable. I would also like to express my gratitude to **Dr. Meera Nair, Dr. Pareeth C M., Dr. Shaji E. M., Dr. Seema Menon., Dr. Silpa Prabha., Dr. Indu M. S., Dr. Ravikumar., Dr. Ramya Haridas., Dr. Ann Mary Joseph.,** and **Dr. Hasna**, whose constant motivation and support greatly assisted me throughout my work.

I would like to acknowledge the contributions of my labmates, **Dr. Leena Chandrashekaran**, **Dr. Safna Hussain**, **Mrs. Anu**, and **Mrs. Jisna Baby**, who have generously shared their knowledge and expertise with me. I extend my thanks to **Mrs. Sneha Das**, **Ms. Gopika Biju**, and **Ms. Athira** for their support. I am also deeply grateful to **Mrs. Sneha K.**, **Mrs. Neethu**, **Mrs. Sisira K. Suresh**, **Mrs. Veena Gopinath**, **Ms. Agnes Ouseph**, **Vignesh**, **Lijith K. P**, **Mrs. Anju Joseph**, **Mrs. Silpa**, **Mrs. Navya**, and **Ms. Haseena** for their continuous help. I sincerely acknowledge the contributions of the many M.Sc. dissertation students who assisted me at various stages

of this journey. I am especially thankful to **Ms. Neethu**, **Ms. Jamsia**, and Trainee **Anajana** for their support and valuable help throughout the research process.

I would like to express my sincere gratitude to **Mrs. Preetha C.G.**for her unwavering support and patience with my animal work. Special thanks to **Mrs. Sumathy**, **Mrs. Sheeba**, **Mrs. Sunitha**, and **Mrs. Hemalatha** for their continuous help and encouragement throughout the process at the **Amala Cancer Research Centre**.

I would like to extend my gratitude to **Dr. Sreed Sharma Kanakkillam**, University of Ljubljana, **Snijesh V.P**., St. John's National Academy of Health Sciences, and **Dr. Faisal Moossa Athikkavil**, Fondazione Istituto Neurologico Nazionale Casimiro Mondino, **Sister Beena,** Manipal Univeristy, for their valuable contributions and incredible support in my research journey.

I am sincerely grateful to CSIR for their generous financial support through the CSIR JRF Fellowship, which was essential in enabling me to complete my research.

I am deeply grateful to the incredible people who have stood by me throughout this journey, offering love, guidance, and unwavering support. I would like to express my heartfelt gratitude to my husband for his unwavering love, support, and encouragement throughout this journey. His belief in me has been a constant source of strength. I am also deeply grateful to my husband's family for their kindness, patience, and the support that has been essential to my journey.

The love, wisdom, and unwavering support of my beloved parents have been the guiding forces in my life. Their belief in me has provided a solid foundation, and their sacrifices and guidance have continuously fuelled my determination to move forward. The encouragement from my sister, and brother-in-law, has provided peace and reassurance, always reminding me that I am not alone.

The boundless joy of my niece, has been a reminder of the importance of love and family, and her laughter has brightened even the toughest days.

My heartfelt gratitude goes to all the individuals who have supported me along the way, offering their time, expertise, encouragement, and kindness throughout this challenging yet rewarding journey.

Soumya V V

Dedicated to

My family, for being my foundation and my strength.

My friends, for standing by me through it all.

The Divine, for his constant presence and blessings.

CONTENTS

List of Tables ..... **i**

List of Figures ..... **ii**

List of Abbreviations ..... **vi**

Abstract ..... **ix**

Abstract (Malayalam) ..... **xiii**

Introduction ..... **xviii**

Chapter 1: Review of literature **01-33**

1.1 Introduction 01
1.2 Palmitic acid: a prime saturated fat 02
1.2.1 Palmitic acid synthesis, dietary uptake, and metabolism 03
1.2.2 PA and health implications 05
1.2.3 Palm oil as a prime source of PA 07
1.3 Endoplasmic reticulum stress: cellular adaptations and pathology 09
1.3.1 Endoplasmic reticulum: protein folding and homeostasis 09
1.3.2 Endoplasmic reticulum stress (ER stress) 10
1.3.3 Unfolded protein responses (UPR) 11
1.3.3.1 PERK pathway 12
1.3.3.2 IRE1 pathway 13
1.3.3.3 ATF6 pathway 14
1.3.4 Integration of ER stress with redox homeostasis and lipotoxicity 15
1.3.4.1 ER stress and redox homeostasis 15
1.3.4.2 ER stress and lipotoxicity 16
1.3.4.3 ER stress and inflammation 18
1.3.5 ER stress and autophagy 19
1.4 Excess palmitic acid intake and ER stress 21
1.5 Colorectal cancer (CRC) 26
1.5.1 ER stress: a dual-edged sword in colon cancer pathology 28
1.5.2 UPR's role in colon cancer progression and drug resistance 30
1.6 Research Problem 32
1.7 Objectives 32

Chapter 2. Materials and methods **34-70**

2.1 Materials 34
2.1.1 Chemicals 34
2.1.2 Diagnostic kits and reagents 36
2.1.3 Instruments 36

2.1.4 Software 37
2.1.5 Cell lines 38
2.1.6 Animals 38
2.1.7 Palm oil 38
2.1.7.1 GC-MS/MS analysis of palm oil 38
2.1.7.2 Direct fame synthesis 38
2.1.7.3 Concentration of palmitic acid in palm oil 39
2.2. Methods 39
2.2.1 Cytology 39
2.2.1.1 Cell culture conditions and treatment procedures 39
2.2.1.1.1 Thawing of cells 39
2.2.1.1.2 Cryopreservation of cells 40
2.2.1.1.3 Cell Harvesting 40
2.2.1.1.4 Cell Seeding Density 40
2.2.1.1.5 Preparation of palmitic acid stock solution 41
2.2.1.2 Cell culture assays 41
2.2.1.2.1 MTT assay 41
2.2.1.2.2 Sulforhodamine B assay 41
2.2.1.2.3 Oil red O staining and quantification of neutral lipids 42
2.2.1.2.4 Trypan blue exclusion method 42
2.2.1.2.5 Colony formation assay 43
2.2.1.2.6 DCFH-DA assay 43
2.2.1.2.7 Thioflavin T assay 44
2.2.1.2.7.1 Determination of misfolded protein aggregates in cells 44
2.2.1.2.7.2 Determination of misfolded protein aggregates in tissues 45
2.2.1.2.8 Acridine orange assay - acidic vacuoles 45
2.2.1.2.9 Monodansyl cadaverine 46
2.2.1.2.10 Hoechst 33342/propidium iodide double fluorescent staining 46
2.2.2 Animal experiments 47
2.2.2.1 Grouping 47
2.2.2.2 Palm oil administration and CT26-pulmonary metastasis induction 47
2.2.2.3 Analysis of body weight, food, and water intake 48
2.2.2.4 Blood, serum, tissue sample collection and storage 49
2.2.2.5 Glucose tolerance test 49
2.2.2.6 Analysis of lung and intestine histopathology 49
2.2.2.7 Collagen specific studies 49
2.2.3 Biochemistry 50
2.2.3.1 Preparation of cell lysates 50
2.2.3.2 Preparation of tissue homogenate 50
2.2.3.3 Biochemical assays for total protein and oxidative stress parameters 50
2.2.3.3.1 Total protein measurement by lowry method 50

2.2.3.3.2 Total protein measurement by BCA method 51
2.2.3.3.3 Determination of total protein by biuret method 52
2.2.3.3.4 Determination of SOD (Superoxide dismutase) activity 52
2.2.3.3.5 Determination of CAT (Catalase) activity 53
2.2.3.3.6 Estimation of GSH (Reduced Glutathione) content..... 53
2.2.3.3.7 Determination of GST..... 54
2.2.3.3.8 Determination of GR (Glutathione Reductase) activity..... 55
2.2.3.3.9 Glutathione peroxidase (GPx) activity assay..... 56
2.2.3.3.10 Determination of lipid peroxidation by TBARS..... 56
2.2.3.4 Analysis of haematological parameters 57
2.2.3.5 Analysis of serum biochemistry..... 58
2.2.3.5.1 Estimation of serum lipid profile 58
2.2.3.5.1.1 Detection of serum total cholesterol 58
2.2.3.5.1.2 Analysis of serum triglycerides..... 59
2.2.3.5.1.3 Detection of serum HDL (High-density lipoprotein)..... 59
2.2.3.5.1.4 Detection of serum LDL (Low-density lipoprotein)..... 60
2.2.3.5.2 Analysis of liver function markers..... 60
2.2.3.5.2.1 Aspartate transaminase (AST) activity 60
2.2.3.5.2.2 Alanine transaminase (ALT) activity 61
2.2.3.5.2.3 Alkaline phosphatase (ALP) activity 61
2.2.3.5.3 Elisa..... 61
2.2.3.5.3.1 Determination of *Il-6* 61
2.2.3.5.3.2 Determination of *Tnfα*..... 62
2.2.4 Molecular biology..... 62
2.2.4.1 Gene expression profiling..... 63
2.2.4.1.1 RNA isolation..... 63
2.2.4.1.1.1 Homogenization/lysate preparation and phase separation..... 63
2.2.4.1.1.1.1 Tissue homogenization..... 63
2.2.4.1.1.1.2 Cell harvesting and lysate preparation..... 63
2.2.4.1.1.2 Phase separation..... 63
2.2.4.1.1.3 Precipitation..... 64
2.2.4.1.1.4 Washing and separation and storage of RNA 64
2.2.4.1.1.5 Quantifying and checking the integrity of RNA..... 64
2.2.4.1.1.5.1 Quantifying RNA..... 64
2.2.4.1.1.5.2 Detection of RNA integrity..... 64
2.2.4.1.2 cDNA synthesis..... 65
2.2.4.1.3 Real-time quantitative PCR 65
2.2.4.1.4 Primers..... 67
2.2.5 Statistical analysis..... 70

Chapter 3: Analysis of Palmitic Acid Uptake, Toxic Effects, and Lipid Accumulation in Normal and Cancerous Gastrointestinal Cells.....71-99

3.1 Introduction.....71

3.2 Materials and methods.....72

3.2.1 Preparation of palmitic acid stock solution and treatment.....72
3.2.2 MTT assay.....73
3.2.3 Trypan blue exclusion analysis.....73
3.2.4 Morphological assessment.....73
3.2.5 Neutral lipid accumulation.....73
3.2.6 Cell death.....73
3.2.7 Colony formation assay.....73
3.2.8 Statistical analysis.....73

3.3 Results.....74

3.3.1 Effect of palmitic acid on cell viability.....74
3.3.2 Morphological alterations.....76
3.3.3 Uptake of palmitic acid and neutral lipid accumulation.....83
3.3.4 Effect of palmitic acid on colony formation.....88

3.4 Discussion.....95

Chapter 4. Analysis of Palmitic Acid-induced Oxidative Stress, Endoplasmic Reticulum Stress (ERS), and Unfolded Protein Response (UPR) in Normal and Colon Cancer Cells.....100-145

4.1 Introduction.....100
4.2 Materials and methods.....101
4.2.1 Analysis of reactive oxygen species.....101
4.2.2 Analysis of misfolded protein accumulation.....102
4.2.3 Analysis of oxidative stress and lipid peroxidation.....102
4.2.4 Analysis of acidic vacuoles.....102

4.2.5 Analysis of autophagic flux.....102
4.2.6 RT-qPCR analysis.....103
4.2.7 Statistical analysis.....103

4.3 Results.....103
4.3.1 Palmitic acid-induced ROS production in normal and colon cancer cells.....103
4.3.2 Effects of palmitic acid on misfolded protein aggregation.....108

4.3.3 Effect of palmitic acid on antioxidant enzyme activity.....112
4.3.4 Effect of palmitic acid on lipid peroxidation.....112
4.3.5 Effects of palmitic acid on the expression of antioxidant genes.....119
4.3.6 Upregulation of ERS markers *Bip, Chop*, and *Atf6*.....119
4.3.7 Activation of *Perk/Atf4* arm of UPR.....120

4.3.8 Palmitic acid-induced acidic vacuoles 124
4.3.9 Effect of palmitic acid on autophagic flux 124
4.3.10 Effect of PA on *Beclin 1* and *LC3B1* expression 125
4.3.11 Influence of PA on the expression of *Ire1/Xbp1* 126
4.4 Discussion 138
Chapter 5: Effects of Excess Palm Oil Intake on the Development of Endoplasmic Reticulum Stress (ERS) and UPR in Murine Intestinal Tissues 146-165
5.1 Introduction 146
5.2 Materials and methods 148
5.2.1 Palm oil 148
5.2.2 Animals 148
5.2.3 Histopathological analysis of small and large intestine and colon 148
5.2.4 Analysis of lipid peroxidation and antioxidants in intestinal tissues 149
5.2.5 Analysis of inflammatory cytokines in intestinal tissues 149
5.2.6 Quantitative real-time PCR 149
5.2.7 Statistical analysis 149
5.3 Results 149
5.3.1 Palmitic acid concentration in heat-treated palm oil 149
5.3.2 HPO alters tissue architecture of mouse intestines 150
5.3.3 *Il-6* and *Tnf-* α levels in Mouse intestine after HPO treatment 151
5.3.4 HPO alters antioxidant activity, GSH levels, and lipid peroxidation 152
5.3.5 HPO induced ER stress in mouse intestines 156
5.3.6 HPO upregulates *perk/atf4* pathway and antioxidant genes 156
5.3.7 HPO upregulates of *ire1/xbp1* and autophagy genes 157
5.4 Discussion. 163
Chapter 6: Impact of Prolonged Excessive Palm Oil Intake on the Development and Progression of CT26-Induced Colon Cancer Metastasis 166-190
6.1. Introduction 166
6.2. Graphical abstract 168
6.3. Materials and methods 168
6.3.1 GC-MS/MS analysis for palmitic acid quantification in palm oil 168
6.3.2 Cell line and culture conditions 168

6.3.3 Animals, grouping, and experimental procedures....168
6.3.4 Analysis of physiological parameters....169
6.3.5. Analysis of haematological parameters....169
6.3.6 Analysis of glucose tolerance....170
6.3.7 Analysis of serum lipid profiles....170
6.3.8 Analysis of Serum cytokines (Il6 and Tnf-α)....170
6.3.9 Analysis of liver toxicity markers, total protein, and total bilirubin....170
6.3.10 Histopathological analysis....170
6.3.11 Analysis of hydroxyproline in lung tissues....171
6.3.11.1 Picrosirius staining of lung tissues....171
6.3.11.2 Analysis of hydroxyproline in lung tissues....171
6.4 Statistical analysis....171
6.5. Results....172
6.5.1 Impact of HPO on CT26 lung metastasis and associated pathology....172
6.5.2 Effects of HPO on collagen deposition....172
6.5.3 Effect of HPO on body weight, food, and water intake in mice....176
6.5.4 Effect of HPO on Glucose tolerance....177
6.5.5 Changes in haematological parameters following HPO oral gavage....180
6.5.6 HPO impact on liver toxicity markers, total protein and total bilirubin....183
6.5.7 Effects of HPO on serum and tissue cytokines IL6 and TNF-α....185
6.5.8 Effects of HPO on serum lipid profile....185
6.6 Discussion....188

Chapter 7: The Role of Palm Oil in Inducing Inflammation, ER Stress and UPR inColonCancerMetastasisinMice....191-207

7.1 Introduction....191
7.2 Materials and methods....193
7.2.1 Analysis of misfolded protein aggregates in lung tissues....193
7.2.2 Analysis of pulmonary redox status....193
7.2.3 Analysis of cytokines in lung tissues....193
7.2.4 RT-qPCR....194
7.3 Statistical analysis....194

7.4 Results 194
7.4.1 Effects of HPO on *Il6* and *tnf-α* in lung tissues 194
7.4.2 Effect of HPO on antioxidants and MDA level in lung tissues 194
7.4.4 HPO-induced ER stress in lung tissues 198
7.4.5 Effect of HPO on the expression of *Perk/Atf4* and antioxidant genes 202
7.4.6 Effect of HPO on the expression of *Ire1/Xbp1* and autophagy 202
7.5 Discussion 205

Chapter 8: Summary and conclusion 208-213
8.1 Summary 208
8.2 Conclusion 213
Chapter 9: Recommendations 214
Bibliography 215-247
Publications and Presentations 248

LIST OF TABLES

Table No	Title	Page No
1.1	Fatty acid composition in palm oil	08
1.2	Estimated new colorectal cancer cases (2020 – 2040)	28
2.1	Cell culture media and its components	39
2.2	Seeding density and medium volumes for cell lines	40
2.3	Experimental group details	47
2.4	Components for RNA isolation	63
2.5	Components for RNA quantification	64
2.6	Components for cDNA synthesis	65
2.7	Components for real-time quantitative PCR	66
2.8	PCR amplification conditions	66
2.9	Human primer sequences	67
2.10	Mouse primer sequences	68
2.11	RAT primer sequences	69
4.1	The level of antioxidants in IEC6, HCT116 and CT26 cells against Palmitic acid	114
5.1	Two-way ANOVA of HPO treatment and tissue type on IL-6 and TNFα	152
5.2.	Levels of antioxidants and MDA in the intestines following HPO gavage	153
5.3.	Two-way ANOVA of HPO treatment and tissue type on anti-oxidant activities and MDA levels	153
6.1	Lipid Profile Parameters in Experimental Groups	186
7.1	The level of antioxidants and MDA in lung tissues of mice	196

LIST OF FIGURES

Figure No	Title	Page No
1.1	Synthesis of palmitic acid	04
1.2	Palmitic acid in disease progression	07
1.3	UPR arms and unfolded protein response pathways	15
.1.4	Colorectal cancer statistics	27
1.5	Divergent cellular responses to ER stress	29
2.1	HPO administration and CT26 cell inoculation in BALB/c mice	48
3.1.	Effects of palmitic acid on IEC6, HCT116, and CT26 Cells	75
3.2.	Morphology of IEC6 cells	77
3.3.	Morphology of HCT116 Cells	78
3.4.	Morphology of CT26 Cells	79
3.5.	Microscopic images of IEC6 cells stained with PI and Hoechst	80
3.6.	Microscopic images of HCT116 cells stained with PI and Hoechst	81
3.7.	Microscopic images of CT26 cells stained with PI and Hoechst	82
3.8.	PA-induced neutral lipid accumulation in IEC6, HCT116, and CT26 cells	84
3.9.	Microscopic images of IEC6 cells stained with Oil Red O	85
3.10.	Microscopic images of neutral lipid accumulation in HCT116 cells stained with Oil Red O	86
3.11.	Neutral lipid accumulation in CT26 cells	87
3.12.	Effect of PA on colony formation in IEC6 cells	89
3.13.	Microscopic images of IEC6 colonies	90
3.14.	Effect of PA on colony formation in HCT116 cells	91
3.15.	Microscopic images of HCT116 colonies	92
3.16.	Effect of PA on colony formation in CT26 cells	93
3.17	Representative images of CT26 cell colonies	94
4.1.	Microscopic images showing DCF fluorescence associated with ROS production IEC6 cells	105

4.2.	Spectrofluorimetric analysis of ROS production in IEC6 cells	105
4.3.	DCF fluorescence images showing ROS production in HCT116	106
4.4.	ROS production in HCT116 cells	106
4.5.	DCF fluorescence images illustrating ROS production in CT26 cells	107
4.6.	Graphical representation of DCF fluorescence showing ROS production in CT26 cells	107
4.7.	Microscopic images showing thioflavin T (ThT) fluorescence in IEC6 cells	109
4.8.	Spectrofluorimetric analysis of misfolded proteins (ER stress) in IEC6 cells	109
4.9.	ThT fluorescence images showing misfolded protein accumulation (ER stress) in HCT116 cells	110
4.10.	Spectrofluorimetric analysis of misfolded proteins in HCT116 cells	110
4.11.	Microscopic images showing ThT fluorescence in CT26 cells	111
4.12.	Spectrofluorimetric analysis of misfolded proteins in CT26 cells	111
4.13.	Effects of PA on antioxidant levels in IEC6 cells	115
4.14.	Effects of PA on antioxidants in HCT116 cells	116
4.15.	Effects of PA on SOD, CAT, GST, GR, GPx, and GSH in CT26 cells.	117
4.16.	Effects of PA on MDA levels, indicating lipid peroxidation in IEC6, HCT116 and CT26 cells	118
4.17.	Effect of PA on antioxidant gene expression in IEC6, HCT116, and CT26 cells.	121
4.18.	Effect of PA on ER stress markers in IEC6, HCT116, and CT26 cells	122
4.19.	Effect of PA on *Perk/Atf4* expression in IEC6, HCT116 and CT26 cells	123
4.20.	PA-induced acidic vacuoles formation in IEC6 cells	127
4.21.	Grayscale intensity profiles of green (nucleic-acid) and red (acidic vacuole) fluorescence in acridine orange stained IEC6 cells	128
4.22.	Fluorescent images of PA-induced acidic vacuoles in HCT116 cells	129

4.23.	Grayscale intensity profiles of green (nucleic-acid) and red (acidic vacuole) fluorescence in acridine orange stained HCT116 cells	130
4.24.	Fluorescent images of PA-induced acidic vacuoles in CT26 cells	131
4.25.	Grayscale intensity profiles of green (nucleic-acid) and red (acidic vacuole) fluorescence in acridine orange stained CT26 cells	132
4.26.	Fluorescent images of PA-induced autophagic flux in IEC6 cells	133
4.27.	Fluorescent images of PA-induced autophagic flux in HCT116 cells	134
4.28	Fluorescent images of PA-induced autophagic flux in CT26 cells	135
4.29	Effect of PA on *Ire1/Xbp1* expression in IEC6, HCT116 and CT26 cells	136
4.30	Effect of PA on autophagy related gene expression in IEC6, HCT116 and CT26 cells	137
5.1.	GC-MS-chromatogram of heat-treated palm oil.	150
5.2.	Histological changes in the small and large intestines of mice after HPO oral administration.	151
5.3.	IL-6 and TNF-α concentrations in the mouse small and large intestines following HPO treatment.	154
5.4.	Antioxidant levels and oxidative stress in the small and large intestines of mice after HPO gavage.	155
5.5.	The effects of HPO treatment on ER stress markers in the small and large intestines	158
5.6.	*Perk* and *Atf4* upregulation in mouse intestines post-HPO	159
5.7.	RT-PCR analysis of *Nrf2*, *Nqo1*, and *Ho-1* expression in mouse intestines after HPO treatment.	160
5.8.	RT-PCR analysis of *Ire1* and *Xbp1* expression in mouse intestines after HPO treatment	161
5.9.	RT-PCR analysis of *Becn1* and *Lc3b1* expression in mouse intestines after HPO treatment	162
6.1.	Histopathological analysis of CT26 pulmonary metastasis	174
6.2.	Ki67 staining of lung histological sections	174
6.3.	Sirius red staining for collagen and Hydroxyproline content in lung tissue	175

6.4.	Body weight, food, and water intake in mice over four months	178
6.5.	OGTT conducted in experimental groups	179
6.6.	The effects of chronic HPO intake on various haematological parameters	181
6.7.	Representation of Lymphocytes and Platelets in Mice Following Chronic HPO Intake.	182
6.8.	The impact of HPO on hepatic enzymes, total protein, and bilirubin levels in mice	184
6.9.	ELISA analysis showing inflammatory cytokines	185
6.10.	Impact of HPO on serum lipid profiles in mice	187
7.1.	Concentrations of IL-6 and TNF-α, in the lung tissues of mice	195
7.2.	Levels of antioxidants and MDA in lung tissues of mice	197
7.3.	Detection of misfolded protein (ER stress) using Thioflavin T	199
7.4	Grayscale intensity plot profiles and bar graph representing Thioflavin T fluorescence	200
7.5	Expression levels of ER stress marker genes, in lung tissues	201
7.6	Expression of the *Perk/Atf4* UPR arm, and antioxidant genes	203
7.7	Expression of the Irel/*Xbpl* UPR arm, and autophagy genes.	204

LIST OF ABBREVIATIONS

4-PBA	:	4-Phenylbutyric acid
ALP	:	Alkaline phosphatase
ALT	:	Alanine transaminase
ANOVA	:	Analysis of Variance
AST	:	Aspartate transaminase
ATF4	:	Activating transcription factor 4
ATF6	:	Activating transcription factor 6
Beclin 1	:	Beclin 1 protein (autophagy marker)
BiP	:	Binding immunoglobulin protein
BSA	:	Bovine serum albumin
CDNB	:	1-Chloro-2,4-dinitrobenzene
CHOP	:	C/EBP Homologous Protein
CRC	:	Colorectal cancer
EDTA	:	Ethylenediaminetetraacetic acid
ELISA	:	Enzyme-linked immunosorbent assay
ER	:	Endoplasmic reticulum
ERAD	:	ER-associated degradation
ERS	:	Endoplasmic reticulum stress
GADD34	:	Gene growth arrest and DNA damage-inducible protein 34
GCMS	:	Gas chromatography-mass spectrometry
GPx	:	Glutathione peroxidase
GR	:	Glutathione reductase
GRP78	:	Glucose-regulated protein 78
GSH	:	Reduced glutathione
GST	:	Glutathione S-transferase
HDL	:	High-density lipoprotein
hr	:	Hour
HO-1	:	Heme oxygenase 1
IL-6	:	Interleukin-6
IRE1	:	Inositol-requiring enzyme 1
JNK	:	C-Jun N-terminal kinase
Keap1	:	Kelch-like ECH-associated protein 1

kg	:	Kilogram
LC3B1	:	Microtubule-associated protein 1A/1B-light chain 3 beta
LDH	:	Lactate dehydrogenase
LDL	:	Low-density lipoprotein
MDA	:	Malondialdehyde
mg	:	Milligram
min	:	Minute
mL	:	Millilitre
mm	:	Millimetre
MTT	:	3-(4,5-Dimethylthiazol-2-yl)-2,5-diphenyltetrazolium bromide
µg	:	Microgram
µm	:	Micrometre
NADPH	:	Nicotinamide adenine dinucleotide phosphate
NACL	:	Sodium chloride
NBT	:	Nitro blue tetrazolium
NCCS	:	National Centre for Cell Science
NF-κB	:	Nuclear transcription factor-κB
nM	:	nanoMoles
NQO1	:	NAD(P)H dehydrogenase quinone 1
NRF-2	:	Nuclear factor erythroid 2–related factor 2
OECD	:	Organisation for Economic Co-operation and Development
OGT	:	Oral glucose tolerance
PA	:	Palmitic acid
PBS	:	Phosphate-buffered saline
PCR	:	Polymerase chain reaction
PDI	:	Protein disulfide isomerase
PERK	:	Protein kinase RNA-like endoplasmic reticulum kinase
PH	:	Potential of hydrogen
qPCR	:	Quantitative polymerase chain reaction
RIDD	:	Regulated IRE1-dependent decay of mRNAs
ROS	:	Reactive oxygen species
RPM	:	Revolutions per minute
S1P	:	Site 1 protease
S2P	:	Site 2 protease

SDS	:	Sodium dodecyl sulfate
SFA	:	Saturated fatty acid
SOD	:	Superoxide dismutase
TBA	:	Thiobarbituric aci
TBARS	:	Thiobarbituric acid reactive substances
TCA	:	Trichloroacetic acid
TC	:	Total cholesterol
TG	:	Triacylglycerol
TM	:	Tunicamycin
TNF-α	:	Tumor necrosis factor-α
TNFR	:	Tumor necrosis factor receptor
TRAF2	:	Tumor necrosis factor receptor-associated factor 2
UPR	:	Unfolded protein response
U	:	Unit of enzyme activity
VLDL	:	Very low-density lipoprotein
XBP1	:	X-box binding protein 1

ABSTRACT

Palmitic acid, a major saturated fatty acid found in palm oil and other dietary sources, plays a crucial role in cellular metabolism, particularly in lipid metabolism, oxidative stress, and endoplasmic reticulum (ER) stress. When excessive palmitic acid induces ER stress, where protein-folding demands surpass the capacity of ER, it may disrupt cellular balance and potentially lead to cell dysfunction or death. Considering the evidence linking ER stress to various pathological conditions, understanding the mechanistic impact of palmitic acid on ER stress and cellular fate is crucial. This study investigates the molecular pathways through which palmitic acid influences ER stress and its downstream effects, providing insights into its potential role in disease progression and metabolic disorders. Additionally, UPR signalling in metastasised tumour-bearing mice administered with palm oil will be analysed.

In vitro experiments revealed a decline in cell viability dose-dependently across all cell lines. Notably, IEC6 cells exhibited greater tolerance (IC_{50}: 342 μM) than cancer cells, with IC_{50} values of 180 μM for HCT116 and 168 μM for CT26. Morphological alterations, including cell structure disruption, were minimal at lower concentrations but became significant at higher doses. Both normal and cancer cells were found to accumulate neutral lipids, indicating the involvement of fatty acid transport proteins. Notably, both normal cells and cancer cells showed significant lipid accumulation even at lower concentrations and retained the ability to form colonies, indicating resilience under metabolic stress. However, at higher concentrations, palmitic acid disrupted lipid metabolism and compromised antioxidant defences, ultimately leading to cell death.

Excess lipid accumulation in cells led to increased ROS and the accumulation of misfolded proteins at both low and high doses. The upregulation of ER stress marker genes *Bip, Chop,* and *Atf6* further indicated ER stress and misfolded protein accumulation. These findings suggest that palmitic acid disrupts protein folding mechanisms and ER functionality at higher concentrations, leading to cellular dysfunction, while cells can withstand the stress at lower concentrations, indicating that oxidative stress-associated metabolic stresses play a crucial role in ER stress in pathological and physiological contexts.

The ER stress-associated UPR pathways, particularly *PERK/ATF4, IRE1/XBP1*, and ATF6, play a crucial role in cell survival under stress. Palmitic acid is found to activate the PERK pathway and enhance the antioxidant enzymes like superoxide dismutase

(SOD), catalase (CAT) etc, at sub-lethal doses. However, the activity declined to its toxic level. The glutathione-based antioxidants were stable at lower doses but dropped significantly at toxic concentrations, emphasising their role in detoxifying palmitic acid metabolites. Lipid peroxidation level was also increased by palmitic acid, diminishing antioxidant defences, compromising membrane integrity, and heightening oxidative stress at higher doses. Stress-responsive factors *Nrf2*, *Nqo1*and *Ho-1,* key antioxidant defence and autophagy regulators, showed variable expression. The cancer cells, HCT116 and CT26, displayed Nrf2 upregulation compared to normal IEC6 cells. This highlights the adaptive responses of cancer cells under toxic stress to maintain homeostasis. This may lead to cell survival mechanisms.

Palmitic acid treatment resulted in the formation of acidic vacuoles, indicating an autophagic response. Further, acidic vacuoles led to autophagy, as evidenced by MDC staining. The expression of autophagy-related genes *Beclin 1* and *Lc3b1*, along with UPR markers *Ire1* and *Xbp1*, was upregulated particularly in cancer cells, suggesting that palmitic acid enhances cellular resistance to stress through the activation of both autophagy and ER stress pathways. This link between autophagy and ER stress is critical, as autophagy alleviates ER stress by degrading damaged cellular components, while the UPR regulates autophagic flux. This interaction may promote cell survival and progression in colon cancer, indicating potential therapeutic strategies for targeting these pathways to inhibit cancer survival mechanisms.

In vivo studies were conducted using a palm oil-rich diet to analyse the impact of prolonged intake of heat-treated palm oil (HPO), which is high in palmitic acid, on colon cancer metastasis. Using gas chromatography-mass spectrometry/mass spectrometry (GC-MS/MS) analysis determined a palmitic acid concentration of 367 mg/mL in HPO. Over four months, mice received 200 µl of HPO, corresponding to 73.4 mg of palmitic acid per mouse. HPO consumption caused oxidative stress and reduced antioxidant levels in the small intestine, leading to increased lipid peroxidation. This oxidative stress was less pronounced in the large intestine due to its limited lipid absorption capacity. Histopathological analysis revealed significant alterations in goblet cell morphology, inflammation, and ER stress development in the intestinal tissues. Prolonged HPO intake led to the upregulation of ER stress markers such as BIP, CHOP, and ATF6 and the activation of different UPR pathways, with the PERK/ATF4

pathway being more active in the small intestine and the IRE1/XBP1 pathway in the large intestine.

The study investigated the effect of HPO on CT26 cell-induced colon cancer pulmonary metastasis. Oral administration of HPO in mice with CT26 inoculated cancer led to metastasis along with inflammatory cell infiltration. Consistent with previous findings, HPO promoted metastasis through the TLR4/TRIF-Peli1-pNF-κB pathway, while CD36 blockade effectively inhibited this process. HPO treatment exhibited significant body weight loss, glucose intolerance, and systemic inflammation, accompanied by elevated counts of white blood cells, monocytes, neutrophils, lymphocytes, and platelets, suggesting immune modulation. Additionally, HPO influenced lipid metabolism in cancer progression, as evidenced by increased serum cholesterol, triglycerides, and LDL levels. Elevated AST and ALT levels indicated liver dysfunction, while increased lung hydroxyproline and collagen deposition suggested a potential link between HPO exposure and pulmonary fibrosis.

The colon cancer pulmonary metastasis further impacted inflammatory responses, oxidative stress, ER stress, and associated signalling pathways by HPO. Palmitic acid-induced inflammation in lung tissues, characterised by elevated levels of IL-6 and TNF-α, creates a microenvironment favourable for metastatic spread. Increased immune cell infiltration and invasion further supported the role of HPO-induced inflammation in facilitating cancer cell aggressiveness. Chronic HPO intake disrupted redox homeostasis in lung tissues, leading to oxidative damage exacerbated by alterations in antioxidant enzymes. Significant changes in glutathione-related enzymes without corresponding adjustments in SOD and CAT underscored a dysregulated antioxidant defence system, potentiating oxidative stress and inflammation. HPO-induced ER stress, evidenced by the upregulation of ER stress markers like *Bip, Chop, Atf6*, and the activation of *Perk/Atf4* and *Ire1*/*Xbp1* signalling pathways, contributed to a pro-tumorigenic microenvironment favouring cancer metastasis.

In conclusion, palmitic acid-induced oxidative and ER stresses disrupt cellular homeostasis, triggering UPR pathways and impairing antioxidant defences. Cancer cells exhibit metabolic resistance, with increased lipid accumulation and stress adaptation mechanisms. *In vivo*, prolonged HPO intake led to systemic inflammation, immune modulation, and liver dysfunction. HPO-driven ER stress and inflammation in lung tissues, characterised by IL-6 and TNF-α elevation, created a tumour-promoting

microenvironment, facilitating metastatic progression. The dysregulation of antioxidant defence systems further exacerbated oxidative damage. CD36 blockade mitigated HPO-induced metastasis, underscoring the potential of targeting fatty acid metabolism in cancer therapy. These findings provide mechanistic insights into the interplay between lipid metabolism, ER stress, and tumour progression, emphasising the need for dietary interventions and therapeutic strategies to counteract palmitic acid-driven cancer aggressiveness.

Keywords: Palmitic Acid, ER Stress, Oxidative Stress, Autophagy, Unfolded Protein Response, Cancer Metastasis.

സംഗ്രഹം

പാം ഓയിലിലും മറ്റ് ഭക്ഷണ സ്രോതസ്സുകളിലും കാണപ്പെടുന്ന ഒരു പ്രധാന പൂരിത ഫാറ്റി ആസിഡായ പാൽമിറ്റിക് ആസിഡ് സെല്ലുലാർ മെറ്റബോളിസത്തിൽ, പ്രത്യേകിച്ച് ലിപിഡ് മെറ്റബോളിസം, ഓക്സിഡേറ്റീവ് സ്ട്രെസ്, എൻഡോപ്ലാസ്മിക് റെറ്റിക്കുലം സമ്മർദ്ദം എന്നിവയിൽ നിർണായക പങ്ക് വഹിക്കുന്നു. അമിതമായ പാൽമിറ്റിക് ആസിഡ് ഇആർ സമ്മർദ്ദത്തിന് കാരണമാകുമ്പോൾ, അവിടെ ശരിയായ പ്രോട്ടീൻ- രൂപികരണം തകരാറിലാവുക്കയും തന്മൂലം ഇആറിന്റെ സ്വാഭാവികമായ ശേഷി മറികടക്കപ്പെടുക്കയും ചെയ്യുന്നു. ഇത് സെല്ലുലാർ സന്തുലിതാവസ്ഥയെ തടസ്സപ്പെടുത്തുകയും സെൽ അപര്യാപ്തതയിലേക്കോ മരണത്തിലേക്കോ നയിച്ചേക്കാം. ഇആർ സമ്മർദ്ദത്തെ വിവിധ പാത്തോളജിക്കൽ അവസ്ഥകളുമായി ബന്ധിപ്പിക്കുന്ന തെളിവുകൾ കണക്കിലെടുക്കുമ്പോൾ, ഇആർ സമ്മർദ്ദത്തിലും കോശത്തിൻ്റെ നിലനില്പുമായി ബന്ധപ്പെട്ട അന്തിമഫലത്തിലും പാൽമിറ്റിക് ആസിഡിന്റെ യാന്ത്രിക സ്വാധീനം മനസിലാക്കുന്നത് നിർണായകമാണ്. പാൽമിറ്റിക് ആസിഡ് ഇആർ സമ്മർദ്ദത്തെയും അതിന്റെ ഡൗൺസ്ട്രീം ഇഫക്റ്റുകളെയും സ്വാധീനിക്കുന്ന തന്മാത്രാ പാതകളെക്കുറിച്ച് ഈ പഠനം അന്വേഷിക്കുന്നു. കൂടാതെ, പാം ഓയിൽ ഉപയോഗിച്ച് നൽകിയ മെറ്റാസ്റ്റാസിസ് ട്യൂമർ ഉള്ള എലികളിലെ യുപിആർ സിഗ്നലിംഗ് വിശകലനം ചെയ്യും.

വിവിധ തരം കോശങ്ങളിൽ, പാൽമിറ്റിക് ആസിഡ് ഉപേയോഗിച്ചു നടത്തിയ പരീക്ഷണങ്ങളിൽ സെൽ വയബിലിറ്റി ഡോസ്-ആശ്രിതമായി കുറയുന്നതായി കണ്ടെത്തി. കോശങ്ങളിൽ നോർമൽ കോശങ്ങളായ IEC6 (IC_{50}: 342 μM) നു ക്യാൻസർ കോശങ്ങളേക്കാൾ HCT116 (180 μM) ആൻഡ് (CT26 168 μM) പാൽമിറ്റിക് ആസിഡിനോട് കൂടുതൽ ടോളറൻസ് ഉള്ളതായി കാണാം. കുറഞ്ഞ അളവിലുള്ള പാൽമിറ്റിക് ആസിഡിന്റെ ഉപയോഗത്തിൽ കോശ ഘടനയിലെ മാറ്റങ്ങൾ വളരെ കുറവായിരുന്നു, എന്നാൽ ഉയർന്ന അളവിൽ ഈ മാറ്റങ്ങൾ ശ്രദ്ധേയമായി കാണപ്പെട്ടു. സാധാരണ സെലുകളും ക്യാൻസർ സെലുകളും ന്യൂട്രൽ ലിപിഡുകൾ എക്യുമുലേറ്റ് ചെയ്യുന്നത് കണ്ടു, ഇത് ഫാറ്റി ആസിഡ് ട്രാൻസ്പോർട്ട് പ്രോട്ടീനുകളുടെ പങ്ക് സൂചിപ്പിക്കുന്നു. പ്രത്യേകിച്ച്, നോർമൽ സെലുകളും ക്യാൻസർ സെലുകളും കുറഞ്ഞ അളവുകളിൽ ഗണ്യമായ ലിപിഡ് സമാഹരണം കാണിച്ചു, കൂടാതെ കോളനി രൂപീകരണത്തിന്റെ കഴിവ് നിലനിർത്തുകയും ചെയ്തു, ഇത് മെടാബോലിക് ദോഷത്തിനിടയിൽ സ്ഥിരത കാണിക്കുന്നതായി സൂചിപ്പിക്കുന്നു. എങ്കിലും, ഉയർന്ന അളവുകളിൽ പാൽമിറ്റിക് ആസിഡ് ലിപിഡ് മെടാബോളിസം തകരാറിലാക്കി ആന്റി-ഓക്സിഡന്റ് പ്രതിരോധങ്ങളെ ദുർബലമാക്കി, ഒടുവിൽ കോശ മരണം ഉണ്ടാക്കുന്നതായി കണ്ടു.

കോശങ്ങളിൽ ലിപിഡുകളുടെ അനാവശ്യമായ സമാഹാരം ROS വർധിപ്പിക്കുകയും, മിസ്ഫോൾഡഡ് പ്രോട്ടീനുകളുടെ സമാഹരണം ഉണ്ടാകുകയും ചെയ്തു. എന്റ്റോപ്ലാസ്മിക് റെറ്റികുലം സ്ട്രെസിന്റെ സൂചകങ്ങളായ *Bip, Chop, Atf6* ജീൻകളുടെ ആധിക്യം മിസ്ഫോൾഡഡ് പ്രോട്ടീനുകളുടെ സമാഹരണവും സൂചിപ്പിച്ചു. ഈ കണ്ടെത്തലുകൾ കാണിക്കുന്നത്, ഉയർന്ന അളവുകളിൽ പാൽമിറ്റിക് ആസിഡ്

പ്രോട്ടീൻ ഫോൾഡിങ് പ്രക്രിയകളും ER-യുടെ പ്രവർത്തനവും തകരാറിലാക്കുകയും കോശ ദോഷത്തിന് കാരണമാകുകയും ചെയ്യുന്നു. എന്നാൽ, താഴ്ന്ന അളവുകളിൽ കോശങ്ങൾക്ക് ഈ സമ്മർദ്ദം താങ്ങാൻ കഴിയുന്നു, അതായത് ഓക്സിഡേറ്റീവ് സ്ട്രെസ്സും ബന്ധിച്ച മെടാബോലിക് സമ്മർദ്ദങ്ങൾ ER ദോഷത്തിൽ പ്രധാന പങ്ക് വഹിക്കുന്നുവെന്ന് സൂചിപ്പിക്കുന്നു.

എന്റ്റോപ്ലാസ്മിക് റെറ്റികുലം സ്ട്രെസുമായി ബന്ധപെട്ട UPR പാതകൾ, പ്രത്യേകിച്ച് PERK/ATF4, IRE1/XBP1, ATF6, കൊശ സംരക്ഷണത്തിൽ പ്രധാന പങ്ക് വഹിക്കുന്നു. പാൽമിറ്റിക് ആസിഡ് PERK പാതയെ കൂടുതൽ സജീവമാക്കുന്നത് കണ്ടു, കൂടാതെ ഉപജീവനകോശങ്ങളെ സഹായിക്കുന്ന ആന്റി-ഓക്സിഡന്റ് എഞ്ചൈമുകളായ സൂപ്പർ ഓക്സൈഡ് ഡിസ്മ്യൂട്ടേസ് (SOD), കാറ്റാലേസ് (CAT) മുതലായവയെ താഴ്ന്ന പാൽമിറ്റിക് ആസിഡിന്റെ അളവു ഉപയോഗിച്ചപ്പോൾ വർദ്ധിപ്പിക്കുകയും ചെയ്തു. കൂടുതലാവുമ്പോൾ വിഷാഭാവത്തിലേക്ക് മാറുന്നതായും കണ്ടു . ഗ്ലുതതയോണിന്റെ സംബന്ധിച്ച ആന്റി-ഓക്സിഡന്റ് പ്രവർത്തനം താഴ്ന്ന അളവുകളിൽ സ്ഥിരമായിരുന്നു, എന്നാൽഉയർന്ന അളവുകളിൽ അത് നാശമുള്ള നിലയിലേക്കു കുറഞ്ഞു, ഇത് പാൽമിറ്റിക് ആസിഡ് മെറ്റബോലൈറ്റുകൾ ഡീറ്റോക്സിഫൈ ചെയ്യുന്നതിൽ അതിന്റെ പങ്ക് സൂചിപ്പിക്കുന്നു. പാൽമിറ്റിക് ആസിഡ് ലിപിഡ് പെറോക്സിഡേഷൻ നില കൂട്ടുകയും, ആന്റി-ഓക്സിഡന്റ് പ്രതിരോധങ്ങളെ ദുർബലമാക്കുകയും, മൈംബ്രെയ്ൻ ഇന്റഗ്രിറ്റിയെ ബാധിക്കുകയും, ഓക്സിഡേറ്റീവ് സ്ട്രെസ് വർദ്ധിപ്പിക്കുകയും ചെയ്തു. സ്ട്രെസ്-പ്രതിസന്ധി ഘടകങ്ങളായ Nrf2, Nqo1, Ho-1,ആന്റി-ഓക്സിഡന്റ് പ്രതിരോധത്തിന്റെ പ്രധാന നിയന്ത്രണകങ്ങളിലും ഓട്ടോഫജിയും പഠനത്തിൽ കണ്ടു. ക്യാൻസർ സെലുകൾ HCT116, CT26, സാധാരണ IEC6 സെലുകൾക്ക് അപേക്ഷിച്ച് Nrf2-യുടെ അപ്പ്ഡെറെഗുലേഷൻ കാണിച്ചു. ഇത് ക്യാൻസർ കോശങ്ങളുടെ അനുകൂലപ്രതിസന്ധി പ്രതികരണങ്ങൾ ഹൈമോസ്റ്റേസിസ് നിലനിർത്തുന്നതിനുള്ള മാർഗ്ഗങ്ങൾ കാണിക്കുന്നു, അതിനാൽ കോശ സംരക്ഷണ മാർഗങ്ങളിലേക്ക് നയിക്കുന്നു

പാൽമിറ്റിക് ആസിഡ് ആസിഡിക് വാക്യൂവോളുകളുടെ രൂപീകരണത്തിന് കാരണമാകുന്നു, ഇത് ഓട്ടോഫാഗി പ്രതികരണത്തെ സൂചിപ്പിക്കുന്നു. MDC സ്റ്റെയിനിങ്ങിലൂടെ ആസിഡിക് വാക്യൂവോളുകൾ ഓട്ടോഫാഗി പ്രക്രിയയുമായി ബന്ധപ്പെട്ടതാണ് എന്ന് കണ്ടെത്തി. ഓട്ടോഫാഗി-ബന്ധപെട്ട ജീൻകൾ Beclin 1, Lc3b1, കൂടാതെ ER സ്ട്രെസ് മാർക്കർ Ire1, Xbp1 എന്നിവയുടെ പ്രകടനം ക്യാൻസർ കോശങ്ങളിൽ കൂടുതൽ ഉയർന്നു. ഇത്, പാൽമിറ്റിക് ആസിഡ് കോശങ്ങളുടെ എന്റ്റോപ്ലാസ്മിക് റെറ്റികുലം (ER) സ്ട്രെസ് പാതയും ഓട്ടോഫാഗി പാതയും സജീവമാക്കുന്നു, ഇത് കോശത്തെ സ്ട്രെസിൽ നിന്നുള്ള സംരക്ഷണം വർദ്ധിപ്പിക്കുന്നുവെന്ന് സൂചിപ്പിക്കുന്നു. ഓട്ടോഫാഗിയും ER സ്ട്രെസ് പാതയും തമ്മിലുള്ള ബന്ധം, ഉണ്ട് എങ്ങനെഎന്നാൽ ഡാമേജ്ഡ് കോശ ഘടകങ്ങളെ ഓട്ടോഫാഗി നശിപ്പിച്ച് ER സ്ട്രെസ് കുറയ്ക്കുകയും, UPR ഓട്ടോഫാഗി പാതയെ നിയന്ത്രിക്കുകയും ചെയ്യുന്നു. ഈ പ്രക്രിയകൾ കോളോൺ ക്യാൻസർ സംരക്ഷണത്തിനും പുരോഗതിക്കും

സഹായകമാകാൻ സാധ്യതയുണ്ട്, അതിനാൽ ഈ പാതകളെ ലക്ഷ്യമിട്ടുള്ള ചികിത്സാ തന്ത്രങ്ങൾ ഉപയോഗിച്ച് ക്യാൻസർ സംരക്ഷണ മാർഗ്ഗങ്ങൾ തടയാനുള്ള സാധ്യത ഉണ്ട്.

പാൽമിറ്റിക് ആസിഡ് കൂടുതൽ ഉള്ള പാമോയിൽ (HPO) ചെറുതായി ചൂടാക്കിയാണ് എലികളിലെ പരീക്ഷണങ്ങളിൽ ഉപയോഗിക്കുന്നത്.ഗ്യാസ് ക്രോമാറ്റോഗ്രാഫി-മാസ്സ് സ്പെക്ട്രോമെട്രി (GC-MS/MS) ഉപയോഗിച്ച് HPOയിൽ 367 mg/mL പാൽമിതിക് ആസിഡിന്റെ അളവ് കണ്ടെത്തി. നാല് മാസക്കാലം, ഓരോ എലിക്കും ഓരോ ദിവസവും 200 µl HPO നൽകിയപ്പോൾ 73.4 mg പാൽമിതിക് ആസിഡ് ഉൾക്കൊള്ളുന്നത് കണ്ടെത്തി .HPO (heat-treated palm oil) ഉപയോഗം ഓക്സിഡേറ്റീവ് സ്ട്രെസ് ഉണ്ടാക്കി, ഇതിന്റെ ഫലമായി ചെറിയ ആന്റസ്റ്റൈനിന്റെ ആന്റിയോക്സിഡന്റ് നില കുറഞ്ഞു, എളുപ്പത്തിൽ ലിപിഡ് പെരോക്സിഡേഷൻ വർദ്ധിച്ചു. വലിയ ആന്റസ്റ്റൈനിന്റെ ലിപിഡ് ആസ്വീകരണ ശേഷി കുറഞ്ഞിരുന്നതിനാൽ അവിടെ ഓക്സിഡേറ്റീവ് സ്ട്രെസ് കുറവായിരുന്നു. ഹിസ്റ്റോപാത്തോളജിക്കൽ പരിശോധനയിൽ ഗോബ്ലെറ്റ് കോശങ്ങളുടെ രൂപഭേദം, അണുബാധ, ER സ്ട്രെസ്സ് എന്നിവയെ കണ്ടെത്തി. ദീർഘകാല HPO ഉപയോഗം ER സ്ട്രെസ് മാർക്കറായ BIP, CHOP, ATF6 എന്നിവയുടെ ഉയർച്ചക്കും UPR പാതകളുടെ സജീവീകരണത്തിനും കാരണമാകുന്നു. PERK/ATF4 പാത ചെറിയ ആന്റസ്റ്റൈൻ, IRE1/XBP1 പാത വലിയ ആന്റസ്റ്റൈൻ പാതയിൽ കൂടുതൽ സജീവമായി പ്രവർത്തിക്കുന്നുവെന്ന് കണ്ടു. ഈ പഠനം HPO ഉപയോഗിച്ച് CT26 സെൽ-പ്രേരിത കോളോൺ കാൻസർ ഓർഗാനുകളിലേക്ക് എങ്ങനെ മെടാസ്റ്റാസിസ് ഉണ്ടാക്കുന്നു എന്നത് പരിശോധിച്ചു.

HPO എലികളിൽ നൽകിയപ്പോൾ, കാൻസർ കോശങ്ങൾ അവയവങ്ങളിലേക്ക് സഞ്ചരിക്കുകയും അണുബാധയും ഉണ്ടാകുകയും ചെയ്തു. HPO, TLR4/TRIF-Peli1-pNF-κB വഴിയിലൂടെ മെടാസ്റ്റാസിസിന് സഹായിക്കുന്നു എന്നും , എന്നാൽ CD36 ബ്ലോക്കുചെയ്യുന്നതിലൂടെ ഈ പ്രക്രിയ തടഞ്ഞുഎന്നും മുമ്പുള്ള മഠങ്ങൾ പഠനങ്ങൾ തെളിയിച്ചിട്ടുണ്ട് . HPO ഉപയോഗം ശരീര ഭാരം കുറയ്ക്കുകയും, ഗ്ലൂക്കോസ് തകരാറാകുകയും, ഇൻഫ്ലമേഷൻ വർദ്ധിപ്പിക്കുകയും ചെയ്തു. ഇതിന് അനുയോജ്യമായി, വെളുത്ത രക്തകോശങ്ങൾ, മൊണോസൈറ്റുകൾ, ന്യൂട്രോഫിലുകൾ, ലിംഫോസൈറ്റുകൾ, പ്ലേറ്റ്ലറ്റുകൾ എന്നിവയുടെ എണ്ണം വർദ്ധിച്ച് ഇമ്യൂൺ സംവിധാനത്തെ ബാധിച്ചു. HPO ഉപയോഗം കോളോൺ കാൻസറിൽ ലിപിഡ് മെറ്റബോളിസത്തിൽ മാറ്റങ്ങൾ ഉണ്ടാക്കി, കൊളസ്ട്രോൾ, ട്രൈഗ്ലിസറൈഡ്, LDL തലങ്ങൾ ഉയർന്നു. AST, ALT ലെവലുകൾ ഉയർന്നത് കരളിന്റെ പ്രയാസം സൂചിപ്പിച്ചു. കൂടാതെ, ഹൈഡ്രോക്സിപ്രോളിൻ, കോളജൻ സ്രാവം എന്നിവയുടെ വർദ്ധന പുല്മണറി ഫൈബ്രോസിസുമായി ബന്ധപ്പെട്ടു.

HPO (ഹീറ്റ്-ട്രീറ്റ് ചെയ്ത പാൽമായിൽ) ഉപയോഗം കോളോൺ കാൻസർ പുല്മണറി മെടാസ്റ്റാസിസിനെ കൂടുതൽ ശക്തമാക്കുകയും ഇൻഫ്ലമേഷൻ, ഓക്സിഡേറ്റീവ് സ്ട്രെസ്, ER സ്ട്രെസ് എന്നിവയെ ബാധിക്കുകയും ചെയ്തു. പാൽമിറ്റിക് ആസിഡ് മൂലമുള്ള ശ്വാസകോശ അണുബാധ IL-6, TNF-α ലെവലുകൾ വർദ്ധിപ്പിച്ച്, കാൻസർ കോശങ്ങൾ വ്യാപിക്കുന്നതിനുള്ള അനുകൂല സാഹചര്യം ഉണ്ടാക്കി. HPO ഉപയോഗം മൂലം പ്രതിരോധ കോശങ്ങൾ കൂടുതൽ ശ്വാസകോശത്തിൽ എത്തുകയും, കാൻസർ

കോശങ്ങളുടെ ആക്രമണശേഷി വർദ്ധിപ്പിക്കുകയും ചെയ്തു. ദീർഘകാലമായി HPO ഉപയോഗിക്കുന്നത് ശ്വാസകോശത്തിലെ ഓക്സിഡേറ്റീവ് ബാലൻസ് തകർക്കുകയും, ആന്റിയോക്സിഡന്റ് എൻസൈമുകളിൽ മാറ്റങ്ങൾ വരുത്തുകയും ചെയ്തു. ഗ്ലൂട്ടത്തയോൺ ബന്ധപ്പെട്ട എൻസൈമുകളിൽ വലിയ വ്യത്യാസമുണ്ടായെങ്കിലും SOD, CAT എന്നിവയിൽ മാറ്റമില്ലാത്തത് ആന്റിഓക്സിഡന്റ് പ്രതിരോധ സംവിധാനം തകരാറിലാണെന്ന് സൂചിപ്പിക്കുന്നു, ഇത് ഓക്സിഡേറ്റീവ് സ്ട്രെസിനും ഇൻഫ്ലമേഷനും കാരണമായി. കൂടാതെ, HPO ഉപയോഗം ER സ്ട്രെസിനെയും വർദ്ധിപ്പിച്ചു. Bip, Chop, Atf6 എന്നീ മാർക്കറുകൾ ഉയർന്നതും, Perk/Atf4, Ire1/Xbp1 പാതകൾ സജീവമായതും കാൻസർ മെടാസ്റ്റാസിസിന് അനുകൂലമായ ഒരു പരിതസ്ഥിതി സൃഷ്ടിച്ചു. ഇതുമൂലം, കാൻസർ കോശങ്ങൾ കൂടുതൽ വ്യാപിക്കുകയും രോഗം കൂടുതൽ കടുത്തതാകുകയും ചെയ്യുന്നു.

പാൽമിറ്റിക് ആസിഡ് ശരീരത്തിൽ ഓക്സിഡേറ്റീവ് സ്ട്രെസ്സും ER സ്ട്രെസ്സും ഉണ്ടാക്കി, കോശങ്ങളുടെ സ്വാഭാവിക നില തകർക്കുന്നു. ഇത് പ്രതിരോധ ശക്തി കുറയ്ക്കുകയും, കാൻസർ കോശങ്ങൾക്ക് കൂടുതൽ വളരാൻ അനുകൂല സാഹചര്യം സൃഷ്ടിക്കുകയും ചെയ്യുന്നു. മൈസ് മേൽ നടത്തിയ പരീക്ഷണത്തിൽ, ദീർഘകാലം HPO ഉപയോഗിച്ചത് ശരീരത്തിൽ അണുബാധ (inflammation), പ്രതിരോധ വ്യതിയാനം, കരളിന്റെ പ്രവർത്തനക്കേടുകൾ എന്നിവ ഉണ്ടാക്കി. ശ്വാസകോശങ്ങളിൽ IL-6, TNF-α എന്ന ഇൻഫ്ലമേറ്ററി മൂലകങ്ങൾ കൂടിയതോടെ, കാൻസർ കോശങ്ങൾ കൂടുതൽ വ്യാപിക്കാനായി അനുയോജ്യമായ അന്തരീക്ഷം സൃഷ്ടിച്ചു. ആന്റിഓക്സിഡന്റ് പ്രതിരോധം തകരാറിലായതോടെ, ഓക്സിഡേറ്റീവ് നാശം കൂടി.

CD36 എന്ന ഒരു പ്രോട്ടീൻ തടഞ്ഞപ്പോൾ, HPO മൂലമുണ്ടാകുന്ന കാൻസർ വ്യാപനം കുറച്ചു. അതിനാൽ, കൊഴുപ്പ് (fat) അനുബന്ധ കാൻസർ ചികിത്സയ്ക്കായി പുതിയ മാർഗങ്ങൾ പരിഗണിക്കേണ്ടതുണ്ടെന്നു മനസ്സിലാക്കാം. ഈ പഠനം, ഭക്ഷണ ശീലങ്ങൾ മാറ്റി HPO മൂലമുണ്ടാകുന്ന കാൻസർ അപകടം കുറയ്ക്കാൻ സഹായിക്കാമെന്ന ആശയം ശക്തിപ്പെടുത്തുന്നു.

പ്രധാന വാക്കുകൾ: പാൽമിറ്റിക് ആസിഡ്, പാം ഓയിൽ, എന്റ്റോപ്ലാസ്മിക് റെറ്റികുലം സ്ട്രെസ്, ഓക്സിഡേറ്റീവ് സ്ട്രെസ്, ഓട്ടോഫാഗി, കാൻസർ മെടാസ്റ്റാസിസ്.

INTRODUCTION

The role of dietary lipids in cancer development has gained considerable attention in recent years, with numerous epidemiological studies highlighting a strong correlation between high-fat consumption and an increased risk of malignancies such as breast, prostate, and colorectal cancers. Among dietary fats, saturated fatty acids like palmitic acid have been extensively studied due to their potential influence on cancer initiation and progression. Palmitic acid, a major component of animal fats and processed foods, has been implicated in various oncogenic processes, including inflammation, oxidative stress, metabolic reprogramming, and modulation of the tumour microenvironment.

Palmitic acid is a 16-carbon saturated fatty acid, one of the most abundant fatty acids. It is a significant component of palm oil, dairy products, and meat and is a key structural component of cell membranes and an energy source. Palmitic acid is a fundamental component of cell membranes, contributing to membrane fluidity and integrity, and is essential for signal transduction and intercellular communication. Palmitic acid is primarily synthesised in the liver through *de novo* lipogenesis and also comes from dietary sources, particularly diets high in saturated fats. Despite its physiological roles, concerns arise regarding its association with health issues such as obesity, insulin resistance, and cardiovascular diseases due to its abundance in diets. Moreover, recent studies emphasise the involvement of palmitic acid in cancer cell survival and proliferation, where altered lipid metabolism provides energy and building blocks for rapid growth (Zeng *et al.*, 2020a, Maly and Hofmann, 2020, Fatima *et al*., 2019b). Palmitic acid reported activating pathways promoting cell survival like the PI3K/Akt pathway while inhibiting regulators of cellular energy homeostasis such as AMP-activated protein kinase (AMPK).

Endoplasmic reticulum (ER) stress and mitochondrial dysfunction contribute to apoptosis, revealing its intricate role in disease pathogenesis. Understanding the metabolic effects of palmitic acid, mainly its association with ER stress, is crucial for elucidating its diverse roles and identifying potential disruptions in cellular physiology and pathology. Hence, exploring the multifaceted functions of palmitic acid emphasises its significance in cellular processes and its implications for health and disease. Understanding the importance of palmitic acid in cancer cell metabolism and signalling is critical for developing targeted therapies and dietary interventions for cancer

prevention and treatment, while strategies to alter lipid metabolism and fatty acid composition offer promising avenues for cancer therapy and prevention.

The endoplasmic reticulum (ER) is a key organelle orchestrating essential cellular processes such as protein synthesis, folding, and lipid metabolism, crucial for maintaining cellular homeostasis (Schröder, 2008b, Celik *et al.*, 2023). However, when confronted with disruptions in its functions, the ER activates intricate stress response pathways, collectively known as the Unfolded Protein Response (UPR), to mitigate cellular stress and restore equilibrium. The significance of ER stress transcends fundamental cellular dynamics, extending into the realm of disease pathogenesis, particularly in the context of cancer. The link between ER stress and cancer biology is evident in various facets of tumour initiation, progression, and response to treatment. Notably, cancer cells exploit adaptive mechanisms triggered by ER stress to facilitate their survival and proliferation, underscoring the Principal role of this process in oncogenesis (Oakes, 2020).

Understanding the molecular mechanisms of ER stress in cancer is crucial due to its significant impact on clinical management and therapeutic strategies. The UPR, a complex signalling network activated in response to ER stress, comprises three principal branches mediated by transmembrane proteins: inositol-requiring enzyme 1 (IRE1), protein kinase RNA-like ER kinase (PERK), and activating transcription factor 6 (ATF6). These sensors detect aberrations in protein folding and initiate signalling cascades to restore ER homeostasis(Chen *et al*., 2023b). Understanding the details of ER stress in cancer necessitates a comprehensive exploration of its molecular underpinnings and functional consequences. This necessitates a thorough investigation into the activation and regulation of the IRE1, PERK, and ATF6 pathways and their implications for tumour biology and therapeutic targeting. In this study, we aimed to analyse the dynamic association between ER stress and cancer progression, focussing on the molecular mechanisms driving tumour development and progression. The study integrates insights from fundamental research and clinical observations to elucidate the basic mechanisms of ER stress pathways to combat cancer effectively.

Palmitic acid induces ER stress in many pathological contexts, perturbing ER membrane composition and integrity and disrupting the redox balance within the ER, thus playing a diverse role in triggering and sustaining ER stress, highlighting its significance in metabolic disorder development(Celik *et al.,* 2023). Numerous

investigations suggest that palmitic acid enhances cancer cell survival and may promote metastasis (Altea-Manzano *et al.*, 2023, Maly and Hofmann, 2020). Our investigation posits a novel hypothesis that colon cancer cells protect themselves under extreme stress induced by palmitic acid, which could contribute to cell survival and metastasis. This underscores the importance of exploring how cancer cells overcome extreme conditions or cytological perturbations by activating the Unfolded Protein Response. Even though the title does not mention colon cancer, this scenario is inherently the subject of our inquiry. To better understand palmitic acid-induced ER stress and its translational implications, we need to contextualise our findings within colon cancer research, as it is considered a better model. Even if our study focused on colon cancer cells, the general implications of palmitic acid-induced ER stress can be applied to all aspects of cancer biology. This study is significant because it provides insight into the molecular mechanisms behind tumour cell adaptability.

Colorectal cancer remains a significant challenge in oncology due to its global impact on morbidity and mortality. The association between high consumption of palmitic acid-rich foods and increased colon cancer risk has drawn attention to the molecular intricacies involved. Recent studies have elucidated the relationship between excess dietary saturated fats, inflammation, alterations in gut microbiota, and the development and progression of colon cancer (Yang *et al*., 2022, Tong *et al.,* 2021, Bojková *et al.*, 2020). Endoplasmic reticulum (ER) stress adaptation mechanisms in cancer biology are vital in promoting cancer cell survival and proliferation. Cancer cells exploit the UPR to cope with ER stress, promoting malignant traits and therapeutic resistance. This adaptive process encompasses alterations such as enhanced protein folding capacity through upregulated chaperone proteins like heat shock proteins (HSPs), increased lipid metabolism facilitating membrane biogenesis, and modulation of calcium homeostasis to regulate ER stress responses.

Dysregulation of ER stress responses fuels various facets of cancer progression, including tumour growth, invasion, and metastasis, and confers resistance to conventional chemotherapy and targeted therapies *(Wang et al., 2012, Bonsignore et al.*, 2023, Wang and Mi, 2023). Understanding the association between dietary fat intake and colon cancer pathogenesis is crucial. Targeting palmitic acid-induced ER stress presents a promising therapeutic approach for colon cancer treatment. By disrupting adaptive mechanisms that promote cancer cell survival and proliferation,

pharmacological inhibitors of the UPR pathway and dietary interventions offer novel strategies to improve patient outcomes and overcome therapeutic resistance. Research into metabolic abnormalities contributing to cancer progression, particularly the effects of palmitic acid on ER stress in colon cancer cells, provides insights into cancer cell survival mechanisms. This exploration contributes to a deeper understanding of colon cancer biology and may inform new treatment strategies.

Elucidating the molecular details underlying ER stress-mediated cancer progression offers promising therapeutic strategies targeting vulnerabilities associated with ER stress adaptation. Integrating data from epidemiological studies, mechanistic investigations, and clinical observations contributes to unravelling the complex link between dietary influences, ER stress responses, and colon cancer pathogenesis. Continued research into the molecular mechanisms underlying ER stress and its role in cancer pathogenesis is essential for developing effective targeted therapies and personalised treatment strategies tailored to individual patient profiles. It enhances our understanding of the complexities of metabolic changes responsible for colon cancer's rapid advancement and contributes to the dynamic field of cancer biology.

Chapter 1

Review of Literature

1.1 Introduction

Numerous epidemiological studies have consistently found that high-fat diets are linked to an increased risk of cancer development and progression (Zhang *et al*., 2021). In addition, certain fats have the potential to facilitate inflammation and oxidative stress, thereby establishing a milieu that is favourable for the proliferation of cancer cells. There has been an increase in studies on saturated fatty acids, particularly palmitic acid, to understand the relationship between lipid metabolism, endoplasmic reticulum stress, and survival of cancer cells (Zeng *et al*., 2020a, Maly and Hofmann, 2020). Since palmitic acid is an integral component of cellular membranes, it plays a significant role in regulating cellular homeostasis and energy storage. Recent reports suggest the involvement of palmitic acid in various cellular pathways of disease progression and development (Fatima *et al*., 2019b). Several studies have demonstrated that the development of endoplasmic reticulum (ER) stress can contribute to pathological conditions and the molecular response across multiple disorders, indicating a common underlying mechanism (Marciniak *et al*., 2022). In this context, investigating the metabolic effects of palmitic acid on cellular processes is significant in revealing its diverse roles in various pathological conditions, especially those associated with endoplasmic reticulum stress.

The endoplasmic reticulum plays a key role in protein synthesis, folding, and lipid metabolism to maintain cellular homeostasis. When any cellular stress condition disrupts homeostasis, the ER activates a response or signalling known as UPR, collectively called the ER stress response pathway (Sicari *et al*., 2020), to resolve the stress and maintain homeostasis. However, if the stress remains unresolved, the UPR disruption may linked to a wide range of clinical diseases, including cancer. The cells, particularly cancer cells, may exploit this as an adaptive mechanism to survive, which is crucial in cancer development and progression (Oakes, 2020). Considering this, the study emphasises the role of ER stress in cellular health and pathology with palmitic acid metabolism.

Among the leading causes of cancer-related morbidity and mortality, colon cancer is a significant challenge. Consuming saturated fats increases the risk of colon cancer and progression, demonstrating how dietary choices are significant in susceptibility to the disease and progression. Evidence shows that these diets primely promote inflammatory response and alter gut microbiota, contributing to colon cancer

development and progression (Yang *et al*., 2022, Tong *et al*., 2021, Bojková *et al*., 2020). An understanding of the complex link between dietary fat intake and colon cancer may help with targeted interventions and preventive measures that may reduce the burden of this disease.

For a better understanding of the translational implications and therapeutic potential, we selected the palmitic acid-induced ER stress model. Although our study focused on colon cancer cells, the findings may apply to various aspects, particularly the molecular mechanisms behind tumour cell adaptability.

Due to the high adaptability nature of cancer cells, particularly in the unique environment of the colon, the exploration of metabolic abnormalities that contribute to cancer progression is of paramount importance. The role of palmitic acid is traditionally known in lipid metabolism, and recent studies have reported its significance in various key cellular mechanisms that regulate the survival of colon cancer. Studies into these molecular pathways also help to provide a more comprehensive understanding of colon cancer biology and to develop new strategies for colon cancer management. Thus, this study aims to analyse the effect of palmitic acid on endoplasmic reticulum (ER) stress in colon cancer for a deeper understanding of cell survival. By elucidating the metabolic changes driving colon cancer progression, this study contributes to the broader field of cancer biology.

1.2 Palmitic acid: A prime saturated fat

Palmitic acid is a saturated fatty acid with a 16-carbon aliphatic chain, one of the most common fatty acids in nature. As a straight-chain saturated fatty acid, its carbon atoms are entirely saturated with hydrogen atoms and have no double bonds. $C_{16}H_{32}O_2$ is the chemical formula for palmitic acid. Palm oil and animal fats are among the many natural fats and oils that are a significant constituent (Loften *et al*., 2014). Palmitic acid, which is frequently esterified to glycerol to produce triglycerides, is the major component of many dietary fats and is essential for the production of lipids. Elevated levels of palmitic acid in the bloodstream have been linked to cardiovascular diseases and insulin resistance, even though it is an essential component for cellular structure and energy storage (Simon *et al*., 1995, Reynoso *et al*., 2003). Excessive consumption of palmitic acid has been associated with adverse health effects. It is an essential

constituent of cell membranes, contributing to their fluidity and structural integrity, and is vital to cellular activity (Carta *et al*., 2017).

In addition, palmitic acid functions as a precursor in synthesising hormones and critical signalling molecules. Nevertheless, an overabundance of palmitic acid may potentially contribute to the pathogenesis and metabolic imbalances (Qiu *et al*., 2022). Thus, understanding palmitic acid's balance and physiological responsibilities is essential for optimal health and avoiding its harmful effects from overconsumption.

1.2.1 Palmitic acid synthesis, dietary uptake and metabolism

Palmitic acid (PA), a crucial saturated fatty acid in human physiology, plays a central role in essential cellular components like membrane phospholipids and adipose triacylglycerols, constituting 20-30% of these structures. It is synthesised through de novo lipogenesis, a metabolic pathway involving acetyl-CoA, malonyl-CoA, and fatty acid synthase (Wakil, 1962, Song *et al*., 2018). It can also be derived from various sources, highlighting its versatility in maintaining lipid balance in the body. PA in the human diet is sourced from palm oil, olive oil, red meat, and dairy products, contributing to about 8-10% of total dietary fat intake (Peiretti, 2014).

Despite dietary fluctuations, tissue PA concentration remains stable, indicating a well-regulated system involving endogenous biosynthesis via de novo lipogenesis (DNL) (Murru *et al*., 2022). However, under certain physiological conditions and in response to specific nutritional factors, DNL can be significantly induced, disrupting tissue PA homeostasis (Wilke *et al*., 2009). Under normal physiological conditions, mechanisms exist to prevent excessive PA accumulation in tissues. These mechanisms involve increased delta-nine desaturation, leading to the conversion of PA into palmitoleic acid or the elongation of PA into stearic acid, which is then converted into oleic acid through Δ9 desaturation (Chong *et al*., 2008). These regulatory processes have been paramount due to PA's fundamental role in various biological functions, particularly in infants (Strable and Ntambi, 2010, Innis, 2016, Carlisle *et al*., 2016) (Fig 1.1).

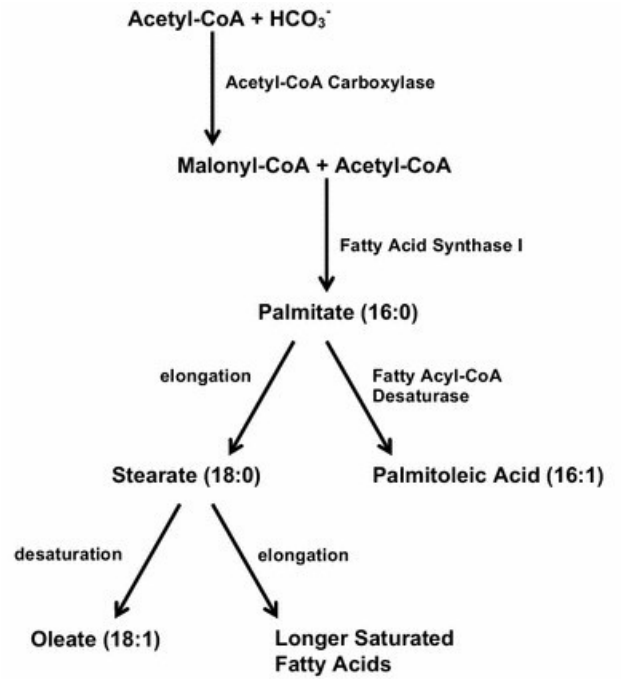

Fig 1.1 Synthesis of palmitic acid. Palmitic acid, a 16-carbon saturated fatty acid, is produced from acetyl-CoA and malonyl-CoA. A subsequent enzymatic process creates palmitoleic acid through double bond introduction and stearate through chain extension. Different fatty acids (oleic acid and others) are synthesised in these sequential steps for crucial cellular functions, such as forming cell membranes, acting as signalling molecules, and storing energy (Carlisle *et al*., 2016).

PA distribution and metabolism within tissues are vital for maintaining and distributing specific tissue concentrations among different lipid classes. An earlier study estimated that approximately 20-30% of daily PA intake, corresponding to 20-30 grams, undergoes beta-oxidation (Mayes *et al*., 2006). The membrane fatty acid transporter CD36, called scavenger receptor B2, is primarily responsible for internalising palmitate. Nevertheless, there are additional pathways by which palmitate can enter cells, including lipoprotein lipase-mediated absorption, direct membrane contacts, and albumin-mediated transfer (Glatz *et al*., 2010, McArthur *et al*., 1999). Additionally, it has been observed that in both the liver and most bodily tissues, a substantial portion of PA (60-70%) is incorporated into phospholipids. This process is centrally controlled by the liver, which finely regulates PA level by managing its conversion into palmitoleic acid or elongation into stearic acid, followed by subsequent desaturation into oleic acid (Carta *et al*., 2015).

Under normal physiological conditions, dietary PA intake does not substantially impact plasma PA concentrations. These findings suggest that the liver utilises a sophisticated homeostatic control mechanism to manage PA concentrations. This involves its production through de novo lipogenesis and subsequent desaturation. This intricate regulation ensures that PA level is carefully maintained within a narrow range, preventing health implications associated with dysregulation (Innis *et al*., 1997, Song *et al*., 2017).

Maintaining the balance between saturated (SAFA) and unsaturated fatty acids (UFA) in membrane phospholipids (PL), particularly PA, is a priority. Excess fatty acids in the liver are packaged into triglycerides (TAG) within very low-density lipoproteins (VLDL), contributing to a coordinated physiological strategy to sustain the homeostatic equilibrium essential for vital functions and the physical-chemical properties of membrane phospholipids (Abbott *et al*., 2012).

1.2.2 PA and health implication

The unique role of PA in various health issues, including metabolic syndrome, cardiovascular disease, type 2 diabetes, obesity, inflammation and cancer, sets it apart from other saturated fats (Lee *et al*., 2015, Siri-Tarino *et al*., 2010). It has been shown that elevated plasma palmitic acid level is associated with metabolic syndrome and insulin resistance, particularly in people with diabetes. Palmitic acid increases cellular uptake, activating non-oxidative metabolic pathways, inhibiting insulin signalling, and ultimately contributing to insulin resistance through downstream effects (Palomer *et al*., 2018). PA-related obesity causes chronic inflammation and metabolic disorders. Palmitic acid (PA) induces insulin resistance by activating Toll-like receptor 4 (TLR4) and producing reactive oxygen species (ROS) (Franchi *et al*., 2009, Ting *et al*., 2008, Cani *et al*., 2007, de Wit *et al*., 2012). In addition to increasing interleukin-1 production, PA promotes insulin resistance through TNF-dependent and TNF-independent mechanisms (Cheng *et al*., 2015).

Through mechanisms such as autophagic degradation of lipid droplets, ER stress, apoptosis, and oxidative stress, PA causes lipotoxicity in non-adipose tissues, causing cellular dysfunction, notably in hepatocytes, pancreatic beta cells, muscle cells, and endothelial cells (Singh and Cuervo, 2012, Borradaile *et al*., 2006). Several complex processes involve PA-induced lipotoxicity, including increased ceramide production,

mitochondrial dysfunction, nitrosative stress, apoptosis and necroptosis (Mancini *et al*., 2015a, Cao *et al*., 2012). PA emerged as a significant factor influencing cancer risk, particularly in breast, colorectal, and prostate cancers. A national case-control study in Scotland demonstrated a dose-dependent positive association between certain fatty acids and colorectal cancer risk (Mancini *et al*., 2015a).

Various proteins are regulated by protein palmitoylation, which occurs when palmitic acid is covalently bound to proteins; dysregulation of this process results in diseases such as cancer, neuronal disorders, and metabolic dysfunction (Thomas and Huganir, 2013, Chamberlain *et al*., 2013, Charest and Bouvier, 2003). Altering the dynamics of protein palmitoylation, exemplified by disrupting Ras membrane interactions and modifying protein trafficking, including protease-activated receptor-2 and metastasis suppressor protein KAI1/CD82, has been implicated in the onset of diseases such as cancer, neuronal disorders, and metabolic disorders (Lin *et al*., 2017, Adams *et al*., 2011, Zhou *et al*., 2004, Anderson and Ragan, 2016, Holland and Thomas, 2017, Mohammed *et al*., 2013).

Even though plasma level of palmitic acid may not differ significantly between obese and non-obese individuals, obesity can cause chronic low-grade inflammation by accumulating excessive amounts of palmitic acid in white adipocytes, disrupting adipocyte function, reducing adiponectin secretion, and releasing pro-inflammatory agents, ultimately causing systemic inflammation. Additionally, PA-filled adipocytes activate macrophages, triggering NF- kB signalling and MAPK signalling pathways, releasing cytokines such as TNF and IL-10. PA induces preadipocyte apoptosis by inducing oxidative pathways, cell death, and ER stress (Kennedy *et al*., 2009, Xi *et al*., 2007, Ajuwon and Spurlock, 2005, Bradley *et al*., 2008).

PA level is altered in cancer cells due to changes in the metabolism of glucose, lipids, and amino acids. Fatty acids are derived from the diet or synthesised from citrate in cancer cells, leading to elevated levels of PA due to increased fatty acid synthase activity (FAS) (Kwan *et al*., 2015, Kwan *et al*., 2013). FAS inhibition induces apoptosis in cancer cells, likely by reducing PA availability, and disruption of FAS affects lipid raft architecture and inhibits key signalling pathways (Ventura *et al*., 2015). Furthermore, cancer cells may receive fatty acids from adipocytes in the tumour microenvironment, with evidence increasingly pointing to specific tumorigenic properties of PA, distinct from those of other saturated fatty acids (Laurent *et al*., 2016). As a signalling molecule,

PA has been implicated in the proliferation and invasiveness of cancer cells through Akt phosphorylation and the TLR4/ROS/NFκB/MMP9 signalling pathway (Binker-Cosen *et al*., 2017a).

Conflicting study outcomes may stem from inadequate sample sizes, diverse biomarkers for fatty acid intake, and variations in study populations with different characteristics and cancer risk factors. While evidence supports the impact of individual PA and their ratios on carcinogenesis and its progression, the specific mechanisms by which PA contributes to cancer development remain poorly understood, potentially involving hormonal changes, cell membrane composition, and cell signalling pathways.

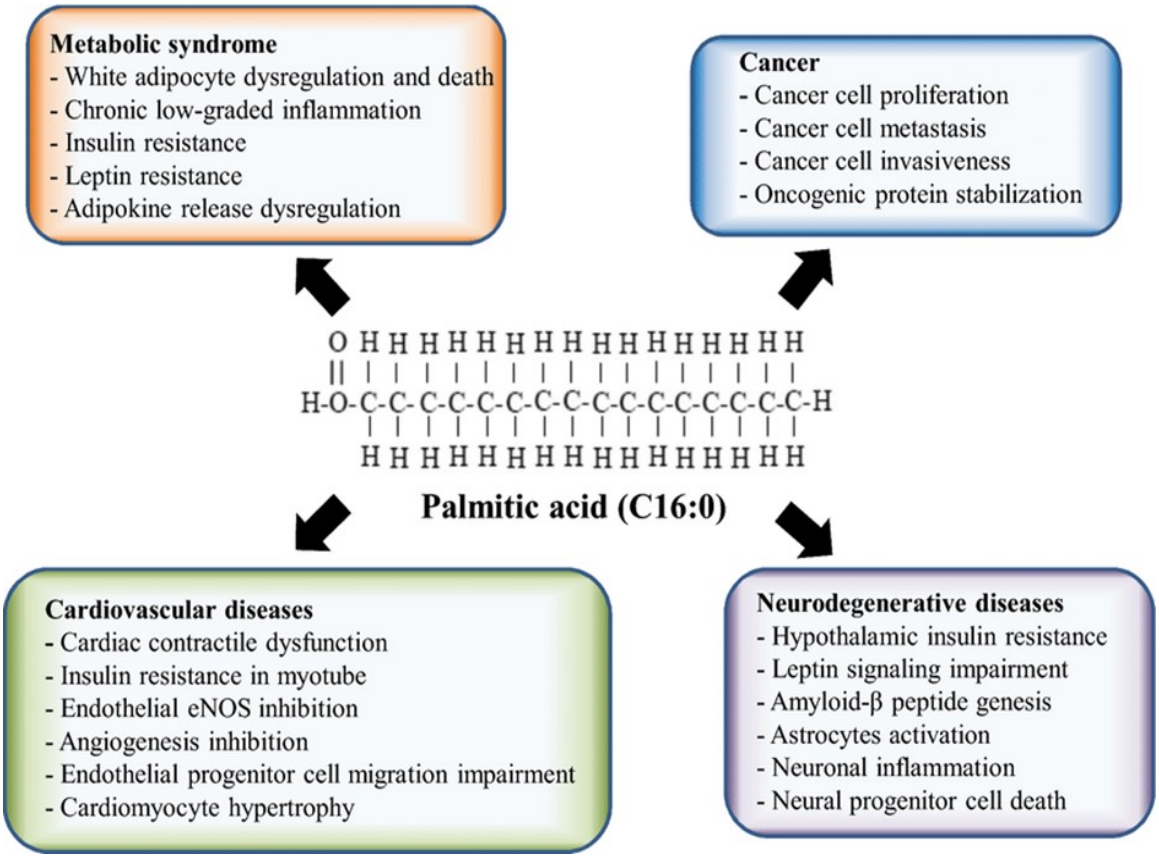

Fig 1.2 The role of palmitic acid in disease progression (Fatima *et al*., 2019a)

1.2.3 Palm oil as a prime source of PA

Despite health concerns, palm oil (PO), a significant source of palmitic acid, is vital to the food industry. Other sources of PA include lard, cocoa butter, etc. Most dietary PA comes from palm oil, containing 44% of its saturated fatty acids. High-fat diets, mainly those high in palm oil, cause gut microbiota alterations that generate pro-inflammatory chemicals such as lipopolysaccharides (LPSs). A PO-rich di*et al*so causes weight gain,

hepatic fat build-up, and reduced microbial diversity, implicating diet in the complicated relationship between obesity, inflammation, and metabolic dysfunction.

In a population-based case-control study of Costa Rican adults, palm oil consumption was associated with an increased risk of acute myocardial infarction (Martínez-Ortiz *et al*., 2006). Further, SFAs in palm oil and palmitic acid have been linked to adverse cardiovascular outcomes, with research demonstrating that unsaturated fatty acids are more beneficial for cardiovascular health (Fattore and Fanelli, 2013). Studies have documented potential adverse health effects of palm oil in recent decades, attributing them to its high palmitic acid content.

According to the data presented in Table 1, PO is composed of the following: 50% saturated fatty acids (SFAs), with palmitic acid (44 per cent) and stearic acid (5%) in smaller proportions; 40% monounsaturated fatty acids (MUFAs), with oleic acid predominately; and 10% polyunsaturated fatty acids (PUFAs), with linoleic acid predominately.

Table 1.1 Fatty acid composition in palm oil

Free Fattyacids			
Group	**Trivial Names**	**Symbol**	**Composition of Fatty acids**
SFA	Caproic acid	C6:0	-
	Caprylic acid	C8:0	-
	Capric acid	C10:0	-
	Lauric acid	C12:0	0.10
	Myristic acid	C14:0	1.00
	Palmitic acid	C16:0	44.00
	Stearic acid	C18:0	5.00
	Arachidic acid	C20:0	0.10
MUFA	Palmitoleic acid	C8::1n9	0.10
	Oleic acid	C8::1n9	41.20
PUFA	Linolenic acid	C8:3n3	0.50
	Linoleic acid	C8:2n6	8.00

Adapted from (Rahman *et al*., 2022)

1.3 Endoplasmic reticulum stress: Cellular adaptation and pathology

Through protein synthesis, folding, and trafficking, the endoplasmic reticulum maintains cellular homeostasis; however, a variety of physiological and pathological factors may result in endoplasmic reticulum stress (ERS), resulting in the accumulation of proteins that have been unfolded or misfolded. UPR is a cascade of signalling events that restore ER function and maintain cellular integrity through this intricate cellular response (Lai *et al*., 2007). Although the UPR is initially adaptive, prolonged or severe ERS can contribute to the pathogenesis of a variety of diseases, including neurodegenerative disorders, metabolic disorders, and cancers (Corazzari *et al*., 2017, Ren *et al*., 2021, Ghemrawi and Khair, 2020).

1.3.1 Endoplasmic reticulum: Protein folding and homeostasis

The endoplasmic reticulum (ER) is a network of membrane-bound organelles that consists of tubules and sacs within the cytoplasm of eukaryotic cells (Mohan *et al*., 2019). The ER plays a vital role in many cellular functions, primarily facilitating membrane and secretory protein synthesis, protein folding with post-translational modifications, quality control of protein folding, intracellular calcium storage, lipid/sterol biosynthesis, calcium storage and detoxification (Schröder, 2008b). Two unique forms of endoplasmic reticulum are rough endoplasmic reticulum (RER) and smooth endoplasmic reticulum (SER). The SER synthesises lipids, phospholipids, and steroids found in organs with active secretion, such as the testes, ovaries, and sebaceous glands (Voeltz *et al*., 2002). In contrast to smooth ER, rough ER is decorated with ribosomes, which allows it to support vital functions like protein synthesis and quality control of protein folding (Garfield and Cardell, 1987). The precise supervision of protein folding is a function of specialised molecular chaperones and folding enzymes within the endoplasmic reticulum. The oxidising environment of the ER lumen is essential for the proper folding and maturation of secretory proteins. It uses specific molecular chaperones and folding enzymes to regulate protein folding precisely. The ubiquitin-proteasome system directs proteins that cannot fold correctly within the allotted time frame toward ER-associated destruction (ERAD) (Hwang and Qi, 2018).

Normally, molecular chaperones and cis-trans peptidyl-prolyl isomerases catalyse critical processes and avoid aggregation to regulate appropriate protein folding. Folding in the ER is driven by the hydrophobic effect, which is affected by the formation of

disulphide bonds and glycosylation; PDIs catalyse slow processes. To prevent stress and toxicity from incompetent chains, a functional protein-folding mechanism collects correctly folded proteins and maintains ER homeostasis (Schröder, 2008a). The three primary hierarchical protein-folding machinery: lectin chaperones (calnexin, calreticulin, and calmegin), HSP70 molecular chaperones Bip/GRP78/Kar2p and Lhs1p/GRP170/ORP150, and HSP90 chaperone GRP94. GRP94 and lectin chaperones preferentially act on partially folded proteins, whereas Bip targets fully unfolded polypeptide chains in these hierarchical systems (Pobre *et al*., 2019, Craven *et al*., 1996, Saris *et al*., 1997, Argon and Simen, 1999, Watanabe *et al*., 1994, Winter and Jakob, 2004). Disulphide bond formation and isomerisation occur in the ER through a quasi-stochastic mechanism that combines oxidative and conformational protein folding. Reactive groups randomly come into contact during this process, impacted by conformational restrictions and polypeptide chain loop entropies. PDIs have thioredoxin-like domains and are involved in redox and chaperone processes. Because most PDI in the ER is found in its reduced dithiol state, isomerase activity plays a crucial role in oxidative protein folding. Reactive oxygen species (ROS) are produced by oxidase activity, which is necessary to create de novo disulphide bonds. FAD-dependent oxidases, such as Ero1p/ERO1-La, ERO1-Lb, and Erv2p, are responsible for this activity and are found in eukaryotic cells (Schröder, 2008a).

1.3.2 Endoplasmic reticulum stress (ER stress)

Various cytological conflicts, including hypoxia, oxidative stress, nutrient deprivation, cellular redox regulation and immune cell infiltration, can disrupt ER homeostasis, accumulating misfolded or unfolded proteins in ER and impairing the protein folding machinery. This represents an evolutionarily conserved adaptive response to address adverse conditions, triggering the activation of signalling pathways within the ER, commonly referred to as the ER stress response pathway or Unfolded Protein Response (Chen *et al*., 2023b, Zhang and Kaufman, 2008b). The length and intensity of ER stress determines the cell's fate: if it lasts for a long time, the cell will start the processes that lead to programmed cell death. In contrast, the cell will activate processes to restore ER equilibrium during brief stress, ultimately increasing cell survival (Xu *et al*., 2005, Boyce and Yuan, 2006).

1.3.3 Unfolded protein responses (UPR)

The UPR is an intracellular signal transduction that monitors protein folding within the endoplasmic reticulum lumen and communicates this information to the cytoplasm and the nucleus. When unfolded proteins build up in the endoplasmic reticulum, local chaperones activate, releasing transmembrane ER proteins essential for initiating the unfolded protein response. Normal conditions prevent transmembrane ER proteins from aggregating because the ER chaperone Grp78 (Bip) firmly binds these proteins' N-termini. But Grp78 loses its grip when misfolded proteins accumulate, making it easier for these transmembrane signalling proteins to aggregate and set off the unfolded protein response (Xu *et al*., 2005). These proteins constitute a structural connection that smoothly connects the two cellular compartments by spanning ER membranes, with their C-terminus in the cytosol and their N-terminus in the ER lumen. Three transmembrane proteins located in the endoplasmic reticulum (ER)-Inositol-requiring element-1 (IRE-1), PKR-like endoplasmic reticulum kinase (PERK), and activated transcription factor 6 become active participants in the Unfolded Protein Response (UPR). All three sensors are dormant at the ER membrane when coupled to Bip. However, Bip separates from ATF6, IRE1, and PERK in reaction to unfolded or misfolded proteins. Misfolded proteins can be handled appropriately thanks to this separation, making it possible for one or more of these transducers to activate them (Lai *et al*., 2007). They regulate the expression of various genes that maintain ER homeostasis or induce apoptosis if ER stress persists.

It is widely accepted that the UPR comprises three main mechanisms: transcriptional activation of UPR genes, translational attenuation of global protein synthesis, and ER-associated degradation (ERAD). When unfolded proteins in the ER cannot attain their final, proper structure, they are translocated to the cytosol. There, they undergo ubiquitination and proteasome-dependent degradation. This process is known as ER-associated degradation (ERAD). It serves as a critical mechanism for disposing of misfolded proteins and alleviating ER stress, contributing to ER homeostasis restoration.

Chronic ER stress, which arises from the inability to manage elevated protein levels and misfolded proteins effectively, has been demonstrated to be linked to a range of pathological disorders (Rovira-Llopis *et al*., 2014, Valdés *et al*., 2014). Furthermore, misfolded proteins often lose their regular physiological activity within the ER, making

them resistant to degradation or proper folding. As a result, neither apoptosis nor internal homeostasis is initiated, ultimately leading to various diseases (Adams *et al*., 2019). Substantial evidence indicates that ER stress and the UPR contribute significantly to the pathogenesis of numerous diseases. These conditions include neurodegenerative diseases, metabolic disorders, malignancies (cancers), cardiovascular diseases, and inflammatory disorders. Dysregulation of ER function and the UPR can disrupt cellular processes and contribute to the development and progression of these diverse pathological conditions (Zeeshan *et al*., 2016b). Understanding and targeting these pathways may hold promise for therapeutic interventions

1.3.3.1 PERK pathway

PERK, a transmembrane type 1 kinase in the ER, is activated upon ER stress by inducing oligomer formation and phosphorylating itself and eIF2α, resulting in eIF2α inactivation and subsequent mRNA translation inhibition (Lavoie *et al*., 2014, Liu *et al*., 2015, Harding *et al*., 1999b). It is believed that this PERK-driven translation inhibition may play a pivotal role in mitigating ER stress by reducing the protein influx into the ER, thus contributing to the alleviation of ER stress. eIF2 recruitment is facilitated by the dimerization and trans-autophosphorylation of the cytosolic domain of PERK in response to endoplasmic reticulum stress. Phosphorylation at Serine 51 stops eIF2 from being recycled to its active GTP-bound state by inhibiting the pentameric guanine exchange factor eIF2B (Harding *et al*., 1999a). Under conditions of eIF2α insufficiency, specific mRNAs featuring upstream open reading frames (uORFs) are preferentially translated, notably ATF4, a transcription factor that activates genes such as GADD34 and CHOP (Vattem and Wek, 2004). GADD34 encodes a regulatory subunit of protein phosphatase PP1C, establishing a negative feedback loop by dephosphorylating eIF2α, counteracting translational attenuation of PERK. CHOP, activated by ATF4, plays a key role in apoptosis regulation. This underlines the dual nature of PERK signalling in pro-survival and pro-apoptotic responses during prolonged ER stress (Bhattarai *et al*., 2021b, Harding *et al*., 1999a, Novoa *et al*., 2001, Yong *et al*., 2021, Malhi *et al*., 2013). Beyond translational control, PERK activates Nrf2 and ATF4, influencing common targets, including CHOP, thus impacting redox homeostasis and apoptosis regulation. The balance between Nrf2 and ATF4 signalling

pathways in response to ER stress can modulate CHOP expression levels, highlighting the intricate nature of PERK-mediated cellular reactions (Cullinan and Diehl, 2006).

1.3.3.2 IRE1 pathway

IRE-1 is a universally conserved, type 1, bifunctional transmembrane kinase/endoribonuclease that serves as a key sensor for ER stress in eukaryotes, contains an amino-terminal luminal domain and a carboxy-terminal cytoplasmic region containing kinase and RNase domains. (Tirasophon *et al*., 1998, Calfon *et al*., 2002). IRE1α and IRE1*β* are two variants of IRE1, distinguished by their unique substrate specificities and RNase domains, which govern their distinct functionalities. IRE1α, ubiquitously present, is implicated in UPR signalling via its cytosolic domains of kinase and endoribonuclease. On the other hand, IRE1*β*, which is exclusively expressed in intestinal epithelial cells, is hypothesised to be involved in UPR specific to digestive tissue via RNA cleavage (Grey *et al*., 2020, Imagawa *et al*., 2008).

When the ER is stressed, IRE1 undergoes self-association of its luminal domain, termed Ire1-LD, which forms higher-order oligomers (Karagöz *et al*., 2017, Amin-Wetzel *et al*., 2017). Initiated by nucleotide binding, this conformational shift serves as a molecular switch, activating the RNase domain. These oligomeric assemblies are essential for the subsequent activation of its cytoplasmic kinase and RNase domains. It is believed that the cytoplasmic domain of IRE1a exhibits endoribonuclease activity upon activation and targets mRNAs encoded by X-box-binding protein (XBP) 1 and catalyses the cleavage of 26 nucleotides, which forms spliced XBP1s (Karagöz *et al*., 2019). XBP1s, which is a transcriptional activator and regulator, is then translocated to the nucleus for transactivation of ER chaperones and secretory genes, as well as activating ER-associated degradation (ERAD) genes, facilitating efficient removal of unfolded and misfolded proteins from the ER for degradation by proteasomes (Calfon *et al*., 2002, Han *et al*., 2009, Hollien *et al*., 2009). As XBP1 translocate to the nucleus, it activates pro-survival gene expression and increases protein secretion in the ER and Golgi compartments (Acosta-Alvear *et al*., 2007). Additionally, IRE1α activity triggers the degradation of other ER-localized mRNAs through regulated IRE1-dependent decay (RIDD) (Maurel *et al*., 2014). Hence, XBP1s are crucial in regulating multiple aspects of endoplasmic reticulum (ER) function, including ER expansion, protein maturation, folding, export from the ER, and the clearance of misfolded proteins (Bertolotti *et al*., 2000, Jurkin *et al*., 2014).

Despite this, IRE1 engages with TRAF2 to initiate an inflammatory response, activating apoptosis-associated protein kinases such as apoptosis signal-regulating kinase 1 (ASK1), ultimately leading to JNK activation (Kim *et al*., 2008). Moreover, IRE1–TRAF2 complexes recruit IκB kinase, inducing the degradation and phosphorylation of IκB, facilitating the translocation of nuclear factor-κB (NF-κB) to the nucleus and thereby regulating the transcription of inflammatory genes(Malhotra and Kaufman, 2007, Kaneko *et al*., 2003). Notably, phosphorylation likely facilitates IRE1 deactivation by potentially destabilising its oligomeric structure. This is possibly through electrostatic repulsion from the localised high concentration of negatively charged phosphate groups. Initially, phosphorylation events may promote oligomeric complexes (Gardner *et al*., 2013).

1.3.3.3 ATF6 pathway

The 90-kDa ATF6 protein in cells is a type 2 transmembrane protein with a significant ER-luminal domain and exhibits a complex response to ER stress (Zhu *et al*., 1997). Mammalian paralogues ATF6α and ATF6*β*, both with distinct transcriptional activation domains, are related to a function in which ATF6*β* functions as a repressor, adjusting the degree and duration of ATF6α-mediated gene regulation in the Unfolded Protein Response (Thuerauf *et al*., 2004). In contrast to Ire1 and PERK, ATF6 contains a stress-sensing luminal domain at the C-terminus and a bZip transcription factor domain at the amino terminus, which serves as redox sensors. It's critical to note that Bip release, significantly during ER stress, modulates ATF6 activation (Yamamoto *et al*., 2007). Following ER stress, ATF6 undergoes transport to the Golgi apparatus, where a carefully orchestrated processing event occurs, guided by S1P and S2P proteases. This complex processing results in the release of ATF6's transcription factor domain, ATF6 (N), which then moves to the nucleus. As soon as ATF6 (N) enters the nucleus, it coordinates the activation of genes critical for ER expansion and the upregulation of chaperones, foldases, and components of the ER-associated degradation pathway. These actions collectively contribute to the cell's response to ER stress. (Haze *et al*., 1999, Walter and Ron, 2011, Chen *et al*., 2023b). ATF6's target genes are crucial ER-resident proteins contributing to protein folding, such as Bip, GRP94, and PDI. Furthermore, following cleavage, ATF6p50, the active form of ATF6α, translocate to the nucleus to activate UPR target genes and forms heterodimers with XBP1s, facilitating the upregulation of ERAD-associated genes (Walter and Ron, 2011).

Additionally, ATF6 regulates and activates genes that are targets of UPR, such as CHOP and GRP78 (Basseri and Austin, 2012b).

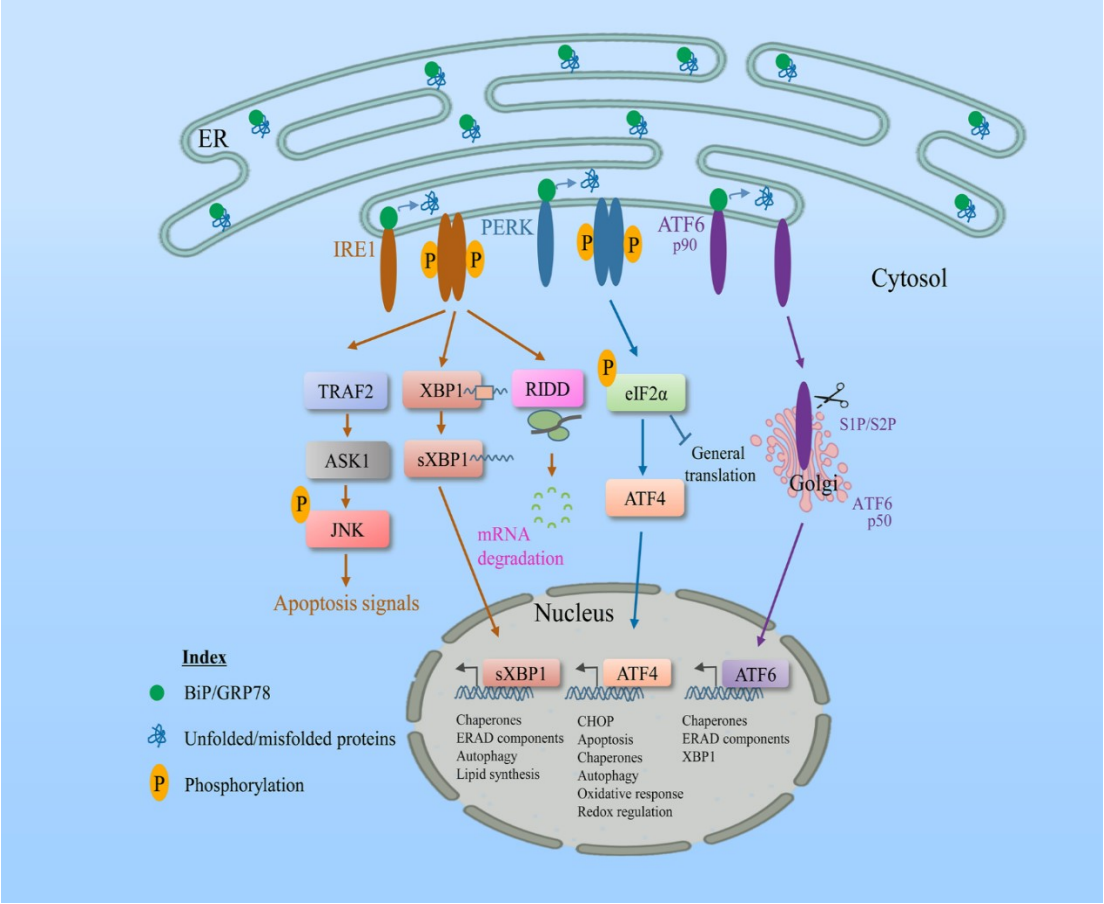

Fig 1.3 UPR arms and unfolded protein response pathways (Bhattarai *et al.*, 2021a)

1.3.4 Integration of ER stress with redox homeostasis and lipotoxicity

The balance between redox homeostasis, lipotoxicity, and ER stress is essential for cell function. Misfolded proteins cause ER stress, activating the UPR to restore balance. Redox signalling is linked to ER stress, and it can reduce antioxidant defences and increase oxidative stress. Lipotoxicity, the accumulation of excess lipids, can amplify oxidative stress and cause a feedback loop that worsens cellular dysfunction. Understanding ER stress's interaction with redox homeostasis and lipotoxicity is crucial for understanding metabolic disorders and neurodegenerative diseases.

1.3.4.1 ER stress and redox homeostasis

ER functions are governed by oxidative protein folding (OPF), which generates H2O2 through proteins such as ERO1 and QSOX. Oxidoreductases such as PRDX4, GPX7/8,

and APX, along with GSH, maintain ER redox homeostasis; however, an imbalance can result in oxidative stress, disrupting this equilibrium and causing misfolded protein accumulation (ER stress) (Zhang *et al*., 2019). During ER stress, PERK activity inhibits both protein synthesis and mRNA translation. Furthermore, PERK-induced synthesis of ATF4 and Nrf2 facilitates amino acid metabolism and GSH production, which is essential for maintaining redox balance (Cullinan *et al*., 2003). Upon activation, NRF2 dissociates from KEAP1 and translocate to the nucleus. Through NRF2, antioxidant response elements are activated, promoting the expression of antioxidant factors while inhibiting the expression of pro-oxidant proteins. In addition, the NRF2-ATF4 heterodimer contributes to the induction of heme oxidase-1 gene expression. As a result of this PERK-NRF2 signalling pathway within the UPR, a regulated antioxidant response has been identified to counterbalance oxidative stress in the ER(Cullinan and Diehl, 2004, Ma, 2013, He *et al*., 2001). PERK-deficient cells exhibit heightened vulnerability to hydrogen peroxide and endoplasmic reticulum (ER) stress. This underscores the critical function of PERK in cellular stress adaptation by reducing reactive oxygen species via GSH synthesis (Zeeshan *et al*., 2016a). Cells lacking PERK exhibit increased oxidative stress due to impaired translation regulation, emphasising the importance of maintaining ER redox homeostasis (Harding *et al*., 2003). The tight linkage between oxidative stress response and UPRER suggests their evolution is likely due to the ER's role as a major source of ROS production during protein folding. The NRF2-UPR axis may serve as a bidirectional signal between the ER and cytoplasm, preparing for potential toxic effects during ER stress or promoting protein folding under cytoplasmic stress.

1.3.4.2 ER stress and lipotoxicity

The ER manages lipids and proteins, with the UPR playing a vital role in maintaining metabolic and lipid balance (Kammoun *et al*., 2009). Lipid metabolism disruptions can cause cellular damage due to interactions between altered redox homeostasis, oxidative stress, lipotoxicity, and ER stress (Burgos-Morón *et al*., 2019, Basseri and Austin, 2012a). Excessive build-up of lipids in the body can lead to metabolic disorders and cell death due to lipotoxicity. This is typically associated with long-term endoplasmic reticulum (ER) stress and abnormal UPR signalling in the ER. Saturated fatty acids such as palmitate activate the UPR-ER, causing harmful effects in pancreatic β-cells, liver, adipose tissue, and muscle cells (Han and Kaufman, 2016).

Numerous studies suggest that the PERK-eIF2α pathway regulates lipogenesis and develops hepatic steatosis (Lauressergues *et al*., 2012). In primary rat pancreatic *β* cells, exposure to palmitate triggers the activation of PERK, which results in increased phosphorylation of eIF2α, splicing of Xbp1s, and activity of ATF4. However, excessive palmitate can induce ER stress and caspase activation, leading to cell death due to heightened palmitoylation (Cnop *et al*., 2007, Karaskov *et al*., 2006). Lipotoxicity and ER dysfunction occur due to altered ER membrane composition, increased ceramide accumulation, and modified sphingolipid metabolism caused by the excess palmitate (Han and Kaufman, 2016, Cunha *et al*., 2008).

The stress caused by saturated fatty acids in the endoplasmic reticulum (ER) significantly contributed to liver lipotoxicity. In liver cell lines such as HepG2 and L02, exposure to saturated fatty acids activates the PERK pathway, which increases the expression of downstream targets ATF4 and CHOP (Cao *et al*., 2012). Reducing ER stress by inhibiting PERK activation or overexpressing Bip can help prevent cell death caused by palmitate. Palmitic acid alters the metabolism of phospholipids in liver cells, which affects ER calcium signalling and leads to abnormal mitochondrial metabolism and increased production of reactive oxygen species (ROS). Restoring ER lipid composition and calcium homeostasis through enzymatic conversion and protein overexpression can help alleviate lipotoxicity (Egnatchik *et al*., 2014, Listenberger *et al*., 2001).

Furthermore, Muscle cells are sensitive to endoplasmic reticulum (ER) stress induced by lipids. In mice fed a high-fat diet, skeletal muscle showed increased ER stress markers. Overexpressing SCD1, a lipid metabolism regulator, improved insulin resistance. However, restoring ER homeostasis may not fully regain insulin signalling during palmitate-induced ER stress (Peter *et al*., 2009, Han and Kaufman, 2016).

IRE1α plays a significant role in lipotoxicity associated with endoplasmic reticulum stress, in addition to PERK. Deleting hepatocyte-specific Ire1α increased hepatic lipid levels and decreased plasma lipids due to the modulation of lipid metabolism-related genes such as C/EBP*β*, C/EBPδ, PPARγ, and enzymes involved in triglyceride biosynthesis (Lee *et al*., 2008, Zhang *et al*., 2011a). IRE1α is necessary for lipid delivery in VLDL assembly. The effects of the IRE1α/XBP1 pathway on lipid accumulation and secretion vary due to the hyperactivation of IRE1α in liver-specific Xbp1−/− mice. It decreases plasma triglycerides and cholesterol by degrading mRNA

related to lipid metabolism. IRE1α/XBP1 also regulates inflammatory cytokines, and blocking them has anti-inflammatory effects (Han and Kaufman, 2016, Wang *et al*., 2015b). Coming to the ATF6 arm of UPR, the ATF6α pathway inhibits lipid accumulation during ER stress. Its deletion leads to prolonged hepatic dysfunction and steatosis due to sustained CHOP expression, C/EBPα suppression, and impaired ATF6α-mediated induction of chaperone and ERAD genes. In high-fat diets, Atf6α−/− mice develop hepatic steatosis and glucose intolerance (Rutkowski *et al*., 2008, Han and Kaufman, 2016, Yamamoto *et al*., 2010).

As discussed, stress in the ER and the UPR pathways plays a significant role in lipid metabolism and lipotoxicity in various tissues. This stress leads to the modulation of critical enzymes involved in lipid synthesis or modification in response to stimuli. However, prolonged unresolved ER stress can be fatal.

1.3.4.3 ER stress and inflammation

Excessive metabolic factors such as lipids, glucose, cytokines, and neurotransmitters can cause inflammation by disrupting the inflammatory and ER-stress responses. This triggers a feedback loop that intensifies inflammation, disrupts metabolic functions, and can lead to chronic inflammation and other health problems. UPR and inflammatory signalling pathways are linked through ROS generation, ER-mediated calcium release, and NF-κB/JNK activation. (JUN N-terminal kinase) within the MAPK pathway and initiating the acute-phase response (Zhang and Kaufman, 2008a). During protein folding, ER stress induces the production of reactive oxygen species (ROS), resulting in oxidative stress, inflammation and glutathione depletion (Raha and Robinson, 2000, Cuozzo and Kaiser, 1999).

NF-κB is a key regulator of inflammation activated by signals, leading to the phosphorylation and degradation of IκB. When there is an increase in protein folding within the Endoplasmic Reticulum (ER), it can cause oxidative stress and the release of calcium. This, in turn, can activate the NF-κB signalling pathway through the PERK–eIF2α pathway, leading to an increase in the ratio of NF-κB to IκB and its translocation into the nucleus. This response occurs when ER stressors or exposure to ultraviolet radiation (Meyer *et al*., 1992, Deng *et al*., 2004, Wu *et al*., 2004).

IRE1α is essential for ER stress and inflammatory responses. Autophosphorylation changes its conformation, forming the IRE1α–TRAF2 complex (Hu *et al*., 2006, Urano

et al., 2000). This complex attracts IKK, resulting in IκB phosphorylation, NF-κB nuclear translocation, and activation. The IRE1α-TRAF2 complex activates JNK, affecting inflammatory gene expression through AP1 phosphorylation. Impairment of ER stress-induced NF-κB activation and TNF-α generation in IRE1α-deficient mouse embryonic fibroblasts highlights the role of the IRE1α–TRAF2 complex in linking ER stress to inflammation. Research is needed to understand how JNK and NF-κB signalling modulate inflammation, metabolism, cell survival, and apoptosis in response to ER stress (Davis, 2000, Hu *et al*., 2006).

1.3.5 ER stress and autophagy

Autophagy is the primary lysosomal degradation mechanism that sequesters damaged cytoplasmic components in double-membrane vacuoles (Glick *et al*., 2010, Mizushima *et al*., 2008). Endoplasmic reticulum stress and autophagy are interrelated processes. Autophagy helps restore balance through the breakdown of damaged segments. But, if this process continues for a longer time, it can lead to excessive autophagy and programmed cell death. To ensure endoplasmic reticulum stability, unfolded protein response mechanisms such as PERK, IRE1, and ATF6 come into play. These mechanisms facilitate the repair of misfolded proteins and autophagy (Liu *et al*., 2016, Høyer-Hansen *et al*., 2007).

Studies have shown a strong link between autophagy and the UPR, with the PERK–eIF2α pathway being a key factor in initiating autophagy after endoplasmic reticulum stress (ERS). CHOP and ATF4 control over a dozen ATG genes, with ATF4-induced CHOP being especially significant (B'Chir *et al*., 2013). During autophagy, alterations in precise UPR signalling regulate the transition from survival to cell death signals. Increased levels of ATF4-directed CHOP are correlated with cell death, while autophagy is a crucial pro-survival mechanism that counteracts excessive UPR signalling (Nijholt *et al*., 2011). In severe endoplasmic reticulum stress cases, autophagy can lead to cell death (Luo and Lee, 2013b, Rubiolo *et al*., 2014, Tomar *et al*., 2013).

It has been reported that PERK plays an essential role in autophagy induced by endoplasmic reticulum stress. This is especially critical in situations involving misfolded proteins and polyglutamine repeats. The PERK-eIF2α pathway is crucial for this process, as it upregulates Atg12 expression and promotes autophagy. Therefore, ER

stress is linked to this mechanism. Furthermore, autophagy is centrally mediated by eIF2α, activated by various stressors. This activation may be achieved via ATF4-induced Atg12 expression (Høyer-Hansen and Jäättelä, 2007). Recent studies have shown that PERK can trigger the movement of essential autophagy transcription factors, TFEB and TFE3, to the nucleus when the endoplasmic reticulum (ER) is under stress. This activation stimulates the expression of autophagy and lysosomal genes, enhancing the resistance of ATF4 and CHOP to apoptosis arising from ER stress (Martina *et al*., 2016).

Recent studies have shown that IRE1, not PERK, is the primary factor responsible for LC3-positive vesicle formation in response to endoplasmic reticulum (ER) stress in MEFs and PERK-deficient embryonic stem cells. LC3 translocation was reduced in TRAF-2-deficient MEFs and with a JNK inhibitor. This suggests that the IRE1-TRAF2-JNK pathway is crucial for Thapsigargin-induced autophagy. These findings highlight the essential role of IRE1 in ER stress-induced autophagy (Høyer-Hansen and Jäättelä, 2007, Li *et al*., 2006, Demarchi *et al*., 2006, Ogata *et al*., 2006).

The activation of IRE1 and JNK is dependent on TRAF2, which phosphorylates Bcl-2, causing beclin-1 dissociation, activating the PI3K complex and initiating autophagy (Deegan *et al*., 2013). Studies have shown that in the absence of IRE1, JNK regulates autophagy in response to oxidative stress (Haberzettl and Hill, 2013). Intestinal epithelial cells of rats with ATG-knockout were found to have increased IRE1 activity and inflammation dependent on IRE1. Dysregulated autophagy can activate IRE1, which activates the sXBP arm of the UPR. This suggests a feedback mechanism in the signalling of UPR (Adolph *et al*., 2013).

Prolonged activation of XBP1 in endothelial cells increases Beclin1 expression, LC1 to LC3 conversion, and autophagic vesicle production. On the other hand, in mouse endothelial cells, XBP1 deficiency decreases LC3 expression and autophagosome formation (Margariti *et al*., 2013). Recent studies have shown that activating lysosomal activity downstream of constitutive UPRER via the overexpression of xbp-1s in neurons is crucial for prolonging lifespan. The overexpression of xbp-1s plays a critical role in preserving proteostasis by increasing the acidity and activity of the intestinal lysosomes (Imanikia *et al*., 2019).

When chemotherapy activates autophagy, tumour cells can become more resistant to cell death and reduce the effectiveness of treatment (Luo and Lee, 2013a). Melanoma cells that respond to BRAF inhibitor (BRAFi) treatment exhibit autophagy-mediated resistance. Overexpression of UPR and autophagy-dependent on protein kinase RNA-like endoplasmic reticulum kinase (PERK) prevents cell death induced by BRAFi. In xenograft models, suppressing autophagy pharmacologically increases BRAFi's anticancer efficacy and makes melanoma cells more vulnerable to cell death (Ma *et al*., 2014).

Intestinal epithelial cells that lack the IRE1 transducer XBP-1 undergo autophagy dependent on PERK and p-eIF2α. This highlights the critical balance in UPR regulation and reveals a feedback loop. Enteritis is caused by paneth cell dysfunction and defective autophagy, triggered by XBP-1 knockdown. Co-deletion of ATG genes exacerbates Crohn's disease-like inflammation, and ATG16L1 mutants exhibit an ERS-autophagy negative feedback loop that adversely regulates the UPR (Adolph *et al*., 2013). The deletion of XBP-1 activates PERK/ATF4, which controls autophagy through FOXO1, inducing autophagy and suggesting that the UPR limits it (Vidal *et al*., 2012). The IRE-TRAF2-JNK pathway or the PERK-eIF2α pathway mediates ER stress-induced autophagy. Disrupting the corresponding pathway reduces the steady-state amount of autophagic vesicles (Ogata *et al*., 2006, Kouroku *et al*., 2007).

1.4 Excess palmitic acid intake and ER stress

High PA intake and cellular accumulation can induce ER stress-related metabolic problems. It may increase lipid build-up, especially triglycerides, affecting ER function for lipid storage and metabolism. Chronic ER stress from high PA may affect cell function and cause diabetes, obesity, and neurodegenerative illnesses. While the cellular response restores ER balance, persistent ER stress has adverse effects. Maintaining a balanced diet and lifestyle is crucial to prevent excessive PA intake and its potential contribution to ER stress-related health issues.

High PA levels exacerbate dyslipidaemia consequences (Staaf *et al*., 2016). It was evident that Protein palmitoylation promotes ER stress signalling in some cell types (Hsiao *et al*., 2014b, Baldwin *et al*., 2012). Studies suggest that protein palmitoylation-mediated PA sensing produces ER stress, which damages the blood testis barrier (BTB) (Ge *et al*., 2022). Furthermore, PA triggers an unfolded protein response in which the

ER chaperone immunoglobulin heavy chain binding protein (Bip) and proapoptotic transcription factor C/EBP homologous protein increase, indicating that PA produces ER stress in podocytes (Sieber *et al*., 2010).

ER stress signalling triggered by FFAs significantly contributes to hepatic insulin resistance in the progression of NAFLD, underscoring its pivotal role in this metabolic disorder (Ozcan *et al*., 2004). It was found that PA induces apoptosis in Saos-2 cells by activating ER stress and autophagy (Yang *et al*., 2018a). Elevated PA levels, stemming from a high-fat diet, exacerbate lung fibrosis by inducing ER stress and lung epithelial cell death, with observed mitigating effects through targeting the fatty acid transporter CD36, suggesting a potential association between dietary saturated fats and pulmonary fibrosis (Chu *et al*., 2019b). It was found that PA induces cell death and ER stress in primary rat hepatocytes, marked by elevated expression of CHOP, GRP78, and GRP94 (Zhang *et al*., 2011b). Furthermore, PA contributed to impaired endothelium-dependent vasodilatation (EDV) in the thoracic aorta, and this effect was reversed by fenofibrate (FF) treatment, which decreased ER stress and increased phosphorylation of endothelial nitric oxide synthase (eNOS) (Lu *et al*., 2015).

PA-induced apoptosis and necrosis in podocytes, contributing to diabetic nephropathy, are associated with ER stress, and the protective effects of monounsaturated palmitoleic and oleic acids, as well as CHOP gene silencing, suggest a potential therapeutic strategy involving dietary shifts toward unsaturated free fatty acids to delay DN progression (Sieber *et al*., 2010). It was found that PA, a prevalent saturated fatty acid in obesity, increased endothelin-1 (ET-1) expression in both in vivo high-fat diet (HFD)--fed mice and in vitro cultured human aortic endothelial cells (HAECs). The induction of ET-1 by PA was observed in both acute and chronic treatments and was associated with ER stress. Furthermore, it was revealed that the PA-induced ET-1 expression was mitigated by pre-treatment with the ER stress inhibitor 4-phenylbutyric acid or the protein kinase C (PKC) inhibitor Gö 6850. These findings offer novel mechanistic insights into the development of obesity-associated hypertension and cardiovascular diseases (Zhang *et al*., 2018a).

It was evident that PA played a central role in inducing endothelial lipotoxicity, and mesenchymal stem cells (MSCs) demonstrated the ability to mitigate this lipotoxicity by reducing ER stress and suppressing endothelial-to-mesenchymal transition (EndMT) in response to PA stimulation (Luo *et al*., 2020). It was found that elevated levels of PA

in the follicular fluid induced apoptosis in mouse granulosa cells, and melatonin exhibited protective effects by mitigating PA-induced cell viability decrease, apoptosis, and ER stress, as well as preserving oestrogen and progesterone levels (Chen *et al.*, 2019b). It was found that O-GlcNAc transferase (OGT) upregulation in non-alcoholic fatty liver disease-associated hepatocellular carcinoma (NAFLD-HCC) was linked to its induction of PA, which, in turn, led to ER stress and activation of oncogenic JNK/c-jun/AP-1 and NF-κB cascades. Inhibition of OGT demonstrated a suppressive effect on cell proliferation, emphasising the critical role of PA in mediating OGT's oncogenic functions in NAFLD-associated HCC (Xu *et al.,* 2017). In addition, the detrimental impact of PA on primary rat hepatocytes, revealing its induction of ER stress and cell death while also highlighting the therapeutic potential of chlorogenic acid in preventing ER stress-mediated apoptosis by reducing key markers, indicating a potential avenue for addressing PA-induced hepatocyte damage (Zhang *et al.*, 2018b).

It was evident that dietary supplementation of PA in mice for two weeks led to significantly decreased glucose tolerance, suppressed glucose-stimulated insulin secretion (GSIS) during pancreatic perfusion, and increased mRNA expression of ER stress markers such as C/EBP homologous protein (CHOP), immunoglobulin heavy-chain binding protein (BIP), and X-box binding protein (XBP)-1 in isolated islets, suggesting that PA may induce early-stage lipotoxicity by influencing GSIS and activating the ER stress pathway in pancreatic *β*-cells (Hirata *et al.*, 2016). Furthermore, PA induces apoptosis in testicular Leydig cells through ER stress. Curcumin, a natural polyphenol, demonstrated significant protective effects against PA-induced toxicity and apoptosis in murine Leydig tumour cell line 1 (MLTC-1) cells. The anti-apoptotic action of curcumin was associated with the inhibition of ER stress markers, such as glucose-regulated protein 78 (GRP78) and CCAAT/enhancer binding protein homologous protein (CHOP). Furthermore, *in vivo* experiments showed that curcumin mitigated the decrease in testosterone levels induced by PA exposure in both MLTC-1 cells and rats fed a high-fat diet. These findings suggest curcumin's potential as a therapeutic agent for addressing obesity-related male infertility by protecting against PA-induced apoptosis through ER stress inhibition in Leydig cells (Chen *et al.,* 2019c).

It was observed that PA-induced cell injury in HepG2 cells resulted in ER stress and triggered calcium overflow from the ER to the mitochondria. However, the protective effects of augmenter of liver regeneration (ALR) against liver steatosis were associated

with its ability to alleviate PA-induced cell injury, downregulate inositol 1,4,5-trisphosphate receptor (IP3R) expression, and inhibit ER stress. ALR's interference with the interaction between BCL-2 and IP3R was identified as a novel mechanism, suggesting a role for ALR in resisting ER stress induced by PA in transfected cells (Xiao *et al*., 2018). It was found that PA-induced apoptotic and necrotic cell death, along with ER stress markers in the renal proximal tubular cell line NRK-52E. However, the unsaturated fatty acids, α-linolenic acid and palmitoleate, significantly reduced cell death and levels of ER stress indicators induced by PA, suggesting a potential protective mechanism for unsaturated fatty acids in countering the lipotoxic effects of PA in renal cells (Katsoulieris *et al*., 2009). Previously, it was found that PA-induced podocyte apoptosis and this effect was mitigated by berberine (BBR) treatment. The results suggested that PA mediated podocyte apoptosis through enhancing ER stress and reactive oxygen species (ROS) production. The protective effects of BBR were associated with the suppression of ROS-dependent ER stress (Katsoulieris *et al*., 2009).

It was evident that PA (C16:0) and TLR2 ligand-induced monocyte activation and ER stress markers, while docosahexaenoic acid (DHA) inhibited these responses. The results suggest that PA-induced ER stress contributes to monocyte activation. DHA's anti-inflammatory effects may be mediated, at least in part, by modulating ER homeostasis in response to different dietary fats (Snodgrass *et al*., 2016). It was found that PA-induced endothelial lipotoxicity and upregulated lectin-like oxidised low-density lipoprotein receptor-1 (LOX-1) in human umbilical vein endothelial cells (HUVECs). Curcumin alleviated PA-induced lipotoxicity and inhibited LOX-1 upregulation, potentially involving the suppression of ER stress (Luo *et al*., 2021). Further, it was found that PA increased the expression of cannabinoid receptor 1 (CB1R) in human renal proximal tubular cells (HK-2 cells). PA-induced CB1R activation was associated with apoptosis, and CB1R blockade was suggested as a potential therapeutic approach for diabetic nephropathy (Lim *et al*., 2010).

It was reported that PA treatment disrupted lipid metabolism homeostasis and triggered ER stress and inflammation in large yellow croaker's intestine or intestinal cells. The decrease in phosphatidylethanolamine (PE) content was identified as contributing to the intestinal homeostatic imbalance induced by PA. PE supplementation was suggested as a potential nutritional strategy to regulate intestinal homeostasis (Fang *et al*., 2022b). Earlier, it was found that PA-induced cell death in human hepatoma cells (HepG2)

through caspase-1 mediated pyroptosis and ER stress. Interestingly, the monounsaturated fatty acid oleic acid (OA) protected against hepatic lipotoxicity by suppressing PA-induced pyroptosis and ERS in HepG2 cells. The down-regulation of gastrin D (GSDMD) expression was identified as a potential mechanism contributing to the protective effects of OA against pyroptosis (Zeng *et al*., 2020b). It was revealed that PA-induced ER stress and autophagy in prefrontal cells, contributing to apoptosis and a decline in neuroplasticity-related proteins. Inhibition of ER stress reduced neuroplasticity-related protein expression, while inhibition of autophagy exacerbated apoptosis and enhanced ER stress in PA-treated prefrontal cells, highlighting the intricate interplay between ER stress and autophagy in the context of lipotoxicity-induced cognitive dysfunction (Xue *et al*., 2021). In a hepatocyte steatosis model with HepG2 cells exposed to PA, various polyphenols and berberine exhibited protective effects by preventing PA-induced steatosis, intracellular reactive oxygen species (ROS) production, and mRNA increase for inducible nitric oxide synthase (iNOS). It was also noted that these polyphenols partially inhibited PA-induced markers of ER stress, along with reductions in mitochondrial content and membrane potential. This suggests that the observed protective mechanisms of polyphenols against PA-induced hepatocyte damage are consistent across these compounds (Rafiei *et al*., 2018).

In the investigation of PA-induced metabolic and lipotoxic changes in human hepatoma cells (Hep3B, Huh7, and HepG2), it was found that PA altered lipid metabolism, induced oxidative stress, and disrupted intracellular $Ca2^{+}$ balance. Previously, it was also observed toxic manifestations, such as changes in $Ca2^{+}$ level, mitochondrial dysfunction, and activation of the PERK-eIF2α-CHOP pathway, with variations in sensitivity among different hepatoma cell lines, highlighting the complex and cell-type-specific responses to PA-induced lipotoxicity (Nissar *et al*., 2015). Moreover, it was evident that obesity-related neurodegenerative diseases, it was found that PA, a saturated fatty acid, induces significant neuron cell cycle arrest in the G2/M phase in SH-SY5Y cells, accompanied by an increase in endoplasmic reticular (ER) stress markers. The research further revealed that this G2/M arrest and associated ER stress were reversed by treatment with 2-bromopalmitate, a protein palmitoylation inhibitor, suggesting a crucial role for protein palmitoylation in PA-induced neuron cell dysfunction (Hsiao *et al*., 2014a). An earlier study reported that on dairy cows during the early postpartum period, it was observed that PA-induced lipotoxicity in calf hepatic

cells could be mitigated by propionate. Propionate enhanced autophagic activity, as evidenced by increased expression of autophagy markers, and suppressed ER stress, ultimately improving cell viability. These findings suggest that propionate's protective effects involve enhancing autophagy and alleviating ER stress, providing insights into potential strategies for addressing liver injury in dairy cows during the transition period (Gao *et al*., 2021).

In PA-challenged pancreatic *β*-cells, kaempferol, a natural flavonoid, demonstrated a lipid-lowering effect by inducing autophagy, specifically through AMPK/mTOR-mediated lipophagy. This mechanism was associated with decreased lipid stores, ER stress alleviation, and restoration of *β*-cell function. Kaempferol's potential to prevent ectopic lipid accumulation and mitigate ER stress suggests its candidacy as a therapeutic agent for addressing obesity-linked diabetic complications (Varshney *et al*., 2018). In well-differentiated human colonic goblet cells, eicosapentaenoic acid (EPA) and docosahexaenoic acid (DHA) were identified as potential protective agents against ER stress-induced alterations in Muc2 secretion caused by PA (PAL). This suggests that EPA and DHA may have therapeutic potential in mitigating the detrimental effects of saturated fatty acids associated with conditions such as type 2 diabetes, obesity, or inflammatory bowel disease. These findings warrant further exploration in *in vivo* studies regarding dietary obesity (Escoula *et al*., 2019). A previous study showed that high-calorie diet-fed mice exhibited adipocyte hypertrophy, inflammation, and ER stress in subcutaneous and visceral adipose tissues. Resveratrol treatment alleviated insulin resistance and ER stress, increased SIRT1 expression, and reversed the expression of adipokines in both adipose tissues. This protective effect of resveratrol was also observed in PA-treated adipocytes, suggesting a potential role for resveratrol in mitigating ER stress and inflammation induced by high-calorie diets or PA in adipose tissues and cells (Chen *et al*., 2017).

1.5 Colorectal cancer (CRC)

CRC originates in the colon or rectum. In 2020, colorectal cancer was the third most common cancer worldwide, with 1.9 million diagnoses and 0.9 million deaths. Westernization has increased the occurrence of this disease in developing countries and industrialised countries, making it a significant public health issue. In addition, early-stage instances are rising (Xi and Xu, 2021a). GLOBOCAN 2020 estimated 1.15 million new instances of colon cancer, 0.7 million rectal cancers, and 50,000 anal

cancers worldwide in 2020. By 2040, 1.92 million new colon, 1.16 million rectal, and 78,000 anal cancer cases are estimated. This shows the expected rise of these cancers over the next two decades (Table 2) (Sung *et al*., 2021). Population-based screening programmes have been pushed and adopted in industrialised countries for over a decade to improve colorectal cancer treatment outcomes by shifting distribution to early stages (Arnold *et al*., 2017, Miller *et al*., 2022, Ahmed, 2020).

CRC rates are four times greater in countries with a very high Human Development Index (HDI) than in those with a low HDI (Khazaei *et al*., 2016, Gullickson *et al*., 2021). However, the incidence rate is rising in developing nations due to risk factor exposure but is constant or declining in wealthy countries. China and the US predicted the most CRC cases in 2020. China will have 0.91 million cases in 2040, up 64% from 2020. CRC is expected to affect 4.4 per cent of males and 4.1 per cent of women in the US. Cases are expected to climb from 0.16 million in 2020 to 0.21 million. The top 10 countries with the most significant CRC incidence in 2020 were Russia, Germany, India, Brazil, the UK, Italy, and France, as depicted in figures 1.4 and 1.5 (Siegel *et al*., 2020, Bray *et al*., 2012, Xi and Xu, 2021b).

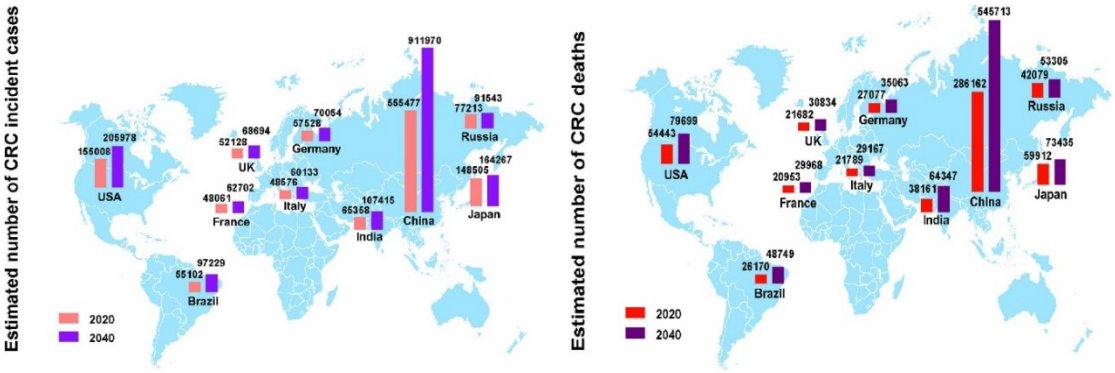

Figure 1.4 Colorectal Cancer Statistics: A Comparison of New Cases and Mortality Rates in the Top 10 Countries for 2020 and Projections for 2040 (Right and Left, respectively). Adapted from (Xi and Xu, 2021a).

Table 1.2 Estimated new colorectal cancers cases (2020 to 2040)

Cancer sites	2020	2040
Colon	1148515	1916781
Rectum	732210	1160296
Anus	50865	77597
Total	1931590	3154674

Adapted from (Xi and Xu, 2021b)

From 2014 to 2021, 74.7 percent of 1028 colorectal cancer patients in India had advanced illness, mainly affecting the rectum (50 %). Of 163 patients, 73% had advanced anal cancer. Colorectal cancer patients received 37.1 % chemotherapy, and anal cancer patients 43.1%. The study found a significant Annual Percentage Change in lower GI cancer incidences increasing (Raj *et al*., 2022).

CRC incidence and mortality arise from a complex interplay of genetic and modifiable factors. Low physical activity, overweight, bad diets, and lifestyle choices, including heavy alcohol and smoking, increase CRC risk. Impaired gut flora and intestinal inflammatory disease (IBD) also contribute (Snider *et al*., 2016, Shaw *et al*., 2018, Lukic *et al*., 2023, Kato and Sun, 2023). Recent research has focused on molecular abnormalities that cause CRC, specifically the UPR and IRE1, PERK, and ATF6 - three necessary ER transmembrane protein sensors (Kato and Sun, 2023, Lukic *et al*., 2023). Understanding these molecular pathways offers insights into the convergence of various risk factors in colorectal cancer development. This makes a holistic approach that combines lifestyle changes with molecular understanding essential for CRC prevention and management.

1.5.1 ER stress: A dual-edged sword in colon cancer pathology

Recent studies indicate that the UPR may significantly impact the progression and development of CRC (Huang *et al*., 2021c). A pro-survival or cell death response is typically induced by ER stress to restore cellular homeostasis and prevent cancer development. However, Prolonged or severe ER stress may enhance cancer cell survival and growth (Siwecka *et al*., 2019) (Fig 1.5). CRC formation is influenced by the UPR, which governs cell survival and adaptation in response to endoplasmic reticulum stress via interrelated yet different pathways; IRE1, PERK, and ATF6 are

involved in the UPR. Identifying the UPR pathways, which govern the interplay between adaptability and apoptosis in the development of colorectal cancer, may facilitate the creation of innovative therapeutic and diagnostic approaches. Therefore, it is necessary to conduct a more comprehensive analysis of the signal exchanges that govern the balance between adaptability and apoptosis in the aetiology of colorectal cancer. Furthermore, by acknowledging that ER stress and UPR cause colorectal cancer, a unique perspective has been offered on the development of therapeutic, preventative, and diagnostic measures (Zhou *et al*., 2016, Geng *et al*., 2023).

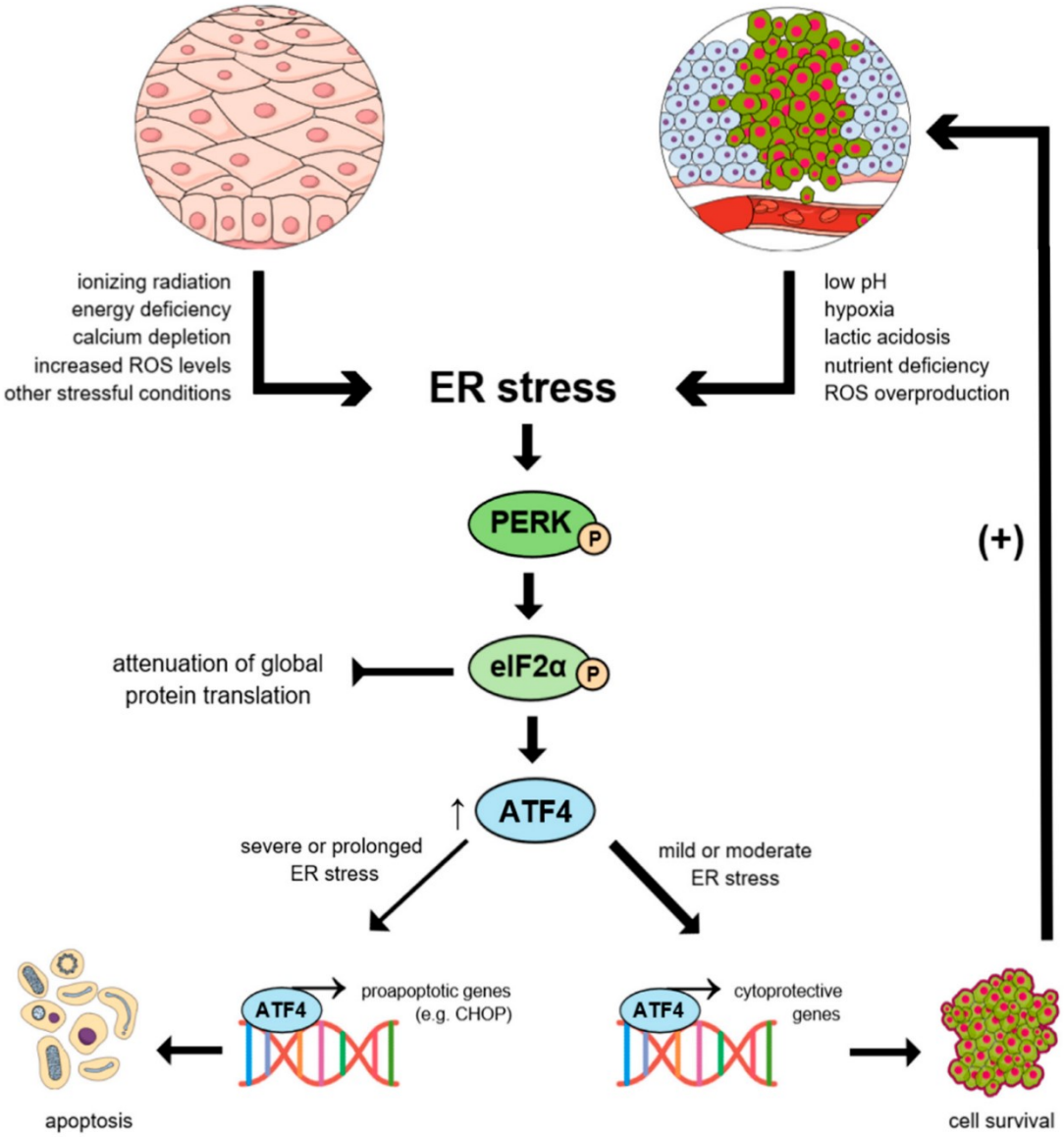

Fig 1.5 Divergent cellular responses to ER stress: Contrasting activation of the PERK-dependent UPR signalling pathway in normal epithelial cells and cancer cells (Siwecka *et al*., 2019).

1.5.2. UPR's role in colon cancer progression and drug resistance

It was shown that overexpression of GRP78, a protein that influences apoptosis and cell proliferation, could be a sign of malignant transformation in colorectal cancer (Mhaidat *et al*., 2016, Huang *et al*., 2021b, Xing *et al*., 2011, Piton *et al*., 2016a). Elevated ER stress associated with treatment resistance is indicated by enhanced ER labelling, increased mitochondrial $Ca2^{+}$ levels, and increased ER stress-related proteins in colon cancer cells. These results suggest that colon cancer treatment resistance is primarily caused by ER stress (Kim *et al*., 2016). Additionally, the PERK-ATF4 pathway contributes considerably to CRC cell treatment resistance, suggesting that this system may aid metastatic spread, too (Shi *et al*., 2019). Research has demonstrated that autophagy, induced by ER stress, removes polyubiquitinated protein aggregates and reduces cellular vacuolisation in colon cancer cells. It results in cell death in embryonic fibroblasts and colon cells, highlighting the context-dependent role of autophagy during ER stress and its potential implications for tumour-specific therapies that attempt to reduce ER-induced cell death (Ding *et al*., 2007).

IRE1α, a critical component of the unfolded protein response, has been recognised as a crucial element in the progression of colonic tumours. This is supported by its inhibitory impact on the growth of intestinal organoids, suppression of proliferation of colon cancer cells, inhibition of the stemness of cancer stem cells, and prevention of the development of colitis-associated colonic tumours in mice. The development of a therapeutic strategy that targets IRE1α selectively with the inhibitor exhibits potential for the management of colon cancer (Li *et al*., 2017). The acceleration of cancer cell invasion in response to XBP1 overexpression using small interfering RNA (siRNA) and the inhibition of XBP1 indicate that XBP1 IRS expression correlates positively with increased tumour invasiveness. Based on these results, XBP1 might emerge as an innovative biomarker for invasion and metastasis of colorectal cancer (Mhaidat *et al*., 2015). XBP1s, a transcription factor, activates the IRE1α-JNK pathway in colon cancer cells by binding to the promoter and activating its expression during ER stress. This regulatory cascade modulates mRNA degradation, encouraging colon cancer cell proliferation. These data indicate that XBP1s may be a promising colon cancer treatment target (Liu *et al*., 2023). Another study found that the IRE1α-XBP1 pathway is crucial for modulating cell proliferation, metastasis, and EMT in CRC. Based on tissue microarray research and functional testing, greater IRE1α expression negatively

correlates with overall survival rates. IRE1α binding to the cyclin D1 promoter directly affects CRC cell mitosis (Jin *et al*., 2016a).

IRE1α facilitates regulating colon cancer cell metastasis *via* modulation of fibronectin-1 (FN1) expression. This is demonstrated by the observation that FN1 expression, migration, and invasion are all inhibited upon IRE1α knockdown, an effect attributable to a decrease in XBP1s production. The molecular operation of XBP1s involves binding to the FN1 promoter, which then regulates signalling pathways associated with the metastatic process (Xie *et al*., 2019). Moreover, EGFR targeting inhibits the activation of the IRE1α-XBP1s signalling pathway via the EGFR-MEK-ERK pathway. Still, the addition of cetuximab to oxaliplatin enhances its effectiveness by further inhibition of the IRE1α-XBP1s pathway. Based on the substantial data supporting combining EGFR targeting with chemotherapy for treating colorectal cancer, these findings suggest that the signalling pathway involving IRE1α-XBP1s holds great promise as a therapeutic target (Huo *et al*., 2020).

A comprehensive investigation that identified and verified fifty ERS differentially expressed genes and eight ERS model genes related to CRC stage and prognosis identified three subtypes of CRC. ATF6 expression was additionally emphasised as a diagnostic indicator for distinguishing non-ulcerative colitis individuals with CRC from those presenting with low-grade dysplasia (Hanaoka *et al*., 2018). Furthermore, the research study developed a nomogram that incorporated the ER score, age, and CRC stage to forecast prognosis across different forms of CRC effectively (Qu *et al*., 2023). It is widely recognised that elevated ATF6 levels in patients with colorectal cancer are associated with a decreased rate of disease-free survival. Chronic ATF6 activation in the colon has also been connected to dysbiosis and tumour growth mediated by the microbiota (Coleman *et al*., 2018). An alternative inquiry has identified ATF6 as a factor that regulates BRCA-1 expression via mTOR activation and protects colon cancer cells from ER stress-induced cytotoxicity. Also, Inhibiting ATF6 increases the vulnerability of colon cancer cells to DNA-damaging agents like Adriamycin and amplifies the lethal effects of endoplasmic reticulum stress inducers, according to research (Benedetti *et al*., 2022).

In colorectal cancer, the expression of the oncogene CIP2A is upregulated due to ER stress-induced activation of ATF6, which creates a direct binding channel between ATF6 and the CIP2A promoter. Potentially improving the prognosis of individuals

diagnosed with colon cancer, CIP2A targeting could impede the mechanisms behind ER stress-mediated survival (Liu *et al*., 2018). Furthermore, research has revealed that GREM1 plays a substantial role in the progression of colorectal cancer through its opposition to BMP2 and differential regulation of ATF6 and ATF4 in unfolded protein response pathways, which are facilitated by the activation of PI3K/AKT/mTOR (Li *et al*., 2022). The induction of epithelial-mesenchymal transition by different stress conditions is supported by an ER-stress response characterised by increased vimentin and GRP78. Both EMT and ER stress are inhibited in the absence of ZEB1, and reoxygenation reverts both processes depending on ZEB1. An elevated intensity of GRP78 in the invasive fronts of colorectal cancer is correlated with the activation of ZEB1 via HIF1α and *β*-catenin. This suggests that cellular stress is arranged hierarchically in response to malnutrition or hypoxia, with extracellular matrix stress preceding endoplasmic reticulum stress (Huo *et al*., 2020) (Fig 1.5).

1.6 Research problem

Palmitic acid, traditionally known for its involvement in lipid metabolism, has been shown to influence various cellular mechanisms that regulate cancer cell survival. However, its impact on endoplasmic reticulum (ER) stress, a key pathway that maintains cellular homeostasis, remains underexplored in the context of colon cancer. ER stress, if unresolved, can lead to cellular dysfunction and has been implicated in the survival and adaptation of cancer cells, particularly in response to metabolic stress. This study addresses the gap in understanding how palmitic acid induces ER stress in colon cancer cells and its role in modulating cellular survival and progression. The study will explore the molecular mechanisms through which palmitic acid affects ER stress responses to provide insights into cancer cell adaptability and identify potential therapeutic targets. By elucidating the complex relationship between palmitic acid metabolism, ER stress, and colon cancer progression, this study aims to contribute to the broader field of cancer biology and open avenues for targeted interventions to mitigate the risk and progression of colon cancer.

1.7 Objectives

1. Anlaysis of ER stress satus in normal and cancer cell by the exposure of different concentration of palmitic acid.

2. Aanalysis of gene alterations related to ER stress mediated cell survival – death pathways

3. Analysis of ER stress signaling pathays in cancerous and non cancerous tissues of CT26 metastsised tumour bearing mice administered with palm oil

Chapter 2

Materials and methods

2.1 Materials

2.1.1 Chemicals

Name of chemicals	**Manufacturer**
Acetic acid (Glacial 99-100%)	: Merck (New Jersey, United States)
Acridine orange	: Sisco Research Laboratories (India)
Acrylamide	: -do-
Agarose	: -do-
Ammonium persulfate	: -do-
β-mercaptoethanol	: Merck (New Jersey, United States)
Bis-acrylamide	: Sisco Research Laboratories (India)
Bovine serum albumin (BSA)	: -do-
Bromophenol blue	: -do-
CDNB(1-chloro-2,4 di nitro benzene)	: -do-
Chloroform	: Merck (New Jersey, United States)
Coomassie brilliant blue	: -do-
Copper sulfate penta hydrate	: -do-
Dextrose	: Sisco Research Laboratories (India)
Dichloro-dihydro-fluorescein diacetate	: Sisco Research Laboratories (India)
Diethyl pyro carbonate (DEPC)	: -do-
Dimethyl sulfoxide	: Sisco Research Laboratories (India)
Dipotassium hydrogen phosphate	: Merck (New Jersey, United States)
Disodium hydrogen phosphate	: Merck (New Jersey, United States)
Direct red 80	: Sigma Aldrich Inc. (St Lois, USA)
Dithiobis (2-nitro benzoic acid) (DTNB)	: Sisco Research Laboratories (India)
Dithiothreitol (DTT)	: -do-
DPX mountant	: Sisco Research Laboratories (India)
Dulbecco's modified eagle medium	: Gibco, Thermo Fisher Scientific, USA
Ethanol	: Merck (New Jersey, United States)
Ethidium bromide (ETBR)	: Sisco Research Laboratories (India)
Ethylene diamine tetra acetic acid (EDTA)	: -do-
Ferric chloride	: Merck (New Jersey, United States)

Foetal bovine serum (FBS)	: Merck (New Jersey, United States)
Folin's Ciocalteau reagent	: -do-
Formaldehyde	: -do-
Four-phenyl butyric acid	: Sisco Research Laboratories (India)
Gel loading dye	: Promega (Wisconsin, United States)
Glutathione reduced (GSH)	: -do-
Glycine	: Sisco Research Laboratories (India)
Hanks balanced salt solution (HBSS)	: Biovision
Hematoxylene	: Sigma Aldrich Inc. (St Lois, USA)
HEPES buffer	: Himedia Laboratories (India)
Hoechst 34580	: Sigma Aldrich Inc. (St Lois, USA)
Hydrochloric acid	: Merck (New Jersey, United States)
Hydrogen peroxide	: -do-
Isopropanol	: -do-
Methanol	: Spectrochem (Mumbai, India)
Monodansyl cadaverine	: Merck (New Jersey, United States)
MTT (3-(4,5-dimethylthiazol-2-yl)-2, 5-diphenyl tetrazolium bromide	: Merck (New Jersey, United States)
N-acetyl-L-cysteine	: Sisco Research Laboratories (India)
Nitrobluetetrazolium (NBT)	: Sisco Research Laboratories (India)
Non-essential amino acids	: Himedia Laboratories (India)
Oil red O	: -do-
Orthophosphoric acid	: Merck (New Jersey, United States)
Palmitic acid	: Merck (New Jersey, United States)
Paraformaldehyde	: Sigma Aldrich Inc. (St Lois, USA)
PCR master mix	: Promega (Wisconsin, United States)
Ponceau stain	: Sisco Research Laboratories (India)
Potassium chloride (KCl)	: Merck (New Jersey, United States)
Potassium dihydrogen phosphate	: -do-
Pricric acid	: Sisco Research Laboratories (India)
Primers	: Integrated DNA Technologies, IA, USA
Propidium iodide	: Sigma Aldrich Inc. (St Lois, USA)

Propylene glycol	: Sisco Research Laboratories (India)
RPMI	: Gibco, Thermo Fisher Scientific, USA
Sodium acetate	: -do-
Sodium azide	: -do-
Sodium bicarbonate	: -do-
Sodium dihydrogen phosphate dehydrate	: -do-
Sodium dodecyl sulphate	: -do-
Sodium hydroxide	: -do-
Sodium potassium tartrate	: -do-
Sodium pyruvate	: Himedia Laboratories (India)
Sulforhodamine B	: Sisco Research Laboratories (India)
Sulfuric acid	: Merck (New Jersey, United States)
Tetramethylethylenediamine	: Sisco Research Laboratories (India)
Thiobarbituric acid (TBA)	: -do-
Thioflavin T	: Sisco Research Laboratories (India)
Trichloro acetic acid (TCA)	: -do-
Tris buffer	: -do-
Tris-HCl	: -do-
Trizol reagent	: -do-
Trypsin	: Merck (New Jersey, United States)
Tunicamycin (TM)	: Merck (New Jersey, United States)

2.1.2 Diagnostic kits and reagents

Name of the diagnostic kits	**Manufacturer**
Mouse interleukin- 6 (IL-6)	: PeproTech, Germany
Mouse TNFα	: -do-
Total RNA isolation kit	: Origin
CDNA synthesis kit	: -do-
ORIonX 2X RT-PCR smart mix	: -do-

2.1.3 Instruments

Name of the instruments	**Make**
Deep freezer (-70 & -20ºC)	: Remi Laboratory Instruments, India

Double distillation unit (Quartz)	: Borosil, India
Electronic balance	: Schimadzu, Genzo Shimadzu
Electrophoresis unit	: Genei, Bangalore, India
ELISA plate reader	: Thermo Scientific, Waltham, USA
Fluorescence microscope	: Leica DMIL, Wetzlar, Germany
Fluorescence spectrophotometer	: PerkinElmer, Massachusetts, USA
FTIR spectrophotometer	: PerkinElmer, Massachusetts, USA
GC-MS/MS	: Thermo Fisher Scientific, Germany
Gel documentation system	: Remi Laboratory Instruments, India
High-speed cooling centrifuge	: Remi Laboratory Instruments, India
Horizontal laminar flow hood	: Clean Air, Chennai, India
Hot air oven	: Rotex Instruments Pvt Ltd, India
Incubator	: Beston Instruments, India
Inverted microscope	: Magnus INVI, Bangalore, India
LC-MS/MS	: Agilent biotech, California, USA
Microcentrifuge	: Tarsons Products Private Limited
Multi dispenser	: Eppendorf, Hamburg, Germany
pH meter	: Eutech, Waltham, USA
PCR (thermal cycler)	: Eppendorf, Hamburg, Germany
Phase contrast microscope	: Magnus INVI, Bangalore, India
Quantitative real-time PCR	: Applied Biosystems, Waltham, USA
Tissue homogenizer	: Yorco Scientific, Chennai, India
Ultra-low deep freezer (-80ºC)	: New Brunswick, Eppendorf, Germany
UV/visible spectrophotometer	PG Instruments Ltd; Systronics India
Vacuum concentrator	: Eppendorf, Hamburg, Germany.

2.1.4 Softwares

Name of the software	**Purpose**
Adobe photoshop CS 5.0,	: Image processing
Endnote X5	: Reference manager
GraphPad Prism 7.0	: Statistics and graph preparation
GraphPad Instat 3.0	: Statistical analysis
IS Capture 3.6.6	: Microscope image capture
Applied Biosystems 7300 software	: Real-time PCR analysis

MS Word 2010	: Text preparation
MS Excel 2010	: Calculation
MS Power Point 2010	: Presentation and artworks
Adobe acrobat DC Pro	: Preparation and edit PDF files
Image J 1.48	: Biological image processing
UV Win spectrophotometer software	: Spectroscopic measurement

2.1.5 Cell lines

IEC6 (normal rat intestinal cells) and HCT116 (human colon cancer cells) were obtained from NCCS Pune. The mouse metastatic colon cancer cell line (CT26) was provided as a gift by Dr. Bipasha Bose, Professor, Yenepoya University, Manipal. All experimental procedures were performed under sterile conditions.

2.1.6 Animals

Male BALB/c mice weighing 24-26 g were purchased from the Kerala Veterinary and Animal Sciences University (KVASU), Mannuthy, Thrissur. Polypropylene cages were used to house the animals. During their acclimatisation, they were fed non-purified rat chow and filtered water for two weeks. The animal experiments are carried out by the approval of institutional animal ethics committee (IAEC) of Amala Cancer Research Centre (No. ACRC/IAEC/21(2)-P11 dt.02-12-2021). All protocols were conducted in accordance with the guidelines of the Committee for the Purpose of Control and Supervision of Animal Experiments (CPCSEA), under the Ministry of Environment, Forest, and Climate Change, Government of India.

2.1.7 Palm oil

Palm oil was purchased from a local market

2.1.7.1 GC-MS/MS analysis

In accordance with traditional cooking practices, palm oil was subjected to a mild heat treatment prior to cooking in order to enhance its palatability.

2.1.7.2 Direct fame synthesis (O'Fallon *et al*., 2007)

To a screw-cap Pyrex culture tube (16 × 125 mm), add 40 μL palm oil, 0.7 mL 10 N KOH in water, and 5.3 mL of Methanol were added. For optimal sample penetration, dissolution, and hydrolysis, the tube was incubated at 55°C for 1.5 hrs with vigorous hand-shaking every 20 min. Add 0.58 mL of 24 N H_2SO_4 in water after cooling in a cold tap water bath. With precipitated K_2SO_4, the tube was incubated for 1.5 hrs at 55°C with hand-shaking every 20 min. The tube was cooled with tap water after FAME

synthesis. Add three millilitres of hexane and vortex-mix for five minutes on a multitube vortex to extract FAME. The FAME-containing hexane layer was carefully transferred to a GC vial after 5 min of tabletop centrifugation. The sealed vial was kept at -20°C until GC analysis.

GC-MS analysis was done using an Agilent Technologies GC model-7890A (USA). The study used a DB-5 column measuring 30 m x 0.25 mm x 0.25 μm. An Agilent 5975C Inert XL MSD was employed as the MS detector. A constant injection volume of 1.0 L was maintained, with an injection temperature of 250°C. The temperature of the column oven was set to 60°C and increased at a rate of 5°C per minute. A constant detector temperature of 250°C was maintained for the duration of the study.

2.1.7.3 Concentration of palmitic acid in palm oil

According to the GC-MS analysis, the palmitic acid concentration in HPO was **367,000 µg/mL (367mg/mL)**

2.2 Methods

2.2.1 Cytology

2.2.1.1 Cell culture conditions and treatment procedures

Culturing was performed in DMEM/RPMI at 37°C with 5% CO_2.

Table 2.1 Cell culture media and its components

Cell line	Medium	Serum	Antibiotics	Additives
IEC6	DMEM (4.5 mg/mL glucose)	10% FBS	1% P/S	4 mM glutamine
HCT116	DMEM	10% FBS	1% P/S	
CT26	RPMI	10% FBS	1% P/S	

P/S; Penicillin and streptomycin, FBS; fetal bovine serum, DMEM: Dulbecco's Modified Eagle Medium, RPMI: Roswell Park Memorial Institute medium.

2.2.1.1.1 Thawing of cells

After cryopreservation, the cells were thawed at 37°C. Centrifugation was performed at 2000 rpm for 3 min in 9 mL of DMEM to exclude DMSO from the suspension. The pellet was then resuspended in 1 mL of complete media and introduced into a T25 tissue culture flask containing 6 mL of media.

2.2.1.1.2 Cryopreservation of cells

The cells were trypsinised, counted, and diluted to $1x10^5$ cells/ml in a cryomedium containing 90% FBS and 10% sterile DMSO. The aliquots were stored in cryovials and kept in an -80°C freezer.

2.2.1.1.3 Cell harvesting

Cells were cultured in a T25 flask with 7 ml of medium. Cell growth was limited to 70% confluence to maintain differentiation capacity, and passages were limited to 15. For passaging, cells were trypsinized with 0.5 mL of trypsin-EDTA after washing with 1 ml of 1x PBS and then resuspended in 1.5 ml of fresh media. Before plating, 4×10^4 cells were counted using 0.04% trypan blue and transferred to a T25 flask with 7 ml medium. Passaging was carried out every three to four days, involving centrifugation at 2000 rpm for three min and resuspension in 10 ml fresh medium. Finally, the cells were stored at -80°C after removing the supernatant.

2.2.1.1.4 Cell seeding density

Due to the doubling process, the standardised seeding densities for the IEC6, CT26, and HCT116 cell lines varied marginally. The table below shows the seeding density and maximum media volume used across well plates to optimise cell line growth for various experiments.

Table 2.2 Seeding density and medium volumes for cell lines

Cell lines	Well plates	Seeding density	Medium/well
IEC6	96	10000-15000	0.1
	48	20000-25000	0.25
	24	50000	0.5
	12	1×10^5	0.7-1.5
	6	1.5×10^5	1.0-2.0
CT26	96	10000-15000	0.1
	48	20000-25000	0.25
	24	50000	0.5
	12	1×10^5	0.7-1.5
	6	1.5×105	1.0-2.0
HCT116	96	5000-10000	0.15
	48	15000-20000	0.35
	24	30000-40000	0.6
	12	0.7×10^5	1
	6	1×10^5	2

Seeding densities (cells/well) and medium volumes (mL) may vary with experimental conditions and cell line.

2.2.1.1.5 Preparation of palmitic acid stock solution (Takahashi *et al*., 2012)

A 100 *m*M palmitic acid stock solution was prepared in absolute alcohol (EtOH). IEC6 cells were treated with different doses of palmitic acid ranging from 100 to 400 μM, while CT26 and HCT116 cells were treated with 50 to 200 μM based on their respective IC_{50} values. The absolute alcohol (vehicle control) concentration was maintained at 0.002%.

2.2.1.2 Cell culture assays

2.2.1.2.1 MTT assay (Marshall *et al*., 1995)

Principle: The MTT assay is a colorimetric assay based on the reduction of yellow tetrazolium salt MTT (3-(4,5-dimethylthiazol-2-yl)-2,5-diphenyltetrazolium bromide) to purple formazan crystals by mitochondrial enzymes, primarily succinate dehydrogenase, thus providing a measure of cellular metabolic activity.

Procedure: The cells were cultured for 24 hrs and then exposed to varying palmitic acid concentrations. They were incubated over the following 24 hrs at 37°C with 5% CO_2. A four-hour treatment with MTT (5 μg/ml) reagent was done on the cells. The formazan crystals formed were dissolved using DMSO. Absorbance was taken at 510 nm. Images were captured with a phase-contrast microscope (Magnification of 10 X with a scale bar of 100 μm). Finally, the endpoint parameters were calculated, including the % cell viability and cytotoxicity (CT%).

$$\text{Cytotoxicity (CT) \%} = (\text{OD Control} - \text{OD sample}) / \text{OD Control} \times 100$$

$$\text{Viability \%} = 100 - \text{cytotoxicity (CT) \%}$$

MTT was used to investigate palmitic acid cytotoxicity against rat intestinal IE-6 cell lines and murine metastatic colon cancer cells CT 26. The quantitative assay determined the IC_{50}.

2.2.1.2.2 Sulforhodamine B assay (Skehan *et al*., 1990)

Principle: The residues of basic amino acids in cells fixed in trichloroacetic acid, pH-dependently and electrostatically bound to Sulforhodamine B.

Procedure: Cells were seeded and exposed to different doses of palmitic acid the following day. After treatment, the cells were fixed at 4°C for one hour using 10% trichloroacetic acid. They were then stained with 0.4% SRB. The excess stain was removed using 1 ml of 1% acetic acid. Following the dissolution of protein-bound dyes in 200 μl of 10 mM Tris, optical density at 510 nm was determined using an ELISA

plate reader. Additionally, images were captured at 10 X magnification using a phase-contrast microscope featuring a 100 μm scale bar. Endpoint parameters such as % cell viability and % cytotoxicity (CT%) were determined for each cell line.

Cytotoxicity (CT) % = (OD Control – OD sample) / OD Control × 100

Viability % = 100 - Cytotoxicity (CT) %

Sulforhodamine B assay measured the IC_{50} of palmitic acid on HCT116 colon cancer cells. Furthermore, it was utilised to standardise fluorescent signals in spectrofluorimetric quantification for DCHDA and thioflavin T staining, using cell numbers to indicate protein content.

2.2.1.2.3 Oil red O staining and quantification of neutral lipids (Kinkel *et al*., 2004, Krishnan *et al*., 2019)

Principle: The oil red O dye (ORO) is a diazo dye used to stain neutral lipids and fat deposits in cells and tissues. In quantitative photometry, oil red O eluted in isopropanol shows maximum absorbance at 510 nm.

Procedure: Cells were cultured and treated with various doses of palmitic acid at 37°C with 5% CO2 for 24 hrs. After PBS wash and 10 min of methanol fixation. The cells were rinsed with distilled water, and 100% polyethylene glycol (PEG) was added and removed after 2 min. Then 500 μl of Oil Red O was applied for 15 min. Wells were then washed in 60% PEG for one minute after stain removal. After washing with distilled water, 1 ml of haematoxylin was added for 10 min. The nuclei were stained with sodium phosphate for five minutes and washed in distilled water. Air-dried wells were mounted on Crystal/MountTM and photographed in an inverted phase-contrast microscope at 40X magnification using a 100 μm scale bar. Isopropanol was used to elute the dye, and washing was done with 60% PEG after treatment. At 510 nm, absorbance was measured and normalised to control.

Normalisation = Absorbance of the sample at 510 nm/absorbance of the control at 510 nm

2.2.1.2.4 Trypan blue exclusion method (Strober, 2001)

Principle: When cell suspension is mixed with trypan blue, it becomes possible to differentiate between live and dead cells on a hemacytometer visually. It shows that living cells have transparent cytoplasm; dead cells absorb dye and turn blue.

Procedure: cell grown in 6 well plates incubated at 37ºC at 5% CO_2. Subsequently, they were subjected to specific doses of palmitic acid and incubated for an additional 24 hrs. After trypsinization, 100 μl of cell suspension was diluted 1:1 with 0.4 per cent trypan

blue. The diluted mixture was then used to count cells using a haemocytometer under an inverted microscope. Finally, comparing the treated and untreated cell counts yielded a relative cell number.

$$Cells/_{ml} = N \times D \times 10^4$$

$$\text{Viable cells (\%)} = \left(\frac{Total\ unstained\ cells}{Total\ \ cells}\right)100$$

Note: N: mean cell counts per square, D: dilution factor

2.2.1.2.5 Colony formation assay (Brix *et al*., 2020)

Principle: The colony formation assay assesses the proliferative potential of a cell by measuring its ability to form a colony or clone.

Procedure: cultured cells in 6 well plates was treated with varying concentrations of palmitic acid for 24 hrs. After trypsinisation, 3000 cells/well were reseeded into duplicate 6-well plates following 15 days of incubation period at 37°C. The developed colonies were subsequently fixed in methanol and stained with 0.5 per cent crystal violet. For calculating the plating efficiency (PE) and survival fraction (SF) colonies with 50 or more cells were exclusively counted, and colony images were captured at 10 X magnification using an inverted phase contrast microscope.

$$\text{PE (\%)} = \left(\frac{Colony\ count}{\text{Seeded cell number)}}\right)100$$

$$\text{SF} = \left(\frac{\textbf{colonies devloped post treatmnet)}}{\textbf{colonies devped for Untreated)}}\right)\left(\frac{\textbf{PE (Untreated)}}{\textbf{PE (Treated)}}\right)$$

2.2.1.2.6 DCFH-DA assay (Ng and Ooi, 2021)

Principle: DCFDA is a fluorescent dye that measures hydroxyl and peroxyl activity in cells. Once it diffuses into cells, the dye is transformed by a cellular esterase into a non-fluorescent compound. ROS later oxidizes this compound into DCF, which is highly fluorescent.

Procedure: Two experiments were conducted using different cell lines to measure intracellular reactive oxygen species generation. The cells were exposed to varying concentrations of palmitic acid (PA) for 24 hrs. One group was pre-treated with either a ROS scavenger (N-acetylcysteine, Nac, 1 mM) or positive control (H_2O_2, 100 μM) six hours before signal detection. After treatment, both groups were exposed to DCFHDA (10 μM) for 30 min at 37°C. ROS fluorescence was quantified at 485/530 nm excitation/emission wavelength using a fluorescent spectrometer. In addition, images were captured using a Leica DMIL fluorescence microscope (Germany).

Calculate DCF corrected and SRB corrected:

DCF corrected =DCF-average (untreated cell control DCF)

SRB corrected =SRB-average (untreated cell control SRB)

Calculate fold change for DCF and SRB

$$\text{DCF foldchange } \left(\frac{DCF}{\text{Average (Untreated cell control DCF}}\right)$$

$$\text{SRB foldchange} = \left(\frac{SRB}{\text{Average (Untreated cell control SRB}}\right)$$

Calculate the ratio of DCF to SRB

$$\text{DCF: SRB} = \left(\frac{DCF\ foldchange}{SRB\ fold\ change}\right)$$

2.2.1.2.7 Thioflavin T (ThT) assay (Beriault and Werstuck, 2013, Cuanalo-Contreras *et al*., 2022)

Principle: When misfolded proteins bind to ThT, a benzothiazole dye displays an increase in green fluorescence. The amount of misfolded/unfolded protein aggregates and the level of UPR activation are directly proportional to the detected rise in ThT fluorescence.

2.2.1.2.7.1 Determination of misfolded protein aggregates in cells

Procedure: Misfolded protein aggregates were detected using Thioflavin fluorescence. In two independent experiments, cells were seeded, incubated overnight and treated with various PA concentrations for 24 hrs. One group received a positive control of 4-phenyl butyric acid, an ER stress inhibitor (2 mM PBA) or tunicamycin (3μg/mL TM), six hours before signal detection. A fixation of 4% paraformaldehyde in cells was conducted following treatment, followed by permeabilization with 0.1% Triton X and staining with Thioflavin (5 μM) for 40 min. ThT fluorescence microscopic pictures were acquired at 485 nm excitation and 535 nm emission. The values were normalised sulforhodamine B assay. The data underwent analysis, and the relative fluorescent intensity was determined using the following calculation method.

Calculate ThT corrected and SRB corrected:

ThT corrected = ThT - average (untreated cell control ThT)

SRB corrected = SRB - average (untreated cell control SRB)

Calculate fold change for ThT and SRB

$$\text{ThT foldchange} = \left(\frac{\text{ThT}}{\text{Average (Untreated cell control ThT}}\right)$$

$$\text{SRB foldchange} = \left(\frac{SRB}{\text{Average (Untreated cell control SRB}}\right)$$

Calculate the ration of ThT to SRB

$$\text{ThT: SRB} = \left(\frac{\text{ThT } foldchange}{SRB\ fold\ change}\right)$$

2.2.1.2.7.2 Determination of misfolded protein aggregates in tissues

Procedure: Tissue samples are homogenized in PBS and centrifuged at 20,000 × g for 1 hour at 4°C to isolate insoluble protein fractions. The supernatant is discarded, and the insoluble pellet is carefully resuspended in a detergent buffer containing 20 mM TRIS–HCl, 100 mM NaCl, 0.1% SDS, 1% sodium deoxycholate, 1% Igepal, and 1X protease inhibitor cocktail. After centrifugation to remove debris, the preparation is ready for further analysis. Normalize the concentration of insoluble protein across the samples. Prepare a stock solution of thioflavin T (Sigma) at a concentration of 5 μM in PBS. Measure the fluorescence signal of the buffer and thioflavin T solution to obtain background values. Incubate the insoluble protein fractions with the thioflavin T solution at 37°C for 30 min to allow binding. Measure the fluorescence of the samples using a spectrofluorometer with excitation at 435 nm and emission at 485 nm. Subtract the background fluorescence values obtained in the absence of thioflavin T from the sample readings. Analyse the relative fluorescence intensity of thioflavin T-bound insoluble protein fractions. Background Correction: Subtract the background fluorescence (F_background) from the fluorescence intensity of each sample (F_sample) to obtain the corrected fluorescence intensity (corrected).

$$F_{\text{corrected}} = F_{\text{sample}} - F_{\text{background}}$$

Normalization of fluorescent intensity: Normalize the corrected fluorescence intensity to the initial protein concentration of each sample.

$$\text{Normalized Fluorescence (X)} = \frac{F\text{corrected}}{Protein\ concentration(\frac{mg}{ml})}$$

2.2.1.2.8 Acridine orange assay – acidic vacuoles (Thomé *et al*., 2016, Klimaszewska-Wisniewska *et al*., 2016, Lu *et al*., 2019b, Traganos and Darzynkiewicz, 1994)

Principle: In an acidic environment, acridine orange (AO) dye emits bright red fluorescence, which is used to stain acidic vacuoles. By staining acidic autophagic vacuoles, AO enables the visualization of autophagosomes and highlights the fusion of autophagosomes and lysosomes in autophagy.

Procedure: Cultured cells were subjected to a specific concentration of palmitic acid for 24 hours, while a positive control was treated with HBSS (Hanks Balanced Salt

Solution) at 37°C with 5% CO^2. Subsequently, the cells underwent a post-wash, followed by the application of 1μg/ml acridine orange for 30 min under identical conditions. Upon removal of the dye, PBS was introduced, and the cells were observed using an inverted fluorescence microscope. Spectrofluorimetric analysis was conducted, utilizing emission filters for green fluorescence (510–530 nm) and red fluorescence (650 nm). The obtained values were normalized against cell proliferation determined by suforhodamine B, based on three independent experiments.

OD corrected= OD sample- OD blank

Normalised Optical density (OD) = OD corrected value/SRB reading

2.2.1.2.9 Monodansyl cadaverine assay (Notaro *et al*., 2023) (Kumari, Kamat *et al.* 2023) (Biederbick *et al*., 1995, Niemann *et al*., 2000).

Principle: MDC staining in autophagy relies on the auto fluorescent compound's accumulation in the acidic environment of mature autophagic vacuoles, facilitated by an ion-trapping mechanism with lipid interaction. Enhanced MDC fluorescence, upon cell uptake and localisation to autophagic vacuoles, indicates increased autophagic activity.

Procedure: Cells were subjected to treatment with palmitic acid and HBSS (Hank's Balanced Salt Solution) as a positive control for 24 hrs at 37°C with 5% CO_2. Following this treatment, MDC stain (50 μM in PBS) was added for 30 min. After two PBS washes, images were captured with an emission and excitation wavelengths of 340-380 nm and a barrier filter set at 430 nm. To quantify the autophagic phenomenon, cells were washed with Hank’s buffer after staining with MDC, and fluorescence was measured using spectrofluorimetric analysis (Ex 340 nm and Em 535 nm). Fluorescence values were normalized based on cell proliferation using the sulforhodamine B (SRB) assay. Three independent experiments were performed for each assay condition.

OD corrected= OD sample- OD blank

Normalised Optical density (OD) = OD corrected value/SRB reading

2.2.1.2.10 Hoechst 33342/propidium iodide double fluorescent staining (Li *et al*., 2021)

Principle: Hoechst stain all cell nuclei blue, while propidium iodide selectively stain dead cell nuclei red. Together, they enable the distinction between live (blue) and dead (red) cells in a population under fluorescence microscopy.

Procedure: Cultured cells were exposed to the selected palmitic acid doses for 24 hrs, followed by a PBS wash and fixation in 4% paraformaldehyde, maintaining 37°C with 5% CO_2. Then, Hoechst (10 μg/mL) was added in the dark for 15 min at 37°C, followed by propidium iodide (10 μg/mL) incubation for further 15 min in the dark. After washing and removing excess dye the cells were observed under fluorescence microscopy using excitation/emission wavelengths specific for Hoechst (350/461) and PI (493/636).

2.2.2 Animal experiments

2.2.2.1 Grouping

Throughout a 4-month, animals were consistently maintained on their respective diets, with unrestricted access to food and water. There were four groups of mice selected at random, each group carrying 12 animals represented as follows;

Table 2.3 Experimental group details

Group	Diet Type	Inoculation
Group 1	Normal chow	None
Group 2	Normal chow + HPO	None
Group 3	Normal chow	CT26 Cells
Group 4	Normal chow + HPO	CT26 Cells

2.2.2.2 Palm oil administration and CT26- pulmonary metastasis induction

Group 1 taken as the normal control, Group 2 received oral gavage of palm oil as the positive control, Group 3 acted as the CT26 metastasis control, and Group 4 received both palm oil oral gavage and CT26 metastasis induction. In groups 2 and 4, 200 μL of palm oil (Ghezzal *et al*., 2020) was administered orally on a daily basis, amounting to a total of 73.6μg of palmitic acid per day over the course of 4 months. After one month of palm oil oral gavage, BALB/c mice in groups 3 and 4 were subjected to intravenous injection with 1×10^5 CT26 tumour cells (in 200 μL PBS via the tail vein) to initiate pulmonary metastases (Chang *et al*., 2004).

At the end of 4 months, animals fasted overnight, oral glucose tolerance test was carried out. The next day, animals were euthanised under CO_2 anaesthesia. The blood was collected; the lung and intestinal tissues were excised and washed in ice-cold saline, a portion was cut immediately and preserved in buffered formalin (8%) for histological analysis, and the remaining tissues were frozen under -80ºC until use.

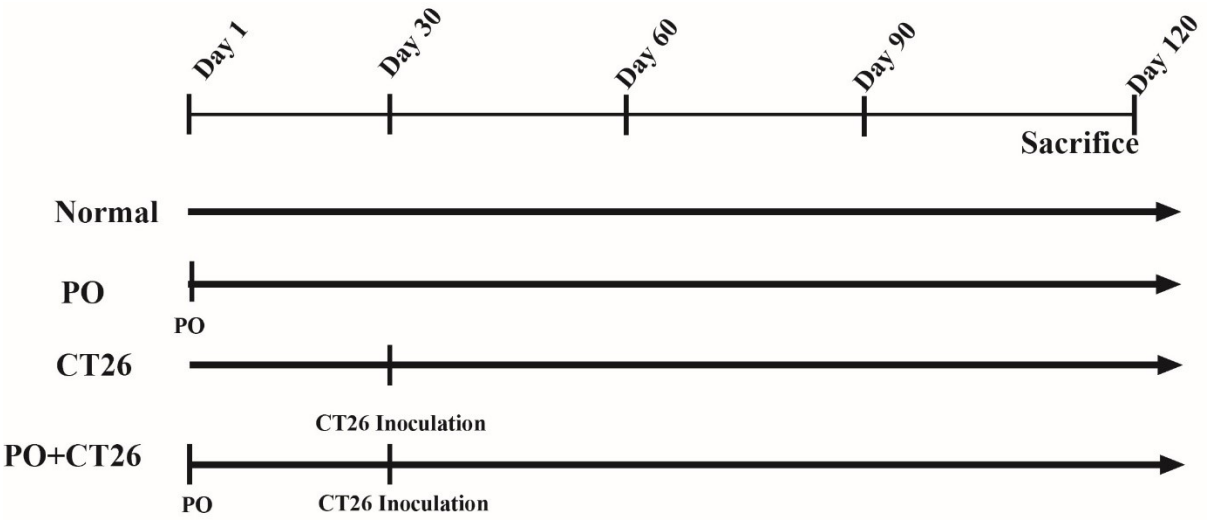

Figure 2.1 HPO administration and CT26 cell inoculation in BALB/c mice.

After 1st month of palm oil administration CT26 cells were inoculated in 4th group animals *via* tail vein for developing pulmonary metastasis.

2.2.2.3 Analysis of body weight, food, and water intake (Yang *et al*., 2014)

Body weight was assessed on a weekly basis for the duration of the four-month study. The mice were weighed for every week at the beginning and end at the same ours. The average body weight was calculated as follows.

$$Average\ body\ weight\ (g) = \frac{Average\ body\ weight\ for\ 16\ weeks\ pergroup}{Total\ number\ of\ anImals\ pergroup}$$

The average food/water intake for each group was calculated weekly by recording it twice a week. Average food/water intake each group was calculated weekly by recording biweekly. Weekly values for each group were added to calculate cumulative consumption. Average food/water intake per group was calculated by dividing total intake by study period.

$$\text{Average food/water intake per group (G) at Week (W)} = \frac{\text{Food/water intake biweekly}}{2}$$

Cumulative food intake/water for group (G) over the 16-week period: = Sum of food/water intake at each week

$$\text{Overall average food intake per group (G) across the 16 weeks} = \frac{\text{Cumulative food/water intake}}{16}$$

2.2.2.4 Blood, serum, tissue sample collection and storage *(Wang et al., 2015a, Sales et al., 2019)*

Following sacrifice, blood samples were collected and fractionated: 1 mL was transferred to an EDTA-coated haematology tube and gently homogenised. The remaining blood, for serum biochemistry, was dispensed into a 2 mL microtube. 0.5 mL of supernatant was collected from the serum by centrifugation at 4000 rpm for 20 min. Blood and serum were analysed for haematological and biochemical factors (detailed in the biochemistry section). After excising and washing the lung and intestinal tissues with ice-cold saline, a section was taken and preserved in 8% buffered formalin for histological examination. The remaining tissues were stored for biochemical and molecular analysis at a temperature of -80ºC.

2.2.2.5 Glucose tolerance test (Rekha *et al*., 2018)

The initial fasting glucose levels of the mice were determined using commercially available strips after they had fasted overnight (One Touch Select, India). Oral glucose concentrations of 1.5 g/kg were supplied to the animals, and blood glucose levels were monitored at intervals of 30, 60, 90, and 120 min. The blood glucose level vs time was used to generate the graph, and the area under the curve was computed using Microsoft Office Excel 2010.

2.2.2.6 Analysis of lung and intestine histopathology *(Elbakary et al., 2018, Clarke et al., 2000)*

The lung and intestinal tissue samples were fixed in 8% buffered formalin after a PBS wash. The fixed tissue was dehydrated using an ascending series of alcohol solutions (10-100 per cent). The clearing was done in xylene and impregnated with molten wax. Serial sections of blocks, each with a thickness of 5 μM, were obtained utilising an automated microtome. In order to rehydrate the serial sections, decreasing grades of alcohol were applied to fresh glass slides containing the sections. The tissue sections were stained with Haematoxylin-Eosin (H & E). After re-hydrating, DPX mountant was added. A pathologist affiliated with the Amala Institute of Medical Science assisted in the pathologic examination of the dried slides, which were observed using a Magnus INVI microscope.

2.2.2.7. Collagen specific studies (Pick *et al*., 1989, Cheng *et al*., 2014)

Collagens in lung sections were locally analysed using picrosirius red staining. Tissue sections were stained with Sirius red at a thickness of 3 μm in order to distinguish

collagen fibres using a phase contrast microscope. To prepare the staining solution, Sirius red was dissolved in a saturated solution of picric acid (0.1%). Collagen deposits were yellow to orange when observed under a microscope.

2.2.3 Biochemistry

2.2.3.1. Preparation of cell lysates (Tangjitjaroenkun *et al*., 2012, Duranti *et al*., 2021) After decanting the medium, 2×10^6 cells/ml were washed in 3-5 mL of PBS. Later a brief trypsinisation, the cells were harvested. After five minutes of centrifugation at 200 g, the cell suspensions were rinsed twice with 5 mL of PBS. Discarded the supernatant and resuspended the cell pellet in 1 ml PBS, iced at 4°C. Cells were lysed using four to five freeze-thaw cycles. Lipid peroxidation analysis was performed on 200 μl of the cell-pelleted lysate. The supernatants obtained from centrifuging 800 μl of cell lysate at 10,000 g for 15 min at 4°C were examined for antioxidant activity.

2.2.3.2. Preparation of tissue homogenate (Kaushik and Kaur, 2003)

A 10 per cent (w/v) 5 ml separate tissue homogenate of the lung, intestine, and colon were prepared immediately with ice-cold 50 mM Tris-HCl (pH 7.3). The homogenate was divided into two: 1 ml for lipid peroxidation analysis and 4 ml centrifuged at 1000 g for 10 min at 4°C. In order to get the post-mitochondrial supernatant, the acquired supernatant was subjected to an additional 20 min of centrifugation at 4ºC at 12,000 H g. Biochemical analyses were conducted on the collected homogenate and supernatant.

2.2.3.3. Biochemical assays for total protein and oxidative stress parameters

Several biochemical analyses were conducted on tissue homogenate and cell lysate, including determination of total protein, analysis of enzymatic antioxidants, like catalase (Beers and Sizer, 1952), superoxide dismutase (McCord and Fridovich, 1969), glutathione s transferase (Habig *et al*., 1974) glutathione reductase (Racker, 1955), glutathione peroxidase (Thompson *et al*., 1976, Hafeman *et al*., 1974) and non-enzymatic antioxidant reduced glutathione (Moron *et al*., 1979). A detection of MDA concentration (Ohkawa *et al*., 1979) was also conducted for lipid peroxidation analysis. Lowry (Lowry *et al*., 1951), BCA (Smith *et al*., 1985) , and Biuret methods (Kingsley *et al*., 1972) were used to determine the total protein in lysates and homogenates.

2.2.3.3.1. Total protein measurement by lowry method *(Lowry et al., 1951)*

Principle: Copper sulphate and –CO-NH- bond in a polypeptide chain reacts to form a blue coloured complex in alkaline medium. Tyrosine and tryptophan residues in proteins

reduce phosphomolybdate and phosphotungstate in Folin-Ciocalteau assays, improving detection sensitivity.

Procedure. Initially, 2% sodium carbonate was dissolved in 0.1 N sodium hydroxide to prepare reagent A, while 0.5% copper sulfate ($CuSO_4.5H_2O$) was dissolved in 1% potassium sodium tartrate to prepare reagent B. The final reagent 1 was obtained by combining reagent A and reagent B in a precise ratio of 50:1. For reagent 2, Folin-Ciocalteau was diluted 1:1 in water. Next, 200 μl samples were added to the test tube, followed by 1 ml reagent 1. Solutions were incubated at 37ºC in the dark for 10 min after vigorous vertexing. Then incubated the solutions by adding 100 μl of reagent 2 at 37ºC for 30 min in the dark. With a UV-visible spectrophotometer at 660 nm, the absorbance was determined.

BSA (1 mg/ml) standard, serially diluted to determine absorbances at 0, 10, 20, 30, 40 and 50 μg/ml. The absorbance at 660 nm was then plotted along the Y-axis and the protein concentration was used to figure the standard curve. The standard curve was created using graph software (excel) and calculates the protein concentration in the given sample as following method.

$$Standard\ curve:\ y = ax + b$$

$$Protein\ content(mg/ml) = [\Delta A_{660}) - b] \div [a \times f]$$

ΔA660 is the standard's optical density, calculated by subtracting the blank's OD from the sample's OD. In this context, y is the standard's optical density, x is its concentration, and the standard curve is defined by slope (a) and intercept (b). The dilution factor (f) adjusts concentrations for sample dilutions.

2.2.3.3.2. Total protein measurement by BCA method (Smith *et al*., 1985)

Principle: In an alkaline medium, Cu^{2+} can be reduced to Cu^{+} by proteins. Cu^{+} can form a water-soluble purple complex with a maximum absorption peak at 560 nm when combined with BCA reagent. Protein concentration is directly proportional to the absorbance value.

Procedure: BCA working reagent constitute reagent A and reagent B in 50:1 ratio. To a 98-well plate, 200 μl of BCA Working reagent were added (8:1) for 25 μl of sample and incubated for 30 min at 37°C in the dark. Following a 10 min equilibration at room temperature, optical density at 562 nm was measured using UV-vis spectrophotometry.

BSA standard at 1 mg/ml was serially diluted to 0, 0.2, 0.4, 0.6, 0.8, 1.0 mg/ml and a duplicate reaction was carried out for each gradient. In order to plot a standard curve,

the various concentration of proteins in the serially diluted standard solutions was plotted on the X-axis, and the absorbance at 562 nm was plotted on the Y-axis, using graph software (excel). The formula for finding standard curve and protein concentration as follows;

$$Standard\ curve:\ y = ax + b$$

$$Protein\ content(mg/ml) = [\Delta A_{562}) - b] \div [a \times f]$$

ΔA562, the absolute optical density of the standard, is obtained by subtracting its OD from the blank sample's OD. Here, y represents the standard's absolute OD, x is its concentration, and the standard curve is defined by slope (a) and intercept (b). The dilution factor (f) adjusts concentrations for sample dilutions.

Note: (Reagent A contains 1% BCA-Na_2, 2% $Na_2CO_3 \cdot H2O$, 0.16% Na2 tartrate, 0.4% NaOH, and 0.95% $NaHCO_3$.Reagent B is 4% w/v $CuSO_4 \cdot 5H_2$)

2.2.3.3.3. Determination of total protein by biuret method (Kingsley *et al*., 1972)

Principle: In alkaline solutions, proteins and copper ions react to form a blue-violet complex. In alkaline solutions, proteins form a blue-violet complex with copper ions. The amount of total proteins present in the sample is reflected by the intensity of the formed colour.

Procedure: Test and standard reaction system was prepared by adding 1 mL of Biuret reagent, to10 μL of sample (serum or tissue sample) and 10 μL of protein standard (6 g/dL), respectively. It was thoroughly mixed and incubated at 37ºC for 5 min. The optical density was measured within 60 min at 555 nm. The quantity of protein in the sample was measured as follows:

$$\text{Total protein (g/dl)} = \left(\frac{Absorbance\ of\ the\ test}{Absorbance\ of\ te\ Standard}\right)(Conc.\ of Standard)$$

2.2.3.3.4 Determination of SOD (superoxide dismutase) activity *(McCord and Fridovich, 1969)*

Principle: Superoxide radicals were produced through the interaction of photoactivated riboflavin and oxygen-reduced nitro blue tetrazolium (NBT). SOD, in turn, inhibited the reduction of nitro blue tetrazolium (NBT).

Procedure: To 2550 μl of 67 mM phosphate buffer (pH 7.8), 100 μl tissue or cell lysate sample was introduced. Next, 100 μl of NBT (0.15 mM) and 200 μl of KCN (0.0015%) were added. The initial absorbance at 560 nm was measured after adding 50 μl of riboflavin (0.12 mM) to the above mixture. Under an incandescent lamp all the test tubes were subjected to uniform illumination for 15 min and final absorbance were

taken at 560 nm. The phosphate buffer served as the blank solution, while a 3 ml mixture containing phosphate buffer, NBT, and KCN was utilized as the control solution.

The percentage inhibition was determined by comparing the absorbance changes between the sample and the control. The enzyme activity was measured as 1 unit, which corresponds to the concentration of sample used to remove 50% of the superoxide anion from the solution and is expressed as U/mg protein.

$$\text{Inhibition of SOD (\%)} = \left(\frac{OD\ value of\ \ control - OD\ value\ \ of\ the\ Sample}{OD\ value\ \ of\ the\ control}\right) \times 100$$

$$\text{SOD activity (U/mg Protein)} = \left(\frac{Inhibition of SOD(\%)}{50\%}\right)\left(\frac{1000}{100}\right)\left(\frac{f}{CPr}\right)$$

2.2.3.3.5 Determination of CAT (catalase) activity (Beers and Sizer, 1952)

Principle: Detection of catalase activity involves measuring the decrease in H2O2 concentration that occurs when standard H_2O_2 solution is added to the analyte sample.

Procedure: To 2.8 mL of 0.1 M phosphate buffer (pH 7.4), cell lysate or tissue homogenate was added. The reaction was initiated by adding 0.3% H_2O_2 solution. A decline in absorbance at 240 nm was observed at 30 sec intervals over a 3 min period. Finally, the molar extinction coefficient of hydrogen peroxide (43.6 mM 1 cm-1) was used to calculate catalase activity. Specific activity was quantified as hydrogen peroxide consumption per gram of protein per minute at 25°C.

$$\text{Specific activity of catalyse} = \left(\frac{\left(\frac{\Delta Ab}{min}\right)1000}{(mg\ protein)43.6}\right)$$

$$\text{Unit activity of catalase} = \left(\frac{\left(\frac{\Delta Ab}{min}\right)[V1]1000}{(43.6\times1\times V2)(mg\ protein\ in\ the\ sample)}\right)$$

The change in absorbance (ΔAb) is determined by subtracting the initial optical density (OD Initial) from the final optical density (OD Final). The molar extinction coefficient for 30 mM H_2O_2 at 240 nm in a 1 cm quartz cuvette is 43.6 L/(mmol·cm). The reaction time is 't' (2 min) with optical path length 1 cm. V1 represents the sample volume in definition, and V2 is the sample volume added to the reaction. The dilution factor of the sample before the test is calculated as df = V1/V2. The result is expressed in mg/ml protein.

2.2.3.3.6 Estimation of GSH (reduced glutathione) content *(Moron et al., 1979)*

Principle: The yellow-coloured complex formed during the interaction between DTNB and GSH showed a maximum absorption at 412 nm.

Procedure: To 50 μL of 25% TCA (final concentration of 5% or less), 200 μL of tissue supernatant was added and kept at 25ºC for 5 min. Following, centrifugation for 10 min at 3000 g, 100 μl of supernatant was introduced to 900 μl of 0.2 M sodium phosphate buffer (pH 8.0). Subsequently, the mixture received the addition of 2.0 mL of DTNB (0.6 mM) and underwent a 20-min incubation period, followed by measuring the absorbance at 412 nm. The GSH content was represented as nmol/mg protein by calculating from the standard curve for reduced glutathione using its slope.

The working solution (1 mM) was prepared from a stock standard of 10 nM GSH. The recommended concentrations were 0.10,20,30,40,50 and 60 μM. The standard curve was generated in Microsoft Excel by plotting GSH concentration on the X-axis against absorbance at 412 nm on the Y-axis. The protein content in the sample was then calculated using the relevant formula.

$$Standard\ curve: \ y = ax + b$$

$$\text{GSH content (concentration/mg protein)} = \left(\frac{\frac{(\Delta A_{412}) - b}{a \times f}}{CPr} \right)$$

For the standard, the absolute OD measurement (y) is linked to the concentration measurement (x) by using a standard curve with slope (a) and intercept (b). The dilution factor is denoted as (f). The calculation of ΔA412 involves determining the difference between the optical density of the sample and the blank. CPr represents the concentration of the protein.

2.2.3.3.7 Determination of GST (Habig *et al*., 1974, Simons and Vander Jagt, 1977)

Principle: The GST catalyses the binding of reduced glutathione (GSH) to dinitrobenzene (CDNB), resulting in an absorption peak of 340 nm. GSH-ST activity can be calculated by measuring the increasing rate of absorbance at 340 nm.

$$\text{G-SH+CDNB} \xrightarrow{\text{GST}} \text{G-SDNB conjugate + HCl}$$

Procedure: The 10 ml reaction cocktail consists of 9.8 ml PBS, 0.1 ml CDNB (100 nM), 0.1 ml GSH (100 mM). PBS was used as a blank and the reaction cocktail was the control. To a 3 ml quartz cuvette 2.95 μl of reaction cocktail was added. Later, 50 μL of the sample was introduced into the cuvette, and the rise in absorbance was observed at 340 nm over a 5-min duration with 2 min intervals. The activity of GST was quantified by taking the molar extinction coefficient of 9.6 x10^3 L/mol/cm and expressed in nanomoles per milligram of protein consumed each minute.

$$\text{Enzyme activity (U/mg protein)} = \left(\frac{\frac{\Delta A}{\epsilon \times path\ lenghth}}{t}\right)\left(\frac{\left(\frac{V1}{V2}\right)df}{Cpr}\right) \text{ OR}$$

$$\text{GST activity U/mg protein} = \left(\frac{\frac{\Delta A}{9.6\times 1}}{2}\right)\left(\frac{\left(\frac{3000}{100}\right)df}{CPr}\right)$$

The change in absorbance (ΔA) is calculated as the subtracting the final absorbance and the initial absorbance. The molar extinction coefficient for 100 mM CDNB at 340 nm in a 1 cm quartz cuvette. The reaction time is 't' (2 min) and the optical path length is 1cm. V1 represents the sample volume in the definition (1 ml = 3000 μl), and V2 is the sample volume (100 μl). The dilution factor of the sample is 'df'. The sample protein concentration is expressed as Cpr (mg protein/ml).

2.2.3.3.8 Determination of GR (glutathione reductase) activity *(Racker, 1955, Mavis and Stellwagen, 1968)*

Principle: Quantification of GR activity involves assessing NADPH consumption during the conversion of oxidized glutathione (GSSG) to reduced glutathione (GSH). The catalysed reaction by GR is represented as follows:

$$GSSG + NADPH + H+ \rightarrow 2GSH + NADP+$$

Procedure: In a 3 ml cuvette, 1.5 ml of phosphate buffer (0.1 M) with EDTA (1 mM), 100 μl of glutathione oxidized (30 mM), 350 μl of NADPH (0.8 mM), 300 μl of BSA (1%), and 2.9 ml of deionized water were added. To initiate the reaction the enzyme was added and absorbance reduction at 340 nm was monitored over a 5 min duration with 2 min intervals. The calculation of GR activity utilized a molar extinction coefficient of 6.22 mm^-1cm^-1, and the results were reported in terms of nanomoles of NADPH consumed per minute per milligram of protein. As a blank solution, phosphate buffer was used. The control solution mixture contains phosphate buffer (0.1M) with EDTA (1 mM), 100 μl of oxidized glutathione or GSSG (30 μl), 350 μl of NADPH (0.8 ml), 400 μl of BSA (1%), and 2.9 ml of deionized water, giving a total volume of 2.9 ml.

$$\text{Enzyme activity (U/mg protein)} = \left(\frac{\frac{\Delta A}{\epsilon \times path\ lenghth}}{t}\right)\left(\frac{\left(\frac{V1}{V2}\right)df}{Cpr}\right) \text{ OR}$$

$$\textit{GR activity (U/mg protein)} = \left(\frac{\frac{\Delta A}{6.22\times 1}}{2}\right)\left(\frac{\left(\frac{3000}{100}\right)df}{CPr}\right)$$

The change in absorbance (ΔA) is calculated as the difference between the initial optical density (OD initial) and the final optical density (OD final). The molar extinction coefficient for 1 mM NADPH at 340 nm in a 1 cm quartz cuvette is 6.22 L/(mmol·cm).

The optical path length is 1 cm. The reaction time is 't' (2 min). V1 represents the sample volume in definition (1 ml = 3000 μl), and V2 is the sample volume added to the reaction (0.100 μl). The dilution factor of the sample before the test is denoted as 'df'. The protein concentration in the sample is expressed as Cpr (mg protein/ml).

2.2.3.3.9 Glutathione peroxidase (GPx) activity assay (Thompson *et al*., 1976, Hafeman *et al*., 1974)

Principle: With GSH, GPx catalyses the reduction of hydrogen peroxide (H_2O_2), and the quantification of the remaining GSH is accomplished using DTNB (dithiol-2-nitrobenzoic acid).

Reaction: H2O2+2GSH→GSSG+2H2OH2O2+2GSH→GSSG+2H2O

Procedure: The assay reaction mixture was prepared by adding 100 μM, 0.1 M phosphate buffer (pH 7.0),100 μM (5 mM) glutathione (GSH), 100 μM 25 mM sodium azide, 100 μM tissue homogenate/cell lysate, and 100 μM 1.2 mM hydrogen peroxide. After a 6 min incubation at 37°C, 2.0 mL of 1.67% meta-phosphoric acid was introduced, and subsequent to a 15 min centrifugation at 2500 rpm, the procedure continued. Following supernatant separation, 2 mL of 0.1 M phosphate buffer with 1 mM DTNB was added, and the mixture was incubated at 37°C for 10 min. A measurement of the optical density at 412 nm was then conducted. A blank sample without tissue was also processed parallel to account for background levels. Enzyme activity, expressed as the decrease in log GSH by 0.001/min, was calculated by subtracting the non-enzymatic reaction's decrease in log GSH per minute. The activity is expressed in U/mg protein.

$$\text{GPx activity (U/mg protein)} = \frac{(Blank\ OD\ \ value - OD\ of\ sample)1000}{mg\ protein \times 10}$$

2.2.3.3.10 Determination of lipid peroxidation by TBARS (Ohkawa *et al*., 1979)

Principle: A pink-coloured complex arises as a result of the reaction between malondialdehyde (MDA), a lipid peroxidation by-product, and the thiobarbituric acid (TBA) reagent, with an absorption maximum at 532 nm.

Procedure: A combined volume of 200 μL tissue homogenate was reacted with 600 μL distilled water, 200 μL sodium lauryl sulfate (8%), and 1.5 mL each of 20% acetic acid (pH 3.5) and Thiobarbituric acid (0.8%). Following incubation at 95°C for 1 hr in a boiling water bath, the samples underwent cooling and subsequent centrifugation at 3000 rpm for 10 min. The clarified supernatant was gathered, and its absorbance at 532 nm was measured against a reagent blank to calculate the concentration of lipid peroxidation products.

From a stock standard solution of 238 g/ml, a 10 g/ml working solution was prepared. For plotting standard graphs, the recommended concentrations are 0.10,20,30,40,50,60 μg/ml. The standard curve was generated by plotting MDA concentration on the X-axis and absorbance at 562 nm on the Y-axis using software, specifically excel.

The protein concentration in an unknown sample was calculated using the following formula.

$$Standard\ curve:\ y = ax + b$$

$$\text{TBARS } (\mu moles/g\ protein) = [([\Delta A_{562}) - b] \div [a \times f])/\text{CPr}$$

The absolute OD value of the standard (y) is related to the concentration of the standard (x) through the standard curve, characterised by the slope (a) and intercept (b). The dilution factor is denoted as (f). ΔA562 is calculated as the difference between the sample's OD value and the blank's OD value. Cpr represents the concentration of protein in the sample.

2.2.3.4 Analysis of haematological parameters

The blood samples collected underwent haematological analysis the same day following the sacrifice. The samples were kept in EDTA-coated vials and proper mixing was ensured by shaking. The analysis was performed in fully automated analyser, BC-20 (Mindray). Analysis included RBC, WBC, Hb, HCT, MCH, MCHC, MCV, LYM, PLT, RDW, and haemoglobin level.

RBC/ WBC count: The analyser measures the electrical resistance as red blood cells pass through a sensor zone for examination using impedance-based technology. IT was detected by using the equation

$$RBC = N \times 10^{12}/L:$$

$$WBC = N \times 10^{9}/L;$$

(Note: N is the number of red blood cells per litre of blood)

Absolute count: Multiplying the overall white blood cell count by the proportion of that cell type yields the absolute count for each specific kind of white blood cell.

$$Absolute\ count = Total\ WBC\ coun\ t\left(\frac{\%\ Specific\ \ cell\ type}{100}\right)$$

Determination of Hb: The colour shift that occurs when haemoglobin reacts with a reagent is often measured by spectrophotometry at 525 nm.It was measured as

Hb = x g/dL (where x is the haemoglobin concentration).

Haematocrit (HCT) %: The volume of red blood cells can be determined by the automated analysers as a proportion of the overall volume of blood and it represented as

$$HCT=x\%$$

MCH (Mean corpuscular haemoglobin): MCH is derived by dividing the quantity of red blood cells by the total haemoglobin and expressed in pg.

MCH = Hb/RBC (where Hb is haemoglobin and RBC is red blood cell count)

Mean corpuscular haemoglobin concentration (MCHC): It is the mean haemoglobin concentration in red blood cells and was computed using the formula provided.

$$MCHC = \left(\frac{Hb}{HCT\%}\right)100$$

MCV (Mean corpuscular volume): It is the mean volume or size of a single red blood cell expressed in femtoliters (fL).

$$MCV=\left(\frac{HCT}{RBC}\right)10$$

2.2.3.5 Analysis of serum biochemistry

The serum biochemistry test evaluated crucial metabolic and organ function parameters, encompassing glucose (mg/dL) for blood sugar levels, urea (mg/dL) for kidney function, total protein (g/L) indicating overall protein status, cholesterol (mg/dL) as a key cardiovascular marker, triglycerides (mg/dL) for lipid metabolism, and enzyme activities such as aspartate aminotransferase (AST), alanine aminotransferase (ALT), and alkaline phosphatase (ALP) in IU/L, reflecting liver and bone health. Additionally, ureic nitrogen (mg/dL), creatine kinase (CK) in IU/L, lactate dehydrogenase (LDH) in IU/L, creatinine (mg/dL), and bilirubin (mg/dL) were analysed to provide insights into kidney function, muscle health, tissue damage, and liver-bile duct health, respectively.

2.2.3.5.1 Estimation of serum lipid profile

2.2.3.5.1.1 Detection of serum total cholesterol

Principle: Cholesterase (CHE) hydrolyses cholesterol esters in the bloodstream, releasing free cholesterol and fatty acids. In the presence of cholesterol oxidase, free cholesterol is oxidised, yielding hydrogen peroxide and cholest-4-en-3-one (H_2O_2). A red chromophore is produced when hydrogen peroxide reacts with 4-amino antipyrine (4-AP) and phenol in the presence of peroxidase (POD). This colorimetric transformation means cholesterol metabolism enzyme activities can be measured.

Reactions:

1. Cholesterol ester + H_2O → free cholesterol + fatty acid
2. Cholesterol + O_2 → cholest-4-en-3-one + H_2O_2
3. H_2O_2 + phenol + 4AP → quinonimine + $4H_2O$

Procedure: In a 90 mmol/L PIPES buffer (pH 6.9), unhemolysed serum was combined with a 1 mL reaction mixture containing phenol (26 mmol/L), cholesterol esterase (1000 U/L), cholesterol oxidase (300 U/L), and 4-aminophenazone (0.4 mmol/L). After thorough mixing, incubation was performed at 37°C for 5 min, followed by a reagent blank measurement at 505 nm.

$$Cholesterol\ concentration\ (mg/dl) = \left(\frac{Sample\ Absorbance}{Blank\ Absorbance}\right) Concentration\ standard$$

2.2.3.5.1.2 Analysis of serum triglycerides

Principle: When incubated with lipoprotein lipase (LPL), Triglycerides in the sample undergo hydrolysis to liberate glycerol and free fatty acids. Glycerol kinase and ATP are responsible for converting glycerol into glycerol-3-phosphate (G3P) and adenosine-5-diphosphate (ADP). Glycerol phosphate dehydrogenase (GPO) catalyses the further conversion of glycerol-3-phosphate (G3P) to dihydroxyacetone phosphate (DAP) and hydrogen peroxide (H_2O_2). A red dye is produced when the hydrogen peroxide combines with 4-aminophenazone (4-AP) and p-chlorophenol in the presence of peroxidase (POD).

Reactions:

1. Triglycerides + H_2O → glycerol + fatty acid
2. Glycerol + ATP → glycerol 3 phosphate + ADP
3. G3P + O_2 → DAP + H_2O_2
4. H_2O_2 + p-chlorophenol + 4AP → quinone + H_2O

Procedure: One millilitre of a reagent comprising lipoprotein lipase (150,000 U/L), p-chlorophenol (2 mmol/L), glycerol kinase (500 U/L), glycerol 3-oxidase (3500 U/L), ATP (0.1 mmol/L), and 4-aminophenazone (0.1 mmol/L) was mixed with a 10 μl aliquot of un-hemolyzed blood sample. The solution was mixed exhaustively, incubated at 37°C for 5 min and subsequently analysed at 505 nm against a reagent blank.

$$Triglycerides\ (mg/dl) = \left(\frac{Sample\ Absorbance}{Blank\ Absorbance}\right) Concentration\ standard$$

2.2.3.5.1.3 Detection of serum HDL (high-density lipoprotein)

Principle: A detergent that solubilises HDL, particularly, is utilized to isolate HDL-c. Colour production results from the interaction between HDL-c and cholesterol esterase, cholesterol oxidase, and chromogens. The reaction of non-HDL lipoproteins, including

chylomicrons, VLDL, and LDL, is impeded due to detergent absorption into their surfaces.

Procedure: From a serum sample, 10 μL was added to 450 μL of reagent 1 containing DSB mT (1 mM) and cholesterol oxidase (1000 U/L) in GOOD buffer (pH 7). The mixture was incubated for 5 min at 37°C. Subsequently, 150 μL of reagent 2, consisting of cholesterol esterase (1500 U/L), detergent (2%), ascorbic oxidase (3000 U/L), peroxidase (1300 U/L), and 4-aminoantipyrine (1 mM) in GOOD buffer (pH 7), was added. After thorough mixing, the solution was incubated at 37°C for 5 min and then measured against a reagent blank at 650 nm.

$$HDL\ Cholesterol\ (mg/dl) = \left(\frac{Sample\ Absorbance}{Blank\ Absorbance}\right) Concentration\ standard$$

2.2.3.5.1.4 Detection of serum LDL (low-density lipoprotein)

The Friedewald formula is a widely used equation for estimating low-density lipoprotein cholesterol (LDL-C) levels in the blood. It was introduced in 1972 by William T. Friedewald, Robert I. Levy, and Donald S. Fredrickson. The formula is as follows:

$$LDL\ cholesterol = \left(Total\ cholesterol - HDL\ Cholesterol - \left(\frac{Triglycerides}{5}\right)\right)$$

2.2.3.5.2 Analysis of liver function markers

2.2.3.5.2.1 Aspartate Transaminase (AST) Activity (Reitman and Frankel, 1957)

Principle: AST facilitates the conversion between L-aspartate and α-ketoglutarate, producing oxaloacetate and L-glutamate. The resulting oxaloacetate reacts with 2,4-dinitrophenylhydrazine (2,4-DNPH) colour reagent, forming a brown-coloured complex.

Procedure: Four reaction systems were maintained, including blank, standard, test, and control. In each test tube, 250 μL of buffered aspartate-α-ketoglutarate substrate (pH 7.4) was added. The tubes were then incubated at 37ºC for 60 min. Subsequently, 250 μL of 2,4-DNPH colour reagent was added, followed by the addition of 2.5 mL of NaOH solution (0.4 N). The absorbance was measured at 505 nm.

AST enzyme activity (IU/L)

$$= \left(\frac{Absorbance\ of\ the\ test - Absorbance\ of\ the\ control}{Absorbance\ of\ the\ standred - Absorbance\ of\ the\ Blank}\right)(Concentration\ of\ the\ standred)$$

2.2.3.5.2.2 Alanine transaminase (ALT) activity (Reitman and Frankel, 1957)

Principle: ALT facilitates the synthesis of pyruvate and L-glutamate through the transamination of L-alanine and α-ketoglutarate. Pyruvate reacts with 2,4-dinitrophenylhydrazine (2,4-DNPH) colour reagent, resulting in the formation of a brown-coloured complex.

Procedure: Four reaction systems were maintained, comprising blank, standard, test, and control. In each test tube, 250 μL of buffered alanine-α-ketoglutarate substrate (pH 7.4) was added. The tubes were then incubated at 37ºC for 30 min. Subsequently, 250 μL of 2,4-DNPH colour reagent was added, followed by the addition of 2.5 mL of NaOH solution (0.4 N). Absorbance was measured at 505 nm.

ALT enzyme activity (IU/L) =

$$\left(\frac{Absorbance\ of\ the\ test - Absorbance\ of\ the\ control}{Absorbance\ of\ the\ standred - Absorbance\ of\ the\ Blank}\right)(Concentration\ of\ the\ standred)$$

2.2.3.5.2.3 Alkaline phosphatase (ALP) activity (Reitman and Frankel, 1957)

Principle: Within serum, ALP facilitates the conversion of phenyl phosphate into inorganic phosphate and phenol under pH 10.0 conditions. The generated phenol subsequently reacts with 4-amino antipyrine in the presence of the oxidizing agent potassium ferricyanide, resulting in the formation of an orange-red coloured complex.

Procedure: A working solution for the substrate was prepared. Four reaction systems were maintained, including blank, standard, test, and control. To all test tubes, 0.5 mL of the working buffered substrate and 1.5 mL of distilled water were added. Incubation took place at 37ºC for 3 min. Following this, 50 μL of serum and 50 μL of phenol standard were added to the test and standard tubes, respectively. Incubation continued for 15 min at 37ºC. Subsequently, 1 mL of chromogen reagent was added, and absorbance was measured at 510 nm.

ALT enzyme activity (IU/L) = $\left(\frac{Absorbance\ of\ the\ test - Absorbance\ of\ the\ control}{Absorbance\ of\ the\ standred - Absorbance\ of\ the\ Blank}\right)(10 \times 7.1)$

2.2.3.5.3 ELISA

2.2.3.5.3.1 Determination of IL-6

Principle: The process relies on the specific binding of IL-6 to its immobilized antibody on the ELISA plate, followed by the quantification of the bound IL-6 utilizing the ABTS kit.

Procedure: IL-6 level was determined using a PeproTech ELISA kit according to the manufacturer's instructions. Capture antibody (1μg/ml) was applied to each well, and the plate was incubated overnight at room temperature. After four washes with 300 μl of wash buffer, block buffer (1% BSA in PBS) was added for 1 hour at room temperature. Following aspiration and four washes, standard or sample (100 μl) was added to each well, incubated for 2 hrs, and washed four times. Subsequently, detection antibody (0.25 μg/ml) was added for 2 hrs, followed by aspiration and four washes. Avidin HRP conjugate (100 μl) was added, incubated for 30 min, and the plate was washed four times. Finally, ABTS substrate solution (100 μl) was added for colour development, and the resulting colour was measured at 405 nm using an ELISA plate reader.

$$\text{Concentration of IL6 (Pg/ml)} = \left(\frac{Absorbance\ of\ the\ sample}{Slope\ of\ the\ standred\ curve}\right)$$

2.2.3.5.3.2 Determination of TNFα

Principle: The reaction relies on the specific binding of TNFα to its immobilized antibody on the ELISA plate, followed by the quantification of the bound TNF-alpha using the ABTS kit.

Procedure: TNFα was assessed using a PeproTech ELISA kit per the manufacturer's guidelines. Capture antibody (1 μg/ml) was added (100 μl) to each well on an ELISA plate, which was then sealed and left overnight at room temperature. After removing the liquid, the plate was washed four times with 300 μl of wash buffer (0.05% Tween 20 in PBS). Subsequently, 300 μl of block buffer (1% BSA in PBS) was added and incubated for 1 hour at room temperature, followed by four washes.

Each well received 100 μl of standard or hemolysate-free sample, followed by a 2 hr incubation at room temperature. After aspirating and washing the plate four times, 100 μl of detection antibody (0.5 μg/ml) was added to each well and incubated for 2 hrs. The liquid was aspirated, and the plate was washed four times. Avidin HRP conjugate (100 μl) was added per well, incubated for 30 min at room temperature, aspirated, and the plate was washed four times. Finally, 100 μl of ABTS substrate solution was added to each well and incubated at room temperature for colour development. The absorbance at 405 nm was measured using an ELISA plate reader.

2.2.4 Molecular biology

2.2.4.1 Gene expression profiling

To isolate RNA and synthesize cDNA, glass and plasticware were treated with diethylpyrocarbonate (DEPC). RNA isolation (ORIonX total RNA isolation kit, spin

column: Cat No: ODP419), cDNA synthesis (Thermo Fisher Scientific, US) and RT-*q*PCR (ORIonX 2X RT-PCR Smart Mix with SYBR Green) were performed using the kit method

2.2.4.1.1 RNA isolation

The RNA was extracted from IEC6, HCT116, and CT26 cells treated with palmitic acid, as well as from lung and intestinal tissues obtained from BALB/c mice. The isolated RNA was then used for gene expression profiling. The following components are included in the RNA extraction kit (ORIonX total RNA isolation kit, spin column: Cat No: ODP419).

Table 2.4 Components for RNA isolation

SI No.	Component	Quantity
1	Buffer RZ	52 ml
2	Buffer RD	13 ml
3	Buffer RW	15 ml
4	RNase free ddH2O	10 ml
5	RNase free Spin column CR3	50 nos
6	Collection Tube (2ml)	50 nos
7	Handbook	1

2.2.4.1.1.1 Homogenization/lysate preparation and phase separation

2.2.4.1.1.1.1 Tissue homogenization

Using a power homogeniser, 50 mg of lung tissue was homogenised with 1 ml of buffer RZ. The homogenate was incubated at 37°C for five min to completely dissociate the nucleoprotein complex.

2.2.4.1.1.1.2 Cell harvesting and lysate preparation

Cells were grown and treated as appropriate in a cell culture flask. A total of 10 million cells were trypsinized and collected as pellets prior to extraction. The cells were lysed directly by pipetting up and down several times in 1ml buffer RZ. The lysate was incubated at 37^0C for 5 min in order to dissociate the nucleoprotein complex completely.

2.2.4.1.1.2 Phase separation

To 1 ml of RZ buffer with tissue homogenate/ cell lysate, 200 μl of chloroform was added and vortexed for 15 sec as per manufacturer protocol. After a 3 min room temperature incubation, centrifugation at 12,000 rpm (13,400 g) and 40°C yielded an interphase between the upper aqueous phase and the lower yellow phenol-chloroform layer.

2.2.4.1.1.3 Precipitation

The aqueous phase was carefully pipetted in a new 1 ml eppendorf tube, and then half the volume of 96-100% ethanol was added. The contents were mixed thoroughly. Subsequently, the solution was transferred to a spin column within a 2 ml collection tube and centrifuged at 12000 rpm (13,400 g) for 30 seconds at 4°C. Finally, the flow-through was discarded.

2.2.4.1.1.4 Washing and separation and storage of RNA

Added 500 μl RD buffer to CR3, centrifuged at 12,000 rpm (13,400 g) for 30 s at 40°C, discarded flow-through. Added 700 μl RW buffer, centrifuged at 12,000 rpm (13,400 Xg) for 30 s at 40°C, and discarded flow-through. Added 500 μl RW buffer, closed the lid, centrifuged at 12,000 rpm (13,400 Xg) for 30 s at 40°C. Returned RNAase-free CR3 to the collection tube and centrifuged at 12,000 rpm (13,400 Xg) for 2 min at 40°C to dry the spin column membrane. Placed CR3 spin column in a 1.5 ml RNAase-free collection tube, added 30 to 100 μl RNAase-free DDW to the spin column membrane. Incubated at room temperature (15-25°C) for 2 min, then centrifuged at 12,000 rpm (13,400 g) for 2 min. Eluted RNA at 40°C and stored purified RNA at -80°C.

2.2.4.1.1.5 Quantifying and checking the integrity of RNA

RNA integrity was assessed by gel- electrophoresis and quantified using the QuantusTM fluorometer kit method consisting of the following components.

2.2.4.1.1.5.1 Quantifying RNA

Table 2.5 Components for RNA quantification

SI No.	Component	Quantity
1	20X TE buffer (PH 7.4)	25 ml
2	QuantiFluor® RNA Dye	1 ml
3	RNA Standard, (100mg)	1 ml

To 200 μl 1X TE buffer, 0.5 μl QuantiFluor® RNA Dye with 1μl of RNA extracted was added to a 500 μl PCR tube. A QuantusTM Fluorometer was used to measure RNA after vertexing and incubating in the dark for 5 min at room temperature.

2.2.4.1.1.5.2 Detection of RNA integrity

Initially, the electrophoresis setup ensured a leak-free environment, with a carefully placed gel comb for subsequent gel preparation. A 1.2% agarose gel in TAE buffer with 0.5 μg/mL ethidium bromide (1 μL) was made, poured into the tray without trapping air bubbles and allowed to solidify. Next, the electrophoretic tank was filled with 1X

TAE buffer. After removing the comb, 10 samples were added, each with 2μL gel loading dye, and electrophoresis was conducted at 60V. Subsequently, the gel underwent observation under a UV/Vis gel documentation system.

Reagents: To prepare TAE buffer, 48.4 g of tris-base was dissolved in 20 ml of 0.5 M EDTA, 11.42 mL of glacial acetic acid and added nuclease-free double-distilled water to make up to IL. To prepare 1.2% agarose gel 0.9 g of agarose was dissolved in TAE buffer.

2.2.4.1.2 cDNA synthesis

To synthesise cDNA, 1 μg of RNA was used with the Verso first strand cDNA synthesis Kit. The reaction mixture consisted of the following components;

Table 2.6 Components for cDNA synthesis

SI No.	Components	Quantity (μl)
1	5X cDNA synthesis buffer	4
2	dNTP Mix	2
3	Anchored oligo dT	1
4	RT Enhancer	1
5	Verso Enzyme Mix	1
6	Template (RNA)	5
7	Water, nuclease-free	6
	Total	20

In order to synthesize cDNA, a thermal cycler was set at 42°C for 45 min. The enzymes were inactivated by cycling at 65°C for one minute and immediately placed on ice following inactivation.

2.2.4.1.3 Real-time quantitative PCR

Applied Biosystems 7300 qPCR was used to selectively amplify the target genes. ORIonX 2X real time PCR smart mix with SYBR Green contains the following components.

Table 2.7 Components for real-time quantitative PCR

SI No.	Component	Quantity (μl)
1	2X Real-time PCR master mix with SYBR green	10
2	Forward primer	1
3	Reverse primer	1
4	Template DNA	1
5	Nuclease-free water	7
	Total	20

Amplification of the master mix with the above components was performed using an Applied Biosystems 7300 qPCR system at the following temperatures.

Table 2.8 PCR Amplification conditions

Steps	Temperature	Time
Step 1	95^0C	5 min
Step 2	95^0C	30 sec
Step 3	52^0C-63^0C	40 sec
Step 4	Go to step 2 and repeat 39 cycles	
Step 5	72^0C	30 sec
Step 6	72^0C	5 min
Step7	4^0C	10 min

Using the Applied Biosystems real-time PCR software package, the Ct values were measured to determine the fold change in expression (Livak and Schmittgen, 2001). Both *β*-actin (mouse and rat) and GAPDH (human) were taken as the reference gene. Specifically, negative and positive ΔΔCT values separately indicate corresponding down and up-regulation respectively (Yuan *et al.*, 2008). Normalisation: $\Delta CT = CT_{(Gene\ of\ interest)} - CT_{(Housekeeping\ gene)}$. After finding the average of the ΔCT of the control, calculated the ΔΔCT relative to the average of the ΔCT of the control as follows:

$$\Delta\Delta CT = \Delta CT_{(Gene\ of\ interest)} - \Delta CT_{(Control\ average)}.$$

$$\text{Fold gene expression} = 2^{\wedge -(\Delta\Delta CT)}$$

2.2.4.1.4 Primers

Table 2.9 Human primer sequences

Gene	Forwarded primer	Reverse primer	Product size
PERK	5'ATTGCATCTGCCTGGTTAC3'	5'GACTCCTTCCTTTGCCTGT3'	650
ATF4	5'CCAGCAAAGCACCGCAACA3'	5'CCATCCACAGCCAGCCATT3'	215
NRF2	5'AGACAAACATTCAAGCCGCT3'	5'CCATCTCTTGTTTGCTGCAG3'	438
NQO1	5'AAGGATGGAAGAAACGCCTGGAGA3'	5'GGCCCACAGAAAGGCCAAATTTCT3'	156
HO1	5'ACGCGTTGTAATTAAGCCTCGCAC3'	5'TTCCGCTGGTCATTAAGGCTGAGT3'	176
IRE1	5'TGCGGCAACGCGTCCAGTAA3'	5'GCAGCGCCGGTTCATCCAGT3'	110
XBP1	5'CGCTTGGGGATGGATGCCCTG3'	5'CCTGCACCTGCTGCGGACT3'	75(u)/101(s)
BECLIN1	5'CAA GAT CCT GGA CCG TGT CA3'	5TGG CAC TTT CTG TGG ACA TCA	191
LC3B1	5'AAGGCGCTTACAGCTCAATG3'	5'CTGGGAGGCATAGACCATGT3'	145
ATF6	5'CAGGGAGAAGGAACTTGTGA3'	5' ACTGACCGAGGAGACGAGA3'	344
BIP	5'CACAGTGGTGCCTACCAAGA 3'	5'TGTCTTTTGTCAGGGGTCTTT 3'	107
CHOP	5'AAGGCACTGAGCGTATCATGT3'	5'TGAAGATACACTTCCTTCTTGAACA3'	105
GAPDH	5'GACATGCCGCCTGGAGAAAC3'	5'AGCCCAGGATGCCCTTTAGT3'	92

Table 2.10 Mouse primer sequences

Gene	Forwarded primer	Reverse primer	Product Size
Perk	5’TGCGGCAACGCGTCCAGTAA3’	5’GCAGCGCCGGTTCATCCAGT3’	279
Atf4	5’CCTTCGACCAGTCGGGTTTG3’	5CTGTCCCGGAAAAGGCATCC3′	189
Nrf2	5’CTGAACTCCTGGACGGGACTA3’	5’CGGTGGGTCTCCGTAAATGG3’	182
Nqo1	5’AGGATGGGAGGTACTCGAATC3’	5'TGCTAGAGATGACTCGGAAGG3'	127
Ho1	5’GGTGATGGCTTCCTTGTACC3’	5’AGTGAGGCCCATACCAGAAG3’	155
Ire1	5’CTGTGGTCAAGATGGACTGG3’	5’GAAGCGGGAAGTGAAGTAGC3’	209
Xbp1	5’GAACACGCTTGGGAATGGACAC3’	5’AGAAAGGGAGGCTGGTAAGGAAC3’	343(u)/317(s)
Beclin 1	5'ATACTGTTCTGGGGGTTTGCG3'	5'GTCTCTCCTTTTTCCACCTCTTC3'	111
Lc3b1	5'TTATAGAGCGATACAAGGGGGAG3'	5'CGCCGTCTGATTATCTTGATGAG3'	109
Atf6	5'GCCGACTGTGGTTCAACTTC3'	5'TCCTCAGCACAGCGATATCC3'	215
Bip	5'CTGGGTACATTTGATCTGACTGG3'	5'GCATCCTGGTGGCTTTCCAGCCATTC3'	398
Chop	5’CTGGAAGCCTGGTATGAGGA3’	5’AGGTGCTTGTGACCTCTGCT3’	175
ß-Actin	5’CTGCCTGACGGCCAGGT3’	5’TGGATGCCACAGGATTCCAT3’	101

Table 2.11 Rat primer sequences

Gene	Forward primer	Reverse primer	Product size (kb)
Perk	5'AAGATGGTACAGTGGACGGC3'	5'CCGTGTTCCTGGTGAAATCT3'	300
Atf4	5'GCTGCTGTCTTGTTTTGCTCC3'	5'AGGTGTTCCTCGTGGTTCTCG3'	123
Nrf2	5'GCAACTCCAGAAGGAACAGG3'	5'TCTCTGCCAAAAGCTGCATA3'	197
Nqo1	5'ACTCGGAGAACTTTCAGTACC3'	5'TTGGAGCAAAGTAGAGTGGT3'	492
Ho1	5'AGGAGATAGAGCGAAACAAGCAGAAC3'	5'GCTGTGTGGCTGGTGTGTGTAAGG3'	150
Ire1	5'AAGTTTTGGAAGAGCCAGCA3'	5'TGTTCTTGCCTCCAAGTGTG3'	215
Xbp1	5'AAACAGAGTAGCAGCACAGACTGC3'	5'TCCTTCTGGGTAGACCTCTGGGAC3'	454(u)/428(s)
Beclin1	5'AGCACGCCATGTATAGCAAAGA3'	5'GGAAGAGGGAAAGGACAGCAT3'	69
Lc3b1	5'GGTCCAGTTGTGCCTTTATTGA3'	5'GTGTGTGGGTTGTGTACGTCG3'	153
Atf6	5'TGCAGGTGTATTACGCTTCGC3'	5'GCAGGTGATCCCTTCGAAATG3'	98
Bip	5'GCGAGGATTGAATTGAGTCCTTC3'	5'GAGCGGAACAGGTCCATGTTCA3'	97
Chop	5'CCAGCAGGGTCACAAGCAC3'	5'CGCACTGACCACTCTGTTTC3'	127
β-actin	5'AAGTCCCTCACCCTCCCAAAAG3'	5'AAGCAATGCTGTCACCTTCCC3'	105

2.2.5 Statistical analysis

The data analysis was performed using Mean ± SEM (standard error of the mean) with GraphPad Prism 8.3.8 (San Diego, CA, USA). For three independent *in vitro* experiments, we conducted a one-way ANOVA for multiple comparisons, followed by Tukey's post-hoc test. In analysing antioxidant levels, lipid peroxidation, and gene expression profiling across HPO and tissue types one-way and a two-way ANOVA followed by post hoc Tukey's test was applied (n=6). Statistically significant results were denoted by P values of * for < 0.05, ** for < 0.01, and *** for < 0.001

Chapter 3

Analysis of palmitic acid uptake, toxic effects, and lipid accumulation in normal and cancerous gastrointestinal cells

3.1 Introduction

Palmitic acid (PA), holds significant implications in gastrointestinal health. This saturated fatty acid is synthesized *de novo* in the cytoplasm from acetyl-CoA and malonyl-CoA with the help of enzymes such as fatty acid synthase (FASN). Then, it undergoes elongation to generate other fatty acid species (>C16). In addition, the palmitic acid is obtained through the diet, and uptake is carried out *via* the fatty acid translocase (CD36). Palmitic acid serves as a crucial component of cell membranes and plays a significant role in energy production, signal transduction, and gene expression regulation. However, excessive intake of palmitic acid has been linked to adverse effects, including insulin resistance, inflammation, cardiovascular diseases, and cancer. Palmitic acid has gained considerable attention due to its potential adverse effects on human health when consumed in excess (Westheim *et al*., 2023). However, there remains a substantial gap in understanding the specific effects of palmitic acid on gastrointestinal cells, particularly concerning cancer development and progression. Investigating these mechanisms could provide valuable insights into potential preventive or therapeutic strategies for gastrointestinal cancers.

Understanding the uptake of palmitic acid in gastrointestinal cells is crucial for comprehending its potential toxic effects. Previous reports have emphasized the detrimental effects of elevated palmitic acid levels on cellular stress, mitochondrial function, and lipid accumulation (Murru *et al*., 2022). For instance, studies have shown that increased palmitic acid exposure can induce endoplasmic reticulum stress (ER stress) and impair mitochondrial respiration, leading to cellular dysfunction and apoptosis (Zhang *et al*., 2012a). Moreover, palmitic acid overload has been associated with aberrant lipid metabolism, contributing to the progression of gastrointestinal cancers (Zhang *et al*., 2023). Despite these findings, a significant gap exists in understanding the molecular pathways underlying palmitic acid-induced toxicity and lipid metabolism dysregulation. In this chapter, we aim to investigate the complex association between the uptake of palmitic acid, its potential toxic effects, and the resulting lipid accumulation in normal and cancerous gastrointestinal cells. We also aimed to understand how palmitic acid uptake affects lipid metabolism and cellular behaviours.

As cancer cells have diverse mutations in various oncogenic/tumour suppressor genes, there may be a potential for metabolic rerouting compared to their normal counterparts.

Studies have demonstrated that excess palmitic acid uptake impacts both normal and cancer cells. However, cancer cells demonstrate an increased intake of free fatty acids and exhibit dysregulated lipid metabolism, leading to distinct metabolic pathways contributing to their survival mechanism (Young *et al*., 2022). Also, the cancer cells, for instance, exhibit higher levels of neutral lipids and lipid droplets (LD) (Lung *et al*., 2022). This lipid accumulation supports the cancer cell survival by providing additional lipid substrates and energy, which are crucial for meeting the metabolic demands of rapidly proliferating cancer cells and initiating metastatic processes. Moreover, the storage of excess fatty acids and cholesterol in LD helps to mitigate lipo-toxicity and oxidative stress, thereby promoting proliferation, invasion, metastasis, and resistance to chemotherapy in various cancer types (Jin *et al*., 2023, Petan, 2023b, Raeisi *et al*., 2022). Apart from sustaining cancer cell survival by providing lipid substrates and metabolic resources, it contributes to metastatic spread and therapy resistance, facilitated by the interaction between palmitic acid and CD36 (Pascual *et al*., 2017, Jiang *et al*., 2019). This dysregulation is driven by alterations in key signalling pathways, including those involving oncogenes such as PI3K/AKT/mTOR and transcription factors like SREBPs are reported (Wagner *et al*., 2017, Rizzo *et al*., 2021).

Based on existing literature and significant advancements, the study hypothesizes that in response to palmitic acid overload, cancerous cells will exhibit adaptive metabolic rerouting to support cell survival. Additionally, we anticipate comparing resistance to palmitic acid cytotoxicity in cancer cells to normal intestinal cells. To test these hypotheses, we conducted cell viability assays using normal and gastric cancer cells in response to palmitic acid. Colony formation assays were carried out to evaluate proliferation rates, while Oil Red O staining was employed to quantify lipid accumulation.

3.2 Materials and methods

3.2.1 Preparation of palmitic acid stock solution and treatment

Palmitic acid stock solution was prepared as described in Chapter 2, Materials and methods, Section 2.2.1.1. 5. Briefly, IEC6 (normal rat intestinal cells), HCT116 (human colon cancer cells) and CT26 (murine metastatic colon cancer cells) were exposed to different concentrations of palmitic acid. The highest vehicle control (ethanol) concentration volume did not exceed 0.02%.

3.2.2 MTT assay

To assess cytotoxicity, MTT assay was conducted with IEC6, HCT116, and CT26 cells, following the procedure outlined in Chapter 2, Materials and methods section 2.2.1.2.1.

3.2.3 Trypan blue exclusion analysis

Trypan blue exclusion cell viability assay was conducted with IEC6, HCT116, and CT26 cells, following the methodology outlined in Chapter 2, Materials and methods section 2.2.1.2.4.

3.2.4 Morphological assessment

The morphology of palmitic acid-treated normal and colon cancer cells was analysed by phase-contrast microscope.

3.2.5 Neutral lipid accumulation

Palmitic acid uptake and neutral lipid accumulation in cells were analysed using phase-contrast microscopy. The quantity of the lipid accumulation was measured in a spectrophotometer by staining with Oil Red O as the procedure outlined in Chapter 2, Materials and methods, Section 2.2.1.2.3.

3.2.6 Cell death

Cell death was determined by propidium iodide and Hoechst (PI/H) double staining, and images were captured with a fluorescent microscope, following the procedures outlined in Chapter 2, Materials and methods, Section 2.2.1.2.10

3.2.7 Colony formation assay

The colony forming ability of palmitic acid-treated cells was evaluated post-treatment. Subsequently, the plating efficiency and surviving fractions associated with developed colonies were also determined, as the protocols outlined in Chapter 2, Materials and methods, Section 2.2.1.2.5. Images were captured using a phase-contrast microscope.

3.2.8 Statistical analysis

The data were presented as mean ± standard deviation (SD) from triplicate measurements. Statistical analysis was conducted using GraphPad Prism software version 9. Significance was determined using one-way ANOVA followed by Tukey's post hoc test. A *p-value of *<0.05, **<0.01, and ***<0.001* was considered statistically significant.

3.3 Results

3.3.1 Effect of palmitic acid on cell viability

In MTT assay, the growth of IEC6 normal cells was inhibited to 16 ±1.2%, 31 ±1.9%, 43 ± 3.2%, and 56 ± 3.7% at 100, 200, 300, and 400 μM concentrations, respectively. The IC_{50} value was calculated at 342 μM (Fig. 3.1 A). Similarly, in the trypan blue exclusion assay, the viability of IEC6 cells found declined to 79.6 ± 6.72%, 68.7 ± 8.4%, 57.8 ± 9.01%, and 47.2 ± 8.7% at the same concentrations relative to the untreated control or vehicle (Fig. 3.1 B).

For HCT116 colon cancer cells, the MTT assay revealed growth inhibition by 19 ± 2.3%, 34 ± 2.1%, 55 ± 3.3%, and 49 ± 3.1% at 50, 100, 150, and 200 μM concentrations, respectively, and the IC_{50} calculated is 180 μM (Fig. 3.1 C). In the trypan blue exclusion assay, the viability of HCT116 cells decreased to 90.94 ± 3.17% at 50 μM, 79.10 ± 4.54% at 100 μM, 63.35 ± 4.78% at 150 μM, and 44.91 ± 3.32% at 200 μM (Fig. 3.1 D).

Similarly, for CT26 murine metastatic colon cancer cells, the MTT assay showed growth inhibition by 15 ± 0.9%, 31 ± 1.7%, 49 ± 1.1%, and 60± 2.3% at 50, 100, 150, and 200 μM concentrations, respectively, with an IC_{50} value of 168 μM (Fig. 3.1 E). In the trypan blue exclusion assay, CT26 cell viability was reduced to 82.61 ± 2.3% at 50 μM, 66.61 ± 7.1% at 100 μM, 57.20 ± 6.67% at 150 μM, and 43.25 ± 5.66% at 200 μM (Fig. 3.1 F).

Based on these cell viability assays, the sublethal doses of palmitic acid were determined to be 100 and 200 μM in IEC6 cells and 50 and 100 μM for HCT116 and CT26 cancer cells. Doses exceeding the IC_{50} values were considered toxic concentrations.

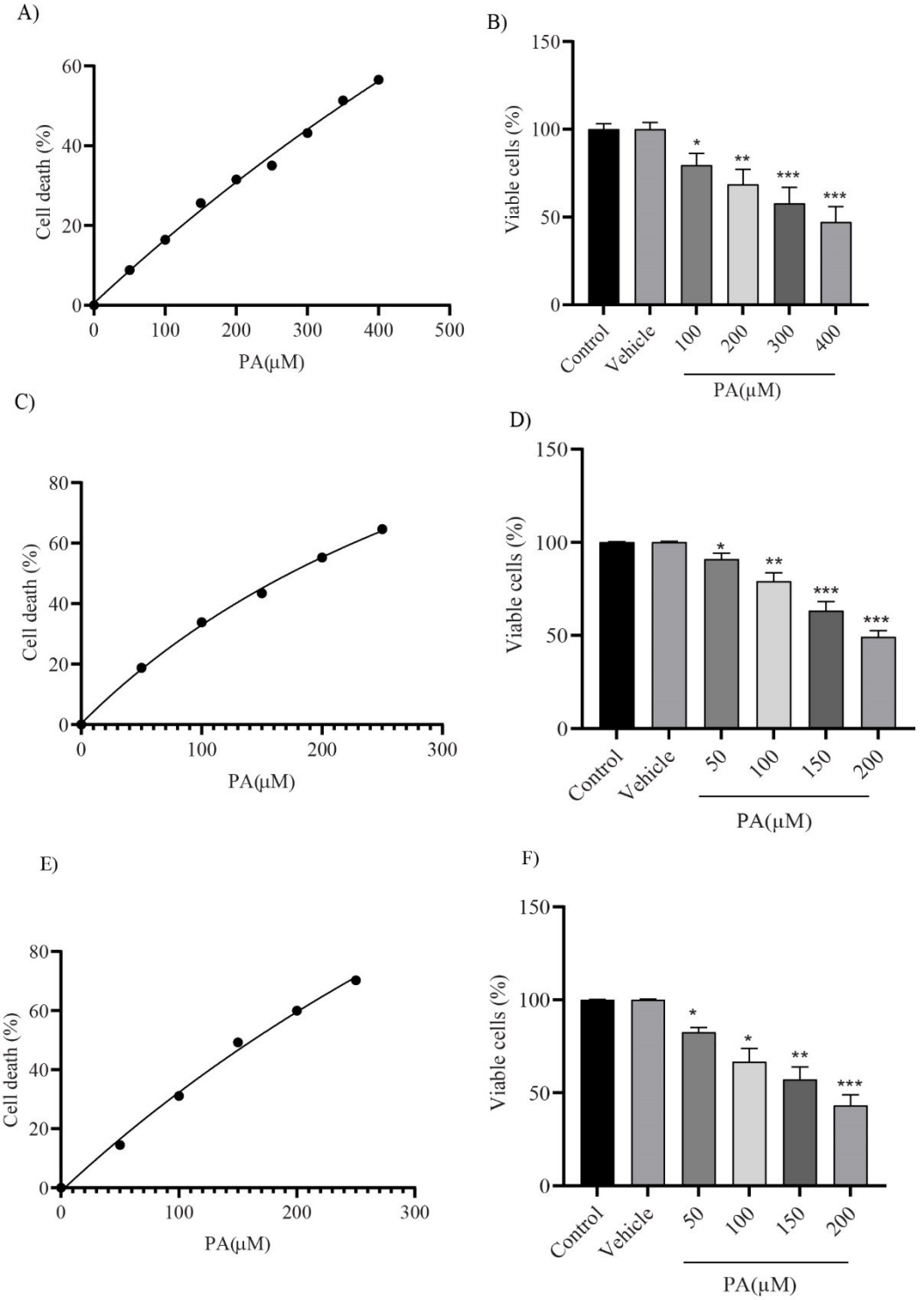

Figure 3.1 Effects of palmitic acid on IEC6, HCT116, and CT26 cells. Cells were treated with various concentrations of palmitic acid for 24 hrs. Cytotoxicity was assessed using the MTT assay (A: IEC6, C: HCT116, E: CT26), and cell viability was evaluated using the Trypan blue exclusion assay (B: IEC6, D: HCT116, F: CT26). Data represent the percentage of cell death or viability relative to untreated controls. Error bars indicate standard deviation from triplicate experiments. Statistical analysis: $*p < 0.05$, $**p < 0.01$, $***p < 0.001$ (one-way ANOVA).

3.3.2 Morphological alterations

The morphology of the cells was assessed after 24 hrs of treatment. IEC6 and HCT116 cells exhibited typical epithelial morphology characterized by tight cell-cell contacts in their untreated state. When exposed to sub-lethal doses of palmitic acid, the cells were observed to be less tightly packed, and the effect became more pronounced as the doses approached toxic concentrations. In addition, these cells displayed elongated cell extrusions and weakened cell-cell contacts (Fig. 3.2 & 3.3). In contrast, CT26 cells consistently exhibited a fibroblast-like morphology characterized by loose intercellular connections under all treatment conditions. Upon exposure to high palmitic acid, these cells transitioned to a fully rounded phenotype. Remarkably, they could sustain this rounded state for an extended period before eventual detachment from the substratum (Fig. 3.4). Notably, when the cells are treated with palmitic acid, they exhibited increased extracellular secretion onto the substratum. This secretion intensified as the concentration of palmitic acid increased. The findings suggest that palmitic acid alters cellular morphology at higher concentrations. This morphological change aligns with the cytotoxic effects observed in previous assessments, further emphasizing the impact of palmitic acid on the studied cell lines.

The cells were also stained with Hoechst 33342 and propidium iodide (PI). Normally, the cells exhibited Hoechst-positive nuclei characterized by uniform and faint blue fluorescence, but the cells emitting red fluorescence indicate the dead cells. However, more cells displayed red fluorescence at 300-400 μM concentrations in IEC6 cells and 150-200 μM in HCT116 and CT26 cells (Fig. 3.5, 3.6 & 3.7). This increase in red fluorescent cells was observed in higher doses, suggesting that palmitic acid leads to increased cell death.

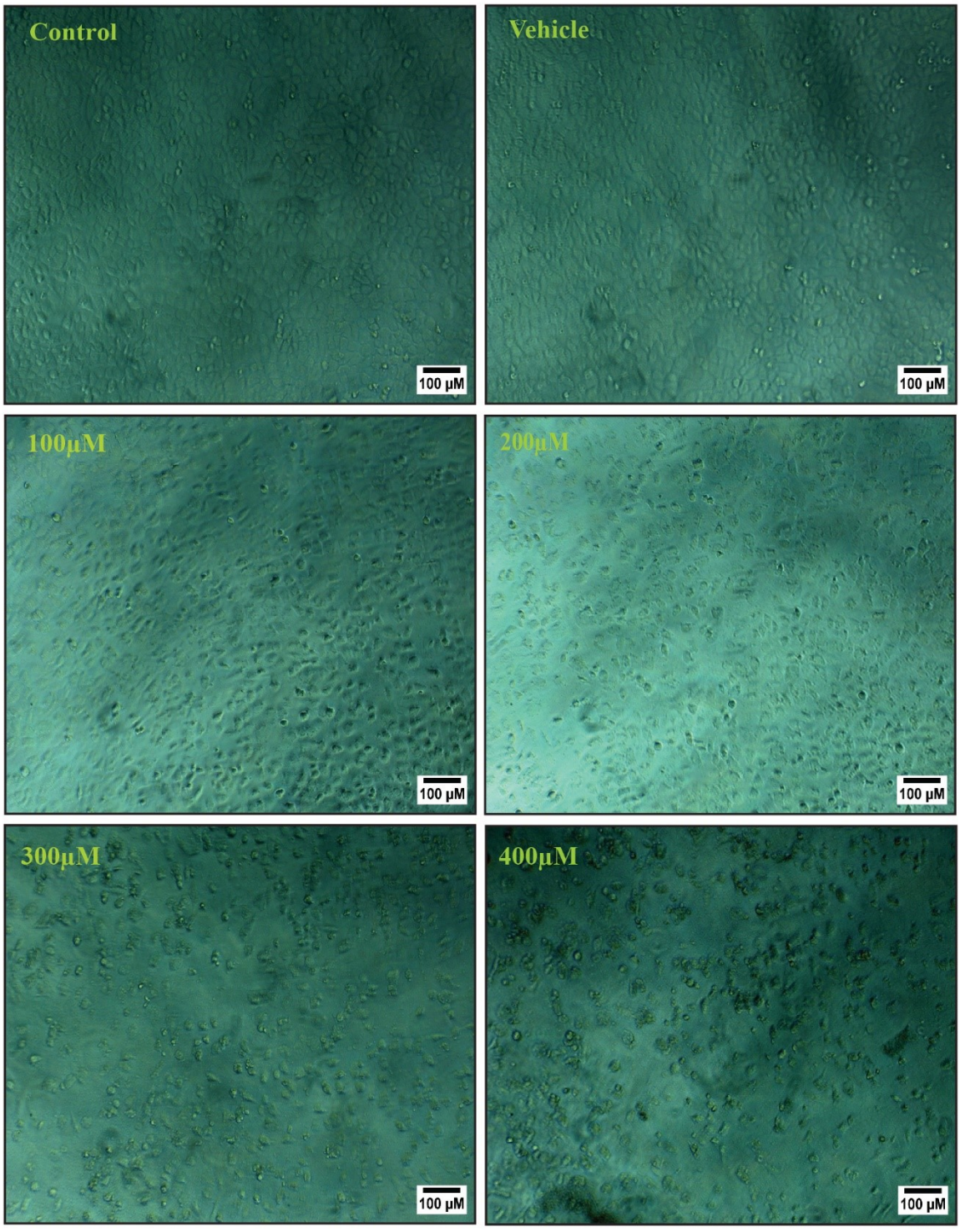

Figure 3.2 Morphology of IEC6 cells. Microscopic images of control, vehicle-treated, and IEC6 cells exposed to 100–400 μM of PA. Scale bar: 100 μm; magnification: 100 X.

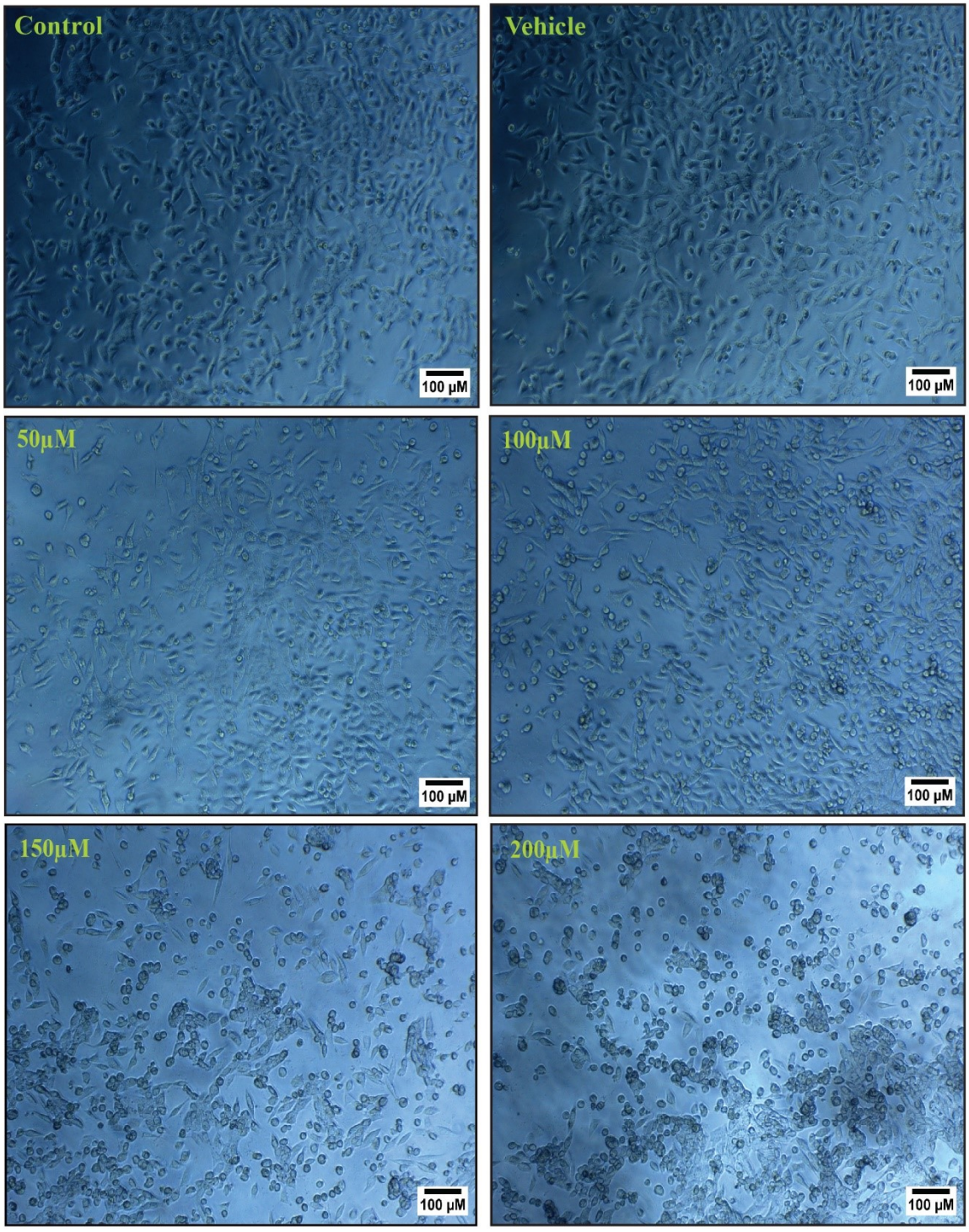

Figure 3.3 Morphology of HCT116 Cells. Microscopic images depict control, vehicle-treated, and HCT116 cells treated with 150–100 μM of PA. Images were captured at 100X magnification with a 100 μm scale bar.

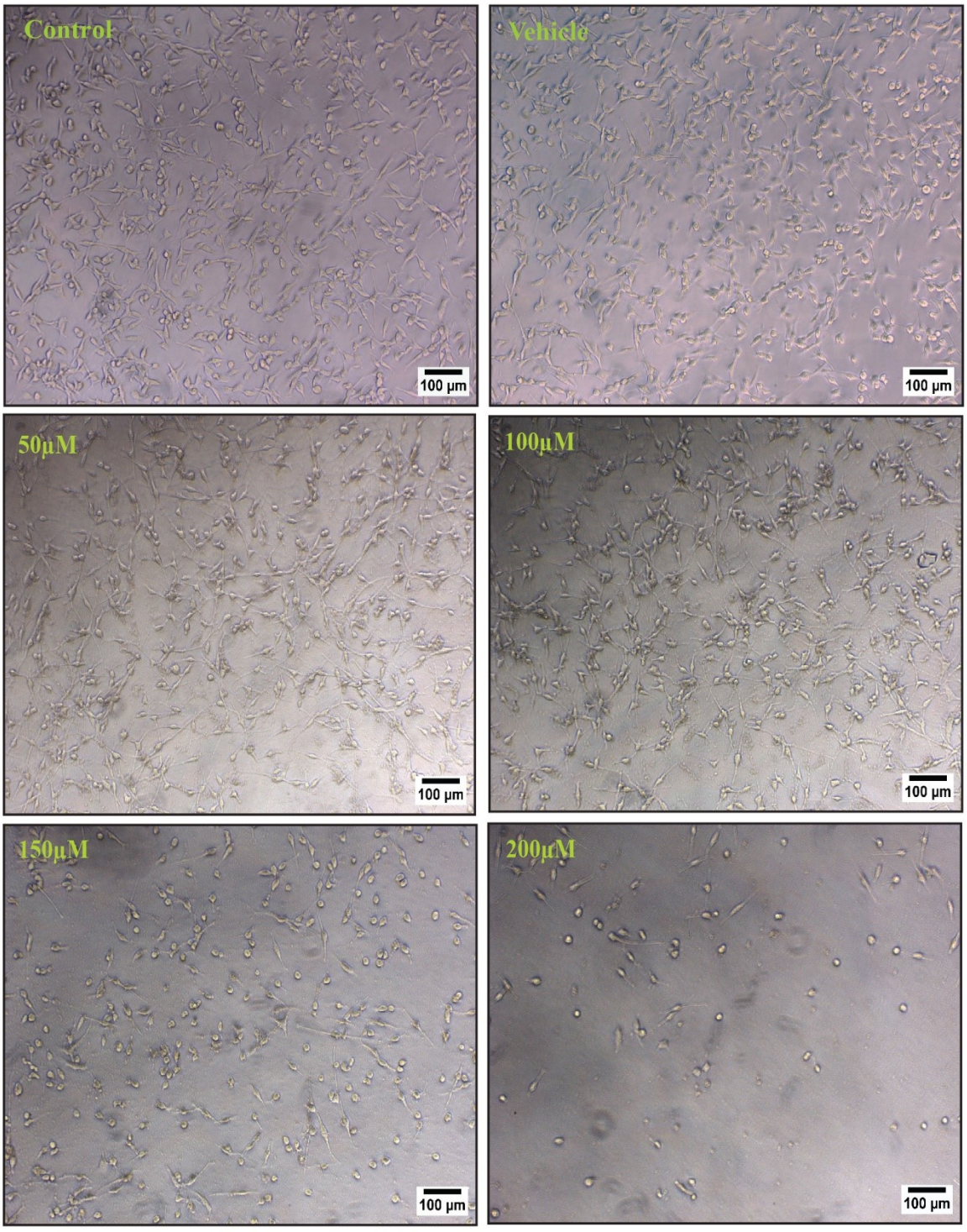

Figure 3.4 Morphology of CT26 Cells. Control, vehicle-treated, and CT26 cells treated with 150–100 μM of PA. Magnification: 100 X; scale bar: 100 μm.

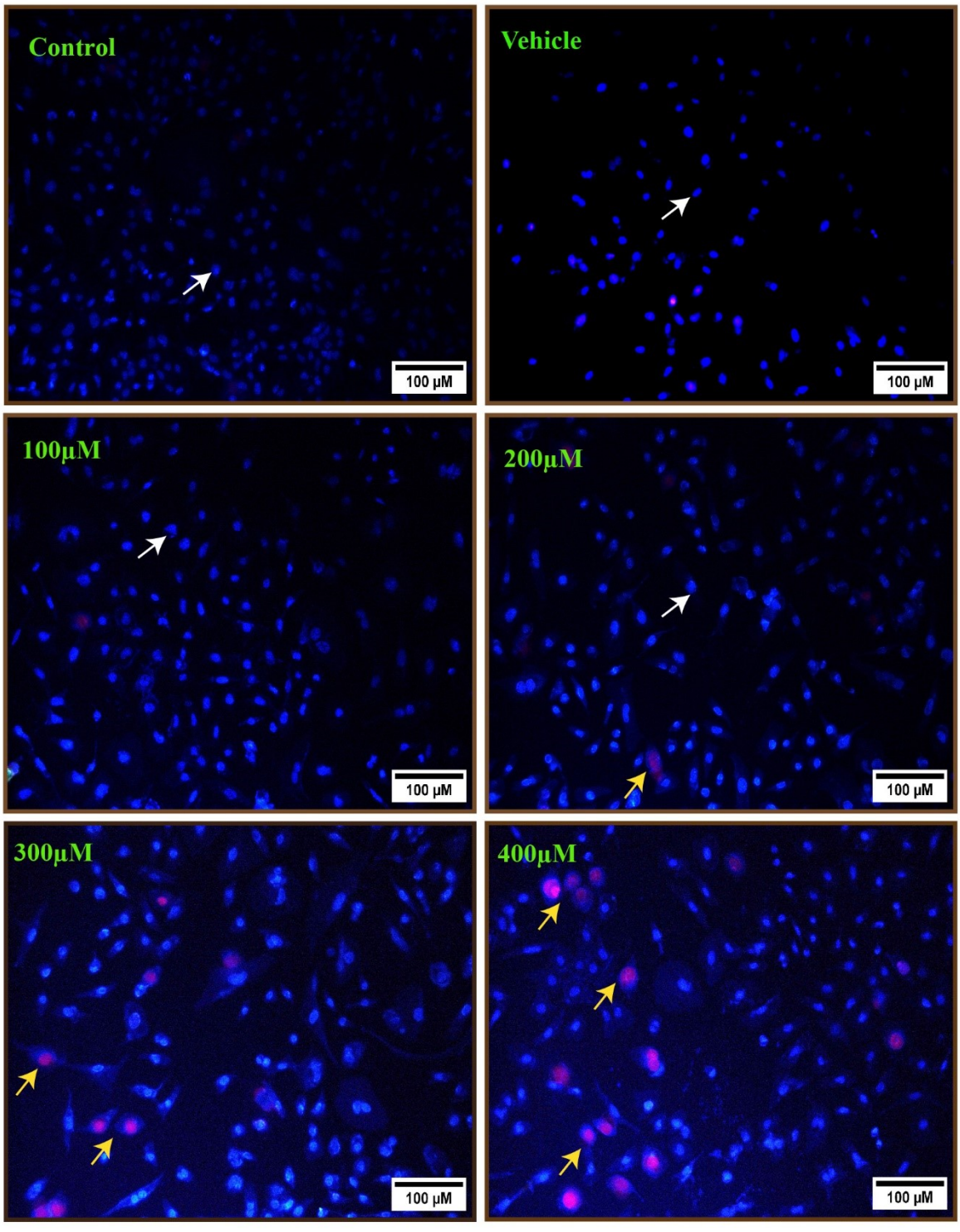

Figure 3.5 Microscopic images of IEC6 cells stained with PI and Hoechst in control vehicle and PA-treated groups (100, 200, 300 and 400 μm). Images were captured at 400 X magnification with a 100 μm scale bar. The white arrow indicates live cells, and the yellow arrow indicate dead cells

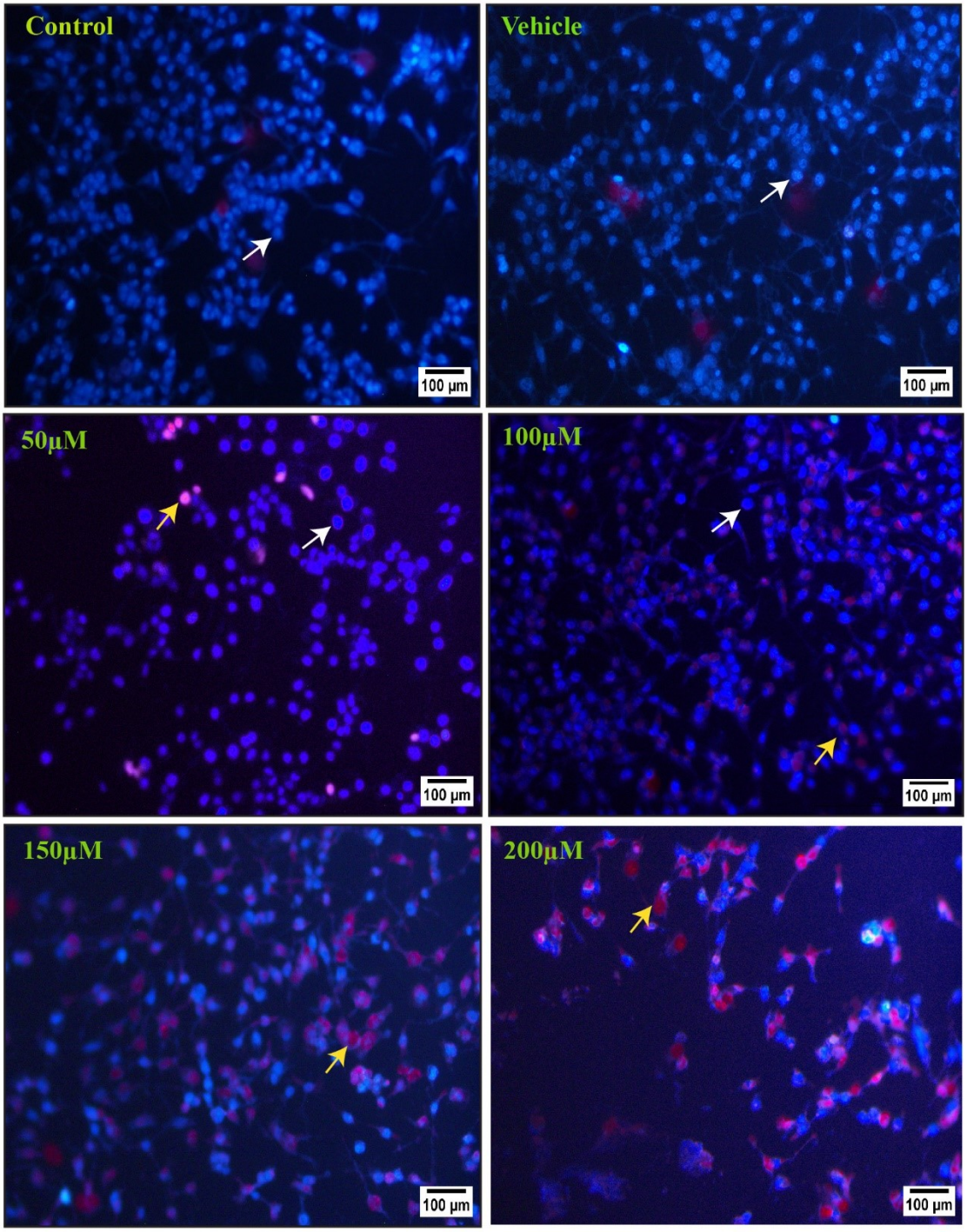

Figure 3.6 Microscopic images of HCT116 cells stained with PI and Hoechst in control vehicle and PA-treated groups (50,100,150 and 200 μm). Images were captured at 400X magnification with a 200 μm scale bar. The white arrow indicates live cells, and the yellow arrow indicates dead cell

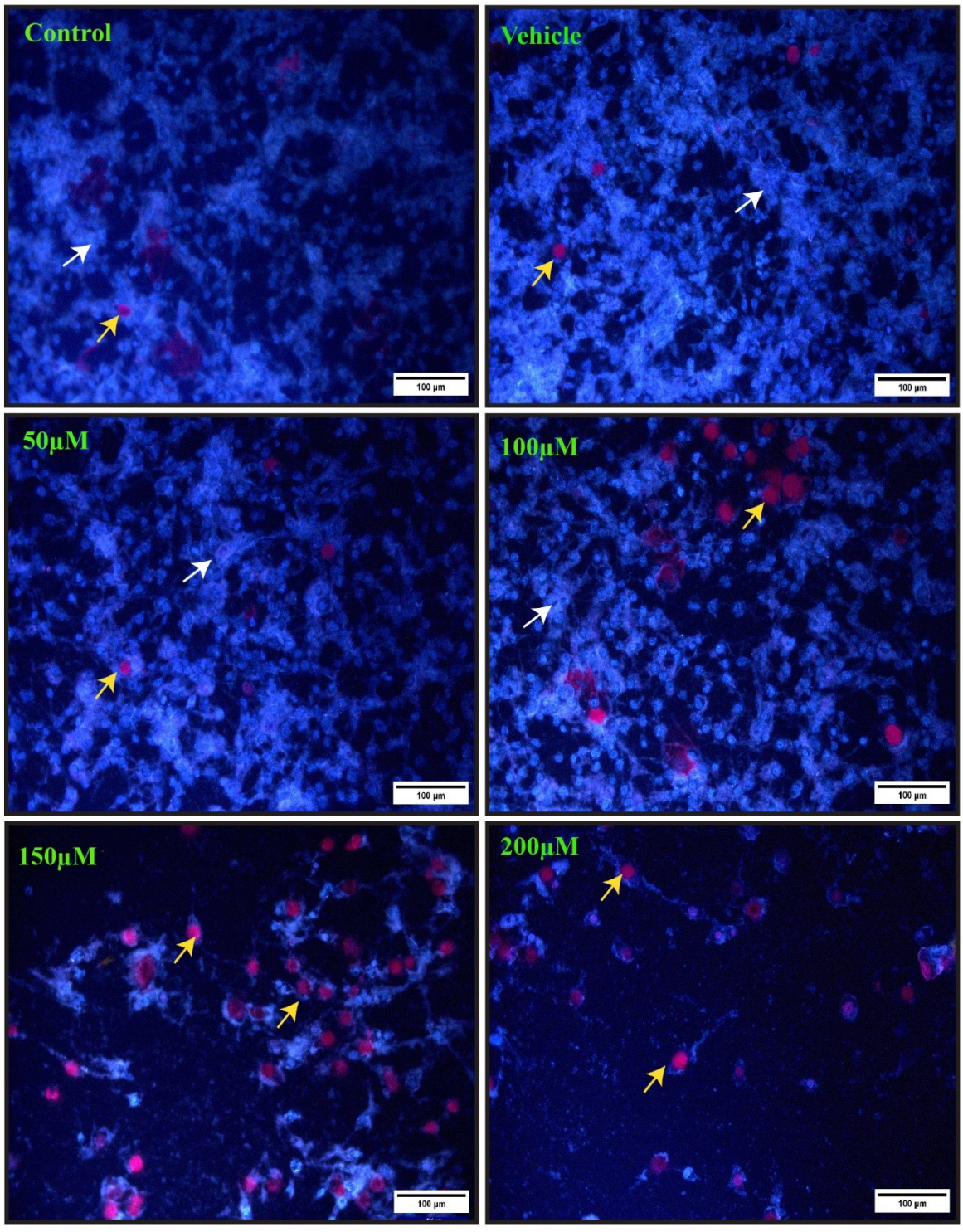

Figure 3.7 Microscopic images of CT26 cells stained with PI and Hoechst in control vehicle and PA-treated groups (50,100,150 and 200 μm). Images were captured at 400X magnification with a 100 μm scale bar. The white arrow indicates live cells, and the yellow arrow indicate dead cells

3.3.3 Uptake of palmitic acid and neutral lipid accumulation

The lipid droplets were analysed by Oil Red O staining and measuring the absorbance at 550 nm (Fig. 3.8). In IEC6 cells, the relative absorbance values were 0.125 ± 0.0012, 0.119 ± 0.0011, 0.280 ± 0.00151, 0.360 ± 0.00139, 0.414 ± 0.00122, and 0.178 ± 0.00169 for the control, vehicle, and 100, 200, 300, and 400 μM palmitic acid, respectively (Fig. 3. 8A & 3.9). The size of the lipid droplets increased with palmitic acid concentration.

In HCT116 cells, the relative absorbance values were 0.098 ± 0.00164, 0.109 ± 0.00157, 0.182 ± 0.00162, 0.261 ± 0.0029, 0.382 ± 0.0031, and 0.204 ± 0.0020 for the control, vehicle, and 50, 100, 150, and 200 μM palmitic acid, respectively (Fig. 3.8 B & 3.10). Unlike IEC6 cells, the size of lipid droplets remained relatively constant, while the number of lipid droplets increased with palmitic acid concentration.

Similarly, in CT26 cells, the relative absorbance values were 0.087 ± 0.0017, 0.092 ± 0.0014, 0.159 ± 0.0036, 0.239 ± 0.0039, 0.337 ± 0.0082, and 0.208 ± 0.0031 for the control, vehicle, and 50, 100, 150, and 200 μM palmitic acid, respectively (Fig. 3.8C & 3.11). As observed in HCT116 cells, the size of lipid droplets remained relatively constant, while the number of lipid droplets increased with increasing palmitic acid concentrations.

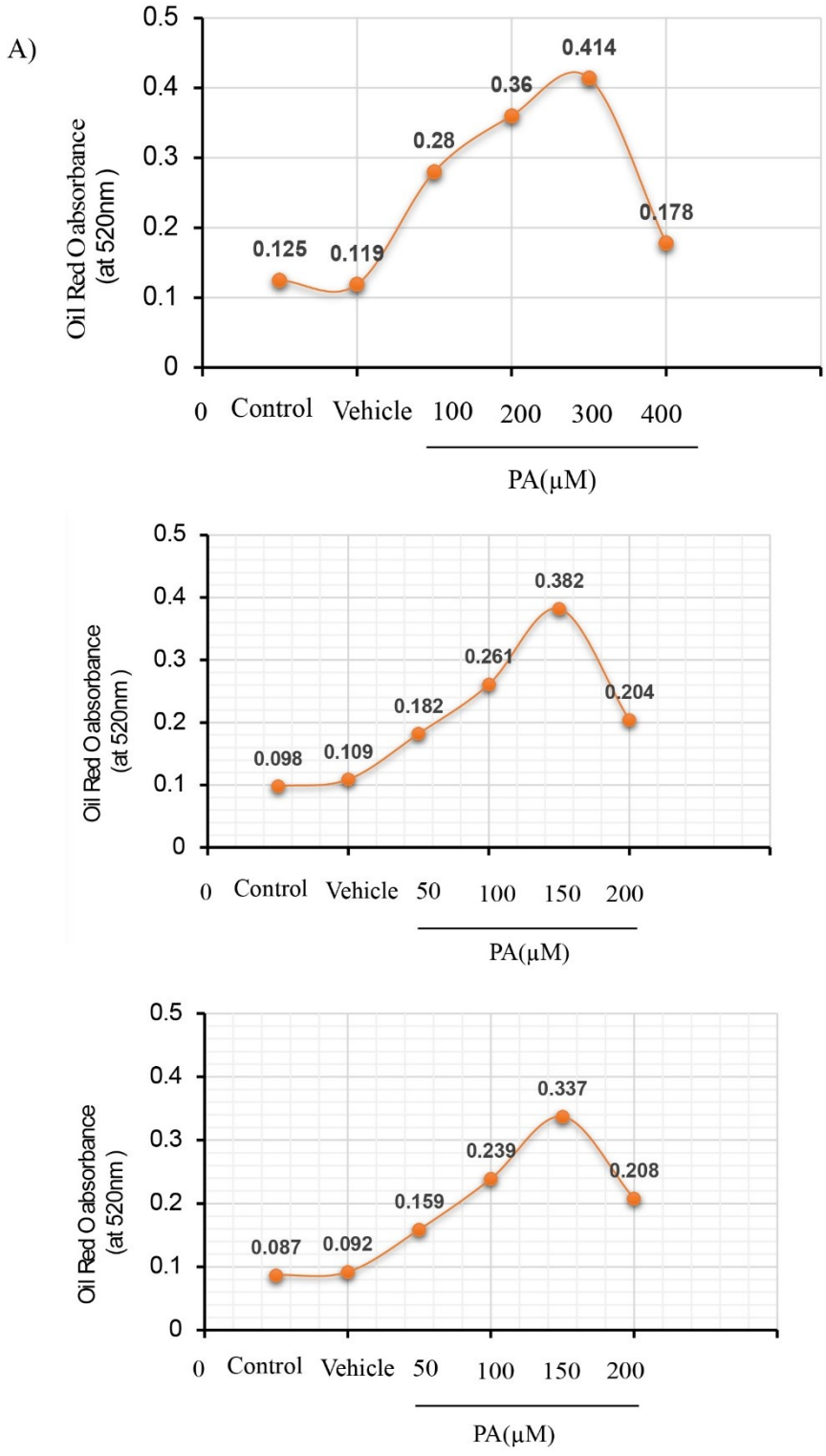

Figure 3.8. PA-induced neutral lipid accumulation in IEC6, HCT116, and CT26 cells after 24 hr treatment. Intracellular lipid content was quantified spectrophotometrically in (A) IEC6 (100-400 μM), (B) HCT116 (50-200 μM), and (C) CT26 (50-200 μM), and represented as absorbance at 520 nm.

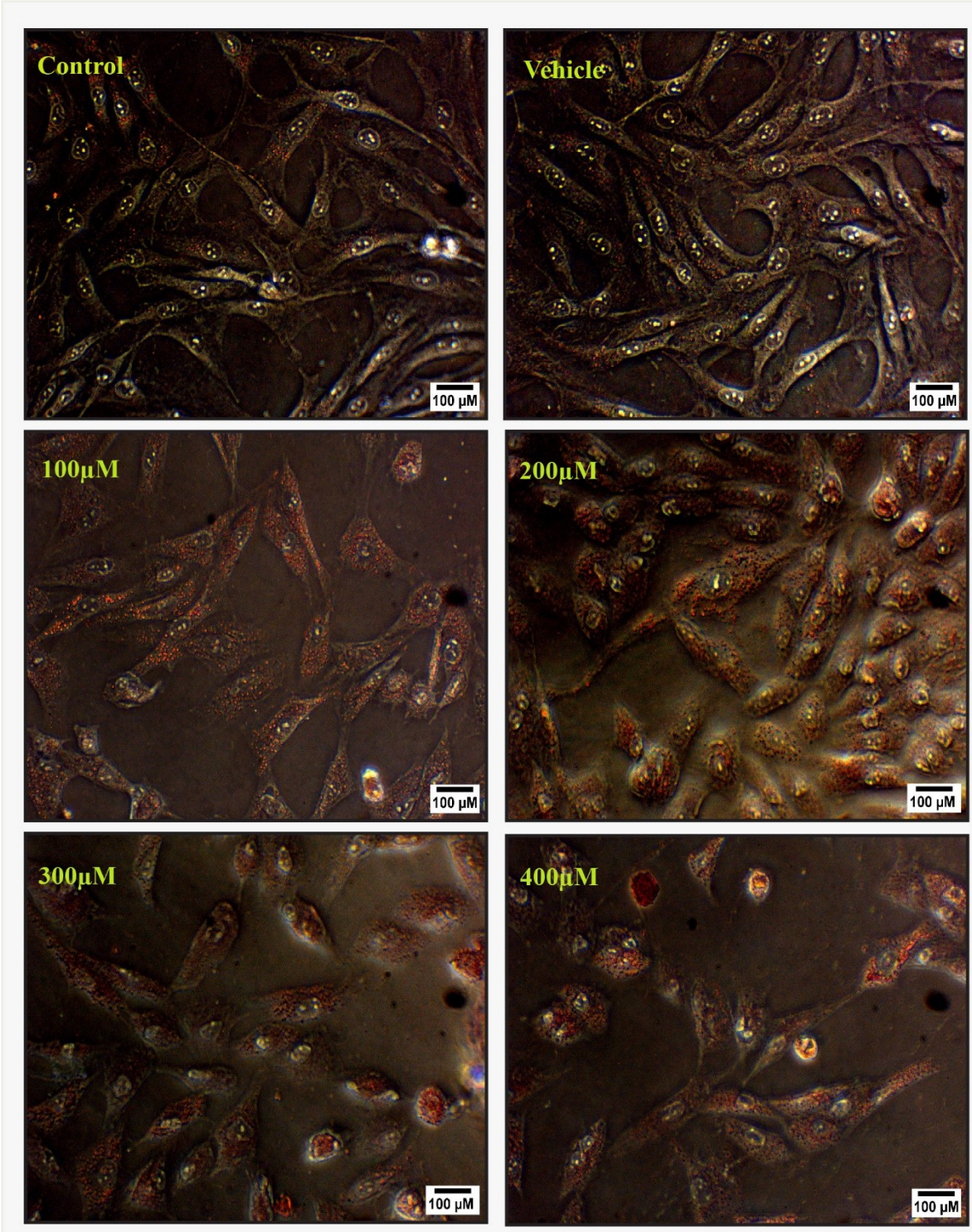

Figure 3.9 Microscopic images of IEC6 cells stained with Oil Red O showing neutral lipid accumulation in the control, vehicle, and PA-treated groups (100, 200, 300 and 400 μM). Images were captured at 400X magnification with a 100 μm scale bar.

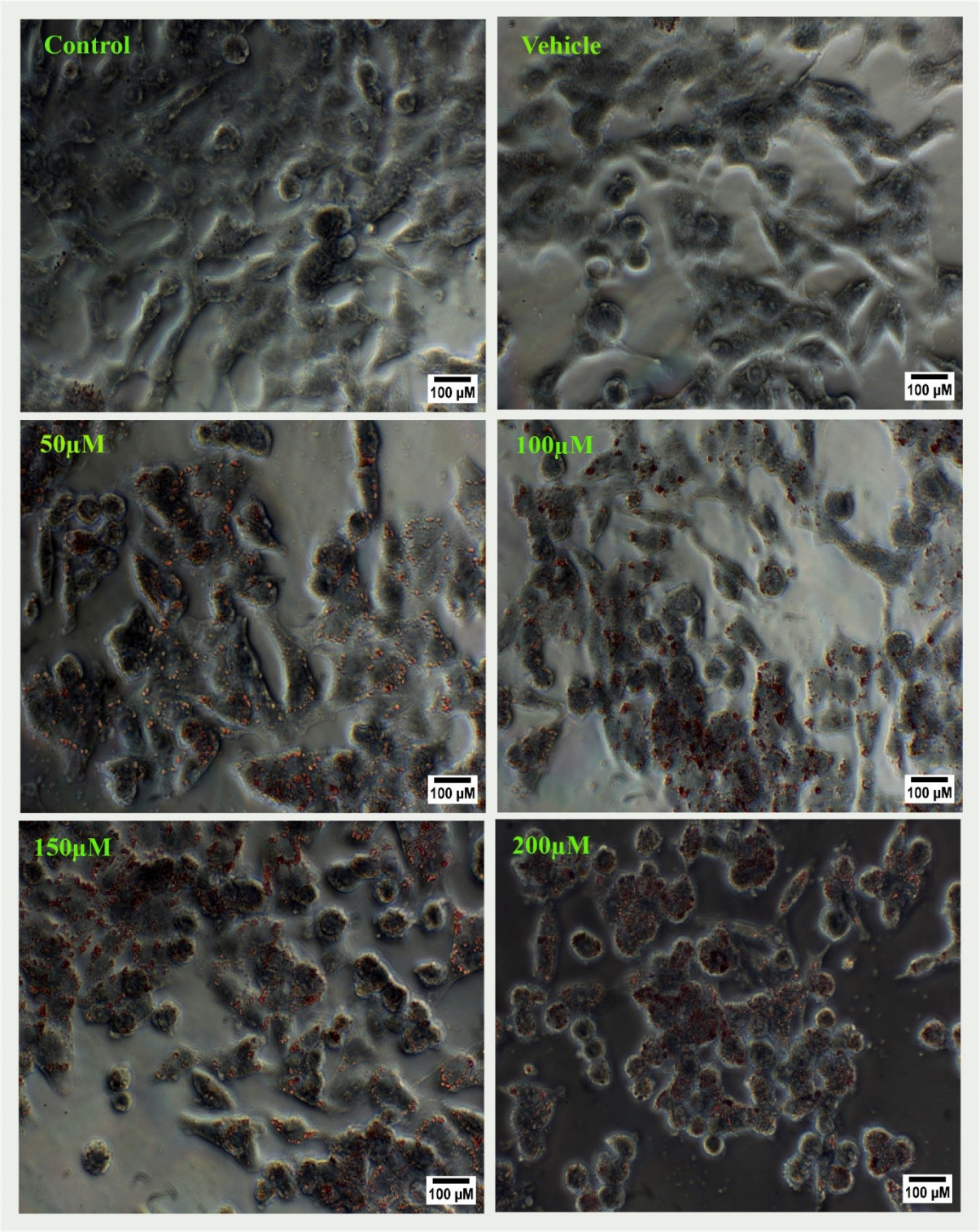

Figure 3.10 Microscopic images of neutral lipid accumulation in HCT116 cells stained with Oil Red O. Control, vehicle, and PA-treated groups (50,100,150 and 200 μM) are shown at 400× magnification with a 100μm scale bar.

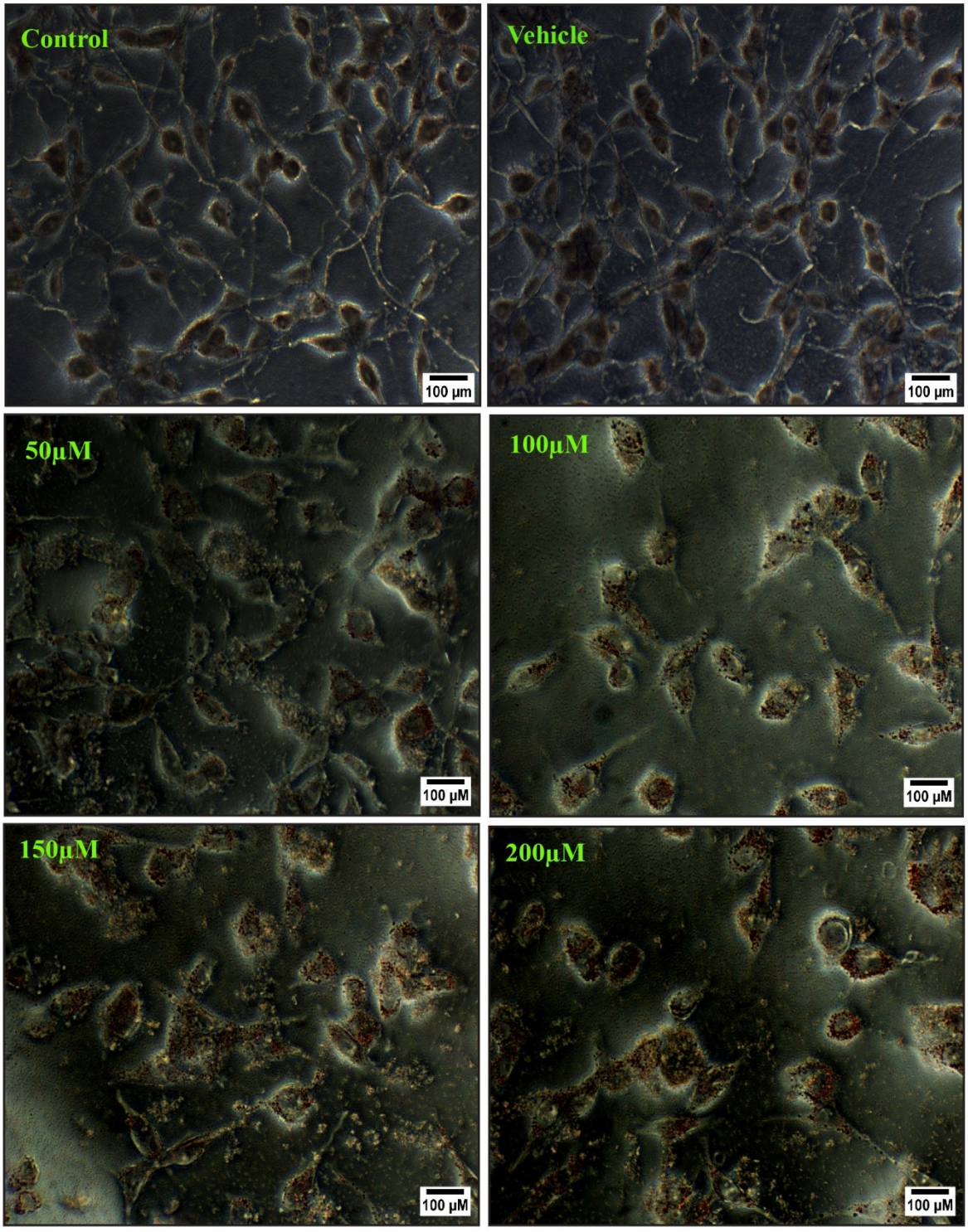

Figure 3.11 Neutral lipid accumulation in CT26 cells at 400X magnification, scale bar 100 μm. Images represent control, vehicle, and PA treated groups (50, 100, 150, and 200 μM).

3.3.4 Effect of palmitic acid on colony formation

The study investigated the impact of palmitic acid on colony formation in cell lines. In all tested cell lines, the study observed a significant reduction in colony formation with increasing concentrations of palmitic acid. This effect was pronounced at specific concentrations ranging from 300 to 400 μM for IEC6 cells and from 150 to 200 μM for HCT116 and CT26 cells. In sublethal doses, the viable colonies of cells were observed (Fig. 3.12- 3.17).

The plating efficiency of IEC6 cells decreased at higher concentrations of palmitic acid. The values determined were 31.7±1.5, 32.1±2.07, 27.66±2.5, 23.16±1.6, 2.8±0.25, and 0.6 ± 0.051 for control, vehicle, 100, 200, 300, and 400 μM, respectively (Fig. 3.12B). The survival fraction was 0.88 ± 0.03, 0.73 ± 0.027, 0.08 ± 0.003, and 0.018 ± 0.002 at the respective palmitic acid concentrations (Fig. 3.12C).

Similarly, HCT116 and CT26 cell lines responded similarly to palmitic acid treatment. The plating efficiency in HCT116 cells decreased with increasing palmitic acid concentrations (50, 100, 150, and 200 μM), with values of 18.56±0.7 for control, 18.27±0.9 for vehicle, 15.53±1.81 for 50 μM, 13.85±0.53 for 100 μM, 0.79±0.050 for 150 μM, and 0.12±0.003 for 200 μM (Fig. 3.14B). Additionally, the survival fraction of HCT116 cells exhibited a similar decreasing trend, with values of 0.76±0.017, 0.718±0.22, 0.042±0.01, and 0.006±0.03 at the corresponding palmitic acid concentrations (Fig. 3.14C).

The plating efficiency in CT26 cells was as follows: control-16.66 ± 1.19, vehicle-16.56 ± 0.7, 50 μM-12.23 ± 1.6, 100 μM-11.4 ± 1.15, 200 μM-11.36 ± 1.09, and 400 μM-0.2 ± 0.030, in comparison to the control and vehicle groups (Fig. 3.16B). Correspondingly, the survival fraction of CT26 cells exhibited a similar decreasing trend, with values of 0.779 ± 0.071, 0.70 ± 0.22, 0.33 ± 0.0062, and 0.008 ± 0.0010 at the respective palmitic acid concentrations (Fig. 3.16C).

This study highlights that palmitic acid treatment exerts a concentration-dependent influence on colony formation in IEC6, HCT116, and CT26 cell lines. The sub-lethal doses of palmitic acid, specifically 100 and 200 μM in IEC6 cells and 50 and 100 μM in HCT116 and CT26 cells, demonstrate a degree of tolerance to the toxic effect of palmitic acid exposure. These sub-lethal doses enable the cell survival, allowing them to form colonies (Fig. 3.13,3.15& 3.17).

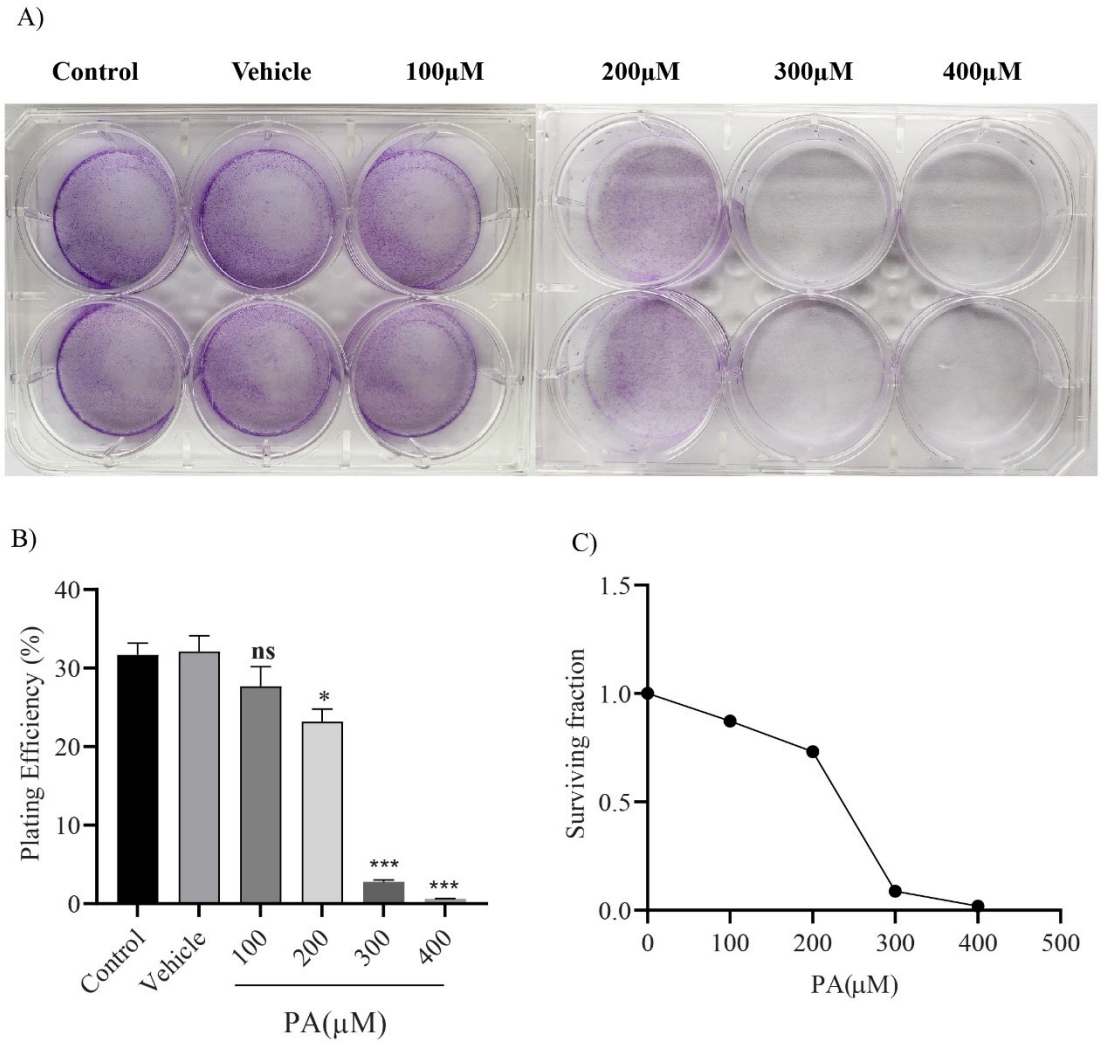

Figure. 3.12 Effect of PA on colony formation in IEC6 cells. Cells were treated with varying PA concentrations (100, 200, 300, 400 μM) or vehicle control for 24 hrs, and colony formation was assessed after 14 days. Colonies were fixed in methanol, stained with crystal violet, and counted. (A) Representative images of colonies on a 6-well plate. (B) Plating efficiency and (C) survival fraction was calculated. Data are mean ± SD (n=3). *(*$p < 0.05$, **$p < 0.01$, ***$p < 0.001$)* compared to the control group.

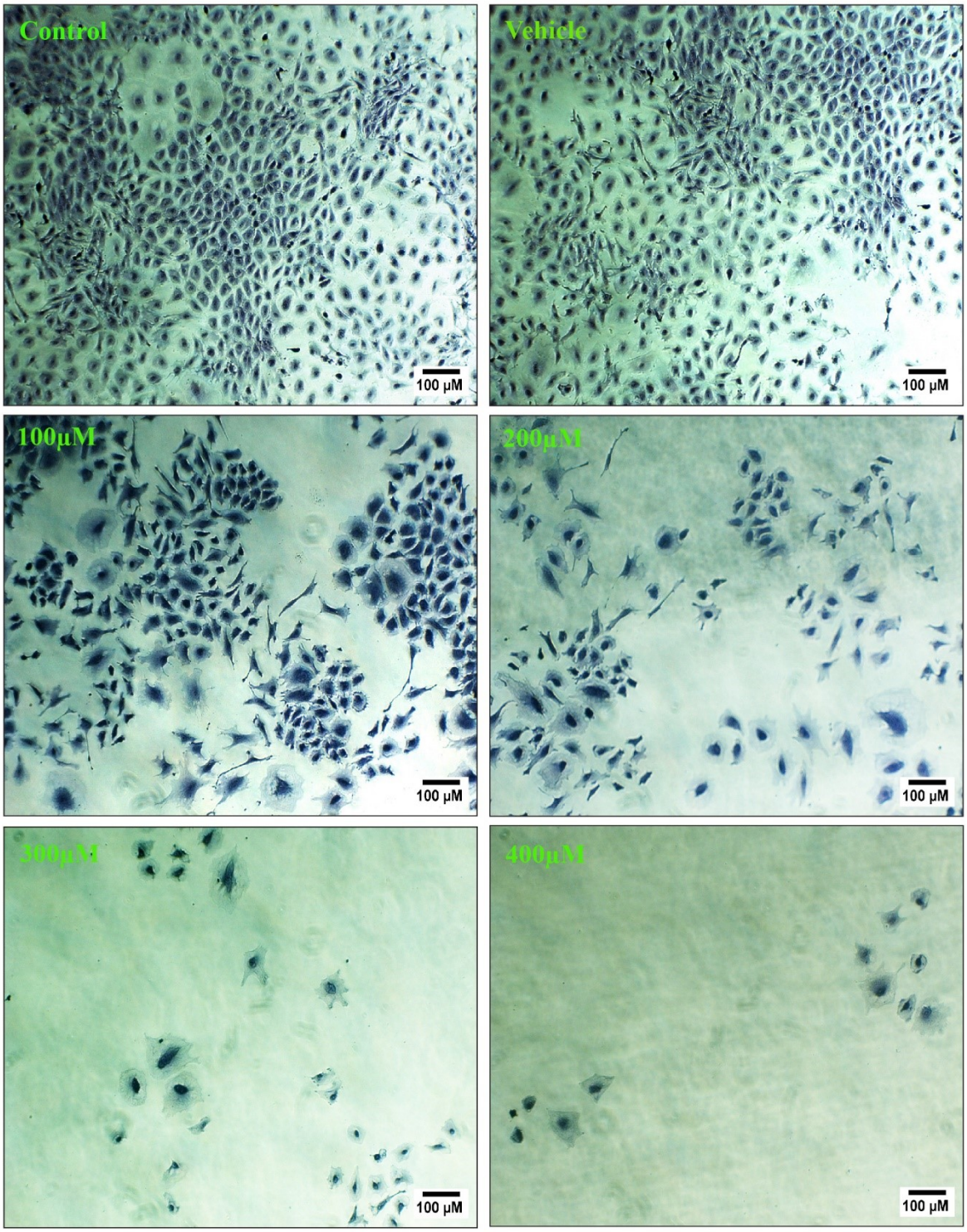

Figure 3.13 Microscopic images of IEC6 colonies in control, vehicle, and palmitic acid-treated groups at 100X magnification. Scale bar: 100 μm.

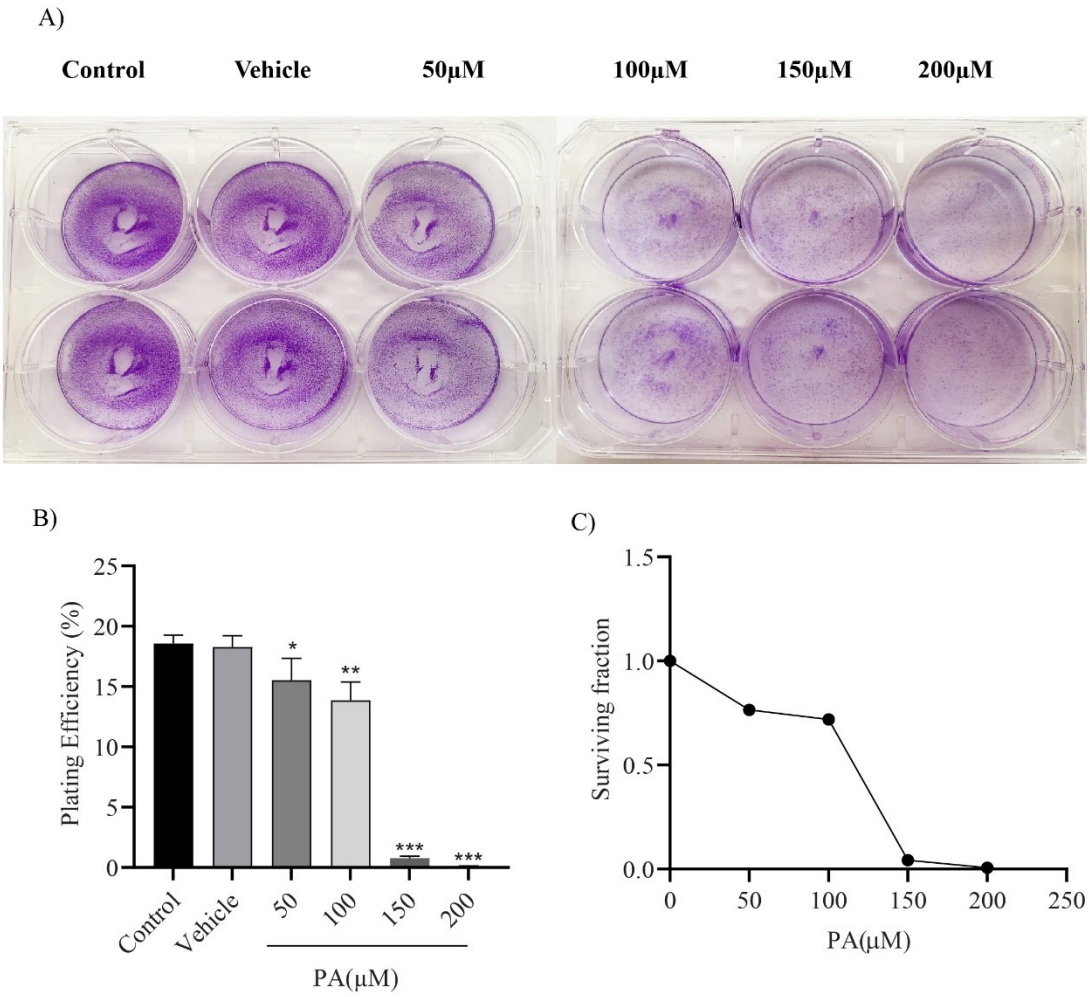

Figure 3.14 Effect of PA on colony formation in HCT116 cells. Cells were treated with PA or vehicle control for 24 hrs, and colonies were assessed after 14 days. (A) Representative images, (B) plating efficiency, and (C) survival fraction were calculated. Data are mean ± SD (n=3). *(*p < 0.05, **p < 0.01, ***p < 0.001).* vs. control.

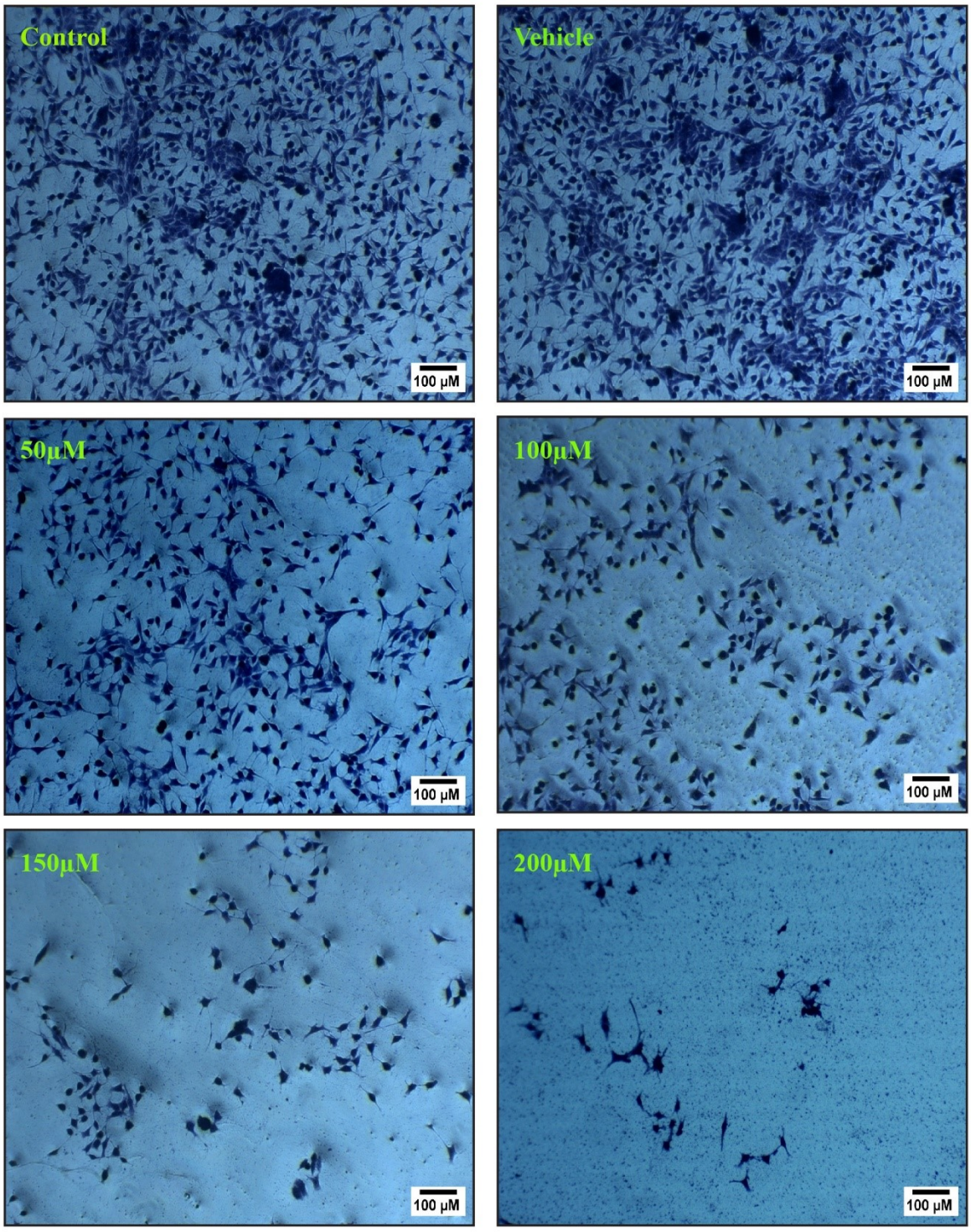

Figure 3.15 Microscopic images of HCT116 colonies in control, vehicle, and palmitic acid-treated groups at 100X magnification. Scale bar: 100 μm.

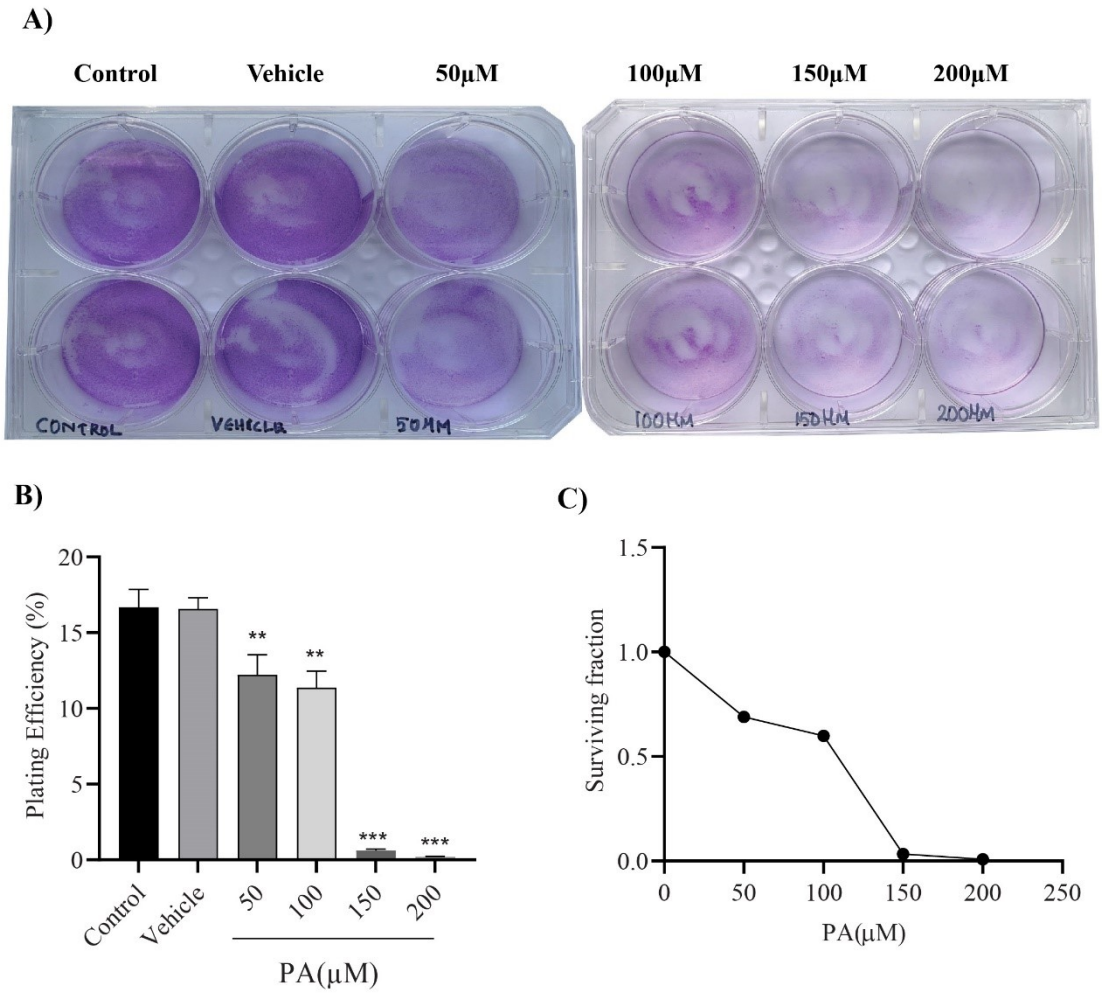

Figure 3.16 Effect of PA on colony formation in CT26 cells. Cells were treated with PA or vehicle for 24 hours, and colonies were assessed after 14 days. (A) Representative images in 6 well plates (B) plating efficiency, and (C) survival fraction. Data are mean ± SEM (n=3). ***p < 0.01,* ****p < 0.001* vs. control.

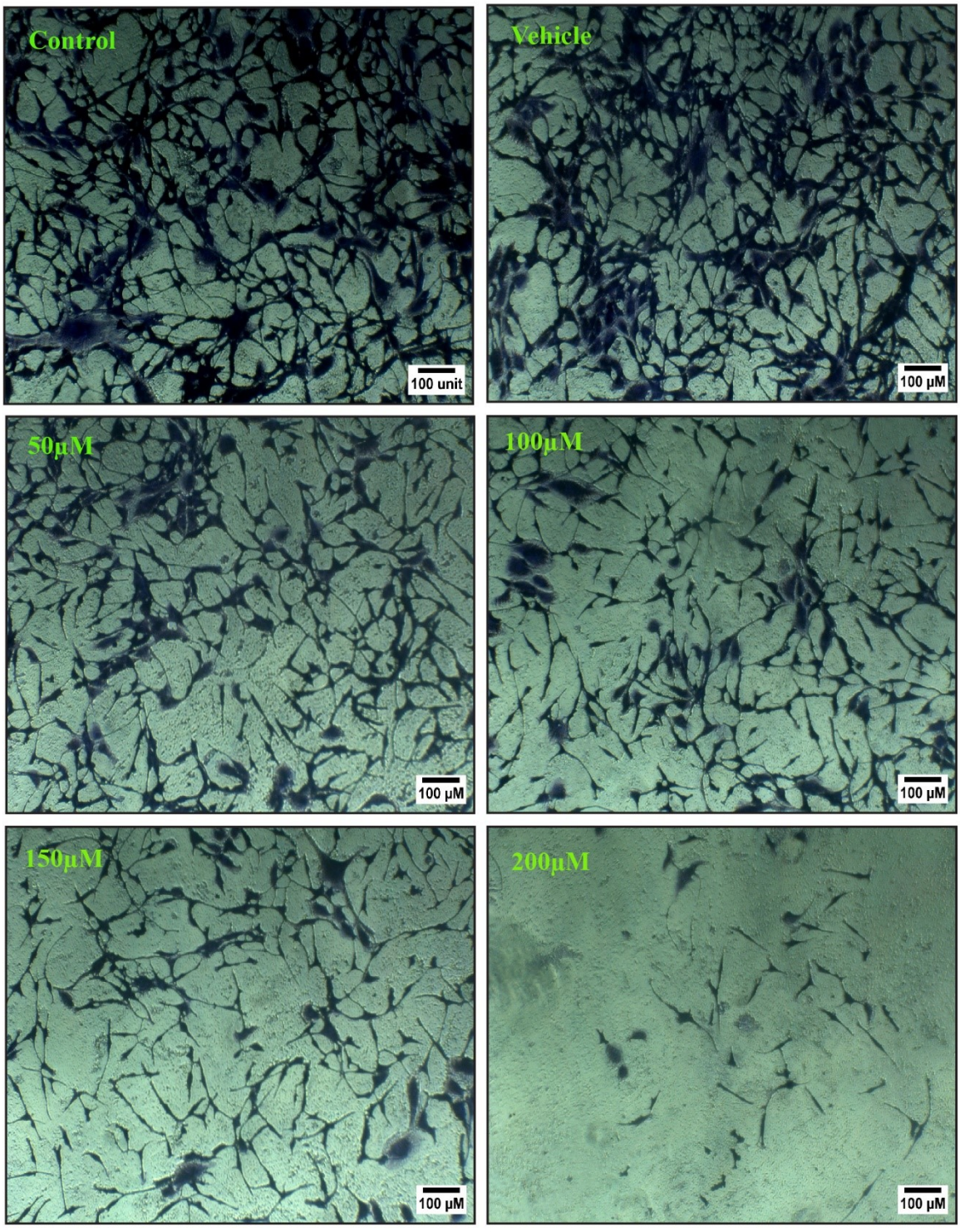

Figure 3. 17. Representative images of CT26 cell colonies in control, vehicle, and palmitic acid-treated groups (50-200 μM) at 100x magnification. Scale bar: 100 μm.

3.4 Discussion

Palmitic acid influences the cellular responses and metabolic pathways in gastrointestinal cells (Gori *et al*., 2020, Ghezzal *et al*., 2020, Kunisawa *et al*., 2014). Several investigations suggested the role of lipid metabolism in cancer progression, especially in gastrointestinal malignancies (Martin-Perez *et al*., 2022, Corn *et al*., 2020, Fu *et al*., 2021). Excess palmitic acid drives metabolic reprogramming and alters the nutrient composition in the tumour microenvironment (Maly and Hofmann, 2020, Binker-Cosen *et al*., 2017b, Kim *et al*., 2019). Hence, understanding the uptake of palmitic acid, toxicity, and consequent accumulation is crucial for understanding the molecular mechanisms of gastrointestinal cancer and discovering innovative therapeutic avenues. Therefore, studying palmitic acid uptake, toxicity, and lipid accumulation in normal and cancer gastrointestinal cells reveals valuable insights into metabolic responses and potential therapeutic targets in these cell lines.

The present chapter assessed the tolerance of palmitic acid and level of toxicity in normal rat intestinal (IEC6) and colon cancer (HCT116 and CT26) cell lines. The trypan blue and MTT assay results indicate a dose-dependent decrease in the viability of cells following the treatment of palmitic acid. Compared to the colon cancer cells, HCT116 and CT26, the normal intestinal cells have a higher tolerance to palmitic acid. Hence, in each case, the doses below the IC_{50} value can withstand induction of cell death. The IC_{50} values for palmitic acid treatment were determined as 342 μM for IEC6 cells, 180 μM for HCT116 cells, and 168 μM for CT26 cells.

The results were consistent with previous findings in normal rat pancreatic beta cells, RIN-5F, demonstrating an IC_{50} range between 0.3-0.5 mM against palmitic acid (Alnahdi *et al*., 2019b). Previous studies have reported that treating various cancer cells with palmitic acid leads to a 50% reduction in viability within the 100 – 800 μM range. The present study observed that the concentration range narrowed to 160-175 μM for HCT116 and CT26 cells. This variability suggests that the specificity of cell response to palmitic acid varies among different cancer cell types (Chen *et al*., 2019a, Aggarwal *et al*., 2022, Ouyang *et al*., 2022, Lu *et al*., 2019a).

Upon analysing the treated cells, including both normal (IEC 6) and colon cancer (HCT116 and CT26) cells, distinct observations were made regarding their morphological changes.

At lower concentrations (100 and 200 μM), minimal disparity was determined in IEC6 cells, whereas pronounced alterations were evident at higher concentrations (300 and 400 μM), characterized by the loss of spindle-shaped morphology. Similarly, in HCT116 and CT26 cells, analogous trends were observed: minimal changes at lower concentrations (50 and 100 μM) contrasted with notable morphological disruptions at higher concentrations (150 and 200 μM), culminating in the loss of cellular morphology. Elevated palmitic acid concentrations increased normal and colon cancer cell secretions, indicating a potential response to palmitic acid uptake. This phenomenon is consistent with the anticipated expulsion of excess palmitic acid, which accumulates due to metabolic constraints, thereby necessitating its extracellular elimination. Lipogenic cells, such as adipocytes and non-adipocytes, release free fatty acids into the tissue microenvironment, as evidenced by studies (Figard *et al*., 1988, Van Harmelen *et al*., 1999), and tumour cells are also known to contribute to this phenomenon as an adaptive response (Spector and Steinberg, 1966, Kleinfeld and Okada, 2005). Consistent with previous studies, palmitic acid is implicated in inducing extracellular vesicle secretion in epithelial cells. Elevated levels of these extracellular vesicles may indicate the activation of apoptotic induction pathways (Cobbs *et al*., 2019). The present findings support previous research, suggesting that at lethal doses of palmitic acid, excess secretion correlates with increased cell death compared to non-lethal doses.

Palmitic acid, while showing potential in sensitizing breast cancer cells to apoptosis and serving as a therapeutic candidate for breast and prostate cancers, is primarily an essential saturated fatty acid obtained through the diet and crucial for cellular survival (Zhu *et al*., 2021, Wang *et al*., 2023a, Yu *et al*., 2023). The paradox of developing a cytotoxic compound from a metabolically essential component raises questions about its therapeutic application. Regardless, studies examining the consequences of palmitic acid excess and its effects on cell signalling mechanisms for pathological transformation become pertinent in this context (Park *et al*., 2014, Ng and Say, 2018, Sergi *et al*., 2022, Alnahdi *et al*., 2019a, Fatima *et al*., 2019a). Furthermore, various investigations indicate that tumours exploit fatty acids, including palmitic acid, to reprogram cancer cells through histone methylation, fostering a neural-like phenotype conducive to tumour innervation and metastasis formation (Pascual *et al*., 2021a, Liu *et al*., 2022, Altea-Manzano *et al*., 2023, Zhang *et al*., 2022b).

It was evident that lipogenic cells tend to accumulate lipids due to their functional specificity, whereas non-lipogenic cells exhibit restricted absorption or metabolize lipids promptly upon absorption (Zhang *et al*., 2016, Suganami *et al*., 2012, van Herpen and Schrauwen-Hinderling, 2008, Granlund *et al*., 2005). Moreover, non-adipogenic cells, such as muscle cells and certain types of epithelial cells, do not have the same capacity for lipid accumulation, as they may be altered or impaired due to various diseases such as diabetes (Fazolini *et al*., 2015). Consistent with the above findings, our study revealed that both normal and colon cancer cells uptake palmitic acid, as confirmed by Oil Red O staining. We also found that palmitic acid in excess induced a significant increase in the accumulation of neutral lipids and the formation of lipid droplets in IEC6, HCT116, and CT26 cells. The uptake of palmitic acid represents a crucial aspect of lipid metabolism, as it serves as a precursor for various cellular processes, including energy production and membrane synthesis. The observed dose-dependent uptake of palmitic acid from the present study hence highlights the regulatory mechanisms governing fatty acid transport in gastrointestinal cells. In many studies, it has been evident that fatty acid transport proteins (FATPs) and fatty acid translocase (FAT/CD36) play crucial roles in mediating the cellular uptake of palmitic acids (Urso and Zhou, 2021, Hua *et al*., 2015, Zhao *et al*., 2018). In our study, lower concentrations (100 and 200 μM for IEC6 and 50 and 100 μM for HCT116 and CT26) resulted in significant lipid droplet formation without affecting the survival of the cells. However, at higher concentrations, cell death occurs. The dose-dependent nature of palmitic acid uptake suggests the existence of saturation kinetics, wherein the transporters exhibit maximal rates of transport at higher concentrations of palmitic acid, which may lead to lipotoxicity.

It has been suggested that lipid droplets have protective properties against various types of cellular stress, including lipotoxic stress, as they play a central role in lipid metabolism (Jarc and Petan, 2019, Listenberger *et al*., 2003). It has been reported that lipid droplets play a crucial role in cancer cells by consolidating lipid acquisition and trafficking pathways, thereby ensuring survival, growth, and metastasis through energy production, redox balance, membrane synthesis, and modulation of autophagy (Petan, 2023a, Jin *et al*., 2023, Koizume and Miyagi, 2016). Moreover, lipid droplets provide metabolic flexibility in cancer cells by efficiently converting excess lipids entering the cells into lipid droplets, thereby regulating lipid storage and utilization to support various cellular functions and

adapt to fluctuating nutrient and energy conditions (Safi *et al*., 2024, Munir *et al*., 2019). The study demonstrates that the non-lipogenic IEC6 cells uptake palmitic acid, forming neutral lipid droplets similar to HCT116 and CT26 cells. Excessive palmitic acid exposure prompts neutral lipid formation in IEC6 cells parallel to lipogenic cells. This emphasizes the potential for metabolic fluctuations in normal cells, leading to pathological shifts if deviations from normal lipid metabolism occur. The findings were consistent with numerous studies indicating that IEC6 cells accumulate neutral lipids in response to abnormal cytological perturbations associated with lipid metabolism, inflammatory responses, and other pathological factors (Moreira *et al*., 2009). Moreover, it was evident that palmitic acid serves as a substrate for *de novo* lipogenesis, wherein it undergoes esterification to form triglycerides and phospholipids within cellular lipid droplets (Ramakrishnan *et al*., 2023). The enhanced lipid accumulation in cancer gastrointestinal cells may be attributed to the upregulation of lipogenic enzymes, such as fatty acid synthase (FASN) and acetyl-CoA carboxylase (ACC), which are frequently dysregulated in cancer to meet the increased demand for membrane biogenesis and energy production (Wang *et al*., 2020, Menendez and Lupu, 2007, Montesdeoca *et al*., 2020).

In the present study, palmitic acid induces lipotoxicity in gastrointestinal cells, resulting in cell death characterized by red staining in PI-HOE assays. This staining indicates apoptosis or necrosis due to lipotoxic effects observed at 300 and 400 μM concentrations in IEC6 cells and 150 and 200 μM in HCT116 and CT26 cells, respectively. The differential susceptibility of normal and cancer gastrointestinal cells to palmitic acid-induced toxicity may arise from variations in lipid metabolism and antioxidant defence mechanisms (Swinnen *et al*., 2006). Cancer cells often exhibit heightened lipogenic activity and altered antioxidant activity, rendering them more susceptible to lipotoxic insults (George and Abrahamse, 2020) (Manoharan *et al*., 2005, Sharma *et al*., 2009, Rysman *et al*., 2010).

The cellular resilience and the proliferative potential of the cells after the palmitic acid treatment were tested *via* colony formation assay. The results indicate that concentrations of 100 and 200 μM of palmitic acid support the formation of healthy colonies in IEC6 cells, while concentrations of 50 and 100 μM are conducive to colony formation in HCT116 and CT26 cells. The study aligns with previous findings, demonstrating palmitic acid's role in promoting cancer cell survival through diverse mechanisms (Binker-Cosen *et al*., 2017b, Maly and Hofmann, 2020, Kim *et al*., 2019). In our investigation, concentrations of 50 and

100 μM palmitic acid in both HCT116 and CT26 cells showed resilience to excessive exposure, forming efficient colonies post-treatment. Additionally, normal IEC6 cells tolerated concentrations of 100 and 200 μM, implying metabolic adaptability in normal cells under extreme conditions. The study suggests that cancer cells effectively mimic normal cells to survive despite lacking several functional cell signalling mechanisms due to various mutations. Therefore, these concentrations represent the survival threshold suitable for further analysis of cell signalling pathways related to cell survival.

In conclusion, the study revealed the uptake, toxicity, and accumulation of palmitic acid in normal and cancer gastrointestinal cells. Targeting fatty acid metabolism, supported by developing inhibitors against key lipid biosynthesis enzymes, holds promise for cancer therapy. Modulating fatty acid uptake and utilization presents a therapeutic strategy to mitigate palmitic acid-induced metabolic flexibility, attenuating cancer progression and offering significant implications for understanding metabolic alterations in gastrointestinal cancer.

Chapter 4

Analysis of palmitic acid-induced oxidative stress, endoplasmic reticulum stress (ERS), and unfolded protein response (UPR) in normal and colon cancer cells

4.1 Introduction

Multiple studies have identified that excess palmitic acid uptake induces oxidative stress and subsequent lipotoxicity in the colon (Mansuri *et al*., 2021, Xu *et al*., 2020). The role of palmitic acid in metabolic diseases like obesity, insulin resistance, and cardiovascular diseases has been well-documented. However, its involvement in cancer pathogenesis is less extensively documented (Binker-Cosen *et al*., 2017b, Liu *et al*., 2022). Palmitic acid has been known to induce ER stress, a condition of misfolded/unfolded protein accumulation in the endoplasmic reticulum, leading to UPR, which is crucial in various cellular processes, including apoptosis, inflammation, and carcinogenesis (Lin *et al*., 2019). In addition, oxidative and ER stresses are critical cellular processes that significantly impact cell function and survival in normal and cancer cells. This chapter investigates how palmitic acid induces oxidative stress and the subsequent accumulation of misfolded proteins, leading to ER stress and UPR in normal and colon cancer cells.

Many physiological or pathological perturbations contribute to disruptions in ER homeostasis. One such distress is oxidative stress, a condition characterised by the excessive production of reactive oxygen species (ROS). These ROS can damage cellular components such as lipids, proteins, and DNA, causing significant harm. In cells, the endoplasmic reticulum (ER) is particularly sensitive to oxidative stress due to its critical role in protein folding and processing. This sensitivity disrupts protein folding, post-translational modifications, and calcium homeostasis. Consequently, the accumulation of misfolded proteins in the lumen of ER causes stress (ER stress) and activates the UPR. The UPR aims to restore ER function by increasing the expression of chaperones, attenuating protein translation, and promoting the degradation of misfolded or unfolded proteins (Pham *et al*., 2023). However, sustained ER stress can activate pro-apoptotic signalling pathways, contributing to cell death. Three canonical branches of the UPR, mediated by protein kinase RNA-like ER kinase (PERK), activating transcription factor 6 (ATF6), and inositol-requiring enzyme 1 (IRE1), pathways are reported as the critical mediators of ER stress-induced survival and apoptosis.

Previous studies have demonstrated the involvement of ER stress and the UPR in the pathogenesis of various cancers, including colon, hepatic, lung, pancreas, and prostate

(Cherubini and Zito, 2022, Luna-Marco *et al*., 2023, Wang *et al*., 2023b, Chen *et al*., 2023a, Cen *et al*., 2023). However, the specific mechanisms underlying palmitic acid-induced ER stress and its consequences in normal and colon cancer remain poorly understood. While some studies have investigated the role of ER stress in response to lipid overload and obesity-associated inflammation, few have explicitly focused on the contribution to the development of colon cancer and progression (Ajoolabady *et al*., 2023). Moreover, existing literature predominantly focuses on the UPR pathway in the context of ER stress induced by pharmacological agents or environmental toxins, with limited research exploring its role in response to dietary factors such as palmitic acid. Therefore, there is a significant gap regarding the molecular mechanisms linking palmitic acid-induced oxidative stress to the activation of the ER stress and associated UPR pathway in normal and cancerous colon cells.

Evidence indicates that palmitic acid induces various cytological perturbations in intestinal tissues and plays a significant role in colon cancer cell progression (Ghezzal *et al*., 2020, Gori *et al*., 2020, Zhang *et al*., 2023). Our study aims to investigate the palmitic acid-induced oxidative stress and its activation of the ER stress and UPR pathway in both normal colon cells and colon cancer cells. We hypothesize that exposure to palmitic acid initiates oxidative stress, which induces endoplasmic reticulum stress and activates the UPR pathway. Although previous research has explored the involvement of ER stress and UPR activation in various cancers, the specific impact of palmitic acid-induced ER stress on colon cancer cells remains poorly understood. Furthermore, the distinct response of normal colon and colon cancer cells to palmitic acid-induced ER stress, primarily through the UPR pathway, requires further exploration**.** This study proposes that colon cancer cells may exhibit an altered response to palmitic acid-induced ER stress compared to normal colon cells, potentially promoting cancer cell survival. Addressing this issue is crucial for identifying potential therapeutic targets and developing strategies to mitigate the influence of dietary factors on colon cancer development and progression. By exploring these gaps, the present chapter aims to provide deeper insights into the relationship between oxidative stress, ER stress, and UPR activation in normal versus colon cancer cells.

4.2 Materials and Methods

4.2.1 Analysis of reactive oxygen species

DCFH-DA was used to detect and measure the intracellular ROS level in cultured cells. Hydrogen peroxide (H_2O_2) served as a positive control, and N-acetyl cysteine (NAC) is used as an inhibitor of ROS production. Images were captured with a fluorescent microscope. Detailed procedures are provided in Chapter 2, Section 2.2.1.2.6.

4.2.2 Analysis of misfolded protein accumulation

Palmitic acid-induced misfolded protein aggregates (ER stress) in the cells were detected by thioflavin (ThT) staining. The fluorescence level was measured post-staining. Tunicamycin™, an ER stress inducer, was used as a positive control, while 4-phenyl butyric acid (PBA) served as an ER stress inhibitor. The images were obtained using a fluorescence microscope. Detailed experimental protocols and calculations are provided in Chapter 2, Section 2.2.1.2.7.1.

4.2.3 Analysis of oxidative stress and lipid peroxidation

The activities of antioxidant enzymes such as superoxide dismutase (SOD), catalase (CAT), glutathione reductase (GR), glutathione S-transferase (GST), and glutathione peroxidase (GPx), and the level of glutathione (GSH) and lipid peroxidation were assessed. Detailed protocol is described in Chapter 2, Sections 2.2.3.3.

4.2.4 Analysis of the acidic vacuoles

Acidic vesicular organelles (AVOs), indicating early-phase autophagy, were identified by acridine orange staining. Following specific treatments, the cells underwent staining with 1 μg/mL acridine orange for 30 min at 37°C and measured excitation/emissions in green (510–530 nm) and red (650 nm) fluorescence filters by fluorescent spectroscopy. The procedures and calculations are explained in detail in Section 2.2.1.2.8 of Chapter 2.

4.2.5 Analysis of autophagic flux

To analyse autophagy, the cells were exposed to palmitic acid and treated with a Monodansylcadverine (MDC), which selectively stains acidic vesicular organelles, including autophagic vacuoles and auto phagolysosomes. Briefly, the cells were stained with 50 μM MDC at 37°C for 15 min, washed with Hanks' buffer, and fluorescence was

measured at Ex 340 nm and Em 535 nm. The values were normalised against cell proliferation using the sulforhodamine B assay. Each condition underwent three independent experiments. The complete procedure is cited in Chapter 2, Section 2.2.1.2.9.

4.2.6 RT- *q*PCR analysis

Total RNA was isolated from palmitic acid-treated normal and cancer cells. cDNA was synthesised using 10 μg of RNA by cDNA synthesis kit. PCR reactions were performed in triplicate for each sample using specific primers targeting *Bip, Chop, Atf6, Perk, Atf4, Nrf2, Nqo-1*, and *Ho-1* genes. The fold changes of the target genes were normalised to β-actin expression, and gene expression levels were determined using the Livak method (2^(-ΔΔCt) method). Detailed procedures and corresponding primer sequences are provided in Chapter 2, Section 2.2.4

4.2.7 Statistical analysis

The results are expressed as mean ± SD from three independent samples. Statistical analysis was performed using one-way ANOVA, followed by Tukey's multiple comparison test for comparisons among all groups or Dunnett's test against a control group. Statistical significance was defined as $p < 0.05$, with significance levels indicated as $*p < 0.05$, $**p < 0.01$, and $***p < 0.001$

4.3 Results

4.3.1 Palmitic acid-induced ROS production in normal and colon cancer cells

Exposure to PA increased ROS production in IEC6, HCT116, and CT26 cells over 24 hrs, as determined by DCF fluorescence staining. By Nac treatment, ROS generation declined, confirming reduced ROS production. In all three cell lines, PA concentrations above the IC_{50} values (IEC6: 342 μM, HCT116: 180 μM, CT26: 168 μM) did not significantly reduce ROS level following Nac treatment. This absence of a reduction in ROS level was attributed to the cytotoxic effects of PA (Fig. 4.1-4.6).

The relative fold change of ROS in IEC6 cells was found to be 1.99 ± 0.053, 2.18 ± 0.094, 2.55 ± 0.0754, and 1.92 ± 0.094 for 100, 200, 300, and 400 μM of PA, respectively. When treated with Nac, the ROS levels reduced to 1.49 ± 0.058, 1.64 ±

0.144, 2.42 ± 0.136, and 1.71 ± 0.225 for the respective concentrations. The fold change for the positive control (H_2O_2) was 3.57 ± 0.242 for the IEC6 ROS level (Fig 4.2).

Similarly, the relative fold change in HCT116 and CT26 cells for 50, 100, 150, and 200 μM concentrations were 1.751 ± 0.1821 and 1.681 ± 0.181, 1.952 ± 0.1704 and 1.971 ± 0.154, 2.621 ± 0.1893 and 2.75 ± 0.1953, and 1.857 ± 0.158 and 1.857 ± 0.148, respectively. The Nac treatment caused a reduction in relative fold change for the aforementioned concentrations in HCT116 and CT26 cells as follows: 1.42 ± 0.1528 and 1.37 ± 0.11, 1.65 ± 0.1594 and 1.603 ± 0.144, 2.54 ± 0.2119 and 2.699 ± 0.129, and 1.736 ± 0.16 and 1.735 ± 0.152, respectively. The relative fold change for H_2O_2 was 2.84 ± 0.248 and 3.319 ± 0.271 in HCT116 and CT26 cells, respectively (Fig 4.4 & Fig 4.6).

The fluorescent images illustrate DCF fluorescence in PA-treated IEC6, HCT116, and CT26 cells with and without Nac, showing a dose-dependent response compared to the control. Nac effectively reduced ROS levels in IEC6 cells treated with 100 and 200 μM PA and HCT116 and CT26 cells exposed to 50 and and100 μM concentrations. However, at concentrations of 300 and 400 μM in IEC6 cells and 150 and 200 μM in HCT116 and CT26 cells, an observable increase in ROS production was noted compared to the control, which Nac supplementation less effectively mitigated (Fig. 4.1, Fig. 4.3, & Fig. 4.5).

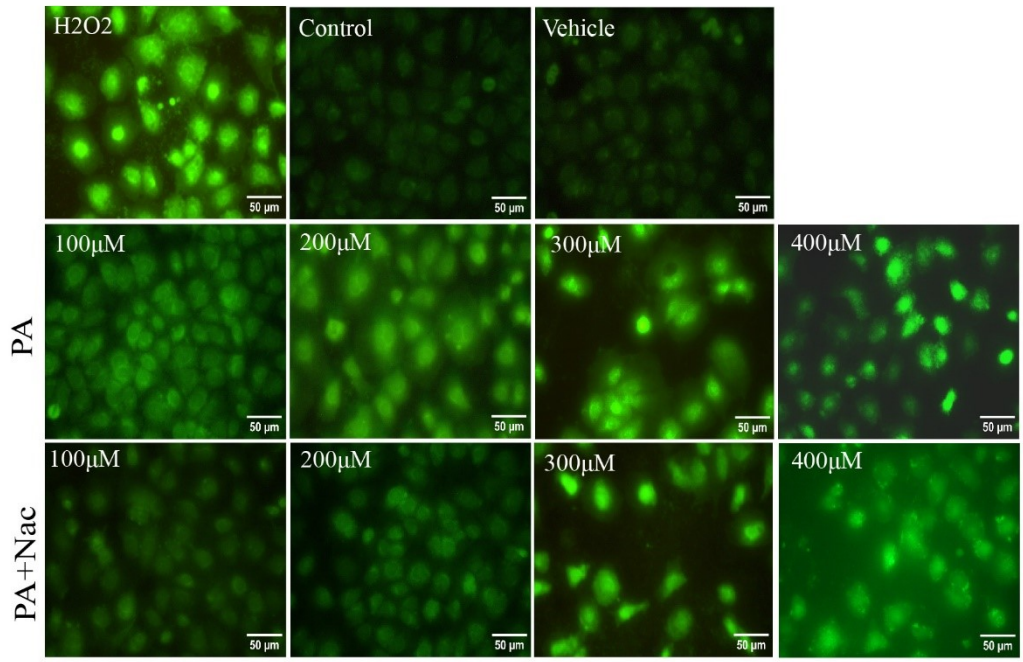

Figure 4.1 Microscopic images showing DCF fluorescence associated with ROS production in IEC6 cells under the following conditions: H_2O_2-treated positive control, untreated control, vehicle-treated, and PA-treated (100-400 µM PA) with or without NAC. Scale bar = 50 µm, magnification = 400x.

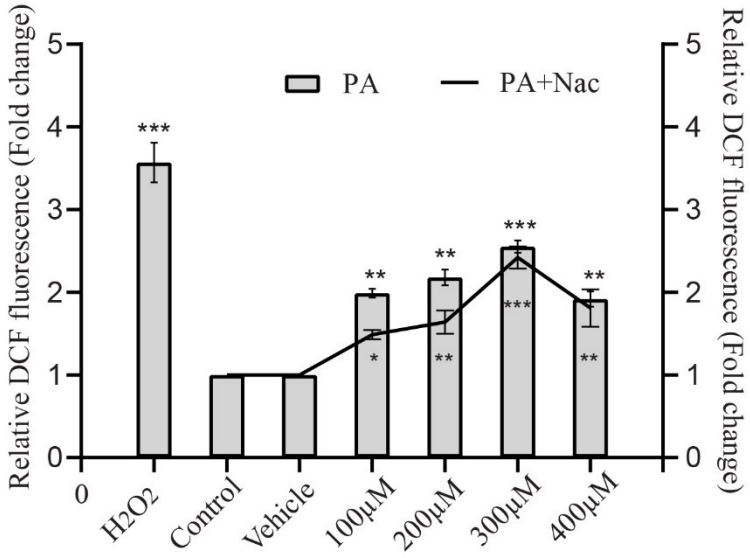

Figure 4.2 Spectrofluorimetric analysis of ROS production in IEC6 cells via DCF fluorescence under H_2O_2, control, vehicle, and PA (100-400 µM) treatments. The bar graph shows ROS levels without NAC, and the line graph shows ROS levels with NAC. Data are presented as mean ± SD (n = 3), analysed by one-way ANOVA with Tukey's test. *$P < 0.05$, **$P < 0.01$, ***$P < 0.001$.

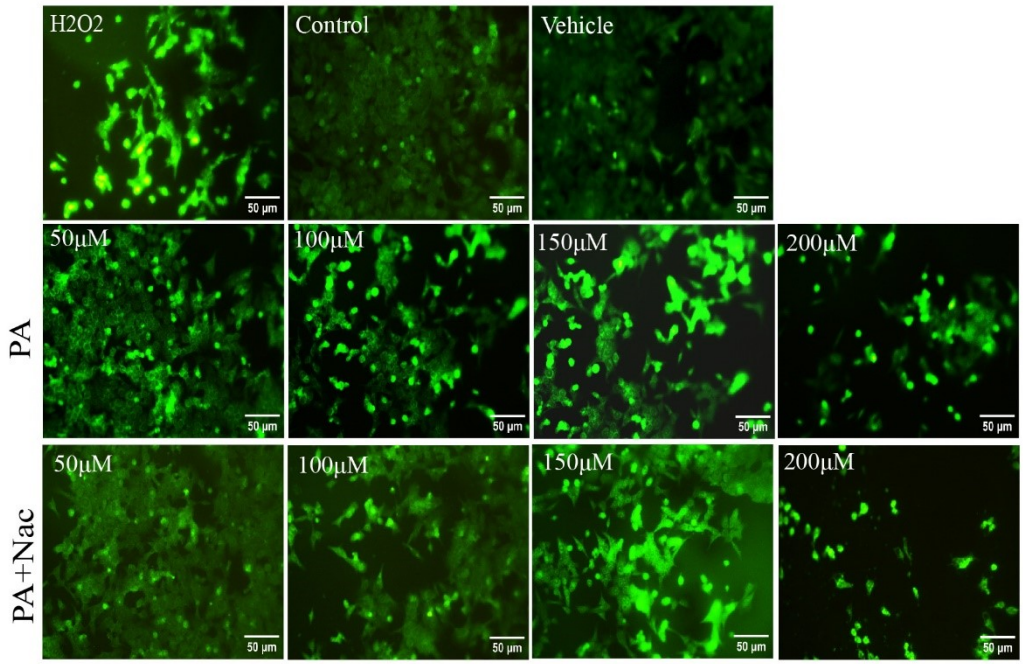

Figure 4.3 DCF fluorescence images showing ROS production in HCT116 cells under H_2O_2-treated, untreated, vehicle-treated, and PA-treated (50-100 µM) conditions, with or without NAC. Scale bar = 50 µm, magnification = 400x.

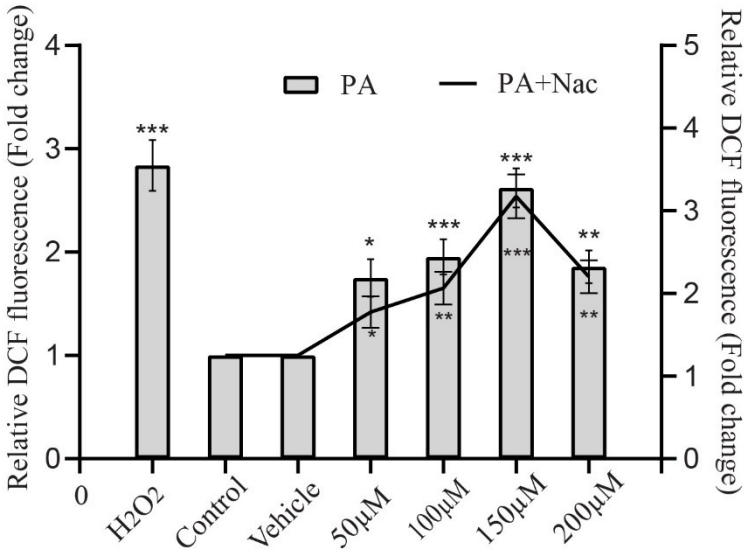

Figure 4.4 ROS production in HCT116 cells via DCF fluorescence under H_2O_2, control, vehicle, and PA (50-200 µM) treatments. Bar graph: ROS levels without NAC; Line graph: ROS levels with NAC. Data are mean ± SD (n = 3), analysed by one-way ANOVA with Tukey's test. *$P < 0.05$, **$P < 0.01$, ***$P < 0.001$.

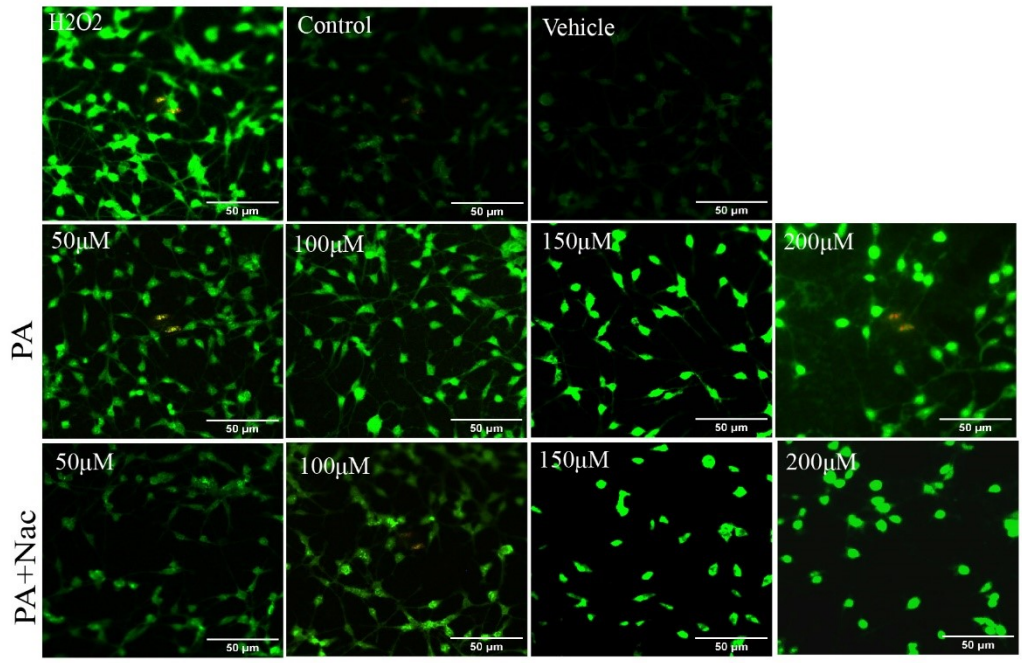

Figure 4.5 DCF fluorescence images illustrating ROS production in CT26 cells under various conditions: untreated, H_2O_2-treated, vehicle-treated, and PA-treated (50–100 µM), with or without NAC. Scale bar: 50 µm; magnification: 200x.

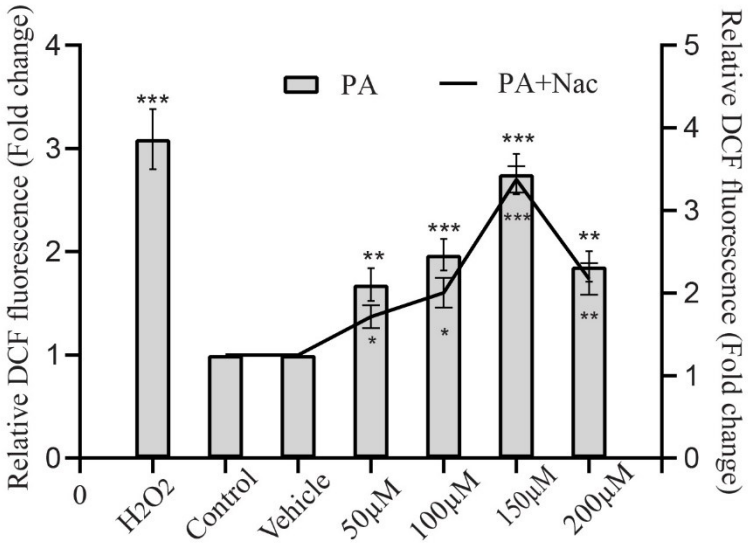

Figure 4.6 DCF fluorescence showing ROS production in CT26 cells under control, H_2O_2, vehicle, and PA (50–200 µM) treatments. Bar graph: ROS levels without NAC; Line graph: ROS levels with NAC. Data are presented as mean ± SD (n = 3) and analysed using one-way ANOVA with Tukey's *test (*P < 0.05, **P < 0.01, ***P < 0.001).*

4.3.2 Effects of palmitic acid on misfolded protein aggregation

Fluorescence microscopy and spectrofluorimetric analysis revealed increased misfolded protein aggregates (ER stress) in PA-treated cells. Tunicamycin™ (positive control) elevated misfolded protein levels, while PBA, an ER stress inhibitor, reduced PA-induced ER stress. The relative fold change in ThT fluorescence in IEC6 cells, indicating misfolded protein aggregate accumulation, was 1.8 ± 192, 2.03 ± 0.211, 2.19 ± 0.23, and 1.68 ± 0.18 for 100, 200, 300, and 400 μM of PA, respectively. The addition of PBA reduced these values to 1.57 ± 0.141, 1.71 ± 0.134, 2.12 ± 0.198, and 1.57 ± 0.141, respectively. For TM treatment, the fold change was 2.9 ± 0.24 relative to the control (Fig. 4.8).

The relative fold change for HCT116 and CT26 cells treated with 50, 100, 150, and 200 μM PA was determined. For HCT116 cells, the fold change was 1.931 ± 0.186, 2.360 ± 0.213, 2.743 ± 0.239, and 1.712 ± 0.143, respectively. For CT26 cells, the corresponding values were 1.627 ± 0.139, 2.113 ± 0.211, 2.307 ± 0.204, and 1.433 ± 0.091. Additionally, the fold change for TM treatment was 3.170 ± 0.340 in HCT116 cells and 2.530 ± 0.237 in CT26 cells. In HCT116 cells, PBA reduced the fold change to 1.647 ± 0.280, 2.109 ± 0.230, 2.661 ± 0.216, and 1.579 ± 0.102 for 50, 100, 150, and 200 μM PA, respectively. In CT26 cells, the fold change declined to 1.389 ± 0.121, 1.780 ± 0.165, 2.250 ± 0.198, and 1.360 ± 0.091 for the same PA concentrations (Fig.10 &12).

Fluorescent images show ThT fluorescence in PA-treated IEC6, HCT116, and CT26 cells, with and without PBA treatment, demonstrating a dose-dependent relationship compared to the control. PBA reduced misfolded protein levels in IEC6 cells at 100 and 200 μM PA and HCT116 and CT26 cells at 50 and 100 μM PA. However, at higher concentrations (300 and 400 μM PA in IEC6 cells and 150 and 200 μM in HCT116 and CT26 cells), an increase in misfolded protein levels was observed, with PBA being less effective in reducing this increase (Fig 4.7,4.9 &4.11).

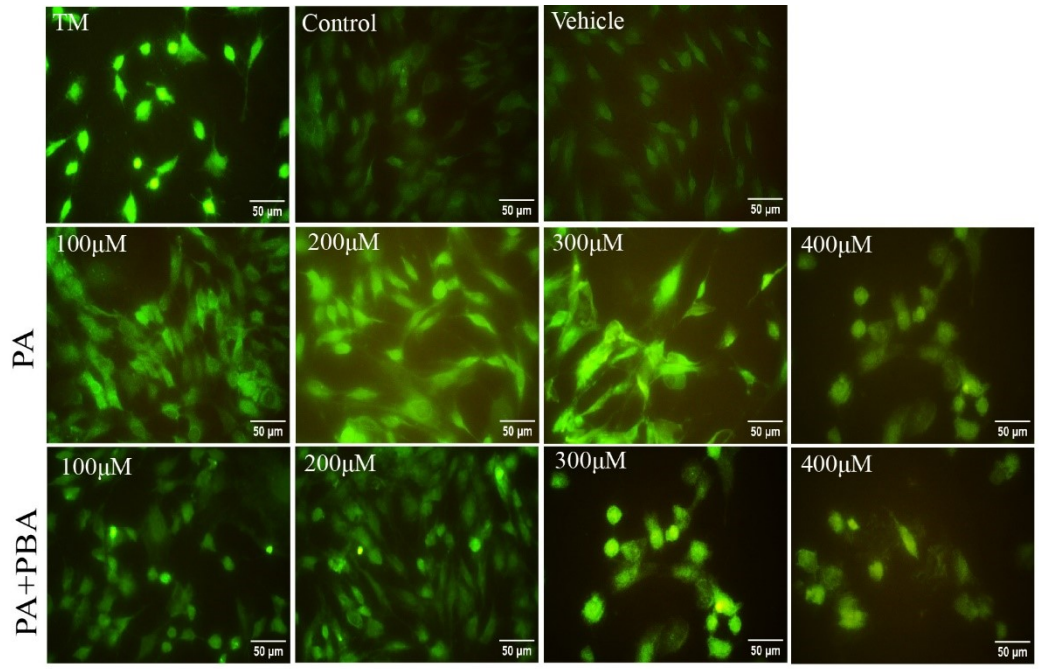

Figure 4.7 Microscopic images showing thioflavin T (ThT) fluorescence, indicating the accumulation of misfolded proteins (ER stress) in IEC6 cells under the following conditions: TM-treated positive control, untreated control, vehicle-treated, and PA-treated (100–400 µM PA), with or without PBA. Scale bar = 50 µm, magnification = 400×.

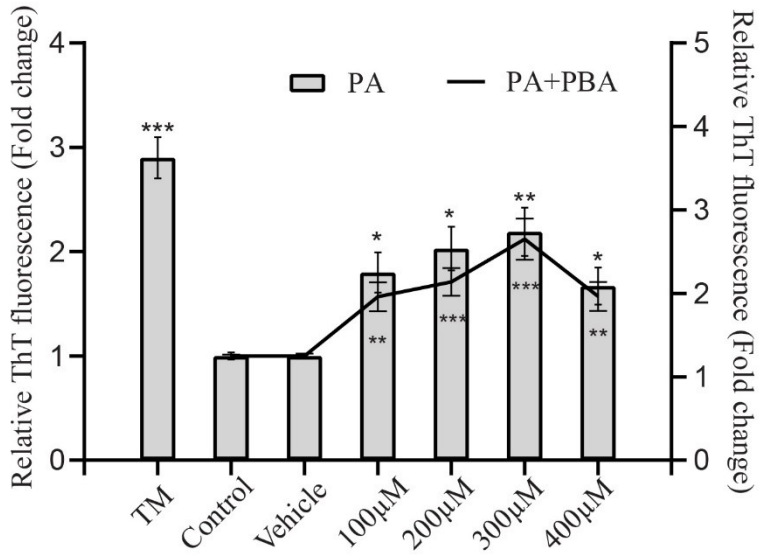

Figure 4.8 Spectrofluorimetric analysis of misfolded proteins (ER stress) in IEC6 cells under TM control, vehicle-treated, and PA-treated (100–400 µM) conditions. The bar graph represents misfolded protein accumulation levels without PBA, while the line graph represents levels with PBA. Data are presented as mean ± SD (n = 3) and analysed using one-way ANOVA. *$P < 0.05$, **$P < 0.01$, ***$P < 0.001$.

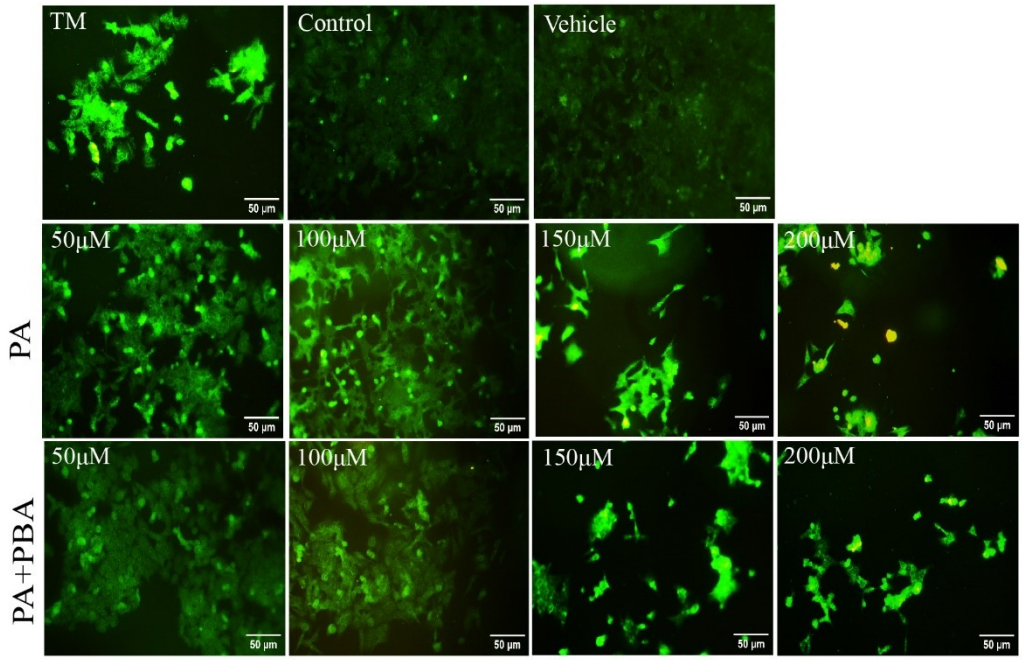

Figure 4.9 ThT fluorescence images showing misfolded protein accumulation (ER stress) in HCT116 cells under TM, untreated, vehicle, and PA (50–200 µM) treatments, with or without PBA. Scale bar = 50 µm, magnification = 400×.

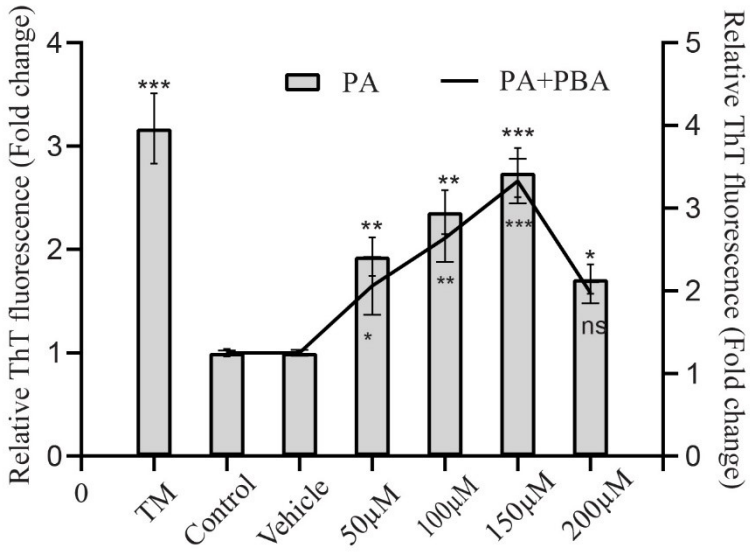

Figure 4.10 Spectrofluorimetric analysis of misfolded proteins in HCT116 cells under TM, vehicle, and PA (50–200 µM) treatments. The bar graph shows misfolded protein accumulation without PBA, and the line graph shows levels with PBA. Data are presented as mean ± SD (n = 3) and analysed by one-way ANOVA. *$P < 0.05$, **$P < 0.01$, ***$P < 0.001$.

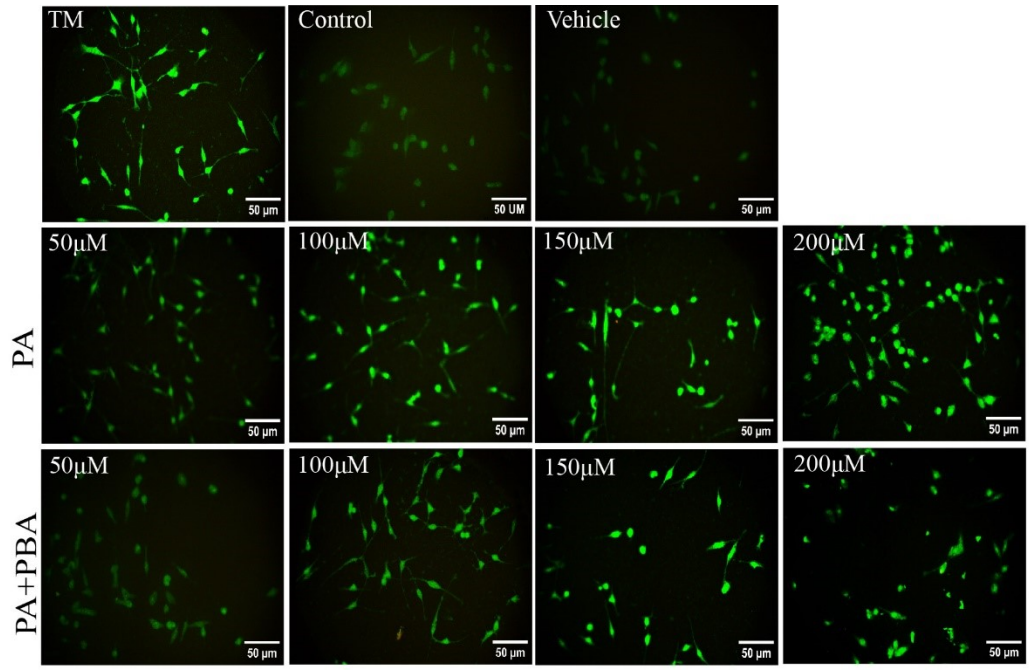

Figure 4.11 Microscopic images showing ThT fluorescence in CT26 cells under the following conditions: TM-treated positive control, untreated control, vehicle-treated, and PA-treated (50–200 µM), with or without PBA. Scale bar = 50 µm, magnification = 200×.

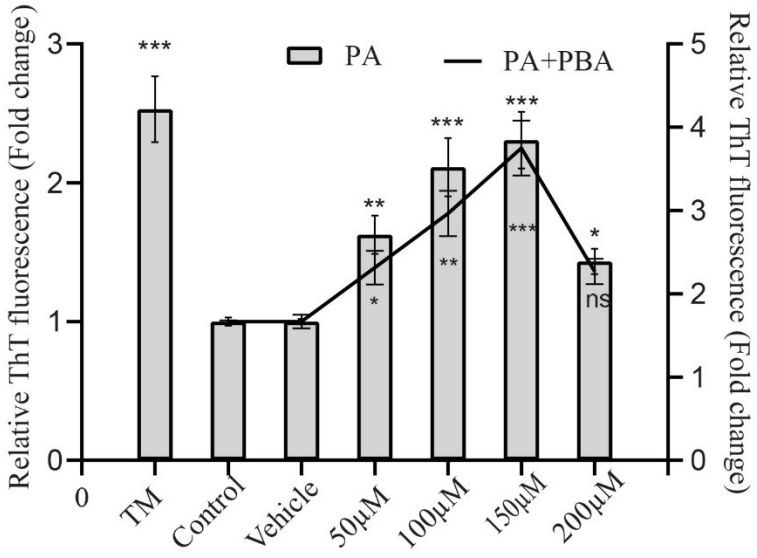

Figure 4.12 Spectrofluorimetric analysis of misfolded proteins in CT26 cells under TM, vehicle, and PA (50–200 µM) treatments. Bar graph shows accumulation without PBA, and line graph shows levels with PBA. Data are mean ± SD (n = 3), analysed by one-way ANOVA. *$P < 0.05$, **$P < 0.01$, ***$P < 0.001$.

4.3.3 Effect of palmitic acid on antioxidant enzyme activity

The levels of antioxidant enzymes SOD, CAT, GST, GR, GPX, and GSH varied in PA-treated IEC6, HCT116, and CT26 cells. SOD and CAT activity increased up to 100-200 μM in IEC6 cells, then declined at 300-400 μM. A similar trend was observed in HCT116 and CT26 cells, with elevations up to 50-100 μM and declines at 150-200 μM compared to untreated or vehicle control cells. In contrast, the levels of glutathione-related antioxidants GST, GR, GPX, and GSH remained stable up to 100-200 μM in IEC6 cells and 50-100 μM in HCT116 and CT26 cells. However, once concentrations exceeded sub-lethal doses or reached their respective IC_{50} values, antioxidant levels drastically declined in all cell types (Fig. 13, 14 & 15, Table 4.1).

4.3.4 Effect of palmitic acid on lipid peroxidation

In all PA-treated cell lines, MDA levels remained stable at sub-lethal doses—100-200 μM for IEC6 cells and 50-100 μM for HCT116 and CT26 cells - indicating no significant lipid peroxidation at these concentrations. However, MDA levels increased substantially at 300 μM in IEC6 cells and 150 μM in HCT116 and CT26 cells. At concentrations above the IC_{50}, MDA levels declined at 400 μM in IEC6 cells and 200 μM in HCT116 and CT26 cells due to extreme toxicity at these higher doses (Fig 4.16).

In untreated and vehicle control IEC6 cells, MDA levels were measured at 22.699 ± 2.305 and 19.679 ± 2.055 nanomoles/mg protein, respectively. At concentrations of 100, 200, 300, and 400 μM, MDA levels were found to be 21.809 ± 1.807, 22.749 ± 2.4, 32.217 ± 2.080, and 15.803 ± 2.301 nanomoles/mg protein, respectively (Fig 4.16 A).

For HCT116 cells, the MDA levels in untreated and vehicle control cells were 27.86 ± 2.28 and 28.51 ± 2.59 nanomoles/mg protein, respectively. After treatment with PA, MDA levels remained stable at 31.04 ± 2.87 and 33.57 ± 2.79 nanomoles/mg protein for 50 and 100 μM concentrations, respectively. However, MDA levels increased to 41.39 ± 4.20 nanomoles/mg protein at 150 μM, then decreased to 17.93 ± 2.92 nanomoles/mg protein at 200 μM (Fig 4.16 B).

Similar trends were observed in CT26 cells, with the control and vehicle-treated MDA levels measured at 38.35 ± 3.10 and 37.82 ± 3.07 nanomoles/mg protein, respectively. At 50 and 100 μM concentrations, MDA levels remained stable at 39.99 ± 3.12 and

41.29 ± 2.91 nanomoles/mg protein, respectively, similar to the baseline levels. However, significant lipid peroxidation occurred at 150 μM and 200 μM concentrations, with MDA levels increasing substantially to 49.67 ± 2.03 and 23.17 ± 1.09 nanomoles/mg protein, respectively (Fig 4.16 C).

Table 4.1 The level of antioxidants in IEC6, HCT116 and CT26 cells against palmitic acid

	Sample	SOD	CAT	GST	GR	GPX	GSH
IEC 6	Control	12.5±1.18	10±1.489	23.39±3.18	11.5±1.23	20.38±1.8	38.1±3.5
	Vehicle	12.08±1.65	9.85±1.65	23.62±2.929	11.27±1.21	19.62±1.28	38.65±2.8
	100μM	19.54±1.92	16.02±1.776	23.23±2.76	10.49±0.83	17.56±2.59	36.94±3.5
	200μM	21.21±2.19	18.44±1.44	22.8±1.89	10.3±0.95	18.46±1.8	33.19±2.7
	300μM	17.8±1.16	14.32±1.13	16.65±1.99	7.08±0.87	14.31±1.54	27.74±3.4
	400μM	8.85±1.33	6.25±0.99	14.34±1.02	5.81±0.92	7.66±1.9	19.29±4.39
HCT116	Control	16.13±1.8	12.5±1.25	15.55±2.12	17.9±1.02	23.26±2.34	94.25±11.07
	Vehicle	17.87±1.93	13.06±1.1	15.01±1.9	17.03±2.5	23.02±2.67	90.05±13.08
	50μM	26.79±2.43	17.62±1.4	16.24±2.25	17.28±2.7	27.97±2.98	94.25±15.93
	100μM	28.61±2.9	19.41±1.77	16.27±2.38	18.21±2.19	30.28±2.43	95.24±15.05
	150μM	22.62±2.54	7.03±2.67	9.24±1.92	10.28±2.28	15.27±2.56	58.74±6.5
	200μM	7.29±2.18	5.46±2.33	5.23±3.02	6.28±2.92	9.27±3.12	28.49±5.95
CT26	Control	15.57±1.63	12.02±1.39	26.37±2.48	23.19±1.28	29.37±3.48	56.974±4.461
	Vehicle	16.67±2.13	11.92±1.79	26.61±2.39	23.63±2.61	28.6±2.39	57.825±3.85
	50μM	21.26±1.53	18.59±1.46	25.76±2.29	23.08±2.45	26.75±2.29	55.787±4.8
	100μM	22.68±2.09	19.84±2.15	24.97±2.48	22.51±2.74	27.97±2.47	53.509±4.15
	150μM	9.52±1.65	7.24±1.13	20.01±1.4	16.96±1.94	21.91±2.47	42.324±3.98
	200μM	4.21±1.17	3.98±1.64	9.68±0.88	12.72±1.77	15.68±2.89	11.243±2.43

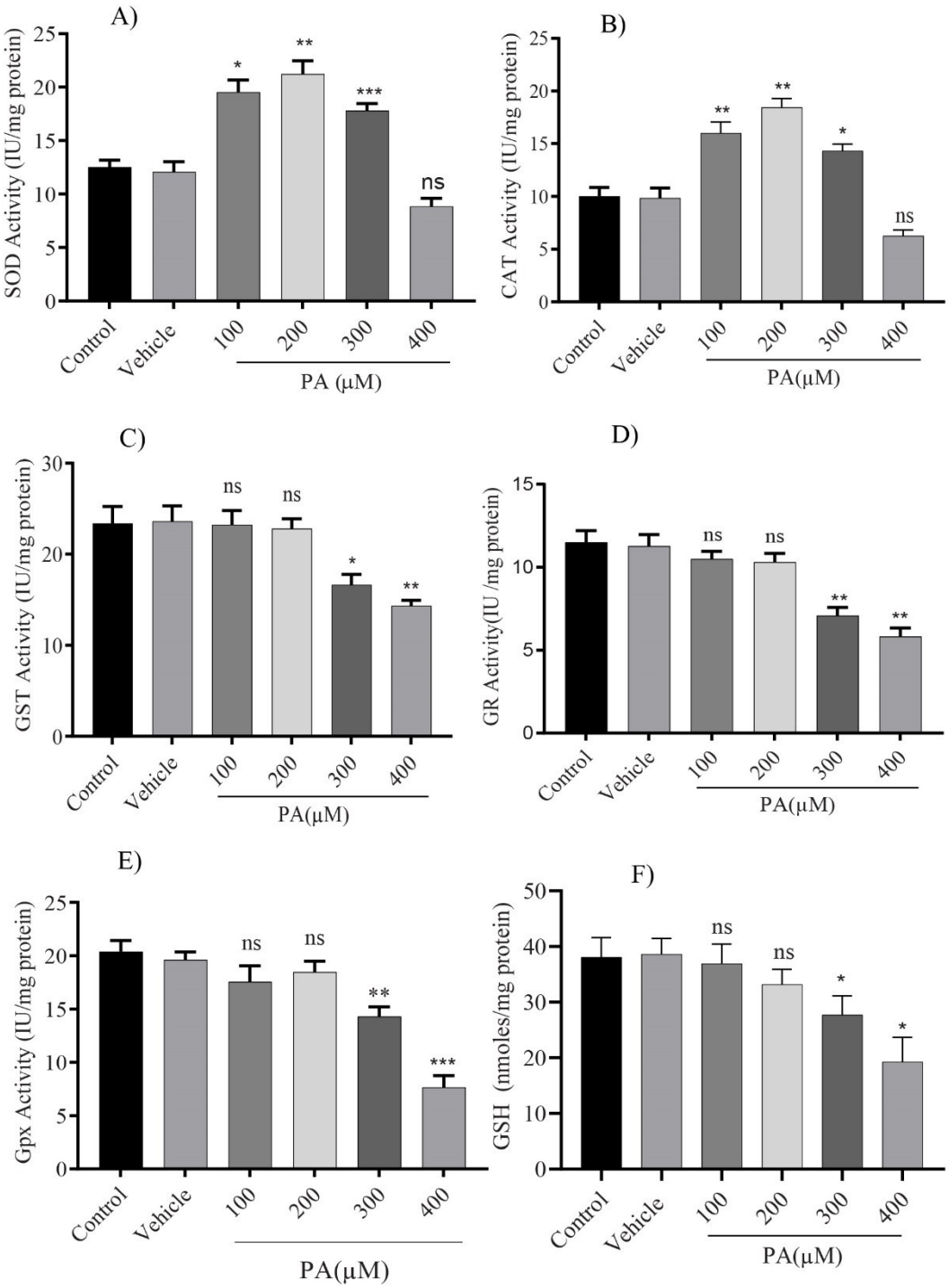

Figure 4.13 Effects of PA on antioxidant levels in IEC6 cells. Bar graphs show (A) SOD, (B) CAT, (C) GST, (D) GR, (E) GPx activities (IU/mg protein), and (F) GSH concentration (nmol/mg protein) under control, vehicle, and PA-treated (100–400 μM) conditions. Data are presented as mean ± SD (n = 3), analysed by one-way ANOVA with Tukey's test. Significance: *$P < 0.05$, **$P < 0.01$, ***$P < 0.001$.

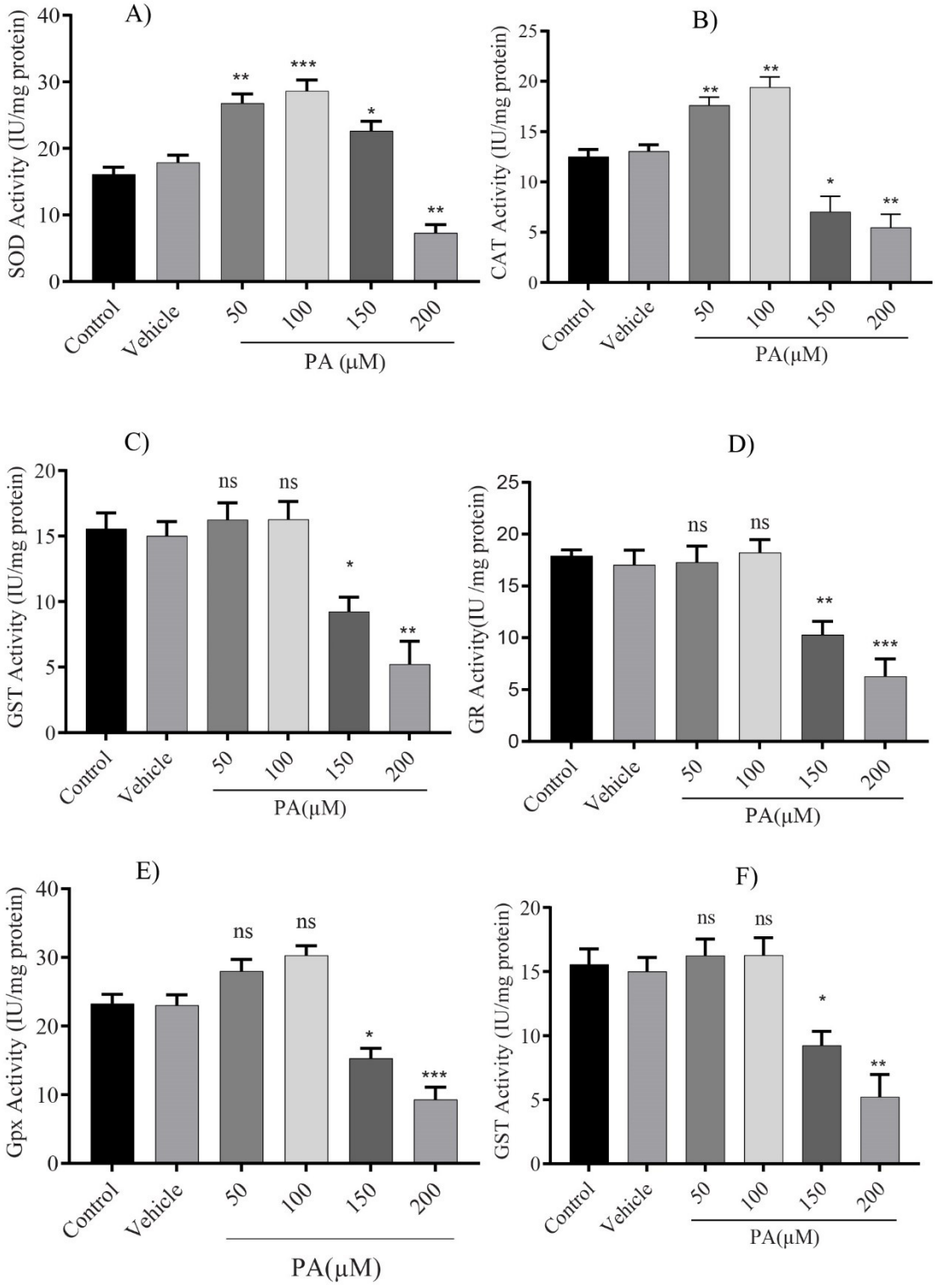

Figure 4.14 Effects of PA (50–100 μM) on antioxidants in HCT116 cells. Bar graphs show (A) SOD, (B) CAT, (C) GST, (D) GR, (E) GPx (IU/mg protein), and (F) GSH (nmol/mg protein). Data are mean ± SD (n = 3), analysed by ANOVA with Tukey's test *(*P < 0.05, **P < 0.01, ***P < 0.001)*.

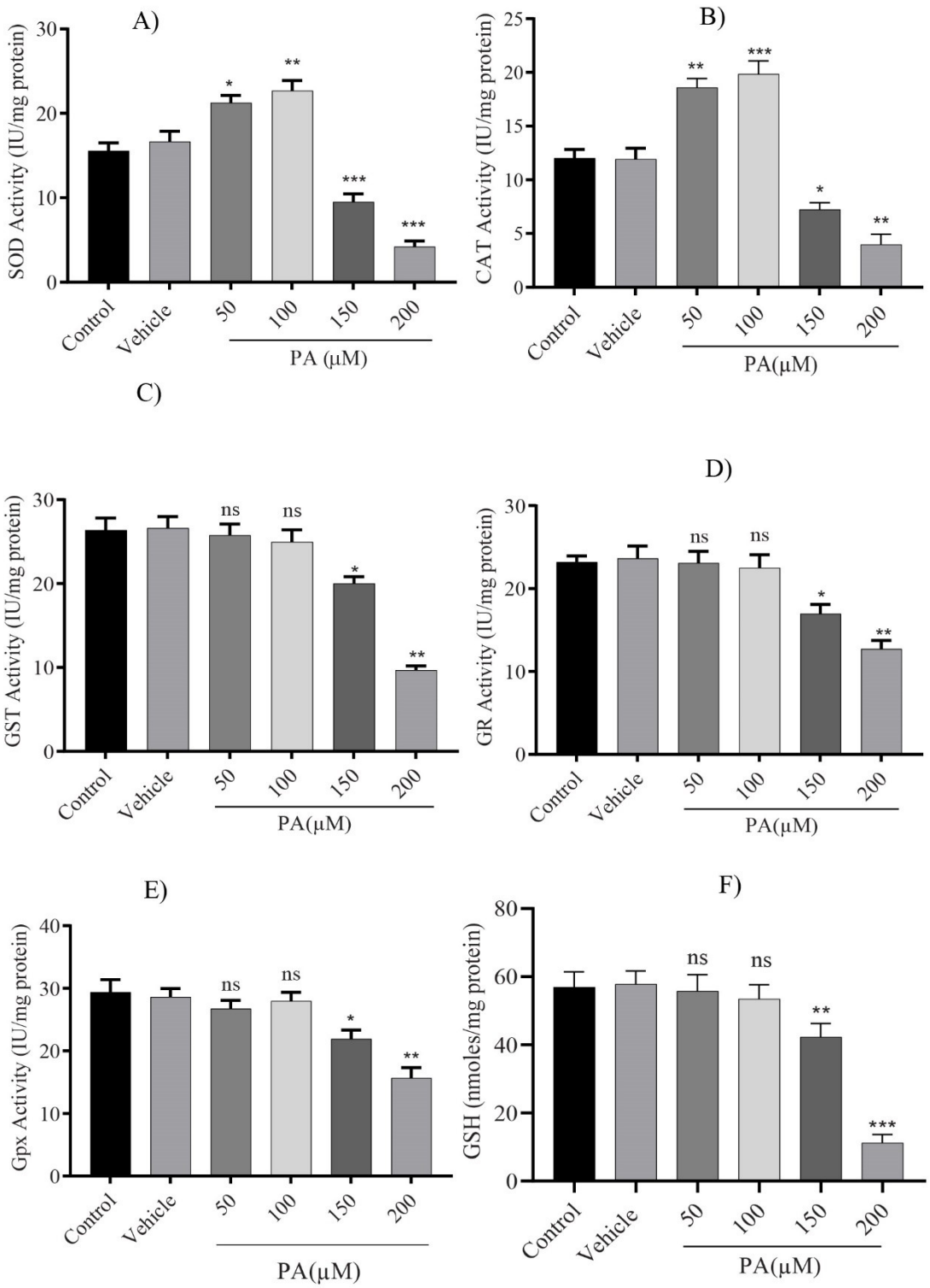

Figure 4.15 Effects of PA (50–100 μM) on (A) SOD, (B) CAT, (C) GST, (D) GR, (E) GPx, and (F) GSH in CT26 cells. Data are mean ± SD (n = 3), analysed by ANOVA *(*P < 0.05, **P < 0.01, ***P < 0.001)*.

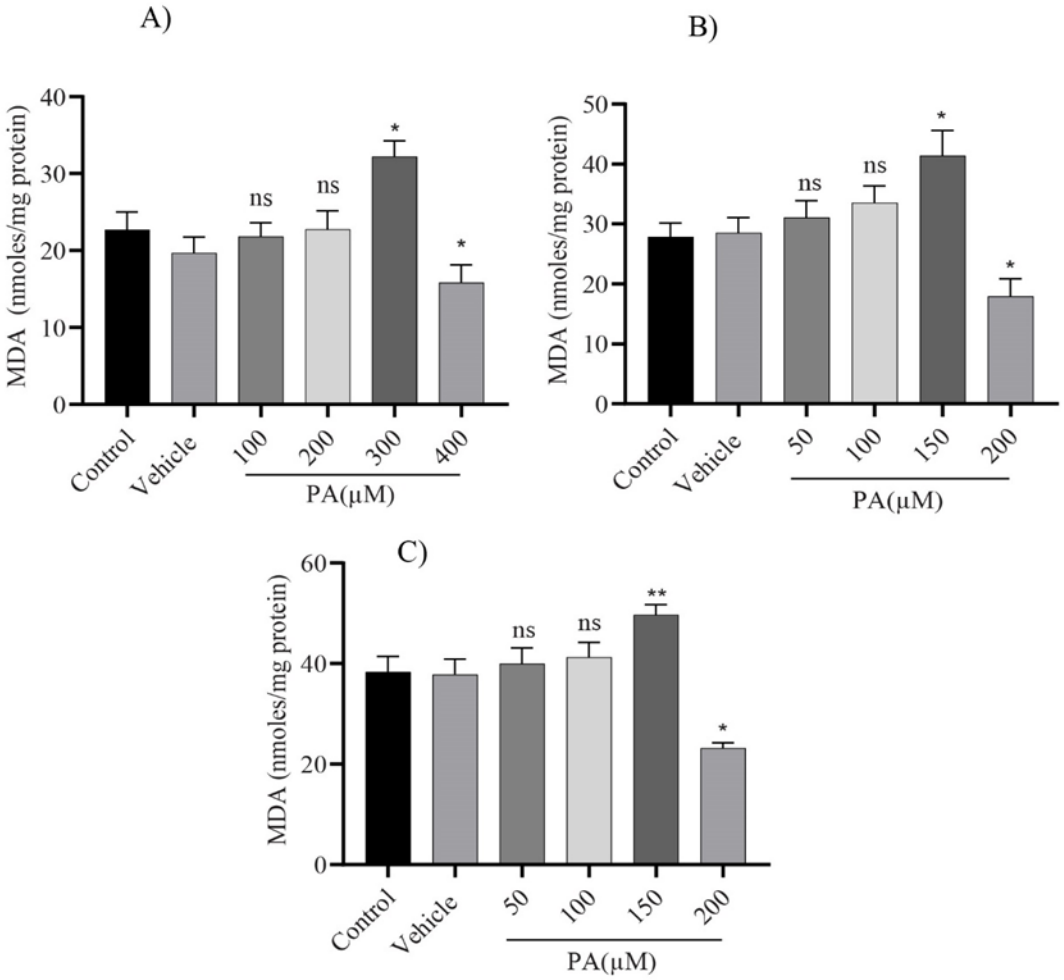

Figure 4.16 Effects of PA on MDA levels, indicating lipid peroxidation, in (A) IEC6 (100–400 μM PA), (B) HCT116 (50–400 μM PA), and (C) CT26 (50–200 μM PA) cells under control, vehicle, and PA-treated conditions. Data are mean ± SD (n = 3), analysed by one-way ANOVA with Tukey's test *(*P < 0.05, **P < 0.01, ***P < 0.001).*

4.3.5 Effects of palmitic acid on the expression of antioxidant genes

Nrf2 expression was up-regulated in IEC6 cells by 2.67 ± 0.31 and 3.31 ± 0.25-fold with 100 and 200 μM of PA, respectively, compared to the control. In HCT116 cells, the expression increased to 8.36 ± 0.14 and 11.00 ± 0.20-fold with 50 and 100 μM of PA. In CT26 cells, the expression was 4.95 ± 0.15 and 5.80 ± 0.10-fold with the same concentrations of PA as in HCT116 (Fig 4.17A-C).

Similarly, the expression of the *Nqo1* gene in IEC6 cells was enhanced by 1.82 ± 0.10 and 2.26 ± 0.09-fold with 100 and 200 μM of PA, respectively. In HCT116 and CT26 cells, *Nqo1* gene expression increased to 5.92 ± 0.16 and 3.4 ± 0.012-fold at 50 μM, but decreased to 5.038 ± 0.075 and 4.17 ± 0.12-fold at 100 μM of PA, compared to the control, respectively (Fig 4.17D-E).

In IEC6 cells, the expression of *Ho-1* increased by 1.95 ± 0.05 and 2.53 ± 0.03-fold with 100 and 200 μM of PA, respectively. In HCT116 cells, the fold change increased to 3.60 ± 0.05 for 50 μM and 2.87 ± 0.03 for 100 μM of PA. In CT26 cells, the fold change rose to 3.88 ± 0.16 for 50 μM and then decreased to 5.77 ± 0.35 for 100 μM of PA compared to the control (Fig 4.17 F-H).

4.3.6. Upregulation of ERS markers *Bip, chop*, and *Atf6*

In IEC6 cells, exposure to PA at 100 and 200 μM concentrations led to a respective increase in *Bip* expression by approximately 1.71 ± 0.07 and 2.60 ± 0.05-fold. Similarly, HCT116 cells showed elevated *Bip* expression of 2.92 ± 0.15 and 3.65 ± 0.05-fold with 50 and 100 μM PA concentrations. CT26 cells exhibited similar trends with fold changes of 2.06 ± 0.07 and 3.09 ± 0.12-fold compared to the control (Fig. 4.18A-C).

Chop gene expression in IEC6 cells increased by 1.78 ± 0.03 and 2.08 ± 0.08-fold under 100 and 200 μM of PA, respectively. Similarly, HCT116 and CT26 cells showed increases of 2.33 ± 0.08 and 1.99 ± 0.02-fold at 50 μM and 3.12 ± 0.13 and 2.90 ± 0.19-fold at 100 μM of PA, respectively, compared to the control (Fig 4.18 D-F).

Furthermore, *Atf6* expression in IEC6 cells was up-regulated by approximately 1.57 ± 0.12 and 1.84 ± 0.07-fold under 100 and 200 μM of PA, respectively. In HCT116 and CT26 cells, similar increases were observed, with fold changes of 2.34 ± 0.12 and 2.63 ± 0.08 for 50 μM and 3.01 ± 0.16 and 3.16 ± 0.17 for 100 μM of PA, respectively (Fig 4.18 G-H).

4.3.7 Activation of *Perk/Atf4* arm of UPR

In IEC6 cells, *Perk* expression increased by 2.66 ± 0.14-fold with 100 μM of PA and decreased at 2.10 ± 0.15-fold with 200 μM compared to the control. In HCT116 cells, *Perk* expression rose to 3.66 ± 0.16-fold with 50 μM and 4.48 ± 1.17-fold with 100 μM of PA. Similarly, in CT26 cells, *Perk* expression levels were 3.11 ± 0.15-fold with 50 μM and 4.20 ± 0.51-fold with 100 μM of PA (Fig 4.19A-C). Additionally, *Atf4* gene expression in IEC6 cells increased by approximately 2.26 ± 0.15-fold with 100 μM and decreased by 1.87 ± 0.13-fold with 200 μM of PA. In HCT116 and CT26 cells, *Atf4* gene expression rose to 3.39 ± 0.51-fold and 3.15 ± 0.36-fold with 50 μM, and 4.10 ± 0.40-fold and 4.30 ± 0.45-fold with 100 μM of PA, respectively (Fig 4.19 D-F).

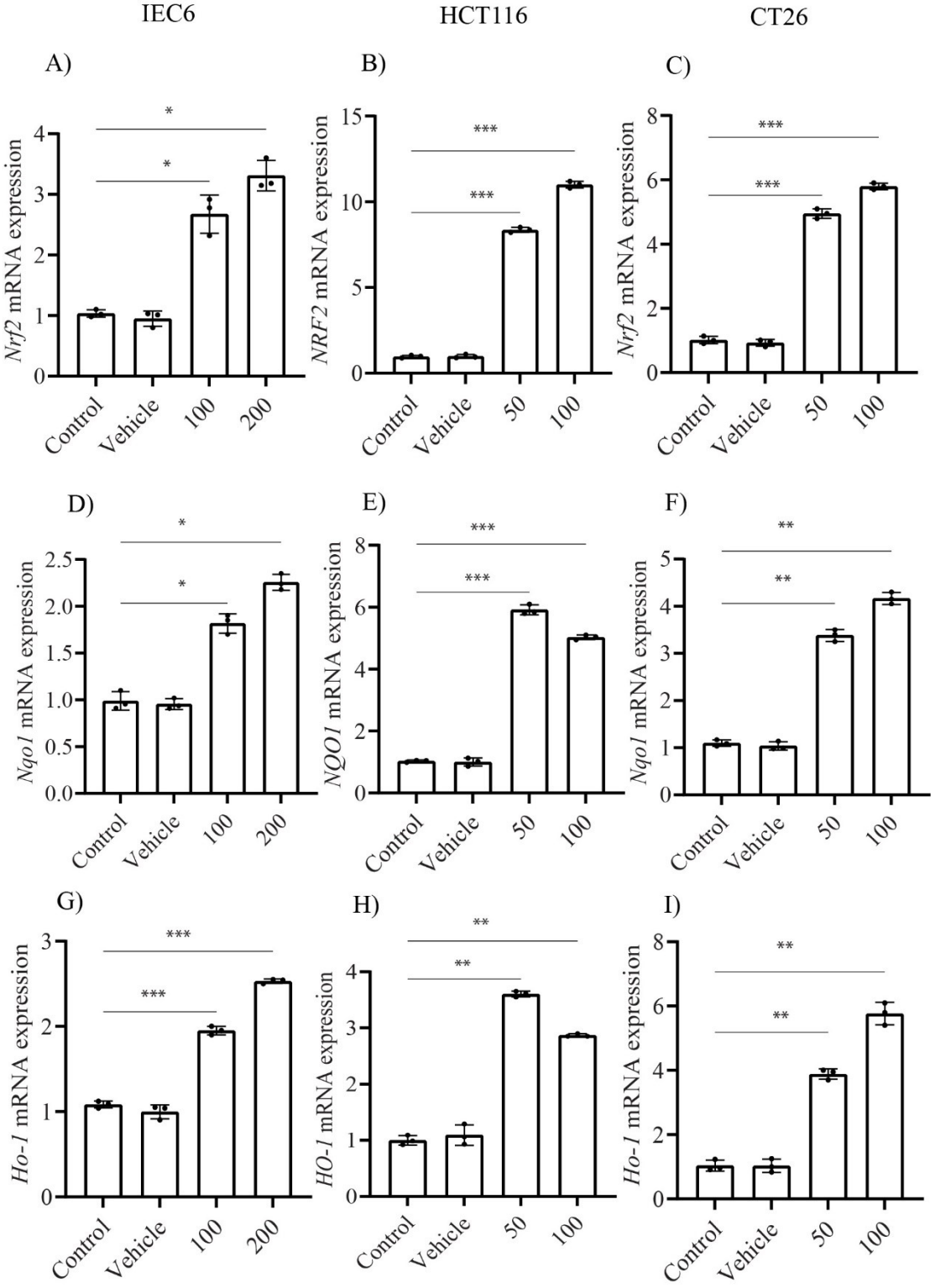

Figure 4.17. Effect of PA on antioxidant gene expression in IEC6, HCT116, and CT26 cells. RT-PCR bar graphs show fold change in gene expression relative to control, with PA concentrations indicated for each cell line: IEC6 (100-200 μM), HCT116 (50-100 μM), and CT26 (50-100 μM). (A–C) *Nrf2,* (D–F) *Nqo1*, and (G–I) *Ho-1* expression. Data are mean ± SD (n = 3), analysed by one-way ANOVA with Dunnett's test. *$P < 0.05$, **$P < 0.01$, ***$P < 0.001$.

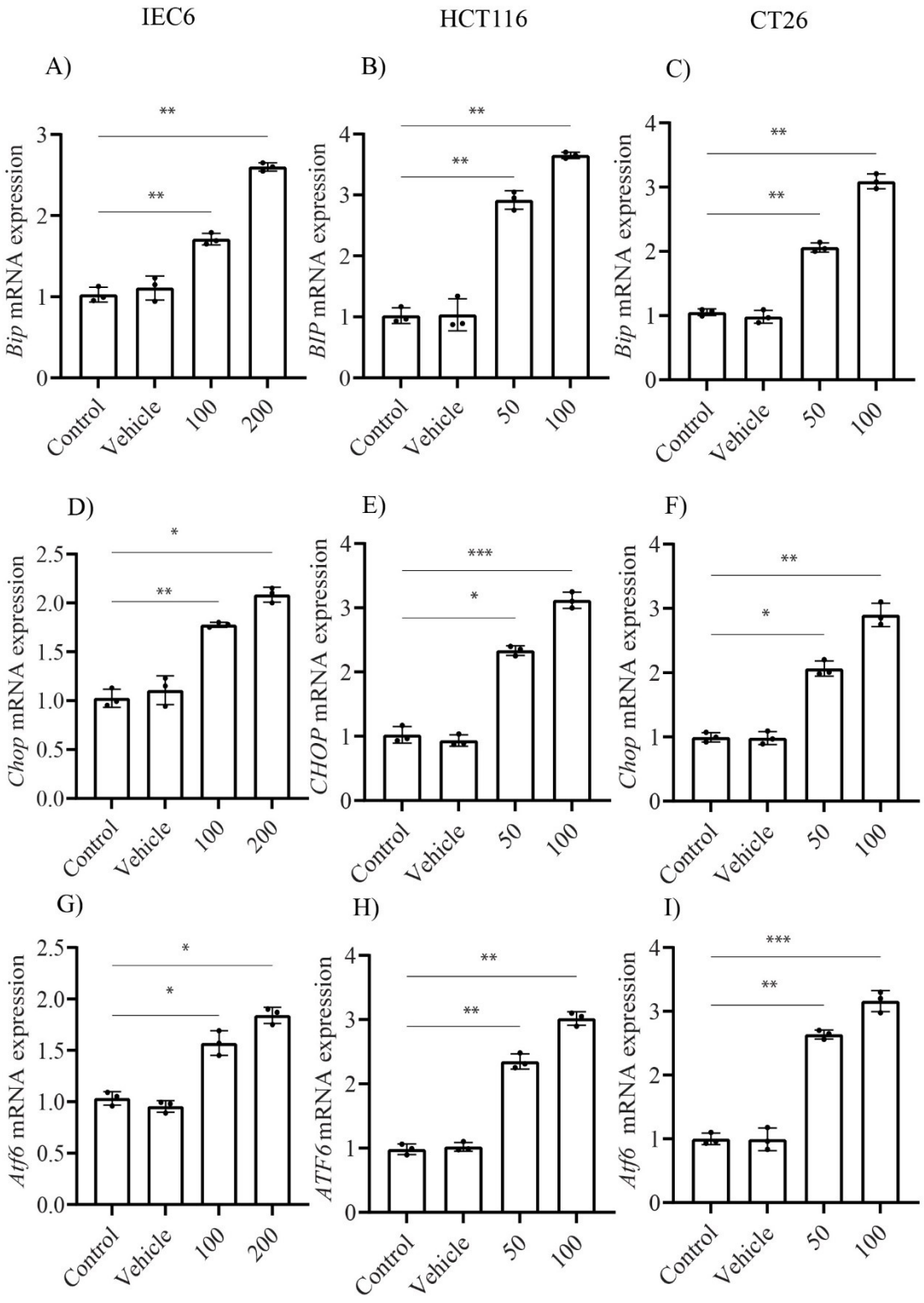

Figure 4.18. Effect of PA on ER stress markers in IEC6 (100-200 µM), HCT116 (50-100 µM), and CT26 (50-100 µM) cells. RT-PCR bar graphs show fold change in *Bip* (A–C), *Chop* (D–F), and *Atf6* (G–I) expression relative to control. Data are mean ± SD (n = 3), analysed by one-way ANOVA with Dunnett's test. *$P < 0.05$, **$P < 0.01$, ***$P < 0.001$.

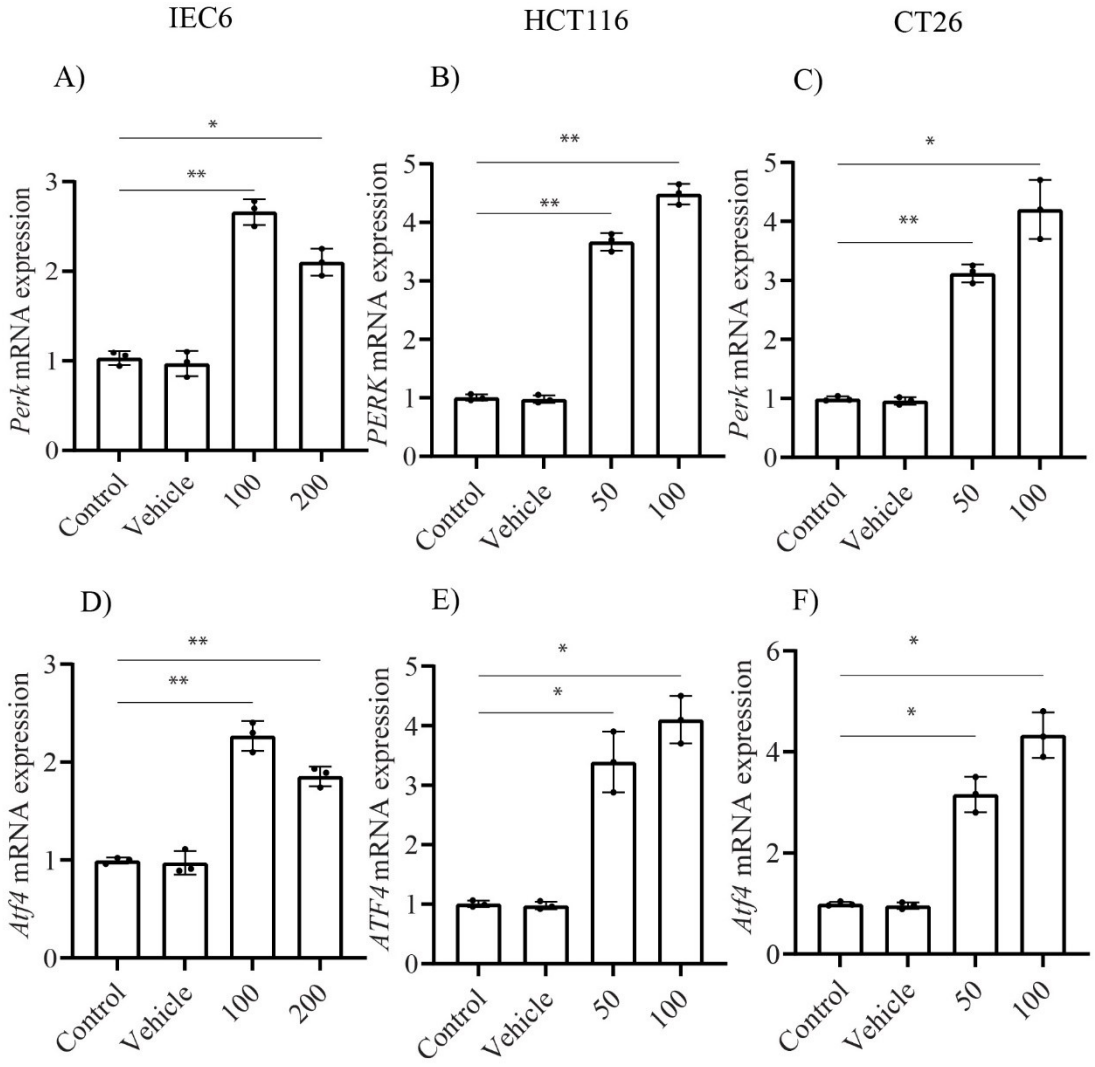

Figure 4.19. Effect of PA on *Perk/Atf4* expression in IEC6 (100-200 µM), HCT116 (50-100 µM), and CT26 (50-100 µM) cells. Bar graphs show fold change in *Perk* (A–C) and *Atf4* (D–F) expression relative to control. Data are mean ± SD (n = 3), analysed by one-way ANOVA with Dunnett's test. *$P < 0.05$, **$P < 0.01$, ***$P < 0.001$.

4.3.8 Palmitic acid-induced acidic vacuoles

This investigation examined the effect of PA on the formation of acidic vacuoles IEC6 HCT116 and CT26 cells as a marker of early-phase autophagic responses. Acridine orange was employed for spectrofluorimetric analysis and fluorescent microscopy, which allowed for detecting the wavelength characteristic of acidic autolysosomes. HBSS treatment served as a positive control to confirm starvation-induced autophagic responses across all cell lines.

In IEC6 cells, the normalized fluorescent intensity in response to various concentrations of PA exhibited a dose-dependent increase. The recorded intensities were as follows: 1.90 ± 0.02 for 100 μM, 2.35 ± 0.03 for 200 μM, 3.10 ± 0.03 for 300 μM, 1.23 ± 0.03 for 400 μM PA, and 4.20 ± 0.02 for HBSS treatment (Fig. 4.20B).In HCT116 cells, the normalized fluorescent intensity across various concentrations of PA was measured as follows: 1.57 ± 0.02 for 50 μM, 1.93 ± 0.02 for 100 μM, 2.16 ± 0.03 for 150 μM, 1.35 ± 0.02 for 200 μM PA concentration, and notably, 3.93 ± 0.03 for HBSS (Fig. 14.21B).In CT26 cells, the normalized fluorescent intensities across various concentrations of PA were recorded as follows: 1.42 ± 0.01 for 50 μM, 1.72 ± 0.02 for 100 μM, 2.04 ± 0.01 for 150 μM, 1.26 ± 0.02 for 200 μM PA concentration, and 2.53 ± 0.02 for HBSS (Fig. 14.22B).

Fluorescent imaging substantiated the dose-dependent trend observed in the spectrofluorimetric analysis. In IEC6 cells, acidic vacuoles were distributed consistently up to 200 μM, whereas in HCT116 and CT26 cells, the distribution was evident up to 100 μM. At higher concentrations, substantial fused autolysosomes became apparent. These findings collectively indicate that PA affects the formation of acidic vacuoles in both normal intestinal and colon cancer cells in a dose-dependent manner, with higher concentrations leading to the formation of larger fused autolysosomes (Fig. 14.20A,14.21A, & 14.22A).

4.3.9 Effect of palmitic acid on autophagic flux

PA treatment triggered autophagic flux in both IEC6 and HCT116 and CT26 cells, which was confirmed through spectrofluorimetric analysis and fluorescent microscopy using Monodansyl-cadaverine as a marker. Treatment with HBSS served as a positive control, resulting in starvation-induced elevation of autophagic flux in the cells. This further supports the role of PA in modulating autophagy in these cells.

The investigation assessed the normalized fluorescent intensity across various concentrations of PA in IEC6 cells. The measured intensities were as follows: 1.65 ± 0.019 for 100 μM, 2.34 ± 0.014 for 200 μM, 2.76 ± 0.013 for 300 μM, 1.76 ± 0.011 for 400 μM, and 3.13 ± 0.033 for HBSS treatment (Fig. 4.14 H). These results demonstrate a dose-dependent increase in fluorescent intensity up to 300 μM PA, followed by a decrease at the highest concentration of 400 μM. HBSS treatment shows the highest intensity (Fig.4.23B).

For HCT116 cells, the normalized fluorescent intensity was measured and recorded as follows: 1.57 ± 0.015 for 50 μM, 1.97 ± 0.012 for 100 μM, 2.59 ± 0.010 for 150 μM, 1.64 ± 0.010 for 200 μM PA, and 2.87 ± 0.012 for HBSS treatment (Fig. 4.24B). Similarly, for CT26 cells, the normalized fluorescent intensity measurements were as follows: 1.43 ± 0.014 for 50 μM PA, 1.81 ± 0.012 for 100 μM, 2.26 ± 0.013 for 150 μM, 1.42 ± 0.013 for 200 μM, and 2.63 ± 0.016 for HBSS treatment (Fig. 4.25B).

Fluorescent imaging substantiated the dose-dependent trend observed in the spectrofluorimetric analysis. Greyscale intensity plot profiles of fluorescent images indicate the corresponding green and red fluorescence in IEC6, HCT116, and CT26 cells associated with acidic vacuole generation in response to PA treatment (Fig. 4.21, 4.23, & 4.25). In IEC6 cells, acidic vacuoles were distributed consistently up to 200 μM, whereas in HCT116 and CT26 cells, the distribution was evident up to 100 μM. At higher concentrations, substantial fused autolysosomes became apparent. These findings collectively indicate that PA affects the formation of acidic vacuoles in both normal intestinal and colon cancer cells in a dose-dependent manner, with higher concentrations leading to the formation of larger fused autolysosomes (Fig. 14.20A,14.21A, & 14.22A).

4.3.10 Effect of PA on *Beclin 1* and *Lc3b1* expression

The study explored the expression of *Beclin 1* and *Lc3b1* genes, key markers for autophagic responses, in IEC6, HCT116, and CT26 cells treated with sublethal doses of PA. IEC6 cells were treated with 100 and 200 μM, while HCT116 and CT26 cells were treated with 50 and 100 μM of PA. The impact of these treatments on the autophagic pathways was assessed by measuring the expression levels of *Beclin* 1 and *Lc3b1,* which are associated with the initiation and progression of autophagy, respectively.

The expression of *Beclin 1* in IEC6 cells showed a dose-dependent up-regulation with 100 and 200 μM of PA, increasing by 1.84 ± 0.13 and 2.36 ± 0.21423-fold, respectively,

compared to the control. In HCT116 cells, *Beclin 1* expression rose to 2.077 ± 0.2081 and 2.853 ± 0.240-fold with 50 and 100 μM of PA, respectively. Similarly, in CT26 cells, the expression of *Beclin 1* increased by 1.9 ± 0.1932 and 2.8 ± 0.274-fold at the same concentrations of PA as observed in HCT116 cells (Fig. 4.26 A, B& C). The expression of the *Lc3b1* gene in IEC6 cells increased by 1.93 ± 0.135 and 2.9474 ± 0.2053-fold with 100 and 200 μM of PA, respectively. In HCT116 and CT26 cells, *Lc3b1* gene expression rose to 2.51 ± 0.227 and 3.436 ± 0.158-fold for 50 μM, and 3.13 ± 0.3743 and 3.74 ± 0.27874-fold for 100 μM of PA, compared to the control, respectively (Fig. 4.26 D, E& F).

4.3.11 Influence of palmitic acid on the expression of *Ire1 /Xbp1*

The study examined the expression of *Ire1* and *Xbp1*, key UPR (unfolded protein response) genes, and their associated endoplasmic reticulum (ER) stress responses in IEC6, HCT116, and CT26 cells exposed to sublethal doses of PA. Specifically, IEC6 cells were treated with 100 and 200 μM, while HCT116 and CT26 cells were treated with 50 and 100 μM of PA. The goal was to assess how PA treatment influences the UPR pathway and ER stress markers across different cell types.

The study observed that IRE1 expression in IEC6 cells was significantly up-regulated by 2.88 ± 0.362-fold and 3.7 ± 0.387-fold when treated with 100 and 200 μM of PA, respectively, compared to the control. In HCT116 cells, *Ire1* expression increased to 3.967 ± 0.363-fold and 4.693 ± 0.24-fold with 50 and 100 μM of PA, respectively. Similarly, CT26 cells showed an increase in *Ire1* expression by 3.497 ± 0.361-fold and 4.127 ± 0.16250-fold with the same concentrations of PA (Fig.4.27A, B&C).

The expression of the *Xbp1* gene in IEC6 cells was significantly enhanced by 1.81 ± 0.139-fold and 2.332 ± 0.242-fold with 100 and 200 μM of PA, respectively. In HCT116 cells, *Xbp1* gene expression increased to 2.343 ± 0.351-fold with 50 μM and 3.19 ± 0.344-fold with 100 μM of PA. Similarly, in CT26 cells, *Xbp1* gene expression rose to 2.897 ± 0.215-fold with 50 μM and 3.980 ± 0.2-fold with 100 μM of PA compared to the control (Fig.4.27D, E&F).

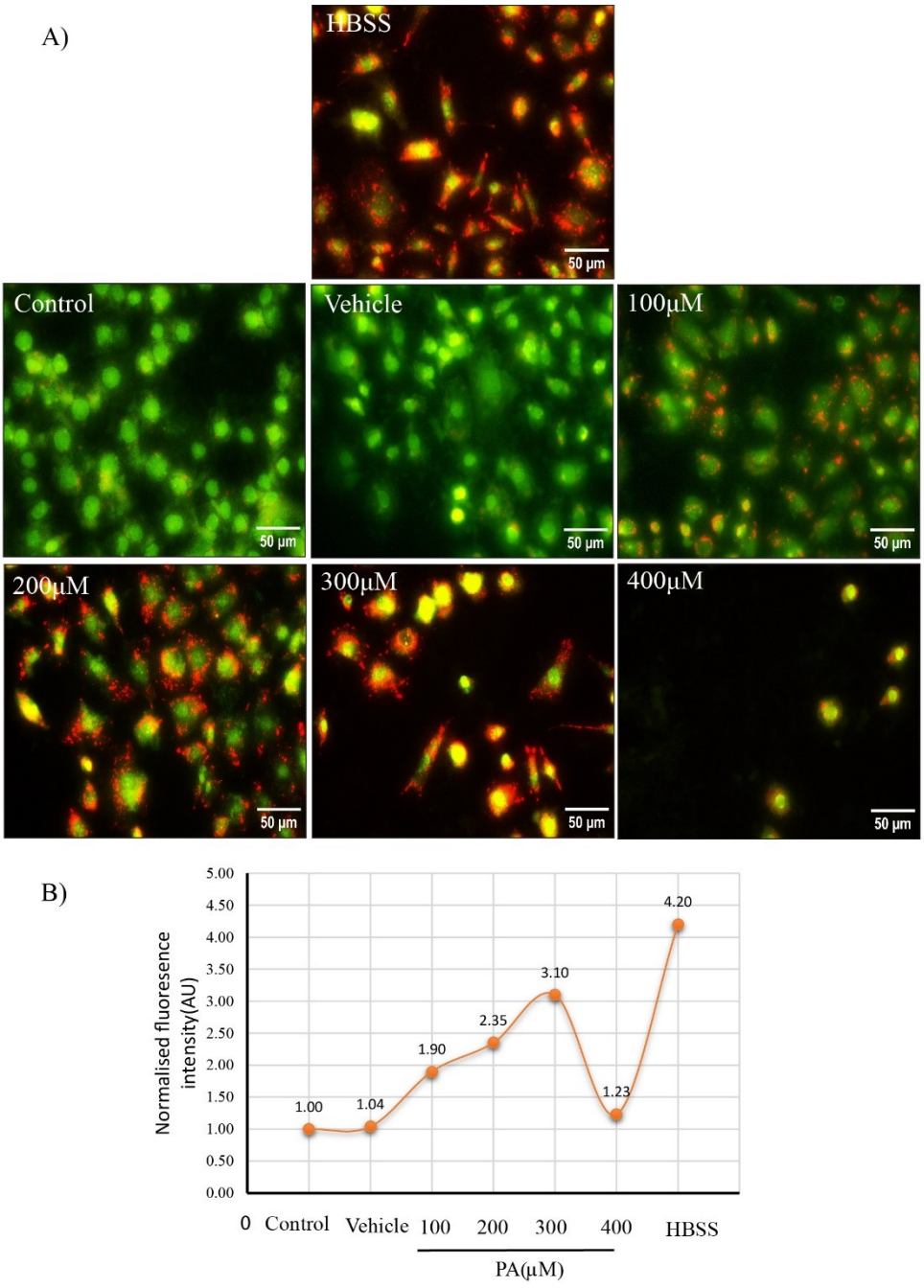

Figure 4.20 PA-induced acidic vacuole formation in IEC6 cells. (A) Fluorescence images show IEC6 cells under different conditions, including control, vehicle, 100–400 µM PA, and HBSS (positive control), with a scale bar of 50 µm and magnification of 400×. (B) Graph depicting background-subtracted fluorescence intensity (arbitrary units) of acridine orange, indicating acidic vacuole formation, as measured by spectrofluorimetric analysis in IEC6 cells. Acridine orange was excited at 488 nm, with emissions at 525 nm (green) and 650 nm (red).

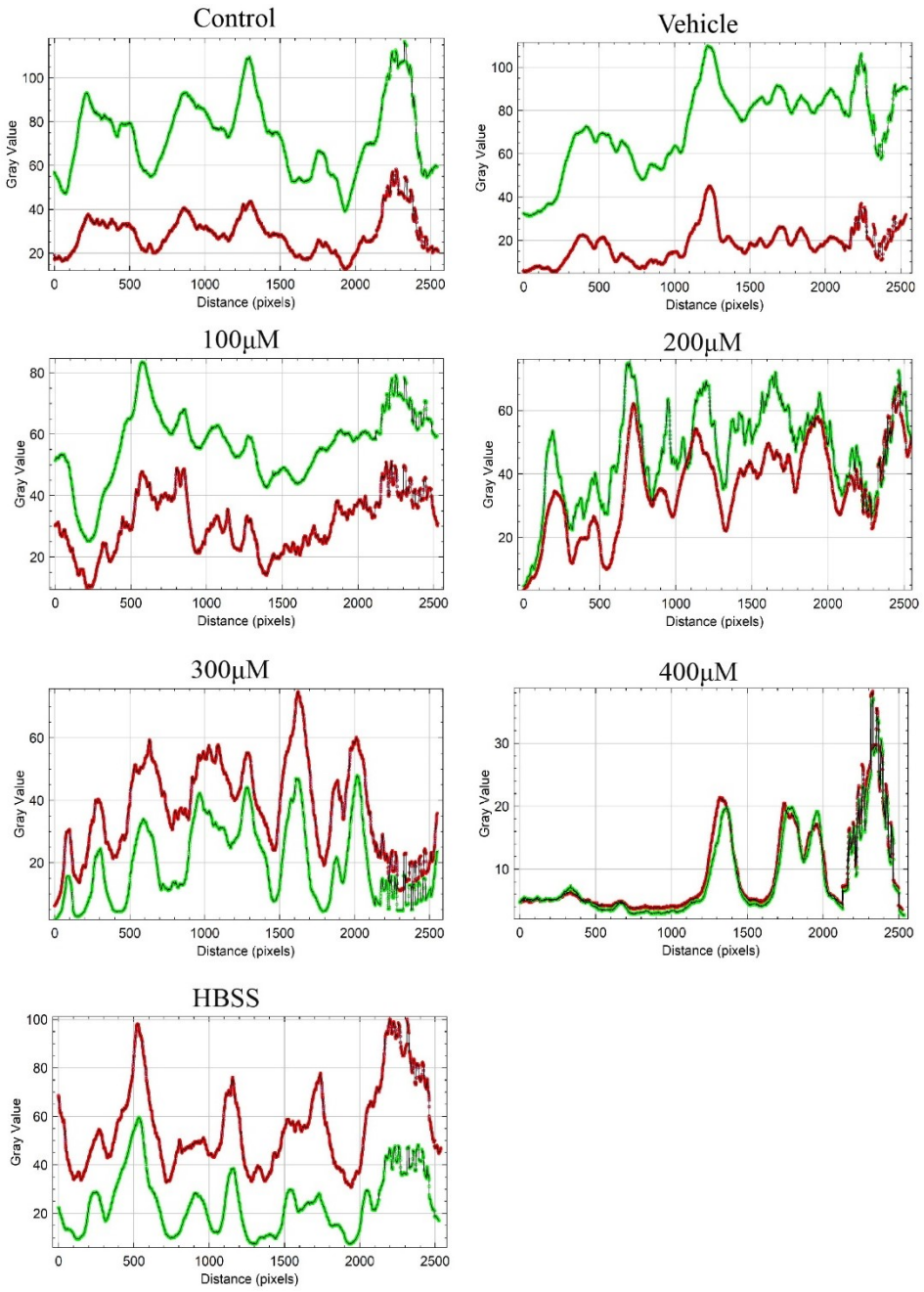

Figure 4.21 Grayscale intensity profiles of green (nucleic acid) and red (acidic vacuole) fluorescence in acridine orange–stained IEC6 cells. ImageJ analysis was performed on fluorescent images from normal, vehicle, and PA-treated cells (100–400 µM), with HBSS as a positive control. The plot compares control, vehicle, and PA-treated conditions, highlighting fluorescence variations related to acidic vacuole accumulation. (Acridine orange excited at 488 nm emissions 525 nm (green) and 650 nm (red)).

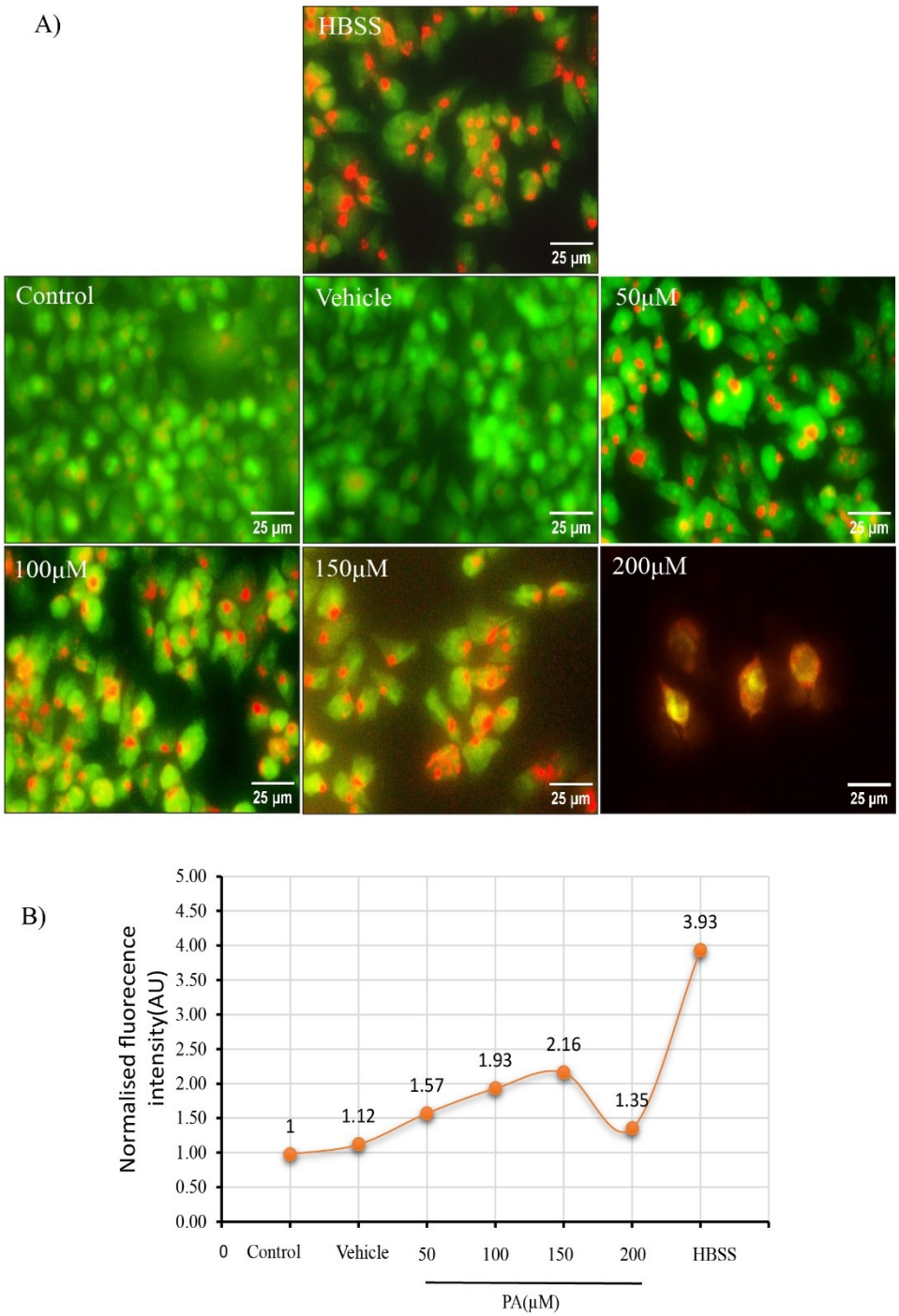

Figure 4.22 (A) Fluorescent images of PA-induced acidic vacuoles in HCT116 cells (control, vehicle, 50-100 µM PA, HBSS), scale bar: 25 µm, magnification: 400x. (B) Graph of background-subtracted fluorescence intensity (AU) of acridine orange, indicating acidic vacuole formation, measured by spectrofluorimetric analysis (excitation: 488 nm, emission: 525 nm and 650 nm).

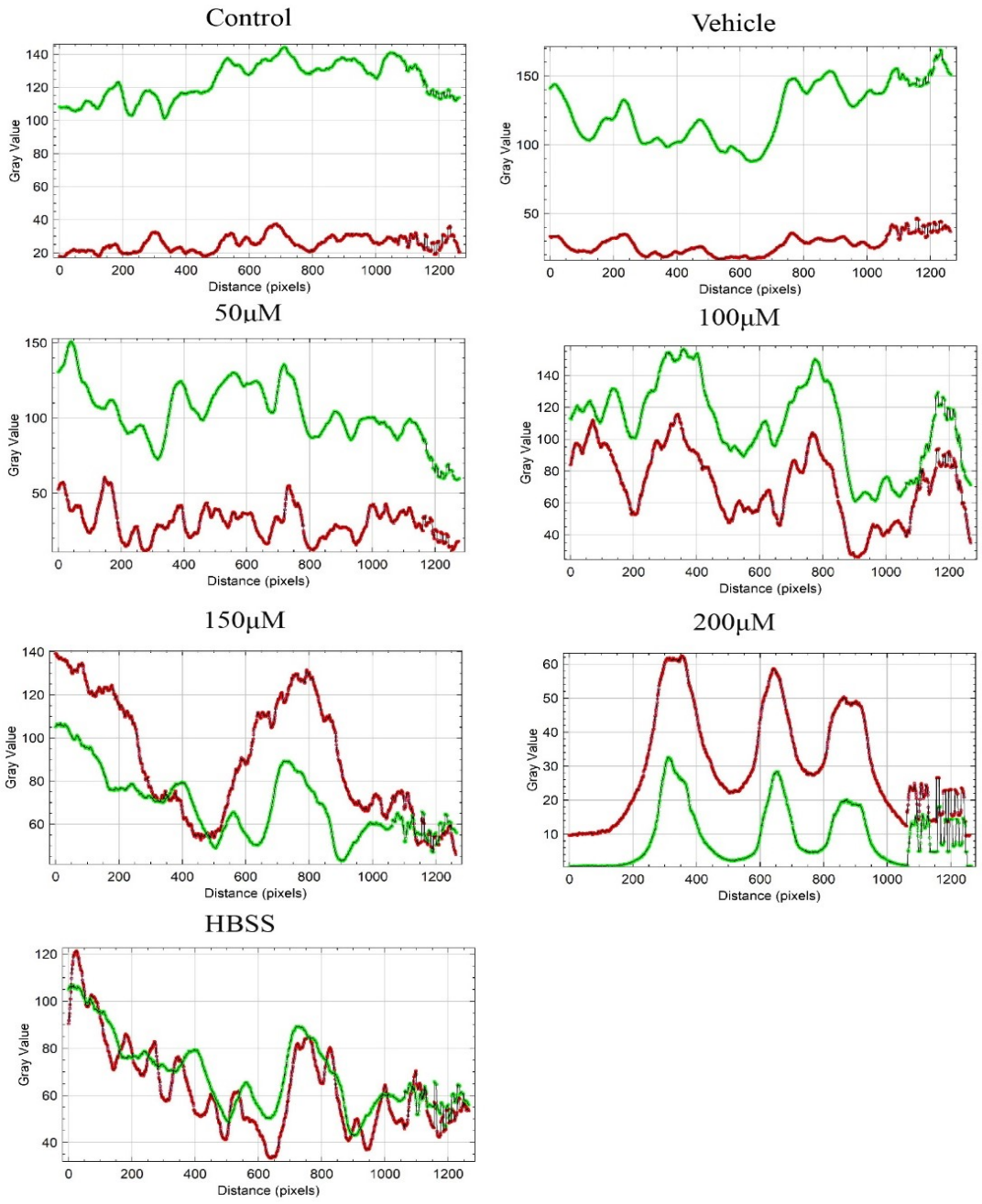

Figure 4.23 Grayscale intensity profiles of green (nucleic acid) and red (acidic vacuole) fluorescence in acridine orange–stained HCT116 cells. ImageJ analysis compared control, vehicle, PA-treated (50–200 μM), and HBSS conditions. (Excitation: 488 nm; Emission: 525 nm, 650 nm).

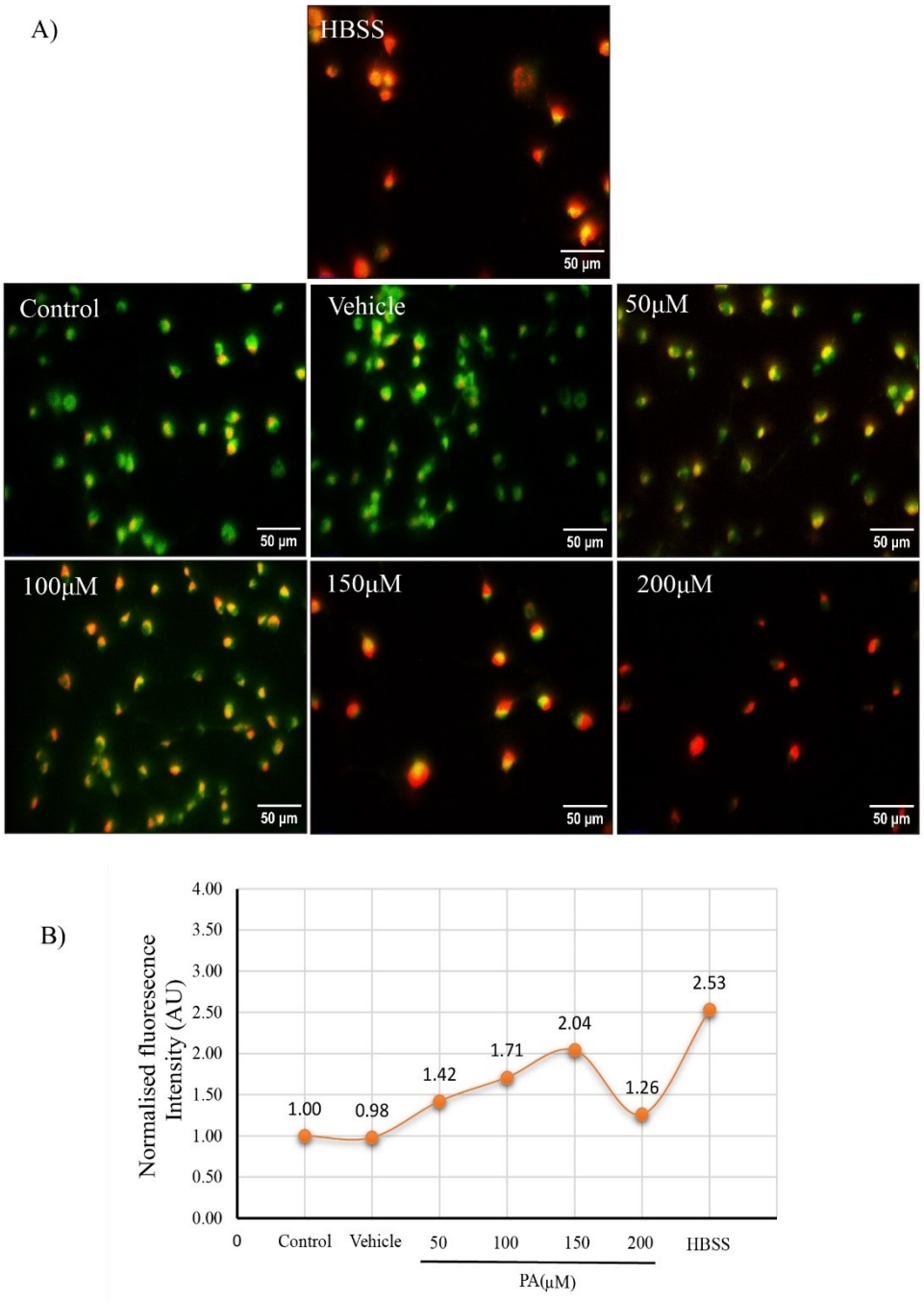

Figure 4.24 (A) Fluorescent images of PA-induced acidic vacuoles in CT26 cells (control, vehicle, 50–200 µM PA, HBSS). Scale bar = 50 µm; magnification = 200x. (B) Line graph shows fluorescence intensity normalized to the background fluorescence.

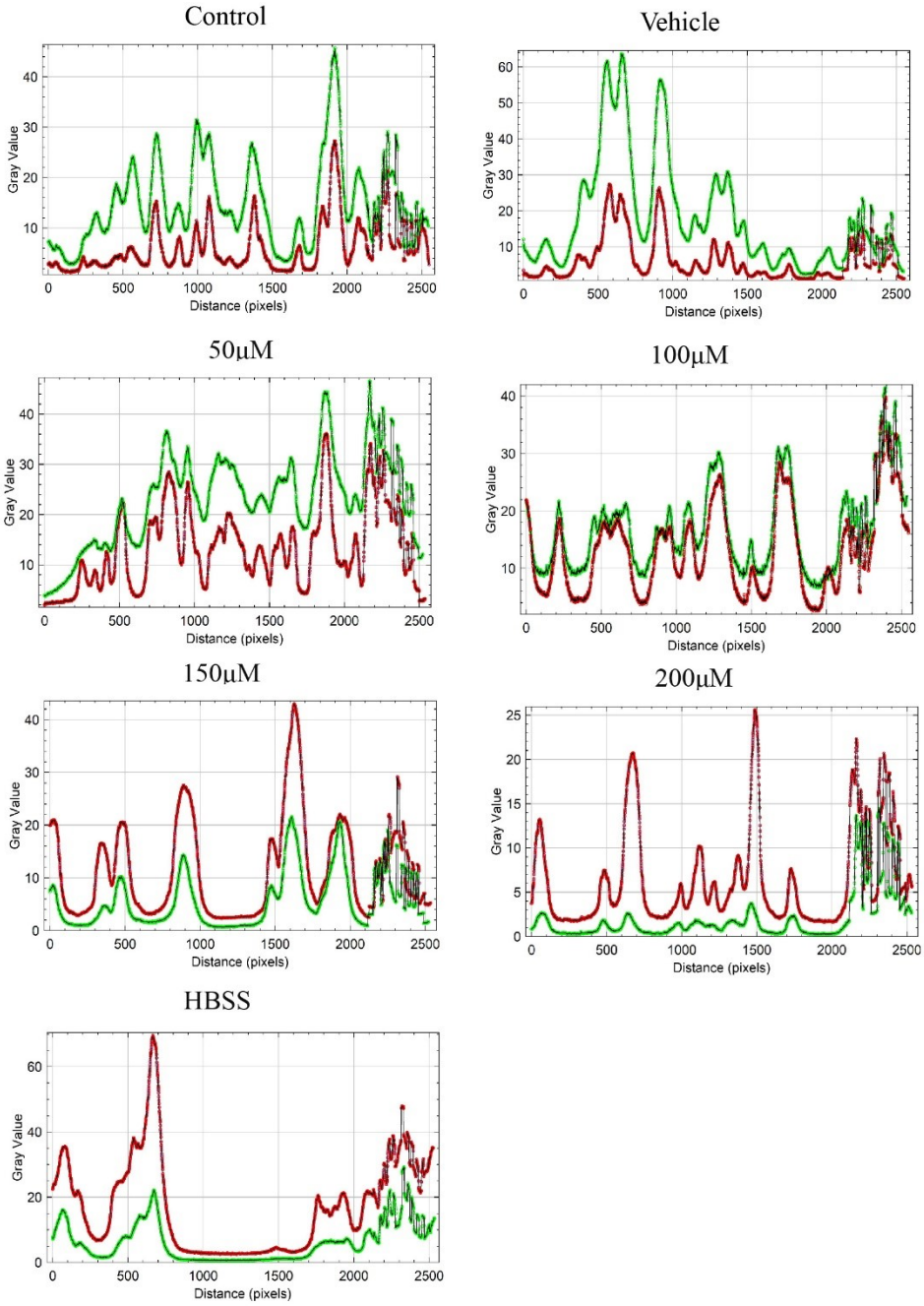

Figure 4.25 Grayscale intensity profiles of nucleic acid (green) and acidic vacuole (red) fluorescence in acridine orange–stained CT26 cells. ImageJ analysis of normal, vehicle, and PA-treated (50–200 μM) cells with HBSS control shows fluorescence variations. Excitation: 488 nm; Emission: 525 nm (green), 650 nm (red).

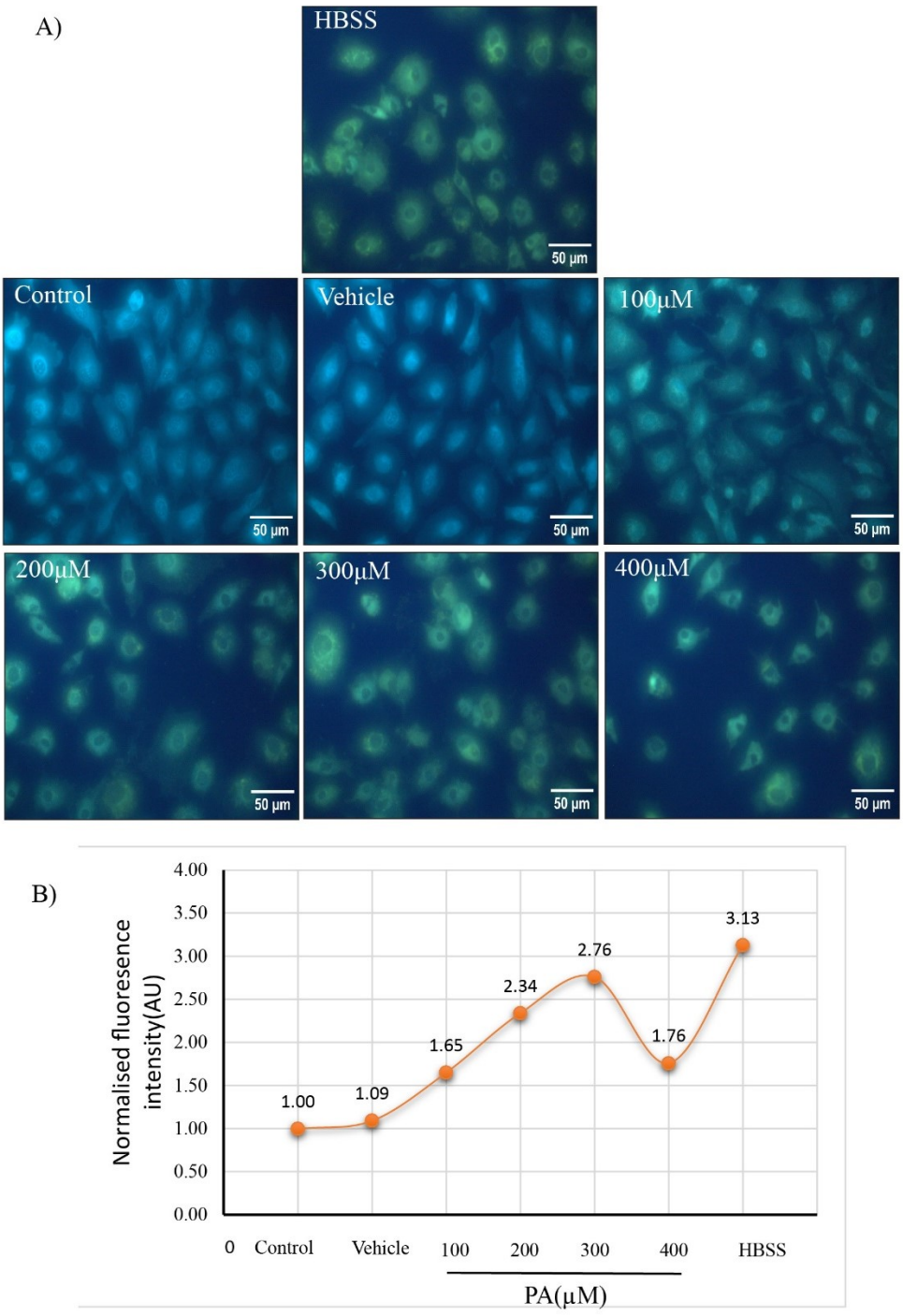

Figure 4.26 (A) Fluorescent images showing PA-induced autophagic flux in IEC6 cells under various conditions, including control, vehicle, 100–400 µM PA, and HBSS (positive control), with a scale bar of 50 µm and magnification of 400x. (B) Line graph indicating normalized fluorescence intensity relative to background fluorescence.

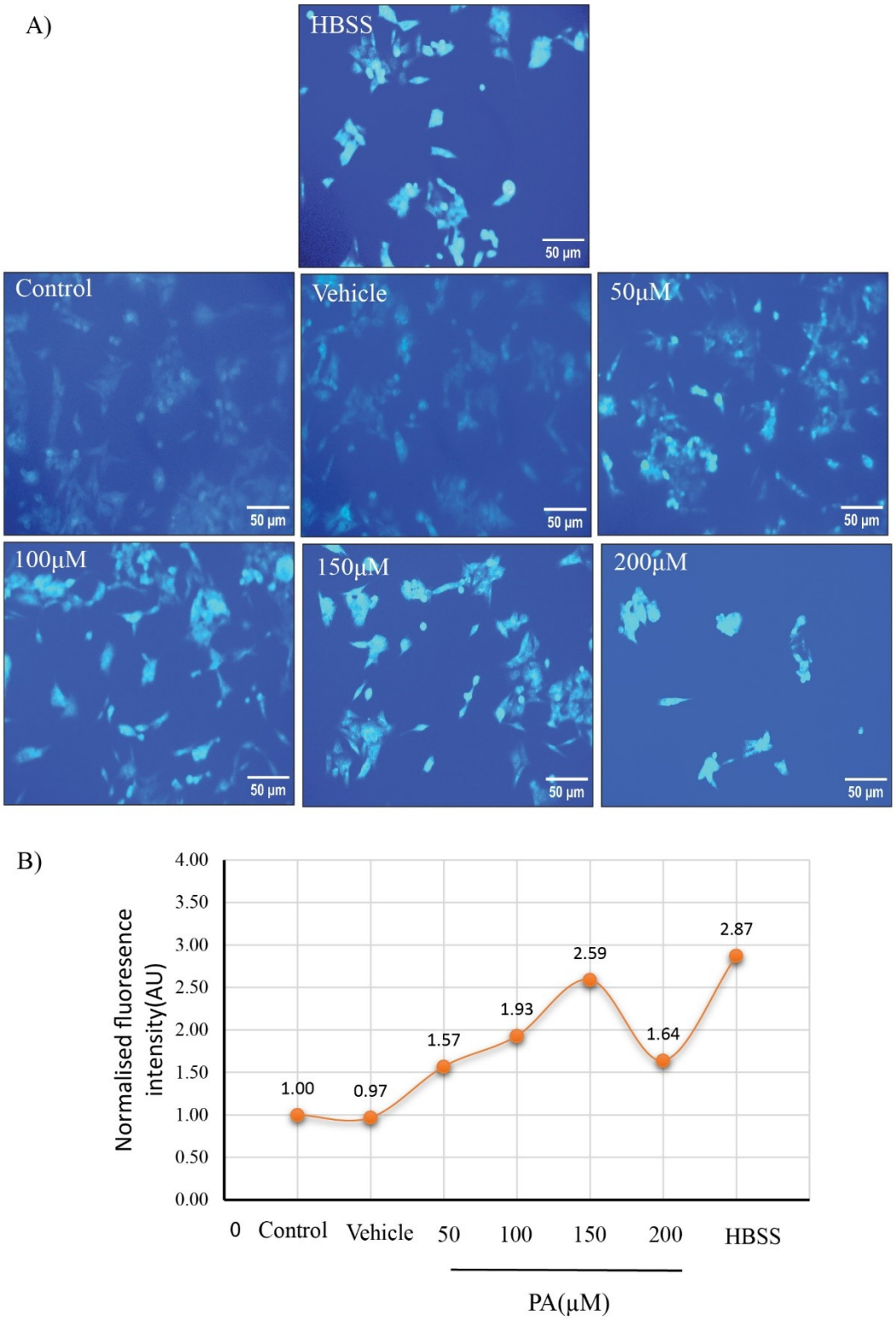

Figure 4.27 (A) Fluorescent images of PA-induced autophagic flux in HCT116 cells: control, vehicle, 50–200 µM PA, and HBSS (positive control), scale bar 50 µm, 400x magnification. (B) Line graph of normalized fluorescence intensity relative to background fluorescence.

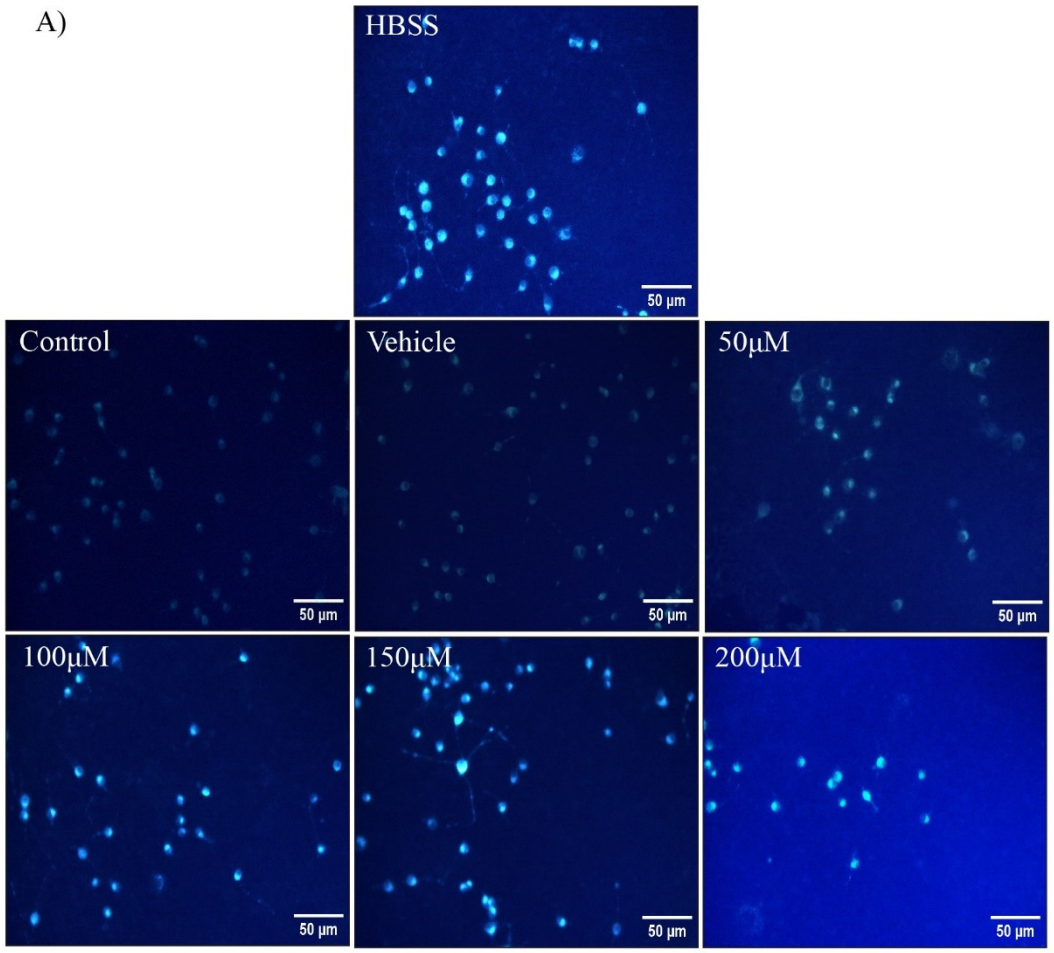

Figure 4.28 (A) Fluorescent images of PA-induced autophagic flux in CT26 cells: control, vehicle, 50–200 µM PA, and HBSS (positive control), scale bar 50 µm, 200x magnification. (B) Line graph of normalized fluorescence intensity relative to background fluorescence.

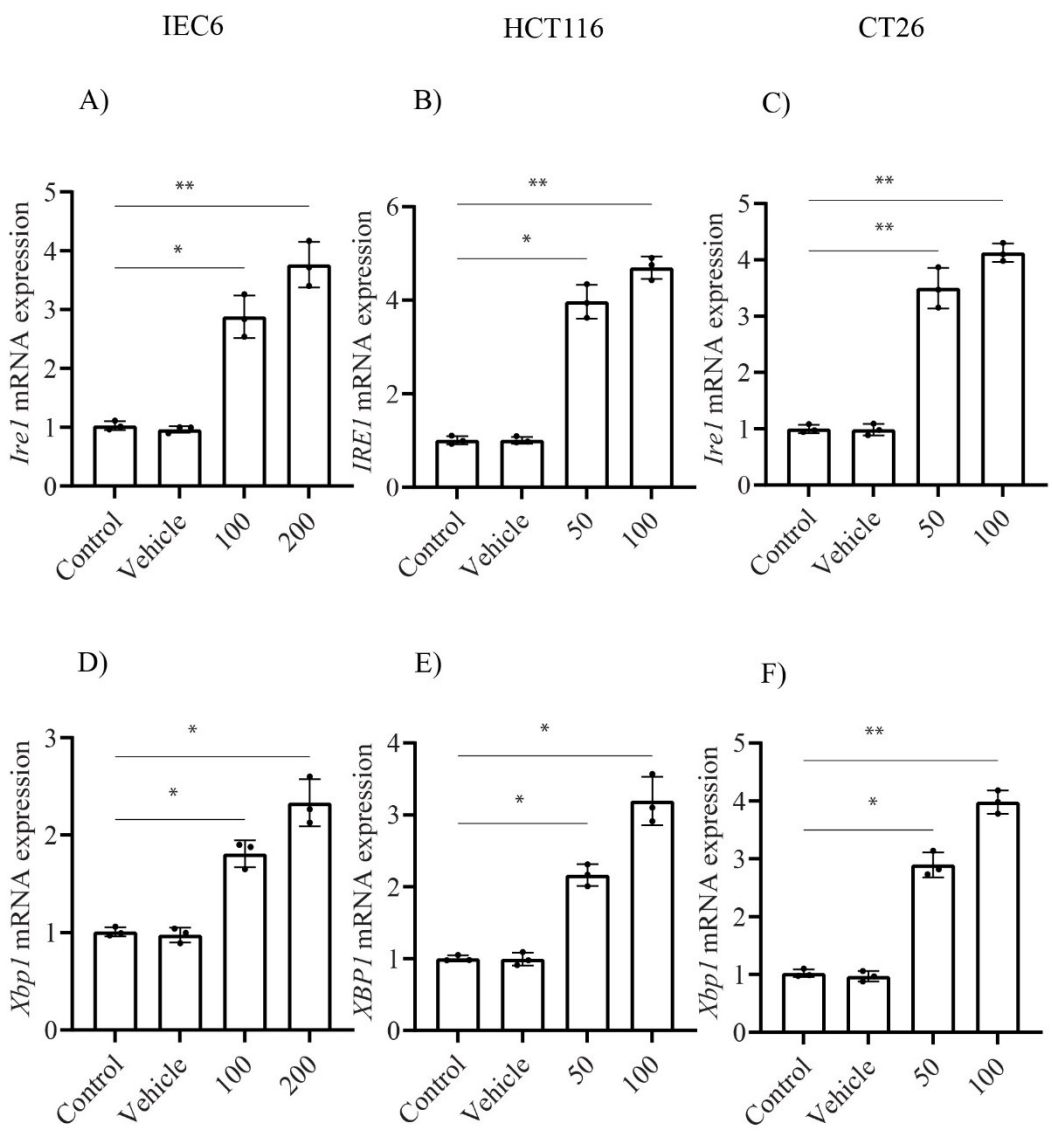

Figure 4.29. Effect of PA on *Ire1*/*Xbp1* expression in IEC6 (100-200 µM), HCT116 (50-100 µM), and CT26 (50-100 µM) cells. Graphs show fold change in *Ire1* (A–C) and *Xbp1* (D–F) expression relative to control. Data are mean ± SD (n = 3), analysed by one-way ANOVA with Dunnett's test. *$P < 0.05$, **$P < 0.01$, ***$P < 0.001$.

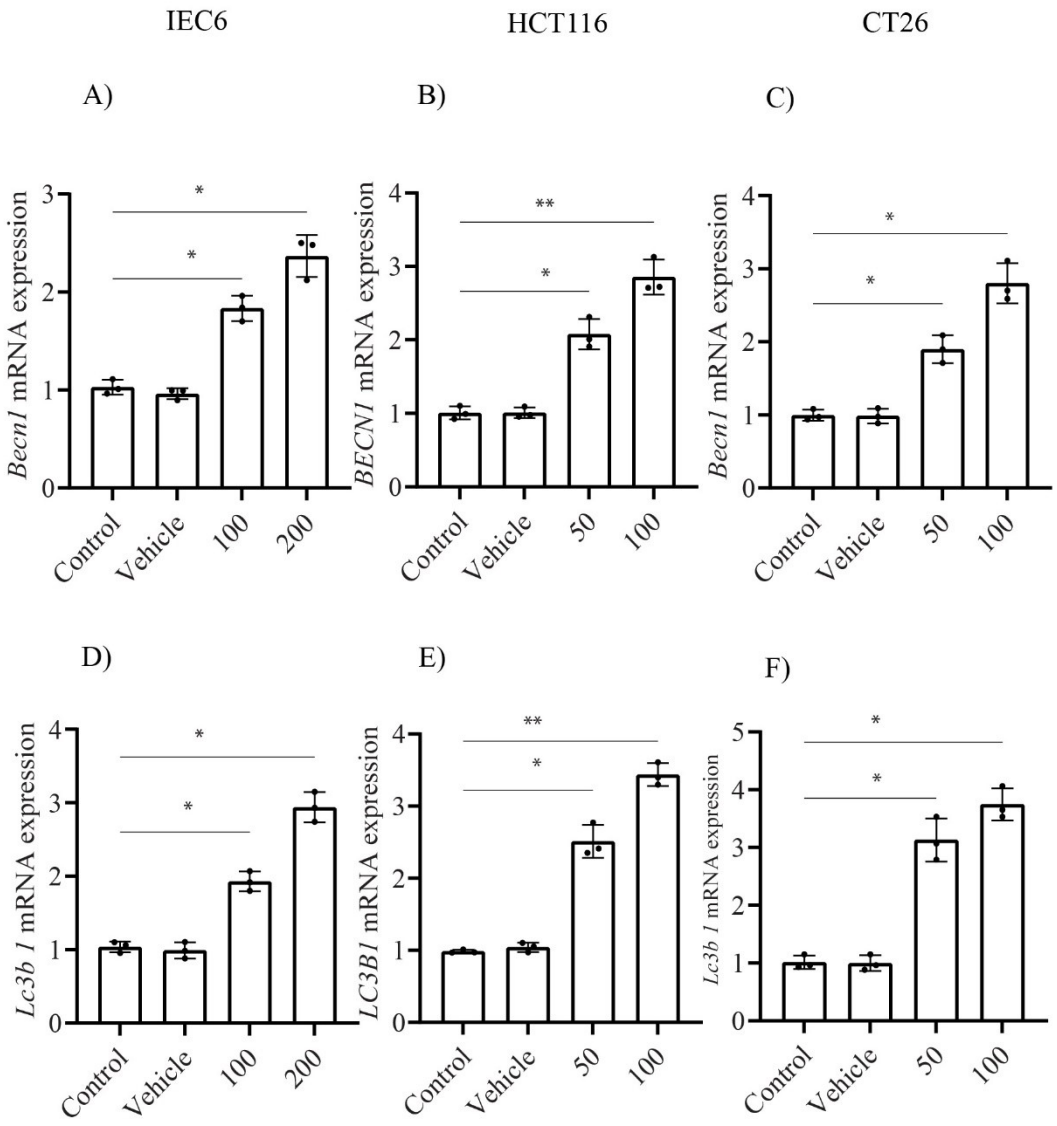

Figure 4.30 Effect of PA on autophagy-related gene expression in IEC6 (100-200 µM), HCT116 (50-100 µM), and CT26 (50-100 µM) cells. Bar graphs show fold change in *Becn1* (A–C) and *Lc3b1* (D–F) expression relative to control. Data are mean ± SD (n = 3), analysed by one-way ANOVA with Dunnett's test. *$P < 0.05$, **$P < 0.01$, ***$P < 0.001$.

4.4 Discussion

Cancer cells exhibit remarkable adaptability and resilience against stressors such as hypoxia, nutrient deprivation, and immune cell infiltration, posing significant challenges in their clinical management. A key adaptive mechanism employed by these cells involves ER stress and the associated UPR, which enable cells to withstand such stressors. These responses are activated in pathological and physiological conditions, with cancer cells exploiting these mechanisms to survive under extreme conditions. Understanding these adaptive mechanisms is crucial for developing effective therapeutic strategies. This study explored the effects of palmitic acid-induced oxidative stress and the subsequent accumulation of misfolded proteins in normal and colon cancer cells. Specifically, we investigated the role of ER stress and the UPR in mediating cellular responses to these conditions. Our results reveal a significant contribution of the UPR signalling pathway in enhancing cell survival under palmitic acid-induced stress, as palmitic acid significantly contributes to various health impacts. Moreover, palmitic acid promotes β-catenin palmitoylation, driving colorectal cancer progression by enhancing β-catenin signalling. This insight underscores the importance of targeting palmitic acid-induced ER stress and UPR pathways in developing therapeutic strategies for colon cancer.

Colon cancer cells exhibit substantial flexibility, allowing them to withstand extreme conditions, evade apoptosis, and develop treatment resistance. Endoplasmic reticulum stress is a primary adaptive response in many cancer cells that is effectively exploited to avoid cell death(Wang *et al*., 2014). Previous findings indicate that both ER stress and the UPR are implicated in the development of tumours, including human colon adenocarcinoma(Xing *et al*., 2006, Piton *et al*., 2016b). Tumours with activated UPR exhibit greater resistance to treatment, increased aggressiveness, and a higher tendency to relapse (Chipurupalli *et al*., 2019). Additionally, ER stress is suspected of triggering epithelial-to-mesenchymal transition (EMT), a phenomenon implicated in cancer pathophysiology(Zhong *et al*., 2011).

Palmitic acid, known for its involvement in diverse cellular mechanisms, has garnered attention for its role in oxidative stress and ER stress/unfolded protein responses. It can induce reactive oxygen species production in normal and cancer cells (Chu *et al*., 2019b, Zeng *et al*., 2020a). The current investigation demonstrates a dose-dependent induction of reactive oxygen species (ROS) by palmitic acid in both normal rat intestinal cells (IEC6)

and colon cancer cells (HCT116 and CT26). The study additionally confirmed that in IEC6 cells, the induction of ROS by palmitic acid was effectively attenuated by N-acetylcysteine (NAC) at concentrations ranging from 100 to 200 μM. However, NAC could not alleviate the elevated ROS levels induced by palmitic acid concentrations of 300 to 400 μM as it approached toxic concentrations. Likewise, In HCT116 and CT26 cells, NAC effectively scavenged ROS induced by palmitic acid at concentrations of 50-100 μM but was ineffective at reducing ROS production at 150-200 μM due to toxicity. This elevation in ROS levels disrupts cellular redox equilibrium, leading to oxidative stress. Furthermore, the production of ROS in response to palmitic acid originates from various sources, such as mitochondrial dysfunction, NADPH oxidase activation, and excessive accumulation of lipid droplets, aligning with previous findings (Ohtsu *et al*., 2017, Xu *et al*., 2016, Sato *et al*., 2014). This highlights palmitic acid's ability to induce oxidative stress, a process associated with developing numerous diseases, particularly concerning cancer pathogenesis and progression (Toyokuni, 2008, Mahalingaiah and Singh, 2014).

Palmitic acid's influence extends to modulating misfolded protein aggregate formation within cells, exacerbating ER stress and initiating the UPR (Park *et al*., 2014, Pardo *et al*., 2015). This accumulation of misfolded proteins is a cellular reaction to proteotoxic stress, instigating signalling cascades to regain protein homeostasis. The heightened presence of misfolded protein aggregates after palmitic acid exposure highlights its capacity to disrupt protein folding mechanisms and ER functionality, consequently fostering cellular dysfunction (Lu *et al*., 2015, Zeng *et al*., 2020a). The study demonstrated that palmitic acid induces the formation of misfolded protein aggregates or ER stress in IEC6, HCT116, and CT26 cells in a dose-dependent manner across specified concentrations. Additionally, treatment with 4-phenyl butyric acid (4-PBA) in palmitic acid-treated cells reduced ERS at 100 to 200 μM concentrations. However, this reduction in ERS was not observed at concentrations of 300 to 400 μM in IEC6 cells. Similarly, in HCT116 and CT26 cells, a decrease in ERS was observed at concentrations of 50 to 100 μM, whereas concentrations of 150 to 200 μM did not exhibit the same effect. The study indicated that the inability of 4-PBA to mitigate stress at higher concentrations may be attributed to cells being unable to tolerate the stress, potentially leading to the activation of apoptotic or necrotic pathways resulting from ERS stress. Overall, this investigation elucidates the effects of palmitic acid

on misfolded protein aggregates, revealing its potential role in disrupting protein homeostasis.

ROS-triggered UPR activates adaptive responses and restores protein-folding homeostasis (Santos *et al*., 2009). The UPR response to oxidative stress involves activating antioxidant defence systems, characterized by the upregulation of enzymes designed to neutralize ROS and counteract potential cellular damage (Ong and Logue, 2023). Palmitic acid exposure influences the activity of antioxidant enzymes, crucial in mitigating oxidative damage and maintaining cellular redox balance (Alnahdi *et al*., 2019b). The observed alterations in antioxidant enzyme activity, such as superoxide dismutase, catalase, and glutathione-related enzymes, suggest a dysregulation of antioxidant defence mechanisms in response to palmitic acid-induced oxidative stress. This dysregulation may compromise the cell's ability to neutralize ROS, exacerbating oxidative damage and contributing to disease progression (Li *et al*., 2019, Palomino *et al*., 2022). The present study observed elevated superoxide dismutase (SOD) and catalase (CAT) enzyme activity up to sub-lethal doses in IEC6 cells (100-200 μM) and HCT116/CT26 cells (50-100 μM). However, enzyme activity was found to decline upon exposure to toxic concentrations. It was evident that SOD primarily converts superoxide radicals into hydrogen peroxide, while catalase decomposes hydrogen peroxide into water and oxygen (Buettner, 2011).

Furthermore, the study revealed that the glutathione-related antioxidants (GST, GR, GPX, and GSH) remain stable in sublethal doses in all cell lines and are found to decline at toxic concentrations. GST aids in the detoxification of palmitic acid metabolites, GR maintains GSH levels for antioxidant regeneration, GPX directly scavenges ROS using GSH as a cofactor, and GSH acts as a primary cellular antioxidant, collectively safeguarding cells against oxidative damage caused by palmitic acid-induced ROS (Deponte, 2013). In addition, lipid peroxidation, a hallmark of oxidative stress, is exacerbated upon exposure to palmitic acid. The unsaturated fatty acid composition of cellular membranes renders them susceptible to attack by ROS, leading to lipid peroxidation and subsequent membrane damage. Palmitic acid-induced lipid peroxidation compromises membrane integrity and amplifies oxidative stress by generating lipid peroxidation by-products, further perpetuating cellular damage and dysfunction (Oh *et al*., 2012, Yan *et al*., 2017). The present study demonstrates that sublethal doses do not lead to a significant elevation in MDA levels. However, MDA levels were significantly elevated at toxic concentrations,

indicating a heightened oxidative stress response. As mentioned in the previous chapter, cells exposed to sublethal doses survived oxidative stress, as evidenced by forming viable colonies even after treatment with palmitic acid. Additionally, stress-responsive transcription factors like Nrf2 and NF-κB regulate the expression of genes involved in antioxidant defence, inflammation, and apoptosis to maintain cellular homeostasis and ensure cell viability (Bryan *et al*., 2013, Choudhury *et al*., 2015).

Palmitic acid modulates the expression of antioxidant genes, critical components of the cellular defence against oxidative stress (Kuda *et al*., 2018). The observed alterations in the expression of antioxidant genes, such as *Nrf2, Ho-1, and Nqo1*, reflect the adaptive response of cells to palmitic acid-induced oxidative stress. However, the precise mechanisms underlying the transcriptional regulation of antioxidant genes by palmitic acid warrant further investigation to elucidate their role in cellular adaptation and survival. Based on the current findings, it is evident that HCT116 and CT26 cells exhibited higher upregulation of *Nrf2* compared to IEC6 cells, with HCT116 demonstrating the highest expression. Regarding *Nqo1* and *Ho-1* expression, both IEC6 cells and CT26 showed elevated levels. However, in HCT116 cells, expression initially increased and then decreased within the range of sublethal doses.

Studies have shown that activation of the UPR pathway has been linked to cancer cell survival (Patel *et al*., 2021). Palmitic acid's induction of ER stress highlights its role in perturbing ER homeostasis and protein folding machinery, which may affect cellular function and viability (Zhang *et al*., 2012b, Pardo *et al*., 2015). Palmitic acid elicits ER stress, as evidenced by the upregulation of ER stress markers, including Bip, CHOP, and ATF6 (Xiang *et al*., 2021). ER stress represents a cellular response to the accumulation of misfolded proteins within the ER lumen, triggering the activation of the UPR (Schröder, 2008b). The study revealed that *Bip, Chop*, and *Atf6* expression was relatively higher in HCT116 and CT26 compared to IEC6 cells. It was evident that the chaperone protein *Bip*, induced by UPR, is crucial for the growth and proliferation of cancer cells (Banach *et al*., 2019). Additionally, the PERK pathway activation is essential for cancer cells undergoing epithelial-mesenchymal transition (EMT), primarily mediated by the *Nrf2* cascade(Feng *et al*., 2017). Recent findings suggest that the PERK-NRF2 pathway is activated in colorectal cancer (CRC) cells under ER stress(Shi *et al*., 2019).

The study revealed that *Perk* expression increased to 100 μm and was relatively stable as it approached 200 μm in IEC6 cells. Conversely, in HCT116 and CT26 cells, a consistent increasing trend in *Perk* gene expression was observed. A similar pattern was noted in the *Atf4* mechanism across the cell lines. These findings suggest a feedback mechanism regulating *Perk* activity in normal cells. However, unresolved ER stress triggers persistent *Perk* activation in cancer cells such as HCT116 and CT26. The study also found that expression of *Atf4*, a canonical downstream factor of the *Perk* kinase, is up-regulated in CRC cells that hold heightened survival possibility in palmitic acid-induced stress. The study further showed that *Perk* and *Atf4* are functionally required for cell survival through palmitic acid-induced stress. Palmitic acid activates the PERK/ATF4 arm of the UPR, leading to the transcriptional upregulation of downstream target genes involved in protein folding, antioxidant defence, and apoptosis. PERK/ATF4 signalling activation represents a cellular attempt to restore protein homeostasis and alleviate ER stress. However, sustained activation of this pathway may contribute to cell death via apoptotic mechanisms, highlighting the dual role of UPR signalling in cell survival and death decisions. The activation of the *Perk/Atf4* arm of the UPR by palmitic acid is particularly interesting, leading to the transcriptional upregulation of downstream target genes involved in protein folding, antioxidant defence, and apoptosis. *Perk/Atf4* signalling activation represents a cellular attempt to restore protein homeostasis and alleviate ER stress. However, prolonged activation of this pathway may contribute to cell death via apoptotic mechanisms, highlighting the dual role of UPR signalling in cell survival and death decisions.

Furthermore, the study investigated the role of palmitic acid-induced *Ire1/Xbp1* arm of UPR pathway activation in normal intestinal cells and colon cancer cell survival through autophagic flux modulation, unveiling intricate cellular responses to lipid-induced signalling rerouting. The study elucidated how survival pathways are implicated in both cancer and normal cells in response to palmitic acid-induced endoplasmic reticulum stress through autophagic responses.

The findings revealed that palmitic acid treatment led to a dose-dependent increase in the formation of acidic vacuoles, indicating early-phase autophagic responses in normal and cancerous intestinal cells with acridine orange staining. Acridine Orange stains acidic vacuoles red, typically showing green fluorescence in the cytoplasm or nucleus. Red fluorescence intensity correlates with acidity, allowing quantification of acidic

compartments. This observation suggests that palmitic acid can initiate autophagy, a cellular process crucial for maintaining homeostasis by degrading damaged organelles and proteins(Chatterjee *et al*., 2019). The observation revealed that HCT116 cells accumulated more acidic vacuoles than HCT116 and IEC6 cells. Palmitic acid triggers acidic vacuoles as a cellular adaptation mechanism. However, a saturation effect was noted beyond specific concentrations, highlighting the complexity of cellular responses to lipotoxicity. Moreover, Monodansylcadaverine (MDC) selectively labels autophagic vacuoles.

Additionally, palmitic acid-induced autophagic flux, as evidenced by the dose-dependent increase in normalized fluorescent intensity of mono dansyl-cadaverine, a marker for autophagosomes. The study observed that the normalized fluorescent intensity of MDC in palmitic acid-treated IEC6 cells was higher than in HCT116 cells and CT26 cells. Hence, the study indicates that not all acidic vacuoles end up in autophagy.

The study revealed that the up-regulation of autophagy-related genes *Beclin 1* and *Lc3b1* further supports the induction of autophagy by sublethal doses of palmitic acid. It was evident from Chapter 1 that the sublethal doses form viable colonies after palmitic acid treatment. The expression levels of both genes were higher in HCT116 and CT26 than in IEC6 cells. These findings suggest that palmitic acid modulates autophagic processes by activating vital regulatory genes involved in autophagosome formation and maturation, thereby enhancing cellular resistance to palmitic acid-induced stress. In addition, palmitic acid treatment also induced ER stress, as demonstrated by the upregulation of *Ire1* and *Xbp1* genes. The IRE1/XBP1 pathway is a critical component of the unfolded protein response (UPR), which is activated in response to ER stress to restore cellular homeostasis. Our findings suggest that palmitic acid-induced ER stress may contribute to cellular adaptation and survival under conditions of lipid-induced stress. The study revealed that both IEC6 cells and CT26 cells exhibited a comparable upregulation of the *Ire1* gene, mirroring the high expression observed in HCT116 cells. However, the downstream activator of *Ire1*, *Xbp1*, was found to be highly expressed in HCT116 and CT26 cells compared to IEC6 cells. The study findings are consistent with previous research demonstrating that *Xbp1* mRNA splicing plays a pivotal role in coordinating autophagic responses through the transcriptional regulation of *Beclin-1,* which is essential for the initiation of autophagy (Margariti *et al*., 2013).

Previous studies have revealed that the IRE1/XBP1 arm of the unfolded protein response (UPR) activates cell survival mechanisms via autophagy (Ogata *et al*., 2006). Interestingly, we observed an interconnection between autophagy and ER stress in response to palmitic acid treatment. Autophagy serves as a mechanism to alleviate ER stress by removing misfolded proteins and damaged organelles, thus reducing the burden on the ER. Conversely, the UPR can regulate autophagic flux by modulating the expression of autophagy-related genes. This crosstalk between autophagy and ER stress highlights the complexity of cellular responses to lipid-induced stress. In colon cancer, our findings suggest that palmitic acid-induced activation of the IRE1/XBP1 pathway and modulation of autophagic flux may contribute to cancer cell survival and progression. It was clear from the study that colon cancer cells mimic the survival strategy of normal cells. Targeting these pathways pharmacologically may offer promising therapeutic approaches for combating colon cancer by restoring cellular homeostasis and inhibiting cancer cell survival mechanisms.

In conclusion, our study provides valuable insights into the molecular mechanisms underlying palmitic acid-induced activation of the IRE1/XBP1 pathway and modulation of autophagic flux in normal intestinal and colon cancer cells. Further research is needed to elucidate the specific molecular targets within these pathways and optimize therapeutic interventions for clinical applications in colon cancer treatment.

Palmitic acid-induced oxidative stress profoundly affects cellular homeostasis, influencing ROS production, protein folding dynamics, antioxidant defence mechanisms, and ER stress response pathways. Understanding the molecular mechanisms underlying these effects is crucial for elucidating the pathophysiological implications of palmitic acid in normal and cancerous colon cells. It may provide insights into potential therapeutic strategies for mitigating palmitic acid-induced cellular dysfunction and disease progression. In summary, this study indicates that palmitic acid can induce oxidative stress without causing lipotoxicity up to a specific concentration, and it can activate the PERK/ATF4 pathway to counteract the ER stress developed by palmitic acid in both normal and colon cancer cells. In addition, our study provides valuable insights into the molecular mechanisms underlying palmitic acid-induced activation of the IRE1/XBP1 pathway and modulation of autophagic flux in normal intestinal and colon cancer cells.

These findings contribute to our scientific comprehension of cancer cells' survival-promoting metabolic and cellular adaptations. Additionally, this study establishes a novel connection between saturated fat and ER stress in both normal and colon cancer cells. Such insights shed light on potential therapeutic targets and strategies for combating the deleterious effects of palmitic acid and enhancing cellular resilience against ER stress in cancer contexts. Further research is needed to elucidate the specific molecular targets within these pathways and optimize therapeutic interventions for clinical applications in colon cancer treatment.

Chapter 5

Effects of excess palm oil intake on the development of ERS and UPR in murine intestinal tissues

5.1 Introduction

Lipids are essential dietary components that provide various nutritional benefits, but excessive consumption may lead to potential toxicity especially from the saturated fatty acids of dietary lipids. Additionally, these lipids can trigger degenerative pathophysiology processes by producing excessive oxygen radicals and subsequent lipid peroxidation. Ultimately, they can cause damage on organ systems, causing inflammation, lipid-associated diseases, and other degenerative conditions, including cancer. Palm oil is a widely consumed vegetable oil primarily composed of triglycerides, with approximately 50% saturated fats, mainly palmitic acid, 40% monounsaturated fats, predominantly oleic acid, and 10% polyunsaturated fats. Palm oil consumption has expanded significantly in recent decades due to its adaptability, economic feasibility, and extensive use in the food industry. Despite being a substantial energy source and vital fatty acids, palm oil has generated considerable interest due to its potential adverse health impacts, especially when it comes to chronic intake and its effects on physiological systems. Further, it is critical to determine whether endoplasmic reticulum stress in stomach tissue is connected with high palm oil consumption, which could affect cellular activities.

Palm oil, widely used in processed foods for its ability to enhance texture, flavor stability, and shelf life, contains high levels of saturated fat, particularly palmitic acid, which has been linked to various lipid-associated diseases when consumed excessively. This raises concerns about chronic palm oil consumption on health implications, particularly its effects on different cellular processes within the body. Many studies have shown that the diets with palm oil induces endothelial dysfunction, arterial stiffness, and hypertrophic inward remodelling, exacerbating obesity-related vascular alterations compared to monounsaturated fat diets in mice (Vega-Martín *et al*., 2021). Furthermore, prolonged palm oil consumption induces destructive enteritis, reduced enterocyte proliferation, decreased serum proteins, and altered lipid profile, leading to minor intestine dysfunction and structural damage (Singh *et al*., 2021b). Some studies have highlighted the involvement of palmitic acid-rich diet in chronic liver disease, diabetes, and Crohn's disease, conditions characterized by compromised intestinal permeability. Extensive evidence from both human studies and animal models indicates that the integrity of the intestinal barrier is highly susceptible to alterations caused by stress, dietary factors, and changes in the microbiota.

Studies have demonstrated that diets high in saturated fats can induce ER stress in various tissues, including the liver and adipose tissue, leading to insulin resistance and inflammation (Kim *et al*., 2015, Ahmed *et al*., 2021). The rationale for investigating the effects of chronic palm oil intake on ER stress in murine intestinal tissues stems from several key considerations. Firstly, palm oil is extensively consumed worldwide, particularly in processed foods, contributing significantly to dietary fat intake. However, despite its widespread use, there remains a gap in understanding the specific impacts of chronic palm oil consumption on cellular processes within the intestine, including ER stress. ER stress occurs when the protein-folding capacity is overwhelmed, accumulating misfolded proteins and activating the UPR. Chronic ER stress has been implicated in the pathogenesis of various diseases, including metabolic disorders and inflammatory conditions. Given that the intestine is a primary site of nutrient absorption and plays a crucial role in metabolic homeostasis and immune function, investigating the effects of palm oil on ER stress in intestinal tissues is pertinent.

With a rapid cell turnover rate, intestinal epithelium is a dynamic tissue continually adapting to dietary changes. As a primary site of nutritional absorption, the intestine takes in dietary components, such as fatty acids from palm oil. A limited study has been undertaken to investigate the impact of chronic palm oil consumption on ER stress in the intestinal tissues of mice. Understanding the molecular pathways that cause ER stress in response to palm oil consumption could shed light on potential dietary-gut health associations.

The primary objective of this study is to evaluate the impact of palm oil consumption on ER stress markers in murine intestinal tissues. Specifically, the study aims to investigate whether prolonged intake of palm oil leads to increased ER stress in the intestine and to elucidate the underlying mechanisms contributing to any observed effects. By examining ER stress markers and related pathways in murine models following palm oil consumption, it seeks to understand better the potential implications of palm oil on intestinal health and its role in the development of metabolic and inflammatory disorders. This study will provide valuable insights into the relationship between palm oil consumption and ER stress in the intestine, contributing to our understanding of the health effects of dietary fats and informing future dietary recommendations and interventions aimed at promoting intestinal health.

Assessing ER stress markers in intestinal tissues employed molecular and histological techniques. It utilized a murine model, typically C57BL/6 mice, which were randomly assigned to a palm oil-fed (palm oil (200 μl) + normal chow) group and a control group receiving a standard diet (normal chow) for four months to mimic chronic dietary exposure. Initially, intestinal tissue samples from the palm oil-fed and control groups followed the designated feeding period. These tissue samples were then subjected to various analyses. Histopathological analysis was conducted to examine tissue morphology and structural changes. Gene expression analysis was also performed using quantitative real-time polymerase chain reaction (RT-*q*PCR) to quantify the mRNA levels of key ER stress markers and UPR genes. Furthermore, we evaluated antioxidant levels, lipid peroxidation, and the expression of other relevant genes involved in antioxidant response, autophagy, and inflammation in both the small and large intestines.

5.2 Materials and methods

5.2.1 Palm oil

Following traditional cooking practices, the palm oil was subjected to mild heat treatment at 75°C for 30 minutes to enhance its palatability before being administered to mice via oral gavage. The detailed procedures are described in Chapter 2, Materials and Methods, Section 2.1.7.

5.2.2 Animals

Chapter 2, Materials and methods, section 2.2.2.1 &2.2.2.2, gave a detailed description of the experiment and procedures. Accordingly, as part of the study mentioned, male BALB/c mice were selected for the study. In group I, which represents the control group, normal chow was provided. For group II, 200 μl of heated palm oil (HPO) was administered orally daily, with normal chow providing 73.6 mg of palmitic acid per day over four monthsz. Tissues from the small intestine and colon were collected from group I and II.

5.2.3 Histopathological analysis of small and large intestine and colon

After sacrifice, the intestine was located, and by cutting the cecum, the small intestine was separated from the large intestine. Following flushing with cold PBS, the small

intestine and colon were longitudinally sectioned . A detailed description of the experiment was given in Chapter 2, Materials and methods, Section 2.2.2.6

5.2.4 Analysis of lipid peroxidation and antioxidants in intestinal tissues

The presence of MDA for detecting lipid peroxidation and the levels of different antioxidants (SOD, CAT, GST, GR, GPx and GSH) were analysed in the small intestine and colon of the tissue collected. Tissue homogenate was prepared as per the protocol described in Chapter 2, Materials and methods, Section 2.2.3.2, 2.2.3.3.3-2.2.3.3.10

5.2.5 Analysis of inflammatory cytokines in intestinal tissues

The inflammatory cytokines IL 6 and TNF α were analysed in small and large intestine tissues. The detailed protocols were described in the chapter section 2.2.3.5.3

5.2.6 Quantitative real-time PCR

Total RNA was extracted from a longitudinal section of the small intestine and colon tissues. cDNA preparation, purity assessment quantitation, and RT-*q*PCR were also performed using the kit method. The expression of target genes was normalized to the expression of *β*-actin and shown as a fold change relative to the control group based on the $2^{-\Delta\Delta Ct}$ method. All the procedures were carried out accordingly, as explained in Chapter 2, Materials and methods, Section 2.2.4. Primers used for the study are mentioned in Chapter 2.

5.2.7 Statistical analysis

The data analysis was performed using Mean ± SD (Standard deviation) with GraphPad Prism 8.3.8 (San Diego, CA, USA). To analyse antioxidant levels and lipid peroxidation across HPO treatment and tissue types (small intestine and colon), a two-way ANOVA followed by post hoc Tukey's test was applied (n=6). Gene expression profiling was analysed using the student's t-test. Statistically significant results were indicated by P values of *<0.05, **<0.01, and ***<0.001.

5.3 Results

5.3.1 Palmitic acid concentration in heat-treated palm oil

In the GC-MS analysis, the chromatogram identified the characteristic peak of palmitic acid in heat-treated palm oil (HPO) (Fig. 5.1). The analysis revealed a concentration of

367,000 μg/mL (367mg/ml) of palmitic acid in HPO. This corresponds to a quantity of 73.4 mg of palmitic acid in a 200 μL sample of HPO (Fig. 5.1).

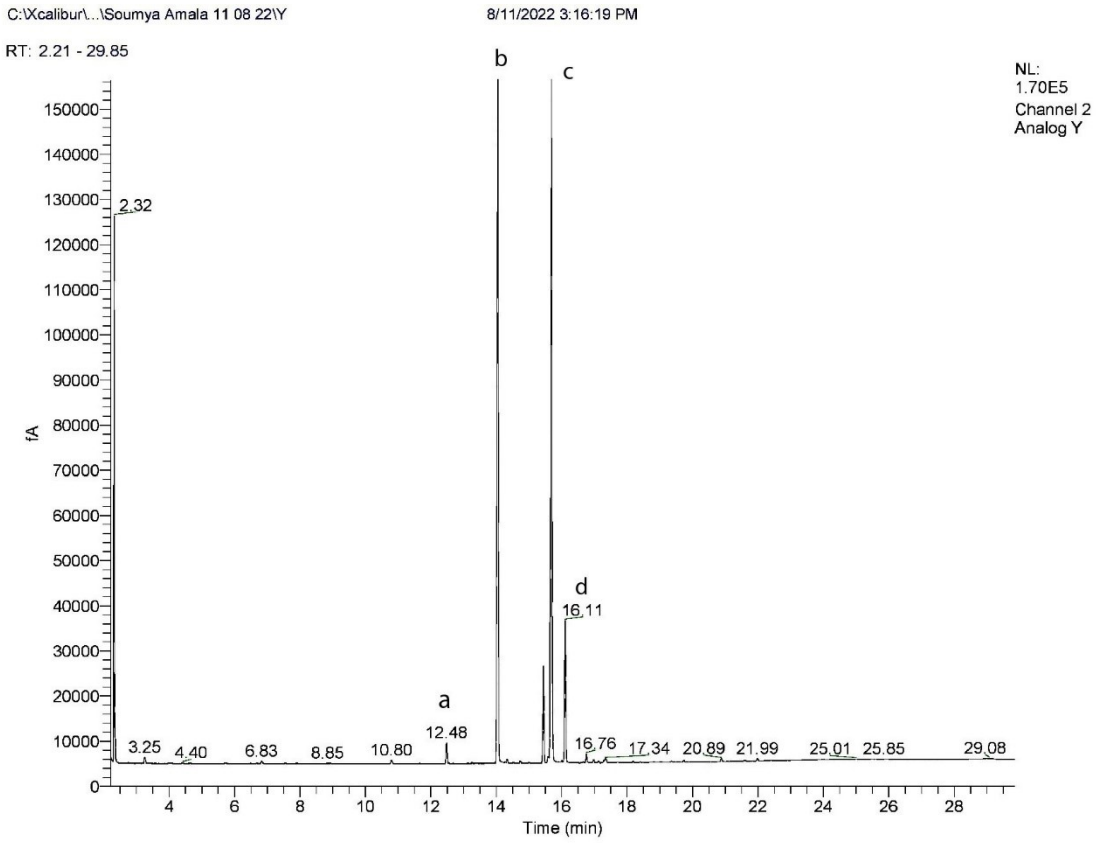

Figure 5.1 GC-MS/MS chromatogram of heat-treated palm oil. (a) Myristic acid, (b) Palmitic acid, (c) Stearic acid, (d) Oleic acid, and (e) Linoleic acid.

5.3.2 HPO alters tissue architecture of mouse intestines

H&E staining revealed mucosal architecture of intestinal tissue in the control group as intact. While, HPO-treated mice exhibited significant inflammatory cell infiltration and disrupted tissue integrity. Specifically, an enlargement goblet cells was predominantly observed in small intestine by HPO (Fig. 5.2).

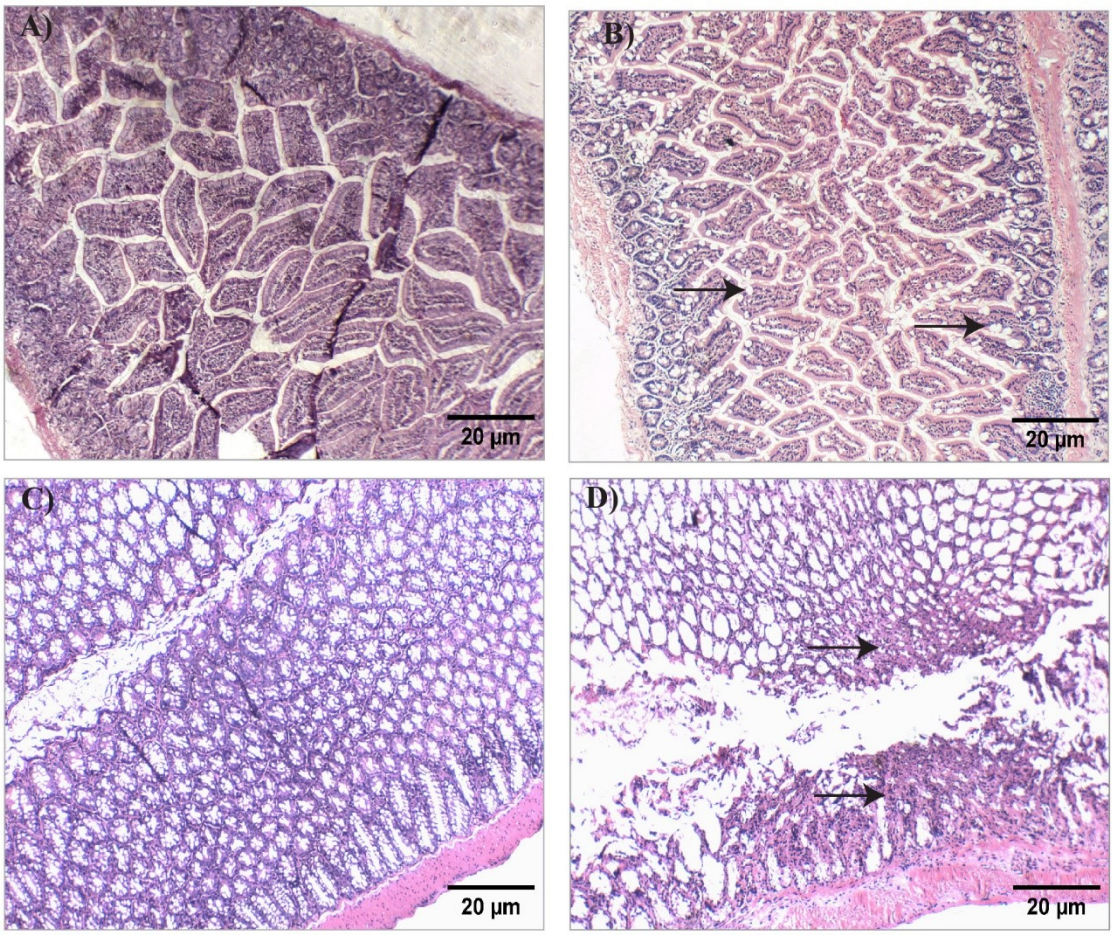

Figure 5.2 Histological changes in the small and large intestines of mice after HPO oral administration. Representative H&E-stained sections of the small (A, B) and large (C, D) intestines from Normal (A, C) and HPO-treated (B, D) mice, imaged at 200X magnification (Magnus Image Capture software), scale bar = 20 µm. HPO treatment for four months led to inflammation, altered tissue structure, and enlarged goblet cells in the small intestine (B, dark arrows), as well as tissue disruption and inflammation in the large intestine (D, dark arrows).

5.3.3 IL-6 and TNFα levels in mouse intestine after HPO treatment

HPO administration significantly elevated IL6 and TNFα levels in the small and large intestines. In the large intestine, IL6 increased from 15.8 ± 2.1 pg/ml to 121.75 ± 8.26 pg/ml, and TNFα rose from 16.5± 2.11 pg/ml to 145.75 ± 6.87 pg/ml. In the small intestine, IL6 levels increased from 12.3 ± 1.9 pg/ml to 98.25 ± 6.12 pg/ml, and TNFα rose from 14.8 ± 1.96 pg/ml to 119 ± 9.9 pg/ml (Fig. 5.3& Tab 5.1). HPO administration significantly elevated IL6 and TNFα levels in both intestinal regions, with a more pronounced increase in the large intestine, indicating a stronger inflammatory response in this tissue. Two-way ANOVA showed that HPO treatment and tissue type

significantly affected IL-6 and TNFα levels, with significant interactions indicating interdependence (Tab 5.1).

Table 5.1 Two-way ANOVA of HPO treatment and tissue type on IL-6 and TNFα

Cytokines	HPO Treatment (F, p)	Tissue Type (F, p)	Interaction
IL6	(F1, 12 = 25.80, p = 0.0003)	(F1,12 = 1303.9, p < 0.0001)	(F1,12 = 14.16, p < 0.0027)
TNFα	(F1, 20 = 30.77, p < 0.0001)	(F1,20 = 2104, p < 0.0001)	(F1,20 = 23.79, p < 0.0001)

The table presents the F-values and associated p-values for cytokines IL-6 and TNFα in HPO-treated small and large intestines.

5.3.4 HPO alters antioxidant activity, GSH level, and lipid peroxidation

HPO treatment had distinct effects on antioxidant activity and oxidative stress markers in the intestinal regions. Under normal conditions, SOD activity was greater in the large intestine compared to the small intestine. However, HPO treatment led to a significant reduction in SOD activity in the large intestine, while levels in the small intestine remained unchanged, highlighting a tissue-specific response. Two-way ANOVA confirmed significant main effects of both HPO treatment and intestinal region on SOD activity, with no significant interaction.

In contrast, CAT activity was naturally higher in the small intestine than in the large intestine. HPO treatment resulted in a significant decrease in CAT activity in both regions. Two-way ANOVA confirmed significant main effects of treatment and intestinal region, again without interaction's, GR, GPX, and GSH levels were significantly reduced in the small intestine following HPO exposure, whereas no significant changes were observed in the large intestine. Two-way ANOVA revealed significant effects of both HPO treatment and intestinal region on GST, GSH, and GPX, while GR was influenced solely by HPO treatment. Notably, GPX exhibited a significant interaction between tissue type and HPO treatment. Under normal conditions, MDA levels were naturally higher in the small intestine compared to the large intestine. HPO treatment further elevated lipid peroxidation in the small intestine, whereas no significant changes were observed in the large intestine, indicating a tissue-specific effect on oxidative damage (Fig. 5.4 Tab 5.2 & Tab 5.3).

Table 5.2 Levels of antioxidants and MDA in the intestines following HPO gavage.

	Sample	SOD (IU/mg P)	CAT (IU/mg P)	GST (IU/mg P)	GR (IU/mg P)	GPX (IU/mg P)	GSH (nmoles/mgP)	MDA (nmoles/mgP)
SI	Normal	12.7±1.5	30.8±1.5	16.6±1.6	16.6±2.1	16.8±1.8	15.6±2.1	26.3±2.4
	HPO	10.7±1.65	24.9±2.4	13.13±1.2	13.5±1.6	12.4±1.4	13.1±1.1	35.2±4.8
LI	Normal	16.7±2.07	25.4±2.9	12.6±1.3	15.6±1.8	20.1±1.8	19.7±1.3	18.6±2.38
	HPO	12.8.6±1.2	18.4±2.15	10.2±1.39	13.7±1.6	19.7±1.4	18.3±1.8	20.6±1.6

Enzyme activities in the small and large intestines (SI: Small intestine, LI: Large intestine) after HPO gavage, including SOD, CAT, GST, GR, and GPX (IU/mg protein), reduced glutathione (nmol/mg protein), and MDA levels (nmol/mg protein) as indicators of lipid peroxidation.

Table 5.3 Two-way ANOVA of HPO treatment and tissue type on antioxidant activities and MDA levels.

Enzymes	HPO Treatment (F, p)	Tissue Type (F, p)	Interaction
SOD	($F_{1, 20} = 24.37$, $p < 0.001$)	($F_{1,20} = 2.23$, $p < 0.001$)	ns
CAT	($F_{1, 20} = 45.20$, $p < 0.001$)	($F_{1,20} = 37.69$, $p < 0.001$)	ns
GST	($F_{1, 20} = 24.19$, $p < 0.001$)	($F_{1,20} = 34$, $p < 0.0001$)	ns
GR	($F_{1, 20} = 13.32$, $p < 0.001$)	ns	ns
GPX	($F_{1, 20} = 12.09$, $p = 0.0024$)	($F_{1,20} = 63.63$, $p < 0.001$)	($F_{1,20} = 7.672$, $p < 0.0118$)
GSH	($F_{1, 20} = 9.577$, $p = 0.0057$)	($F_{1,20} = 56.90$, $p < 0.0001$)	ns
MDA	($F_{1, 20} = 17.05$, $p < 0.0005$)	($F_{1,20} = 82.7$, $p < 0.0001$).	ns

The table presents the F and associated p values for enzyme activity and MDA levels of HPO-treated small and large intestines.

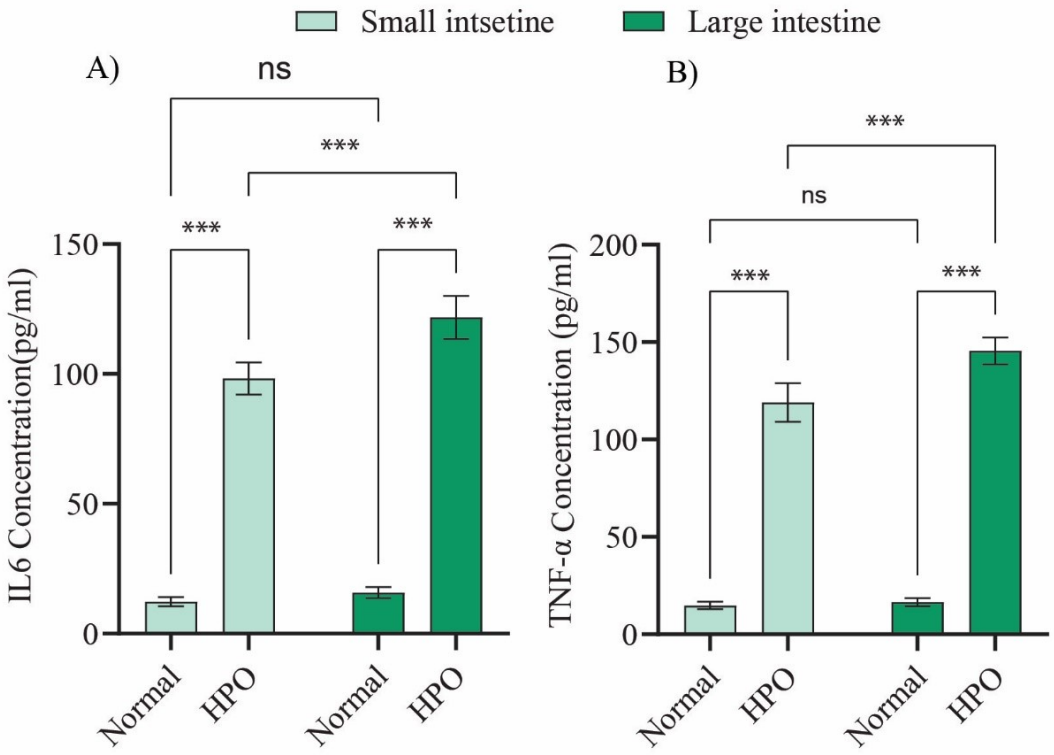

Figure 5.3 A) IL-6 and B) TNF-α concentrations in the mouse small and large intestines following HPO treatment. Results are presented as mean ± SD. Significant differences were observed in both the small and large intestines, analysed using two-way ANOVA, with ***$P < 0.001$ compared to untreated normal mice.

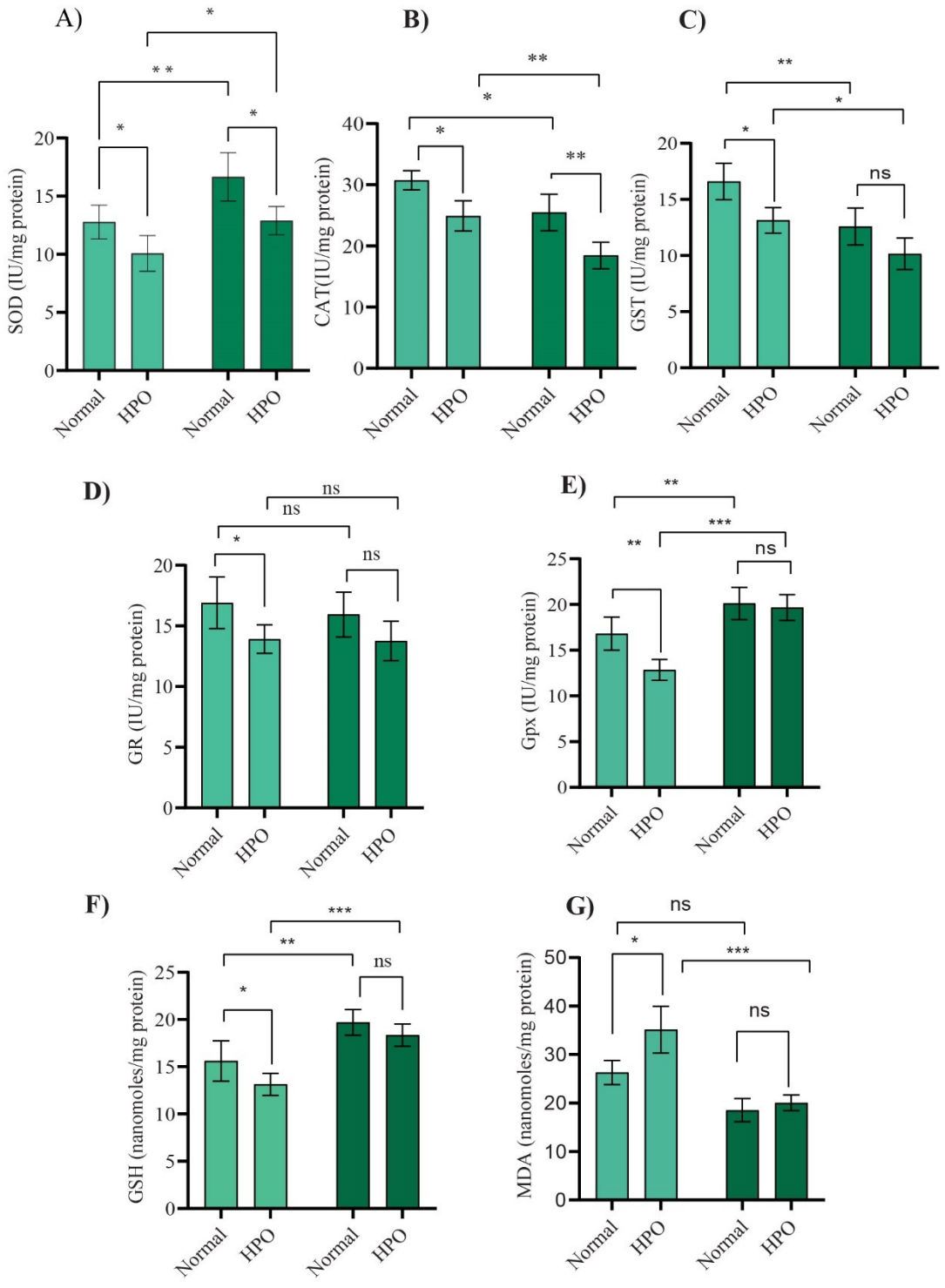

Figure 5.4 Antioxidant levels and oxidative stress in the small and large intestines of mice after HPO gavage. Graphical representation of antioxidant activities, including (A) SOD, (B) CAT, (C) GST, (D) GR, (E) GPx, (F) GSH, and (G) MDA levels in the small and large intestines following HPO gavage. Two-way ANOVA was used to assess the effects of HPO treatment and tissue type on antioxidant and MDA levels. Data are presented as mean ± SD. *$p < 0.05$, **$p < 0.01$, ***$p < 0.001$ vs Normal.

5.3.5 HPO induced ER stress in mouse intestines

RT-qPCR analysis revealed significant upregulation of ER stress markers *Bip*, *Chop*, and *Atf6* in intestines following HPO oral gavage. Specifically, the relative fold change for *Bip* was 2.97±0.36 in the small intestine and 3.08±0.46 in the large intestine (Fig 5.5A&B); for *Chop*, it was 2.75±0.3 in the small intestine and 2.00±0.3 in the large intestine (Fig 5.5C&D); and for *Atf6*, it was 1.95±0.154 in the small intestine and 1.98±0.27 in the large intestine (Fig 5.5E&F). The student's t-test analysis confirmed significant changes in the expression of these ER stress markers between the normal and HPO groups.

5.3.6 HPO upregulates *Perk/Atf4* pathway and antioxidant genes

The study investigated the activation of genes within the *Perk/Atf4* pathway and its association with the upregulation of antioxidant genes, including *Nrf2*, *Nqo1*, and *Ho-1*. In the small intestine, the relative fold change for *Perk* was 3.34 ± 0.47, while in the large intestine, it was 2.35 ± 0.37 (Fig 5.6 A&B). Similarly, *Atf4* expression showed a relative fold change of 2.08 ± 0.34 in the small intestine and 2.5 ± 0.42 in the large intestine (Fig 5.6 C&D).

The significantly higher *Perk* expression in the small intestine suggests greater cellular stress or protein misfolding in this region, or a more active response to specific physiological conditions. In contrast, the higher *Atf4* expression in the large intestine (2.5 ± 0.42 vs. 2.08 ± 0.34) indicates a stronger adaptive response to stressors such as nutrient deprivation, hypoxia, or inflammation. Additionally, *Perk* expression is higher than *Atf4* in the small intestine, whereas *Atf4* expression exceeds *Perk* in the large intestine, highlighting tissue-specific differences in the stress response.

The downstream mediators of the *Perk*/ *Atf4* pathway, *Nrf2*, *Nqo1*, and *Ho-1*, were analysed. *Nrf2* showed a relative fold change of 5.2 ± 0.5 in the small intestine and 4.16 ± 0.2 in the large intestine, indicating significant upregulation in both regions following HPO treatment (Fig 5.7 A&B). Similarly, *Nqo1* expression was 2.32 ± 0.20 in the HPO group compared to 1.8 ± 0.18 in the normal large intestine, with significant differences observed between the normal and HPO groups (Fig 5.7 C&D). The relative fold change for *Ho-1* was 2.03 ± 0.2 in the small intestine and 1.77 ± 0.1 in the large intestine, also showing significant upregulation in both tissues (Fig 5.7 E&F). Notably, *Nrf2*, *Nqo1*, and *Ho-1* expression levels were higher in the small intestine than in the large intestine (Fig 5.7).

5.4.7 HPO upregulates *Ire1/Xbp1* pathway and autophagy genes

The analysis next focused on the activation of the *Ire1/Xbp1, the* UPR arm and the upregulation of autophagy-associated genes *Becn1* and *Lc3b1 Ire1* exhibited significant relative fold changes of 2.4 ± 0.4 in the small intestine and 3.3 ± 0.2 in the large intestine compared to normal conditions (Fig 5.8 A&B). Similarly, *Xbp1* showed significant relative fold changes of 2.1 ± 0.3 in the small intestine and 2.3 ± 0.1 in the large intestine, with a substantial difference in *Xbp1* expression levels between the control and HPO groups (Fig 5.8 C&D).

Additinlly, the study examined autophagy genes *Becn1* and *Lc3b1* activation The expression of *Becn1* showed a relative fold change of 1.8 ± 0.12 in the small intestine, which increased to 1.94 ± 0.2 in the large intestine with HPO treatment (Fig 5.9 A&B). Similarly, the relative fold change in *Lc3b1* between the HPO group and the control was 1.82 ± 0.15 in the small intestine and 1.90 ± 0.16 in the large intestine. Notably, there was no apparent correlation between tissue type and HPO treatment in *Lc3b1* expression levels (Fig 5.9 C&D). It was evident that *Becn1* expression was higher in the HPO-treated large intestine compared to the small intestine. However, the expression of *Lc3b1* was approximately similar between the small and large intestines following HPO treatment.

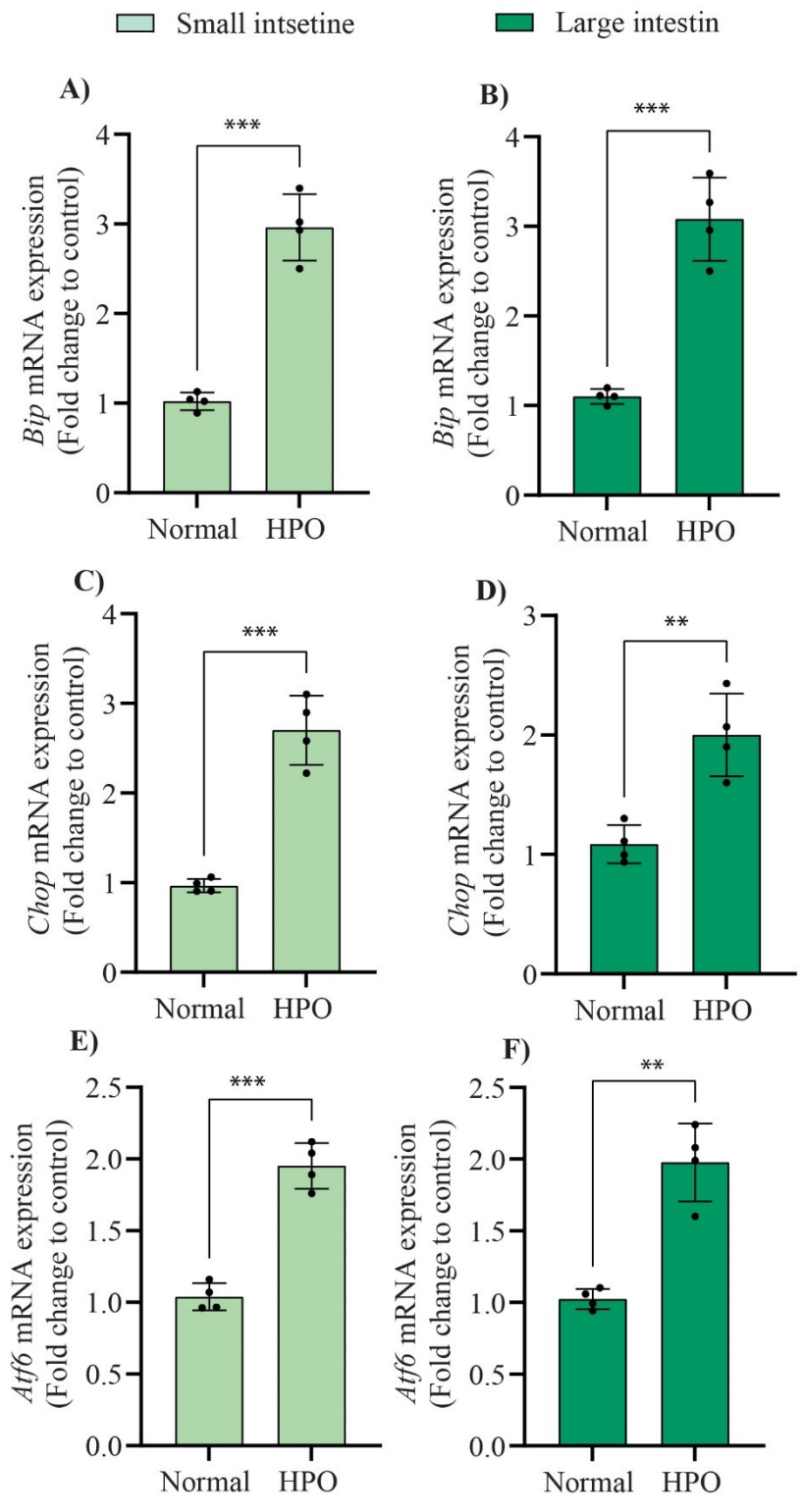

Figure 5.5 The effects of HPO treatment on ER stress markers in the small and large intestines— (A, B) *Bip*, (C, D) *Chop*, and (E, F) *Atf6*—were evaluated by RT-PCR. Student's t-test revealed significant upregulation of *Bip, Chop*, and *Atf6* in both tissues compared to Normal. Data are presented as mean ± SD, with $^{**}p < 0.01$ and $^{***}p < 0.001$ indicating significance

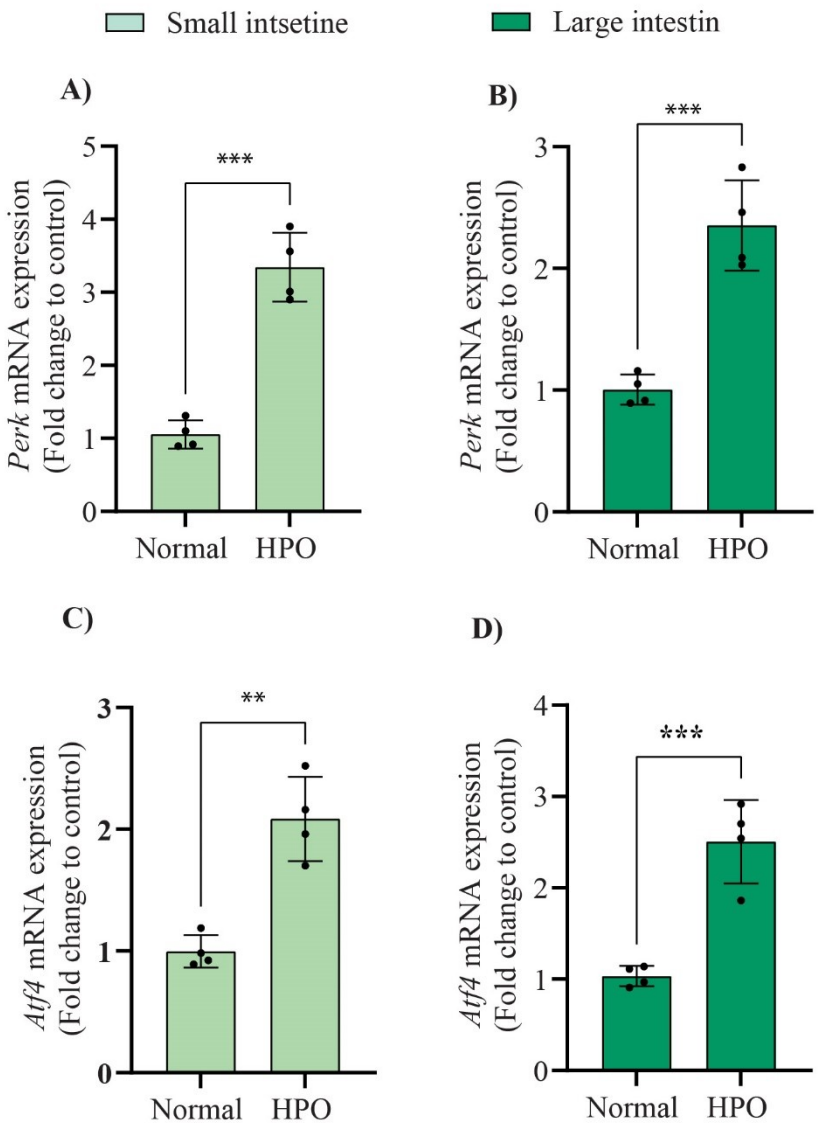

Figure 5.6 *Perk* (A, B) and *Atf4* (C, D) upregulation in mouse intestines post-HPO treatment were analysed via RT-PCR. Genes were significantly upregulated vs Normal (Student's t-test; $^{**}p < 0.01$, $^{***}p < 0.001$). Data are mean ± SD.

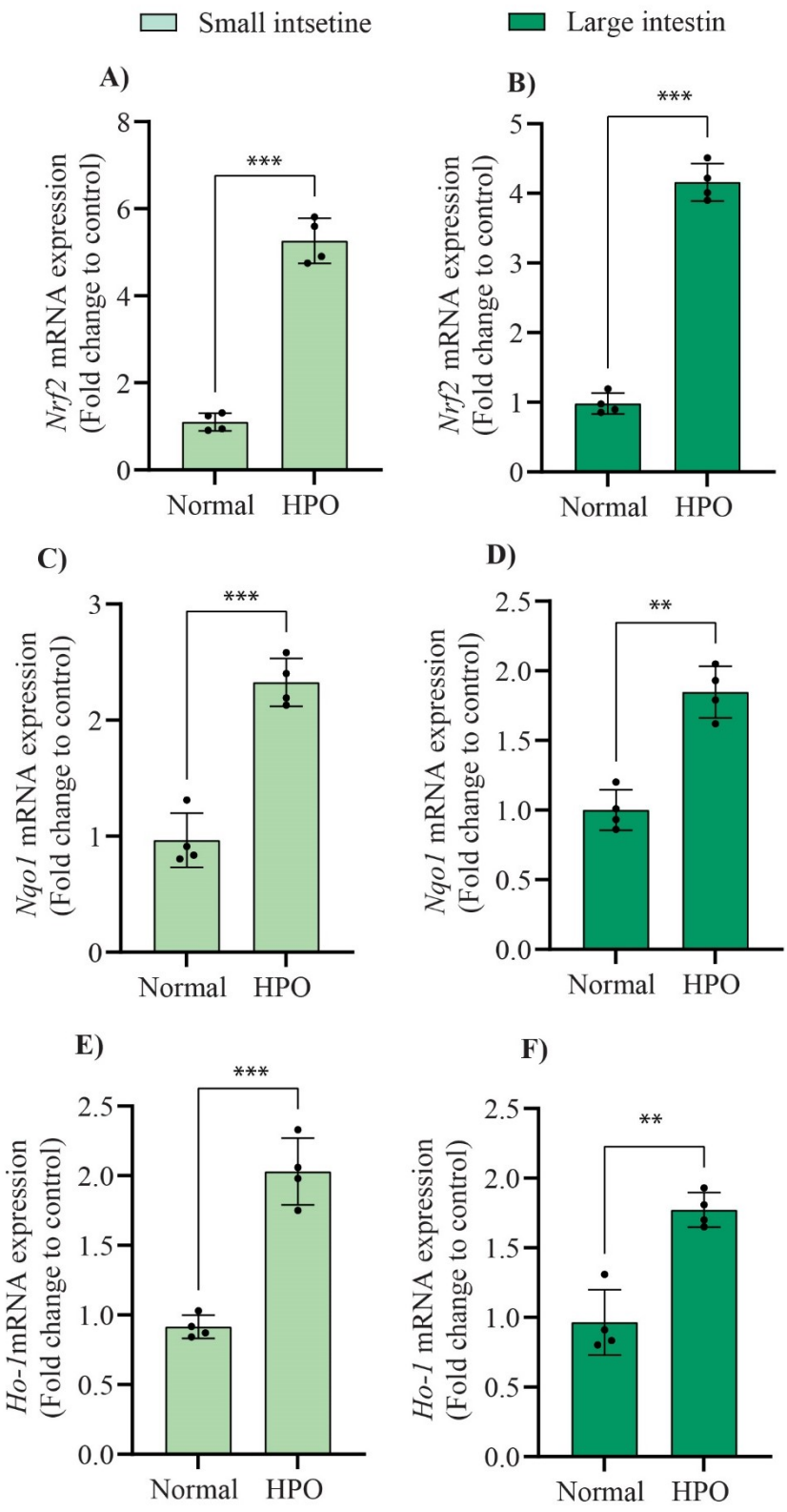

igure 5.7 RT-PCR analysis of *Nrf2* (A, B), *Nqo1* (C, D), and *Ho-1* (E, F) expression in mouse intestines ter HPO treatment. *Nrf2*, *Chop*, and *Ho-1* were significantly upregulated (**$p < 0.01$; ***$p < 0.001$, udent's t-test). Data are mean ± SD.

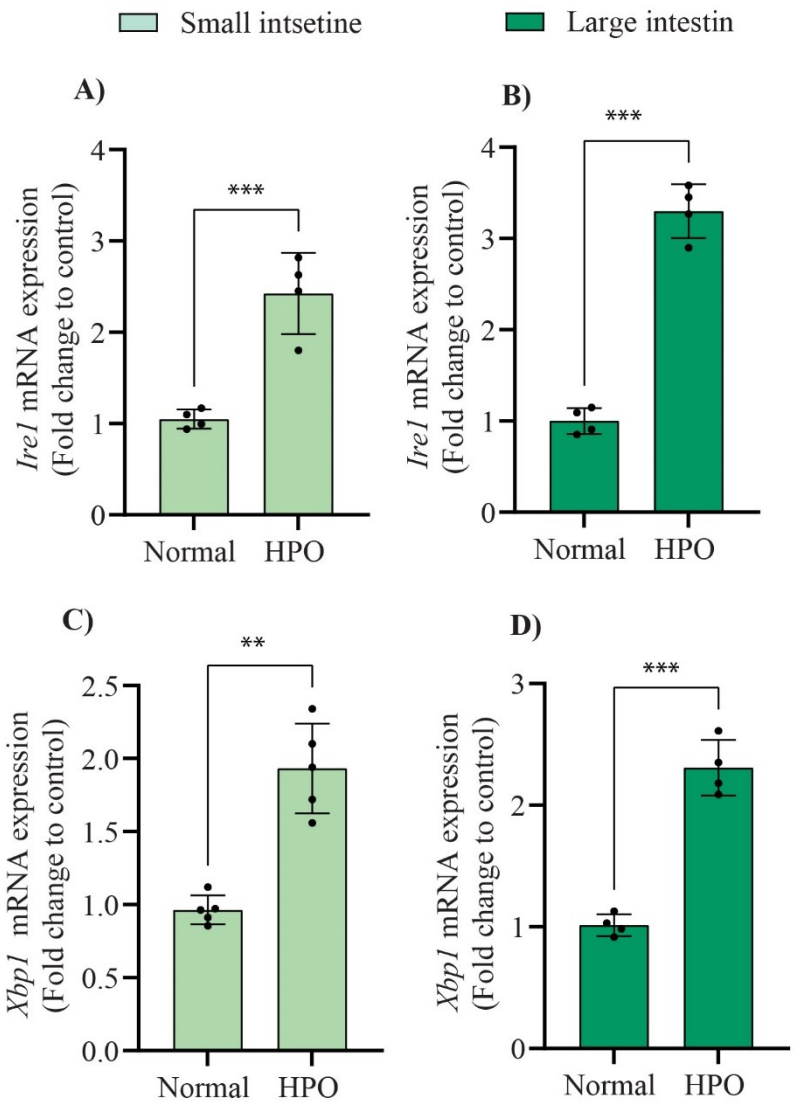

Figure 5.8 RT-PCR analysis of *Ire1* (A, B) and *Xbp1* (C, D) expression in mouse intestines after HPO treatment. Both *Ire1* and *Xbp1* were significantly upregulated *(**$p < 0.01$; ***$p < 0.001$*, Student's t-test). Data are mean ± SD.

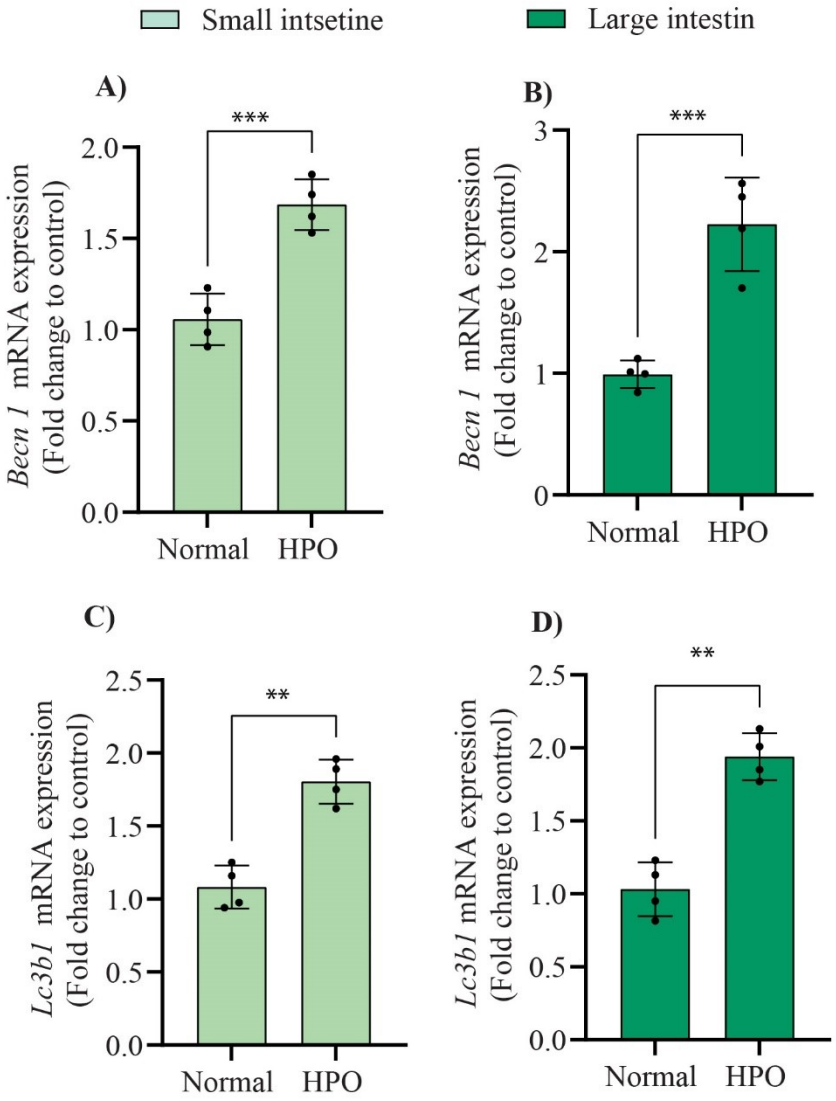

5.4

Figure 5.9 RT-PCR analysis of *Becn1* (A, B) and *Lc3b1* (C, D) expression in mouse intestines after HPO treatment. Both *Becn1* and *Lc3b1* were significantly upregulated *(**p < 0.01; *p < 0.001*, Student's t-test). Data are mean ± SD.

5.4 Discussion

In recent decades, concerns have emerged regarding the safety of palm oil, a highly consumed product, due to its elevated level of saturated palmitic acid. It was evident that palm oil in the diet can result in excess fat accumulation in the distal intestine. Persistent palm oil consumption can result in notable damage and dysfunction within the small intestine, characterized by destructive enteritis, diminished cell proliferation, and compromised absorptive function (Singh *et al*., 2021a). Palmitic acid, abundant in palm oil, is identified as a significant contributor to the adverse effects associated with its consumption, potentially leading to various diseases (Fang *et al*., 2022a, Mancini *et al*., 2015b). This experimental study aimed to evaluate whether prolonged consumption of heat-treated palm oil induces the development of endoplasmic reticulum stress and influences the corresponding morphology and function of the small intestine.

Heated palm oil (HPO) was found to induce notable structural and functional alterations in mice intestines. The findings indicate oxidative stress, immune cell infiltration, and tissue destruction. In the small intestine, a reduction in superoxide dismutase (SOD), catalase (CAT), and glutathione-related antioxidants was observed, accompanied by an increase in lipid peroxidation level. These results suggest enhanced lipotoxicity in the small intestine, while the large intestine exhibits a more pronounced inflammatory response. Thus, it is assumed that the large intestine is less susceptible to oxidative stress-induced lipotoxicity owing to its restricted lipid absorption and unprocessed lipids in cells. Evidently, palmitic acid resulted in lipotoxicity, decreasing goblet cell numbers and significantly reducing *MUC2*, the gene associated with mucin production (Filippello *et al*., 2022). Moreover, it is reported that saturated high-fat diets can amplify paracellular ion permeability and increase macrophage intrusion in the colon (Ghezzal *et al*., 2020). This highlights the detrimental effects of specific dietary components on intestinal barrier function and immune homeostasis. This difference in vulnerability also reflects the functional disparities between the two regions.

The study revealed that palm oil-induced oxidative stress triggers ERS, as evidenced by elevated ER stress markers like *Bip, Chop, and Atf6*. Further, we find alteration of UPR arm components by the administration of HPO, predominantly *Perk/Atf4* in the small and *Ire1/Xbp1* pathway in the large intestine, respectively. ER stress response resulted in the necrosis of intestinal epithelial cells (IECs). This process leads to the depletion of goblet

cells, a diminished mucus barrier, increased microbial infiltration into the epithelium, and the initiation of various proinflammatory cytokines (Kennelly *et al*., 2021).

The *PERK/ATF4* pathway is pivotal in the highly regenerative small intestine, which serves as the primary site for nutrient absorption as it mitigates the stress and enhances regeneration (Jin *et al*., 2016b). Unlike the small intestine, the large intestine, which focuses on water absorption and electrolyte regulation, is less susceptible to oxidative stress-induced lipotoxicity owed to its limited lipid absorption and unprocessed lipids in cells (Utsunomiya *et al*., 2017, Snipes, 1977). However, high ROS was due to the enteric bacteria in gut epithelia (Jones and Neish, 2017, Zhang and Kaufman, 2008b). The presence of oxidative stress in small and large intestines is evidenced by *Nrf2* activation and subsequent upregulation of *Nqo-1* and *Ho-1*. It revealed discernible variations in the extent of activation in the *PERK/ATF4* branch, indicating different sources of reactive oxygen species development attributed to excess palm oil intake in both intestinal segments.

This increased *Ire1* and *Xbp1* expression potentially strengthens ER-associated degradation and protein folding, signalling a preference for cellular survival (Sun *et al*., 2015). The IRE1/XBP1 expression was comparatively high in the large intestine when HPO was administered. This upregulation indicates a significant role in ER stress response and autophagic regulation. As mentioned, limited lipid absorption and its unprocessed state or altered gut microbiota may induce heightened XBP1 splicing, reflected in increased *Beclin 1* and *Lc3b1* expression, indicating a sustained autophagic response and substantial immune cell infiltration. It was reported that disturbed autophagy in epithelial cells changes the intestinal flora and immune responses (Yang *et al*., 2018b). Moreover, a palm oil-enriched diet induces gut dysbiosis, enhances the translocation of lipopolysaccharide to tissues, and elevates plasma concentration of pro/anti-inflammatory cytokines like IL-6 (Laugerette *et al*., 2012). The current study observed significant production of IL-6 and TNF-α by the infiltrated immune cells in the intestine. It is assumed the damage is associated with the output of the proinflammatory cytokines. From the examination of the small and large intestines, it is apparent that there is a distinct role for *Ire1/Xbp1* activation, with consistently lower activation observed in the small intestine compared to the large intestine. Palmitic acid, hence, has the potential to influence gut disturbances ignificantly. The study elucidates the role of palm oil in influencing gut disturbances significantly, including ER stress and UPR signalling in oxidative stress-mediated lipotoxicity and the subsequent

inflammatory response in the gut. The study reveals the role of ER stress and UPR signalling in oxidative stress-directed lipotoxicity and consequent inflammatory response in the gut.

Chapter 6

Impact of prolonged excessive palm oil intake on the development and progression of CT26 cells induced colon cancer metastasis

6.1 Introduction

Palm oil is a rich source of vitamin E, tocotrienols, antioxidants, beta-carotene, and palmitic acid, which support heart health, skin, and immune function. Palmitic acid, a saturated fatty acid, positively affects energy production, cell membrane integrity, protein regulation, immune modulation, lipid transport, and wound healing in specific contexts. However, prolonged consumption of palm oil, due to its high palmitic acid content may contribute to metabolic diseases and promote cancer progression and metastasis. While its impact on cancer, particularly colon cancer, has been studied, the underlying mechanisms remain largely unexplored. The previous chapters emphasized increased generation of oxidative and subsequent ER stress and inflammation and alteration in mice's histopathological architecture of intestinal tissues by excessive consumption of palm oil in intestines, demonstrating its harmful effect on intestinal health. These findings place the groundwork for exploring its broader role in cancer progression and metastasis.

High-fat diets (HFDs) enriched with high palm oil content have been widely used to study and analyse the effects of palm oil on the physiology and health of experimental animals (Fattore *et al*., 2013, Forman *et al*., 2010). While extensive research has focused on the impact of dietary factors on cancer risk, the specific role of palm oil in colon cancer metastasis remains largely unexplored. This emphasizes the need for further research to elucidate how prolonged dietary exposure to HPO may impact the tumour microenvironment and enhance metastatic potential in colon cancer. Recent studies have revealed that palmitic acid ~~can~~ induce colorectal cancer progression by the activation of the *β*-catenin signalling pathway through dephosphorylation of ACOX1 and palmitoylation of *β*-catenin, key drivers of cancer progression (Zhang *et al*., 2023). Dietary palmitic acid has been shown to induce a pro-metastatic memory through its interaction with Schwann cells (Pascual *et al*., 2021b).

Additionally, palmitic acid has been implicated in melanoma metastasis to the lungs *via* the TLR4/TRIF-Peli1-pNF-κB signalling pathway, highlighting its role in cancer progression in melanomas (Zhang *et al*., 2022a). Furthermore, palmitic acid contributes to cancer cell migration by repressing desmoplakin, and clinical data correlates this mechanism to poor patient outcomes (Nath *et al*., 2021). Considering these, the study is aimed to explore how a palm oil-rich diet influences the progression and metastasis

of colon cancer. For this, the physiological, haematological, and biochemical aspects are examined to clarify the mechanisms underlying the association of palm oil consumption with progression. The study uses heated palm oil, processed at temperatures below 750°C for 30 min, which aligns with traditional cooking practices that preserve its nutritional properties without significant thermal oxidation. Heated palm oil is used in this study, making it relevant to explore its potential health impacts. Based on prior findings, it is hypothesized that prolonged exposure to palm oil rich in palmitic acid influences cancer cell behaviour, potentially exacerbating metastatic progression.

We utilised a multidisciplinary approach integrating animal models and molecular analyses to test this hypothesis. Four groups of animals were selected: Group 1 (normal), group 2 (HPO-heated palm oil positive control), group 3 (CT26 - metastasis control), and group 4 (HPO+CT26). The HPO group received oral gavage of heated palm oil for four months, after which CT26 murine metastatic colon cancer cells were inoculated into the second and third groups to induce pulmonary metastasis. The study design incorporates physiological, biochemical, and haematological assessments, along with histopathological analysis, to evaluate the effects of palm oil on cancer progression. By advancing our understanding of how dietary fat influences cancer progression, we aim to uncover new therapeutic strategies to combat colon cancer metastasis. However, the study's limitations, such as potential confounding factors, variability in dietary patterns, and complex tumour-host interactions, must be acknowledged.

6.2 Graphical abstract

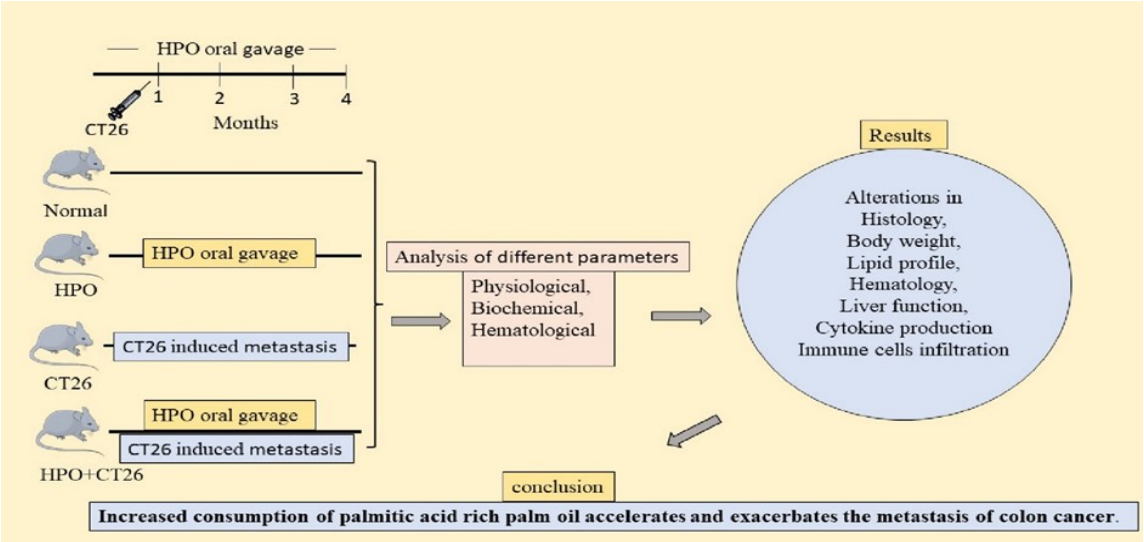

6.3 Materials and Methods

6.3.1 GC-MS/MS analysis for palmitic acid quantification in palm oil

GC-MS/MS analysis was carried out in palm oil to detect and quantify the amount of palmitic acid in it as per the protocol mentioned in Chapter 2, Materials and methods, Section 2.1.7

6.3.2 Cell line and culture condition

The CT26 mouse metastatic colon cancer cell line was a gift by Dr. Bipasha Bose, Professor, Yenepoya Hospital, Manipal. All experiments were conducted under sterile conditions. The cells were cultured in RPMI media supplemented with 100 u/mL penicillin, 100 μg/mL streptomycin, and 10% heat-inactivated FBS and maintained at 37°C in a 5% CO_2 incubator.

6.3.3 Animals, grouping, and experimental procedures

Male BALB/c mice weighing 28-32 g were purchased from the Kerala Veterinary and Animal Sciences University (KVASU), Mannuthy, Thrissur. Polypropylene cages were used to house the animals at the Animal House Facility of Amala Cancer Research Centre. During their acclimatisation, they were fed non-purified rat chow and filtered water for two weeks. The Institutional Animal Ethics Committee (IAEC) approved all the animal experiments before they were carried out (No. ACRC/IAEC/21(2)-P11 Dt. 2-12-2021). Every protocol was done according to the rules of the Committee for

Control and Supervision of Animal Experiments (CCSAE), Ministry of Environment, Forest, and Climate Change, Gov. of India.

In this experimental setup, group 1 is the standard control, and group 2 is the positive control, receiving daily oral gavage of 200 μL palm oil, equivalent to 73.4 mg of palmitic acid per day, over 4 months. Group 3 acts as the CT26 metastasis control, and Group 4 undergoes both heated palm oil (HPO) oral gavage and CT26 for tumour initiation and subsequent metastasis. Group 3 was inoculated with 1×10^5 CT26 cells in 200 μL PBS *via* the tail vein to initiate pulmonary metastases after one month. Group 4 was given oral gavage of palm oil with normal chow, and after one month of palm oil oral gavage, 1×10^5 CT26 cells were inoculated to develop pulmonary metastasis. The present experimental design facilitates the investigation of the distinct and combined impacts of CT26 metastases and palm oil. Detailed explanation was given in Chapter 2, Materials and Methods, Section 2.2.2

6.3.4 Analysis of physiological parameters - body weight, food and water intake

Body weight was assessed every week for the duration of the four-month study. At the end of the study, the average body weight per group and % change in body weight was calculated. Each group's average food/water intake was recorded twice weekly. Group-specific food/water consumption was calculated by subtracting the residual food/volume of water from the initial amount/volume given. The average daily food/water intake per group was calculated by dividing total consumption by the study duration. Chapter 2, Materials and Methods, Section 2.2.2.3 mentions detailed procedures and equations.

6.3.5 Analysis of haematological parameters

The haematological test evaluated a comprehensive range of parameters for analysing different aspects of blood composition and cellular characteristics. These parameters encompass red blood cells (RBC) measured in 10^6 cells/µL, reticulocytes as a percentage (%), haemoglobin concentration in g/dL, haematocrit percentage (%), mean corpuscular volume (MCV) in femtoliters (fL), mean corpuscular haemoglobin (MCH) in picograms (pg.), mean corpuscular haemoglobin concentration (MCHC) in grams per litre (g/L), red cell distribution width (RDW) as a percentage (%), platelet count in $\times 10^3/\mu$L, mean platelet volume (MPV) in femtoliters (fL), platelet crit percentage (%), platelet distribution width (PDW) as a percentage (%), white blood cells (WBC) count

in × $10^3/\mu$L, and a white blood cell differential count. These parameters collectively offer valuable insights into blood cellular composition. Detailed procedures were mentioned in Chapter 2, Materials and methods, Section 2.2.2.4

6.3.6 Analysis of glucose tolerance

The fasting glucose levels of mice were evaluated utilising One Touch Select strips after an overnight fast. Blood glucose levels were monitored at 30, 60, 90, and 120 min after administering 1.5 g/kg glucose; the collected data were used to generate a graph and compute the area under the curve in Microsoft Office Excel 2010. As detailed in Chapter 2, Materials and methods, Section 2.2.2.5

6.3.7 Analysis of serum lipid profiles

Initial measurements were taken of total cholesterol (TC), low-density lipoprotein (LDL) cholesterol, and high-density lipoprotein (HDL) cholesterol. Low-density lipoprotein (VLDL) cholesterol concentration was calculated using the data above. A detailed description is given in Chapter 2, Materials and methods, Section 2.2.3.5

6.3.8 Analysis of serum and tissue cytokines-IL6 and TNF-ά

The serum cytokines IL-6 TNF-ά were determined. Chapter 2, Materials and methods, Section 2.2.3.5.3, wrote the detailed protocol.

6.3.9 Analysis of liver toxicity markers, total protein and total bilirubin

The enzyme activities such as aspartate aminotransferase (AST), alanine aminotransferase (ALT), alkaline phosphatase (ALP) in IU/L, Total protein, and bilirubin reflecting liver function were performed in serum. Detailed procedures are mentioned in Chapter 2, Materials and Methods, Section 2.2.3.5.2.

6.3.10 Histopathological analysis

The tissue specimens underwent the following procedures: fixation in 8% buffered formalin, dehydration, xylene clearance, wax impregnation, and automated microtome sectioning at a 5μm thickness. The sections were rehydrated on glass slides, subjected to H&E staining, mounted with DPX, and scrutinised under a Magnus INVI microscope at the Amala Institute of Medical Science, under the supervision of a pathologist, as detailed in Chapter 2, Materials and methods, Section 2.2.2.6

6.3.11 Analysis of lung fibrosis

6 .3.11.1 Picrosirius staining of lung tissues

To examine collagen deposition, lung tissues were stained with picrosirius red (dispersed in a 0.1 per cent picric acid solution, with a thickness of 3 μm). Under a phase-contrast microscope, collagen fibres were identified as yellow-orange colour. Detailed procedures are mentioned in Chapter 2, Materials and Methods, Section 2.2.2.7

6.3.11.2 Analysis of hydroxyproline in lung tissues

Lung tissue samples from various experimental groups were harvested, digested, and then neutralised overnight at 110°C in 1 ml of 6N HCl. The pH of all samples was carefully adjusted to below 6. To initiate the collagen determination process, 100 μl of the prepared samples were mixed with 1ml of a chloramine T solution comprising 1.4% chloramine T, 10% isopropanol, and 0.5 M sodium acetate, all at pH 6, and left to react for 20 minutes at room temperature. Subsequently, 1ml of Ehrlich's solution (containing 14.9% p-dimethylaminobenzaldehyde, 70% isopropanol, and 20% perchloric acid from Sigma-Aldrich) was added to each sample, followed by an incubation period at 65°C for 15 min.

After incubation, 200 μl aliquots were carefully transferred to a 96-well plate, and the absorbance was measured at 570 nm. The collagen content in each sample was determined by comparing its absorbance with standards prepared with cis-hydroxyproline in concentrations ranging from 0.01 to 110 μg/ml. The conversion factor of 1 μg hydroxyproline, equivalent to 6.94 μg collagen, was employed for calculations (reference 61). Finally, the total collagen content was expressed as μg collagen per mg of wet tissue.

6.4 Statistical analysis

Results are expressed as Mean ± SD. Statistical analyses were performed using GraphPad Prism 6.0. Multiple group comparisons were conducted using one-way analysis of variance (ANOVA) followed by post hoc analysis. A p-value of $*P < 0.05$, $**P < 0.01$, *and* $***P < 0.001$ was considered statistically significant.

6.5 Results

6.5.1 Impact of HPO on CT26 lung metastasis and associated pathology

Histopathological analysis revealed an increased level of metastatic distribution in the HPO+CT26 group compared to the CT26 metastatic control. Additionally, increased infiltration of inflammatory cells was observed in the HPO group compared to the control group. Within the CT26 group, a moderate level of inflammatory cells was evident, forming a component of the metastatic process (Fig 6.1). Additionally, Ki-67 staining of lung histological sections revealed a significantly higher incidence of metastasis in the HPO+CT26 group compared to the CT26 group alone, suggesting that HPO enhances cancer cell metastasis (Fig 6.2).

6.5.2 Effect of HPO on collagen deposition

Excessive HPO consumption led to increased lung hydroxyproline content, a prominent collagen component and fibrosis marker, in both the HPO (13.6 ± 1.4) and HPO+CT26 (12.7± 2.05) groups compared to the normal (1.3 ± 3.14) and CT26 (4.1 ± 0.933) groups (Fig 6.3B). Sirius Red staining demonstrated heightened collagen deposition in lung tissues induced by palm oil intake compared to the normal and CT26 groups (Fig 8e). These findndings indicate palm oil's role in promoting fibrosis in lung tissues (Fig 6.3A).

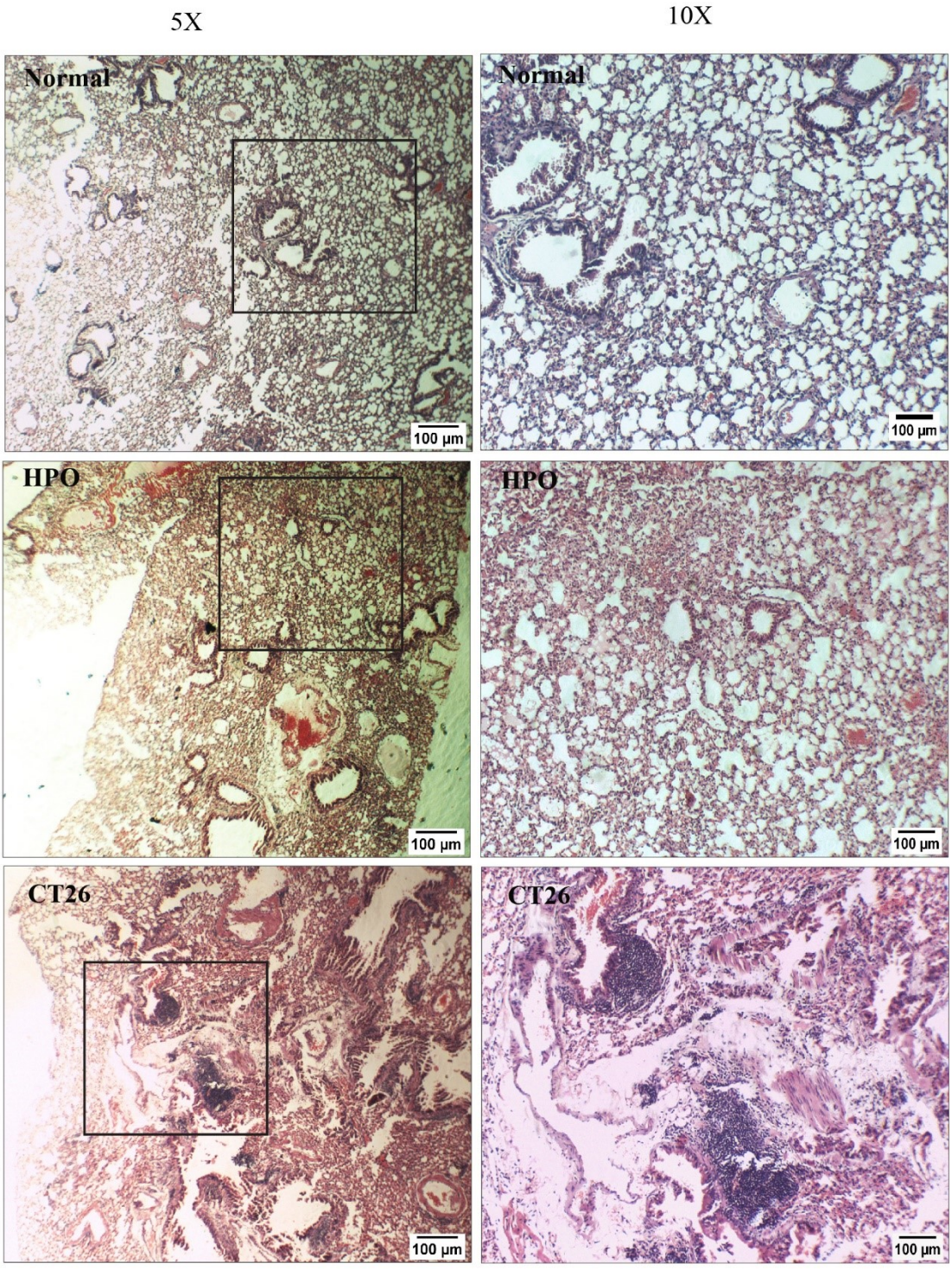
5X
10X
Normal
Normal
100 µm
100 µm
HPO
HPO
100 µm
100 µm
CT26
CT26
100 µm
100 µm

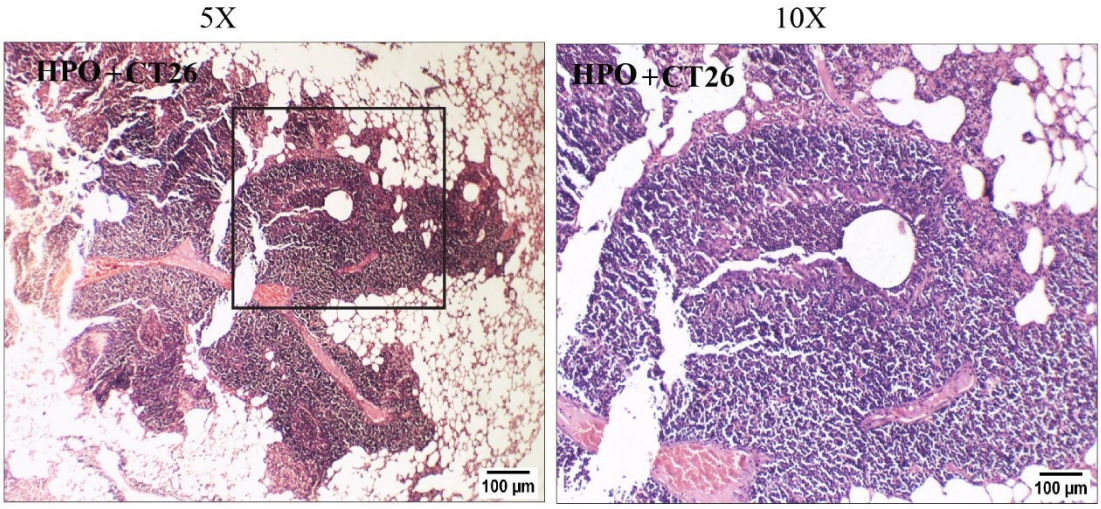

Figure 6.1 Histopathological analysis of CT26 pulmonary metastasis showing lung tissue sections from Normal, HPO, CT26 (previous page), and HPO+CT26 groups, captured using phase-contrast microscopy at 50X (left) and 100X (right) magnification, with a 100µm scale bar. The rectangular area in the left panel (5X) is enlarged in the right panel (10X).

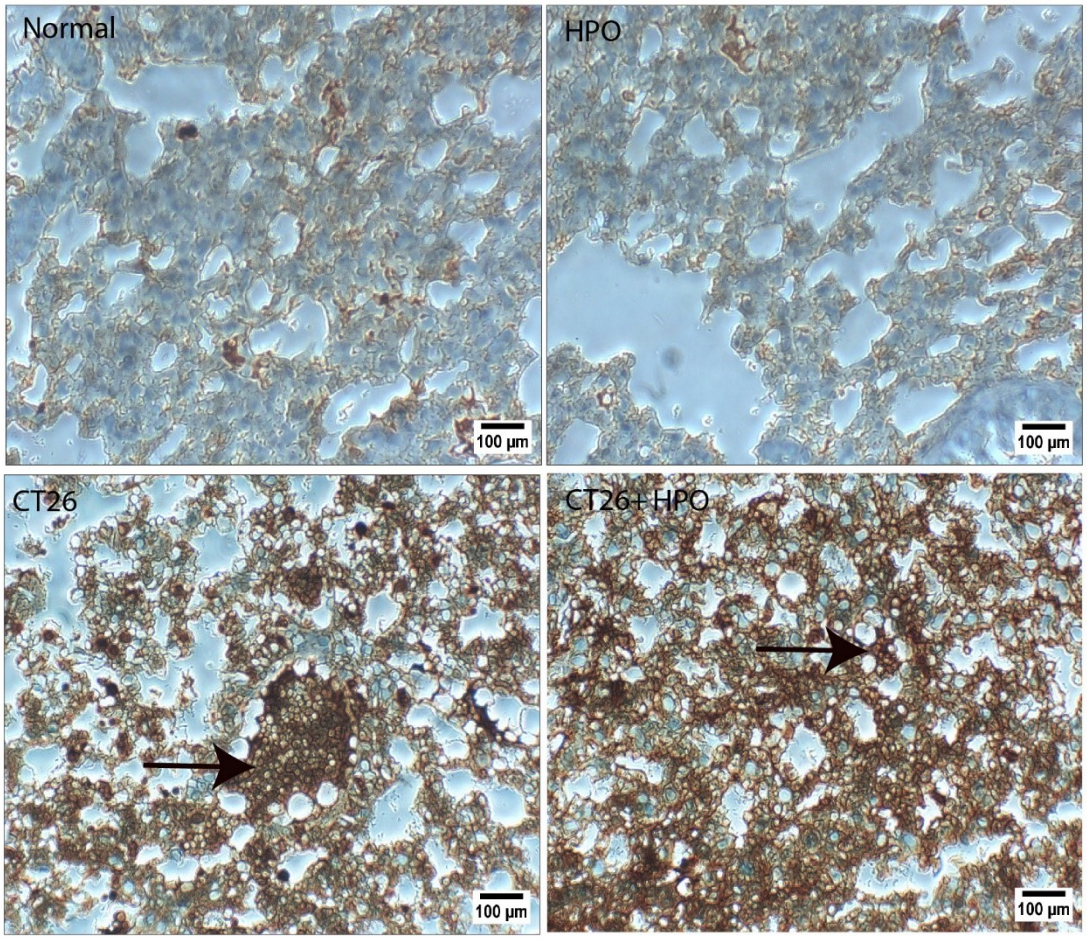

Figure 6.2 Ki-67 staining of lung histological sections in Normal, HPO, CT26, and HPO+CT26 groups, captured using phase-contrast microscopy at 200X magnification, with a 100µm scale bar. Metastatic activity is observed in the CT26 and HPO+CT26 groups. Black arrows indicate metastatic cells.

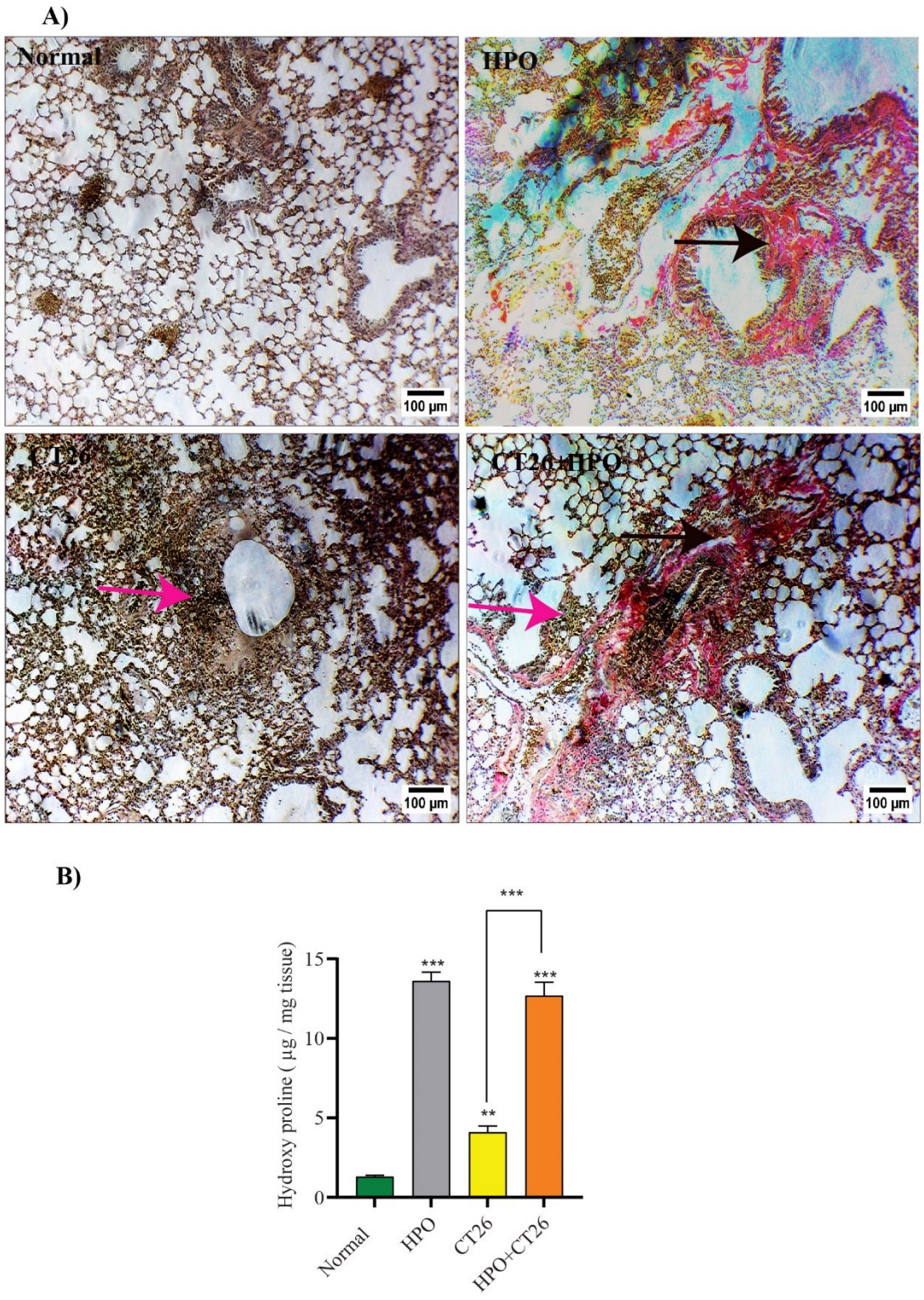

Figure 6.3 (A) Sirius red staining for collagen (100X, scale bar 100 µm) showing collagen deposition (black arrows) in HPO and HPO+CT26 groups. (B) Hydroxyproline content in lung tissue of Normal, HPO, CT26, and HPO+CT26 groups post-HPO, with metastatic cells marked by pink arrows in CT26 and HPO+CT26. Data as mean ± SD. Statistical analysis: One-way ANOVA, Tukey's post hoc test; $**p \leq 0.01$, $***p \leq 0.001$.

6.5.3 Effect of HPO on body weight, food and water intake in mice

The study assessed the changes in body weight of mice across four experimental groups: normal, HPO, CT26, and HPO + CT26, over 16 weeks. Initially, all groups had similar baseline average weights: normal (25.14 ± 0.58 g), HPO (25.05 ± 0.63 g), CT26 (24.99 ± 0.57 g), and HPO + CT26 (24.79 ± 0.55 g). By week 8, the normal group showed significant weight gain, averaging 28.41 ± 0.75 g, followed by HPO (27.03 ± 0.65 g), HPO + CT26 (27.09 ± 0.71 g), and CT26 (26.90 ± 0.68 g). At week 16, the normal group maintained the highest weight (31.11 ± 0.89 g), followed by CT26 (30.65 ± 0.84 g), HPO (30.03 ± 0.87 g), and HPO + CT26 (29.43 ± 0.92 g). The normal group exhibited consistent and significant weight gain, while the HPO + CT26 group showed reduced weight gain, suggesting a potential interaction between HPO and CT26 (Fig 6.4A). The percentage change in body weight confirmed these trends: normal (23.85 ± 2.13%), CT26 (22.71 ± 2.50%), HPO (19.91 ± 1.97%), and HPO + CT26 (18.67 ± 3.39%). The HPO and HPO + CT26 groups experienced diminished weight gain compared to the control group, with the HPO + CT26 group showing a significant weight gain reduction compared to the CT26 group alone (Fig 6.4B).

It was evident that the normal group exhibited significant weight gain, indicating typical growth. The HPO group had reduced weight gain, suggesting HPO treatment may moderate body weight increase. The CT26 group, representing tumour-bearing mice, showed slightly reduced weight gain, indicating the tumour may affect metabolism but not ultimately impair growth. However, the HPO + CT26 group had the lowest weight gain, significantly lower than the CT26 group, suggesting HPO treatment in combination with the tumour suppresses weight gain. These findings imply that HPO may influence growth and energy balance in tumour-bearing mice, potentially affecting tumour-related changes in body weight.

Consistent with the weight gain changes, food intake was 5.7 ± 1.3 g/mouse/day in the Normal group and 5 ± 0.9 g/mouse/day in the CT26 group, while it was significantly reduced in the HPO and HPO + CT26 groups, with values of 4.4 ± 1.2 and 2.8 ± 1.4 g/mouse/day, respectively (Fig 6.4C). Similarly, water intake was 3.8 ± 1.1 ml/mouse/day in the Normal group and 3.5 ± 1.2 ml/mouse/day in the CT26 group, but decreased significantly in the HPO and HPO + CT26 groups, measuring 1.4 ± 0.7 and 1.8 ± 1.1 ml/mouse/day, respectively (Fig 6.4D). These findings suggest that the HPO and HPO + CT26 groups exhibit significant reductions in food and water intake

compared to the Normal and CT26 groups, with the most pronounced decrease observed in the HPO + CT26 group. This could indicate a potential synergistic effect between HPO and CT26, leading to greater disruptions in food and water consumption. The suppression of weight gain in the HPO and HPO+CT26 groups, compared to the control and CT26 groups, was attributed to reduced food and water intake in mice that consumed oil.

6.5.4 Effect of HPO on glucose tolerance

After a 16-week experimental period, OGTT (oral glucose tolerance test) was conducted to assess fasting blood glucose levels in mice groups. The pre-treatment analysis demonstrated no observable glucose intolerance across the normal, HPO, CT26, and HPO+CT26 groups, with glucose levels returning to near-fasting levels within 120 min (Fig 6.5A). Consequently, no significant changes were noted in the area under the curve among the four groups following glucose administration (Fig 6.5B). In post-treatment OGTT, the normal group displayed a response consistent with pre-treatment analysis. Significant hypoglycaemia was observed in the CT26 metastatic control group, with glucose levels increasing from an initial 86.75 ± 12.21 mg/dL to 216 ± 15.56 mg/dL and then returning to 96.52 ± 9.12 mg/dL within 120 min after oral glucose administration.

Conversely, both the HPO and HPO+CT26 groups exhibited initial glucose levels of 126 ± 13.94 mg/dL and 123 ± 16.34 mg/dL, respectively, which rose to 487.26 ± 15.45 mg/dL and 410 ± 12.21 mg/dL before declining to 167.6 ± 14.36 mg/dL and 145.69 ± 14.03 mg/dL, respectively, after oral glucose administration (Fig 6.5C). The HPO and HPO+CT26 groups displayed significant glucose intolerance, as indicated by the area under the curve analysis (Fig 6.5D).

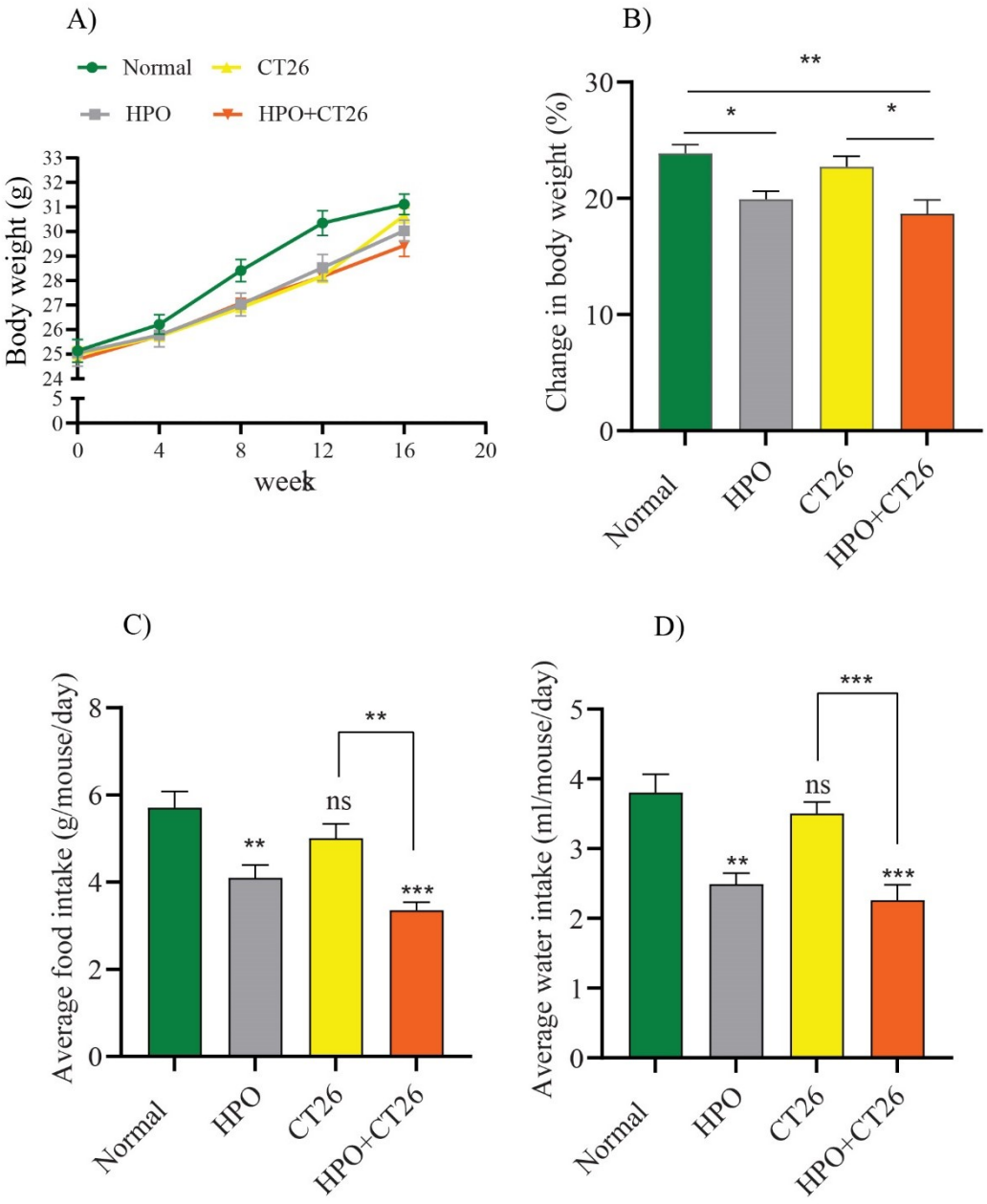

Figure 6.4 Body weight, food, and water intake in mice over four months. (A) Bi-weekly body weight measurements, (B) percentage body weight change at study end of the study (C) average food consumption (g/mouse/day), and (E) average water intake (ml/mouse/day). Data are mean ± SD; *$p \leq 0.05$, **$p \leq 0.0$, ***$p \leq 0.001$ (one-way ANOVA, Tukey's posthoc).

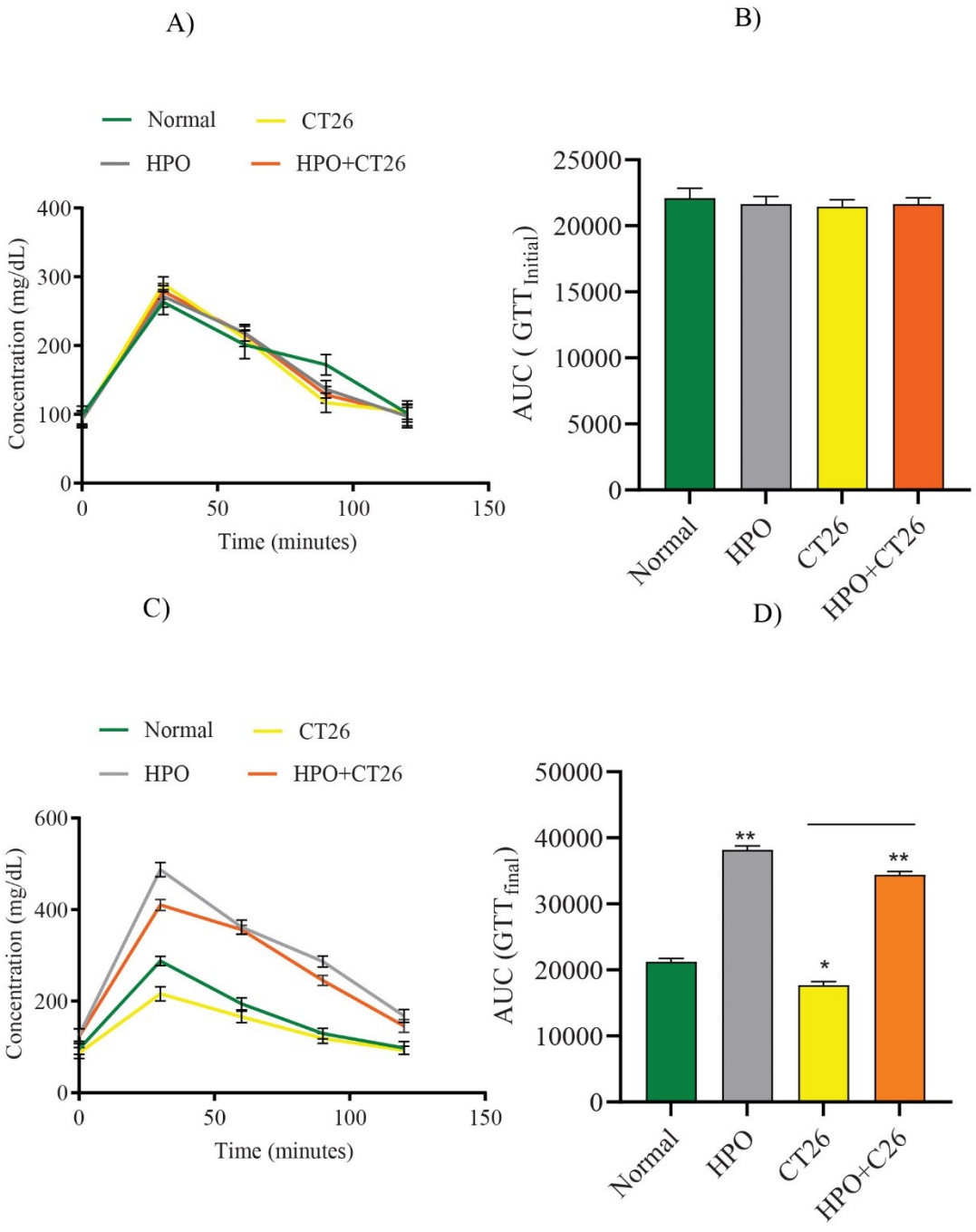

Figure 6.5. OGTT was conducted in experimental groups after overnight fasting, both before and at the end of the experiment. Line graphs (A) and (C) depict glucose tolerance before and after the experiment, respectively. Bar graphs (B) and (D) show the area under the curve (AUC) for initial and final glucose tolerance in the Normal, HPO, CT26, and HPO+CT26 groups. Results are mean ± SEM, with significance *(*$p \leq 0.05$, **$p \leq 0.005$)* analysed using one-way ANOVA and Tukey's posthoc test.

6.5.5 Changes in haematological parameters following HPO oral gavage

Haematological analysis showed no significant changes in haemoglobin (Hb), haematocrit (HCT), mean corpuscular haemoglobin (MCH), mean corpuscular haemoglobin concentration (MCHC), mean corpuscular volume (MCV), and red blood cell (RBC) counts (Fig. 6.6A). However, significant changes were observed in WBC, monocytes, neutrophils, lymphocytes, and platelets (Figs. 6.64 & 6.7(A & B)).

Total WBC counts significantly increased in the CT26 and HPO + CT26 groups compared to baseline levels. In contrast, the HPO group showed values similar to the normal group (Fig. 6.4b). Both the CT26 and HPO + CT26 groups showed a significant increase in total WBC counts, indicating a heightened immune response likely due to tumour presence and the combined effect of HPO treatment. Additionally, the HPO + CT26 group exhibited higher WBC counts than the CT26 group alone, suggesting an enhanced influence of HPO treatment (Fig. 6.6B).

Monocyte counts were elevated in the CT26 and HPO + CT26 groups compared to the normal level. The HPO group showed a mild decrease in trend monocyte count, though this reduction was insignificant (Fig. 6.6B). These results suggest that HPO in a metastasized condition is pro-inflammatory.

Neutrophil counts were significantly increased only in the HPO + CT26 group, with no significant changes observed in the HPO and CT26 groups compared to the normal group. The elevated neutrophil count in the HPO + CT26 group suggests that HPO treatment may influence the metastatic condition, possibly by enhancing the immune response in the presence of tumour growth (Fig. 6.6B).

Lymphocyte counts were significantly increased only in the HPO + CT26 group, while the HPO and CT26 groups were comparable to the normal group (Fig. 6.7A). Platelet counts significantly increased in the HPO and HPO + CT26 groups, whereas the CT26 group was similar to the normal group (Fig. 6.7B). These findings indicate distinct haematological responses to tumour growth and HPO treatment, highlighting their combined influence on lymphocyte and platelet dynamics.

A)

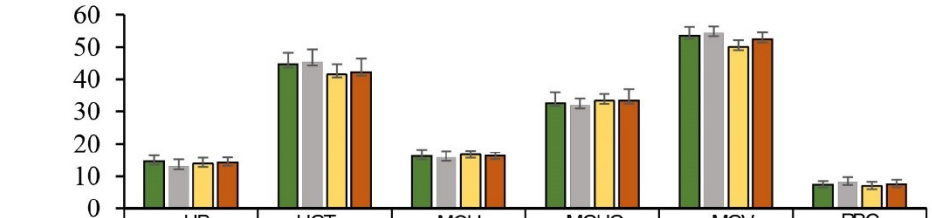

	HB (g/dL)	HCT (%)	MCH (pg/cell)	MCHC (%)	MCV (fl)	RBC (10^6/µL)
Normal	14.59 ± 1.8	44.61 ± 3.73	16.21 ± 2.01	32.67 ± 3.41	53.6 ± 2.62	7.42 ± 1.09
HPO	13.12 ± 2.1	45.32 ± 4.06	15.74 ± 1.99	31.9 ± 2.25	54.4 ± 2.01	8.32 ± 1.37
CT26	13.9 ± 1.84	41.56 ± 3.04	16.7 ± 1.13	33.44 ± 2.09	50.1 ± 2.08	7.03 ± 1.21
HPO+CT26	14.21 ± 1.61	42.13 ± 4.23	16.3 ± 1.04	33.49 ± 3.46	52.42 ± 2.17	7.59 ± 1.35

B)

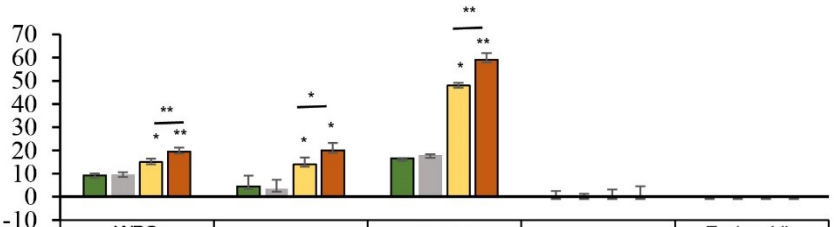

	WBC 10^3/µl)	MONO (%)	Neutrophils (%)	Basophils (%)	Eosinophils (%)
Normal	9.2	4.39	16.49	0.003	0.0009
HPO	9.5	3.27	17.92	0.0088	0.00016
CT26	18.6 ± 1.4	14.3 ± 1.13	48.14 ± 3.09	0.28 ± 0.0071	0.93 ± 0.059
HPO+CT26	23.7 ± 1.7	18.94 ± 2.94	59.03 ± 4.46	0.28 ± 0.0068	0.95 ± 0.0812

Figure 6.6 The effects of chronic HPO intake on various haematological parameters are presented. Panel (A) depicts a grouped bar graph showing haemoglobin (Hb, g/dL), haematocrit (HCT, %), mean corpuscular haemoglobin (MCH, pg/cell), mean corpuscular haemoglobin concentration (MCHC, %), mean corpuscular volume (MCV, fL), and red blood cell count (RBC, 10^6/µL). Panel (B) illustrates white blood cell (WBC) differential counts, including total WBC (10^3/µL), monocytes (%), neutrophils (%), basophils (%), and eosinophils (%). Data are expressed as mean ± SD, and statistical significance was assessed using one-way ANOVA followed by Tukey's post hoc test *(*$p \leq 0.05$, **$p \leq 0.01$)*.

A)

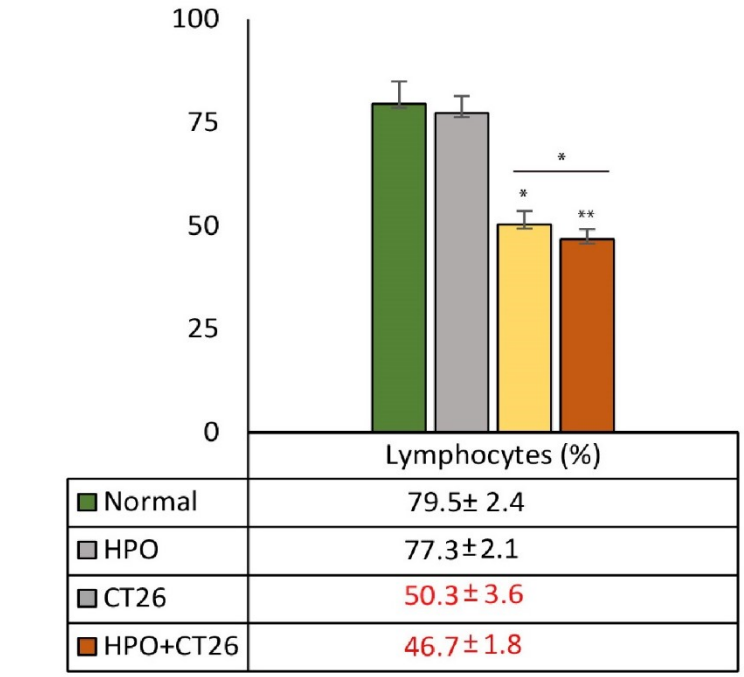

	Lymphocytes (%)
Normal	79.5± 2.4
HPO	77.3±2.1
CT26	50.3±3.6
HPO+CT26	46.7±1.8

B)

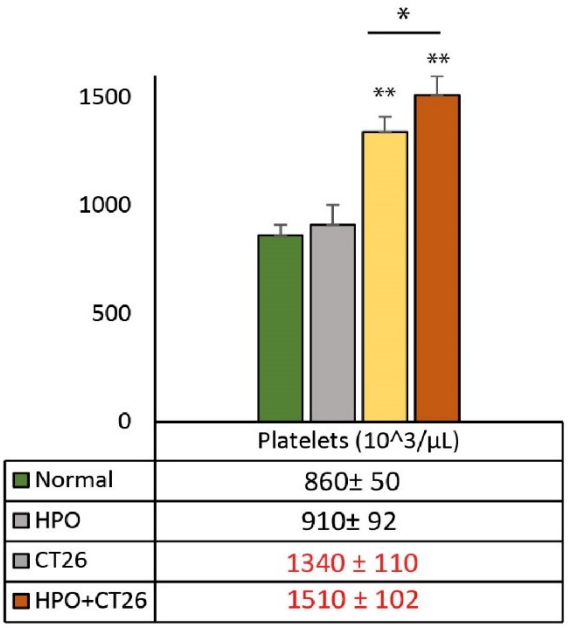

	Platelets (10^3/µL)
Normal	860± 50
HPO	910± 92
CT26	1340 ± 110
HPO+CT26	1510 ± 102

Figure 6.7 Representation of (A) Lymphocytes (%) and (B) Platelets (10^3/µL) in Mice Following Chronic HPO Intake. Results are shown as mean ± SD. Significance assessed using one way-ANOVA with Tukey's posthoc test: *$p \leq 0.05$; and **$p \leq 0.01$.

6.5.6 HPO impact on liver toxicity markers, total protein and total bilirubin

The serum analysis of liver function markers, total protein, and total bilirubin revealed significant alterations in the activities of AST (aspartate aminotransferase) and ALT (alanine aminotransferase) across the experimental groups. ALP (alkaline phosphatase) level remained relatively stable. In the CT26, HPO, and HPO + CT26 groups, AST and ALT activities were significantly increased compared to the Normal group. Precisely, AST activity was measured at 135 ± 21.56 IU/L in the Normal group, 276 ± 30.84 IU/L in the HPO group, 269 ± 49.53 IU/L in the CT26 group, and 61.23 ± 61.23 IU/L in the HPO + CT26 group. Similarly, ALT activity was significantly elevated in the HPO (89 ± 15.2 IU/L), CT26 (62 ± 11.28 IU/L), and HPO + CT26 (114 ± 26.29 IU/L) groups compared to the Normal group, which showed a value of 31 ± 3.25 IU/L (Fig. 6.8A).

Regarding total protein levels, significant declines were observed in the CT26 and HPO + CT26 groups, with values of 5.1 ± 0.35 g/dl and 3.4 ± 0.2 g/dl, respectively, compared to the Normal group (5.6 ± 0.1 g/dl). The HPO group showed a total protein level of 3.6 ± 0.32 g/dl (Fig. 6.8B). However, no significant alterations were noted in serum bilirubin levels across the experimental groups compared to the Normal. These results suggest potential liver dysfunction, particularly in the CT26 and HPO + CT26 groups, as evidenced by the elevated AST and ALT activities and decreased total protein levels.

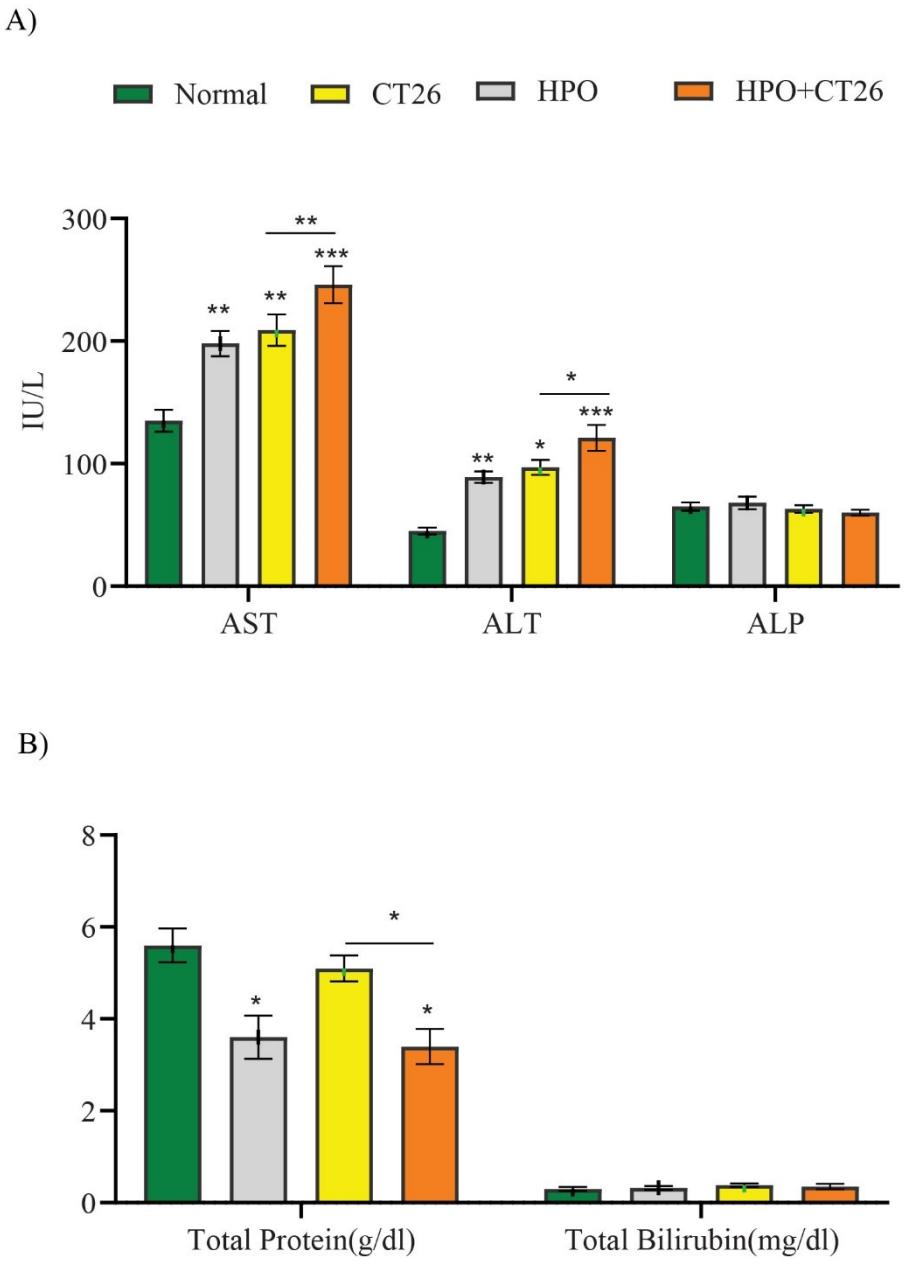

Figure 6.8 Illustrates the impact of HPO on hepatic enzymes, total protein, and bilirubin levels in mice across Normal, HPO, CT26, and HPO+CT26 groups. The grouped bar graph in (A) depicts the levels of aspartate aminotransferase (AST), alanine aminotransferase (ALT), and alkaline phosphatase (ALP), while (B) shows total protein and total bilirubin levels. Statistical significance was determined using one-way ANOVA followed by Tukey's post hoc test, with significance levels indicated by asterisks *(*P < 0.05, **P < 0.01* and ****p < 0.001*). All values are presented as Mean ± SD.

6.5.7 Effects of HPO on serum cytokines IL6 and TNFα

Serum cytokine analysis showed significant increases in IL-6 and TNF-α levels across the treatment groups. IL-6 levels were elevated in the HPO (39 ± 6.4 pg/ml), CT26 (54.5 ± 9.74 pg/ml), and HPO + CT26 (91 ± 12.22 pg/ml) groups compared to the normal group (9.6 ± 1.61 pg/ml) (Fig. 6.9A). Similarly, TNF-α concentrations were higher in the HPO (60.25 ± 9.9 pg/ml), CT26 (57.3 ± 10.06 pg/ml), and HPO + CT26 (110.7 ± 7.1 pg/ml) groups compared to the normal group (10.45 ± 1.4 pg/ml) (Fig. 6.9B). These results suggest that HPO treatment significantly enhances cytokine levels compared to the CT26 group, which also exhibited elevated levels relative to the normal group.

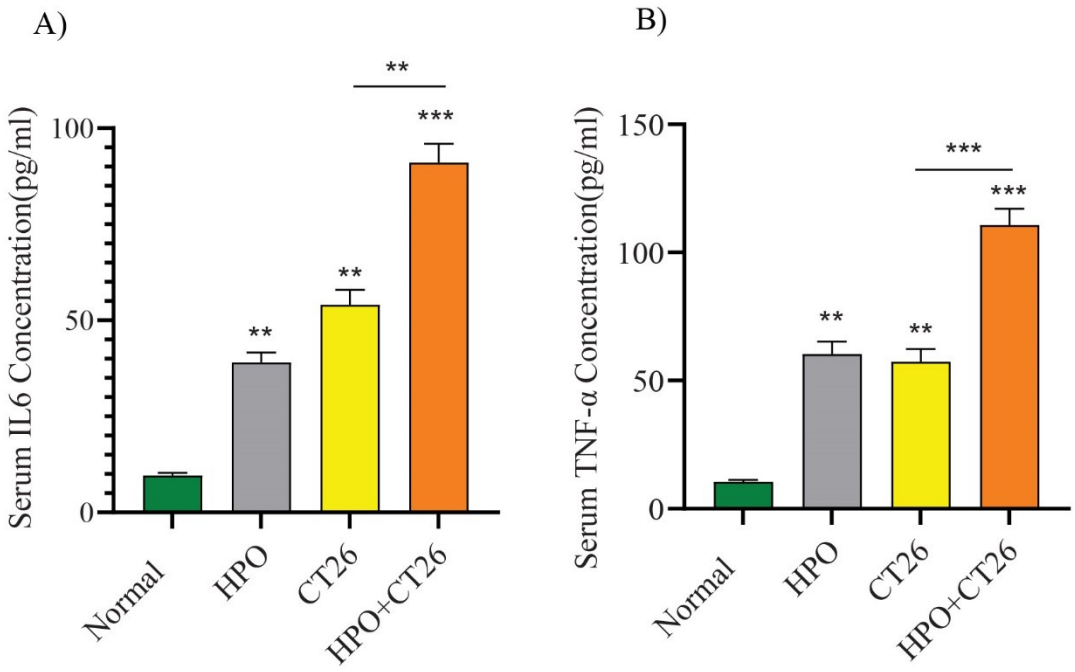

Figure 6.9 ELISA analysis showing inflammatory cytokines A) IL6 and B) TNF-α in the serum of mice groups: normal, HPO, CT26, and HPO+CT26. Data are represented as Mean ± SD *(**p < 0.01; ***p < 0.001).*

6.5.8 Effect of HPO on serum lipid profile

Serum lipid profile analysis revealed significant alterations in total cholesterol, triglycerides, LDL, HDL, and VLDL levels among the experimental groups. Total cholesterol and triglyceride levels were significantly higher in the HPO and HPO + CT26 groups than in the normal and CT26 groups. LDL levels also showed a marked

increase in the HPO and HPO + CT26 groups, whereas HDL levels were significantly reduced compared to the normal and CT26 groups. VLDL levels were elevated in all experimental groups, with the highest levels observed in the HPO and HPO + CT26 groups. These results highlight significant disruptions in lipid metabolism associated with HPO treatment and tumour growth (Fig. 6.10 & Tab 6.1).

Table 6.1 Lipid profile parameters in experimental groups

Lipid Parameters	Normal (mg/dl)	HPO (mg/dl)	CT26 (mg/dl)	HPO + CT26 (mg/dl)
Total Cholesterol	126 ± 18	260 ± 32	118 ± 14	275 ± 38
Triglycerides	34 ± 3.5	182 ± 23	41 ± 4.8	176 ± 17
LDL	50 ± 5.9	176 ± 28	52 ± 8.3	183 ± 21
HDL	62 ± 11	38 ± 4.6	64 ± 9.5	38 ± 5.3
VLDL	8 ± 2.02	38 ± 5.3	10 ±2.6	35 ± 4.5

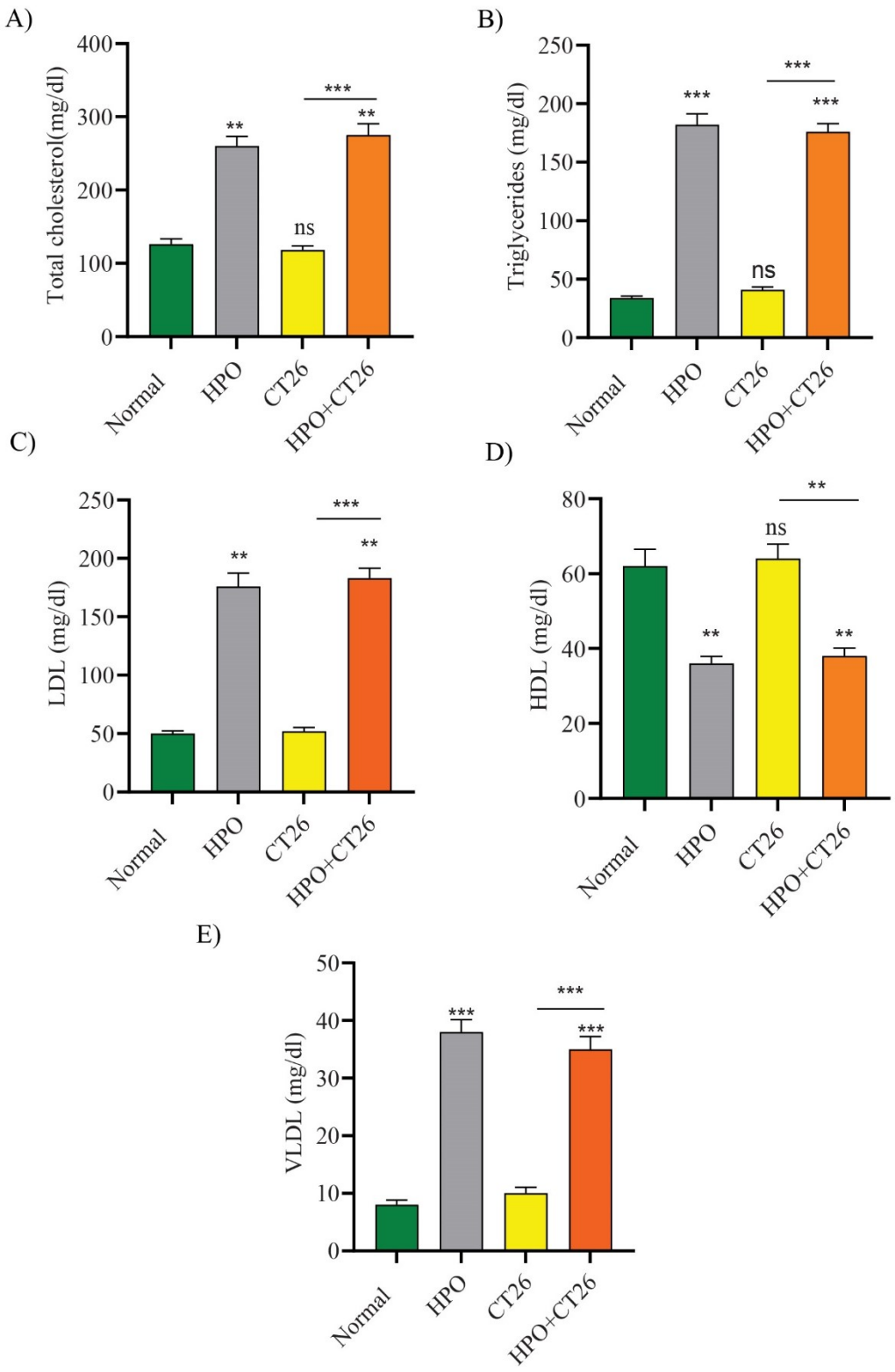

Figure 6.10 Impact of HPO on serum lipid profiles in mice: normal, HPO, CT26, and HPO+CT26 groups. Serum lipid profiles include total cholesterol, triglycerides, HDL, LDL, and VLDL. Data are presented as Mean ± SD. Significance assessed using ANOVA with Tukey's post hoc test: *$*p \leq 0.05$; **$**p \leq 0.005$; and ***$***p \leq 0.001$.

6.6. Discussion

This study investigates the complex interplay between prolonged intake of excessive heat-treated palm oil (HPO) and the progression of colon cancer metastasis, specifically in the context of CT26-induced pulmonary metastasis. The use of palm oil, which is rich in palmitic acid, as a model for dietary influence saturated fat on cancer progression is grounded in prior research indicating that palmitic acid plays a crucial role in promoting metastasis in various cancer types, including oral carcinomas and melanomas (Kim *et al*., 2019, Pascual *et al*., 2021a, Zhang *et al*., 2022c, Pascual *et al*., 2021b, Huang *et al*., 2021a). The study provides new evidence that the consumption of HPO exacerbates lung metastasis in a murine model of colon cancer, suggesting that prolonged exposure to HPO may facilitate the spread and progression of cancer cells.

The observed increase in metastatic distribution and inflammatory cell infiltration in the HPO+CT26 group, as compared to the CT26 control group, strongly supports the hypothesis that HPO accelerates cancer metastasis. Histopathological analyses showed more prominent metastatic lesions in the lungs of animals receiving HPO, aligning with findings from other studies suggesting that dietary palmitic acid enhances metastatic potential through inflammatory pathways (Zhang *et al*., 2022a, Pascual *et al*., 2021a, Alkan *et al*., 2022). This inflammatory response, coupled with increased cell infiltration, suggests that HPO may influence cancer progression by inducing a pro-inflammatory environment that facilitates metastasis.

Furthermore, the data on body weight changes support the hypothesis that HPO intake induces metabolic alterations that may exacerbate cancer progression. The significant weight reduction in the HPO and HPO+CT26 groups suggests that HPO may impair metabolic functions and nutritional intake, which are critical components in cancer progression. Previous research has shown that metabolic disturbances such as obesity and altered energy balance can promote cancer metastasis (Barone *et al*., 2020, Annett *et al*., 2020). In this study, the reduced food and water intake observed in these groups further implicates HPO as a potential disruptor of metabolic homeostasis, which could fuel cancer progression through altered cellular energy states.

The glucose tolerance tests revealed significant disturbances in glucose metabolism post-treatment, with the HPO and HPO+CT26 groups exhibiting pronounced glucose intolerance. The transient hypoglycemia in the CT26 group suggests that cancer

progression may alter systemic glucose control. Still, the exacerbated glucose intolerance in the HPO groups further underscores the influence of dietary factors on cancer metabolism. Hyperglycemia stimulates epithelial-mesenchymal transition (EMT) and promotes migration and invasion in colorectal cancer cells (Wu *et al*., 2018, Choi *et al*., 2018, Nishii *et al*., 2001). These findings highlight the role of glucose metabolism in the metastatic process, with HPO-induced glucose intolerance potentially amplifying the metastatic potential of CT26 cells.

Haematological parameters also provided insights into the systemic effects of tumour growth and HPO intake. The marked increase in white blood cell counts, particularly neutrophils, in the HPO+CT26 group suggests that HPO may modulate immune responses favouring metastasis. Neutrophil counts are often elevated in cancer patients and have been implicated in promoting tumour growth and metastasis (Abu-Shawer *et al*., 2019, Wen *et al*., 2021). The immune modulation observed in the HPO+CT26 group and the platelet increase further highlight the potential impact of HPO on the tumour microenvironment and immune system. Elevated platelet counts have been associated with cancer metastasis, suggesting that platelet-mediated mechanisms might play a role in the metastasis-promoting effects of HPO.

Another critical aspect of cancer progression involves lipid metabolism, particularly in the context of serum lipid profiles. The significant increases in total cholesterol, triglycerides, and LDL-C levels in the HPO and HPO+CT26 groups point to the influence of HPO intake on lipid metabolism. These alterations in lipid profiles are known to impact processes such as cell migration, invasion, and angiogenesis, all of which are critical for metastasis (Adam *et al*., 2008, Hisham *et al*., 2020, Li *et al*., 2016, Irshad *et al*., 2023, Fernández *et al*., 2020). The findings suggest that HPO-induced changes in lipid metabolism may contribute to the metastatic potential of CT26 cells, emphasizing the complex interplay between diet and tumour biology.

Additionally, the liver function markers indicated potential hepatic dysfunction in the HPO and HPO+CT26 groups. The increases in AST and ALT levels, along with reduced serum total protein levels, point to liver damage or impaired function as a consequence of both tumour growth and HPO intake. Previous studies have shown that liver dysfunction is common in cancer patients and can exacerbate the progression of metastasis (Ojo *et al*., 2016). The liver's role in detoxification and metabolism suggests

that alterations in liver function may influence systemic factors that support cancer metastasis.

Finally, the analysis of lung hydroxyproline content and collagen deposition in the HPO and HPO+CT26 groups provides compelling evidence for the role of HPO in promoting pulmonary fibrosis. The elevated hydroxyproline levels and increased collagen deposition observed in the lung tissues of these groups suggest that HPO may contribute to fibrotic changes in the lung. This process has been associated with the progression of metastatic disease. The observed effects are consistent with findings from other studies showing that palmitic acid-rich diets contribute to lung fibrosis (Atanasov *et al*., 2022, Chu *et al*., 2019a). This further underscores the potentially harmful effects of prolonged HPO intake on pulmonary health and metastasis.

In conclusion, this study provides robust evidence for the complex and detrimental effects of prolonged heated palm oil intake on colon cancer metastasis. The interplay between dietary factors, metabolic changes, inflammatory responses, immune modulation, and lipid metabolism all contribute to the enhanced metastatic potential of CT26 colon cancer cells in the presence of HPO. The findings underscore the importance of understanding how dietary fat, particularly palmitic acid-rich palm oil, may exacerbate cancer progression and metastasis, suggesting potential therapeutic avenues targeting metabolic and inflammatory pathways in metastatic disease. Further research is necessary to elucidate the underlying molecular mechanisms and to validate these findings in clinical settings, which could ultimately lead to more effective interventions in cancer therapy.

Chapter 7

The role of palm oil in inducing inflammation, ER stress and UPR in colon cancer metastasis in mouse

7.1 Introduction

Colorectal cancer poses a significant global health challenge, with factors such as age, family history, inflammatory bowel diseases, and dietary habits contributing to its widespread occurrence and propensity for metastasis (Samadder *et al*., 2019). Metastatic growth originating from primary tumours is influenced by many factors, extending beyond genetics to encompass lifestyle choices and environmental exposures. Indeed, pre-clinical models have demonstrated that high-fat diets can promote tumorigenesis, while obesity is linked to increased aggressiveness in specific cancer types (Tong *et al*., 2021, Narita *et al*., 2019). Furthermore, cancer progression can be fuelled by alterations in fatty acid uptake and metabolism. Saturated fatty acids and their interaction with key proteins and transporters, such as CD36, are pivotal in tumorigenesis, chemotherapy resistance, and metastasis (Feng *et al*., 2023). The chronic consumption of palm oil, a widely used cooking oil and ingredient in processed foods, is increasingly linked to a heightened risk of colorectal cancer progression due to high palmitic acid content (Pascual *et al*., 2021a). However, further investigation is required to understand how palmitic acid-rich palm oil promotes metastasis and unravel the underlying mechanisms.

The widespread use of palm oil has contributed significantly to dietary fat intake worldwide, particularly in regions where it is heavily consumed, particularly in Asia and Africa. Palm oil is rich in saturated fats, with approximately 50% of its fat content comprising saturated fatty acids. This makes it a concern for public health, as high intake of saturated fats has been associated with an increased risk of various cancers. Numerous studies have linked palm oil, rich in palmitic acid, to be a significant contributor to various cancers, prompting further investigation into its role in disease development.

Colon cancer manifests through the malignant transformation of cells in the colon or rectum, leading to tumour formation that can invade neighbouring tissues and spread to distant organs like the liver and lungs. Metastasis encompasses a multifaceted series of steps, including the spread of cancer cells from the primary tumour site, invasion into neighbouring tissues, entry into blood or lymphatic vessels (intravasation), circulation to distant organs, exit from vessels (extravasation), and establishment of secondary tumours.

Many studies have demonstrated that ERS and the activation of UPR play crucial roles in the metastasis of various cancers. The unfolded protein response is identified as a primary contributor to addressing cytological perturbations during tumour development and progression, as it serves as a stress-adaptive mechanism in normal cells that cancer cells exploit for their benefit during metastasis. In addition, the dysregulation of UPR has been implicated in various aspects of tumour development and progression, including proliferation, survival, angiogenesis, and metastasis.

Despite the increasing evidence linking chronic palm oil consumption and the risk associated with saturated fatty acids to cancer progression, the precise molecular mechanisms underlying this association, particularly regarding colorectal cancers, remain incompletely understood. Furthermore, the impact of chronic palm oil exposure on the unfolded protein response (UPR)-mediated metastatic potential of colon cancer cells remains largely unexplored. Closing this knowledge gap is crucial for understanding the intricate relationship between dietary factors, cellular stress responses, and the metastatic progression of cancer. Hence, the study hypothesises that chronic consumption of palm oil, rich in saturated fatty acids, exacerbates colorectal cancer progression through modulation of the unfolded protein response (UPR), consequently enhancing metastatic potential in colon cancer cells.

This study aims to investigate the impact of chronic palm oil consumption on colorectal cancer progression and metastasis using relevant animal models. Firstly, the study assesses the effect of long-term palm oil intake on colorectal tumour growth, invasion, and metastasis *in vivo*, utilising appropriate animal models that mimic human colorectal cancer progression. The BALB/C mice were inoculated with CT26 murine metastatic colon cancer cells and administered heated palm oil (HPO) at 250 μl for four months, starting one month before inoculation, as outlined in Chapter 6.

Specifically, it aims to elucidate how palm oil exposure modulates the unfolded protein response (UPR) pathway in colon cancer cells, which plays a crucial role in cellular stress responses and tumorigenesis. Through detailed molecular analyses, the study seeks to decipher the association between palm oil-induced UPR activation and the metastatic potential of colon cancer cells in association with inflammation, altered redox status and misfolded protein aggregates development. The methodology utilised in this study involved ELISA, fluorescent microscopy, spectrofluorimetry, biochemical analysis, and RT-*q*PCR techniques. This comprehensive approach will provide valuable

insights into the complex relationship between dietary factors, cellular stress responses, and cancer progression, potentially paving the way for novel therapeutic strategies to combat colorectal cancer metastasis associated with palm oil consumption.

7.2 Materials and methods

7.2.1 Analysis of misfolded protein aggregates in lung tissues

Tissue samples are thinly sliced (10-20 μm) using a cryostat or microtome, placed on slides, and air-dried. They're then incubated with 0.05% Thioflavin T in PBS for 5-10 min, washed thrice with PBS, and mounted with glycerol under a coverslip. Slides are sealed, dried, and examined under a fluorescence microscope (excitation/emission: 450-490 nm/515-535 nm). Fluorescence intensity and distribution are analysed, with safety precautions like gloves and waste disposal. The detailed procedure is described in Chapter 2, Methodology, Section 2.2.1.2.7.2.

7.2.2 Analysis of pulmonary redox status

Lung tissue was excised and rinsed with ice-cold saline. Portions were fixed in 10% buffered formalin for histopathological analysis. Lung homogenate (10% w/v) was prepared in Tris-HCl buffer (0.1 M, pH 7.4) for lipid peroxidation. The homogenates were centrifuged at 10,000 rpm for 15 min at 4°C, and the supernatant was collected for assays of GSH,GST, GR, GPX, SOD, and catalase. The protocol is described in Chapter 2, Materials and methods, Sections 2.2.3.2, 2.2.3.3.3 to 2.2.3.3.10.

7.2.3 Analysis of cytokines in lung tissues

For cytokine measurement, the lungs were subsequently homogenised with a 10 mM potassium phosphate buffer (pH 7.4) containing 0.1 mM EDTA, 0.1 mM phenylmethanesulfonylfluoride fluoride, 1 µM aprotinin, 1 μM pepstatin A, and 2 μM leupeptin. The homogenates were centrifuged at 10,500 × g for 1 hour, and the supernatants were stored at -80°C. IL6 and TNFά concentrations in lung tissue were quantitatively assessed using the enzyme-linked immunosorbent assay (ELISA, PeproTech) technique according to their recommended protocols. Detailed procedures can be found in Chapter 2, Materials and methods, Section 2.2.3.5.3.

7.2.4 RT-*q*PCR

RT-PCR was conducted to assess the expression of antioxidant, autophagy, ER stress marker, and UPR genes, following the protocol outlined in Chapter 2, Materials and methods, Section 2.2.4. The primers used are listed in table 2.10.

7.3 Statistical analysis

The data are presented as mean ± SD. Differences among groups were assessed using one-way ANOVA and Tukey's post hoc analysis for multiple comparisons. Statistically significant results are indicated by P values of *$*<0.05$, **<0.01, and ***<0.001.

7.4 Results

7.4.1 Effects of HPO on IL6 and TNFα in lung tissues

The histopathological analysis of lung tissues from the various groups revealed the recruitment of inflammatory cells in the HPO, CT26, and HPO + CT26 groups compared to the normal group. The findings indicated elevated production of IL-6 and TNFα in HPO and HPO + CT26. In normal animals, the concentration of IL6 in lung tissue was quantified at 7.75 ± 2.14 pg/ml. Following treatment, this concentration showed significant elevation to 57 ± 9.11pg/ml in HPO-treated animals, 50.5 ± 14.15 pg/ml in animals inoculated with CT26 metastatic cells, and 76.5 ± 10.06 pg/ml in animals subjected to HPO treatment and CT26 inoculations (Fig 7.1A). Similarly, the TNFα level in lung tissue of normal animals was measured at 10.83 ± 1.54 pg/ml. Post-treatment, this level significantly rose to 66.17 ± 10.23 pg/ml for HPO-treated animals, 56.83 ± 6.77pg/ml for CT26 inoculated animals, and 93.83 ± 11.33 pg/ml for animals subjected to both HPO and CT26 (Fig 7.1B). These results indicate that IL6 and TNFα levels were elevated in all treatment groups compared to the normal group. Among the treatment groups, HPO and HPO + CT26 exhibited the highest levels of these cytokines. This suggests that high HPO intake contributes to increased inflammatory responses, with a synergistic effect observed in the presence of CT26 metastasis.

7.4.2 Effect of HPO on antioxidants and MDA levels in lung tissues

The levels of various antioxidants, including SOD, CAT, and glutathione-related antioxidants, GST, GR, GPx, and GSH, as well as lipid peroxidation levels were determined in lung tissue homogenates. The results indicated that there was no change in activity observed for SOD and CAT enzymes in the four groups (Fig 7.2 A&B, Table

7.1). However, the activity of glutathione-related enzymes was significantly altered in the HPO, CT26, and HPO+CT26 groups compared to the control group.

The glutathione-related enzymes showed a more pronounced reduction in the HPO+CT26 group, followed by the HPO-treated group, and finally, the CT26 group. The results revealed that both HPO treatment and CT26 inoculation reduce the activity of antioxidant levels. However, for GPx, no reduction was observed in the CT26 inoculated group compared to the HPO-treated group (Fig 7.2 C D E&F Table 7.1). The study also analysed the level of MDA, which was found to increase drastically in the HPO+CT26 group compared to the other groups. Additionally, both the HPO-treated and CT26 groups also showed elevated levels of peroxidation (Fig 7.2G, Table 7.1).

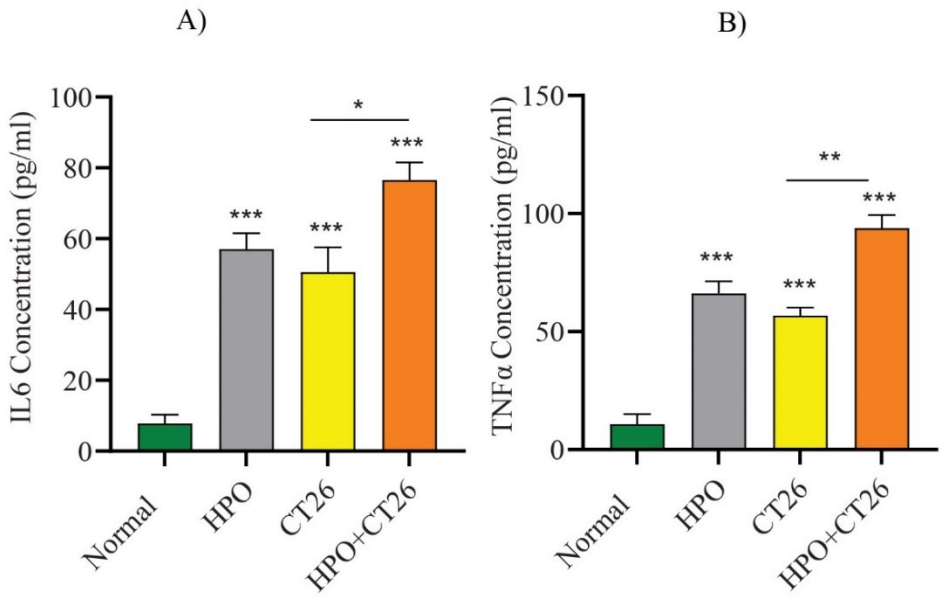

Figure 7.1 Concentrations of (A) IL-6 and (B) TNF-α in lung tissues of Normal, HPO, CT26, and HPO+CT26 mouse groups, measured by ELISA and normalized to the Normal group. Data are Mean ± SD; *$p < 0.05$, **$p < 0.01$, ***$p < 0.001$.

Table 7.1 The level of antioxidants and MDA (lipid peroxidation) in lung tissues of mice

Level of antioxidants and lipid peroxidation							
Sample	**SOD (IU/mg P)**	**CAT IU/mg P**	**GST IU/mg P**	**GR IU/mg P**	**GPX IU/mg P**	**GSH nmoles/mgP**	**MDA nmoles/mgP**
Normal	52.83±5.04	31.51±2.07	98.83±12.47	10.33±1.5	83.2±6.4	6.06±0.7	1.8±0.059
HPO	51.17±4.3	30.11±5.04	64±10.9	5.66±0.83	65.5±8.7	3.5±0.47	3.2±0.058
CT26	50.04±7.78	31.33±3.26	72±10.48	7.13±0.30	75±7.96	4.6±0.5	2.72±0.018
HPO+CT26	50.35± 5.7	29.13±4.51	51.33±4.89	3.5±0.064	57±10.9	2.46±0.076	3.58±0.0396

The table lists enzyme activities, including superoxide dismutase, catalase, glutathione-s-transferase, glutathione reductase, and glutathione peroxidase, measured in IU/mg protein, along with reduced glutathione levels expressed in nanomoles/mg protein in different experimental groups.

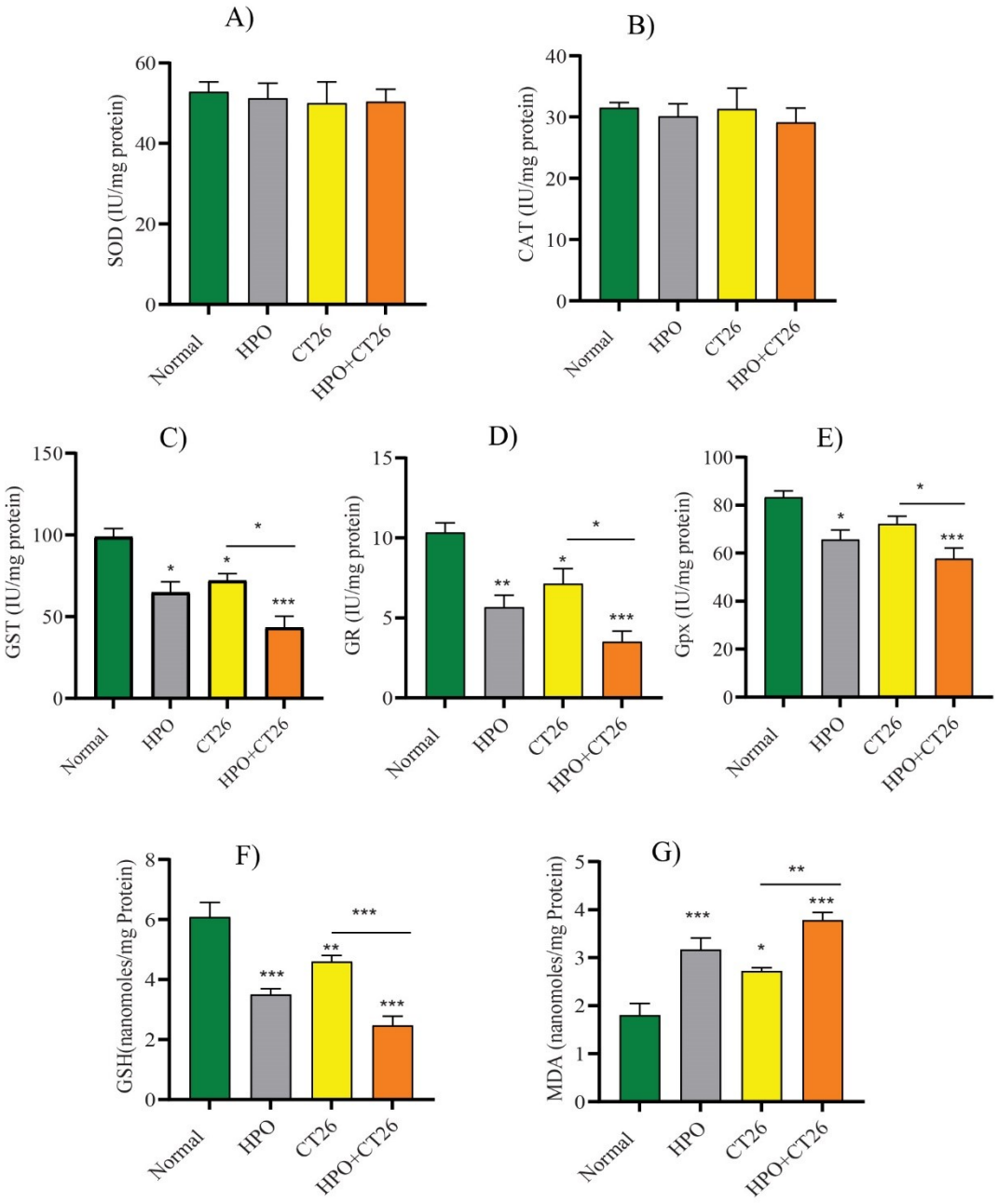

Figure 7.2 Levels of antioxidants A) SOD, B) CAT, C) GST, D) GR, E) GPX) and F) MDA in lung tissues of experimental mice groups (Normal, HPO, CT26, HPO+CT26). Data are expressed as activity (IU/mg protein) for SOD, CAT, GST, GR, GPX, and concentration (nmol/mg protein) for GSH and MDA, relative to normal animals. Data are shown as Mean ± SD. Statistical significance: *$p < 0.05$, **$p < 0.01$, ***$p < 0.001$.

7.4.4 HPO-induced ER stress in lung tissues

The accumulation of misfolded proteins and the development of ER stress were analysed in lung tissues. The results indicated that misfolded protein aggregation significantly increased in the HPO+CT26 group compared to the CT26 metastatic control group. The HPO group also exhibited aggregated misfolded proteins, though to a lesser extent than both the CT26 and HPO+CT26 groups, as demonstrated by the fluorescent images (Fig 7.3A). The normalised fluorescent intensity calculated for the normal, HPO, CT26, and HPO+CT26 groups were 0.20 ± 0.150, 0.266 ± 0.180, 0.47 ± 0.0165, and 0.769 ± 0.0199, respectively (Fig 7.3B).

Subsequent RT-*q*PCR analysis was conducted to confirm the development of ER stress in lung tissue by analysing the expression of *Bip*, *CHOP*, and *ATF6*, ER stress marker genes. The relative fold changes calculated for *Bip* in HPO, CT26, and HPO+CT26 were 2.05 ± 0.37, 2.28 ± 0.34, and 3.33 ± 0.46, respectively. For *CHOP*, the relative fold changes in HPO, CT26, and HPO+CT26 were 1.99 ± 0.19, 2.28 ± 0.45, and 3.50 ± 0.43, respectively. For *ATF6*, the relative fold changes were 1.58 ± 0.188, 1.53 ± 0.162, and 2.4 ± 0.258, respectively (Fig. 7.4).

A)

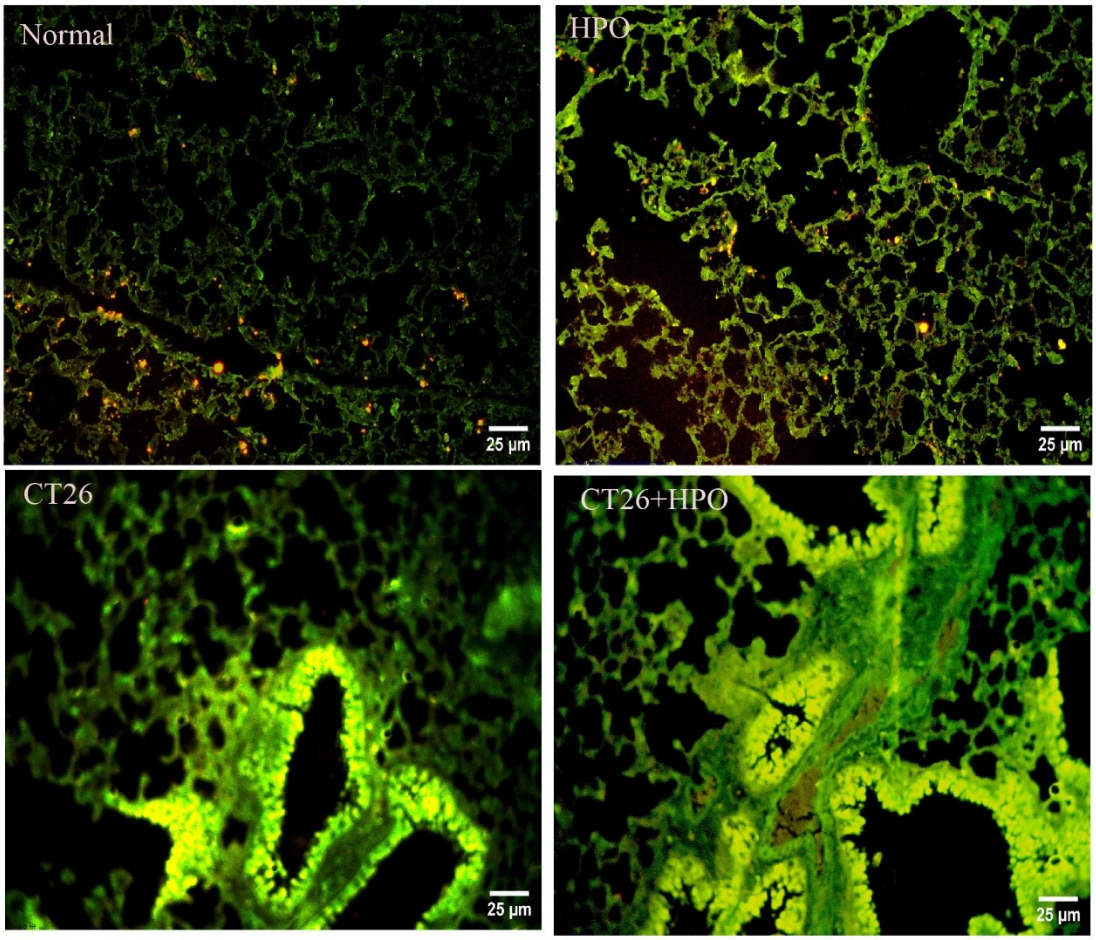

B)

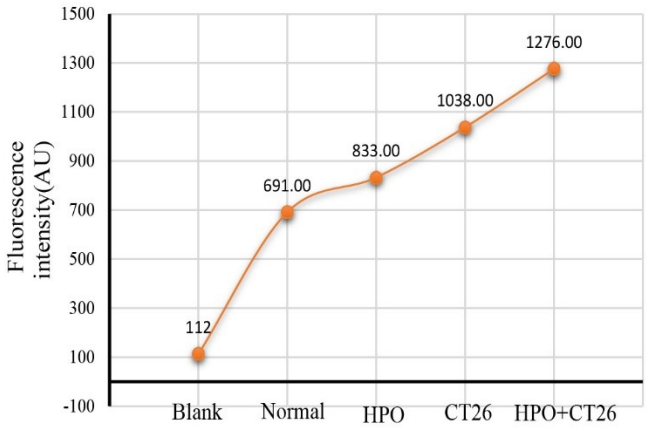

Figure 7.3 Detection of misfolded protein ER stress using Thioflavin T stain in lung tissues of mice during metastasis following excess HPO intake. A) Normal, HPO, CT26, HPO+CT26. Magnification: 400x, scale bar: 25 µm. B) Line graph showing fluorescence intensity in the experimental groups.

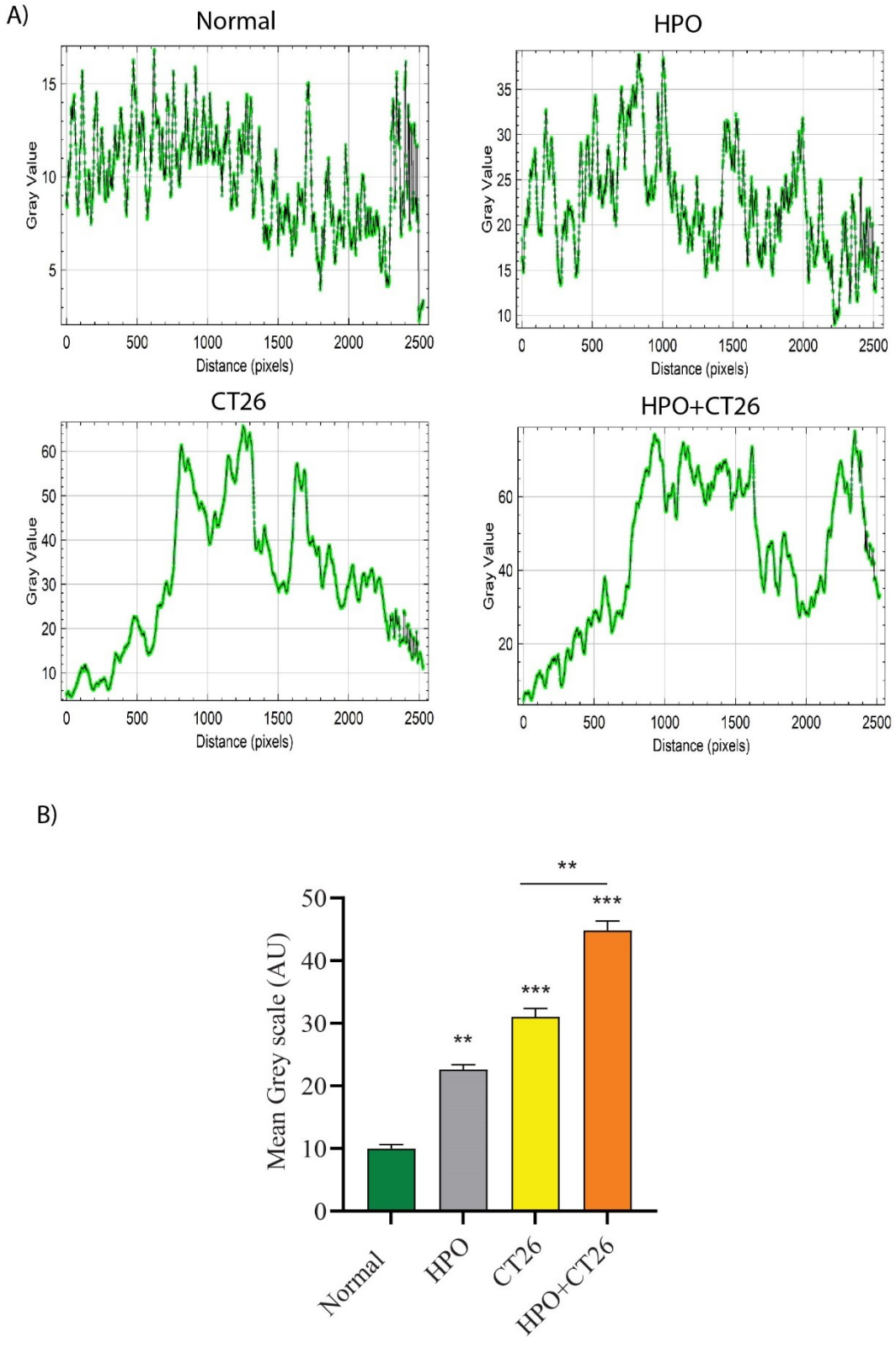

Figure 7.4 A) Grayscale intensity plot and B) bar graph representing the intensity obtained from the plot of thioflavin T fluorescence in normal, HPO, CT26, and HPO+CT26 mice. Results are mean ± SD, with significance *(**p ≤ 0.01, ***p ≤ 0.001)* analysed using one-way ANOVA and Tukey's posthoc test.

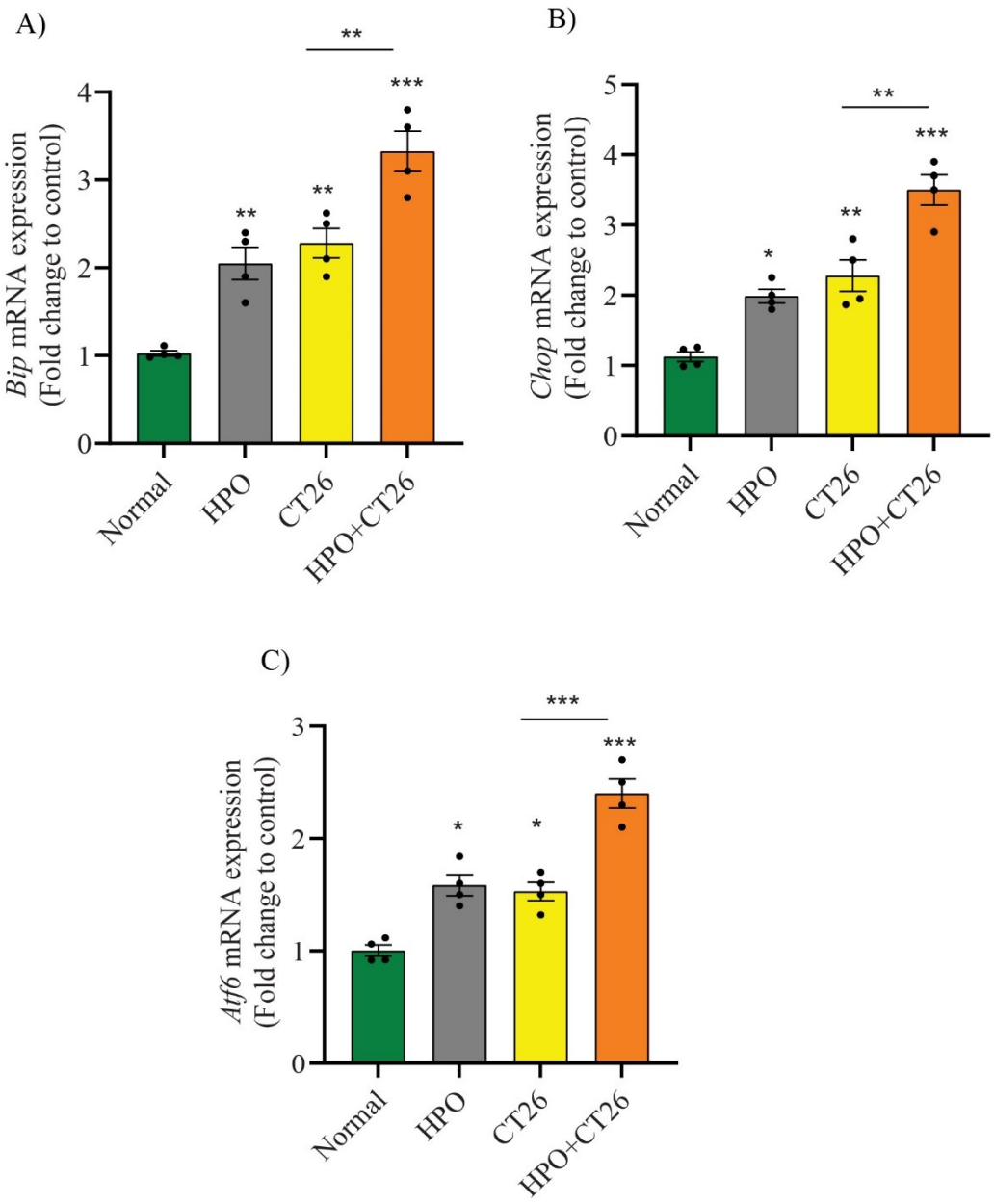

Figure 7.5 Expression levels of ER stress marker genes, including *Bip*, *Chop*, and *Atf6*, in lung tissues of mice: Normal, HPO, CT26, and HPO+CT26. Data represent fold change in expression relative to the Normal group. Values are shown as mean ± SD. Statistical analysis was performed using one -way ANOVA followed by Tukey's post-hoc test. Statistical significance: *$p < 0.05$, **$p < 0.01$, ***$p < 0.001$.

7.4.5. Effect of HPO on the expression of *Perk/Atf4* and antioxidant genes

Following the detection of ER stress markers, the study investigated the *Perk/Atf4* pathway and associated expression of antioxidant genes. The expression of *Perk* and *Atf4* genes was upregulated in lung tissues, with relative fold changes in HPO, CT26, and HPO+CT26 as follows: 2.275 ± 0.26, 2.7 ± 0.322, and 3.395 ± 0.436 for *PERK*, and 1.73 ± 0.32, 1.855 ± 0.34, and 2.63 ± 0.32 for *ATF4* (Fig. 7.5A & B).

Subsequently, expression analysis was performed for antioxidant genes, including *Nrf2*, *Nqo1*, and *Ho-1*. It was found that *Nrf2*, *Nqo1*, and *Ho-1* were upregulated in lung tissue, with fold changes of 1.82 ± 0.15, 2.25 ± 0.298, and 3.12 ± 0.32 for *Nrf2*; 1.73 ± 0.18, 1.25 ± 0.12, and 2 ± 0.44 for *Nqo1*; and 2.1 ± 0.399, 2.4 ± 0.41, and 3.91 ± 0.335 for *Ho-1* in HPO, CT26, and HPO+CT26, respectively (Fig. 7.5C, D & E).

7.4.6. Effect of HPO on the expression of *Ire1/Xbp1* and autophagy

As part of the UPR analysis, the study next analysed the activation of the *Ire1*/*Xbp1* pathway and the subsequent processes associated with autophagy in lung tissues. It was found that *Ire1*/*Xbp1* activate autophagy-associated genes *Beclin 1* and *Lc3b1*. The RT-qPCR results revealed that the relative fold changes calculated in HPO, CT26, and HPO+CT26 were as follows: 2.185 ± 0.35, 3.2 ± 0.47, and 4.04 ± 0.35 for *Ire1*, and 1.75 ± 0.288, 2.5 ± 0.365, and 3.35 ± 0.369 for *Xbp1* (Fig. 7.6A & B).

Regarding autophagy, *Beclin 1* and *Lc3b1* were upregulated as follows: 1.675 ± 0.2, 2.025 ± 0.359, and 2.75 ± 0.36 for *Beclin 1*, and 1.7 ± 0.21, 1.9 ± 0.33, and 2.66 ± 0.23 for *Lc3b1* in HPO, CT26, and HPO+CT26, respectively. Both *Ire1*/*Xbp1* and *Beclin 1*, as well as *Lc3b1*, exhibited significant upregulation in HPO, CT26, and HPO+CT26 lung tissues, indicating more pronounced activation in HPO+CT26 (Fig. 7.6C & D).

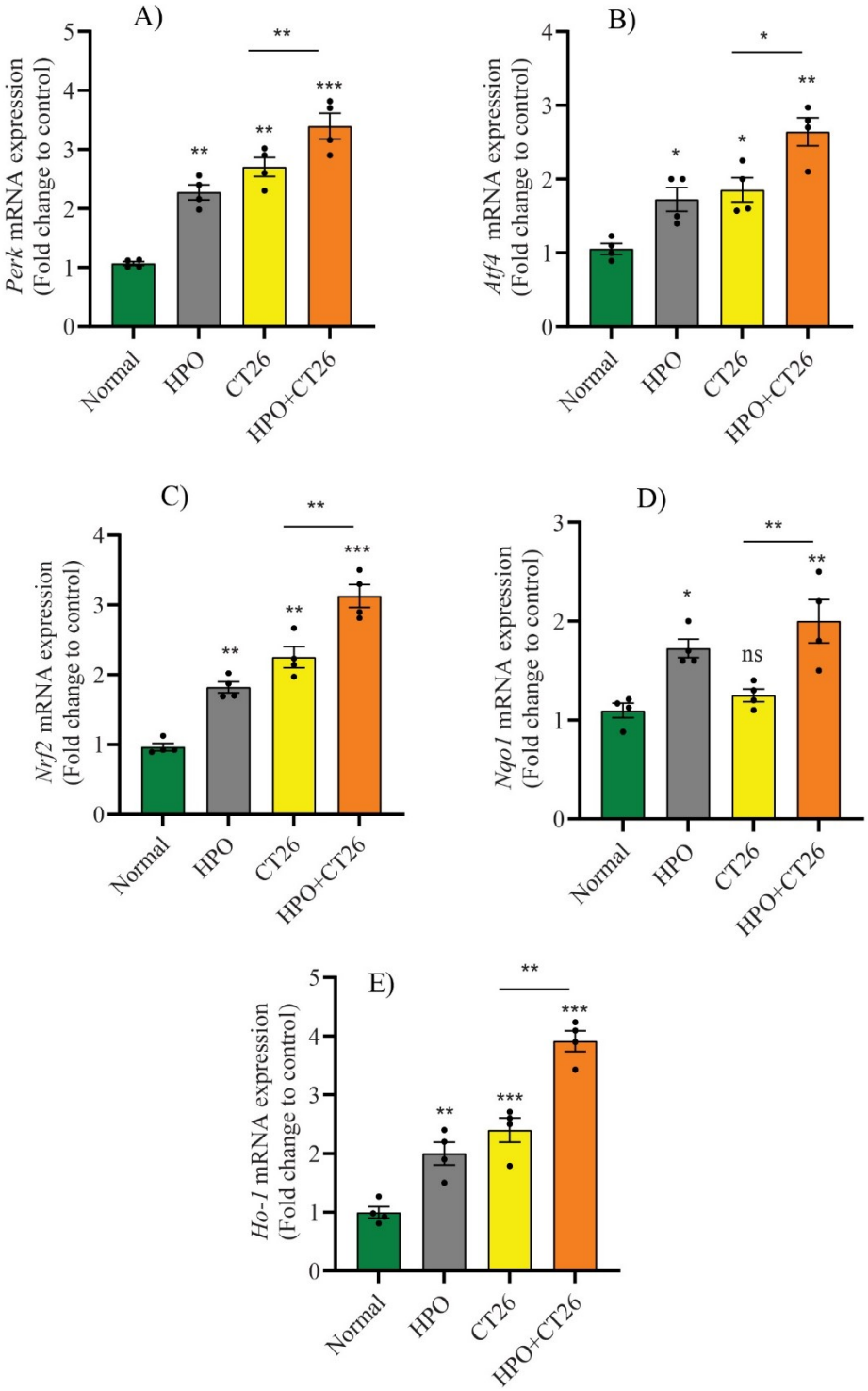

Figure 7.6 Expression of the (A) *Perk*, (B) *Atf4* UPR arm, and antioxidant genes (C) *Nrf2*, (D) *Nqo1*, and (E) *Ho-1* in lung tissues of Normal, HPO, CT26, and HPO+CT26 mice. Data are presented as fold change relative to Normal mice and shown as mean ± SD. Statistical significance: * $p < 0.05$, ** $p < 0.01$, *** $p < 0.001$.

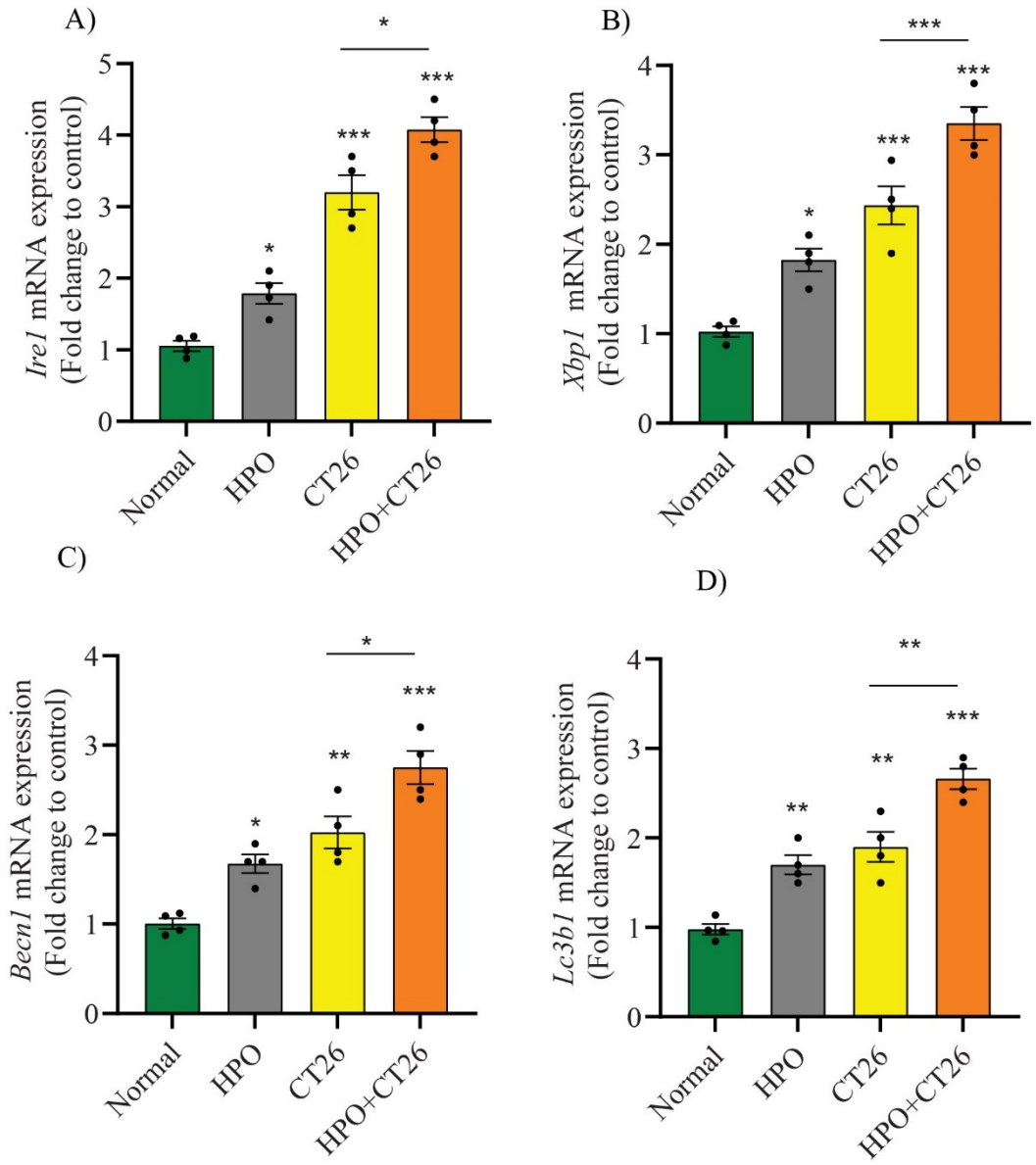

Figure 7.7 Expression of the (A) *Ire1*, (B) *Xbp1* UPR arm, and antioxidant genes (C) *Becn1* and (D) *Lc3b1* in lung tissues of Normal, HPO, CT26, and HPO+CT26 mice. Data are presented as fold change relative to Normal mice and shown as mean ± SD. Statistical significance: * $p < 0.05$, ** $p < 0.01$, *** $p < 0.001$.

7.5. Discussion

Palm oil consumption has recently been identified as a risk factor for various health impacts(Menta *et al*., 2022, Singh *et al*., 2021b). Given its abundance in palmitic acid, debates arise regarding whether palm oil directly contributes to cancer or plays a role in cancer progression. No comprehensive study has explored the potential relationship between palm oil consumption and cancer progression. However, numerous studies have indicated that the saturated fatty acid, palmitic acid, abundant in palm oil, may play a significant role in cancer, especially colon cancer progression, highlighting the complexity of its potential impact (Fattore and Fanelli, 2013, Theodoratou *et al*., 2007, Menta *et al*., 2022). The study of chronic palm oil (HPO) intake-induced inflammation on colon cancer metastasis has revealed complex molecular mechanisms, showing the interaction between palmitic acid-rich dietary factors and cancer progression. This study examines cellular processes such as inflammation, oxidative stress, ER stress, and cellular signalling pathways, offering crucial insights into the mechanisms underlying tumour metastasis in response to HPO consumption.

Studies have shown that dietary saturated fatty acids, especially palmitic acid, are linked to elevated plasma IL-6 levels, potentially influencing systemic inflammation and disease susceptibility (Domínguez-López *et al*., 2022). Another study revealed that palm oil or palmitic acid exposure induces inflammation in various organs, including the liver, intestine, and endothelial cells (Ghezzal *et al*., 2020, Lu *et al*., 2022, Florescu *et al*., 2023). Firstly, the observed elevation in IL-6 and tumour necrosis TNF-α levels within lung tissues following chronic HPO intake underscores the pro-inflammatory nature of palmitic acid, a prominent component of palm oil. The upregulation of these cytokines implicates HPO-induced inflammation as a pivotal contributor to establishing a tumour-permissive microenvironment conducive to metastatic spread. Notably, IL-6 and TNF-α have promoted tumour growth, angiogenesis, and metastasis, emphasising their significance in cancer progression (Rašková *et al*., 2022, Ray *et al*., 2018, Cui *et al*., 2023). The findings revealed that CT26 metastasis was associated with increased immune cell infiltration and invasion. However, HPO treatment enhanced lung tissue inflammation, potentially promoting metastatic cell establishment. Consequently, the study observed aggressive spreading of CT26 cells in HPO-treated lung tissues.

Subsequently, the alterations in antioxidants and lipid peroxidation levels observed also reflected changes in the tissue's redox status induced by inflammation (Ahn and Kim,

2021, Bondia-Pons *et al*., 2012, Muro *et al*., 2024, Scarian *et al*., 2024). Previous studies revealed the relationship between inflammation-induced alterations in antioxidants like SOD, CAT, and glutathione-related antioxidants and the consequential impact on lipid peroxidation in oxidative stress dynamics (Yang *et al*., 2024, Dzięgielewska-Gęsiak *et al*., 2024, Svobodová *et al*., 2024). Moreover, the perturbation of antioxidant status in lung tissues after HPO consumption highlights the intricate balance between oxidative stress and antioxidant defence mechanisms. While the antioxidant system endeavours to counteract the deleterious effects of reactive oxygen species generated during lipid peroxidation, chronic HPO intake may overwhelm these defences, leading to oxidative damage and cellular dysfunction. The study further revealed that lung tissues from HPO, CT26, and HPO+CT26 groups exhibited alterations in glutathione-related enzymes (GST, GR, GPX, and GSH) but showed no changes in SOD and CAT enzymes, accompanied by significant lipid peroxidation. These findings suggest an altered redox status associated with inflammation in the lung tissues. This dysregulation of redox homeostasis may exacerbate inflammation, fuelling a vicious cycle of oxidative stress and inflammation that potentiates cancer metastasis.

In line with previous findings, excess palmitic acid and a diet rich in palm oil have been demonstrated to induce ER stress in various tissues (Chen *et al*., 2024, Vidrio-Huerta *et al*., 2024, Molonia *et al*., 2024, Sahoo *et al*., 2024, Zhao *et al*., 2024b, Tan *et al*., 2024, Li *et al*., 2024). In the present study, the induction of ER stress and misfolded protein aggregation in response to HPO consumption further explains the complex link between metabolic stress pathways and tumour progression. ER, stress is a critical mediator of cellular adaptation to environmental insults, yet prolonged activation of the UPR may exacerbate inflammation and promote tumorigenesis(Acosta-Alvear *et al*., 2024, Minjares *et al*., 2025, Zhang *et al*., 2024, Yuan *et al*., 2024). The upregulation of ER stress marker genes such as *Bip*, *CHOP* and *ATF6* suggests a convergence of metabolic and inflammatory pathways, wherein HPO-induced ER stress fuels a pro-tumorigenic microenvironment conducive to cancer metastasis. Furthermore, the dysregulation of *PERK*/ *ATF4, Ire1*/ *Xbp1 and ATF6* signalling pathways associated with HPO intake emphasise the intricate regulatory mechanisms governing cellular responses to dietary stressors. The *PERK*/ *ATF4* axis activation may potentiate oxidative stress and inflammation. In contrast, activation of the *Ire1*/ *Xbp1* pathway

may modulate autophagy with inflammation and cell survival in response to ER stress (Xu *et al*., 2022, Narayanan *et al*., 2022, Zhao *et al*., 2024a, Stevens *et al*., 2023, Fang *et al*., 2024, Wan *et al*., 2025, Chipurupalli *et al*., 2021). In this context, the concomitant upregulation of antioxidant genes and enhanced autophagy observed in the HPO+CT group (Fig. 7.6) highlights a coordinated adaptive mechanism. The antioxidant response appears to counteract excessive ROS generated by HPO-driven lipid peroxidation and tumor-associated oxidative stress, while autophagy facilitates the clearance of damaged organelles and provides metabolic substrates to sustain tumor cell survival. Together, these dual adaptations enable CT26 cells to withstand dietary oxidative burden, thereby strengthening redox homeostasis and promoting metastatic potential. These findings highlight the multifaceted nature of cellular responses to HPO-induced stress, implicating diverse signalling cascades in the regulation of cancer metastasis.

In conclusion, elucidating these molecular mechanisms underscores the complex interplay between dietary factors, inflammation, oxidative stress, and ER stress in driving cancer metastasis in response to chronic HPO intake. From the study, it became evident that chronic intake of HPO induces inflammation in lung tissues, altering the redox status and enhancing inflammation. This, in turn, induces ER stress and creates a conducive environment for metastatic cells to establish themselves in the lung tissue and propagate vigorously within the tissues. By Unravelling the intricate signalling networks implicated in HPO-induced tumorigenesis, this study provides a foundation for developing targeted therapeutic strategies to disrupt key molecular pathways underlying cancer metastasis. However, further research is warranted to elucidate the precise mechanisms by which HPO modulates tumour progression and to identify potential therapeutic targets for intervention in metastatic disease.

Chapter 8

Summary and conclusion

8.1 Summary

Palmitic acid, a saturated fatty acid abundant in dietary sources like palm oil, influences cellular metabolism and health. It plays crucial roles in lipid metabolism, oxidative stress, and, notably, in triggering endoplasmic reticulum (ER) stress. ER stress develops when the protein folding capacity of the ER is overwhelmed. The stress affects cellular homeostasis and potentially leads to dysfunction of cells or lead to death. Although reports suggest that palmitic acid induces oxidative and ER stresses, understanding how enhanced ER stress affects cancer cells, especially their survival, remains limited. Considering this, the study hypothesised palmitic acid-induced ER stress plays a role in adapting the cancer cell in survival by modulating stress response pathways, UPR, thereby promoting mechanisms that support tumour progression. Hence, this study aims to investigate ER stress responses in normal and cancer cell lines exposed to palmitic acid by exploring gene alterations especially linked to cell fate decisions. The study also envisaged assessing UPR signalling pathways in metastasised tumour-bearing mice treated with palm oil. These findings illuminate strategies for potentially targeting fatty acid metabolism and stress response mechanisms to enhance cancer therapies and cellular resilience.

The initial phase of the study examined the effects of palmitic acid on normal rat intestinal (IEC6) and colon cancer (HCT116 and CT26) cell lines, focusing on tolerance, toxicity, and lipid accumulation. Normal colon cells (IEC6) exhibited greater tolerance to palmitic acid, showing a dose-dependent decrease in cell viability with an IC_{50} of 342 μM. In contrast, cancer cells were a little more sensitive, with IC_{50} values of 180 μM for HCT116 and 168 μM for CT26. These results suggest that normal colon cells may be more resistant to lipid overload due to more efficient lipid metabolism and stress response mechanisms that help maintain cellular homeostasis.

In contrast, cancer cells exhibited a heterogeneous population, with most of the cells undergoing death. However, a subset of more resilient cancer cells survived and contributed to the population's recovery. This highlights the efficacy of some cancer cells in a population in enabling faster and more progressive tumour growth. These resilient cancer cells uniquely withstand palmitic acid-induced ER stress, highlighting the need to target them to better understand their survival mechanisms.

The cells accumulated with neutral lipids and formed lipid droplets upon exposure to palmitic acid. This accumulation was dose-dependent. The substantial accumulation of lipid droplets at lower concentrations of palmitic acid intake was excessive in both normal and cancer cells. Lower concentrations found supported the formation of healthy colonies. This indicates that the cancer cells may survive and proliferate under certain conditions despite metabolic stress. However, higher concentrations of palmitic acid alter lipid metabolism and antioxidant defences and may lead to death. Therefore, the lower concentrations with significant lipid accumulation were chosen for further study.

Further, the excess lipid accumulation in cells induced oxidative stress, and more misfolded proteins and ER stress were assessed by respective markers. A preliminary indication of ER stress development. This ER stress developed was confirmed by reducing the stress with 4-phenyl butyric acid (4-PBA), especially at lower concentrations of palmated acid. This suggests that ER stress is well tolerated at lower concentrations of palmitic acid, indicating that oxidative stress-associated metabolic stresses play a significant role in ER stress under both pathological and physiological conditions.

The study further explores ER stress-associated UPR responses, focusing on the PERK/ATF4, IRE1/XBP1, and ATF6 pathways and their roles in supporting cell survival. The ROS generated triggers PERK, and the UPR activates adaptive responses, including antioxidant defence systems, by restoring protein-folding homeostasis. Palmitic acid exposure affects the antioxidant enzyme activity, including SOD and CAT crucial for mitigating oxidative stress. Our study observed elevated SOD and CAT activities at sub-lethal doses but a decline at toxic concentrations. Similarly, glutathione-related antioxidants also remained stable at sub-lethal doses but declined at toxic levels, highlighting the role of these enzymes in detoxifying excess palmitic acid metabolites and scavenging ROS. Lipid peroxidation, a hallmark of oxidative stress, was also exacerbated by palmitic acid, accompanied by declining antioxidants that compromised membrane integrity and amplified oxidative stress at higher concentrations. Stress-responsive transcription factors like Nrf2 and NF-κB also regulate antioxidant defence, inflammation, and apoptosis to maintain cellular homeostasis. Palmitic acid modulates the expression of antioxidant genes in HCT116 and CT26 cells by showing upregulation of Nrf2 compared to normal colon cells. The

expression of NQO1 and HO-1 also varied, reflecting the adaptive response to oxidative stress.

Considering the selected doses, PERK expression remains stable in IEC6 cells at 100 and 200 μM, while expression increased in HCT116 and CT26 colon cancer cells from 50 to 100 μM. The study revealed a feedback mechanism regulating PERK activity in normal cells, while unresolved ER stress triggered persistent PERK activation in cancer cells. Moreover, this study indicates that palmitic acid can induce oxidative stress without causing lipotoxicity up to a specific concentration and can activate the PERK/ATF4 pathway to counteract ER stress in normal and colon cancer cells. These findings enhance our understanding of cancer cell metabolic and cellular adaptations and establish a link between saturated fat and ER stress. This offers potential therapeutic targets for combating the deleterious effects of palmitic acid and enhancing cellular resilience in cancer.

Palmitic acid-induced ER stress *via* the IRE1/XBP1 pathway associated autophagic flux *via* the IRE1/XBP1 pathway. Palmitic acid treatment increased acidic vacuoles, indicating early autophagic responses. Not all acidic vacuoles are transformed into autophagic vacuoles; hence, MDC staining was carried out further to confirm the development of autophagic flux in treated cells. Palmitic acid also upregulated autophagy-related genes BECLIN 1 and LC3B1 and ER stress markers IRE1 and XBP1, particularly in cancer cells. This suggests palmitic acid enhances cellular resistance to stress through autophagy and ER stress pathways. The study highlights the crosstalk between autophagy and ER stress, where autophagy alleviates ER stress by degrading damaged components, and UPR regulates autophagic flux. In colon cancer, this interplay may promote cell survival and progression. Targeting these pathways could offer therapeutic strategies to restore cellular homeostasis and inhibit cancer survival mechanisms. Further research is needed to identify specific molecular targets within these pathways and develop optimised treatments for colon cancer.

The study chose palm oil to analyse the impact of a palmitic acid-rich diet *in vivo* in mice due to its high fatty acid levels. Palm oil, a palmitic acid-rich oil, was chosen as a dietary model. The objective of the study was to validate the development of ER stress and UPR responses in intestinal tissues due to heat-treated palm oil (HPO) and second, to examine the role of HPO in colon cancer pulmonary metastasis and its contribution to ER stress and UPR activation in cancer cell survival.

GC-MS/MS analysis determined a palmitic acid concentration of 367 mg/mL in HPO. Each mouse received 200 μl, corresponding to 73.4 mg per mouse. HPO causes oxidative stress and reduced antioxidant levels in the small intestine, leading to increased lipid peroxidation. This oxidative stress was less pronounced in the large intestine, which may be due to its limited lipid absorption. Palmitic acid exposure resulted in lipotoxicity, alterations in goblet cell morphology, and inflammation. The study also found that HPO-induced oxidative stress triggered ER stress, marked by elevated BIP, CHOP, and ATF6 levels, and activated different UPR pathways (PERK/ATF4 in the small intestine and IRE1/XBP1 in the large intestine). The large intestine exhibited a more pronounced inflammatory response with increased autophagy-related gene expression (Beclin 1 and LC3B1) and immune cell infiltration. Significant IL-6 and TNF-α production by infiltrated immune cells, indicating an inflammatory response due to palm oil consumption. The role of ER stress and UPR signalling in oxidative stress-mediated lipotoxicity and the subsequent inflammatory response in the gut suggests that palm oil consumption significantly influences gut health and contributes to various pathologies.

Prolonged consumption of heat-treated palm oil induces ER stress and alters the morphology and function of the small intestine, leading to lipotoxicity, inflammation, and impaired barrier function. The differential activation of UPR pathways in the small and large intestines reflects their distinct roles and susceptibilities. The findings highlight the distinct roles of the PERK/ATF4, IRE1/XBP1, and ATF6 pathways in different intestinal regions. These emphasise the adverse effects of palm oil consumption on gut health, highlighting the need for further research to develop targeted therapeutic strategies for mitigating these effects.

The study also investigated the impact of prolonged intake of heat-treated palm oil (HPO), rich in palmitic acid, on colon cancer metastasis. Previous research has shown that dietary palmitic acid promotes metastasis in various cancers. The present study revealed that tumours from mice on a palm oil-rich diet exhibit sustained high metastatic activity. Histopathological analysis revealed altered metastatic distribution and increased inflammatory cell infiltration, suggesting that HPO exacerbates metastatic spread. The findings align with previous studies indicating that palmitic acid-rich palm oil promotes lung metastasis *via* TLR4/TRIF-Peli1-pNF-κB pathway and that

blocking CD36 inhibits metastasis, emphasising the role of palmitic acid in promoting metastasis.

After four months, body weight metastasised mice were found to be reduced by HPO. The decreased food and water intake suggested metabolic alterations and a potential link to metastasis progression. The glucose intolerance observed highlights the connection between dietary changes, cancer advancement, and glucose control. Haematological analysis showed significant increases in white blood cell counts, monocytes, neutrophils, lymphocytes, and platelets, indicative of systemic inflammation and immune modulation. Serum lipid profile analysis revealed significant increases in total cholesterol, triglycerides, and LDL levels, suggesting an impact on lipid metabolism associated with cancer progression. Elevated liver function markers (AST, ALT) levels indicated hepatic injury or dysfunction. The findings of increased lung hydroxyproline content and collagen deposition in the HPO and HPO+CT26 groups suggest a direct association between HPO intake and pulmonary fibrosis, highlighting the need for awareness of the potential adverse effects of dietary factors on pulmonary health.

The intake of HPO resulting in colon cancer lung metastasis further impacts inflammatory responses, oxidative stress, ER stress, and associated signalling pathways. It was found that palmitic acid induces inflammation in lung tissues, characterised by elevated levels of IL6 and TNFα, which create a microenvironment conducive to metastatic spread. Increased immune cell infiltration and invasion further supported the role of HPO-induced inflammation in facilitating cancer cell aggressiveness. Furthermore, chronic HPO intake disrupted redox homeostasis in lung tissues, leading to oxidative damage exacerbated by alterations in antioxidant enzymes. The study highlighted significant changes in glutathione-related enzymes without corresponding adjustments in SOD and CAT, underscoring a dysregulated antioxidant defence system that potentiated oxidative stress and inflammation. Moreover, HPO-induced ER stress, evidenced by the upregulation of ER stress markers like BIP, CHOP, ATF6, and activation of PERK/ATF4 and IRE1/XBP1 signalling pathways, contributed to a pro-tumorigenic microenvironment favouring cancer metastasis.

8.2 Conclusion

The study comprehensively elucidates the role of palmitic acid, mainly through the consumption of heat-treated palm oil, inducing ER stress and its implications for cancer cell survival and metastasis. Prolonged intake of HPO leads to significant ER stress in intestinal tissues, evidenced by the upregulation of stress markers such as *Bip, Chop*, and *Atf6* and the differential activation of UPR pathways. The differential expression of *Perk/Atf4* in the small intestine and *Ire1/Xbp1* in the large intestine under HPO gavage reflects the distinct roles these pathways play in managing region-specific stresses. *Perk/Atf4* in the small intestine regulates protein synthesis and cellular homeostasis under increased metabolic demand. In contrast, *Ire1/Xbp1* in the large intestine modulates inflammatory responses and maintains mucosal integrity in response to microbial stress and gut inflammation induced by the high-fat diet.

This stress response is coupled with oxidative stress, lipotoxicity, and inflammation, altering intestinal morphology and function. Additionally, HPO exacerbates colon cancer metastasis, as shown by increased inflammatory cell infiltration, systemic inflammation, and metabolic disturbances. These findings highlight the detrimental impact of dietary palmitic acid on gut health and cancer progression, emphasising the need for targeted therapeutic strategies to mitigate these effects. The study underscores the complex interplay between dietary components, ER stress, and cancer cell survival, providing a foundational understanding of how chronic consumption of palmitic acid-rich diets can contribute to cancer metastasis.

Chapter 9

Recommendations

9.1 Future Recommendations

1. The signalling pathways linking ER stress and cancer progression are driven by key mediators like GRP78, PERK, IRE1, and ATF6, which regulate tumour growth, survival, and metastasis. Investigating their interactions with lipid metabolism may reveal vital insights into cancer pathology.

2. Targeting lipid metabolism and ER stress in cancer involves small molecules, gene therapies, and combination treatments to disrupt tumour growth and survival mechanisms, exploiting these dual vulnerabilities.

3. The bidirectional relationship between autophagy and ER stress in cancer is crucial, particularly in how autophagy mitigates or exacerbates lipid-induced ER stress. Understanding this interplay could reveal therapeutic opportunities, with the potential to modulate these mechanisms to enhance anti-cancer strategies.

4. Identifying biomarkers linked to ER stress and lipid metabolism dysregulation in cancer can aid early diagnosis, prognostication, and prediction of treatment responses, enhancing therapies targeting ER stress pathways.

5. Lipid-induced ER stress influences immune cell function in the tumour microenvironment, contributing to immune evasion. Investigating these effects may uncover therapeutic strategies to enhance anti-tumour immunity by modulating ER stress pathways.

6. Comparing the effects of saturated, unsaturated, and trans fats on ER stress, lipid metabolism, and cancer progression may reveal fatty acids with distinct roles, uncovering potential cancer prevention and therapy targets.

BIBLIOGRAPHY

ABBOTT, S. K., ELSE, P. L., ATKINS, T. A. & HULBERT, A. J. 2012. Fatty acid composition of membrane bilayers: importance of diet polyunsaturated fat balance. *Biochim Biophys Acta,* 1818**,** 1309-17.

ABU-SHAWER, M., ABU-SHAWER, O., SOULEIMAN, M., AKKAWI, M., ALSHAKHATREH, O., ALTAMIMI, T., AL-OMARI, A. & AL-HUSSAINI, M. 2019. Hematologic Markers of Lung Metastasis in Stage IV Colorectal Cancer. *Journal of Gastrointestinal Cancer,* 50**,** 428-433.

ACOSTA-ALVEAR, D., HARNOSS, J. M., WALTER, P. & ASHKENAZI, A. J. N. R. M. C. B. 2024. Homeostasis control in health and disease by the unfolded protein response. 1-20.

ACOSTA-ALVEAR, D., ZHOU, Y., BLAIS, A., TSIKITIS, M., LENTS, N. H., ARIAS, C., LENNON, C. J., KLUGER, Y. & DYNLACHT, B. D. 2007. XBP1 controls diverse cell type- and condition-specific transcriptional regulatory networks. *Mol Cell,* 27**,** 53-66.

ADAM, S. K., SOELAIMAN, I. N., UMAR, N. A., MOKHTAR, N., MOHAMED, N. & JAARIN, K. 2008. Effects of repeatedly heated palm oil on serum lipid profile, lipid peroxidation and homocysteine levels in a post-menopausal rat model. *Mcgill J Med,* 11**,** 145-51.

ADAMS, C. J., KOPP, M. C., LARBURU, N., NOWAK, P. R. & ALI, M. M. U. 2019. Structure and Molecular Mechanism of ER Stress Signaling by the Unfolded Protein Response Signal Activator IRE1. *Front Mol Biosci,* 6**,** 11.

ADAMS, M. N., CHRISTENSEN, M. E., HE, Y., WATERHOUSE, N. J. & HOOPER, J. D. 2011. The role of palmitoylation in signalling, cellular trafficking and plasma membrane localization of protease-activated receptor-2. *PLoS One,* 6**,** e28018.

ADOLPH, T. E., TOMCZAK, M. F., NIEDERREITER, L., KO, H. J., BÖCK, J., MARTINEZ-NAVES, E., GLICKMAN, J. N., TSCHURTSCHENTHALER, M., HARTWIG, J., HOSOMI, S., FLAK, M. B., CUSICK, J. L., KOHNO, K., IWAWAKI, T., BILLMANN-BORN, S., RAINE, T., BHARTI, R., LUCIUS, R., KWEON, M. N., MARCINIAK, S. J., CHOI, A., HAGEN, S. J., SCHREIBER, S., ROSENSTIEL, P., KASER, A. & BLUMBERG, R. S. 2013. Paneth cells as a site of origin for intestinal inflammation. *Nature,* 503**,** 272-6.

AGGARWAL, R., PENG, Z., ZENG, N., SILVA, J., HE, L., CHEN, J., DEBEBE, A., TU, T., ALBA, M., CHEN, C.-Y., STILES, E. X., HONG, H. & STILES, B. L. 2022. Chronic Exposure to Palmitic Acid Down-Regulates AKT in Beta-Cells through Activation of mTOR. *The American Journal of Pathology,* 192**,** 130-145.

AHMED, B., SULTANA, R., GREENE, M. W. J. B. & PHARMACOTHERAPY 2021. Adipose tissue and insulin resistance in obese. 137**,** 111315.

AHMED, M. 2020. Colon Cancer: A Clinician's Perspective in 2019. *Gastroenterology Res,* 13**,** 1-10.

AHN, Y. J. & KIM, H. J. A. 2021. Lutein as a modulator of oxidative stress-mediated inflammatory diseases. 10**,** 1448.

AJOOLABADY, A., LEBEAUPIN, C., WU, N. N., KAUFMAN, R. J. & REN, J. 2023. ER stress and inflammation crosstalk in obesity. *Med Res Rev,* 43**,** 5-30.

AJUWON, K. M. & SPURLOCK, M. E. 2005. Palmitate activates the NF-kappaB transcription factor and induces IL-6 and TNFalpha expression in 3T3-L1 adipocytes. *J Nutr,* 135**,** 1841-6.

ALKAN, H. F., ALTEA-MANZANO, P. & FENDT, S. M. 2022. Palmitic acid: Enabling the tumor's nerves. *Cell Metab,* 34**,** 7-9.

ALNAHDI, A., JOHN, A. & RAZA, H. 2019a. Augmentation of Glucotoxicity, Oxidative Stress, Apoptosis and Mitochondrial Dysfunction in HepG2 Cells by Palmitic Acid. *Nutrients* [Online], 11.

ALNAHDI, A., JOHN, A. & RAZA, H. 2019b. N-acetyl cysteine attenuates oxidative stress and glutathione-dependent redox imbalance caused by high glucose/high palmitic acid treatment in pancreatic Rin-5F cells. *PLoS One,* 14**,** e0226696.

ALTEA-MANZANO, P., DOGLIONI, G., LIU, Y., CUADROS, A. M., NOLAN, E., FERNÁNDEZ-GARCÍA, J., WU, Q., PLANQUE, M., LAUE, K. J., CIDRE-ARANAZ, F., LIU, X.-Z., MARIN-BEJAR, O., VAN ELSEN, J., VERMEIRE, I., BROEKAERT, D., DEMEYER, S., SPOTBEEN, X., IDKOWIAK, J., MONTAGNE, A., DEMICCO, M., ALKAN, H. F., RABAS, N., RIERA-DOMINGO, C., RICHARD, F., GEUKENS, T., DE SCHEPPER, M., LEDUC, S., HATSE, S., LAMBRECHTS, Y., KAY, E. J., LILLA, S., ALEKSEENKO, A., GELDHOF, V., BOECKX, B., DE LA CALLE ARREGUI, C., FLORIS, G., SWINNEN, J. V., MARINE, J.-C., LAMBRECHTS, D., PELECHANO, V., MAZZONE, M., ZANIVAN, S., COOLS, J., WILDIERS, H., BAUD, V., GRÜNEWALD, T. G. P., BEN-DAVID, U., DESMEDT, C., MALANCHI, I. & FENDT, S.-M. 2023. A palmitate-rich metastatic niche enables metastasis growth via p65 acetylation resulting in pro-metastatic NF-κB signaling. *Nature Cancer,* 4**,** 344-364.

AMIN-WETZEL, N., SAUNDERS, R. A., KAMPHUIS, M. J., RATO, C., PREISSLER, S., HARDING, H. P. & RON, D. 2017. A J-Protein Co-chaperone Recruits BiP to Monomerize IRE1 and Repress the Unfolded Protein Response. *Cell,* 171**,** 1625-1637.e13.

ANDERSON, A. M. & RAGAN, M. A. 2016. Palmitoylation: a protein S-acylation with implications for breast cancer. *NPJ Breast Cancer,* 2**,** 16028.

ANNETT, S., MOORE, G. & ROBSON, T. 2020. Obesity and Cancer Metastasis: Molecular and Translational Perspectives. *Cancers* [Online], 12.

ARGON, Y. & SIMEN, B. B. 1999. GRP94, an ER chaperone with protein and peptide binding properties. *Semin Cell Dev Biol,* 10**,** 495-505.

ARNOLD, M., SIERRA, M. S., LAVERSANNE, M., SOERJOMATARAM, I., JEMAL, A. & BRAY, F. 2017. Global patterns and trends in colorectal cancer incidence and mortality. *Gut,* 66**,** 683-691.

ATANASOV, K. S., GÓMEZ, C., VIVES, J. T., MARTÍN-MEDINA, A., ESCARRER, G., SALA-LLINĀS, E. & MERCADER-BARCELÓ, J. 2022. Effects of a palmitate and fructose rich diet on lung fibrosis and inflammation markers in a murine model. Eur Respiratory Soc.

B'CHIR, W., MAURIN, A. C., CARRARO, V., AVEROUS, J., JOUSSE, C., MURANISHI, Y., PARRY, L., STEPIEN, G., FAFOURNOUX, P. & BRUHAT, A. 2013. The eIF2α/ATF4 pathway is essential for stress-induced autophagy gene expression. *Nucleic Acids Res,* 41**,** 7683-99.

BALDWIN, A. C., GREEN, C. D., OLSON, L. K., MOXLEY, M. A. & CORBETT, J. A. 2012. A role for aberrant protein palmitoylation in FFA-induced ER stress and β-cell death. *Am J Physiol Endocrinol Metab,* 302**,** E1390-8.

BANACH, A., JIANG, Y. P., ROTH, E., KUSCU, C., CAO, J. & LIN, R. Z. 2019. CEMIP upregulates BiP to promote breast cancer cell survival in hypoxia. *Oncotarget,* 10**,** 4307-4320.

BARONE, I., GIORDANO, C., BONOFIGLIO, D., ANDÒ, S. & CATALANO, S. 2020. The weight of obesity in breast cancer progression and metastasis: Clinical and molecular perspectives. *Seminars in Cancer Biology,* 60**,** 274-284.

BASSERI, S. & AUSTIN, R. C. 2012a. Endoplasmic Reticulum Stress and Lipid Metabolism: Mechanisms and Therapeutic Potential. *Biochemistry Research International,* 2012**,** 841362.

BASSERI, S. & AUSTIN, R. C. 2012b. Endoplasmic reticulum stress and lipid metabolism: mechanisms and therapeutic potential. *Biochem Res Int,* 2012**,** 841362.

BEERS, R. F. & SIZER, I. W. 1952. A SPECTROPHOTOMETRIC METHOD FOR MEASURING THE BREAKDOWN OF HYDROGEN PEROXIDE BY CATALASE. *Journal of Biological Chemistry,* 195**,** 133-140.

BENEDETTI, R., ROMEO, M. A., ARENA, A., GILARDINI MONTANI, M. S., DI RENZO, L., D'ORAZI, G. & CIRONE, M. 2022. ATF6 prevents DNA damage and cell death in colon cancer cells undergoing ER stress. *Cell Death Discovery,* 8**,** 295.

BERIAULT, D. R. & WERSTUCK, G. H. 2013. Detection and quantification of endoplasmic reticulum stress in living cells using the fluorescent compound, Thioflavin T. *Biochimica et Biophysica Acta (BBA) - Molecular Cell Research,* 1833**,** 2293-2301.

BERTOLOTTI, A., ZHANG, Y., HENDERSHOT, L. M., HARDING, H. P. & RON, D. 2000. Dynamic interaction of BiP and ER stress transducers in the unfolded-protein response. *Nat Cell Biol,* 2**,** 326-32.

BHATTARAI, K. R., RIAZ, T. A., KIM, H.-R. & CHAE, H.-J. 2021a. The aftermath of the interplay between the endoplasmic reticulum stress response and redox signaling. *Experimental & Molecular Medicine,* 53**,** 151-167.

BHATTARAI, K. R., RIAZ, T. A., KIM, H. R. & CHAE, H. J. 2021b. The aftermath of the interplay between the endoplasmic reticulum stress response and redox signaling. *Exp Mol Med,* 53**,** 151-167.

BIEDERBICK, A., KERN, H. F. & ELSÄSSER, H. P. 1995. Monodansylcadaverine (MDC) is a specific in vivo marker for autophagic vacuoles. *Eur J Cell Biol,* 66**,** 3-14.

BINKER-COSEN, M. J., RICHARDS, D., OLIVER, B., GAISANO, H. Y., BINKER, M. G. & COSEN-BINKER, L. I. 2017a. Palmitic acid increases invasiveness of pancreatic cancer cells AsPC-1 through TLR4/ROS/NF-κB/MMP-9 signaling pathway. *Biochem Biophys Res Commun,* 484**,** 152-158.

BINKER-COSEN, M. J., RICHARDS, D., OLIVER, B., GAISANO, H. Y., BINKER, M. G. & COSEN-BINKER, L. I. 2017b. Palmitic acid increases invasiveness of pancreatic cancer cells AsPC-1 through TLR4/ROS/NF-κB/MMP-9 signaling pathway. *Biochemical and Biophysical Research Communications,* 484**,** 152-158.

BOJKOVÁ, B., WINKLEWSKI, P. J. & WSZEDYBYL-WINKLEWSKA, M. 2020. Dietary Fat and Cancer—Which Is Good, Which Is Bad, and the Body of Evidence. *International Journal of Molecular Sciences* [Online], 21.

BONDIA-PONS, I., RYAN, L., MARTINEZ, J. A. J. J. O. P. & BIOCHEMISTRY 2012. Oxidative stress and inflammation interactions in human obesity. 68**,** 701-711.

BONSIGNORE, G., MARTINOTTI, S. & RANZATO, E. 2023. Endoplasmic Reticulum Stress and Cancer: Could Unfolded Protein Response Be a Druggable Target for Cancer Therapy? *International Journal of Molecular Sciences* [Online], 24.

BORRADAILE, N. M., HAN, X., HARP, J. D., GALE, S. E., ORY, D. S. & SCHAFFER, J. E. 2006. Disruption of endoplasmic reticulum structure and integrity in lipotoxic cell death. *J Lipid Res,* 47**,** 2726-37.

BOYCE, M. & YUAN, J. 2006. Cellular response to endoplasmic reticulum stress: a matter of life or death. *Cell Death & Differentiation,* 13**,** 363-373.

BRADLEY, R. L., FISHER, F. F. & MARATOS-FLIER, E. 2008. Dietary fatty acids differentially regulate production of TNF-alpha and IL-10 by murine 3T3-L1 adipocytes. *Obesity (Silver Spring),* 16**,** 938-44.

BRAY, F., JEMAL, A., GREY, N., FERLAY, J. & FORMAN, D. 2012. Global cancer transitions according to the Human Development Index (2008-2030): a population-based study. *Lancet Oncol,* 13**,** 790-801.

BRIX, N., SAMAGA, D., HENNEL, R., GEHR, K., ZITZELSBERGER, H. & LAUBER, K. 2020. The clonogenic assay: robustness of plating efficiency-based analysis is strongly compromised by cellular cooperation. *Radiation Oncology,* 15**,** 248.

BRYAN, H. K., OLAYANJU, A., GOLDRING, C. E. & PARK, B. K. 2013. The Nrf2 cell defence pathway: Keap1-dependent and -independent mechanisms of regulation. *Biochemical Pharmacology,* 85**,** 705-717.

BUETTNER, G. R. 2011. Superoxide dismutase in redox biology: the roles of superoxide and hydrogen peroxide. *Anticancer Agents Med Chem,* 11**,** 341-6.

BURGOS-MORÓN, E., ABAD-JIMÉNEZ, Z., MARTÍNEZ DE MARAÑÓN, A., IANNANTUONI, F., ESCRIBANO-LÓPEZ, I., LÓPEZ-DOMÈNECH, S., SALOM, C., JOVER, A., MORA, V., ROLDAN, I., SOLÁ, E., ROCHA, M. & VÍCTOR, V. M. 2019. Relationship between Oxidative Stress, ER Stress, and Inflammation in Type 2 Diabetes: The Battle Continues. *Journal of Clinical Medicine* [Online], 8.

CALFON, M., ZENG, H., URANO, F., TILL, J. H., HUBBARD, S. R., HARDING, H. P., CLARK, S. G. & RON, D. 2002. IRE1 couples endoplasmic reticulum load to secretory capacity by processing the XBP-1 mRNA. *Nature,* 415**,** 92-6.

CANI, P. D., AMAR, J., IGLESIAS, M. A., POGGI, M., KNAUF, C., BASTELICA, D., NEYRINCK, A. M., FAVA, F., TUOHY, K. M., CHABO, C., WAGET, A., DELMÉE, E., COUSIN, B., SULPICE, T., CHAMONTIN, B., FERRIÈRES, J., TANTI, J. F., GIBSON, G. R., CASTEILLA, L., DELZENNE, N. M., ALESSI, M. C. & BURCELIN, R. 2007. Metabolic endotoxemia initiates obesity and insulin resistance. *Diabetes,* 56**,** 1761-72.

CAO, J., DAI, D. L., YAO, L., YU, H. H., NING, B., ZHANG, Q., CHEN, J., CHENG, W. H., SHEN, W. & YANG, Z. X. 2012. Saturated fatty acid induction of endoplasmic reticulum stress and apoptosis in human liver cells via the PERK/ATF4/CHOP signaling pathway. *Mol Cell Biochem,* 364**,** 115-29.

CARLISLE, S., TRAINOR, P., YIN, X., DOLL, M., STEPP, M., STATES, J. C., ZHANG, X. & HEIN, D. 2016. Untargeted polar metabolomics of transformed MDA-MB-231 breast cancer cells expressing varying levels of human arylamine N-acetyltransferase 1. *Metabolomics,* 12.

CARTA, G., MURRU, E., BANNI, S. & MANCA, C. 2017. Palmitic Acid: Physiological Role, Metabolism and Nutritional Implications. *Front Physiol,* 8**,** 902.

CARTA, G., MURRU, E., LISAI, S., SIRIGU, A., PIRAS, A., COLLU, M., BATETTA, B., GAMBELLI, L. & BANNI, S. 2015. Dietary triacylglycerols with palmitic acid in the sn-2 position modulate levels of N-acylethanolamides in rat tissues. *PLoS One,* 10**,** e0120424.

CELIK, C., LEE, S. Y. T., YAP, W. S. & THIBAULT, G. 2023. Endoplasmic reticulum stress and lipids in health and diseases. *Progress in Lipid Research,* 89**,** 101198.

CEN, S., JIANG, D., LV, D., XU, R., HOU, J., YANG, Z., WU, P., XIONG, X. & GAO, X. 2023. Comprehensive analysis of the biological functions of endoplasmic reticulum stress in prostate cancer. *Front Endocrinol (Lausanne),* 14**,** 1090277.

CHAMBERLAIN, L. H., LEMONIDIS, K., SANCHEZ-PEREZ, M., WERNO, M. W., GORLEKU, O. A. & GREAVES, J. 2013. Palmitoylation and the trafficking of peripheral membrane proteins. *Biochem Soc Trans,* 41**,** 62-6.

CHANG, K. H., LIAO, H. F., CHANG, H. H., CHEN, Y. Y., YU, M. C., CHOU, C. J. & CHEN, Y. J. 2004. Inhibitory effect of tetrandrine on pulmonary metastases in CT26 colorectal adenocarcinoma-bearing BALB/c mice. *Am J Chin Med,* 32**,** 863-72.

CHAREST, P. G. & BOUVIER, M. 2003. Palmitoylation of the V2 vasopressin receptor carboxyl tail enhances beta-arrestin recruitment leading to efficient receptor endocytosis and ERK1/2 activation. *J Biol Chem,* 278**,** 41541-51.

CHATTERJEE, T., PATTANAYAK, R., UKIL, A., CHOWDHURY, S. & BHATTACHARYYA, M. 2019. Autophagy protects peripheral blood mononuclear cells against inflammation, oxidative and nitrosative stress in diabetic dyslipidemia. *Free Radic Biol Med,* 143**,** 309-323.

CHEN, H., XU, N., XU, J., ZHANG, C., LI, X., XU, H., ZHU, W., LI, J., LIANG, D. & ZHOU, W. 2023a. A risk signature based on endoplasmic reticulum stress-associated genes predicts prognosis and immunity in pancreatic cancer. *Front Mol Biosci,* 10**,** 1298077.

CHEN, L., WANG, T., CHEN, G., WANG, N., GUI, L., DAI, F., FANG, Z., ZHANG, Q. & LU, Y. 2017. Influence of resveratrol on endoplasmic reticulum stress and expression of adipokines in adipose tissues/adipocytes induced by high-calorie diet or palmitic acid. *Endocrine,* 55**,** 773-785.

CHEN, X., CHEN, K., HU, J., DONG, Y., ZHENG, M., JIANG, J., HU, Q. & ZHANG, W. J. C. B. 2024. Palmitic acid induces lipid droplet accumulation and senescence in nucleus pulposus cells via ER-stress pathway. 7**,** 539.

CHEN, X., SHI, C., HE, M., XIONG, S. & XIA, X. 2023b. Endoplasmic reticulum stress: molecular mechanism and therapeutic targets. *Signal Transduction and Targeted Therapy,* 8**,** 352.

CHEN, Z., LEI, L., WEN, D. & YANG, L. 2019a. Melatonin attenuates palmitic acid-induced mouse granulosa cells apoptosis via endoplasmic reticulum stress. *Journal of Ovarian Research,* 12**,** 43.

CHEN, Z., LEI, L., WEN, D. & YANG, L. 2019b. Melatonin attenuates palmitic acid-induced mouse granulosa cells apoptosis via endoplasmic reticulum stress. *J Ovarian Res,* 12**,** 43.

CHEN, Z., WEN, D., WANG, F., WANG, C. & YANG, L. 2019c. Curcumin protects against palmitic acid-induced apoptosis via the inhibition of endoplasmic reticulum stress in testicular Leydig cells. *Reproductive Biology and Endocrinology,* 17**,** 71.

CHENG, L., YU, Y., SZABO, A., WU, Y., WANG, H., CAMER, D. & HUANG, X. F. 2015. Palmitic acid induces central leptin resistance and impairs hepatic glucose and lipid metabolism in male mice. *J Nutr Biochem,* 26**,** 541-8.

CHENG, T., LIU, Q., ZHANG, R., ZHANG, Y., CHEN, J., YU, R. & GE, G. 2014. Lysyl oxidase promotes bleomycin-induced lung fibrosis through modulating inflammation. *Journal of Molecular Cell Biology,* 6**,** 506-515.

CHERUBINI, A. & ZITO, E. 2022. ER stress as a trigger of UPR and ER-phagy in cancer growth and spread. *Front Oncol,* 12**,** 997235.

CHIPURUPALLI, S., KANNAN, E., TERGAONKAR, V., D'ANDREA, R. & ROBINSON, N. J. I. J. O. M. S. 2019. Hypoxia induced ER stress response as an adaptive mechanism in cancer. 20**,** 749.

CHIPURUPALLI, S., SAMAVEDAM, U. & ROBINSON, N. J. F. I. M. 2021. Crosstalk between ER stress, autophagy and inflammation. 8**,** 758311.

CHOI, Y. J., LEE, D. H., HAN, K.-D., SHIN, C. M. & KIM, N. 2018. Abdominal obesity, glucose intolerance and decreased high-density lipoprotein cholesterol as components of the metabolic syndrome are associated with the development of colorectal cancer. *European Journal of Epidemiology,* 33**,** 1077-1085.

CHONG, M. F., HODSON, L., BICKERTON, A. S., ROBERTS, R., NEVILLE, M., KARPE, F., FRAYN, K. N. & FIELDING, B. A. 2008. Parallel activation of de novo lipogenesis and stearoyl-CoA desaturase activity after 3 d of high-carbohydrate feeding. *Am J Clin Nutr,* 87**,** 817-23.

CHOUDHURY, S., GHOSH, S., GUPTA, P., MUKHERJEE, S. & CHATTOPADHYAY, S. 2015. Inflammation-induced ROS generation causes pancreatic cell death through modulation of Nrf2/NF-κB and SAPK/JNK pathway. *Free Radic Res,* 49**,** 1371-83.

CHU, S. G., VILLALBA, J. A., LIANG, X., XIONG, K., TSOYI, K., ITH, B., AYAUB, E. A., TATITURI, R. V., BYERS, D. E. & HSU, F.-F. 2019a. Palmitic acid–rich high-fat diet exacerbates experimental pulmonary fibrosis by modulating endoplasmic reticulum stress. *American Journal of Respiratory Cell and Molecular Biology,* 61**,** 737-746.

CHU, S. G., VILLALBA, J. A., LIANG, X., XIONG, K., TSOYI, K., ITH, B., AYAUB, E. A., TATITURI, R. V., BYERS, D. E., HSU, F. F., EL-CHEMALY, S., KIM, E. Y., SHI, Y. & ROSAS, I. O. 2019b. Palmitic Acid-Rich High-Fat Diet Exacerbates Experimental Pulmonary Fibrosis by Modulating Endoplasmic Reticulum Stress. *Am J Respir Cell Mol Biol,* 61**,** 737-746.

CLARKE, S. J., FARRUGIA, D. C., AHERNE, G. W., PRITCHARD, D. M., BENSTEAD, J. & JACKMAN, A. L. 2000. Balb/c mice as a preclinical model for raltitrexed-induced gastrointestinal toxicity. *Clin Cancer Res,* 6**,** 285-96.

CNOP, M., LADRIERE, L., HEKERMAN, P., ORTIS, F., CARDOZO, A. K., DOGUSAN, Z., FLAMEZ, D., BOYCE, M., YUAN, J. & EIZIRIK, D. L. 2007. Selective inhibition of eukaryotic translation initiation factor 2 alpha dephosphorylation potentiates fatty acid-induced endoplasmic reticulum stress and causes pancreatic beta-cell dysfunction and apoptosis. *J Biol Chem,* 282**,** 3989-97.

COBBS, A., CHEN, X., ZHANG, Y., GEORGE, J., HUANG, M.-B., BOND, V., THOMPSON, W. & ZHAO, X. 2019. Saturated fatty acid stimulates production of extracellular vesicles by renal tubular epithelial cells. *Molecular and Cellular Biochemistry,* 458**,** 113-124.

COLEMAN, O. I., LOBNER, E. M., BIERWIRTH, S., SORBIE, A., WALDSCHMITT, N., RATH, E., BERGER, E., LAGKOUVARDOS, I., CLAVEL, T., MCCOY, K. D., WEBER, A., HEIKENWALDER, M., JANSSEN, K. P. & HALLER, D. 2018. Activated ATF6 Induces Intestinal Dysbiosis and Innate Immune Response to Promote Colorectal Tumorigenesis. *Gastroenterology,* 155**,** 1539-1552.e12.

CORAZZARI, M., GAGLIARDI, M., FIMIA, G. M. & PIACENTINI, M. 2017. Endoplasmic Reticulum Stress, Unfolded Protein Response, and Cancer Cell Fate. *Front Oncol,* 7**,** 78.

CORN, K. C., WINDHAM, M. A. & RAFAT, M. 2020. Lipids in the tumor microenvironment: From cancer progression to treatment. *Progress in Lipid Research,* 80**,** 101055.

CRAVEN, R. A., EGERTON, M. & STIRLING, C. J. 1996. A novel Hsp70 of the yeast ER lumen is required for the efficient translocation of a number of protein precursors. *Embo j,* 15**,** 2640-50.

CUANALO-CONTRERAS, K., SCHULZ, J., MUKHERJEE, A., PARK, K. W., ARMIJO, E. & SOTO, C. 2022. Extensive accumulation of misfolded protein aggregates during natural aging and senescence. *Front Aging Neurosci,* 14**,** 1090109.

CUI, G., LIU, H. & LAUGSAND, J.-B. J. I. I. 2023. Endothelial cells-directed angiogenesis in colorectal cancer: Interleukin as the mediator and pharmacological target. 114**,** 109525.

CULLINAN, S. B. & DIEHL, J. A. 2004. PERK-dependent activation of Nrf2 contributes to redox homeostasis and cell survival following endoplasmic reticulum stress. *J Biol Chem,* 279**,** 20108-17.

CULLINAN, S. B. & DIEHL, J. A. 2006. Coordination of ER and oxidative stress signaling: The PERK/Nrf2 signaling pathway. *The International Journal of Biochemistry & Cell Biology,* 38**,** 317-332.

CULLINAN, S. B., ZHANG, D., HANNINK, M., ARVISAIS, E., KAUFMAN, R. J. & DIEHL, J. A. 2003. Nrf2 is a direct PERK substrate and effector of PERK-dependent cell survival. *Mol Cell Biol,* 23**,** 7198-209.

CUNHA, D. A., HEKERMAN, P., LADRIÈRE, L., BAZARRA-CASTRO, A., ORTIS, F., WAKEHAM, M. C., MOORE, F., RASSCHAERT, J., CARDOZO, A. K., BELLOMO, E., OVERBERGH, L., MATHIEU, C., LUPI, R., HAI, T., HERCHUELZ, A., MARCHETTI, P., RUTTER, G. A., EIZIRIK, D. L. & CNOP, M. 2008. Initiation and execution of lipotoxic ER stress in pancreatic beta-cells. *J Cell Sci,* 121**,** 2308-18.

CUOZZO, J. W. & KAISER, C. A. 1999. Competition between glutathione and protein thiols for disulphide-bond formation. *Nat Cell Biol,* 1**,** 130-5.

DAVIS, R. J. 2000. Signal transduction by the JNK group of MAP kinases. *Cell,* 103**,** 239-52.

DE WIT, N., DERRIEN, M., BOSCH-VERMEULEN, H., OOSTERINK, E., KESHTKAR, S., DUVAL, C., DE VOGEL-VAN DEN BOSCH, J., KLEEREBEZEM, M., MÜLLER, M. & VAN DER MEER, R. 2012. Saturated fat stimulates obesity and hepatic steatosis and affects gut microbiota composition by an enhanced overflow of dietary fat to the distal intestine. *Am J Physiol Gastrointest Liver Physiol,* 303**,** G589-99.

DEEGAN, S., SAVELJEVA, S., GORMAN, A. M. & SAMALI, A. 2013. Stress-induced self-cannibalism: on the regulation of autophagy by endoplasmic reticulum stress. *Cell Mol Life Sci,* 70**,** 2425-41.

DEMARCHI, F., BERTOLI, C., COPETTI, T., TANIDA, I., BRANCOLINI, C., ESKELINEN, E. L. & SCHNEIDER, C. 2006. Calpain is required for macroautophagy in mammalian cells. *J Cell Biol,* 175**,** 595-605.

DENG, J., LU, P. D., ZHANG, Y., SCHEUNER, D., KAUFMAN, R. J., SONENBERG, N., HARDING, H. P. & RON, D. 2004. Translational repression mediates activation of nuclear factor kappa B by phosphorylated translation initiation factor 2. *Mol Cell Biol,* 24**,** 10161-8.

DEPONTE, M. 2013. Glutathione catalysis and the reaction mechanisms of glutathione-dependent enzymes. *Biochimica et Biophysica Acta (BBA) - General Subjects,* 1830**,** 3217-3266.

DING, W. X., NI, H. M., GAO, W., HOU, Y. F., MELAN, M. A., CHEN, X., STOLZ, D. B., SHAO, Z. M. & YIN, X. M. 2007. Differential effects of endoplasmic reticulum stress-induced autophagy on cell survival. *J Biol Chem,* 282**,** 4702-4710.

DOMÍNGUEZ-LÓPEZ, I., ARANCIBIA-RIVEROS, C., CASAS, R., TRESSERRA-RIMBAU, A., RAZQUIN, C., MARTÍNEZ-GONZÁLEZ, M. Á., HU, F. B., ROS, E., FITÓ, M., ESTRUCH, R., LÓPEZ-SABATER, M. C. & LAMUELA-RAVENTÓS, R. M. 2022. Changes in plasma total saturated fatty acids and palmitic acid are related to

pro-inflammatory molecule IL-6 concentrations after nutritional intervention for one year. *Biomedicine & Pharmacotherapy,* 150**,** 113028.

DURANTI, G., MALDINI, M., CROGNALE, D., HORNER, K., DIMAURO, I., SABATINI, S. & CECI, R. 2021. Moringa oleifera Leaf Extract Upregulates Nrf2/HO-1 Expression and Ameliorates Redox Status in C2C12 Skeletal Muscle Cells. *Molecules,* 26.

DZIĘGIELEWSKA-GĘSIAK, S., WYSOCKA, E., FATYGA, E. & MUC-WIERZGOŃ, M. J. M. 2024. Relationship of SOD-1 Activity in Metabolic Syndrome and/or Frailty in Elderly Individuals. 14**,** 514.

EGNATCHIK, R. A., LEAMY, A. K., JACOBSON, D. A., SHIOTA, M. & YOUNG, J. D. 2014. ER calcium release promotes mitochondrial dysfunction and hepatic cell lipotoxicity in response to palmitate overload. *Mol Metab,* 3**,** 544-53.

ELBAKARY, R. H., OKASHA, E. F., HASSAN RAGAB, A. M. & RAGAB, M. H. 2018. Histological Effects of Gold Nanoparticles on the Lung Tissue of Adult Male Albino Rats. *J Microsc Ultrastruct,* 6**,** 116-122.

ESCOULA, Q., BELLENGER, S., NARCE, M. & BELLENGER, J. 2019. Docosahexaenoic and Eicosapentaenoic Acids Prevent Altered-Muc2 Secretion Induced by Palmitic Acid by Alleviating Endoplasmic Reticulum Stress in LS174T Goblet Cells. *Nutrients* [Online], 11.

FANG, W., LIU, Y., CHEN, Q., XU, D., LIU, Q., CAO, X., HAO, T., ZHANG, L., MAI, K. & AI, Q. 2022a. Palmitic acid induces intestinal lipid metabolism disorder, endoplasmic reticulum stress and inflammation by affecting phosphatidylethanolamine content in large yellow croaker Larimichthys crocea. *Front Immunol,* 13**,** 984508.

FANG, W., LIU, Y., CHEN, Q., XU, D., LIU, Q., CAO, X., HAO, T., ZHANG, L., MAI, K. & AI, Q. 2022b. Palmitic acid induces intestinal lipid metabolism disorder, endoplasmic reticulum stress and inflammation by affecting phosphatidylethanolamine content in large yellow croaker Larimichthys crocea. *Frontiers in Immunology,* 13.

FANG, Y., LI, W., DONG, C., GAO, B., GUO, W., LI, M. & JIAO, Z. J. R. R. 2024. Inhibition of SLC40A1 represses osteoblast formation via inducing iron accumulation and activating the PERK/ATF4/CHOP pathway mediated oxidative stress. 29**,** 2428147.

FATIMA, S., HU, X., GONG, R.-H., HUANG, C., CHEN, M., WONG, H. L. X., BIAN, Z. & KWAN, H. Y. 2019a. Palmitic acid is an intracellular signaling molecule involved in disease development. *Cellular and Molecular Life Sciences,* 76**,** 2547-2557.

FATIMA, S., HU, X., GONG, R. H., HUANG, C., CHEN, M., WONG, H. L. X., BIAN, Z. & KWAN, H. Y. 2019b. Palmitic acid is an intracellular signaling molecule involved in disease development. *Cell Mol Life Sci,* 76**,** 2547-2557.

FATTORE, E. & FANELLI, R. 2013. Palm oil and palmitic acid: a review on cardiovascular effects and carcinogenicity. *Int J Food Sci Nutr,* 64**,** 648-59.

FATTORE, E., FANELLI, R. J. I. J. O. F. S. & NUTRITION 2013. Palm oil and palmitic acid: a review on cardiovascular effects and carcinogenicity. 64**,** 648-659.

FAZOLINI, N. P., CRUZ, A. L., WERNECK, M. B., VIOLA, J. P., MAYA-MONTEIRO, C. M. & BOZZA, P. T. 2015. Leptin activation of mTOR pathway in intestinal epithelial cell triggers lipid droplet formation, cytokine production and increased cell proliferation. *Cell Cycle,* 14**,** 2667-76.

FENG, W. W., ZUPPE, H. T. & KUROKAWA, M. 2023. The Role of CD36 in Cancer Progression and Its Value as a Therapeutic Target. *Cells* [Online], 12.

FENG, Y.-X., JIN, D. X., SOKOL, E. S., REINHARDT, F., MILLER, D. H. & GUPTA, P. B. 2017. Cancer-specific PERK signaling drives invasion and metastasis through CREB3L1. *Nature Communications,* 8**,** 1079.

FERNÁNDEZ, L. P., GOMEZ DE CEDRON, M. & RAMIREZ DE MOLINA, A. 2020. Alterations of lipid metabolism in cancer: implications in prognosis and treatment. *Frontiers in oncology,* 10**,** 577420.

FIGARD, P. H., HEJLIK, D. P., KADUCE, T. L., STOLL, L. L. & SPECTOR, A. A. 1988. Free fatty acid release from endothelial cells. *Journal of Lipid Research,* 27**,** 771-780.

FILIPPELLO, A., DI MAURO, S., SCAMPORRINO, A., TORRISI, S. A., LEGGIO, G. M., DI PINO, A., SCICALI, R., DI MARCO, M., MALAGUARNERA, R., PURRELLO, F. & PIRO, S. 2022. Molecular Effects of Chronic Exposure to Palmitate in Intestinal Organoids: A New Model to Study Obesity and Diabetes. *Int J Mol Sci,* 23.

FLORESCU, D. N., BOLDEANU, M.-V., ȘERBAN, R.-E., FLORESCU, L. M., SERBANESCU, M.-S., IONESCU, M., STREBA, L., CONSTANTIN, C. & VERE, C. C. J. L. 2023. Correlation of the Pro-Inflammatory Cytokines IL-1β, IL-6, and TNF-α, Inflammatory Markers, and Tumor Markers with the Diagnosis and Prognosis of Colorectal Cancer. 13**,** 2261.

FORMAN, M. R., MAHABIR, S. J. B. C. & CANCER 2010. Saturated fatty acids and cancer. 213-233.

FRANCHI, L., EIGENBROD, T., MUÑOZ-PLANILLO, R. & NUÑEZ, G. 2009. The inflammasome: a caspase-1-activation platform that regulates immune responses and disease pathogenesis. *Nature Immunology,* 10**,** 241-247.

FU, Y., ZOU, T., SHEN, X., NELSON, P. J., LI, J., WU, C., YANG, J., ZHENG, Y., BRUNS, C., ZHAO, Y., QIN, L. & DONG, Q. 2021. Lipid metabolism in cancer progression and therapeutic strategies. *MedComm (2020),* 2**,** 27-59.

GAO, W., FANG, Z., LEI, L., JU, L., JIN, B., LOOR, J. J., LIANG, Y., SHI, Z., SHEN, T., YU, H., CHEN, M., OUYANG, H., SONG, Y., WANG, Z., LIU, G., LI, X. & DU, X. 2021. Propionate alleviates palmitic acid–induced endoplasmic reticulum stress by enhancing autophagy in calf hepatic cells. *Journal of Dairy Science,* 104**,** 9316-9326.

GARDNER, B. M., PINCUS, D., GOTTHARDT, K., GALLAGHER, C. M. & WALTER, P. 2013. Endoplasmic reticulum stress sensing in the unfolded protein response. *Cold Spring Harb Perspect Biol,* 5**,** a013169.

GARFIELD, S. A. & CARDELL, R. R. 1987. Endoplasmic Reticulum: Rough and Smooth. *In:* BOURNE, G. H. (ed.) *Cytology and Cell Physiology (Fourth Edition).* San Diego: Academic Press.

GE, X., HE, Z., CAO, C., XUE, T., JING, J., MA, R., ZHAO, W., LIU, L., JUERAITETIBAIKE, K., MA, J., FENG, Y., QIAN, Z., ZOU, Z., CHEN, L., FU, C., SONG, N. & YAO, B. 2022. Protein palmitoylation-mediated palmitic acid sensing causes blood-testis barrier damage via inducing ER stress. *Redox Biology,* 54**,** 102380.

GENG, J., GUO, Y., XIE, M., LI, Z., WANG, P., ZHU, D., LI, J. & CUI, X. 2023. Characteristics of endoplasmic reticulum stress in colorectal cancer for predicting prognosis and developing treatment options. *Cancer Med,* 12**,** 12000-12017.

GEORGE, S. & ABRAHAMSE, H. 2020. Redox Potential of Antioxidants in Cancer Progression and Prevention. *Antioxidants* [Online], 9.

GHEMRAWI, R. & KHAIR, M. 2020. Endoplasmic Reticulum Stress and Unfolded Protein Response in Neurodegenerative Diseases. *International Journal of Molecular Sciences* [Online], 21.

GHEZZAL, S., POSTAL, B. G., QUEVRAIN, E., BROT, L., SEKSIK, P., LETURQUE, A., THENET, S. & CARRIÈRE, V. 2020. Palmitic acid damages gut epithelium integrity and initiates inflammatory cytokine production. *Biochimica et Biophysica Acta (BBA) - Molecular and Cell Biology of Lipids,* 1865**,** 158530.

GLATZ, J. F., LUIKEN, J. J. & BONEN, A. 2010. Membrane fatty acid transporters as regulators of lipid metabolism: implications for metabolic disease. *Physiol Rev,* 90**,** 367-417.

GLICK, D., BARTH, S. & MACLEOD, K. F. 2010. Autophagy: cellular and molecular mechanisms. *J Pathol,* 221**,** 3-12.

GORI, M., ALTOMARE, A., COCCA, S., SOLIDA, E., RIBOLSI, M., CAROTTI, S., RAINER, A., FRANCESCONI, M., MORINI, S., CICALA, M. & PIER LUCA GUARINO, M. 2020. Palmitic Acid Affects Intestinal Epithelial Barrier Integrity and Permeability In Vitro. *Antioxidants* [Online], 9.

GRANLUND, L., LARSEN, L. N., NEBB, H. I. & PEDERSEN, J. I. 2005. Effects of structural changes of fatty acids on lipid accumulation in adipocytes and primary hepatocytes. *Biochimica et Biophysica Acta (BBA) - Molecular and Cell Biology of Lipids,* 1687**,** 23-30.

GREY, M. J., CLOOTS, E., SIMPSON, M. S., LEDUC, N., SEREBRENIK, Y. V., DE LUCA, H., DE SUTTER, D., LUONG, P., THIAGARAJAH, J. R., PATON, A. W., PATON, J. C., SEELIGER, M. A., EYCKERMAN, S., JANSSENS, S. & LENCER, W. I. 2020. IRE1β negatively regulates IRE1α signaling in response to endoplasmic reticulum stress. *J Cell Biol,* 219.

GULLICKSON, C., GOODMAN, M., JOKO-FRU, Y. W., GNANGNON, F. H. R., N'DA, G., WOLDEGEORGIS, M. A., BUZIBA, N. G., KARUGU, C., MANRAJ, S. S., LORENZONI, C. F., HANSEN, R., FINESSE, A., SOMDYALA, N. I. M., BUKIRWA, P., CHINGONZOH, T., CHOKUNONGA, E., LIU, B., KANTELHARDT, E., PARKIN, D. M. & JEMAL, A. 2021. Colorectal cancer survival in sub-Saharan Africa by age, stage at diagnosis and Human Development Index: A population-based registry study. *Int J Cancer,* 149**,** 1553-1563.

HABERZETTL, P. & HILL, B. G. 2013. Oxidized lipids activate autophagy in a JNK-dependent manner by stimulating the endoplasmic reticulum stress response. *Redox Biol,* 1**,** 56-64.

HABIG, W. H., PABST, M. J. & JAKOBY, W. B. 1974. Glutathione S-transferases. The first enzymatic step in mercapturic acid formation. *J Biol Chem,* 249**,** 7130-9.

HAFEMAN, D. G., SUNDE, R. A. & HOEKSTRA, W. G. 1974. Effect of dietary selenium on erythrocyte and liver glutathione peroxidase in the rat. *J Nutr,* 104**,** 580-7.

HAN, D., LERNER, A. G., VANDE WALLE, L., UPTON, J. P., XU, W., HAGEN, A., BACKES, B. J., OAKES, S. A. & PAPA, F. R. 2009. IRE1alpha kinase activation modes control alternate endoribonuclease outputs to determine divergent cell fates. *Cell,* 138**,** 562-75.

HAN, J. & KAUFMAN, R. J. 2016. The role of ER stress in lipid metabolism and lipotoxicity. *J Lipid Res,* 57**,** 1329-38.

HANAOKA, M., ISHIKAWA, T., ISHIGURO, M., TOKURA, M., YAMAUCHI, S., KIKUCHI, A., UETAKE, H., YASUNO, M. & KAWANO, T. 2018. Expression of ATF6 as a marker of pre-cancerous atypical change in ulcerative colitis-associated colorectal cancer: a potential role in the management of dysplasia. *Journal of Gastroenterology,* 53**,** 631-641.

HARDING, H. P., ZHANG, Y. & RON, D. 1999a. Protein translation and folding are coupled by an endoplasmic-reticulum-resident kinase. *Nature,* 397**,** 271-4.

HARDING, H. P., ZHANG, Y. & RON, D. 1999b. Protein translation and folding are coupled by an endoplasmic-reticulum-resident kinase. *Nature,* 397**,** 271-274.

HARDING, H. P., ZHANG, Y., ZENG, H., NOVOA, I., LU, P. D., CALFON, M., SADRI, N., YUN, C., POPKO, B., PAULES, R., STOJDL, D. F., BELL, J. C., HETTMANN, T., LEIDEN, J. M. & RON, D. 2003. An integrated stress response regulates amino acid metabolism and resistance to oxidative stress. *Mol Cell,* 11**,** 619-33.

HAZE, K., YOSHIDA, H., YANAGI, H., YURA, T. & MORI, K. 1999. Mammalian transcription factor ATF6 is synthesized as a transmembrane protein and activated by proteolysis in response to endoplasmic reticulum stress. *Mol Biol Cell,* 10**,** 3787-99.

HE, C. H., GONG, P., HU, B., STEWART, D., CHOI, M. E., CHOI, A. M. K. & ALAM, J. 2001. Identification of Activating Transcription Factor 4 (ATF4) as an Nrf2-interacting Protein: IMPLICATION FOR HEME OXYGENASE-1 GENE REGULATION*. *Journal of Biological Chemistry,* 276**,** 20858-20865.

HIRATA, T., KAWAI, T., HIROSE, H., TANAKA, K., KUROSAWA, H., FUJII, C., FUJITA, H., SETO, Y., MATSUMOTO, H. & ITOH, H. 2016. Palmitic acid-rich diet suppresses glucose-stimulated insulin secretion (GSIS) and induces endoplasmic reticulum (ER) stress in pancreatic islets in mice. *Endocr Res,* 41**,** 8-15.

HISHAM, M. D. B., AZIZ, Z., HUIN, W. K., TEOH, C. H. & JAMIL, A. H. A. 2020. The effects of palm oil on serum lipid profiles: A systematic review and meta-analysis. *Asia Pac J Clin Nutr,* 29**,** 523-536.

HOLLAND, S. M. & THOMAS, G. M. 2017. Roles of palmitoylation in axon growth, degeneration and regeneration. *J Neurosci Res,* 95**,** 1528-1539.

HOLLIEN, J., LIN, J. H., LI, H., STEVENS, N., WALTER, P. & WEISSMAN, J. S. 2009. Regulated Ire1-dependent decay of messenger RNAs in mammalian cells. *J Cell Biol,* 186**,** 323-31.

HØYER-HANSEN, M., BASTHOLM, L., SZYNIAROWSKI, P., CAMPANELLA, M., SZABADKAI, G., FARKAS, T., BIANCHI, K., FEHRENBACHER, N., ELLING, F., RIZZUTO, R., MATHIASEN, I. S. & JÄÄTTELÄ, M. 2007. Control of macroautophagy by calcium, calmodulin-dependent kinase kinase-beta, and Bcl-2. *Mol Cell,* 25**,** 193-205.

HØYER-HANSEN, M. & JÄÄTTELÄ, M. 2007. Connecting endoplasmic reticulum stress to autophagy by unfolded protein response and calcium. *Cell Death & Differentiation,* 14**,** 1576-1582.

HSIAO, Y.-H., LIN, C.-I., LIAO, H., CHEN, Y.-H. & LIN, S.-H. 2014a. Palmitic Acid-Induced Neuron Cell Cycle G2/M Arrest and Endoplasmic Reticular Stress through Protein Palmitoylation in SH-SY5Y Human Neuroblastoma Cells. *International Journal of Molecular Sciences,* 15**,** 20876-20899.

HSIAO, Y. H., LIN, C. I., LIAO, H., CHEN, Y. H. & LIN, S. H. 2014b. Palmitic acid-induced neuron cell cycle G2/M arrest and endoplasmic reticular stress through protein palmitoylation in SH-SY5Y human neuroblastoma cells. *Int J Mol Sci,* 15**,** 20876-99.

HU, P., HAN, Z., COUVILLON, A. D., KAUFMAN, R. J. & EXTON, J. H. 2006. Autocrine tumor necrosis factor alpha links endoplasmic reticulum stress to the membrane death receptor pathway through IRE1alpha-mediated NF-kappaB activation and down-regulation of TRAF2 expression. *Mol Cell Biol,* 26**,** 3071-84.

HUA, W., HUANG, H. Z., TAN, L. T., WAN, J. M., GUI, H. B., ZHAO, L., RUAN, X. Z., CHEN, X. M. & DU, X. G. 2015. CD36 Mediated Fatty Acid-Induced Podocyte Apoptosis via Oxidative Stress. *PLoS One,* 10**,** e0127507.

HUANG, F., SUN, B., WANG, X., JIAN, X., DU, Q. & CHEN, J. 2021a. Dietary palmitic acid promotes tumor growth and epithelial-mesenchymal transformation in prostate cancer.

HUANG, J., PAN, H., WANG, J., WANG, T., HUO, X., MA, Y., LU, Z., SUN, B. & JIANG, H. 2021b. Unfolded protein response in colorectal cancer. *Cell Biosci,* 11**,** 26.

HUANG, J., PAN, H., WANG, J., WANG, T., HUO, X., MA, Y., LU, Z., SUN, B. & JIANG, H. 2021c. Unfolded protein response in colorectal cancer. *Cell & Bioscience,* 11**,** 26.

HUO, M., ZHAO, Y., LIU, X., GAO, Y., ZHANG, D., CHANG, M., LIU, M., XU, N. & ZHU, H. 2020. EGFR targeting enhances the efficiency of chemotherapy through inhibiting IRE1α-XBP1s pathway in colorectal cancer cells. *J Cancer,* 11**,** 4464-4473.

HWANG, J. & QI, L. 2018. Quality Control in the Endoplasmic Reticulum: Crosstalk between ERAD and UPR pathways. *Trends Biochem Sci,* 43**,** 593-605.

IMAGAWA, Y., HOSODA, A., SASAKA, S., TSURU, A. & KOHNO, K. 2008. RNase domains determine the functional difference between IRE1alpha and IRE1beta. *FEBS Lett,* 582**,** 656-60.

IMANIKIA, S., ÖZBEY, N. P., KRUEGER, C., CASANUEVA, M. O. & TAYLOR, R. C. 2019. Neuronal XBP-1 Activates Intestinal Lysosomes to Improve Proteostasis in C. elegans. *Curr Biol,* 29**,** 2322-2338.e7.

INNIS, S. M. 2016. Palmitic Acid in Early Human Development. *Crit Rev Food Sci Nutr,* 56**,** 1952-9.

INNIS, S. M., DYER, R. A. & LIEN, E. L. 1997. Formula containing randomized fats with palmitic acid (16:0) in the 2-position increases 16:0 in the 2-position of plasma and chylomicron triglycerides in formula-fed piglets to levels approaching those of piglets fed sow's milk. *J Nutr,* 127**,** 1362-70.

IRSHAD, R., TABASSUM, S. & HUSAIN, M. 2023. Aberrant Lipid Metabolism in Cancer: Current Status and Emerging Therapeutic Perspectives. *Curr Top Med Chem,* 23**,** 1090-1103.

JARC, E. & PETAN, T. 2019. Lipid Droplets and the Management of Cellular Stress. *Yale J Biol Med,* 92**,** 435-452.

JIANG, M., WU, N., XU, B., CHU, Y., LI, X., SU, S., CHEN, D., LI, W., SHI, Y., GAO, X., ZHANG, H., ZHANG, Z., DU, W., NIE, Y., LIANG, J. & FAN, D. 2019. Fatty acid-induced CD36 expression via O-GlcNAcylation drives gastric cancer metastasis. *Theranostics,* 9**,** 5359-5373.

JIN, C., JIN, Z., CHEN, N.-Z., LU, M., LIU, C.-B., HU, W.-L. & ZHENG, C.-G. 2016a. Activation of IRE1α-XBP1 pathway induces cell proliferation and invasion in colorectal carcinoma. *Biochemical and Biophysical Research Communications,* 470**,** 75-81.

JIN, C., JIN, Z., CHEN, N. Z., LU, M., LIU, C. B., HU, W. L. & ZHENG, C. G. 2016b. Activation of IRE1α-XBP1 pathway induces cell proliferation and invasion in colorectal carcinoma. *Biochem Biophys Res Commun,* 470**,** 75-81.

JIN, Y., TAN, Y., WU, J. & REN, Z. 2023. Lipid droplets: a cellular organelle vital in cancer cells. *Cell Death Discovery,* 9**,** 254.

JONES, R. M. & NEISH, A. S. 2017. Redox signaling mediated by the gut microbiota. *Free Radical Biology and Medicine,* 105**,** 41-47.

JURKIN, J., HENKEL, T., NIELSEN, A. F., MINNICH, M., POPOW, J., KAUFMANN, T., HEINDL, K., HOFFMANN, T., BUSSLINGER, M. & MARTINEZ, J. 2014. The mammalian tRNA ligase complex mediates splicing of XBP1 mRNA and controls antibody secretion in plasma cells. *Embo j,* 33**,** 2922-36.

KAMMOUN, H. L., CHABANON, H., HAINAULT, I., LUQUET, S., MAGNAN, C., KOIKE, T., FERRÉ, P. & FOUFELLE, F. 2009. GRP78 expression inhibits insulin and ER stress-induced SREBP-1c activation and reduces hepatic steatosis in mice. *J Clin Invest,* 119**,** 1201-15.

KANEKO, M., NIINUMA, Y. & NOMURA, Y. 2003. Activation signal of nuclear factor-kappa B in response to endoplasmic reticulum stress is transduced via IRE1 and tumor necrosis factor receptor-associated factor 2. *Biol Pharm Bull,* 26**,** 931-5.

KARAGÖZ, G. E., ACOSTA-ALVEAR, D., NGUYEN, H. T., LEE, C. P., CHU, F. & WALTER, P. 2017. An unfolded protein-induced conformational switch activates mammalian IRE1. *eLife,* 6**,** e30700.

KARAGÖZ, G. E., ACOSTA-ALVEAR, D. & WALTER, P. 2019. The Unfolded Protein Response: Detecting and Responding to Fluctuations in the Protein-Folding Capacity of the Endoplasmic Reticulum. *Cold Spring Harb Perspect Biol,* 11.

KARASKOV, E., SCOTT, C., ZHANG, L., TEODORO, T., RAVAZZOLA, M. & VOLCHUK, A. 2006. Chronic palmitate but not oleate exposure induces endoplasmic reticulum stress, which may contribute to INS-1 pancreatic beta-cell apoptosis. *Endocrinology,* 147**,** 3398-407.

KATO, I. & SUN, J. 2023. Microbiome and Diet in Colon Cancer Development and Treatment. *Cancer J,* 29**,** 89-97.

KATSOULIERIS, E., MABLEY, J. G., SAMAI, M., GREEN, I. C. & CHATTERJEE, P. K. 2009. α-Linolenic acid protects renal cells against palmitic acid lipotoxicity via inhibition of endoplasmic reticulum stress. *European Journal of Pharmacology,* 623**,** 107-112.

KAUSHIK, S. & KAUR, J. 2003. Chronic cold exposure affects the antioxidant defense system in various rat tissues. *Clin Chim Acta,* 333**,** 69-77.

KENNEDY, A., MARTINEZ, K., CHUANG, C. C., LAPOINT, K. & MCINTOSH, M. 2009. Saturated fatty acid-mediated inflammation and insulin resistance in adipose tissue: mechanisms of action and implications. *J Nutr,* 139**,** 1-4.

KENNELLY, J. P., CARLIN, S., JU, T., VAN DER VEEN, J. N., NELSON, R. C., BUTEAU, J., THIESEN, A., RICHARD, C., WILLING, B. P. & JACOBS, R. L. 2021. Intestinal Phospholipid Disequilibrium Initiates an ER Stress Response That Drives Goblet Cell Necroptosis and Spontaneous Colitis in Mice. *Cellular and Molecular Gastroenterology and Hepatology,* 11**,** 999-1021.

KHAZAEI, S., REZAEIAN, S., KHAZAEI, S., MANSORI, K., SANJARI MOGHADDAM, A. & AYUBI, E. 2016. Effects of Human Development Index and Its Components on Colorectal Cancer Incidence and Mortality: a Global Ecological Study. *Asian Pac J Cancer Prev,* 17**,** 253-6.

KIM, I., XU, W. & REED, J. C. 2008. Cell death and endoplasmic reticulum stress: disease relevance and therapeutic opportunities. *Nat Rev Drug Discov,* 7**,** 1013-30.

KIM, J. K., KANG, K. A., PIAO, M. J., RYU, Y. S., HAN, X., FERNANDO, P. M. D. J., OH, M. C., PARK, J. E., SHILNIKOVA, K., BOO, S. J., NA, S.-Y., JEONG, Y. J., JEONG, S. U. & HYUN, J. W. 2016. Endoplasmic reticulum stress induces 5-fluorouracil resistance in human colon cancer cells. *Environmental Toxicology and Pharmacology,* 44**,** 128-133.

KIM, O.-K., JUN, W., LEE, J. J. A. O. N. & METABOLISM 2015. Mechanism of ER stress and inflammation for hepatic insulin resistance in obesity. 67**,** 218-227.

KIM, S., YANG, X., YIN, A., ZHA, J., BEHARRY, Z., BAI, A., BIELAWSKA, A., BARTLETT, M. G., YIN, H. & CAI, H. 2019. Dietary palmitate cooperates with Src kinase to promote prostate tumor progression. *Prostate,* 79**,** 896-908.

KINGSLEY, G. R., DEMETRIOU, J. A., BEATTIE, J. M., WILCOX, A. A., NOTRICA, S. & DOUMAS, B. T. 1972. Procedure for Serum Protein Determinations with a Triphosphate Biuret Reagent1 1The Editorial Committee invited Dr. Kingsley to submit a chapter on the determination of total protein with the triphosphate biuret reagent, to complement the sodium hydroxide biuret reagent chapter previously written on the biuret determination of total protein by Reinhold (1). This study by the Submitter and Checkers confirmed that both the sodium hydroxide biuret reagent of Reinhold (1) and this one of Kingsley are satisfactory. Thus, the choice of reagent is left to the investigator. *In:* COOPER, G. R. (ed.) *Standard Methods of Clinical Chemistry.* Elsevier.

KINKEL, A. D., FERNYHOUGH, M. E., HELTERLINE, D. L., VIERCK, J. L., OBERG, K. S., VANCE, T. J., HAUSMAN, G. J., HILL, R. A. & DODSON, M. V. 2004. Oil red-O stains non-adipogenic cells: a precautionary note. *Cytotechnology,* 46**,** 49-56.

KLEINFELD, A. M. & OKADA, C. 2005. Free fatty acid release from human breast cancer tissue inhibits cytotoxic T-lymphocyte-mediated killing. *J Lipid Res,* 46**,** 1983-90.

KLIMASZEWSKA-WISNIEWSKA, A., HALAS-WISNIEWSKA, M., TADROWSKI, T., GAGAT, M., GRZANKA, D. & GRZANKA, A. 2016. Paclitaxel and the dietary flavonoid fisetin: a synergistic combination that induces mitotic catastrophe and autophagic cell death in A549 non-small cell lung cancer cells. *Cancer Cell Int,* 16**,** 10.

KOIZUME, S. & MIYAGI, Y. 2016. Lipid Droplets: A Key Cellular Organelle Associated with Cancer Cell Survival under Normoxia and Hypoxia. *International Journal of Molecular Sciences* [Online], 17.

KOUROKU, Y., FUJITA, E., TANIDA, I., UENO, T., ISOAI, A., KUMAGAI, H., OGAWA, S., KAUFMAN, R. J., KOMINAMI, E. & MOMOI, T. 2007. ER stress (PERK/eIF2alpha phosphorylation) mediates the polyglutamine-induced LC3 conversion, an essential step for autophagy formation. *Cell Death Differ,* 14**,** 230-9.

KRISHNAN, V., BASKARAN, P. & THYAGARAJAN, B. 2019. Troglitazone activates TRPV1 and causes deacetylation of PPARγ in 3T3-L1 cells. *Biochimica et Biophysica Acta (BBA) - Molecular Basis of Disease,* 1865**,** 445-453.

KUDA, O., BREZINOVA, M., SILHAVY, J., LANDA, V., ZIDEK, V., DODIA, C., KREUCHWIG, F., VRBACKY, M., BALAS, L., DURAND, T., HÜBNER, N., FISHER, A. B., KOPECKY, J. & PRAVENEC, M. 2018. Nrf2-Mediated Antioxidant Defense and Peroxiredoxin 6 Are Linked to Biosynthesis of Palmitic Acid Ester of 9-Hydroxystearic Acid. *Diabetes,* 67**,** 1190-1199.

KUNISAWA, J., HASHIMOTO, E., INOUE, A., NAGASAWA, R., SUZUKI, Y., ISHIKAWA, I., SHIKATA, S., ARITA, M., AOKI, J. & KIYONO, H. 2014. Regulation of intestinal IgA responses by dietary palmitic acid and its metabolism. *J Immunol,* 193**,** 1666-71.

KWAN, H. Y., CHAO, X., SU, T., FU, X. Q., LIU, B., TSE, A. K., FONG, W. F. & YU, Z. L. 2015. Dietary lipids and adipocytes: potential therapeutic targets in cancers. *J Nutr Biochem,* 26**,** 303-11.

KWAN, H. Y., YANG, Z., FONG, W. F., HU, Y. M., YU, Z. L. & HSIAO, W. L. 2013. The anticancer effect of oridonin is mediated by fatty acid synthase suppression in human colorectal cancer cells. *J Gastroenterol,* 48**,** 182-92.

LAI, E., TEODORO, T. & VOLCHUK, A. 2007. Endoplasmic reticulum stress: signaling the unfolded protein response. *Physiology (Bethesda),* 22**,** 193-201.

LAUGERETTE, F., FURET, J. P., DEBARD, C., DAIRA, P., LOIZON, E., GÉLOËN, A., SOULAGE, C. O., SIMONET, C., LEFILS-LACOURTABLAISE, J., BERNOUD-HUBAC, N., BODENNEC, J., PERETTI, N., VIDAL, H. & MICHALSKI, M. C. 2012. Oil composition of high-fat diet affects metabolic inflammation differently in connection with endotoxin receptors in mice. *Am J Physiol Endocrinol Metab,* 302**,** E374-86.

LAURENT, V., GUÉRARD, A., MAZEROLLES, C., LE GONIDEC, S., TOULET, A., NIETO, L., ZAIDI, F., MAJED, B., GARANDEAU, D., SOCRIER, Y., GOLZIO, M., CADOUDAL, T., CHAOUI, K., DRAY, C., MONSARRAT, B., SCHILTZ, O., WANG, Y. Y., COUDERC, B., VALET, P., MALAVAUD, B. & MULLER, C. 2016. Periprostatic adipocytes act as a driving force for prostate cancer progression in obesity. *Nat Commun,* 7**,** 10230.

LAURESSERGUES, E., BERT, E., DURIEZ, P., HUM, D., MAJD, Z., STAELS, B. & CUSSAC, D. 2012. Does endoplasmic reticulum stress participate in APD-induced hepatic metabolic dysregulation? *Neuropharmacology,* 62**,** 784-96.

LAVOIE, H., LI, J. J., THEVAKUMARAN, N., THERRIEN, M. & SICHERI, F. 2014. Dimerization-induced allostery in protein kinase regulation. *Trends Biochem Sci,* 39**,** 475-86.

LEE, A. H., SCAPA, E. F., COHEN, D. E. & GLIMCHER, L. H. 2008. Regulation of hepatic lipogenesis by the transcription factor XBP1. *Science,* 320**,** 1492-6.

LEE, J. J., LAMBERT, J. E., HOVHANNISYAN, Y., RAMOS-ROMAN, M. A., TROMBOLD, J. R., WAGNER, D. A. & PARKS, E. J. 2015. Palmitoleic acid is elevated in fatty liver disease and reflects hepatic lipogenesis. *Am J Clin Nutr,* 101**,** 34-43.

LI, C., CAPAN, E., ZHAO, Y., ZHAO, J., STOLZ, D., WATKINS, S. C., JIN, S. & LU, B. 2006. Autophagy is induced in CD4+ T cells and important for the growth factor-withdrawal cell death. *J Immunol,* 177**,** 5163-8.

LI, G., DA, M., ZHANG, W., WU, H., YE, J., CHEN, J., MA, L., GU, N., WU, Y. & SONG, X. 2016. Alteration of serum lipid profile and its prognostic value in head and neck squamous cell carcinoma. *J Oral Pathol Med,* 45**,** 167-72.

LI, L., WANG, F., ZHANG, J., WANG, K., DE, X., LI, L. & ZHANG, Y. 2021. Typical phthalic acid esters induce apoptosis by regulating the PI3K/Akt/Bcl-2 signaling pathway in rat insulinoma cells. *Ecotoxicol Environ Saf,* 208**,** 111461.

LI, P., LI, L., ZHANG, C., CHENG, X., ZHANG, Y., GUO, Y., LONG, M., YANG, S. & HE, J. 2019. Palmitic Acid and β-Hydroxybutyrate Induce Inflammatory Responses in Bovine Endometrial Cells by Activating Oxidative Stress-Mediated NF-κB Signaling. *Molecules* [Online], 24.

LI, R., ZHOU, H., LI, M., MAI, Q., FU, Z., JIANG, Y., LI, C., GAO, Y., FAN, Y., WU, K., COSTA, C. D., SHENG, X., HE, Y. & LI, N. 2022. Gremlin-1 Promotes Colorectal Cancer Cell Metastasis by Activating ATF6 and Inhibiting ATF4 Pathways. *Cells* [Online], 11.

LI, X., MAI, K., AI, Q. J. B. E. B. A.-M. & LIPIDS, C. B. O. 2024. Palmitic acid activates NLRP3 inflammasome through NF-κB and AMPK-mitophagy-ROS pathways to induce IL-1β production in large yellow croaker (Larimichthys crocea). 1869**,** 159428.

LI, X. X., ZHANG, H. S., XU, Y. M., ZHANG, R. J., CHEN, Y., FAN, L., QIN, Y. Q., LIU, Y., LI, M. & FANG, J. 2017. Knockdown of IRE1α inhibits colonic tumorigenesis

through decreasing β-catenin and IRE1α targeting suppresses colon cancer cells. *Oncogene,* 36**,** 6738-6746.

LIM, J. C., LIM, S. K., HAN, H. J. & PARK, S. H. 2010. Cannabinoid receptor 1 mediates palmitic acid-induced apoptosis via endoplasmic reticulum stress in human renal proximal tubular cells. *J Cell Physiol,* 225**,** 654-63.

LIN, D., DAVIS, N. & CONIBEAR, E. 2017. Targeting the Ras palmitoylation/depalmitoylation cycle in cancer. *Biochemical Society Transactions,* 45**,** BST20160303.

LIN, Y., JIANG, M., CHEN, W., ZHAO, T., WEI, Y. J. B. & PHARMACOTHERAPY 2019. Cancer and ER stress: Mutual crosstalk between autophagy, oxidative stress and inflammatory response. 118**,** 109249.

LISTENBERGER, L. L., HAN, X., LEWIS, S. E., CASES, S., FARESE, R. V., JR., ORY, D. S. & SCHAFFER, J. E. 2003. Triglyceride accumulation protects against fatty acid-induced lipotoxicity. *Proc Natl Acad Sci U S A,* 100**,** 3077-82.

LISTENBERGER, L. L., ORY, D. S. & SCHAFFER, J. E. 2001. Palmitate-induced apoptosis can occur through a ceramide-independent pathway. *J Biol Chem,* 276**,** 14890-5.

LIU, C. Y., HSU, C. C., HUANG, T. T., LEE, C. H., CHEN, J. L., YANG, S. H., JIANG, J. K., CHEN, W. S., LEE, K. D. & TENG, H. W. 2018. ER stress-related ATF6 upregulates CIP2A and contributes to poor prognosis of colon cancer. *Mol Oncol,* 12**,** 1706-1717.

LIU, M. Q., CHEN, Z. & CHEN, L. X. 2016. Endoplasmic reticulum stress: a novel mechanism and therapeutic target for cardiovascular diseases. *Acta Pharmacol Sin,* 37**,** 425-43.

LIU, S., GAO, Q., LI, Y., LUN, J., YU, M., ZHANG, H. & FANG, J. 2023. XBP1s acts as a transcription factor of IRE1α and promotes proliferation of colon cancer cells. *Archives of Biochemistry and Biophysics,* 737**,** 109552.

LIU, X.-Z., RULINA, A., CHOI, M. H., PEDERSEN, L., LEPLAND, J., TAKLE, S. T., MADELEINE, N., PETERS, S. D. M., WOGSLAND, C. E., GRØNDAL, S. M., LORENS, J. B., GOODARZI, H., LØNNING, P. E., KNAPPSKOG, S., MOLVEN, A. & HALBERG, N. 2022. C/EBPB-dependent adaptation to palmitic acid promotes tumor formation in hormone receptor negative breast cancer. *Nature Communications,* 13**,** 69.

LIU, Z., LV, Y., ZHAO, N., GUAN, G. & WANG, J. 2015. Protein kinase R-like ER kinase and its role in endoplasmic reticulum stress-decided cell fate. *Cell Death Dis,* 6**,** e1822.

LOFTEN, J. R., LINN, J. G., DRACKLEY, J. K., JENKINS, T. C., SODERHOLM, C. G. & KERTZ, A. F. 2014. Invited review: Palmitic and stearic acid metabolism in lactating dairy cows. *Journal of Dairy Science,* 97**,** 4661-4674.

LOWRY, O. H., ROSEBROUGH, N. J., FARR, A. L. & RANDALL, R. J. 1951. Protein measurement with the Folin phenol reagent. *J Biol Chem,* 193**,** 265-75.

LU, C.-W., NGUYEN, N. T., SHEN, S.-C., WU, Y.-B., LIANG, H.-J. & WU, C.-H. 2022. Botanical Antcin K Alleviates High-Fat Damage in Palm Acid Oil-Treated Vascular Endothelial Cells and Macrophages. *Plants* [Online], 11.

LU, J., MENG, Z., CHENG, B., LIU, M., TAO, S. & GUAN, S. 2019a. Apigenin reduces the excessive accumulation of lipids induced by palmitic acid via the AMPK signaling pathway in HepG2 cells. *Exp Ther Med,* 18**,** 2965-2971.

LU, L., ARRANZ-TRULLÉN, J., PRATS-EJARQUE, G., PULIDO, D., BHAKTA, S. & BOIX, E. 2019b. Human Antimicrobial RNases Inhibit Intracellular Bacterial Growth

and Induce Autophagy in Mycobacteria-Infected Macrophages. *Front Immunol,* 10**,** 1500.

LU, Y., CHENG, J., CHEN, L., LI, C., CHEN, G., GUI, L., SHEN, B. & ZHANG, Q. 2015. Endoplasmic reticulum stress involved in high-fat diet and palmitic acid-induced vascular damages and fenofibrate intervention. *Biochemical and Biophysical Research Communications,* 458**,** 1-7.

LUKIC, M., LICAJ, I., LAAKSONEN, M. A., WEIDERPASS, E., BORCH, K. B. & RYLANDER, C. 2023. The burden of colon cancer attributable to modifiable factors-The Norwegian Women and Cancer Study. *Int J Cancer,* 152**,** 195-202.

LUNA-MARCO, C., UBINK, A., KOPSIDA, M. & HEINDRYCKX, F. 2023. Endoplasmic Reticulum Stress and Metabolism in Hepatocellular Carcinoma. *The American Journal of Pathology,* 193**,** 1377-1388.

LUNG, J., HUNG, M. S., WANG, T. Y., CHEN, K. L., LUO, C. W., JIANG, Y. Y., WU, S. Y., LEE, L. W., LIN, P. Y., CHEN, F. F., LIAO, H. F. & LIN, Y. C. 2022. Lipid Droplets in Lung Cancers Are Crucial for the Cell Growth and Starvation Survival. *Int J Mol Sci,* 23.

LUO, B. & LEE, A. S. 2013a. The critical roles of endoplasmic reticulum chaperones and unfolded protein response in tumorigenesis and anticancer therapies. *Oncogene,* 32**,** 805-18.

LUO, B. & LEE, A. S. 2013b. The critical roles of endoplasmic reticulum chaperones and unfolded protein response in tumorigenesis and anticancer therapies. *Oncogene,* 32**,** 805-818.

LUO, R., LI, L., LIU, X., YUAN, Y., ZHU, W., LI, L., LIU, J., LU, Y., CHENG, J. & CHEN, Y. 2020. Mesenchymal stem cells alleviate palmitic acid-induced endothelial-to-mesenchymal transition by suppressing endoplasmic reticulum stress. *Am J Physiol Endocrinol Metab,* 319**,** E961-e980.

LUO, R., ZHAO, L., LI, S., CHEN, P., WANG, L., YU, H., CAI, K., YU, Q. & TIAN, W. 2021. Curcumin Alleviates Palmitic Acid-Induced LOX-1 Upregulation by Suppressing Endoplasmic Reticulum Stress in HUVECs. *BioMed Research International,* 2021**,** 9983725.

MA, Q. 2013. Role of nrf2 in oxidative stress and toxicity. *Annu Rev Pharmacol Toxicol,* 53**,** 401-26.

MA, X. H., PIAO, S. F., DEY, S., MCAFEE, Q., KARAKOUSIS, G., VILLANUEVA, J., HART, L. S., LEVI, S., HU, J., ZHANG, G., LAZOVA, R., KLUMP, V., PAWELEK, J. M., XU, X., XU, W., SCHUCHTER, L. M., DAVIES, M. A., HERLYN, M., WINKLER, J., KOUMENIS, C. & AMARAVADI, R. K. 2014. Targeting ER stress-induced autophagy overcomes BRAF inhibitor resistance in melanoma. *J Clin Invest,* 124**,** 1406-17.

MAHALINGAIAH, P. K. & SINGH, K. P. 2014. Chronic oxidative stress increases growth and tumorigenic potential of MCF-7 breast cancer cells. *PLoS One,* 9**,** e87371.

MALHI, H., KROPP, E. M., CLAVO, V. F., KOBROSSI, C. R., HAN, J., MAUER, A. S., YONG, J. & KAUFMAN, R. J. 2013. C/EBP homologous protein-induced macrophage apoptosis protects mice from steatohepatitis. *J Biol Chem,* 288**,** 18624-42.

MALHOTRA, J. D. & KAUFMAN, R. J. 2007. The endoplasmic reticulum and the unfolded protein response. *Seminars in Cell & Developmental Biology,* 18**,** 716-731.

MALY, I. V. & HOFMANN, W. A. 2020. Effect of Palmitic Acid on Exosome-Mediated Secretion and Invasive Motility in Prostate Cancer Cells. *Molecules* [Online], 25.

MANCINI, A., IMPERLINI, E., NIGRO, E., MONTAGNESE, C., DANIELE, A., ORRÙ, S. & BUONO, P. 2015a. Biological and Nutritional Properties of Palm Oil and Palmitic Acid: Effects on Health. *Molecules* [Online], 20.

MANCINI, A., IMPERLINI, E., NIGRO, E., MONTAGNESE, C., DANIELE, A., ORRÙ, S. & BUONO, P. 2015b. Biological and Nutritional Properties of Palm Oil and Palmitic Acid: Effects on Health. *Molecules,* 20**,** 17339-61.

MANOHARAN, S., KOLANJIAPPAN, K., SURESH, K. & PANJAMURTHY, K. 2005. Lipid peroxidation & antioxidants status in patients with oral squamous cell carcinoma. *Indian J Med Res,* 122**,** 529-34.

MANSURI, M. L., SHARMA, G., PARIHAR, P., DUBE, K. T., SHARMA, T., PARIHAR, A. & PARIHAR, M. S. 2021. Increased oxidative stress and mitochondrial impairments associated with increased expression of TNF-α and caspase-3 in palmitic acid-induced lipotoxicity in myoblasts. *J Biochem Mol Toxicol,* 35**,** e22744.

MARCINIAK, S. J., CHAMBERS, J. E. & RON, D. 2022. Pharmacological targeting of endoplasmic reticulum stress in disease. *Nature Reviews Drug Discovery,* 21**,** 115-140.

MARGARITI, A., LI, H., CHEN, T., MARTIN, D., VIZCAY-BARRENA, G., ALAM, S., KARAMARITI, E., XIAO, Q., ZAMPETAKI, A., ZHANG, Z., WANG, W., JIANG, Z., GAO, C., MA, B., CHEN, Y. G., COCKERILL, G., HU, Y., XU, Q. & ZENG, L. 2013. XBP1 mRNA splicing triggers an autophagic response in endothelial cells through BECLIN-1 transcriptional activation. *J Biol Chem,* 288**,** 859-72.

MARSHALL, N. J., GOODWIN, C. J. & HOLT, S. J. 1995. A critical assessment of the use of microculture tetrazolium assays to measure cell growth and function. *Growth Regul,* 5**,** 69-84.

MARTIN-PEREZ, M., URDIROZ-URRICELQUI, U., BIGAS, C. & BENITAH, S. A. 2022. The role of lipids in cancer progression and metastasis. *Cell Metab,* 34**,** 1675-1699.

MARTINA, J. A., DIAB, H. I., BRADY, O. A. & PUERTOLLANO, R. 2016. TFEB and TFE3 are novel components of the integrated stress response. *Embo j,* 35**,** 479-95.

MARTÍNEZ-ORTIZ, J. A., FUNG, T. T., BAYLIN, A., HU, F. B. & CAMPOS, H. 2006. Dietary patterns and risk of nonfatal acute myocardial infarction in Costa Rican adults. *Eur J Clin Nutr,* 60**,** 770-7.

MAUREL, M., CHEVET, E., TAVERNIER, J. & GERLO, S. 2014. Getting RIDD of RNA: IRE1 in cell fate regulation. *Trends Biochem Sci,* 39**,** 245-54.

MAVIS, R. D. & STELLWAGEN, E. 1968. Purification and subunit structure of glutathione reductase from bakers' yeast. *J Biol Chem,* 243**,** 809-14.

MAYES, C., BURDGE, G. C., BINGHAM, A., MURPHY, J. L., TUBMAN, R. & WOOTTON, S. A. 2006. Variation in [U-13C] α Linolenic Acid Absorption, β-oxidation and Conversion to Docosahexaenoic Acid in the Pre-Term Infant Fed a DHA-Enriched Formula. *Pediatric Research,* 59**,** 271-275.

MCARTHUR, M. J., ATSHAVES, B. P., FROLOV, A., FOXWORTH, W. D., KIER, A. B. & SCHROEDER, F. 1999. Cellular uptake and intracellular trafficking of long chain fatty acids. *J Lipid Res,* 40**,** 1371-83.

MCCORD, J. M. & FRIDOVICH, I. 1969. Superoxide dismutase. An enzymic function for erythrocuprein (hemocuprein). *J Biol Chem,* 244**,** 6049-55.

MENENDEZ, J. A. & LUPU, R. 2007. Fatty acid synthase and the lipogenic phenotype in cancer pathogenesis. *Nature Reviews Cancer,* 7**,** 763-777.

MENTA, P. L. R., ANDRADE, M. E. R., DE CASTRO, L. F., TRINDADE, L. M., DIAS, M. T. S., MIYAMOTO, J. É., DOS SANTOS, R. M., CASSALI, G. D., LEAL, R. F. &

RIBEIRO, A. P. B. J. F. R. I. 2022. Interesterified palm oil increases intestinal permeability, promotes bacterial translocation, alters inflammatory parameters and tight-junction protein genic expression in Swiss mice. 151**,** 110897.

MEUNIER, C., CAI, J., FORTIN, A., KWAN, T., MARQUIS, J. F., TURBIDE, C., VAN DER KRAAK, L., JOTHY, S., BEAUCHEMIN, N. & GROS, P. 2010. Characterization of a major colon cancer susceptibility locus (Ccs3) on mouse chromosome 3. *Oncogene,* 29**,** 647-61.

MEYER, M., CASELMANN, W. H., SCHLÜTER, V., SCHRECK, R., HOFSCHNEIDER, P. H. & BAEUERLE, P. A. 1992. Hepatitis B virus transactivator MHBst: activation of NF-kappa B, selective inhibition by antioxidants and integral membrane localization. *Embo j,* 11**,** 2991-3001.

MHAIDAT, N. M., ALZOUBI, K. H. & ABUSHBAK, A. 2015. X-box binding protein 1 (XBP-1) enhances colorectal cancer cell invasion. *J Chemother,* 27**,** 167-73.

MHAIDAT, N. M., ALZOUBI, K. H., KHABOUR, O. F., BANIHANI, M. N., AL-BALAS, Q. A. & SWAIDAN, S. 2016. GRP78 regulates sensitivity of human colorectal cancer cells to DNA targeting agents. *Cytotechnology,* 68**,** 459-67.

MILLER, K. D., NOGUEIRA, L., DEVASIA, T., MARIOTTO, A. B., YABROFF, K. R., JEMAL, A., KRAMER, J. & SIEGEL, R. L. 2022. Cancer treatment and survivorship statistics, 2022. *CA Cancer J Clin,* 72**,** 409-436.

MINJARES, M., THEPSUWAN, P., ZHANG, K., WANG, J.-M. J. P. & THERAPEUTICS 2025. Unfolded protein responses: Dynamic machinery in wound healing. 108798.

MIZUSHIMA, N., LEVINE, B., CUERVO, A. M. & KLIONSKY, D. J. 2008. Autophagy fights disease through cellular self-digestion. *Nature,* 451**,** 1069-1075.

MOHAMMED, A. M., CHEN, F. & KOWLURU, A. 2013. The two faces of protein palmitoylation in islet β-cell function: potential implications in the pathophysiology of islet metabolic dysregulation and diabetes. *Recent Pat Endocr Metab Immune Drug Discov,* 7**,** 203-12.

MOHAN, S., R, P. R. M., BROWN, L., AYYAPPAN, P. & G, R. K. 2019. Endoplasmic reticulum stress: A master regulator of metabolic syndrome. *European Journal of Pharmacology,* 860**,** 172553.

MOLONIA, M. S., SALAMONE, F. L., SPECIALE, A., SAIJA, A. & CIMINO, F. J. I. J. O. M. S. 2024. D-Allulose Reduces Hypertrophy and Endoplasmic Reticulum Stress Induced by Palmitic Acid in Murine 3T3-L1 Adipocytes. 25**,** 4059.

MONTESDEOCA, N., LÓPEZ, M., ARIZA, X., HERRERO, L. & MAKOWSKI, K. 2020. Inhibitors of lipogenic enzymes as a potential therapy against cancer. *Faseb j,* 34**,** 11355-11381.

MOREIRA, L. S., PIVA, B., GENTILE, L. B., MESQUITA-SANTOS, F. P., D'AVILA, H., MAYA-MONTEIRO, C. M., BOZZA, P. T., BANDEIRA-MELO, C. & DIAZ, B. L. 2009. Cytosolic phospholipase A2-driven PGE2 synthesis within unsaturated fatty acids-induced lipid bodies of epithelial cells. *Biochimica et Biophysica Acta (BBA) - Molecular and Cell Biology of Lipids,* 1791**,** 156-165.

MORON, M. S., DEPIERRE, J. W. & MANNERVIK, B. 1979. Levels of glutathione, glutathione reductase and glutathione S-transferase activities in rat lung and liver. *Biochim Biophys Acta,* 582**,** 67-78.

MUNIR, R., LISEC, J., SWINNEN, J. V. & ZAIDI, N. 2019. Lipid metabolism in cancer cells under metabolic stress. *British Journal of Cancer,* 120**,** 1090-1098.

MURO, P., ZHANG, L., LI, S., ZHAO, Z., JIN, T., MAO, F. & MAO, Z. J. F. I. E. 2024. The emerging role of oxidative stress in inflammatory bowel disease. 15**,** 1390351.

MURRU, E., MANCA, C., CARTA, G. & BANNI, S. 2022. Impact of Dietary Palmitic Acid on Lipid Metabolism. *Front Nutr,* 9**,** 861664.

NARAYANAN, S., ELESELA, S., RASKY, A. J., MORRIS, S. H., KUMAR, S., LOMBARD, D. & LUKACS, N. W. J. J. O. L. B. 2022. ER stress protein PERK promotes inappropriate innate immune responses and pathogenesis during RSV infection. 111**,** 379-389.

NARITA, S., NARA, T., SATO, H., KOIZUMI, A., HUANG, M., INOUE, T. & HABUCHI, T. 2019. Research Evidence on High-Fat Diet-Induced Prostate Cancer Development and Progression. *Journal of Clinical Medicine* [Online], 8.

NATH, A., OAK, A., CHEN, K. Y., LI, I., SPLICHAL, R. C., PORTIS, J., FOSTER, S., WALTON, S. P. & CHAN, C. 2021. Palmitate-Induced IRE1-XBP1-ZEB Signaling Represses Desmoplakin Expression and Promotes Cancer Cell Migration. *Mol Cancer Res,* 19**,** 240-248.

NG, N. S. & OOI, L. 2021. A Simple Microplate Assay for Reactive Oxygen Species Generation and Rapid Cellular Protein Normalization. *Bio Protoc,* 11**,** e3877.

NG, Y. W. & SAY, Y. H. 2018. Palmitic acid induces neurotoxicity and gliatoxicity in SH-SY5Y human neuroblastoma and T98G human glioblastoma cells. *PeerJ,* 6**,** e4696.

NIEMANN, A., TAKATSUKI, A. & ELSÄSSER, H. P. 2000. The lysosomotropic agent monodansylcadaverine also acts as a solvent polarity probe. *J Histochem Cytochem,* 48**,** 251-8.

NIJHOLT, D. A., DE GRAAF, T. R., VAN HAASTERT, E. S., OLIVEIRA, A. O., BERKERS, C. R., ZWART, R., OVAA, H., BAAS, F., HOOZEMANS, J. J. & SCHEPER, W. 2011. Endoplasmic reticulum stress activates autophagy but not the proteasome in neuronal cells: implications for Alzheimer's disease. *Cell Death Differ,* 18**,** 1071-81.

NISHII, T., KONO, S., ABE, H., EGUCHI, H., SHIMAZAKI, K., HATANO, B. & HAMADA, H. 2001. Glucose intolerance, plasma insulin levels, and colon adenomas in Japanese men. *Jpn J Cancer Res,* 92**,** 836-40.

NISSAR, A. U., SHARMA, L. & TASDUQ, S. A. 2015. Palmitic acid induced lipotoxicity is associated with altered lipid metabolism, enhanced CYP450 2E1 and intracellular calcium mediated ER stress in human hepatoma cells. *Toxicology Research,* 4**,** 1344-1358.

NOTARO, A., LAURICELLA, M., DI LIBERTO, D., EMANUELE, S., GIULIANO, M., ATTANZIO, A., TESORIERE, L., CARLISI, D., ALLEGRA, M., DE BLASIO, A., CALVARUSO, G. & D'ANNEO, A. 2023. A Deadly Liaison between Oxidative Injury and p53 Drives Methyl-Gallate-Induced Autophagy and Apoptosis in HCT116 Colon Cancer Cells. *Antioxidants* [Online], 12.

NOVOA, I., ZENG, H., HARDING, H. P. & RON, D. 2001. Feedback inhibition of the unfolded protein response by GADD34-mediated dephosphorylation of eIF2alpha. *J Cell Biol,* 153**,** 1011-22.

O'FALLON, J. V., BUSBOOM, J. R., NELSON, M. L. & GASKINS, C. T. 2007. A direct method for fatty acid methyl ester synthesis: application to wet meat tissues, oils, and feedstuffs. *J Anim Sci,* 85**,** 1511-21.

OAKES, S. A. 2020. Endoplasmic Reticulum Stress Signaling in Cancer Cells. *The American Journal of Pathology,* 190**,** 934-946.

OGATA, M., HINO, S., SAITO, A., MORIKAWA, K., KONDO, S., KANEMOTO, S., MURAKAMI, T., TANIGUCHI, M., TANII, I., YOSHINAGA, K., SHIOSAKA, S., HAMMARBACK, J. A., URANO, F. & IMAIZUMI, K. 2006. Autophagy is activated for cell survival after endoplasmic reticulum stress. *Mol Cell Biol,* 26**,** 9220-31.

OH, J. M., CHOI, J. M., LEE, J. Y., OH, S. J., KIM, H. C., KIM, B. H., MA, J. Y. & KIM, S. K. 2012. Effects of palmitic acid on TNF-α-induced cytotoxicity in SK-Hep-1 cells. *Toxicology in Vitro,* 26**,** 783-790.

OHKAWA, H., OHISHI, N. & YAGI, K. 1979. Assay for lipid peroxides in animal tissues by thiobarbituric acid reaction. *Anal Biochem,* 95**,** 351-8.

OHTSU, A., TANAKA, H., SENO, K., IWATA, H., KUWAYAMA, T. & SHIRASUNA, K. 2017. Palmitic acid stimulates interleukin-8 via the TLR4/NF-κB/ROS pathway and induces mitochondrial dysfunction in bovine oviduct epithelial cells. *Am J Reprod Immunol,* 77.

OJO, O., ASAOLU, M., AKINLUA, O. A. & ATIBA, A. 2016. Serum marker enzymes activities in cancer patients. *Journal of Chemistry and Biochemistry,* 4**,** 15-21.

ONG, G. & LOGUE, S. E. 2023. Unfolding the Interactions between Endoplasmic Reticulum Stress and Oxidative Stress. *Antioxidants* [Online], 12.

OUYANG, F., LI, B., WANG, Y., XU, L., LI, D., LI, F. & SUN-WATERHOUSE, D. 2022. Attenuation of Palmitic Acid-Induced Intestinal Epithelial Barrier Dysfunction by 6-Shogaol in Caco-2 Cells: The Role of MiR-216a-5p/TLR4/NF-κB Axis. *Metabolites* [Online], 12.

OZCAN, U., CAO, Q., YILMAZ, E., LEE, A. H., IWAKOSHI, N. N., OZDELEN, E., TUNCMAN, G., GÖRGÜN, C., GLIMCHER, L. H. & HOTAMISLIGIL, G. S. 2004. Endoplasmic reticulum stress links obesity, insulin action, and type 2 diabetes. *Science,* 306**,** 457-61.

PALOMER, X., PIZARRO-DELGADO, J., BARROSO, E. & VÁZQUEZ-CARRERA, M. 2018. Palmitic and Oleic Acid: The Yin and Yang of Fatty Acids in Type 2 Diabetes Mellitus. *Trends Endocrinol Metab,* 29**,** 178-190.

PALOMINO, O. M., GIORDANI, V., CHOWEN, J., FERNÁNDEZ-ALFONSO, M. S. & GOYA, L. 2022. Physiological Doses of Oleic and Palmitic Acids Protect Human Endothelial Cells from Oxidative Stress. *Molecules* [Online], 27.

PARDO, V., GONZÁLEZ-RODRÍGUEZ, Á., MUNTANÉ, J., KOZMA, S. C. & VALVERDE, Á. M. 2015. Role of hepatocyte S6K1 in palmitic acid-induced endoplasmic reticulum stress, lipotoxicity, insulin resistance and in oleic acid-induced protection. *Food and Chemical Toxicology,* 80**,** 298-309.

PARK, E.-J., LEE, A. Y., PARK, S., KIM, J.-H. & CHO, M.-H. 2014. Multiple pathways are involved in palmitic acid-induced toxicity. *Food and Chemical Toxicology,* 67**,** 26-34.

PASCUAL, G., AVGUSTINOVA, A., MEJETTA, S., MARTÍN, M., CASTELLANOS, A., ATTOLINI, C. S.-O., BERENGUER, A., PRATS, N., TOLL, A., HUETO, J. A., BESCÓS, C., DI CROCE, L. & BENITAH, S. A. 2017. Targeting metastasis-initiating cells through the fatty acid receptor CD36. *Nature,* 541**,** 41-45.

PASCUAL, G., DOMÍNGUEZ, D., ELOSÚA-BAYES, M., BECKEDORFF, F., LAUDANNA, C., BIGAS, C., DOUILLET, D., GRECO, C., SYMEONIDI, A., HERNÁNDEZ, I., GIL, S. R., PRATS, N., BESCÓS, C., SHIEKHATTAR, R., AMIT, M., HEYN, H., SHILATIFARD, A. & BENITAH, S. A. 2021a. Dietary palmitic acid promotes a prometastatic memory via Schwann cells. *Nature,* 599**,** 485-490.

PASCUAL, G., DOMÍNGUEZ, D., ELOSÚA-BAYES, M., BECKEDORFF, F., LAUDANNA, C., BIGAS, C., DOUILLET, D., GRECO, C., SYMEONIDI, A. &

HERNÁNDEZ, I. J. N. 2021b. Dietary palmitic acid promotes a prometastatic memory via Schwann cells. 599**,** 485-490.

PATEL, A., OSHI, M., YAN, L., MATSUYAMA, R., ENDO, I. & TAKABE, K. 2021. The Unfolded Protein Response Is Associated with Cancer Proliferation and Worse Survival in Hepatocellular Carcinoma. *Cancers* [Online], 13.

PEIRETTI, P. G. 2014. Effect of Diet Supplementation and Occurrence in Animal Origin Food.

PETAN, T. 2023a. Lipid Droplets in Cancer. *In:* PEDERSEN, S. H. F. & BARBER, D. L. (eds.) *Organelles in Disease.* Cham: Springer International Publishing.

PETAN, T. 2023b. Lipid Droplets in Cancer. *Rev Physiol Biochem Pharmacol,* 185**,** 53-86.

PETER, A., WEIGERT, C., STAIGER, H., MACHICAO, F., SCHICK, F., MACHANN, J., STEFAN, N., THAMER, C., HÄRING, H. U. & SCHLEICHER, E. 2009. Individual stearoyl-coa desaturase 1 expression modulates endoplasmic reticulum stress and inflammation in human myotubes and is associated with skeletal muscle lipid storage and insulin sensitivity in vivo. *Diabetes,* 58**,** 1757-65.

PHAM, T. N. M., PERUMAL, N., MANICAM, C., BASOGLU, M., EIMER, S., FUHRMANN, D. C., PIETRZIK, C. U., CLEMENT, A. M., KÖRSCHGEN, H. & SCHEPERS, J. J. R. B. 2023. Adaptive responses of neuronal cells to chronic endoplasmic reticulum (ER) stress. 67**,** 102943.

PICK, R., JALIL, J. E., JANICKI, J. S. & WEBER, K. T. 1989. The fibrillar nature and structure of isoproterenol-induced myocardial fibrosis in the rat. *Am J Pathol,* 134**,** 365-71.

PITON, N., WASON, J., COLASSE, É., CORNIC, M., LEMOINE, F., LE PESSOT, F., MARGUET, F. & SABOURIN, J.-C. 2016a. Endoplasmic reticulum stress, unfolded protein response and development of colon adenocarcinoma. *Virchows Archiv,* 469**,** 145-154.

PITON, N., WASON, J., COLASSE, É., CORNIC, M., LEMOINE, F., LE PESSOT, F., MARGUET, F. & SABOURIN, J.-C. J. V. A. 2016b. Endoplasmic reticulum stress, unfolded protein response and development of colon adenocarcinoma. 469**,** 145-154.

POBRE, K. F. R., POET, G. J. & HENDERSHOT, L. M. 2019. The endoplasmic reticulum (ER) chaperone BiP is a master regulator of ER functions: Getting by with a little help from ERdj friends. *J Biol Chem,* 294**,** 2098-2108.

QIU, T., YANG, X., WANG, J., PAN, C., CHU, X., XIONG, J., XIE, J., CHANG, Y., WANG, C. & ZHANG, J. 2022. Obesity-induced elevated palmitic acid promotes inflammation and glucose metabolism disorders through GPRs/NF-κB/KLF7 pathway. *Nutrition & Diabetes,* 12**,** 23.

QU, Z., CHU, J., WU, Y., ZHUANG, J., LIU, J., HAN, S., WU, W. & HAN, S. 2023. Classification of colorectal cancer subtypes based on endoplasmic reticulum stress. *Digestion*.

RACKER, E. 1955. Glutathione reductase from bakers' yeast and beef liver. *J Biol Chem,* 217**,** 855-65.

RAEISI, M., ZEHTABI, M., VELAEI, K., FAYYAZPOUR, P., AGHAEI, N. & MEHDIZADEH, A. 2022. Anoikis in cancer: The role of lipid signaling. *Cell Biol Int,* 46**,** 1717-1728.

RAFIEI, H., OMIDIAN, K. & BANDY, B. 2018. Protection by different classes of dietary polyphenols against palmitic acid-induced steatosis, nitro-oxidative stress and endoplasmic reticulum stress in HepG2 hepatocytes. *Journal of Functional Foods,* 44**,** 173-182.

RAHA, S. & ROBINSON, B. H. 2000. Mitochondria, oxygen free radicals, disease and ageing. *Trends Biochem Sci,* 25**,** 502-8.

RAHMAN, H., SITOMPUL, J. & TJOKRODININGRAT, S. 2022. The composition of fatty acids in several vegetable oils from Indonesia. *Biodiversitas Journal of Biological Diversity,* 23.

RAJ, S., SINGH, R. K., KUMAR, S., DEVI, S., KISHOR, K., SINHA, D. K., MADHAWI, R., KUMAR, P., CHOUBEY, S. & PRAKASH, A. 2022. Clinical and demographic profile of lower gastrointestinal malignancies: A retrospective observational study from Eastern India. *Cancer Research, Statistics, and Treatment,* 5.

RAMAKRISHNAN, S., MOOLI, R. G. R., HAN, Y., FIORENZA, E., KUMAR, S., BELLO, F., NALLANAGULAGARI, A., KARRA, S., TENG, L. & JURCZAK, M. 2023. Hepatic ketogenesis regulates lipid homeostasis via ACSL1-mediated fatty acid partitioning. *Res Sq*.

RAŠKOVÁ, M., LACINA, L., KEJÍK, Z., VENHAUEROVÁ, A., SKALIČKOVÁ, M., KOLÁŘ, M., JAKUBEK, M., ROSEL, D., SMETANA JR, K. & BRÁBEK, J. J. C. 2022. The role of IL-6 in cancer cell invasiveness and metastasis—overview and therapeutic opportunities. 11**,** 3698.

RAY, K., UJVARI, B., RAMANA, V., DONALD, J. J. C. & REVIEWS, G. F. 2018. Cross-talk between EGFR and IL-6 drives oncogenic signaling and offers therapeutic opportunities in cancer. 41**,** 18-27.

REITMAN, S. & FRANKEL, S. 1957. A colorimetric method for the determination of serum glutamic oxalacetic and glutamic pyruvic transaminases. *Am J Clin Pathol,* 28**,** 56-63.

REKHA, B., VELMURUGAN, G., FREDDY, A. J., ANUSHA, S., RAMPRASATH, T., KARTHIK, K. V., SURESH, S., KULSHRESTHA, P., MITHIEUX, G., LYON, A. R., SELVAM, G. S. & RAMASAMY, S. 2018. Chronic intake of 4-Methylimidazole induces Hyperinsulinemia and Hypoglycaemia via Pancreatic Beta Cell Hyperplasia and Glucose Dyshomeostasis. *Scientific Reports,* 8**,** 17037.

REN, J., BI, Y., SOWERS, J. R., HETZ, C. & ZHANG, Y. 2021. Endoplasmic reticulum stress and unfolded protein response in cardiovascular diseases. *Nature Reviews Cardiology,* 18**,** 499-521.

REYNOSO, R., SALGADO, L. M. & CALDERÓN, V. 2003. High levels of palmitic acid lead to insulin resistance due to changes in the level of phosphorylation of the insulin receptor and insulin receptor substrate-1. *Mol Cell Biochem,* 246**,** 155-62.

RIZZO, A. M., COLOMBO, I., MONTORFANO, G., ZAVA, S. & CORSETTO, P. A. 2021. Exogenous Fatty Acids Modulate ER Lipid Composition and Metabolism in Breast Cancer Cells. *Cells* [Online], 10.

ROVIRA-LLOPIS, S., BAÑULS, C., APOSTOLOVA, N., MORILLAS, C., HERNANDEZ-MIJARES, A., ROCHA, M. & VICTOR, V. M. 2014. Is glycemic control modulating endoplasmic reticulum stress in leukocytes of type 2 diabetic patients? *Antioxid Redox Signal,* 21**,** 1759-65.

RUBIOLO, J. A., LÓPEZ-ALONSO, H., MARTÍNEZ, P., MILLÁN, A., CAGIDE, E., VIEYTES, M. R., VEGA, F. V. & BOTANA, L. M. 2014. Yessotoxin induces ER-stress followed by autophagic cell death in glioma cells mediated by mTOR and BNIP3. *Cell Signal,* 26**,** 419-32.

RUTKOWSKI, D. T., WU, J., BACK, S. H., CALLAGHAN, M. U., FERRIS, S. P., IQBAL, J., CLARK, R., MIAO, H., HASSLER, J. R., FORNEK, J., KATZE, M. G., HUSSAIN, M. M., SONG, B., SWATHIRAJAN, J., WANG, J., YAU, G. D. & KAUFMAN, R. J.

2008. UPR pathways combine to prevent hepatic steatosis caused by ER stress-mediated suppression of transcriptional master regulators. *Dev Cell,* 15**,** 829-40.

RYSMAN, E., BRUSSELMANS, K., SCHEYS, K., TIMMERMANS, L., DERUA, R., MUNCK, S., VAN VELDHOVEN, P. P., WALTREGNY, D., DANIËLS, V. W., MACHIELS, J., VANDERHOYDONC, F., SMANS, K., WAELKENS, E., VERHOEVEN, G. & SWINNEN, J. V. 2010. De novo lipogenesis protects cancer cells from free radicals and chemotherapeutics by promoting membrane lipid saturation. *Cancer Res,* 70**,** 8117-26.

SAFI, R., MENÉNDEZ, P. & POL, A. 2024. Lipid droplets provide metabolic flexibility for cancer progression. *FEBS Lett*.

SAHOO, P. K., KRISHNAMOORTHY, C., WOOD, J. R., HANSON, C., ANDERSON-BERRY, A., MOTT, J. L., NATARAJAN, S. K. J. C. D. & DISEASE 2024. Palmitate induces integrated stress response and lipoapoptosis in trophoblasts. 15**,** 31.

SALES, R. C., MEDEIROS, P. C., SPREAFICO, F., DE VELASCO, P. C., GONÇALVES, F. K. A., MARTÍN-HERNÁNDEZ, R., MANTILLA-ESCALANTE, D. C., GIL-ZAMORANO, J., PERES, W. A. F., DE SOUZA, S. A. L., DÁVALOS, A. & TAVARES DO CARMO, M. G. 2019. Olive Oil, Palm Oil, and Hybrid Palm Oil Distinctly Modulate Liver Transcriptome and Induce NAFLD in Mice Fed a High-Fat Diet. *International Journal of Molecular Sciences* [Online], 20.

SAMADDER, N. J., VALENTINE, J. F., GUTHERY, S., SINGH, H., BERNSTEIN, C. N., LEIGHTON, J. A., WAN, Y., WONG, J., BOUCHER, K., PAPPAS, L., ROWE, K., BURT, R. W., CURTIN, K. & SMITH, K. R. 2019. Family History Associates With Increased Risk of Colorectal Cancer in Patients With Inflammatory Bowel Diseases. *Clinical Gastroenterology and Hepatology,* 17**,** 1807-1813.e1.

SANTOS, C. X., TANAKA, L. Y., WOSNIAK, J. & LAURINDO, F. R. 2009. Mechanisms and implications of reactive oxygen species generation during the unfolded protein response: roles of endoplasmic reticulum oxidoreductases, mitochondrial electron transport, and NADPH oxidase. *Antioxid Redox Signal,* 11**,** 2409-27.

SARIS, N., HOLKERI, H., CRAVEN, R. A., STIRLING, C. J. & MAKAROW, M. 1997. The Hsp70 homologue Lhs1p is involved in a novel function of the yeast endoplasmic reticulum, refolding and stabilization of heat-denatured protein aggregates. *J Cell Biol,* 137**,** 813-24.

SATO, Y., FUJIMOTO, S., MUKAI, E., SATO, H., TAHARA, Y., OGURA, K., YAMANO, G., OGURA, M., NAGASHIMA, K. & INAGAKI, N. 2014. Palmitate induces reactive oxygen species production and β-cell dysfunction by activating nicotinamide adenine dinucleotide phosphate oxidase through Src signaling. *J Diabetes Investig,* 5**,** 19-26.

SCARIAN, E., VIOLA, C., DRAGONI, F., DI GERLANDO, R., RIZZO, B., DIAMANTI, L., GAGLIARDI, S., BORDONI, M. & PANSARASA, O. J. I. J. O. M. S. 2024. New insights into oxidative stress and inflammatory response in neurodegenerative diseases. 25**,** 2698.

SCHRÖDER, M. 2008a. Endoplasmic reticulum stress responses. *Cell Mol Life Sci,* 65**,** 862-94.

SCHRÖDER, M. 2008b. Endoplasmic reticulum stress responses. *Cellular and Molecular Life Sciences,* 65**,** 862-894.

SERGI, D., ZAULI, E., CASCIANO, F., SECCHIERO, P., ZAULI, G., FIELDS, M. & MELLONI, E. 2022. Palmitic Acid Induced a Long-Lasting Lipotoxic Insult in Human Retinal Pigment Epithelial Cells, which Is Partially Counteracted by TRAIL. *Antioxidants* [Online], 11.

SHARMA, A., TRIPATHI, M., SATYAM, A. & KUMAR, L. 2009. Study of antioxidant levels in patients with multiple myeloma. *Leuk Lymphoma,* 50**,** 809-15.

SHAW, E., FARRIS, M. S., STONE, C. R., DERKSEN, J. W. G., JOHNSON, R., HILSDEN, R. J., FRIEDENREICH, C. M. & BRENNER, D. R. 2018. Effects of physical activity on colorectal cancer risk among family history and body mass index subgroups: a systematic review and meta-analysis. *BMC Cancer,* 18**,** 71.

SHI, Z., YU, X., YUAN, M., LV, W., FENG, T., BAI, R. & ZHONG, H. 2019. Activation of the PERK-ATF4 pathway promotes chemo-resistance in colon cancer cells. *Scientific Reports,* 9**,** 3210.

SICARI, D., DELAUNAY-MOISAN, A., COMBETTES, L., CHEVET, E. & IGBARIA, A. 2020. A guide to assessing endoplasmic reticulum homeostasis and stress in mammalian systems. *Febs j,* 287**,** 27-42.

SIEBER, J., LINDENMEYER, M. T., KAMPE, K., CAMPBELL, K. N., COHEN, C. D., HOPFER, H., MUNDEL, P. & JEHLE, A. W. 2010. Regulation of podocyte survival and endoplasmic reticulum stress by fatty acids. *Am J Physiol Renal Physiol,* 299**,** F821-9.

SIEGEL, R. L., MILLER, K. D. & JEMAL, A. 2020. Cancer statistics, 2020. *CA Cancer J Clin,* 70**,** 7-30.

SIMON, J. A., HODGKINS, M. L., BROWNER, W. S., NEUHAUS, J. M., BERNERT, J. T., JR. & HULLEY, S. B. 1995. Serum fatty acids and the risk of coronary heart disease. *Am J Epidemiol,* 142**,** 469-76.

SIMONS, P. C. & VANDER JAGT, D. L. 1977. Purification of glutathione S-transferases from human liver by glutathione-affinity chromatography. *Anal Biochem,* 82**,** 334-41.

SINGH, R. & CUERVO, A. M. 2012. Lipophagy: connecting autophagy and lipid metabolism. *Int J Cell Biol,* 2012**,** 282041.

SINGH, R., GUBINA-VAKULYCK, G. & GORBACH, T. 2021a. Pathological changes in the mucous membrane of the small intestine due to prolonged consumption of palm oil. *Comparative Clinical Pathology,* 30**,** 41-47.

SINGH, R., GUBINA-VAKULYCK, G. & GORBACH, T. J. C. C. P. 2021b. Pathological changes in the mucous membrane of the small intestine due to prolonged consumption of palm oil. 30**,** 41-47.

SIRI-TARINO, P. W., SUN, Q., HU, F. B. & KRAUSS, R. M. 2010. Saturated fatty acids and risk of coronary heart disease: modulation by replacement nutrients. *Curr Atheroscler Rep,* 12**,** 384-90.

SIWECKA, N., ROZPĘDEK, W., PYTEL, D., WAWRZYNKIEWICZ, A., DZIKI, A., DZIKI, Ł., DIEHL, J. A. & MAJSTEREK, I. 2019. Dual role of Endoplasmic Reticulum Stress-Mediated Unfolded Protein Response Signaling Pathway in Carcinogenesis. *International Journal of Molecular Sciences* [Online], 20.

SKEHAN, P., STORENG, R., SCUDIERO, D., MONKS, A., MCMAHON, J., VISTICA, D., WARREN, J. T., BOKESCH, H., KENNEY, S. & BOYD, M. R. 1990. New colorimetric cytotoxicity assay for anticancer-drug screening. *J Natl Cancer Inst,* 82**,** 1107-12.

SMITH, P. K., KROHN, R. I., HERMANSON, G. T., MALLIA, A. K., GARTNER, F. H., PROVENZANO, M. D., FUJIMOTO, E. K., GOEKE, N. M., OLSON, B. J. & KLENK, D. C. 1985. Measurement of protein using bicinchoninic acid. *Anal Biochem,* 150**,** 76-85.

SNIDER, A. J., BIALKOWSKA, A. B., GHALEB, A. M., YANG, V. W., OBEID, L. M. & HANNUN, Y. A. 2016. Murine Model for Colitis-Associated Cancer of the Colon. *Methods Mol Biol,* 1438**,** 245-54.

SNIPES, R. L. 1977. Limited fat absorption in the large intestine of mice. A morphological study. *Acta Anat (Basel),* 99**,** 435-9.

SNODGRASS, R. G., HUANG, S., NAMGALADZE, D., JANDALI, O., SHAO, T., SAMA, S., BRÜNE, B. & HWANG, D. H. 2016. Docosahexaenoic acid and palmitic acid reciprocally modulate monocyte activation in part through endoplasmic reticulum stress. *The Journal of Nutritional Biochemistry,* 32**,** 39-45.

SONG, X., HUANG, Y., NEUHOUSER, M. L., TINKER, L. F., VITOLINS, M. Z., PRENTICE, R. L. & LAMPE, J. W. 2017. Dietary long-chain fatty acids and carbohydrate biomarker evaluation in a controlled feeding study in participants from the Women's Health Initiative cohort1,2. *The American Journal of Clinical Nutrition,* 105**,** 1272-1282.

SONG, Z., XIAOLI, A. M. & YANG, F. 2018. Regulation and Metabolic Significance of De Novo Lipogenesis in Adipose Tissues. *Nutrients* [Online], 10.

SPECTOR, A. A. & STEINBERG, D. 1966. Release of free fatty acids from Ehrlich ascites tumor cells. *J Lipid Res,* 7**,** 649-56.

STAAF, J., UBHAYASEKERA, S. J., SARGSYAN, E., CHOWDHURY, A., KRISTINSSON, H., MANELL, H., BERGQUIST, J., FORSLUND, A. & BERGSTEN, P. 2016. Initial hyperinsulinemia and subsequent β-cell dysfunction is associated with elevated palmitate levels. *Pediatr Res,* 80**,** 267-74.

STEVENS, S. A., GONZALEZ AGUIAR, M. K., TORO, A. L., YERLIKAYA, E. I., SUNILKUMAR, S., VANCLEAVE, A. M., PFLEGER, J., BRADLEY, E. A., KIMBALL, S. R., DENNIS, M. D. J. A. J. O. P.-E. & METABOLISM 2023. PERK/ATF4-dependent expression of the stress response protein REDD1 promotes proinflammatory cytokine expression in the heart of obese mice. 324**,** E62-E72.

STRABLE, M. S. & NTAMBI, J. M. 2010. Genetic control of de novo lipogenesis: role in diet-induced obesity. *Crit Rev Biochem Mol Biol,* 45**,** 199-214.

STROBER, W. 2001. Trypan blue exclusion test of cell viability. *Curr Protoc Immunol,* Appendix 3**,** Appendix 3B.

SUGANAMI, T., TANAKA, M. & OGAWA, Y. 2012. Adipose tissue inflammation and ectopic lipid accumulation. *Endocr J,* 59**,** 849-57.

SUN, S., SHI, G., SHA, H., JI, Y., HAN, X., SHU, X., MA, H., INOUE, T., GAO, B., KIM, H., BU, P., GUBER, R. D., SHEN, X., LEE, A.-H., IWAWAKI, T., PATON, A. W., PATON, J. C., FANG, D., TSAI, B., YATES III, J. R., WU, H., KERSTEN, S., LONG, Q., DUHAMEL, G. E., SIMPSON, K. W. & QI, L. 2015. IRE1α is an endogenous substrate of endoplasmic-reticulum-associated degradation. *Nature Cell Biology,* 17**,** 1546-1555.

SUNG, H., FERLAY, J., SIEGEL, R. L., LAVERSANNE, M., SOERJOMATARAM, I., JEMAL, A. & BRAY, F. 2021. Global Cancer Statistics 2020: GLOBOCAN Estimates of Incidence and Mortality Worldwide for 36 Cancers in 185 Countries. *CA Cancer J Clin,* 71**,** 209-249.

SVOBODOVÁ, G., HORNÍ, M., VELECKÁ, E. & BOUŠOVÁ, I. J. A. O. T. 2024. Metabolic dysfunction-associated steatotic liver disease-induced changes in the antioxidant system: a review. 1-22.

SWINNEN, J. V., BRUSSELMANS, K. & VERHOEVEN, G. 2006. Increased lipogenesis in cancer cells: new players, novel targets. *Curr Opin Clin Nutr Metab Care,* 9**,** 358-65.

TAKAHASHI, H. K., CAMBIAGHI, T. D., LUCHESSI, A. D., HIRABARA, S. M., VINOLO, M. A., NEWSHOLME, P. & CURI, R. 2012. Activation of survival and apoptotic signaling pathways in lymphocytes exposed to palmitic acid. *J Cell Physiol,* 227**,** 339-50.

TAN, Y., HUANG, Z., JIN, Y., WANG, J., FAN, H., LIU, Y., ZHANG, L., WU, Y., LIU, P. & LI, T. J. N. C. 2024. Lipid droplets sequester palmitic acid to disrupt endothelial ciliation and exacerbate atherosclerosis in male mice. 15**,** 8273.

TANGJITJAROENKUN, J., CHANTARASRIWONG, O. & CHAVASIRI, W. 2012. Chemical constituents of the stems of Zanthoxylum limonella Alston. *Phytochemistry Letters,* 5**,** 443-445.

THEODORATOU, E., MCNEILL, G., CETNARSKYJ, R., FARRINGTON, S. M., TENESA, A., BARNETSON, R., PORTEOUS, M., DUNLOP, M. & CAMPBELL, H. 2007. Dietary fatty acids and colorectal cancer: a case-control study. *Am J Epidemiol,* 166**,** 181-95.

THOMAS, G. M. & HUGANIR, R. L. 2013. Palmitoylation-dependent regulation of glutamate receptors and their PDZ domain-containing partners. *Biochem Soc Trans,* 41**,** 72-8.

THOMÉ, M. P., FILIPPI-CHIELA, E. C., VILLODRE, E. S., MIGLIAVACA, C. B., ONZI, G. R., FELIPE, K. B. & LENZ, G. 2016. Ratiometric analysis of Acridine Orange staining in the study of acidic organelles and autophagy. *J Cell Sci,* 129**,** 4622-4632.

THOMPSON, R. H., MCMURRAY, C. H. & BLANCHFLOWER, W. J. 1976. The levels of selenium and glutathione peroxidase activity in blood of sheep, cows and pigs. *Research in Veterinary Science,* 20**,** 229-231.

THUERAUF, D. J., MORRISON, L. & GLEMBOTSKI, C. C. 2004. Opposing roles for ATF6alpha and ATF6beta in endoplasmic reticulum stress response gene induction. *J Biol Chem,* 279**,** 21078-84.

TING, J. P., WILLINGHAM, S. B. & BERGSTRALH, D. T. 2008. NLRs at the intersection of cell death and immunity. *Nat Rev Immunol,* 8**,** 372-9.

TIRASOPHON, W., WELIHINDA, A. A. & KAUFMAN, R. J. 1998. A stress response pathway from the endoplasmic reticulum to the nucleus requires a novel bifunctional protein kinase/endoribonuclease (Ire1p) in mammalian cells. *Genes Dev,* 12**,** 1812-24.

TOMAR, D., PRAJAPATI, P., SRIPADA, L., SINGH, K., SINGH, R., SINGH, A. K. & SINGH, R. 2013. TRIM13 regulates caspase-8 ubiquitination, translocation to autophagosomes and activation during ER stress induced cell death. *Biochim Biophys Acta,* 1833**,** 3134-3144.

TONG, Y., GAO, H., QI, Q., LIU, X., LI, J., GAO, J., LI, P., WANG, Y., DU, L. & WANG, C. 2021. High fat diet, gut microbiome and gastrointestinal cancer. *Theranostics,* 11**,** 5889-5910.

TOYOKUNI, S. 2008. Molecular mechanisms of oxidative stress-induced carcinogenesis: from epidemiology to oxygenomics. *IUBMB Life,* 60**,** 441-7.

TRAGANOS, F. & DARZYNKIEWICZ, Z. 1994. Lysosomal proton pump activity: supravital cell staining with acridine orange differentiates leukocyte subpopulations. *Methods Cell Biol,* 41**,** 185-94.

URANO, F., WANG, X., BERTOLOTTI, A., ZHANG, Y., CHUNG, P., HARDING, H. P. & RON, D. 2000. Coupling of stress in the ER to activation of JNK protein kinases by transmembrane protein kinase IRE1. *Science,* 287**,** 664-6.

URSO, C. J. & ZHOU, H. 2021. Role of CD36 in Palmitic Acid Lipotoxicity in Neuro-2a Neuroblastoma Cells. *Biomolecules* [Online], 11.

UTSUNOMIYA, H., YAMAMOTO, Y., TAKESHITA, E., TOKUMOTO, Y., TADA, F., MIYAKE, T., HIROOKA, M., ABE, M., KUMAGI, T., MATSUURA, B., IKEDA, Y. & HIASA, Y. 2017. Upregulated absorption of dietary palmitic acids with changes in intestinal transporters in non-alcoholic steatohepatitis (NASH). *Journal of Gastroenterology,* 52**,** 940-954.

VALDÉS, P., MERCADO, G., VIDAL, R. L., MOLINA, C., PARSONS, G., COURT, F. A., MARTINEZ, A., GALLEGUILLOS, D., ARMENTANO, D., SCHNEIDER, B. L. & HETZ, C. 2014. Control of dopaminergic neuron survival by the unfolded protein response transcription factor XBP1. *Proc Natl Acad Sci U S A,* 111**,** 6804-9.

VAN HARMELEN, V., REYNISDOTTIR, S., CIANFLONE, K., DEGERMAN, E., HOFFSTEDT, J., NILSELL, K., SNIDERMAN, A. & ARNER, P. 1999. Mechanisms involved in the regulation of free fatty acid release from isolated human fat cells by acylation-stimulating protein and insulin. *J Biol Chem,* 274**,** 18243-51.

VAN HERPEN, N. A. & SCHRAUWEN-HINDERLING, V. B. 2008. Lipid accumulation in non-adipose tissue and lipotoxicity. *Physiology & Behavior,* 94**,** 231-241.

VARSHNEY, R., VARSHNEY, R., MISHRA, R., GUPTA, S., SIRCAR, D. & ROY, P. 2018. Kaempferol alleviates palmitic acid-induced lipid stores, endoplasmic reticulum stress and pancreatic β-cell dysfunction through AMPK/mTOR-mediated lipophagy. *The Journal of Nutritional Biochemistry,* 57**,** 212-227.

VATTEM, K. M. & WEK, R. C. 2004. Reinitiation involving upstream ORFs regulates ATF4 mRNA translation in mammalian cells. *Proc Natl Acad Sci U S A,* 101**,** 11269-74.

VEGA-MARTÍN, E., GIL-ORTEGA, M., GONZÁLEZ-BLÁZQUEZ, R., BENEDITO, S., FERNÁNDEZ-FELIPE, J., RUIZ-GAYO, M., DEL OLMO, N., CHOWEN, J. A., FRAGO, L. M., SOMOZA, B. & FERNÁNDEZ-ALFONSO, M. S. 2021. Differential Deleterious Impact of Highly Saturated Versus Monounsaturated Fat Intake on Vascular Function, Structure, and Mechanics in Mice. *Nutrients* [Online], 13.

VENTURA, R., MORDEC, K., WASZCZUK, J., WANG, Z., LAI, J., FRIDLIB, M., BUCKLEY, D., KEMBLE, G. & HEUER, T. S. 2015. Inhibition of de novo Palmitate Synthesis by Fatty Acid Synthase Induces Apoptosis in Tumor Cells by Remodeling Cell Membranes, Inhibiting Signaling Pathways, and Reprogramming Gene Expression. *EBioMedicine,* 2**,** 808-24.

VIDAL, R. L., FIGUEROA, A., COURT, F. A., THIELEN, P., MOLINA, C., WIRTH, C., CABALLERO, B., KIFFIN, R., SEGURA-AGUILAR, J., CUERVO, A. M., GLIMCHER, L. H. & HETZ, C. 2012. Targeting the UPR transcription factor XBP1 protects against Huntington's disease through the regulation of FoxO1 and autophagy. *Hum Mol Genet,* 21**,** 2245-62.

VIDRIO-HUERTA, B., PLÖTZ, T. & LORTZ, S. J. J. O. M. E. 2024. Oxidative and ER stress by elevated insulin biosynthesis and palmitic acid in insulin-producing cells. 72.

VOELTZ, G. K., ROLLS, M. M. & RAPOPORT, T. A. 2002. Structural organization of the endoplasmic reticulum. *EMBO Rep,* 3**,** 944-50.

WAGNER, R., STÜBIGER, G., VEIGEL, D., WUCZKOWSKI, M., LANZERSTORFER, P., WEGHUBER, J., KARTERIS, E., NOWIKOVSKY, K., WILFINGER-LUTZ, N., SINGER, C. F., COLOMER, R., BENHAMÚ, B., LÓPEZ-RODRÍGUEZ, M. L., VALENT, P. & GRUNT, T. W. 2017. Multi-level suppression of receptor-PI3K-mTORC1 by fatty acid synthase inhibitors is crucial for their efficacy against ovarian cancer cells. *Oncotarget,* 8**,** 11600-11613.

WAKIL, S. J. 1962. Enzymatic synthesis of fatty acids. *Comparative Biochemistry and Physiology,* 4**,** 123-158.

WALTER, P. & RON, D. 2011. The unfolded protein response: from stress pathway to homeostatic regulation. *Science,* 334**,** 1081-6.

WAN, Y., LIU, H., JIN, J., ZHANG, Z., YANG, Y., ZHU, X., XIE, S. & HAN, D. J. A. 2025. New insights into ER stress mediated by ATF6 and IRE1-XBP1 signals in yellow catfish under hypoxia. 597**,** 741926.

WANG, C., CHEN, Y. G., GAO, J. L., LYU, G. Y., SU, J., ZHANG, Q. I., JI, X., YAN, J. Z., QIU, Q. L., ZHANG, Y. L., LI, L. Z., XU, H. T. & CHEN, S. H. 2015a. Low local blood perfusion, high white blood cell and high platelet count are associated with primary tumor growth and lung metastasis in a 4T1 mouse breast cancer metastasis model. *Oncol Lett,* 10**,** 754-760.

WANG, G., LIU, G., WANG, X., SETHI, S., ALI-FEHMI, R., ABRAMS, J., ZHENG, Z., ZHANG, K., ETHIER, S. & YANG, Z.-Q. 2012. ERLIN2 promotes breast cancer cell survival by modulating endoplasmic reticulum stress pathways. *BMC Cancer,* 12**,** 225.

WANG, H. & MI, K. 2023. Emerging roles of endoplasmic reticulum stress in the cellular plasticity of cancer cells. *Front Oncol,* 13**,** 1110881.

WANG, S., PARK, S., KODALI, V. K., HAN, J., YIP, T., CHEN, Z., DAVIDSON, N. O. & KAUFMAN, R. J. 2015b. Identification of protein disulfide isomerase 1 as a key isomerase for disulfide bond formation in apolipoprotein B100. *Mol Biol Cell,* 26**,** 594-604.

WANG, W.-A., GROENENDYK, J. & MICHALAK, M. J. B. E. B. A.-M. C. R. 2014. Endoplasmic reticulum stress associated responses in cancer. 1843**,** 2143-2149.

WANG, W., BAI, L., LI, W. & CUI, J. 2020. The Lipid Metabolic Landscape of Cancers and New Therapeutic Perspectives. *Front Oncol,* 10**,** 605154.

WANG, X., ZHANG, C. & BAO, N. 2023a. Molecular mechanism of palmitic acid and its derivatives in tumor progression. *Front Oncol,* 13**,** 1224125.

WANG, Y., NIE, J., DAI, L., HU, W., HAN, S., ZHANG, J., CHEN, X., MA, X., TIAN, G., WU, D., ZHANG, Z., LONG, J. & FANG, J. 2023b. Construction of an endoplasmic reticulum stress-related signature in lung adenocarcinoma by comprehensive bioinformatics analysis. *BMC Pulmonary Medicine,* 23**,** 172.

WATANABE, D., YAMADA, K., NISHINA, Y., TAJIMA, Y., KOSHIMIZU, U., NAGATA, A. & NISHIMUNE, Y. 1994. Molecular cloning of a novel Ca(2+)-binding protein (calmegin) specifically expressed during male meiotic germ cell development. *J Biol Chem,* 269**,** 7744-9.

WEN, S., CHEN, N., HU, Y., HUANG, L., PENG, J., YANG, M., SHEN, X., SONG, Y. & XU, L. 2021. Elevated peripheral absolute monocyte count related to clinicopathological features and poor prognosis in solid tumors: Systematic review, meta-analysis, and meta-regression. *Cancer Med,* 10**,** 1690-1714.

WESTHEIM, A. J. F., STOFFELS, L. M., DUBOIS, L. J., VAN BERGENHENEGOUWEN, J., VAN HELVOORT, A., LANGEN, R. C. J., SHIRI-SVERDLOV, R. & THEYS, J. 2023. The Modulatory Effects of Fatty Acids on Cancer Progression. *Biomedicines,* 11.

WILKE, M. S., FRENCH, M. A., GOH, Y. K., RYAN, E. A., JONES, P. J. & CLANDININ, M. T. 2009. Synthesis of specific fatty acids contributes to VLDL-triacylglycerol composition in humans with and without type 2 diabetes. *Diabetologia,* 52**,** 1628-1637.

WINTER, J. & JAKOB, U. 2004. Beyond transcription--new mechanisms for the regulation of molecular chaperones. *Crit Rev Biochem Mol Biol,* 39**,** 297-317.

WU, J., CHEN, J., XI, Y., WANG, F., SHA, H., LUO, L., ZHU, Y., HONG, X. & BU, S. 2018. High glucose induces epithelial-mesenchymal transition and results in the migration and invasion of colorectal cancer cells. *Exp Ther Med,* 16**,** 222-230.

WU, S., TAN, M., HU, Y., WANG, J. L., SCHEUNER, D. & KAUFMAN, R. J. 2004. Ultraviolet light activates NFkappaB through translational inhibition of IkappaBalpha synthesis. *J Biol Chem,* 279**,** 34898-902.

XI, L., QIAN, Z., XU, G., ZHOU, C. & SUN, S. 2007. Crocetin attenuates palmitate-induced insulin insensitivity and disordered tumor necrosis factor-alpha and adiponectin expression in rat adipocytes. *Br J Pharmacol,* 151**,** 610-7.

XI, Y. & XU, P. 2021a. Global colorectal cancer burden in 2020 and projections to 2040. *Translational Oncology,* 14**,** 101174.

XI, Y. & XU, P. 2021b. Global colorectal cancer burden in 2020 and projections to 2040. *Transl Oncol,* 14**,** 101174.

XIANG, X. Y., LIU, T., WU, Y., JIANG, X. S., HE, J. L., CHEN, X. M. & DU, X. G. 2021. Berberine alleviates palmitic acid-induced podocyte apoptosis by reducing reactive oxygen species-mediated endoplasmic reticulum stress. *Mol Med Rep,* 23.

XIAO, W. C., ZHANG, J., CHEN, S. L., SHI, Y. J., XIAO, F. & AN, W. 2018. Alleviation of palmitic acid-induced endoplasmic reticulum stress by augmenter of liver regeneration through IP3R-controlled Ca(2+) release. *J Cell Physiol,* 233**,** 6148-6157.

XIE, Y., LIU, C., QIN, Y., CHEN, J. & FANG, J. 2019. Knockdown of IRE1α suppresses metastatic potential of colon cancer cells through inhibiting FN1-Src/FAK-GTPases signaling. *The International Journal of Biochemistry & Cell Biology,* 114**,** 105572.

XING, X., LAI, M., WANG, Y., XU, E. & HUANG, Q. J. C. C. A. 2006. Overexpression of glucose-regulated protein 78 in colon cancer. 364**,** 308-315.

XING, X., LI, Y., LIU, H., WANG, L. & SUN, L. 2011. Glucose regulated protein 78 (GRP78) is overexpressed in colorectal carcinoma and regulates colorectal carcinoma cell growth and apoptosis. *Acta Histochem,* 113**,** 777-82.

XU, C., BAILLY-MAITRE, B. & REED, J. C. 2005. Endoplasmic reticulum stress: cell life and death decisions. *J Clin Invest,* 115**,** 2656-64.

XU, D., LIU, L., ZHAO, Y., YANG, L., CHENG, J., HUA, R., ZHANG, Z. & LI, Q. 2020. Melatonin protects mouse testes from palmitic acid-induced lipotoxicity by attenuating oxidative stress and DNA damage in a SIRT1-dependent manner. *J Pineal Res,* 69**,** e12690.

XU, W., GUO, Y. B., LI, X., HE, M. R. & LIU, S. D. 2016. [Palmitic acid induces hepatocellular oxidative stress and activation of inflammasomes]. *Nan Fang Yi Ke Da Xue Xue Bao,* 36**,** 655-9.

XU, W., ZHANG, X., WU, J.-L., FU, L., LIU, K., LIU, D., CHEN, G. G., LAI, P. B.-S., WONG, N. & YU, J. 2017. O-GlcNAc transferase promotes fatty liver-associated liver cancer through inducing palmitic acid and activating endoplasmic reticulum stress. *Journal of Hepatology,* 67**,** 310-320.

XU, X. F., MENG SHI, M., YING LUO, M., DAN LIU, D., MING GUO, D., LING, C., ZHONG, X. L., XU, Y. & CAO, W. Y. J. I. I. 2022. Targeting PERK mediated endoplasmic reticulum stress attenuates neuroinflammation and alleviates lipopolysaccharide-induced depressive-like behavior in male mice. 111**,** 109092.

XUE, X., LI, F., CAI, M., HU, J., WANG, Q. & LOU, S. 2021. Interactions between Endoplasmic Reticulum Stress and Autophagy: Implications for Apoptosis and

Neuroplasticity-Related Proteins in Palmitic Acid-Treated Prefrontal Cells. *Neural Plasticity,* 2021**,** 8851327.

YAMAMOTO, K., SATO, T., MATSUI, T., SATO, M., OKADA, T., YOSHIDA, H., HARADA, A. & MORI, K. 2007. Transcriptional induction of mammalian ER quality control proteins is mediated by single or combined action of ATF6alpha and XBP1. *Dev Cell,* 13**,** 365-76.

YAMAMOTO, K., TAKAHARA, K., OYADOMARI, S., OKADA, T., SATO, T., HARADA, A. & MORI, K. 2010. Induction of liver steatosis and lipid droplet formation in ATF6alpha-knockout mice burdened with pharmacological endoplasmic reticulum stress. *Mol Biol Cell,* 21**,** 2975-86.

YAN, P., TANG, S., ZHANG, H., GUO, Y., ZENG, Z. & WEN, Q. 2017. Palmitic acid triggers cell apoptosis in RGC-5 retinal ganglion cells through the Akt/FoxO1 signaling pathway. *Metabolic Brain Disease,* 32**,** 453-460.

YANG, J., WEI, H., ZHOU, Y., SZETO, C.-H., LI, C., LIN, Y., COKER, O. O., LAU, H. C. H., CHAN, A. W. H., SUNG, J. J. Y. & YU, J. 2022. High-Fat Diet Promotes Colorectal Tumorigenesis Through Modulating Gut Microbiota and Metabolites. *Gastroenterology,* 162**,** 135-149.e2.

YANG, L., GUAN, G., LEI, L., LV, Q., LIU, S., ZHAN, X., JIANG, Z. & GU, X. 2018a. Palmitic acid induces human osteoblast-like Saos-2 cell apoptosis via endoplasmic reticulum stress and autophagy. *Cell Stress and Chaperones,* 23**,** 1283-1294.

YANG, L., LIU, C., ZHAO, W., HE, C., DING, J., DAI, R., XU, K., XIAO, L., LUO, L., LIU, S., LI, W. & MENG, H. 2018b. Impaired Autophagy in Intestinal Epithelial Cells Alters Gut Microbiota and Host Immune Responses. *Appl Environ Microbiol,* 84.

YANG, Y., SMITH, D. L., JR., KEATING, K. D., ALLISON, D. B. & NAGY, T. R. 2014. Variations in body weight, food intake and body composition after long-term high-fat diet feeding in C57BL/6J mice. *Obesity (Silver Spring),* 22**,** 2147-55.

YANG, Y., WANG, Y., ZHOU, Y., DENG, J., WU, L. J. M. & BIOCHEMISTRY, C. 2024. Tirzepatide alleviates oxidative stress and inflammation in diabetic nephropathy via IL-17 signaling pathway. 1-14.

YONG, J., PAREKH, V. S., REILLY, S. M., NAYAK, J., CHEN, Z., LEBEAUPIN, C., JANG, I., ZHANG, J., PRAKASH, T. P., SUN, H., MURRAY, S., GUO, S., AYALA, J. E., SATIN, L. S., SALTIEL, A. R. & KAUFMAN, R. J. 2021. Chop/Ddit3 depletion in β cells alleviates ER stress and corrects hepatic steatosis in mice. *Sci Transl Med,* 13.

YOUNG, R. S. E., BOWMAN, A. P., TOUSIGNANT, K. D., POAD, B. L. J., GUNTER, J. H., PHILP, L. K., NELSON, C. C., ELLIS, S. R., HEEREN, R. M. A., SADOWSKI, M. C. & BLANKSBY, S. J. 2022. Isomeric lipid signatures reveal compartmentalized fatty acid metabolism in cancer. *J Lipid Res,* 63**,** 100223.

YU, X., PENG, W., WANG, Y., XU, W., CHEN, W., HUANG, L., XU, H., HE, X., WANG, S., SUN, Q., LU, W. & XU, Y. 2023. Palmitic Acid Inhibits the Growth and Metastasis of Gastric Cancer by Blocking the STAT3 Signaling Pathway. *Cancers (Basel),* 15.

YUAN, S., SHE, D., JIANG, S., DENG, N., PENG, J. & MA, L. J. M. M. 2024. Endoplasmic reticulum stress and therapeutic strategies in metabolic, neurodegenerative diseases and cancer. 30**,** 40.

ZEESHAN, H. M., LEE, G. H., KIM, H.-R. & CHAE, H.-J. 2016a. Endoplasmic Reticulum Stress and Associated ROS. *International Journal of Molecular Sciences* [Online], 17.

ZEESHAN, H. M., LEE, G. H., KIM, H. R. & CHAE, H. J. 2016b. Endoplasmic Reticulum Stress and Associated ROS. *Int J Mol Sci,* 17**,** 327.

ZENG, X., ZHU, M., LIU, X., CHEN, X., YUAN, Y., LI, L., LIU, J., LU, Y., CHENG, J. & CHEN, Y. 2020a. Oleic acid ameliorates palmitic acid induced hepatocellular lipotoxicity by inhibition of ER stress and pyroptosis. *Nutrition & Metabolism,* 17**,** 11.

ZENG, X., ZHU, M., LIU, X., CHEN, X., YUAN, Y., LI, L., LIU, J., LU, Y., CHENG, J. & CHEN, Y. 2020b. Oleic acid ameliorates palmitic acid induced hepatocellular lipotoxicity by inhibition of ER stress and pyroptosis. *Nutr Metab (Lond),* 17**,** 11.

ZHANG, J., ZHAO, W. S., WANG, X., XU, L. & YANG, X. C. 2018a. Palmitic Acid Increases Endothelin-1 Expression in Vascular Endothelial Cells through the Induction of Endoplasmic Reticulum Stress and Protein Kinase C Signaling. *Cardiology,* 140**,** 133-140.

ZHANG, K. & KAUFMAN, R. J. 2008a. From endoplasmic-reticulum stress to the inflammatory response. *Nature,* 454**,** 455-62.

ZHANG, K. & KAUFMAN, R. J. 2008b. From endoplasmic-reticulum stress to the inflammatory response. *Nature,* 454**,** 455-462.

ZHANG, K., WANG, S., MALHOTRA, J., HASSLER, J. R., BACK, S. H., WANG, G., CHANG, L., XU, W., MIAO, H., LEONARDI, R., CHEN, Y. E., JACKOWSKI, S. & KAUFMAN, R. J. 2011a. The unfolded protein response transducer IRE1α prevents ER stress-induced hepatic steatosis. *Embo j,* 30**,** 1357-75.

ZHANG, Q., YANG, X., WU, J., YE, S., GONG, J., CHENG, W. M., LUO, Z., YU, J., LIU, Y., ZENG, W., LIU, C., XIONG, Z., CHEN, Y., HE, Z. & LAN, P. 2023. Reprogramming of palmitic acid induced by dephosphorylation of ACOX1 promotes β-catenin palmitoylation to drive colorectal cancer progression. *Cell Discovery,* 9**,** 26.

ZHANG, W., SHI, Y., OYANG, L., CUI, S., LI, S., LI, J., LIU, L., LI, Y., PENG, M. & TAN, S. J. C. D. D. 2024. Endoplasmic reticulum stress—a key guardian in cancer. 10**,** 343.

ZHANG, X., LI, X., XIONG, G., YUN, F., FENG, Y., NI, Q., WU, N., YANG, L., YI, Z., ZHANG, Q., YANG, Z., KUANG, Y., SAI, B. & ZHU, Y. 2022a. Palmitic Acid Promotes Lung Metastasis of Melanomas via the TLR4/TRIF-Peli1-pNF-κB Pathway. *Metabolites,* 12.

ZHANG, X., LI, X., XIONG, G., YUN, F., FENG, Y., NI, Q., WU, N., YANG, L., YI, Z., ZHANG, Q., YANG, Z., KUANG, Y., SAI, B. & ZHU, Y. 2022b. Palmitic Acid Promotes Lung Metastasis of Melanomas via the TLR4/TRIF-Peli1-pNF-κB Pathway. *Metabolites* [Online], 12.

ZHANG, X., LI, X., XIONG, G., YUN, F., FENG, Y., NI, Q., WU, N., YANG, L., YI, Z. & ZHANG, Q. J. M. 2022c. Palmitic acid promotes lung metastasis of melanomas via the TLR4/TRIF-Peli1-pNF-κB pathway. 12**,** 1132.

ZHANG, Y., LI, S., LI, F., LV, C. & YANG, Q.-K. 2021. High-fat diet impairs ferroptosis and promotes cancer invasiveness via downregulating tumor suppressor ACSL4 in lung adenocarcinoma. *Biology Direct,* 16**,** 10.

ZHANG, Y., MIAO, L., ZHANG, H., WU, G., ZHANG, Z. & LV, J. 2018b. Chlorogenic acid against palmitic acid in endoplasmic reticulum stress-mediated apoptosis resulting in protective effect of primary rat hepatocytes. *Lipids in Health and Disease,* 17**,** 270.

ZHANG, Y., XUE, R., ZHANG, Z., YANG, X. & SHI, H. 2012a. Palmitic and linoleic acids induce ER stress and apoptosis in hepatoma cells. *Lipids Health Dis,* 11**,** 1.

ZHANG, Y., XUE, R., ZHANG, Z., YANG, X. & SHI, H. 2012b. Palmitic and linoleic acids induce ER stress and apoptosis in hepatoma cells. *Lipids in Health and Disease,* 11**,** 1.

ZHANG, Y., YANG, X., SHI, H., DONG, L. & BAI, J. 2011b. Effect of α-linolenic acid on endoplasmic reticulum stress-mediated apoptosis of palmitic acid lipotoxicity in primary rat hepatocytes. *Lipids in Health and Disease,* 10**,** 122.

ZHANG, Y., YU, H., GAO, P., CHEN, J., YU, C., ZONG, C., LU, S., LI, X., MA, X., LIU, Y. & WANG, X. 2016. The Effect of Growth Hormone on Lipid Accumulation or Maturation in Adipocytes. *Cell Physiol Biochem,* 39**,** 2135-2148.

ZHANG, Z., ZHANG, L., ZHOU, L., LEI, Y., ZHANG, Y. & HUANG, C. 2019. Redox signaling and unfolded protein response coordinate cell fate decisions under ER stress. *Redox Biol,* 25**,** 101047.

ZHAO, J., ZHAO, G., LANG, J., SUN, B., FENG, S., LI, D. & SUN, G. J. J. O. I. M. 2024a. Astragaloside IV ameliorated neuroinflammation and improved neurological functions in mice exposed to traumatic brain injury by modulating the PERK-eIF2α-ATF4 signaling pathway. 72**,** 747-762.

ZHAO, L., ZHANG, C., LUO, X., WANG, P., ZHOU, W., ZHONG, S., XIE, Y., JIANG, Y., YANG, P., TANG, R., PAN, Q., HALL, A. R., LUONG, T. V., FAN, J., VARGHESE, Z., MOORHEAD, J. F., PINZANI, M., CHEN, Y. & RUAN, X. Z. 2018. CD36 palmitoylation disrupts free fatty acid metabolism and promotes tissue inflammation in non-alcoholic steatohepatitis. *Journal of Hepatology,* 69**,** 705-717.

ZHAO, Z., LI, B., CHEN, Q., XIANG, X., XU, X., HAN, S., LAI, W., LI, Y., XU, W. & MAI, K. J. B. J. O. N. 2024b. Dietary palm oil enhances Sterol regulatory element-binding protein 2-mediated cholesterol biosynthesis through inducing endoplasmic reticulum stress in muscle of large yellow croaker (Larimichthys crocea). 131**,** 553-566.

ZHONG, Q., ZHOU, B., ANN, D. K., MINOO, P., LIU, Y., BANFALVI, A., KRISHNAVENI, M. S., DUBOURD, M., DEMAIO, L., WILLIS, B. C. J. A. J. O. R. C. & BIOLOGY, M. 2011. Role of endoplasmic reticulum stress in epithelial–mesenchymal transition of alveolar epithelial cells: effects of misfolded surfactant protein. 45**,** 498-509.

ZHOU, B., LIU, L., REDDIVARI, M. & ZHANG, X. A. 2004. The palmitoylation of metastasis suppressor KAI1/CD82 is important for its motility- and invasiveness-inhibitory activity. *Cancer Res,* 64**,** 7455-63.

ZHOU, X., XING, X., ZHANG, S., LIU, L., WANG, C., LI, L., JI, Q. & LIU, H. 2016. Glucose-regulated protein 78 contributes to the proliferation and tumorigenesis of human colorectal carcinoma via AKT and ERK pathways. *Oncol Rep,* 36**,** 2723-2730.

ZHU, C., JOHANSEN, F. E. & PRYWES, R. 1997. Interaction of ATF6 and serum response factor. *Mol Cell Biol,* 17**,** 4957-66.

ZHU, S., JIAO, W., XU, Y., HOU, L., LI, H., SHAO, J., ZHANG, X., WANG, R. & KONG, D. 2021. Palmitic acid inhibits prostate cancer cell proliferation and metastasis by suppressing the PI3K/Akt pathway. *Life Sci,* 286**,** 120046.

Publications and Presentations

Peer reviewed publications

1. **Valappan Veetil Soumya** , Snijesh Valiya Parambath , Chevookaren Francis Binoy Achuthan C Raghavamenon , Suraj Kadunganattil and Thekkekara Devassy Babu. Palmitic acid induced endoplasmic reticulum stress links metabolic stress to senescence and regulates cell fate via PERK signaling in colon cancer cells *Mapana Journal of Sciences.*

2. **Valappan Veetil Soumya** , Baby Jisna , Davis Anu , Chevookaren Francis Binoy and Thekkekara Devassy Babu IRE1α signalling activation of UPR as an adaptive strategy in gastric cancer progression: Impact on cellular dynamics and therapeutic opportunities. *Drug Discovery Today*.

3. Illam, S P ., Kandiyil S. P., Narayanankutty A ., **Veetil, S P,** Babu T D., Uppu R.M, and Raghavamenon, A.C.,2022. Virgin coconut oil complements with its polyphenol components mitigates sodium fluoride toxicity in vitro and in vivo. Drug and Chemical toxicology,45(6),pp 2528-2534.

4. Anu, D., Rennis, K.D., Soumya, V.V., Jisna, B., Hussan, K.S., Chandrasekharan, L. and Babu, T.D., 2025. Targeting the Tumor Microenvironment in Lung Cancer with a Focus on Immune Evasion, Hypoxia, and Treatment Resistance. Journal of Advanced Health Research & Clinical Medicine, 2(1), pp.3-14.

Non peer-reviewed publications

1. **V V Soumya,** C F Binoy, Jisna Baby, A Archana and Achuthan C Raghavamenon and T D Babu Palmitic acid induced ERS and UPR activate PERK/ATF4-NRF2 to promote colon cancer cell survival . 42nd Annual Conference of the Indian Association for Cancer Research, ACTREC,MUMBAI, January 12–16, 2023.(Poster presentataion)

2. **V V Soumya ,** T D Babu , and C F Binoy Re-establishing Cellular Homeostasis: Unfolded Protein Responses in Rat Intestinal Cells address Palmitic Acid-Induced Endoplasmic Reticulum Stress. Society of Toxicology India (STOX) 42 Annual Conference, Calicut University, Malappuram 23-25 November 2023 (oral presentation)

ELSEVIER

IRE1α-mediated UPR activation in gastrointestinal cancers: Adaptive mechanisms and therapeutic potential

Valappan Veetil Soumya [1], Baby Jisna [1], Davis Anu [1], Chevookaren Francis Binoy [2], Thekkekara Devassy Babu [1,*]

[1] Department of Biochemistry, Amala Cancer Research Centre (Recognised Research Centre, University of Calicut), Thrissur - 680 555, Kerala, India
[2] Research and Post Graduate Department of Zoology, St Thomas College (Autonomous), Thrissur - 680 001, Affiliated to University of Calicut, Kerala, India

The endoplasmic reticulum (ER) plays a crucial role in protein synthesis, folding and quality control. Disruptions in these processes lead to ER stress (ERS) and activate the unfolded protein response (UPR) to restore cellular homeostasis. In gastrointestinal cancers, inositol-requiring enzyme 1α (IRE1α) is a key regulator of the UPR, enabling cancer cells to adapt to hostile conditions such as hypoxia, oxidative stress and chemotherapy. Elevated IRE1α activity supports tumor survival, progression and metastasis by mitigating ERS-induced apoptosis. However, targeting IRE1α signaling presents a promising therapeutic strategy by impairing cancer cell adaptation to stress, offering promising therapeutic opportunities for gastrointestinal cancers.

Keywords: Endoplasmic reticulum stress; unfolded protein response; inositol-requiring enzyme 1α; gastrointestinal cancer; therapeutic potential

Introduction

Gastrointestinal cancers (GC) are amoung the most prevalent malignancies of the digestive system, characterised by high mortality, late detection and poor prognosis.(p1) Targeted therapies, including monoclonal antibodies (trastuzumab, ramucirumab, rilotumumab, onartuzumab), EGFR inhibitors (cetuximab, panitumumab), PD-1/PD-L1 (programmed death-1/PD-ligand 1) blockers (pembrolizumab, nivolumab) and PI3K/AKT/mTOR (phosphoinositide 3-kinase/protein kinase B (AKT)/mechanistic target of rapamycin) pathway inhibitors (everolimus), have shown promise.(p2) However, survival rates remain low owing to late diagnosis and drug resistance. Emerging evidence highlights the role of the unfolded protein response (UPR) in GC pathogenesis, particularly in cancer cell survival, adaptation and therapeutic resistance.(p3) Targeting the UPR might offer novel therapeutic strategies.

The endoplasmic reticulum (ER) plays a vital role in protein synthesis, folding and processing. The accumulation of misfolded proteins triggers the UPR to restore cellular balance.(p4) The UPR enhances protein folding, promotes ER-associated degradation (ERAD) and, if necessary, induces apoptosis. It operates through three main pathways: IRE1α, PERK and ATF6, which reinforce ER capacity and regulate cell fate.(p5) Among these, IRE1α, a key UPR sensor, is overexpressed in various cancers, supporting cell proliferation. GC cells face stressors such as oncogene-driven protein synthesis, hypoxia and nutrient scarcity, which disrupt protein homeostasis. The IRE1α pathway aids in adaptation by enhancing protein folding and degradation, promoting survival and proliferation.(p6),(p7)

GC cells are particularly adept at utilizing the UPR to withstand adverse conditions. They employ diverse survival strategies, such as metabolic rerouting, increased proliferation and aggressive metastasis, to thrive in the hostile tumor microenvironment.(p8) The IRE1α pathway is integral to these adaptive responses, enabling cancer cells to withstand ER stress (ERS) more effectively.(p9) Elevated IRE1α activity in GC cells triggers

* Corresponding author. Babu, T.D. (babutd@amalaims.org)

https://doi.org/10.1016/j.drudis.2025.104335

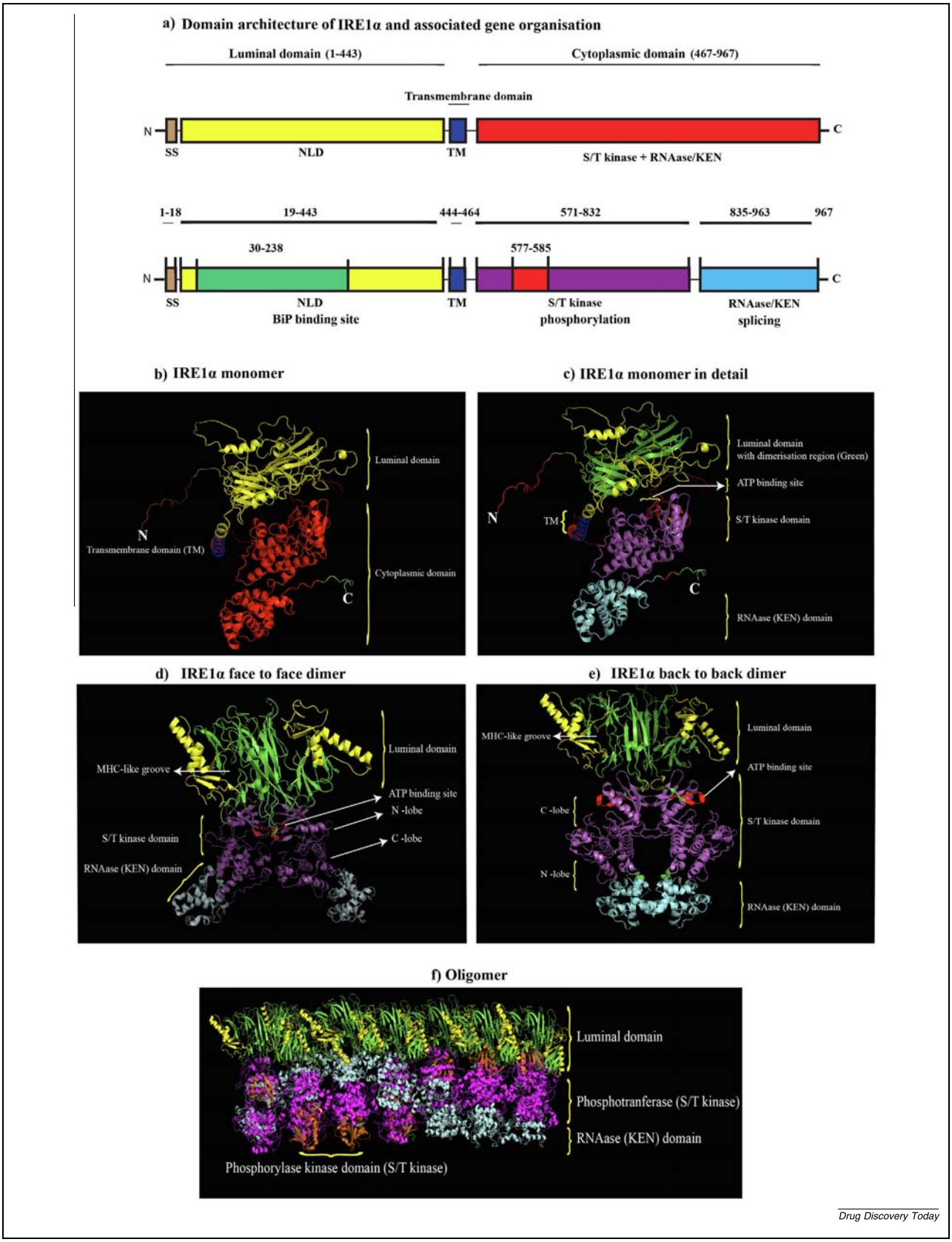

Drug Discovery Today

adaptive mechanisms that support tumor growth and metastasis, including enhanced protein folding, elimination of misfolded proteins and modulation of survival and proliferation signaling pathways.

Given the crucial role of the IRE1α pathway in GC progression, it presents a promising therapeutic target. Targeting IRE1α signaling could impair the ability of cancer cells to handle ERS, potentially leading to decreased survival and proliferation. Understanding the functional significance of IRE1α activation in GC provides valuable insights into potential therapeutic strategies. This review explores the link between IRE1α-directed signaling and the UPR, elucidating their impact on cancer cell dynamics and highlighting potential avenues for therapeutic intervention.

IRE1α: Molecular events in activation and signal transduction

Structure

IRE1, a type I transmembrane protein in the ER, is present in two distinct variants: IRE1α, widely expressed throughout various tissues, and IRE1β, exclusively seen in the intestinal epithelium.[p10],[p11] Like transforming growth factor (TGF)-β, both forms showcase dual enzymatic functions comprising serine/threonine kinase and endoribonuclease activities, activated through ligand-induced dimerization within their cytoplasmic domain. The N-terminal luminal domain (NLD: residues 1–443) acts as an ERS detector, activating independently of ligands. Remarkably, IRE1α proteins possess a signal sequence (SS: residues 1–18) at their N terminus, potentially directing their localization to the ER, and residues 30–238 are the BiP binding site. The cytoplasmic region comprises a kinase domain spanning residue 571–832, featuring a distinctive ATP-binding site (residues 577–585) and a kinase-extension nuclease (KEN)/RNase domain (residues 835–963), distinguished by its helical structure.[p12],[p13],[p14] The kinase domain showcases specific structural elements such as the C-helix, activation segment and disordered residues containing potential phosphorylation sites, whereas the RNase domain exhibits ordered helices and connections.[p6],[p15] The kinase function of IRE1α initiates autophosphorylation, triggering activation of its endonuclease domain to cleave XBP1 (X-box binding protein 1) mRNA, ultimately leading to the generation of the transcriptionally active isoform XBP1s.[p16] Another study reveals a unique structure featuring an amphipathic helix (AH) within its transmembrane helix (TMH: residues 444–464) region. Positioned on the ER-luminal side, this AH enables IRE1α to sense changes in lipid bilayer properties such as thickness and packing density in addition to misfolded protein sensing[p17],[p18],[p19],[p20] (Figure 1a–c).

Activation

The BiP chaperone binds to the NLD of IRE1α, maintaining it in a monomeric conformation. Under ERS, BiP dissociates from IRE1α, allowing dimerization *via* H-bonding and hydrophobic interactions within the NLD. This dimerization forms a stable complex with an MHC-like (major histocompatibility complex) groove that does not require peptide binding, serving as a precursor to oligomerization. Oligomerization enhances IRE1α *trans*-autophosphorylation, a key step in activating its ribonuclease (RNase) activity.[p21],[p22] While phosphorylation has traditionally been viewed as the primary activator of IRE1α, recent studies suggest that conformational changes within its kinase domain play a more central role. RNase activity depends on intermolecular and intramolecular autophosphorylation, with specific amino acid residues being essential for function, independent of kinase activity.

Structural studies highlight differences between yeast and human IRE1α. Yeast IRE1α forms a back-to-back dimer facilitated by the αE0 helix, enabling higher-order oligomerization. By contrast, human IRE1α adopts a face-to-face dimer, where kinase domains interact and position Mg^{2+}-ADP-bound inter-lobe clefts in opposition. This configuration is crucial for transphosphorylation at Ser724. Unlike yeast IRE1α, which binds ADP only in a phosphorylated state, human IRE1α can bind Mg^{2+}-ADP even when dephosphorylated. Mutations in key interfacial residues impair autophosphorylation, underscoring the functional importance of this dimerization mode.[p6],[p23] These structural variations illustrate evolutionary differences in IRE1α activation across species.

During ERS, IRE1α oligomerizes within the ER membrane, forming clusters that act as temporary storage compartments, buffering against overactivation and selectively targeting mRNA substrates. Prolonged stress attenuates IRE1α signaling by dissolving oligomers, leading to dephosphorylation and reduced RNase activity. This refractive state is reversible upon stress resolution, reflecting dynamic regulation. IRE1α activation involves intricate molecular interactions and structural changes, making it a crucial component of cellular stress responses (Figure 1b–f). Understanding these mechanisms could provide therapeutic avenues for ERS-related diseases.

FIGURE 1

Structural insights into IRE1α. **(a)** IRE1α consists of an N-terminal luminal domain (NLD) with a BiP binding site, a transmembrane region (TM) and a C-terminal cytoplasmic domain containing S/T kinase and RNase (KEN) domains. **(b)** The monomer includes a luminal domain (yellow), a transmembrane domain (blue) and a cytoplasmic domain (red). **(c)** Within the luminal domain, a dimerization domain (green) facilitates interactions, whereas the cytoplasmic domain contains an ATP-binding site (red) within the S/T kinase domain (violet) and the RNase (KEN) domain (cyan). **(d)** Under ER stress, misfolded proteins bind to the luminal domain, promoting face-to-face dimerization and *trans*-autophosphorylation of the kinase domains, which activates the RNase function, leading to XBP1 mRNA splicing and unfolded protein response (UPR) activation. **(e)** Back-to-back dimerization facilitates IRE1α oligomerization, contributing to its structural organization and regulation during ER stress, enabling dynamic control of its kinase and RNase activities. **(f)** Higher-order oligomers stabilize this activation, amplifying the UPR signal to enhance protein folding capacity and degrade misfolded proteins. (For interpretation of the references to colour in this figure legend, the reader is referred to the web version of this article)

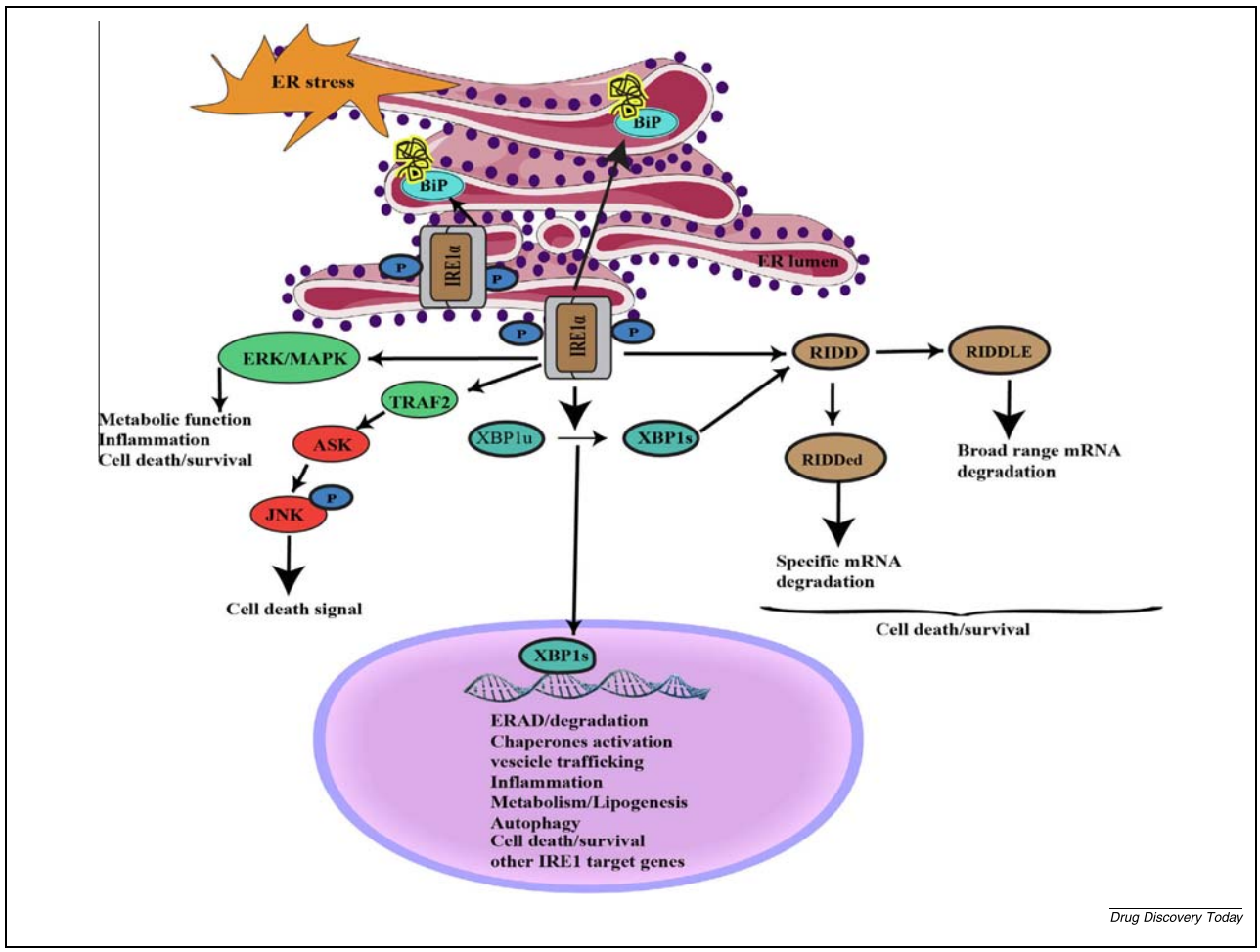

FIGURE 2

IRE1α signaling pathway. Dimerized and phosphorylated IRE1α activates its RNase, processing XBP1u mRNA into active XBP1s transcription factor. XBP1s regulates protein folding, ERAD, chaperone activity, inflammation and cell survival decisions. IRE1α mediates RIDD, degrading mRNAs dependent on RIDD end motifs and those that are RIDD RIDDLE. Additionally, IRE1α activates stress pathways such as TRAF2/ASK/JNK and ERK/MAPK pathways.

Signaling

IRE1α exhibits both RNase and kinase activities, with phosphorylation within its activation loop triggering self-association and signal transduction. Conformational changes shift IRE1α from face-to-face to back-to-back dimers, activating the kinase domain and segregating the RNase domains.[p10] IRE1α signaling has two significant outcomes: XBP1 splicing and regulated IRE1α-dependent decay (RIDD).[p24] Additionally, IRE1α can activate the TRAF2/ASK1/JNK (TNF receptor-associated factor 2/apoptosis signal-regulating kinase 1/c-Jun N-terminal kinase) and ERK/MAPK (extracellular signal-regulated kinase/mitogen-activated protein kinase) pathways.[p25],[p26]

During ERS, IRE1α splices XBP1 mRNA, producing the transcriptionally active XBP1s, which regulate genes involved in ERAD, chaperone expression, vesicle trafficking and inflammation.[p27],[p28] XBP1s promotes cell survival, whereas its unspliced form, XBP1u, acts as a negative regulator.[p29] RNase activity of IRE1α also mediates regulated IRE1-dependent decay (RIDD), which selectively degrades mRNAs, miRNAs and rRNAs. RIDD operates through two mechanisms: endomotif-directed degradation (RIDDed) and the broader, motif-independent RIDDLE pathway.[p30],[p31] Notably, despite its role in degrading ER-targeted mRNAs, RIDD does not cleave XBP1 mRNA, ensuring XBP1 stability during UPR activation.[p32],[p33] MANF (mesencephalic astrocyte-derived neurotrophic factor) has been shown to inhibit the phospho-oligomer-dependent RIDDLE pathway, promoting cell survival[p34] (Figure 2).

IRE1α-mediated RIDD can be cytoprotective or proapoptotic, depending on ERS intensity and duration. Whereas basal RIDD maintains ER homeostasis, excessive stress hyperactivates RIDD, promoting apoptosis by degrading survival-related mRNAs. Prolonged IRE1α activation shifts its function from stress alleviation to apoptotic signaling.[p35] Small-molecule inhibitors targeting the IRE1α RNase and kinase domains have been explored, with ATP mimetics modulating RNase activity independently of phosphorylation.[p36],[p37] The balance between XBP1 splicing and

RIDD determines cell fate, with mild stress favoring cytoprotective responses, whereas prolonged ERS shifts IRE1α toward apoptotic pathways.[p38],[p39] IRE1α also activates JNK signaling by recruiting TRAF2 and ASK1 independently of RNase activity.[p40],[p41],[p42] RNH1 (ribonuclease/angiogenin inhibitor 1) modulates IRE1α by suppressing RNase activity during ERS, whereas USP14 (ubiquitin-specific protease 14), a deubiquitinating enzyme (DUB) acts as an ERAD inhibitor under normal conditions but is inactivated during ERS (Figure 2). IRE1α interacts with heat shock proteins (HSPs), PARP16, RNF13, Bax, Bak and BI-1, further influencing its activity and signaling pathways.

IRE1α signaling: Driving adaptation and survival in GC cells

GC cells adapt and survive through ERS and the UPR. In GCs, IRE1α plays a crucial part, with its reduced expression inhibiting growth and invasion. However, its function remains debated, requiring comprehensive analysis. IRE1α activation regulates key pathways, including XBP1 mRNA processing, RIDD and TRAF2/JNK-MAPK/ERK signaling, preserving ER function and cellular homeostasis without triggering apoptosis. Additionally, IRE1α activation promotes autophagy, inflammation and chemoresistance, facilitating tumor survival and progression.

Proliferation

Inhibition or genetic depletion of IRE1α reduces proliferation, impairs intestinal organoid growth and diminishes colon cancer stem cell (CSC) stemness. Chronic ER stress-induced activation of the IRE1α/XBP1 pathway enhances colorectal cancer (CRC) progression by promoting cell proliferation.[p43] Upregulated XBP1s and cyclin D1 drive the G1-to-S phase transition, facilitating tumor growth.[p44],[p45] The IRE1α–XBP1 axis also advances cancer proliferation *via* JNK phosphorylation and mRNA decay regulation.[p46] Additionally, the XBP1s–TAp73 (transactivation isoform of p73, a member of the p53 tumor suppressor family) axis, involving XBP1s interaction with the tumor suppressor TAp73, plays a crucial part in GC proliferation and colony formation.[p47]

XBP1 overexpression in colorectal adenocarcinomas disrupts cell differentiation regulation, contributing to colon carcinogenesis. Its elevated expression in post-resection patients with CRC or adenoma further supports its role in disease progression.[p48],[p49] Activated XBP1 oncogenic pathways regulate PIN1, a prolyl isomerase, highlighting its potential as a therapeutic target.[p50] PIN1 interacts with XBP1s in a phosphorylation-dependent manner, stabilizing XBP1 and promoting cancer cell proliferation and transformation.[p51] Notably, IRE1α inhibition suppresses colon cancer cell proliferation and CSC properties, preventing colitis-associated tumorigenesis[p52] (Figure 3a).

Studies reveal a regulatory interplay between XBP1 and Fbw7, forming a negative feedback loop in colon cancer progression. XBP1 interacts with Fbw7 (F-box and WD repeat domain-containing 7), leading to ubiquitination and degradation, highlighting the role of Fbw7 as a substrate recognition unit within the SKP1–Cullin–F-box-type-E3-ligase complex. This phosphorylation-dependent interaction underscores the significance of post-translational modifications in cancer regulation, facilitating XBP1 degradation and tumor development.[p53] Additionally, XBP1 variant 1 (Xv1) promotes colon cancer progression by upregulating tubulin tyrosine ligase like 6 (TTLL6), a polyglutamylase essential for mitosis, driving cancer cell division and proliferation[p54] (Figure 3a).

Epithelial-to-mesenchymal transition, metastasis and angiogenesis

XBP1 expression induced by ERS correlates with colon cancer invasiveness and angiogenesis during epithelial-to-mesenchymal transition (EMT). Elevated XBP1s in CRC indicates heightened ERS, marking it as a tumor progression factor.[p55] The IRE1α/XBP1 pathway drives CRC progression and EMT by promoting proliferation *via* the XBP1–cyclin-D1 axis. XBP1s directly binds to the cyclin D1 promoter, enhancing its expression and facilitating invasion and mitosis. Additionally, IRE1α–XBP1 signaling modulates EMT by reducing E-cadherin and increasing N-cadherin levels, underscoring its role in gastrointestinal metastasis.[p44],[p56]

Additionally, IRE1α regulates fibronectin-1 (FN1) expression, a key factor in colon cancer metastasis. Inhibiting IRE1α reduces XBP1s production, leading to decreased FN1 expression and impaired migration and invasion of colon cancer cells. This attenuation suppresses Src, FAK phosphorylation and downstream effectors, including RhoA, Rac1 and CDC42. Exogenous FN1 reverses Src/FAK phosphorylation and restores migration in IRE1α-knockdown cells. Additionally, XBP1s directly binds to the FN1 promoter, initiating its expression. These findings highlight the role of IRE1α in modulating metastatic potential by regulating FN1, influencing cell adhesion and extracellular matrix interactions.[p57]

A novel regulatory framework involving hypoxia-inducible factor (HIF)-1α and p53-responsive miR-34a governs tumor cell transitions between EMT and mesenchymal-epithelial transition (MET) under hypoxic conditions. Hypoxia-induced IRE1α/XBP1, coupled with mutated miR-34a, drives EMT, migration, invasion and chemoresistance in p53-mutated or deficient CRC cells, promoting lung metastasis.[p58] Additionally, dysregulated long non-coding RNAs (lncRNAs) and microRNAs (miRNAs) in CRC probably interact with IRE1α, affecting XBP1 splicing and disrupting proliferation and apoptosis regulation, contributing to CRC progression and metastasis.[p59]

In solid tumors including GC, angiogenesis supports growth and metastasis by forming new blood vessels in response to ischemia, hypoxia and nutrient deprivation. The UPR is activated under these conditions, with IRE1α playing a key part in coordinating cellular adaptation to ERS. The IRE1α/XBP1 pathway significantly influences angiogenesis and tumor progression by upregulating proangiogenic factors such as vascular endothelial growth factor (VEGF), fibroblast growth factor 2 (FGF2), interleukin 6 (IL6), IL8 and connective tissue growth factor (CTGF) in colorectal cancer (CRC).[p60],[p61] Overexpression of XBP1 enhances cancer cell invasiveness, which is suppressed by XBP1 knockout using small interfering RNA (siRNA). Additionally, XBP1 inhibition reduces VEGF receptor-2 (VEGF-R2) levels, suggesting XBP1 as a predictive biomarker for CRC invasion and metastasis. The correlation between XBP1 and VEGF-R2 is fur-

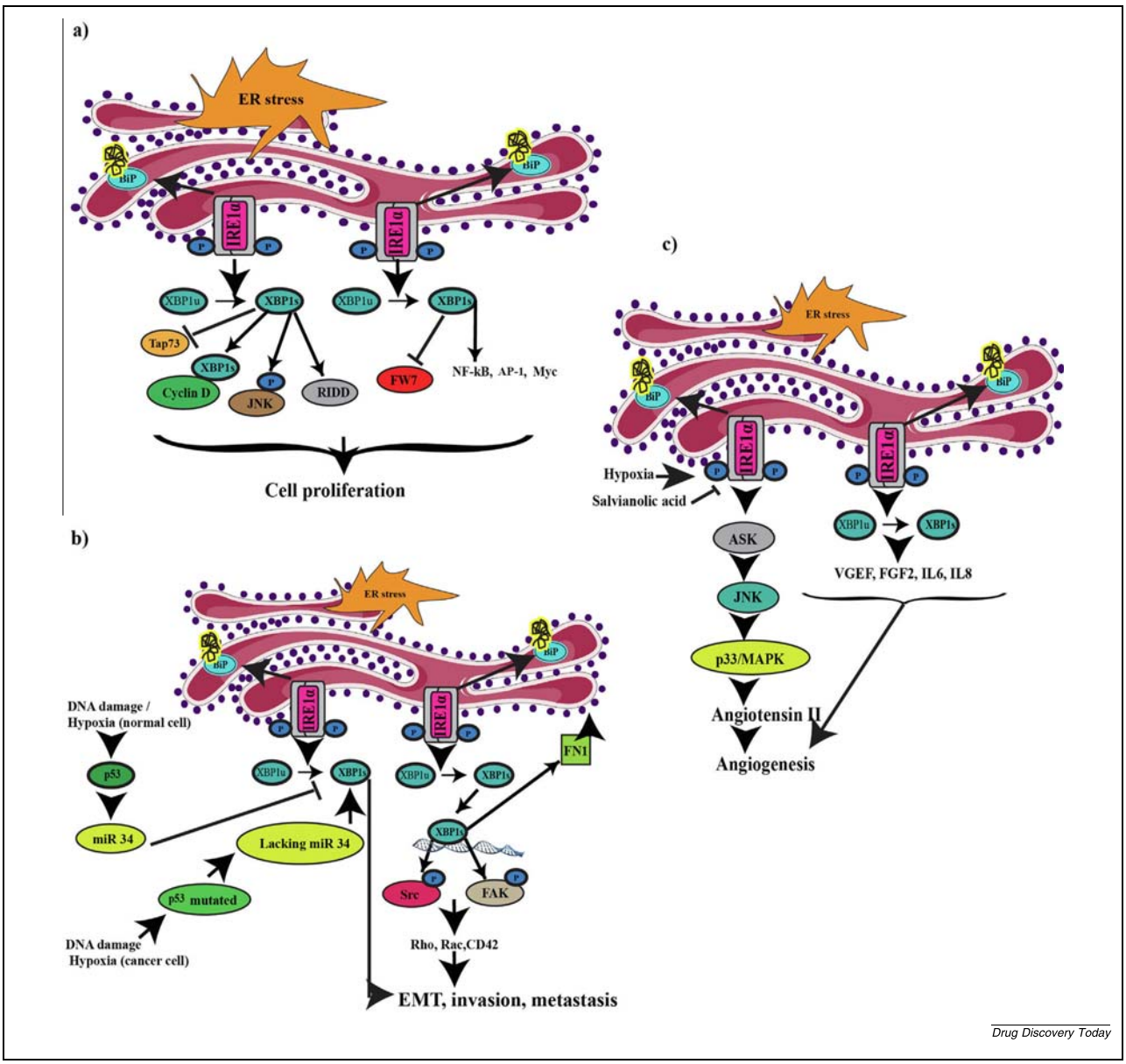

FIGURE 3

Role of IRE1α in GC progression. **(a)** Under extreme ER stress, IRE1α activation splices XBP1 mRNA into XBP1s, promoting cell cycle progression *via* cyclins, JNK phosphorylation and RIDD activation while enhancing proliferation through nuclear factor (NF)-κB, AP-1 and c-Myc. XBP1s inhibits TAp73 and prevents its degradation by FW7. **(b)** During metastasis, XBP1s drive epithelial-mesenchymal transition (EMT) by interacting with cyclin D, upregulating FN1 to enhance invasion and phosphorylating Src and FAK, influencing Rho, Rac and Cdc42. p53-deficient cells lack miR-34, which usually inhibits XBP1s. **(c)** Independently, IRE1α dimerization activates the ASK/JNK/p38/MAPK pathway, promoting angiogenesis via angiotensin II and angiogenic factors (VEGF, FGF2, IL6, IL8, CTGF), enhanced by hypoxia and inhibited by salvianolic acid.

ther evidenced in colon cancer cell lines treated with tunicamycin, highlighting its regulatory role in angiogenesis.[p61]

Experimental evidence highlights IRE1α activation as a crucial link between hypoxia, glucose deprivation and the upregulation of vascular endothelial growth factor-A (VEGF-A), a key regulator of angiogenesis.[p62],[p63] Cancer cells with dominant-negative or absent IRE1α exhibit impaired VEGF-A upregulation under ischemic conditions, emphasizing the role of IRE1α-dependent signaling in tumor adaptation.[p64] Inhibiting IRE1α signaling could disrupt these adaptive responses, attenuating angiogenesis and tumor growth. Additionally, hyperactivated IRE1α, independent of XBP1, drives regenerative intestinal stem cell (ISC) expansion under pathological UPR conditions.[p65] Targeting the IRE1/XBP1 pathway could thus serve as a promising

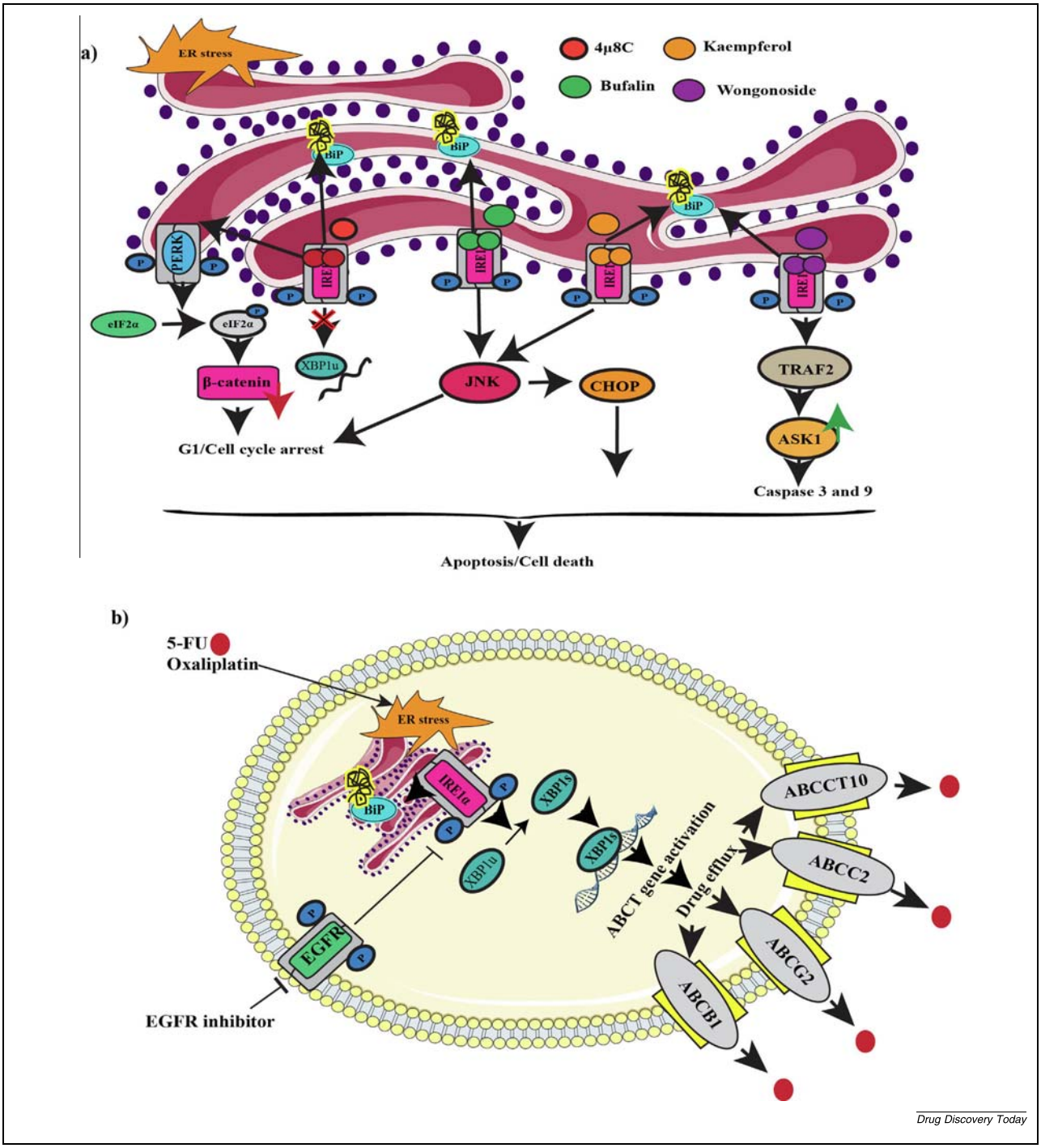

FIGURE 4

Targeting the IRE1α/XBP1 pathway and drug resistance in gastrointestinal cancer (GC). **(a)** 4μ8C inhibits IRE1α post-autophosphorylation, blocking XBP1u to XBP1s conversion, activating the PERK pathway, leading to eIF2α phosphorylation, reduced β-catenin levels, cell-cycle arrest and apoptosis. Bufalin and kaempferol inhibit phosphorylation and activate JNK/CHOP, inducing cell-cycle arrest, wogonoside activates TRAF2 and ASK1, triggering caspase-3/-6 and BAX/BCL2 pathways, ultimately leading to cell death. **(b)** XBP1s activate ABC transporter genes (ABCC10, ABCC2, ABCG2, ABCB1), promoting drug efflux and reducing 5-FU and oxaliplatin efficacy. EGFR inhibitors block XBP1s-induced drug resistance, highlighting EGFR activation as a driver of XBP1s-mediated resistance.

therapeutic approach for controlling angiogenesis and colon cancer progression. Salvianolic acid B (Sal B) demonstrates antiangiogenic effects by mitigating angiotensin II-induced angiogenesis, protecting endothelial cells from hypoxia-induced damage, and modulating the IRE1/ASK1/JNK/p38MAPK pathway, underscoring its therapeutic potential[p66] (Figure 3b,c).

Inhibitors of IRE1α

IRE1α inhibitors, categorized into type I and II kinase and RNase inhibitors, offer promising therapeutic potential with distinct mechanisms and applications.[p67],[p68]

Kinase inhibitors. Two distinct classes of kinase inhibitors, known as types I and II, have been identified, each stabilizing different conformational states of the kinase active site across various protein kinase targets. Type I kinase inhibitors bind to the ATP-binding site within the IRE1α kinase domain, preventing autophosphorylation and suppressing its RNase function. These inhibitors modulate the enzyme's activity by inducing conformational changes in the C-helix, shifting it from an active 'C-helix in' state to an inactive 'C-helix out' state. Key type I inhibitors include APY29, AT9283, sunitinib, dasatinib and VX-680 (MK-0457). Conversely, type II kinase inhibitors attach to an allosteric site near the ATP-binding pocket, stabilizing the kinase domain in its inactive state. This interaction inhibits autophosphorylation and RNase activity by preserving the DFG motif in the inward conformation (DFG-in) and engaging with the ATP-binding site and the adjacent allosteric site. Furthermore, these inhibitors obstruct other IRE1 phosphorylation-dependent processes, including TRAF2 binding.[p6],[p69] Type II inhibitors include1-(4-(8-amino-3-isopropylimidazo[1,5-a]pyrazin-1-yl) naphthalen-1-yl)-3-(3-(trifluoromethyl) phenyl) urea and kinase-inhibiting RNase attenuators (KIRAs).[p6],[p68],[p70]

RNase inhibitors. IRE1α RNase inhibitors are crucial in the cellular response to ERS by inhibiting the endonuclease activity of IRE1, thereby preventing XBP1 mRNA splicing and RIDD functions. These inhibitors can allosterically disrupt or stabilize the active dimeric unit of IRE1, thereby inhibiting or stimulating its RNase activity. HTS utilizing luciferase-based reporter assays in cells and recombinant proteins *in vitro* has revealed several direct inhibitors. These inhibitors are distinguished by a common hydroxy-aryl-aldehyde (HAA) group, which selectively interacts with a specific lysine residue (Lys907) in the RNase domain. This interaction forms a stable imine through Schiff base linkage, effectively preventing site-specific mRNA splicing induced by ERS.[p71] The principal RNase inhibitors include 4μ8C, salicylaldehydes, HNA, OICR573, OICR464, B-I09, STF-083010, as well as the MKC analogs, namely MKC9989, MKC8866 and MKC3946.[p6],[p71],[p72],[p73]

Targeting IRE1α for GC therapy and drug resistance

Inhibitors targeting the kinase or RNase domain of IRE1α have shown promising results in treating gastric cancer.[p71],[p74] Inhibiting the IRE1α/XBP1 pathway activation, alone or in combination with conventional treatments, improves patient outcomes in gastric cancer by enhancing drug sensitivity and inducing cancer cell death.[p75] Targeting IRE1α with inhibitors like 4μ8C offers a promising strategy for treating colon cancer, reducing β-catenin levels and suppressing cancer cell proliferation and stemness through the PERK/eIF2 cascade. 4μ8C inhibits β-catenin signaling, triggers G1 cell-cycle arrest and reduces the formation of colon cancer cell spheres. Moreover, *in vivo* studies show that 4μ8C blocks tumor formation in xenograft assays, suggesting its potential as a treatment for colon cancer by targeting IRE1α RNase activity.[p52]

Bufalin, a cardiac glycoside derived from toads, explicitly binds the kinase domain of IRE1 in gastric cancer cells. This action induces apoptosis and halts proliferation by activating the IRE1/JNK pathway by triggering ERS. Autophagy is also implicated in bufalin-induced apoptosis.[p76] Similarly, kaempferol, a natural flavonoid, has been found to activate the IRE1/JNK/CHOP pathway, leading to autophagic cell death in gastric cancer.[p77] A bioactive compound, wogonoside, has demonstrated potential in inhibiting tumor growth and inducing apoptosis in gastric cancer cells by activating IRE1α-TRAF2-ASK1 signaling. Wogonoside treatment prompts apoptosis and ERS by upregulating caspase-3 and -9, modulating Bax/Bcl-2 expression and activating the ASK1/JNK pathway. Notably, it amplifies interactions between IRE1α, TRAF2 and ASK1, emphasizing the pivotal role of the IRE1α/TRAF2/ASK1 pathway as a crucial mediator of the antitumor effects of wogonoside.[p78] Furthermore, XBP1 peptide vaccination with immunomodulatory medicines might treat stomach tumors.[p79]

Moreover, exosome-mediated delivery of microRNA, miR-3184-5p, targets XBP1, modulating IRE1 activity in gastric cancer. This indicates that targeting IRE1α could suppress gastric cancer growth through the AKT and STAT3 pathways. Decreased expression of miR-3184-5p in gastric cancer patients can lead to dysregulation of the AKT, STAT3 and IRE1 pathways, thereby promoting the vitality of gastric cancer cells.[p80] Another significant finding is that the overexpression of ATP-binding cassette (ABC) transporters, particularly P-glycoprotein (P-gp), driven by XBP1, promotes ERS-associated multidrug resistance (MDR) in colon cancer by actively pumping out chemotherapeutic agents, thereby reducing their intracellular concentration and effectiveness.[p81],[p82] Furthermore, the drugs 5-fluorouracil (5-FU) and oxaliplatin stimulate IRE1α–XBP1s in CRC, enhancing resistance to chemotherapy.[p83],[p84] It was evident that 5-FU and oxaliplatin resistance in CRC treatment can arise through altered drug metabolism, increased DNA repair capacity, enhanced drug efflux and dysregulated apoptotic pathways.[p85] 5-FU-induced IRE1α–XBP1 signaling upregulates ABC transporter expression, including ABCB1, ABCC1 and ABCG2, in colon cancer cells.[p81] Along with that, IRE1α inhibition decreases ABCC10 expression and enhances oxaliplatin sensitivity.[p84],[p86]

EGFR is a transmembrane protein vital in cell growth, proliferation and survival. Inhibitors of EGFR effectively target CD44v9-expressing gastric cancer cells, potentially eradicating drug-resistant populations that withstand cytotoxic anticancer therapies.[p87] Moreover, the investigation highlights that targeting EGFR inhibits the IRE1α/XBP1s pathway, evading chemotherapy resistance in CRC cells and enhancing therapeutic efficacy[p84] (Figure 4).

Targeting IRE1α through inhibitors shows the potential to disrupt key signaling pathways, thereby enhancing the responsiveness of gastric cancer cells to therapeutic agents. The complex

interplay between IRE1α and drug resistance mechanisms, particularly involving ABC transporters and chemotherapy efficacy, underscores the need for targeted research to unravel how IRE1α modulation influences drug resistance and impacts therapeutic effectiveness in cancer treatment.

RACK1, an IRE1α-mediated biomarker, enhances IRE1α signaling by promoting its phosphorylation and XBP1 splicing, contributing to tumor progression therapy resistance, and serving as a potential therapeutic target in advanced hepatocellular carcinoma.[p88] Machine learning identified an XBP1s/LEF1-based prognostic signature, underscoring the IRE1α–XBP1s axis as a key driver and promising therapeutic target, particularly in cases with hyperactivated Wnt/LEF1 signaling.[p89]

IRE1α supports tumor survival by mitigating ER stress but can also induce apoptosis and autophagy when excessively activated, leading to cancer cell death. This threshold-dependent effect presents a therapeutic strategy for tumor regression. Overexpressing IRE1α in tumor cells enhances apoptosis and limits growth in immunocompetent mice, highlighting its potential as a target. Additionally, inhibiting ERO1L (endoplasmic reticulum oxidoreductin 1-like), linked to IRE1α signaling, increases autophagy and apoptosis in CRC cells, suggesting a synergistic approach to tumor suppression.[p90],[p91] Additionally, ERS-inducing agents are being tested in clinical trials for cancer treatment by exploiting the UPR to target cancer cells selectively. A small therapeutic molecule, ERX-41 acts on LIPA (lysosomal acid lipase A) to trigger ERS, sparing normal cells.[p92] Traditional chinese medicine (TCM) products show promise in enhancing drug sensitivity and reducing tumors.[p93] Similarly, FeC_2 selectively induces ERS in cancer cells without harming healthy ones.[p94]

Concluding remarks and future perspectives

In summary, investigating IRE1α signaling activation and its exploitation in GC cells reveals promising avenues for therapeutic intervention. By unravelling the intricate mechanisms underlying IRE1α-mediated adaptive responses, such as apoptosis and autophagy, researchers can develop targeted strategies to disrupt tumor progression. Notably, some downstream pathways of IRE1α are enhanced in survival and death pathways, leading to complexities in determining which cellular phenomenon predominates. One exciting possibility is that the crosstalk between IRE1α and other UPR arms could dictate whether the pathway promotes survival or triggers cell death. Future studies should focus on clarifying these interactions to refine precision medicine approaches tailored to individual patients. Ultimately, exploiting the vulnerabilities of IRE1α signaling offers a substantial opportunity to improve the effectiveness of current treatment approaches and improve patient outcomes in GC.

Author contributions

VVS: conceptualization, data curation, funding acquisition, investigation, writing – original draft. **BJ:** literature search, formatting. **AD:** editing, formatting. **CFB:** supervision, investigation. **TDB:** conceptualization, formal analysis, investigation, project administration, resources, supervision, validation, writing – review & editing.

Conflicts of interest

The authors affirm that they do not have any identifiable conflicting financial interests or personal affiliations that could potentially have influenced the findings presented in this manuscript.

Data availability

No data were used for the research described in the article.

Data availability

Data will be made available on request.

Acknowledgments

The authors acknowledge the Department of Biochemistry, Amala Cancer Research Centre, Thrissur, Kerala, for providing the necessary facilities and a supportive environment for this work. The first author is thankful to the Council of Scientific and Industrial Research (CSIR), New Delhi, for the financial support (no: 21/12/2014(ii)EU-V dt. 24/7/2015).

References

1. Thrift AP, Nguyen TH. Gastric cancer epidemiology. *Gastrointest Endosc Clin N Am*. 2021;31:425–439.
2. Apicella M, Corso S, Giordano S. Targeted therapies for gastric cancer: failures and hopes from clinical trials. *Oncotarget*. 2017;8:57654–57669. https://doi.org/10.18632/oncotarget.14825.
3. Yang WJ et al. Updates on global epidemiology, risk and prognostic factors of gastric cancer. *World J Gastroenterol*. 2023;29:2452–2468. https://doi.org/10.3748/wjg.v29.i16.2452.
4. Hetz C, Zhang K, Kaufman RJ. Mechanisms, regulation and functions of the unfolded protein response. *Nat Rev Mol Cell Biol*. 2020;21:421–438. https://doi.org/10.1038/s41580-020-0250-z.
5. Chen X, Shi C, He M, Xiong S, Xia X. Endoplasmic reticulum stress: molecular mechanism and therapeutic targets. *Signal Transduct Target Ther*. 2023;8:352. https://doi.org/10.1038/s41392-023-01570-w.
6. Siwecka N, Rozpędek-Kamińska W, Wawrzynkiewicz A, Pytel D, Diehl JA, Majsterek I. The structure, activation and signaling of IRE1 and its role in determining cell fate. *Biomedicines*. 2021;9. https://doi.org/10.3390/biomedicines9020156.
7. Zhang K et al. The UPR transducer IRE1 promotes breast cancer malignancy by degrading tumor suppressor microRNAs. *iScience*. 2020;23, 101503. https://doi.org/10.1016/j.isci.2020.101503.
8. Wang Y, Wang K, Jin Y, Sheng X. Endoplasmic reticulum proteostasis control and gastric cancer. *Cancer Lett*. 2019;449:263–271. https://doi.org/10.1016/j.canlet.2019.01.034.
9. Huang J et al. Unfolded protein response in colorectal cancer. *Cell Biosci*. 2021;11:26. https://doi.org/10.1186/s13578-021-00538-z.
10. Siwecka N, Rozpędek-Kamińska W, Wawrzynkiewicz A, Pytel D, Diehl JA, Majsterek I. The structure, activation and signaling of IRE1 and its role in determining cell fate. *Biomedicines*. 2021;9. https://doi.org/10.3390/biomedicines9020156.
11. Le Goupil S, Laprade H, Aubry M, Chevet E. Exploring the IRE1 interactome: from canonical signaling functions to unexpected roles. *J Biol Chem*. 2024;300, 107169. https://doi.org/10.1016/j.jbc.2024.107169.
12. Liu CY, Xu Z, Kaufman RJ. Structure and intermolecular interactions of the luminal dimerization domain of human IRE1alpha. *J Biol Chem*. 2003;278:17680–17687. https://doi.org/10.1074/jbc.M300418200.

13. Zhou J et al. The crystal structure of human IRE1 luminal domain reveals a conserved dimerization interface required for activation of the unfolded protein response. *Proc Natl Acad Sci U S A*. 2006;103:14343–14348. https://doi.org/10.1073/pnas.0606480103.
14. Lee KP, Dey M, Neculai D, Cao C, Dever TE, Sicheri F. Structure of the dual enzyme Ire1 reveals the basis for catalysis and regulation in nonconventional RNA splicing. *Cell*. 2008;132:89–100. https://doi.org/10.1016/j.cell.2007.10.057.
15. Adams CJ, Kopp MC, Larburu N, Nowak PR, Ali MMU. Structure and molecular mechanism of ER stress signaling by the unfolded protein response signal activator IRE1. *Front Mol Biosci*. 2019;6:11. https://doi.org/10.3389/fmolb.2019.00011.
16. Bartoszewska S, Sławski J, Collawn JF, Bartoszewski R. Dual RNase activity of IRE1 as a target for anticancer therapies. *J Cell Commun Signaling*. 2023;17:1145–1161. https://doi.org/10.1007/s12079-023-00784-5.
17. Halbleib K et al. Activation of the unfolded protein response by lipid bilayer stress. *Mol Cell*. 2017;67:673–684.e8. https://doi.org/10.1016/j.molcel.2017.06.012.
18. Ali MM et al. Structure of the Ire1 autophosphorylation complex and implications for the unfolded protein response. *Embo J*. 2011;30:894–905. https://doi.org/10.1038/emboj.2011.18.
19. Simpson MS et al. IRE1α recognizes a structural motif in cholera toxin to activate an unfolded protein response. *J Cell Biol*. 2024;223. https://doi.org/10.1083/jcb.202402062.
20. Bashir S, Pal D, Qadri O, Banday M, Fazili K. Quaternary structure analysis of IRE1. *microPubl Biol*. 2023;2023. https://doi.org/10.17912/micropub.biology.000763.
21. Dawes S et al. Molecular chaperone BiP controls activity of the ER stress sensor Ire1 through interactions with its oligomers. *bioRxiv*. 20242024.02.16.579620.
22. Kepp O, Bezu L, Kroemer G. The endoplasmic reticulum chaperone BiP: a target for immunogenic cell death inducers? *Oncoimmunology*. 2022;11, 2092328. https://doi.org/10.1080/2162402x.2022.2092328.
23. Li Y et al. Phosphorylation at Ser724 of the ER stress sensor IRE1α governs its activation state and limits ER stress–induced hepatosteatosis. *J Biol Chem*. 2022;298.
24. Iwakoshi NN, Lee AH, Vallabhajosyula P, Otipoby KL, Rajewsky K, Glimcher LH. Plasma cell differentiation and the unfolded protein response intersect at the transcription factor XBP-1. *Nat Immunol*. 2003;4:321–329. https://doi.org/10.1038/ni907.
25. Fung TS, Liu DX. The ER stress sensor IRE1 and MAP kinase ERK modulate autophagy induction in cells infected with coronavirus infectious bronchitis virus. *Virology*. 2019;533:34–44. https://doi.org/10.1016/j.virol.2019.05.002.
26. Fu F, Doroudgar S. IRE1/XBP1 and endoplasmic reticulum signaling — from basic to translational research for cardiovascular disease. *Curr Opin Physiol*. 2022;28, 100552. https://doi.org/10.1016/j.cophys.2022.100552.
27. Yoshida H, Matsui T, Yamamoto A, Okada T, Mori K. XBP1 mRNA is induced by ATF6 and spliced by IRE1 in response to ER stress to produce a highly active transcription factor. *Cell*. 2001;107:881–891. https://doi.org/10.1016/s0092-8674(01)00611-0.
28. Lin JH et al. IRE1 signaling affects cell fate during the unfolded protein response. *Science*. 2007;318:944–949. https://doi.org/10.1126/science.1146361.
29. Yoshida H, Uemura A, Mori K. pXBP1(U), a negative regulator of the unfolded protein response activator pXBP1(S), targets ATF6 but not ATF4 in proteasome-mediated degradation. *Cell Struct Funct*. 2009;34:1–10. https://doi.org/10.1247/csf.06028.
30. Le Thomas A et al. Noncanonical mRNA decay by the endoplasmic-reticulum stress sensor IRE1α promotes cancer-cell survival. *bioRxiv*. 2021.
31. Ottens F, Efstathiou S, Hoppe T. Cutting through the stress: RNA decay pathways at the endoplasmic reticulum. *Trends Cell Biol*. 2023. https://doi.org/10.1016/j.tcb.2023.11.003.
32. Cairrão F, Santos CC, Le Thomas A, Marsters S, Ashkenazi A, Domingos PM. Pumilio protects Xbp1 mRNA from regulated Ire1-dependent decay. *Nat Commun*. 2022;13:1587. https://doi.org/10.1038/s41467-022-29105-x.
33. Fu F, Doroudgar S. IRE1/XBP1 and endoplasmic reticulum signaling – from basic to translational research for cardiovascular disease. *Curr Opin Physiol*. 2022;28. https://doi.org/10.1016/j.cophys.2022.100552.
34. Kovaleva V et al. MANF regulates neuronal survival and UPR through its ER-located receptor IRE1α. *Cell Rep*. 2023;42, 112066. https://doi.org/10.1016/j.celrep.2023.112066.
35. Upton JP et al. IRE1α cleaves select microRNAs during ER stress to derepress translation of pro-apoptotic Caspase-2. *Science*. 2012;338:818–822. https://doi.org/10.1126/science.1226191.
36. Ghosh R et al. Allosteric inhibition of the IRE1α RNase preserves cell viability and function during endoplasmic reticulum stress. *Cell*. 2014;158:534–548. https://doi.org/10.1016/j.cell.2014.07.002.
37. Tomasio SM, Harding HP, Ron D, Cross BC, Bond PJ. Selective inhibition of the unfolded protein response: targeting catalytic sites for Schiff base modification. *Mol Biosyst*. 2013;9:2408–2416. https://doi.org/10.1039/c3mb70234k.
38. Maurel M, Chevet E, Tavernier J, Gerlo S. Getting RIDD of RNA: IRE1 in cell fate regulation. *Trends Biochem Sci*. 2014;39:245–254. https://doi.org/10.1016/j.tibs.2014.02.008.
39. Gómora-García JC, Gerónimo-Olvera C, Pérez-Martínez X, Massieu L. IRE1α RIDD activity induced under ER stress drives neuronal death by the degradation of 14-3-3 θ mRNA in cortical neurons during glucose deprivation. *Cell Death Discovery*. 2021;7:131. https://doi.org/10.1038/s41420-021-00518-9.
40. Nishitoh H et al. ASK1 is essential for endoplasmic reticulum stress-induced neuronal cell death triggered by expanded polyglutamine repeats. *Genes Dev*. 2002;16:1345–1355. https://doi.org/10.1101/gad.992302.
41. McQuiston A, Diehl JA. Recent insights into PERK-dependent signaling from the stressed endoplasmic reticulum. *F1000Res*. 2017;6:1897. https://doi.org/10.12688/f1000research.12138.1.
42. Urano F et al. Coupling of stress in the ER to activation of JNK protein kinases by transmembrane protein kinase IRE1. *Science*. 2000;287:664–666. https://doi.org/10.1126/science.287.5453.664.
43. Zarafshani M, Mahmoodzadeh H, Soleimani V, Moosavi MA, Rahmati M. Expression and clinical significance of IRE1-XBP1s, p62, and Caspase-3 in colorectal cancer patients. *Iran J Med Sci*. 2024;49:10–21. https://doi.org/10.30476/ijms.2023.96922.2856.
44. Jin C et al. Activation of IRE1α-XBP1 pathway induces cell proliferation and invasion in colorectal carcinoma. *Biochem Biophys Res Commun*. 2016;470:75–81. https://doi.org/10.1016/j.bbrc.2015.12.119.
45. Zuazo-Gaztelu I et al. A nonenzymatic dependency on inositol-requiring enzyme 1 controls cancer cell cycle progression and tumor growth. *bioRxiv*. 20232023.11.22.567905.
46. Liu S et al. XBP1s acts as a transcription factor of IRE1α and promotes proliferation of colon cancer cells. *Arch Biochem Biophys*. 2023;737, 109552. https://doi.org/10.1016/j.abb.2023.109552.
47. Ji H, Huang C, Wu S, Kasim V. XBP1-s promotes colorectal cancer cell proliferation by inhibiting TAp73 transcriptional activity. *Biochem Biophys Res Commun*. 2019;508:203–209. https://doi.org/10.1016/j.bbrc.2018.11.112.
48. Fujimoto T et al. Overexpression of human X-box binding protein 1 (XBP-1) in colorectal adenomas and adenocarcinomas. *Anticancer Res*. 2007;27:127–131.
49. Wang X, Song Y, Lu X, Zhang H, Wang T. Microcystin-LR regulates interaction between tumor cells and macrophages via the IRE1α/XBP1 signaling pathway to promote the progression of colorectal cancer. *Cells*. 2024;13. https://doi.org/10.3390/cells13171439.
50. Li Y et al. Prolyl isomerase Pin1 sculpts the immune microenvironment of colorectal cancer. *Cell Signal*. 2024;115, 111041. https://doi.org/10.1016/j.cellsig.2024.111041.
51. Chae U et al. Critical role of XBP1 in cancer signalling is regulated by PIN1. *Biochem J*. 2016;473:2603–2610. https://doi.org/10.1042/bcj20160482.
52. Li XX et al. Knockdown of IRE1α inhibits colonic tumorigenesis through decreasing β-catenin and IRE1α targeting suppresses colon cancer cells. *Oncogene*. 2017;36:6738–6746. https://doi.org/10.1038/onc.2017.284.
53. Chae U et al. A negative feedback loop between XBP1 and Fbw7 regulates cancer development. *Oncogenesis*. 2019;8:12. https://doi.org/10.1038/s41389-019-0124-4.
54. Zhong Y et al. XBP1 variant 1 promotes mitosis of cancer cells involving upregulation of the polyglutamylase TTLL6. *Hum Mol Genet*. 2022;31:2639–2654. https://doi.org/10.1093/hmg/ddac010.
55. Zarafshani M, Mahmoodzadeh H, Soleimani V, Moosavi MA, Rahmati M. Expression and clinical significance of IRE1-XBP1s, p62, and Caspase-3 in colorectal cancer patients. *Iran J Med Sci*. 2024;49:10.
56. Bahadori S et al. Application of XBP1s decoy oligodeoxynucleotide attenuates cancerous phenotype in Huh-7 hepatocellular carcinoma cells. *Cell J*. 2024;26:505–514.
57. Xie Y, Liu C, Qin Y, Chen J, Fang J. Knockdown of IRE1α suppresses metastatic potential of colon cancer cells through inhibiting FN1-Src/FAK-GTPases signaling. *Int J Biochem Cell Biol*. 2019;114, 105572. https://doi.org/10.1016/j.biocel.2019.105572.
58. Bouznad N, Rokavec M, Öner MG, Hermeking H. miR-34a and IRE1A/XBP-1(S) form a double-negative feedback loop to regulate hypoxia-induced EMT, metastasis, chemo-resistance and autophagy. *Cancers*. 2023;15. https://doi.org/10.3390/cancers15041143.

59. Wang Y, Zhang J, Zheng S. The role of XBP-1-mediated unfolded protein response in colorectal cancer progression-a regulatory mechanism associated with lncRNA-miRNA-mRNA network. *Cancer Cell Int*. 2021;21:488. https://doi.org/10.1186/s12935-021-02167-5.
60. Silvestre JS. Vascular endothelial growth factor and angiogenesis: the XBP1 games. *Circulation*. 2013;127:1644–1646. https://doi.org/10.1161/circulationaha.113.002336.
61. Mhaidat NM, Alzoubi KH, Abushbak A. X-box binding protein 1 (XBP-1) enhances colorectal cancer cell invasion. *J Chemother*. 2015;27:167–173. https://doi.org/10.1179/1973947815y.0000000006.
62. Drogat B et al. IRE1 signaling is essential for ischemia-induced vascular endothelial growth factor-A expression and contributes to angiogenesis and tumor growth in vivo. *Cancer Res*. 2007;67:6700–6707. https://doi.org/10.1158/0008-5472.Can-06-3235.
63. Chen X et al. Gastric cancer-secreted exosomal X26nt increases angiogenesis and vascular permeability by targeting VE-cadherin. *Cancer Sci*. 2021;112:1839–1852. https://doi.org/10.1111/cas.14740.
64. Chalmers F, Mogre S, Son J, Blazanin N, Glick AB. The multiple roles of the unfolded protein response regulator IRE1α in cancer. *Mol Carcinog*. 2019;58:1623–1630. https://doi.org/10.1002/mc.23031.
65. Niederreiter L et al. ER stress transcription factor Xbp1 suppresses intestinal tumorigenesis and directs intestinal stem cells. *J Exp Med*. 2013;210:2041–2056. https://doi.org/10.1084/jem.20122341.
66. Fan F, Liu F, Shen P, Tao L, Zhang H, Wu H. Salvianolic acid B, a new type I IRE1 kinase inhibitor, abrogates AngII-induced angiogenesis by interacting with IRE1 in its active conformation. *Clin Exp Pharmacol Physiol*. 2023;50:82–95. https://doi.org/10.1111/1440-1681.13726.
67. Wiese W, Siwecka N, Wawrzynkiewicz A, Rozpędek-Kamińska W, Kucharska E, Majsterek I. IRE1α inhibitors as a promising therapeutic strategy in blood malignancies. *Cancers (Basel)*. 2022;14. https://doi.org/10.3390/cancers14102526.
68. Wang L et al. Divergent allosteric control of the IRE1α endoribonuclease using kinase inhibitors. *Nat Chem Biol*. 2012;8:982–989. https://doi.org/10.1038/nchembio.1094.
69. Treiber DK, Shah NP. Ins and outs of kinase DFG motifs. *Chem Biol*. 2013;20:745–746. https://doi.org/10.1016/j.chembiol.2013.06.001.
70. Treiber Daniel K, Shah NP. Ins and outs of kinase DFG motifs. *Chem Biol*. 2013;20:745–746. https://doi.org/10.1016/j.chembiol.2013.06.001.
71. Raymundo DP, Doultsinos D, Guillory X, Carlesso A, Eriksson LA, Chevet E. Pharmacological targeting of IRE1 in cancer. *Trends Cancer*. 2020;6:1018–1030. https://doi.org/10.1016/j.trecan.2020.07.006.
72. Rong J et al. Cell-based high-throughput luciferase reporter gene assays for identifying and profiling chemical modulators of endoplasmic reticulum signaling protein, IRE1. *J Biomol Screen*. 2015;20:1232–1245. https://doi.org/10.1177/1087057115600414.
73. Tomasio SM, Harding HP, Ron D, Cross BC, Bond PJ. Selective inhibition of the unfolded protein response: targeting catalytic sites for Schiff base modification. *Mol BioSyst*. 2013;9:2408–2416.
74. Kim J et al. A novel and potent IRE1α RNase inhibitor, HM100168 as a promising therapeutic strategy in solid cancers. *Cancer Res*. 2024;84:3335.
75. Langlais T et al. Structural and molecular bases to IRE1 activity modulation. *Biochem J*. 2021;478:2953–2975. https://doi.org/10.1042/bcj20200919.
76. Zhao H, Li Q, Pang J, Jin H, Li H, Yang X. Blocking autophagy enhances the pro-apoptotic effect of bufalin on human gastric cancer cells through endoplasmic reticulum stress. *Biol Open*. 2017;6:1416–1422. https://doi.org/10.1242/bio.026344.
77. Kim TW, Lee SY, Kim M, Cheon C, Ko SG. Kaempferol induces autophagic cell death via IRE1-JNK-CHOP pathway and inhibition of G9a in gastric cancer cells. *Cell Death Dis*. 2018;9:875. https://doi.org/10.1038/s41419-018-0930-1.
78. Gu Q, Zhu C, Wu X, Peng L, Huang G, Hu R. Wogonoside promotes apoptosis and ER stress in human gastric cancer cells by regulating the IRE1α pathway. *Exp Ther Med*. 2021;21:411. https://doi.org/10.3892/etm.2021.9842.
79. Bae J et al. Heteroclitic XBP1 peptides evoke tumor-specific memory cytotoxic T lymphocytes against breast cancer, colon cancer, and pancreatic cancer cells. *Oncoimmunology*. 2014;3, e970914. https://doi.org/10.4161/21624011.2014.970914.
80. Lin S, Que Y, Que C, Li F, Deng M, Xu D. Exosome miR-3184-5p inhibits gastric cancer growth by targeting XBP1 to regulate the AKT, STAT3, and IRE1 signalling pathways. *Asia Pac J Clin Oncol*. 2023;19:e27–e38. https://doi.org/10.1111/ajco.13663.
81. Gao Q et al. IRE1α-targeting downregulates ABC transporters and overcomes drug resistance of colon cancer cells. *Cancer Lett*. 2020;476:67–74. https://doi.org/10.1016/j.canlet.2020.02.007.
82. Zhao N et al. Pharmacological targeting of MYC-regulated IRE1/XBP1 pathway suppresses MYC-driven breast cancer. *J Clin Invest*. 2018;128:1283–1299. https://doi.org/10.1172/jci95873.
83. Abbasi S et al. Inhibition of IRE1 RNase activity modulates tumor cell progression and enhances the response to chemotherapy in colorectal cancer. *Med Oncol*. 2023;40:247. https://doi.org/10.1007/s12032-023-02105-7.
84. Huo M et al. EGFR targeting enhances the efficiency of chemotherapy through inhibiting IRE1α-XBP1s pathway in colorectal cancer cells. *J Cancer*. 2020;11:4464–4473. https://doi.org/10.7150/jca.44234.
85. Blondy S, David V, Verdier M, Mathonnet M, Perraud A, Christou N. 5-Fluorouracil resistance mechanisms in colorectal cancer: from classical pathways to promising processes. *Cancer Sci*. 2020;111:3142–3154. https://doi.org/10.1111/cas.14532.
86. Kryczka J, Boncela J. Integrated bioinformatics analysis of the hub genes involved in irinotecan resistance in colorectal cancer. *Biomedicines*. 2022;10. https://doi.org/10.3390/biomedicines10071720.
87. Mashima T et al. In silico chemical screening identifies epidermal growth factor receptor as a therapeutic target of drug-tolerant CD44v9-positive gastric cancer cells. *Br J Cancer*. 2019;121:846–856. https://doi.org/10.1038/s41416-019-0600-9.
88. Pavlović N, Heindryckx FJB. Exploring the role of endoplasmic reticulum stress in hepatocellular carcinoma through mining of the human protein atlas. *Biology (Basel)*. 2021;10:640.
89. Zhang T et al. Targeting the IRE1α-XBP1s axis confers selective vulnerability in hepatocellular carcinoma with activated Wnt signaling. *Oncogene*. 2024;43:1233–1248. https://doi.org/10.1038/s41388-024-02988-4.
90. Martinez-Turtos A et al. IRE1α overexpression in malignant cells limits tumor progression by inducing an anti-cancer immune response. *Oncoimmunology*. 2022;11, 2116844.
91. Chen P, Chen Y, Sharma A, Maria A-G-C, Schmidt-Wolf IG. Inhibition of ERO1L induces autophagy and apoptosis via endoplasmic reticulum stress in colorectal cancer. *Cell Signal*. 2025;127, 111560.
92. Eslami M, Memarian M, Yousefi BJV. ERX-41; Promising compound by targeting LIPA is a new achilles heel therapeutic strategy for hard-to-treat solid tumors by induction of endoplasmic reticulum stress. *Vacunas (English Ed)*. 2023;24:348–357.
93. Li Q, Zhao X, Yang H, Zhu X, Sui X, Feng J. Modulating endoplasmic reticulum stress in gastrointestinal cancers: insights from traditional Chinese Medicine. *Pharmaceuticals (Basel)*. 2024;17:1599.
94. Klemt I et al. 3D-shaped binders of unfolded proteins inducing cancer cell-specific endoplasmic reticulum stress in vitro and in vivo. *J Am Chem Soc*. 2023;145:22252–22264.

Glossary

ABCB1: ATP-binding cassette subfamily B member 1
ATF4: activating transcription factor 4
ATF6: activating transcription factor 6
BAX: BCL2-associated X protein (proapoptotic)
BCL2: B-cell lymphoma 2 (antiapoptotic)
BiP: binding immunoglobulin protein
CHOP: C/EBP homologous protein
EGFR: Epidermal growth factor receptor
eIF2a: eukaryotic initiation factor 2 alpha
GRP78: glucose-regulated protein 78
IRE1a: inositol-requiring enzyme type 1 alpha
PERK: protein kinase RNA-like ER kinase
XBP1u: unspliced X-box binding protein 1

Mapana – Journal of Sciences
2025, Vol. 24, No. 1, 1-22
ISSN 0975-3303 | https://doi.org/10.12723/mjs.72.1

Palmitic acid-induced endoplasmic reticulum stress links metabolic stress to senescence and regulates cell fate via PERK signalling in colon cancer cells

Valappan Veetil Soumya*, Snijesh Valiya Parambath†, Chevookaren Francis Binoy‡ Achuthan C Raghavamenon*, Suraj Kadunganattil* and Thekkekara Devassy Babu*

Abstract

Palmitic acid, a saturated fatty acid, promotes cancer progression and induces endoplasmic reticulum stress, which is associated with a misfolded/unfolded protein response. The study aims to explore the impact of metabolic stress induced by palmitic acid on cell fate decisions in colon cancer cell HCT15, with a specific focus on PERK signalling that connects metabolic stress to senescence. In the MTT assay, the $IC_{50\ was}$ determined to be 186 µM. The uptake of palmitic acid was confirmed by Oil Red O staining. Based on MTT and colony formation assays, the survival doses were identified as 50–100 µM, while lethal doses were determined to be 150–200 µM. Palmitic acid-induced oxidative stress is evidenced by increased ROS production, elevated MDA levels, and alterations in antioxidant activities. ER stress, driven by protein misfolding, was further confirmed through Thioflavin T staining. Gene expression analysis at survival doses revealed upregulation of ER stress and oxidative stress-related genes, including *Bip, CHOP, PERK, ATF4, Nrf2*, and *HO-1*, highlighting their role in promoting stress tolerance. Bioinformatics analysis of GEO datasets on senescence in HCT15 cells revealed a PERK-mediated pathway, supporting a link

* Department of Biochemistry, Amala Cancer Research Centre (Recognized Centre of University of Calicut), Thrissur - 680 555, Kerala, India, Email: soumyavvknr@gmail.com, raghav@amalaims.org, surajk@amalaims.org, babutharakan@gmail.com.

† Division of Molecular Medicine, St. John's Research Institute, Bangalore - 560 034 Karnataka, India. Email: snijesh@gmail.com.

‡ Research and Post-Graduate Department of Zoology, St. Thomas College (Autonomous), Thrissur – 680 001, Affiliated to University of Calicut, Kerala, India. Email: drcfbinoy@gmail.com.

between palmitic acid-induced metabolic stress and senescence. This study emphasises the critical role of palmitic acid-induced ER stress in connecting metabolic stress to senescence in colon cancer cells and the involvement of PERK signalling as a key mediator in this process. These insights provide a deeper understanding of how metabolic stress contributes to senescence, potentially revealing new therapeutic targets for managing colon cancer progression.

Keywords: Palmitic acid; ER stress; UPR; senescence; PERK pathway; colon cancer

1. Introduction

Palmitic acid, a saturated fatty acid prevalent in diets, has been linked to various cancers, influencing tumour growth and metastasis [1, 2]. This dietary component, commonly found in palm oil, dairy products, meats and processed food, has been reported to affect cellular functions by modulating lipid metabolism and promoting the development of a pro-tumorigenic microenvironment. Among its diverse biological effects, it was evident that palmitic acid induces endoplasmic reticulum (ER) stress by overwhelming the protein-folding machinery, thereby activating the unfolded protein response (UPR)[3]. Usually, the UPR is an adaptive mechanism designed to restore cellular balance; however, prolonged or dysregulated ER stress can significantly affect cell fate, potentially promoting either survival or cell death [4].

The UPR is a complex signalling network regulated by three key stress regulators, including protein kinase R-like ER kinase (PERK), activating transcription factor 4 (ATF4), and C/EBP homologous protein (CHOP) [5, 6]. These sensors regulate cell fate under ER stress by balancing protein-folding and cellular needs, promoting survival under mild stress, and initiating apoptosis under extreme stress [7, 8]. Among these, the PERK signalling axis is critical in modulating cell fate. Activation of PERK phosphorylates the eukaryotic initiation factor 2α (eIF2α), which reduces overall protein synthesis by selectively promoting the translation of activating transcription factor 4 (ATF4).ATF4, in turn, modulates genes involved in redox homeostasis, autophagy, and apoptosis, with downstream effectors such as C/EBP homologous protein (CHOP) playing pivotal roles in determining cell survival or death [5, 6].

In cancer, sustained ER stress often shifts the function of UPR from a transient adaptive response to a chronic survival mechanism, enabling tumour cells to endure unfavourable conditions such as nutrient deprivation, hypoxia, and therapeutic stress [9, 10]. Metabolic stress in cancer, caused by factors like nutrient deprivation and altered metabolism, exacerbates cellular

challenges [11, 12]. This disrupts homeostasis and triggers a maladaptive shift in the UPR, leading to chronic activation of UPR pathways due to misfolded protein accumulation. The interplay between metabolic and ER stress creates a cycle that promotes tumour cell survival and adaptability, enhancing resistance to therapeutic interventions[13, 14]. Palmitic acid-induced metabolic stress adds another layer of complexity to ER stress in cancer. By altering lipid composition and disrupting ER membrane integrity, palmitic acid exacerbates protein misfolding and oxidative stress, leading to heightened ER stress. Oxidative stress, driven by excessive reactive oxygen species (ROS) production, was found to synergise with ER stress in promoting cancer cell survival and resistance to apoptosis [2]. Furthermore, the interplay between oxidative stress and UPR pathways enhances tumour cell adaptability, contributing to chemoresistance and disease progression [3].

Senescence, characterised by irreversible cell cycle arrest, is a crucial cellular response to various stressors. [15] Recent evidence indicates that ER stress, mediated through the PERK signalling pathway, significantly drives senescence under stress conditions.[16, 17]. Despite growing insights into ER stress in cancer, the role of palmitic acid-induced metabolic stress in colon cancer cell survival and its link to senescence remains unexplored. Furthermore, colon cancer is the most prevalent malignancy worldwide, with its progression significantly influenced by metabolic and inflammatory factors[18, 19]. This study investigates the effects of palmitic acid-induced metabolic and ER stress on HCT15 colon cancer cells, focusing on how UPR signalling modulates cell survival under these conditions. Through bioinformatics analysis of relevant GEO datasets examining factors such as hypoxia and glucose deprivation in HCT15 cells, this research delves into the contribution of ER stress to cellular senescence. The findings highlight a critical connection between the PERK/ATF4 pathway and senescence, emphasising its central role in metabolic stress responses and colorectal cancer progression. These insights pave the way for identifying novel therapeutic targets to overcome treatment resistance and curb cancer progression.

2. Materials and methods

2.1. Cell culture and treatment

HCT15 colon cancer cells, obtained from NCCS, were maintained in RPMI-1640 medium supplemented with FBS (10%) and penicillin/streptomycin (1%) under controlled conditions of 37°C and 5% CO_2. Cells were treated for 24 hours with palmitic acid (100 mM in ethanol stock), ensuring the final vehicle concentration in the culture medium remained below 0.2%.

2.2 Cytotoxicity and viability assays

Cell viability in HCT15 cells was assessed using the MTT assay and trypan blue exclusion [20, 21]. For the MTT assay, cells (5×10^3/well) were treated with increasing palmitic acid concentrations for 24 hrs, followed by MTT addition (5 mg/mL, 20 µL/well) and 4-hr incubation. Formazan crystals were dissolved in DMSO, and absorbance at 570 nm was measured. The viability of cells after palmitic acid treatment was confirmed using trypan blue exclusion by counting viable and dead cells with a hemacytometer at 50-200 µm.

2.3. Lipid uptake analysis by Oil Red O staining

Neutral lipid accumulation was assessed using the Oil Red O staining method [22]. Post palmitic acid treatment, cells were washed with PBS, fixed with 4% formaldehyde, and stained with Oil Red O for 30 minutes. The stained cells were imaged, and lipid content was quantified by extracting the dye with isopropanol and measuring absorbance at 510 nm using a microplate reader.

2.4. Colony formation assay

Treated cells were PBS-washed, trypsinised, and reseeded at 3,000 cells per well in duplicate 6-well plates. After 15 days of incubation at 37°C, colonies were fixed with methanol and stained with 0.5% crystal violet. Images were captured using a phase-contrast microscope, colonies were counted, and the surviving fractions were calculated [23].

2.5. Reactive oxygen species (ROS) analysis

Treated cells were incubated with 10 µM DCFH-DA (2′,7′-dichlorodihydrofluorescein diacetate) for 30 minutes at 37°C. DCFH-DA was deacetylated intracellularly to DCFH, which ROS oxidised to form the fluorescent DCF. Fluorescence intensity was measured using a BioTek plate reader (excitation: 485 nm; emission: 530 nm). H2O2 (100µM) was treated as positive control 6 hrs before reading. ROS generation was quantified from normalised fluorescence intensity [24].

2.6. Analysis of antioxidant status and lipid peroxidation

Cell lysates were prepared, and total protein content was quantified [25]. Antioxidants, including catalase (CAT)[26], superoxide dismutase (SOD) [27], glutathione S-transferase (GST) [28, 29], glutathione reductase (GR) [30, 31], reduced glutathione (GSH)[32], and glutathione peroxidase (GPx) [33], were measured as described in the respective references. Lipid peroxidation was assessed by determining malondialdehyde (MDA) level using the TBARS method [34].

2.7. Thioflavin T staining for misfolded protein aggregation

Thioflavin T (ThT) staining was performed to visualise misfolded protein aggregates indicative of ER stress. Treated cells were fixed with 4% paraformaldehyde. After washing, cells were incubated with 0.01% ThT for 30 minutes in the dark. The cells were rewashed and imaged using a fluorescence microscope with excitation at 450 nm and emission at 482 nm. ThT fluorescence intensity was quantified using spectrofluorimetric analysis. Tunicamycin (3 µM) was used as a positive control and applied 6 hours before the reading [35].

2.8. Gene expression analysis by RT-*q*PCR

For gene expression analysis, cells treated with 50 µM and 100 µM palmitic acid were harvested for total RNA extraction using the RNeasy Mini Kit (Qiagen) following the manufacturer's protocol. RNA concentrations and purity were determined by spectrophotometry (Nanodrop 2000). Reverse transcription was performed using the Superscript IV Reverse Transcriptase, and RT-PCR was carried out with specific primers for genes involved in ER stress (BIP, CHOP, PERK, ATF4, IRE1, XBP1), oxidative stress (NQO1, HO-1, NRF2), and drug resistance markers. The reaction was performed on a Step OnePlus™ Real-Time PCR System. Relative Gene expression was measured using the $2^{-\Delta\Delta Ct}$ method, normalised to GAPDH [36].

Table 1: Human primer sequences used in the study were as follows:

Gene	Forwarded primer	Reverse primer	Product size
PERK	5'ATTGCATCTGCCTGGTTAC3'	5'GACTCCTTCCTTTGCCTGT3'	650
ATF4	5'CCAGCAAAGCACCGCAACA3'	5'CCATCCACAGCCAGCCATT3'	215
NRF2	5'AGACAAACATTCAAGCCGCT3'	5'CCATCTCTTGTTTGCTGCAG3'	438
NQO1	5'AAGGATGGAAGAAACGCCTGGAGA3'	5'GGCCCACAGAAAGGCCAAATTTCT3'	156
HO1	5'ACGCGTTGTAATTAAGCCTCGCAC3'	5'TTCCGCTGGTCATTAAGGCTGAGT3'	176
ATF6	5'CAGGGAGAAGGAACTTGTGA3'	5' ACTGACCGAGGAGACGAGA3'	344
CHOP	5'AAGGCACTGAGCGTATCATGT3'	5'TGAAGATACACTTCCTTCTTGAACA3'	105
GAPDH	5'GACATGCCGCCTGGAGAAAC3'	5'AGCCCAGGATGCCCTTTAGT3'	92

2.9. Analysis of GEO data from HCT15 colon cancer cells under ER Stress conditions

Gene expression data for HCT15 colon cancer cells under ER stress conditions (GSE227379) were analysed [37]. The dataset, generated on the Illumina NovaSeq 6000 platform, included nine samples: three biological replicates each for control, hypoxia ($CoCl_2$ treatment), and low-glucose conditions. Differential expression analyses compared hypoxia vs. control and low-glucose vs. control groups. Raw FASTQ files underwent quality control with FastQC, and low-quality reads, and adaptor sequences were removed using Trim Galore [38, 39]. High-quality reads were aligned to the GRCh38 reference genome using STAR, followed by gene quantification with feature

counts [40, 41].

Differential expression analysis was performed with DESeq2, which accounts for biological variability and library size differences [42, 43]. Genes with a fold change ≥1.5 and adjusted p-value <0.05 were identified as significantly differentially expressed. Common DEGs between hypoxia and low-glucose conditions were determined using a Venn diagram. KEGG signalling pathway analysis using ShinyGO 0.82 identified significantly enriched pathways (FDR < 0.05), excluding genes without KEGG annotations. Functional analysis of the shared DEGs was conducted using ShinyGO for pathway enrichment, and a network visualisation of gene-pathway interactions was created in Cytoscape. (Shinygo: http://bioinformatics.sdstate.edu/go77/)

2.10. Statistical analysis

The data analysis utilised Mean ± SEM (Standard Error of the Mean) with GraphPad Prism. For three independent in vitro experiments, one-way ANOVA was conducted for multiple comparisons, followed by Tukey's post-hoc test. Statistically significant results were indicated by p-values of * < *0.05,* ** < *0.01,* and *** < *0.001.*

3. Results

3.1 Impact of palmitic acid on cell viability, neutral lipid accumulation, and colony formation in HCT15 colon cancer cells

The toxicity of palmitic acid was initially evaluated in HCT15 colon cancer cells using the MTT assay, which revealed a dose-dependent effect with an IC50 of 186 µM (Fig. 1A). Based on this IC_{50} value, doses of 50, 100, 150, and 200 µM were selected for further analysis. The trypan blue assay confirmed dose-dependent cell viability with the following results: 79.63 ± 0.52%, 68.72 ± 1.45%, 57.87 ± 1.01%, and 47.24 ± 1.7% at 50, 100, 150, and 200 µM, respectively (Fig. 1B). Palmitic acid uptake was measured using Oil Red O staining, which proved the accumulation of neutral lipids in cells at the specified concentrations (Fig.1C). Spectrophotometric analysis of lipid uptake revealed a progressive increase in intracellular lipid content up to 150 µM, with relative values of 2.02 ± 0.31, 2.53 ± 0.51, and 2.80 ± 0.38, respectively. However, at 200 µM, lipid accumulation decreased to 2.23 ± 0.29, suggesting significant toxicity at this concentration (Fig. 1D).

A colony formation assay was performed to evaluate cell survival doses further. Results showed that the cells formed healthy colonies at 50 and 100 µM palmitic acid after treatment, while colony formation was significantly reduced at 150 and 200 µM (Figure 1E). The survival fractions were 0.88 ± 0.02, 0.79 ± 0.19, 0.05 ± 0.009, and 0.005 ± 0.001 for 50, 100, 150, and 200 µM, respectively (Fig. 1F), indicating a sharp decline in survival at 150 and 200 µM.

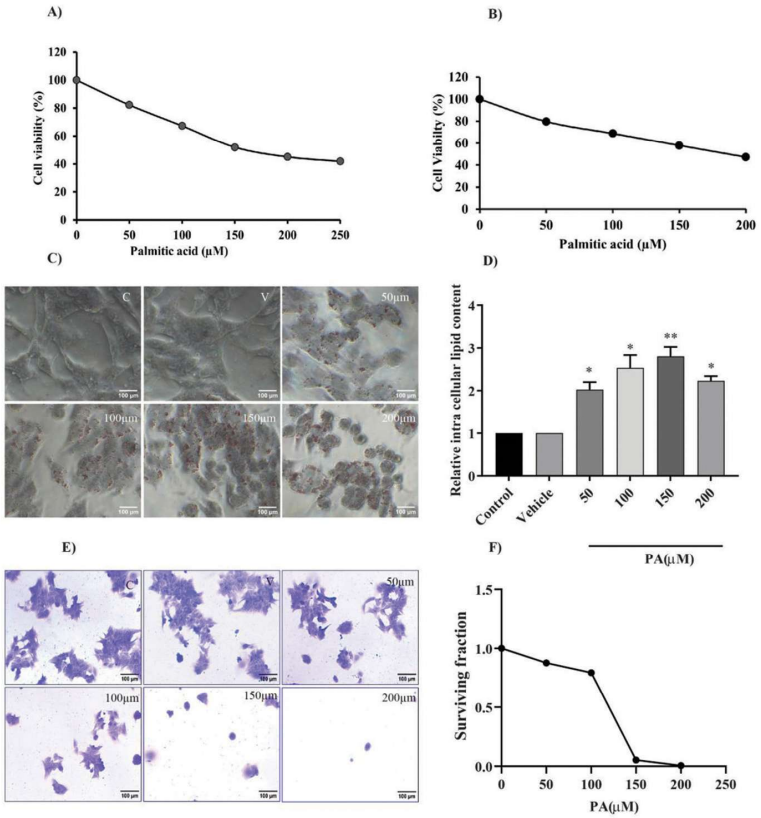

Figure 1: Effects of PA on viability, lipid accumulation, and colony formation in HCT15 cells. HCT15 cells treated with varying PA concentrations of 50,100,150 and 200 were assessed for cytotoxicity by MTT assay (A) and viability by Trypan blue exclusion (B). Lipid accumulation was evaluated through Oil Red O staining with phase-contrast microscopy (magnification 400x, scale bar 100um) (C) and quantified as relative intracellular lipid content (D). Colony formation was examined via crystal violet staining (E), and the survival fraction was calculated relative to controls (F). Statistical significance was assessed using one-way ANOVA and Tukey's post-hoc test, with significance levels indicated as **P < 0.01, *P < 0.05.

3.2 Palmitic acid triggers oxidative stress in colon cancer cells

The exposure of HCT15 cells to palmitic acid resulted in a marked elevation of ROS levels, as indicated by a dose-dependent increase in the green fluorescence intensity of DCFH-DA (Fig.2A). Spectrofluorimetric analysis of palmitic acid-treated cells revealed the following relative fold changes in fluorescence intensity: 1.92 ± 0.15, 2.21 ± 0.21, 2.35 ± 0.29, and 1.94 ± 0.32 at palmitic acid concentrations of 50, 100, 150, and 200 µM, respectively. The reduction in fluorescence intensity at 200 µM is likely attributed to reduced cell viability due to the extreme toxicity of palmitic acid (Fig.2B).

Further analysis of antioxidant levels demonstrated an increase in SOD and CAT at 50 and 100 µM palmitic acid, followed by a decline at 150 µM. Glutathione-related antioxidants, including GST, GR, GPx, and GSH, remained stable up to 100 µM but decreased significantly at 150 µM. The MDA level, a lipid peroxidation marker, remained stable up to 100 µM but increased substantially at 150 µM (Fig. 2C & Table 2).

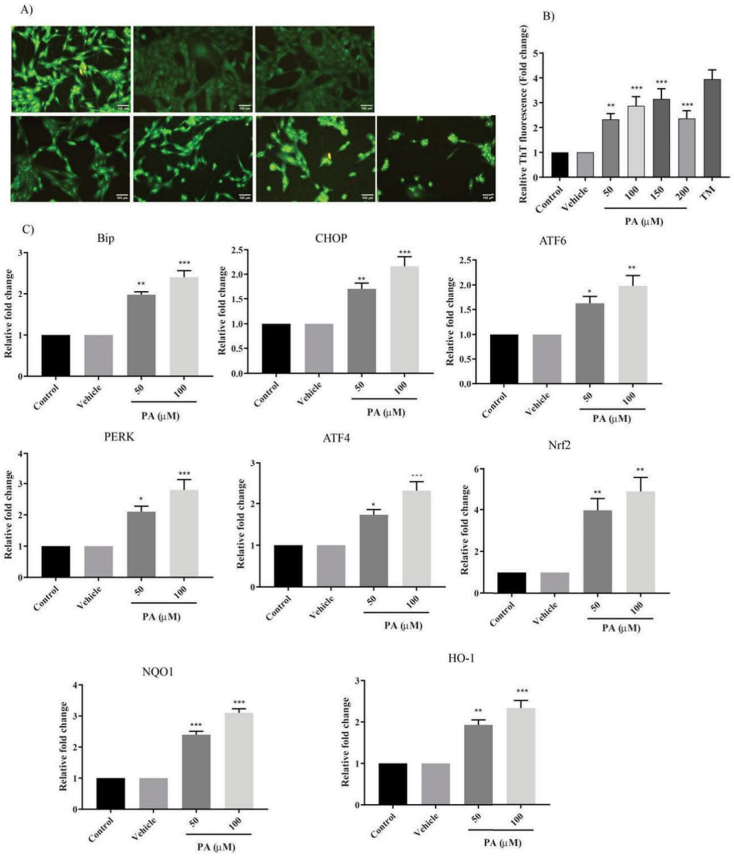

Figure 2: Palmitic acid-induced oxidative stress in colon cancer cells. HCT15 cells treated with PA were subjected to oxidative stress analysis. **(A)** Fluorescent microscopic images of DCFH-DA staining for ROS detection, captured at 400× magnification (scale bar: 100 µm). **(B)** Quantitative spectrofluorimetric analysis of relative DCF fluorescence expressed as relative fold change. **(C)** Graphical representation of the levels of different antioxidants and MDA following PA treatment. Data are presented as mean ± SEM, with statistical significance indicated by ***$p < 0.001$, *$p < 0.05$ and **$p < 0.01$.

Table 2: Elevated antioxidant levels and MDA in palmitic acid-treated HCT15 cell lysates:

Enzymes	Control	Vehicle	50μm	100μm	150μm	200μm
SOD	15.23±2.97	16.12±3.07	27.53±3.59*	35.9±4.02***	41.23±4.62***	24.38±3.71
CAT	9.26±0.93	9.18±1.11	16.91±1.99**	19.17±2.37**	22.86 ±3.2***	10.60±2.48
GST	3.24± 0.31	3.36±0.35	3.412±0.21	3.324±0.34	2.34±0.23*	2.19±0.239**
GR	4.24±0.52	4.39±0.416	4.647±0.52	4.72±0.39	3.02±0.31*	2.36±0.34**
GPX	15.2±2.14	15.02±2.37	14.09±2.38	13.72±2.13	8.56±2.16*	3.41±0.52
GSH	15.23±2.5	15.41±2.42	14.92±3.33	14.80±3.46	12.9±2.74*	7.49±2.95**
MDA	115.33±9.8	114.27±7.99	126.36±11.75	130.26±10.88	161.17±12.05**	91.33±10.3

3.3 Palmitic acid-induced metabolic stress in HCT15 colon cancer cells

palmitic acid-induced metabolic stress in HCT15 colon cancer cells across all tested concentrations (50, 100, 150, and 200 μM), as evidenced by increased lipid accumulation, elevated reactive oxygen species (ROS) production, and altered antioxidant levels. At 50 and 100 μM, cells demonstrated tolerance to the induced stress, characterised by upregulated antioxidant responses. However, exposure to 150 and 200 μM palmitic acid led to significant cytotoxicity, as reflected by a reduced colony-forming ability. These findings demonstrate the dose-dependent nature of palmitic acid-induced metabolic stress, where lower concentrations promote tolerance while higher concentrations induce cytotoxicity.

3.4 Influence of palmitic acid on ER stress and PERK/ATF4 Signalling in regulating antioxidant responses

The influence of palmitic acid on ER stress and PERK/ATF4 signalling in regulating antioxidant responses was investigated in HCT15 cells. Increased misfolded protein aggregates in palmitic acid-treated HCT15 cells were indicated by enhanced green fluorescence from Thioflavin T staining, reflecting elevated ER stress (Fig.3A). Quantitative analysis revealed relative fluorescence intensities of 2.33 ± 0.24, 2.87 ± 0.37, 3.15 ± 0.41, and 2.36 ± 0.31 for palmitic acid concentrations of 50, 100, 150, and 200 μM, respectively, with the positive control (Tunicamycin™) showing intensity of 3.95 ± 0.37. A dose-dependent increase in misfolded protein aggregates was observed up to 150 μM palmitic acid, with a decline in intensity at 200 μM due to extreme toxicity and cell loss (Fig.3A).

The levels of ER stress markers were measured for survival doses of palmitic acid at 50 and 100 μM. BIP expression exhibited fold changes of 1.98 ± 0.12 and 2.4 ± 0.27 at these doses. CHOP expression levels were 1.71 ± 0.20 and 2.16 ± 0.33, while ATF6 expression levels were 1.63 ± 0.23 and 1.98 ± 0.36. PERK expression levels were 2.1 ± 0.31 and 2.8 ± 0.57, and ATF4

expression levels were 1.73 ± 0.22 and 2.31 ± 0.37 for the 50 and 100 µM treatments, respectively. The antioxidant genes Nrf2, NQO1, and HO-1 were upregulated in response to palmitic acid. Nrf2 expression was 4.01 ± 0.98 and 4.93 ± 1.17, NQO1 expression was 2.40 ± 0.19 and 3.10 ± 0.23, and HO-1 expression was 1.93 ± 0.21 and 2.33 ± 0.32 at the two concentrations, respectively (Fig. 3C).

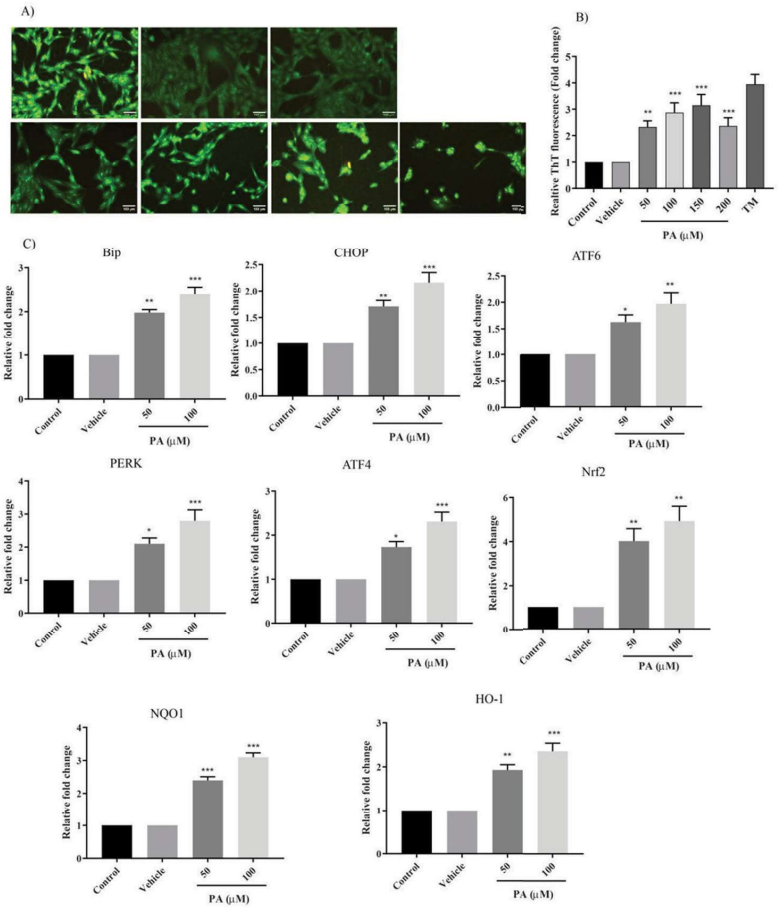

Figure 3: Development of ER stress in HCT15 cells upon PA treatment. HCT15 cells were treated with palmitic acid to assess ER stress markers. **(A)** Fluorescent microscopic images of ThT staining, visualising misfolded protein aggregation, captured at 400× magnification (scale bar: 100 µm). **(B)** Quantification of misfolded protein aggregation in cells represented as relative fold change. **(C)** RT-PCR analysis showing the relative fold change in the expression of ER stress, UPR, and antioxidant genes (BIP, CHOP, ATF6, PERK, ATF4) in response to PA treatment at 50 and 100 µM concentrations. Data are presented as mean ± SE, with statistical significance denoted by ***$p < 0.001$, *$p < 0.05$ and **$p < 0.01$.

3.5. Identification of shared upregulated genes in response to hypoxia and nutrient deprivation in HCT-15 colon cancer cells

Boxplot analysis of normalised gene expression data under hypoxia and nutrient deprivation conditions demonstrated consistent median values and no significant outliers. The uniform distribution of gene expression values across biological replicates, as well as their clustering in PCA plots, further validated the dataset's reliability for differential expression analysis (*Suppl. Fig. 1& Fig. 4A*). Differential expression (DEG) analysis identified 1,073 and 3733 genes as significantly upregulated under hypoxia and nutrient deprivation conditions, respectively. Among these, 1,034 genes were commonly upregulated under both conditions, suggesting shared transcriptional responses to these ER stress conditions (Fig. 4B & C).

3.6. PERK-mediated stress response and negative regulation resulting in senescence in HCT15 cells

Gene ontology analysis of commonly upregulated genes under hypoxia and nutrient deprivation revealed the activation of the PERK-mediated UPR, pathways of negative regulation, and signal transduction by the p53 class, all associated with senescence-induced cell cycle arrest. Specifically, the PERK-mediated unfolded protein response, under ER stress conditions, influences negative regulation and p53 pathways, which are critical in various cellular processes to overcome unfavourable conditions, indicating stress tolerance[17, 44, 45]. In addition, apoptotic pathways are also activated, suggesting severe ER stress in some cells. This observation highlights the heterogeneity of cancer cells, as some exhibit stress tolerance while others undergo cell death, as seen in HCT15 colon cancer cells (Fig. 4D).

Enrichment and network analyses revealed seven significantly enriched pathways (adjusted p-value < 0.05), three directly relevant to the study. The p53 signalling pathway (FDR = 1.2E-04, Fold Enrichment = 5.3) and transcriptional misregulation in cancer (FDR = 6.9E-03, Fold Enrichment = 2.7) were prominently enriched, highlighting their roles in regulating cell cycle arrest and senescence. Key p53 pathway genes, including *CDKN1A (p21)*, *GADD45A*, *BBC3*, and *SESN1*, were upregulated under stress, driving HCT15 cells into senescence by halting proliferation to prevent damage. *CDKN1A* mediated cell cycle arrest, *GADD45A* facilitated DNA repair, while *BBC3* and *SESN1* promoted stress-induced senescence. The transcriptional misregulation in cancer pathways involving *CDKN1A*, *GADD45A*, *MDM2*, and *CCND2* highlighted the contribution of dysregulated transcriptional pathways, notably p53, to senescence. Enrichment of the ferroptosis pathway (FDR = 1.2E-04, Fold Enrichment = 7.3) indicated oxidative stress-induced cell death driven by lipid peroxide accumulation, with severe ER stress triggering cell death in some cells. Significant pathways, including one-carbon folate,

ribosome, and COVID-19, were not central to the study's objectives (Fig. 4E, F). Analysis of the KEGG p53 signalling pathway (hsa04115) revealed that hypoxia and nutrient deprivation activate p53 signalling, upregulating effectors such as *p21* and *GADD45*, inducing cell cycle arrest and senescence under ER stress in HCT15 colon cancer cells (Fig. 5).

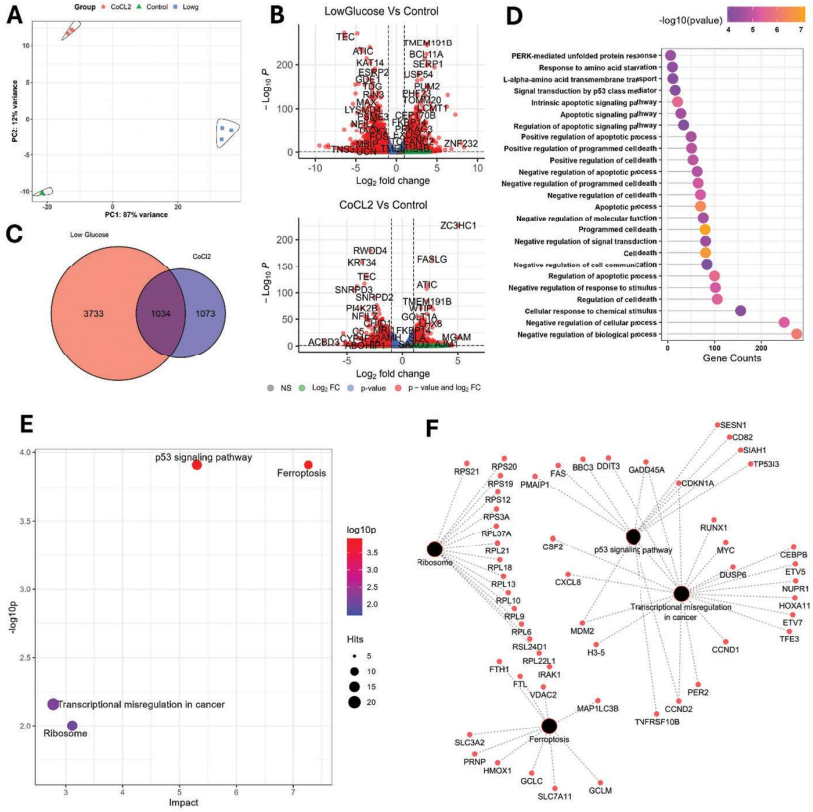

Figure 4: GEO data analysis of two ER stress conditions: hypoxia ($CoCl_2$) and nutrient deprivation (low glucose) in HCT15 colon cancer cells.

Gene expression data from GEO were analysed to assess the impact of hypoxia ($CoCl_2$) and nutrient deprivation (low glucose) on ER stress in HCT15 cells. **(A)** PCA analysis of gene expression in response to hypoxia and nutrient deprivation. **(B)** Volcano plot illustrating differentially expressed genes under hypoxic ($CoCl_2$) and nutrient-deprived (low glucose) conditions. **(C)** Venn diagram showing common DEGs identified in both hypoxia and nutrient deprivation conditions. **(D)** Dot plot displaying the biological processes associated with differentially expressed genes. **(E)** Fold Enrichment analysis highlighting significantly enriched pathways **(F)** Network analysis of genes from enriched pathways.

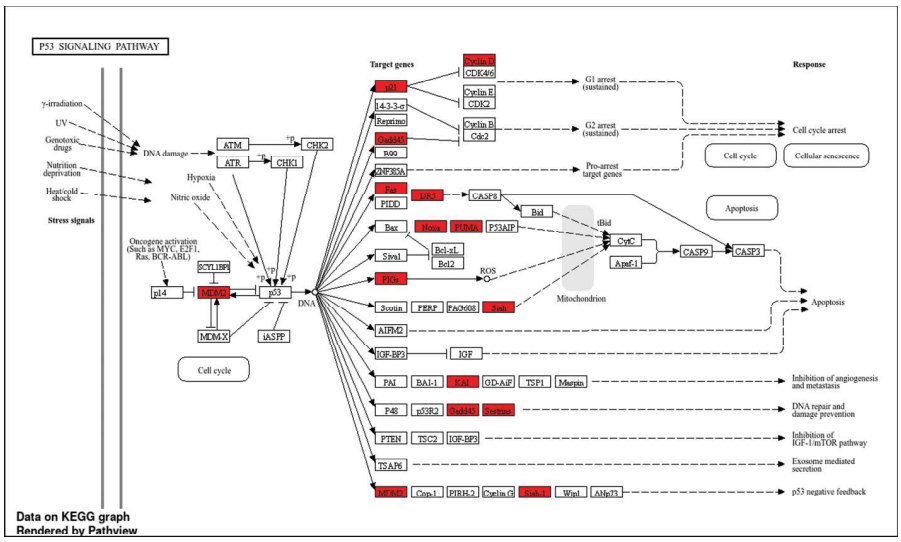

Figure 5: KEGG pathway analysis of common genes from hypoxia and nutrient deprivation. The KEGG analysis identified the *p53 signalling pathway* (hsa04115) as significantly enriched among the common differentially expressed genes under hypoxic ($CoCl_2$) and nutrient-deprived (low glucose) conditions.

4. Discussion

Palmitic acid significantly influences various cellular processes, including metabolism, oxidative stress, and protein homeostasis [46, 47]. In cancer cells, palmitic acid-induced metabolic reprogramming supports rapid growth and tumour progression, with ER stress playing a pivotal role in adapting to these metabolic challenges [48-50]. The current study examined the impact of palmitic acid on metabolic and ER stress in HCT15 colon cancer cells, focusing on the interplay between lipid accumulation, antioxidant responses, and the UPR. The study specifically examined how palmitic acid-induced metabolic stress activates the PERK arm of the UPR, linking lipid overload and metabolic stress to cellular senescence. The findings highlight the critical role of PERK signalling in coordinating cellular adaptation to PA-induced metabolic stress, driving senescence under moderate stress conditions while triggering cell death under extreme stress. Studying senescence, characterised by a permanent or premature exit from the cell cycle, is crucial as it allows cancer cells to adapt to stress, survive adverse conditions, and contribute to drug resistance[51, 52]. Understanding these mechanisms is vital for developing strategies to overcome therapeutic resistance and enhance treatment outcomes.

Our findings demonstrate that palmitic acid induces dose-dependent responses in HCT15 cells, promoting survival at lower concentrations (50 and

100 µM) and cytotoxicity at higher doses (150 and 200 µM). PA triggered lipid accumulation and increased ROS levels at all doses, indicating metabolic and oxidative stress [53-55]. A post-treatment colony formation assay revealed that lower concentrations supported colony formation while higher doses inhibited it. At "survival doses" (50 and 100 µM), adaptive mechanisms such as increased antioxidant enzyme activity (SOD and catalase) and lipid droplet formation mitigated ROS-induced damage. The lack of significant changes in glutathione-related antioxidants suggests the cell manages oxidative stress without depleting glutathione reserves. At "lethal doses" (150 and 200 µM), ROS accumulation overwhelmed antioxidant defences, leading to lipid peroxidation, glutathione depletion (measured by MDA), cellular damage, and reduced viability. The accumulation of oxidative stress surpasses compensatory mechanisms and may trigger apoptosis or necrosis[56, 57]. These dose-dependent effects highlight the balance between adaptive responses and oxidative damage, where excessive stress can overwhelm the cell's capacity to maintain homeostasis, leading to cell death, consistent with prior studies on metabolic stress [58-60].

As palmitic acid induces oxidative and metabolic stress, it contributes to toxicity in cancer cells while simultaneously promoting tumour progression and metastasis [2, 61-64]. This dual effect raises important questions about how palmitic acid can both promote cell death and facilitate cancer progression, highlighting the need for further investigation into the underlying mechanisms. In this context, ER stress, a key oxidative or metabolic stress consequence, is critical in cellular responses, influencing survival or apoptosis through the UPR. It also facilitates tumour initiation, progression, and metastasis by enabling cancer cells to adapt to adverse conditions. Moreover, UPR pathways such as IRE1/XBP1, PERK/ATF4, and ATF6 regulate survival, proliferation, and migration [9, 65]. Activation of the UPR, particularly the PERK pathway, has been identified in response to palmitic acid-induced stress [66, 67]. The PERK arm is crucial for cancer-related cellular stress, supporting proliferation progression [68, 69]. Consistent with previous findings, the current study also identified misfolded protein aggregates at survival doses, confirming palmitic acid-induced ER stress. The stress is accompanied by the upregulation of ER stress and UPR markers, such as BIP, CHOP, PERK, ATF4, and ATF6, and the activation of the PERK pathway, which promotes stress adaptation by reducing protein synthesis and enhancing protein folding [7, 70].

The study focused on adaptive responses, so RT-*q*PCR was not performed due to extreme toxicity and limited cell availability at lethal doses. CHOP expression was dose-dependent at survival doses, where adaptive responses predominated, though some cells still underwent death, as indicated by low CHOP levels. These findings are consistent with previous research showing that prolonged stress overwhelms PERK-mediated protective mechanisms,

leading to chronic ER stress and the upregulation of CHOP-induced pro-apoptotic factors. [71, 72]. This shift from adaptation to toxicity drives cell death, highlighting the dual role of the UPR in promoting survival under moderate stress and apoptosis under excessive stress [3, 73]. In line with previous studies, our study reported that the PERK/ATF4 pathway upregulated antioxidant genes (NRF2, NQO1, HO-1), essential for cellular homeostasis under oxidative stress [74-77].

One ER stress survival pathway involves tissue-specific UPR activation, leading to senescence in cancer cells, which can result from drug resistance or stressors independent of drug influx[55, 78, 79]. The PERK/ATF4 axis induces senescence under various stress conditions in cancer cells [17, 80]. GEO analysis of common genes under two ER stress conditions—$CoCl_2$-induced hypoxia and low-glucose-induced glucose deprivation—in HCT15 colon cancer cells demonstrated PERK-mediated activation of unfolded protein responses, negative regulation of cellular processes, p53 signalling, and apoptosis, as identified through Gene Ontology analysis. This negative regulatory mechanism suggests a slowdown in cellular processes and cell cycle arrest, consistent with previous research linking PERK-mediated unfolded protein responses to the p53 signalling pathway, contributing to senescence [44, 81, 82].

The study highlights the role of the p53 signalling pathway and transcriptional misregulation in cancer during ER stress in HCT15 cells. KEGG analysis indicates that the activation of p53 leads to cell cycle arrest and senescence, supported by the upregulation of key genes like p21 and GADD45 [83, 84]. Transcriptional misregulation involving CDKN1A, GADD45A, MDM2, and CCND2 further promotes senescence through dysregulated p53 pathways[85]. The ferroptosis pathway, linked to oxidative stress, involves SESN1 and BBC3, driving stress-induced senescence and cell death [86, 87]. This dual response reflects population heterogeneity, with stress-tolerant cells entering senescence and stress-intolerant cells dying. Overall, the findings confirm that ER stress activates PERK-mediated unfolded protein responses leading to senescence, with palmitic acid-induced metabolic stress also triggering PERK responses and linking metabolic stress to senescence in HCT15 cells.

5. Conclusion

Palmitic acid-induced ER stress in HCT15 colon cancer cells is mediated through the PERK-mediated pathway, establishing a connection between metabolic stress, cellular senescence, and cell death. Under tolerable stress, cells activate adaptive antioxidant responses to promote survival, while chronic or severe stress leads to irreversible damage and cell death. This study suggests that targeting the PERK-mediated UPR pathway may present

a novel therapeutic strategy for overcoming senescence-induced treatment resistance in colon cancer. However, a limitation of this study is the inability to perform RT-*q*PCR at higher palmitic acid concentrations due to toxicity, restricting the analysis to adaptive senescence mechanisms observed at lower concentrations.

Declaration of competing interest

The authors declare that they have no competing interests.

Appendix A. Supplementary data

Supplementary data for this article are provided in Supplementary Fig 1 and Supplementary Fig 2

Availability of data and materials

The original contributions of this study are detailed in the article, and further inquiries are available upon request.

Acknowledgement

The authors acknowledge the Department of Biochemistry, Amala Cancer Research Centre, Thrissur, Kerala, for providing all the facilities to conduct the research work. The first author is thankful to the Council of Scientific and Industrial Research (CSIR), New Delhi for the financial support (No: 21/12/2014(ii)EU-V dt. 24/7/2015).

Credit authorship contribution statement

Soumy V V: Conceptualization, Data curation, Funding acquisition, Investigation, Methodology, Validation, Writing – original draft. Snijesh V P: methodology, Software, Data Curation, Binoy C F: supervision, investigation, validation. Achuthan C R: Formal analysis, investigation, resource, supervision and validation. Dr. Suraj K: Former analysis, resources, supervision, validation, review & editing. Babu T D: Conceptualization, formal analysis, investigation, methodology, project administration, resources, supervision, validation, writing – review & editing.

Funding

Council of Scientific and Industrial Research (CSIR), India

References

[1]. F. Huang, B. Sun, X. Wang, X. Jian, Q. Du, and J. Chen, "Dietary palmitic acid promotes tumor growth and epithelial-mesenchymal transformation in prostate cancer," 2021.

[2]. S. Fatima *et al.*, "High-fat diet feeding and palmitic acid increase CRC growth in β2AR-dependent manner," vol. 10, no. 10, p. 711, 2019.

[3]. L. Yang, G. Guan, L. Lei, J. Liu, L. Cao, and X. J. B. r. Wang, "Oxidative and endoplasmic reticulum stresses are involved in palmitic acid-induced H9c2 cell apoptosis," vol. 39, no. 5, p. BSR20190225, 2019.

[4]. C. Hetz, K. Zhang, and R. J. J. N. r. M. c. b. Kaufman, "Mechanisms, regulation and functions of the unfolded protein response," vol. 21, no. 8, pp. 421-438, 2020.

[5]. M.-Z. Wu *et al.*, "LncRNA GOLGA2P10 is induced by PERK/ATF4/CHOP signaling and protects tumor cells from ER stress-induced apoptosis by regulating Bcl-2 family members," vol. 11, no. 4, p. 276, 2020.

[6]. A. Tóth *et al.*, "Activation of PERK/eIF2α/ATF4/CHOP branch of endoplasmic reticulum stress response and cooperation between HIF-1α and ATF4 promotes Daprodustat-induced vascular calcification," vol. 15, p. 1399248, 2024.

[7]. R. Ernst, M. F. Renne, A. Jain, and A. J. C. S. H. P. i. B. von der Malsburg, "Endoplasmic reticulum membrane homeostasis and the unfolded protein response," p. a041400, 2024.

[8]. S. Bernales, F. R. Papa, and P. J. A. R. C. D. B. Walter, "Intracellular signaling by the unfolded protein response," vol. 22, no. 1, pp. 487-508, 2006.

[9]. W. Zhang *et al.*, "Endoplasmic reticulum stress—a key guardian in cancer," vol. 10, no. 1, p. 343, 2024.

[10]. B. Yang, S. Wang, Y. Yang, X. Li, F. Yu, and T. J. F. i. I. Wang, "Endoplasmic reticulum stress in breast cancer: a predictive model for prognosis and therapy selection," vol. 15, p. 1332942, 2024.

[11]. C. Panico *et al.*, "Single-cell RNA sequencing reveals metabolic stress-dependent activation of cardiac macrophages in a model of dyslipidemia-induced diastolic dysfunction," vol. 150, no. 19, pp. 1517-1532, 2024.

[12]. W. G. Glanzner *et al.*, "NRF2 attenuation aggravates detrimental consequences of metabolic stress on cultured porcine parthenote embryos," vol. 14, no. 1, p. 2973, 2024.

[13]. Y. Shi, B. Jiang, J. J. B. Zhao, and Pharmacotherapy, "Induction mechanisms of autophagy and endoplasmic reticulum stress in intestinal ischemia-reperfusion injury, inflammatory bowel disease, and colorectal cancer," vol. 170, p. 115984, 2024.

[14]. R. J. de Boer, J. v. L. de Jeude, and J. J. C. L. Heijmans, "ER stress and the unfolded protein response in gastrointestinal stem cells and carcinogenesis," p. 216678, 2024.

[15]. D. Li *et al.*, "Interactions between oxidative stress and senescence in cancer: mechanisms, therapeutic implications, and future perspectives," vol. 73, p. 103208, 2024.

[16]. R. Di Micco, V. Krizhanovsky, D. Baker, and F. J. N. r. M. c. b. d'Adda di Fagagna, "Cellular senescence in ageing: from mechanisms to therapeutic opportunities," vol. 22, no. 2, pp. 75-95, 2021.

[17]. M. Ketkar *et al.*, "Inhibition of PERK-mediated unfolded protein response acts as a switch for reversal of residual senescence and as senolytic therapy in glioblastoma," vol. 26, no. 11, pp. 2027-2043, 2024.

[18]. A. M. Burgos-Molina, T. Téllez Santana, M. Redondo, and M. J. J. I. J. o. M. S. Bravo Romero, "The Crucial Role of Inflammation and the Immune System in Colorectal Cancer Carcinogenesis: A Comprehensive Perspective," vol. 25, no. 11, p. 6188, 2024.

[19]. A. L. Theiss and C. S. J. G. Williams, "Burn the fat: colon cancer tumors are skilled at lipid storage during obesity," 2024.

[20]. M. Zafaryab, K. U. Fakhri, M. A. Khan, K. Hajela, and M. M. A. J. I. J. L. S. R. Rizvi, "In vitro assessment of cytotoxic and apoptotic potential of palmitic acid for breast cancer treatment," vol. 7, no. 1, pp. 166-174, 2019.

[21]. G. Sharma, A. Parihar, P. Parihar, M. S. J. J. o. B. Parihar, and M. Toxicology, "Downregulation of sirtuin 3 by palmitic acid increases the oxidative stress, impairment of mitochondrial function, and apoptosis in liver cells," vol. 33, no. 8, p. e22337, 2019.

[22]. Y. Chen *et al.*, "PNPLA3 148M/M Is More Susceptible to Palmitic Acid-Induced Endoplasmic Reticulum Stress-Associated Apoptosis in HepG2 Cells," vol. 2023, no. 1, p. 2872408, 2023.

[23]. N. Brix, D. Samaga, R. Hennel, K. Gehr, H. Zitzelsberger, and K. Lauber, "The clonogenic assay: robustness of plating efficiency-based analysis is strongly compromised by cellular cooperation," *Radiation Oncology,* vol. 15, no. 1, p. 248, 2020/10/29 2020.

[24]. X. Hu *et al.*, "Effects of saturated palmitic acid and omega-3 polyunsaturated fatty acids on Sertoli cell apoptosis," (in eng), *Syst Biol Reprod Med,* vol. 64, no. 5, pp. 368-380, Oct 2018.

[25]. O. H. Lowry, N. J. Rosebrough, A. L. Farr, and R. J. Randall, "Protein measurement with the Folin phenol reagent," (in eng), *J Biol Chem,* vol. 193, no. 1, pp. 265-75, Nov 1951.

[26]. R. F. Beers, Jr. and I. W. Sizer, "A spectrophotometric method for measuring the breakdown of hydrogen peroxide by catalase," (in eng), *J Biol Chem,* vol. 195, no. 1, pp. 133-40, Mar 1952.

[27]. J. M. McCord and I. Fridovich, "Superoxide dismutase. An enzymic function for erythrocuprein (hemocuprein)," (in eng), *J Biol Chem,* vol. 244, no. 22, pp. 6049-55, Nov 25 1969.

[28]. W. H. Habig, M. J. Pabst, and W. B. J. J. o. b. C. Jakoby, "Glutathione S-transferases: the first enzymatic step in mercapturic acid formation," vol. 249, no. 22, pp. 7130-7139, 1974.

[29]. P. C. Simons and D. L. J. A. B. Vander Jagt, "Purification of glutathione S-transferases from human liver by glutathione-affinity chromatography," vol. 82, no. 2, pp. 334-341, 1977.

[30]. R. D. Mavis and E. J. J. o. B. C. Stellwagen, "Purification and subunit structure of glutathione reductase from bakers' yeast," vol. 243, no. 4, pp. 809-814, 1968.

[31]. E. Racker, "[127] Glutathione reductase1 (liver and yeast)," 1955.

[32]. I. Rahman, A. Kode, and S. K. J. N. p. Biswas, "Assay for quantitative determination of glutathione and glutathione disulfide levels using enzymatic recycling method," vol. 1, no. 6, pp. 3159-3165, 2006.

[33]. D. E. Paglia, W. N. J. T. J. o. l. Valentine, and c. medicine, "Studies on the quantitative and qualitative characterization of erythrocyte glutathione peroxidase," vol. 70, no. 1, pp. 158-169, 1967.

[34]. H. Ohkawa, N. Ohishi, and K. J. A. b. Yagi, "Assay for lipid peroxides in animal tissues by thiobarbituric acid reaction," vol. 95, no. 2, pp. 351-358, 1979.

[35]. D. R. Beriault and G. H. J. B. e. B. A.-M. C. R. Werstuck, "Detection and quantification of endoplasmic reticulum stress in living cells using the fluorescent compound, Thioflavin T," vol. 1833, no. 10, pp. 2293-2301, 2013.

[36]. K. J. Livak and T. D. J. m. Schmittgen, "Analysis of relative gene expression data using real-time quantitative PCR and the 2− ΔΔCT method," vol. 25, no. 4, pp. 402-408, 2001.

[37]. B. Xu *et al.*, "Inositol hexaphosphate enhances chemotherapy by reversing senescence induced by persistently activated PERK and diphthamide modification of eEF2," vol. 582, p. 216591, 2024.

[38]. S. Andrews, "FastQC: a quality control tool for high throughput sequence data. 2010," ed, 2017.

[39]. F. Krueger, "TrimGalore: A wrapper tool around Cutadapt and FastQC to consistently apply quality and adapter trimming to FastQ files. Babraham Bioinformatics," ed, 2015.

[40]. A. Dobin *et al.*, "STAR: ultrafast universal RNA-seq aligner," vol. 29, no. 1, pp. 15-21, 2013.

[41]. Y. Liao, G. K. Smyth, and W. J. B. Shi, "featureCounts: an efficient general purpose program for assigning sequence reads to genomic features," vol. 30, no. 7, pp. 923-930, 2014.

[42]. M. I. Love, W. Huber, and S. J. G. b. Anders, "Moderated estimation of fold change and dispersion for RNA-seq data with DESeq2," vol. 15, pp. 1-21, 2014.

[43]. V. P. Nimbalkar *et al.*, "Premenopausal women with breast cancer in the early post-partum period show molecular profiles of invasion and are associated with poor prognosis," vol. 200, no. 1, pp. 139-149, 2023.

[44]. L. Fusée *et al.*, "The p53 endoplasmic reticulum stress-response pathway evolved in humans but not in mice via PERK-regulated p53 mRNA structures," *Cell Death & Differentiation,* vol. 30, no. 4, pp. 1072-1081, 2023/04/01 2023.

[45]. G. Alasiri *et al.*, "Reciprocal regulation between GCN2 (eIF2AK4) and PERK (eIF2AK3) through the JNK-FOXO3 axis to modulate cancer drug resistance and clonal survival," *Molecular and Cellular Endocrinology,* vol. 515, p. 110932, 2020/09/15/ 2020.

[46]. L. D. Ly *et al.*, "Oxidative stress and calcium dysregulation by palmitate in type 2 diabetes," (in eng), *Exp Mol Med,* vol. 49, no. 2, p. e291, Feb 3 2017.

[47]. G. Carta, E. Murru, S. Banni, and C. Manca, "Palmitic Acid: Physiological Role, Metabolism and Nutritional Implications," (in eng), *Front Physiol,* vol. 8, p. 902, 2017.

[48]. S. Beloribi-Djefaflia, S. Vasseur, and F. J. O. Guillaumond, "Lipid metabolic reprogramming in cancer cells," vol. 5, no. 1, pp. e189-e189, 2016.

[49]. C. Schiliro and B. L. J. C. Firestein, "Mechanisms of metabolic reprogramming in cancer cells supporting enhanced growth and proliferation," vol. 10, no. 5, p. 1056, 2021.

[50]. M. Correia de Sousa, E. Delangre, M. Türkal, M. Foti, and M. J. I. J. o. M. S. Gjorgjieva, "Endoplasmic reticulum stress in renal cell carcinoma," vol. 24, no. 5, p. 4914, 2023.

[51]. J. Mikuła-Pietrasik, A. Niklas, P. Uruski, A. Tykarski, K. J. C. Książek, and M. L. Sciences, "Mechanisms and significance of therapy-induced and spontaneous senescence of cancer cells," vol. 77, pp. 213-229, 2020.

[52]. S. Lee and C. A. J. N. c. b. Schmitt, "The dynamic nature of senescence in cancer," vol. 21, no. 1, pp. 94-101, 2019.

[53]. S. Chen *et al.*, "New insights into the role of mitochondrial dynamics in oxidative stress-induced diseases," vol. 178, p. 117084, 2024.

[54]. L. V. Bel'skaya and E. I. J. C. I. i. M. B. Dyachenko, "Oxidative Stress in Breast Cancer: A Biochemical Map of Reactive Oxygen Species Production," vol. 46, no. 5, pp. 4646-4687, 2024.

[55]. X. Chen *et al.*, "Palmitic acid induces lipid droplet accumulation and senescence in nucleus pulposus cells via ER-stress pathway," vol. 7, no. 1, p. 539, 2024.

[56]. J. M. Matés, J. A. Segura, F. J. Alonso, and J. J. A. o. t. Márquez, "Intracellular redox status and oxidative stress: implications for cell proliferation, apoptosis, and carcinogenesis," vol. 82, pp. 273-299, 2008.

[57]. M. R. Chaudhary *et al.*, "Aging, oxidative stress and degenerative diseases: mechanisms, complications and emerging therapeutic strategies," vol. 24, no. 5, pp. 609-662, 2023.

[58]. S. X. Mthembu *et al.*, "Low levels and partial exposure to palmitic acid improves mitochondrial function and the oxidative status of cultured cardiomyoblasts," vol. 12, pp. 234-243, 2024.

[59]. B. Vidrio-Huerta, T. Plötz, and S. J. J. o. M. E. Lortz, "Oxidative and ER stress by elevated insulin biosynthesis and palmitic acid in insulin-producing cells," vol. 72, no. 2, 2024.

[60]. M. D. Yener, T. Çolak, Ö. D. Özsoy, and F. C. J. J. o. I. F. o. M. Eraldemir, "ALTERATIONS IN CATALASE, SUPEROXIDE DISMUTASE, GLUTATHIONE PEROXIDASE AND MALONDIALDEHYDE LEVELS IN SERUM AND LIVER TISSUE UNDER STRESS CONDITIONS," vol. 87, no. 2, pp. 145-152, 2024.

[61]. A. Alnahdi, A. John, and H. J. N. Raza, "Augmentation of glucotoxicity, oxidative stress, apoptosis and mitochondrial dysfunction in HepG2 cells by palmitic acid," vol. 11, no. 9, p. 1979, 2019.

[62]. E.-J. Park, A. Y. Lee, S. Park, J.-H. Kim, M.-H. J. F. Cho, and C. Toxicology, "Multiple pathways are involved in palmitic acid-induced toxicity," vol. 67, pp. 26-34, 2014.

[63]. Q. Zhang *et al.*, "Reprogramming of palmitic acid induced by dephosphorylation of ACOX1 promotes β-catenin palmitoylation to drive colorectal cancer progression," vol. 9, no. 1, p. 26, 2023.

[64]. X. Zhang *et al.*, "Palmitic acid promotes lung metastasis of melanomas via the TLR4/TRIF-Peli1-pNF-κB pathway," vol. 12, no. 11, p. 1132, 2022.

[65]. G. Porter, "Dissecting the role of endoplasmic reticulum stress in cancer progression," UNSW Sydney, 2024.

[66]. A. Griffiths *et al.*, "ATF4-mediated CD36 upregulation contributes to palmitate-induced lipotoxicity in hepatocytes," vol. 324, no. 5, pp. G341-G353, 2023.

[67]. H. Cho, M. Wu, L. Zhang, R. Thompson, A. Nath, and C. Chan, "Signaling dynamics of palmitate-induced ER stress responses mediated by ATF4 in HepG2 cells," *BMC Systems Biology,* vol. 7, no. 1, p. 9, 2013/01/22 2013.

[68]. Y. Wang *et al.*, "The unfolded protein response induces the angiogenic switch in human tumor cells through the PERK/ATF4 pathway," vol. 72, no. 20, pp. 5396-5406, 2012.

[69]. A. Nagelkerke *et al.*, "Hypoxia stimulates migration of breast cancer cells via the PERK/ATF4/LAMP3-arm of the unfolded protein response," vol. 15, pp. 1-13, 2013.

[70]. L. Carciero *et al.*, "The interplay of extracellular vesicles in the pathogenesis of metabolic impairment and type 2 diabetes," p. 111837, 2024.

[71]. Y. Fang *et al.*, "Inhibition of SLC40A1 represses osteoblast formation via inducing iron accumulation and activating the PERK/ATF4/CHOP pathway mediated oxidative stress," vol. 29, no. 1, p. 2428147, 2024.

[72]. L. Liu *et al.*, "Qing Hua Chang Yin ameliorates chronic colitis in mice by inhibiting PERK–ATF4–CHOP pathway of ER stress and the NF-κB signalling pathway," vol. 62, no. 1, pp. 607-620, 2024.

[73]. Y. Zhang, R. Xue, Z. Zhang, X. Yang, H. J. L. i. h. Shi, and disease, "Palmitic and linoleic acids induce ER stress and apoptosis in hepatoma cells," vol. 11, pp. 1-8, 2012.

[74]. C. Sarcinelli *et al.*, "ATF4-dependent NRF2 transcriptional regulation promotes antioxidant protection during endoplasmic reticulum stress," vol. 12, no. 3, p. 569, 2020.

[75]. S. B. Cullinan, J. A. J. T. i. j. o. b. Diehl, and c. biology, "Coordination of ER and oxidative stress signaling: the PERK/Nrf2 signaling pathway," vol. 38, no. 3, pp. 317-332, 2006.

[76]. S. B. Cullinan *et al.*, "Nrf2 is a direct PERK substrate and effector of PERK-dependent cell survival," vol. 23, no. 20, pp. 7198-7209, 2003.

[77]. J. Wang *et al.*, "Up-regulation of PERK/Nrf2/HO-1 axis protects myocardial tissues of mice from damage triggered by ischemia-reperfusion through ameliorating endoplasmic reticulum stress," vol. 10, no. 3, p. 500, 2020.

[78]. J. H. Lee and J. Lee, "Endoplasmic Reticulum (ER) Stress and Its Role in Pancreatic β-Cell Dysfunction and Senescence in Type 2 Diabetes," (in eng), *Int J Mol Sci,* vol. 23, no. 9, Apr 27 2022.

[79]. Z. Z. Ei *et al.*, "GRP78/BiP determines senescence evasion cell fate after cisplatin-based chemotherapy," *Scientific Reports,* vol. 11, no. 1, p. 22448, 2021/11/17 2021.

[80]. D. R. Fels, C. J. C. b. Koumenis, and therapy, "The PERK/eIF2α/ATF4 module of the UPR in hypoxia resistance and tumor growth," vol. 5, no. 7, pp. 723-728, 2006.

[81]. S. Courtois-Cox *et al.*, "A negative feedback signaling network underlies oncogene-induced senescence," vol. 10, no. 6, pp. 459-472, 2006.

[82]. J. J. A. r. o. p. Campisi, "Aging, cellular senescence, and cancer," vol. 75, no. 1, pp. 685-705, 2013.

[83]. X. W. Wang *et al.*, "GADD45 induction of a G2/M cell cycle checkpoint," vol. 96, no. 7, pp. 3706-3711, 1999.

[84]. X. Palomer, J. M. Salvador, C. Griñán-Ferré, E. Barroso, M. Pallàs, and M. J. M. R. R. Vázquez-Carrera, "GADD45A: With or without You," vol. 44, no. 4, pp. 1375-1403, 2024.

[85]. N. Wechter *et al.*, "Single-cell transcriptomic analysis uncovers diverse and dynamic senescent cell populations," (in eng), *Aging (Albany NY),* vol. 15, no. 8, pp. 2824-2851, Apr 19 2023.

[86]. M. J. P. B. Rusin, "The p53 protein–not only the guardian of the genome," vol. 70, no. 1, pp. 71-87, 2024.

[87]. S. Martello *et al.*, "Developing an RNA Signature for Radiation Injury Using a Human Liver-on-a-Chip Model," vol. 202, no. 3, pp. 489-502, 2024.